NANYANG TECHNOLOGICAL UNIVERSITY
SINGAPORE

Suction, hydraulic and strength properties of compacted soils

KIZZA RICHARD

School of Civil and Environmental Engineering

2019

Suction, hydraulic and strength properties of compacted soils

KIZZA RICHARD

School of Civil and Environmental Engineering

A thesis submitted to the Nanyang Technological University
in partial fulfilment of the requirement for the degree of
Doctor of Philosophy

Statement of Originality

I hereby certify that the work embodied in this thesis is the result of original research, is free of plagiarized materials and has not been submitted for a higher degree to any other University or Institution

5th December 2019

Kizza Richard

Supervisor Declaration Statement

I have reviewed the content and presentation style of this thesis and declare it free of plagiarism and of sufficient grammatical clarity to be examined. To the best of my knowledge, the research and writing are those of the candidate except as acknowledged by the Author Attribution Statement. I confirm that the investigations were conducted in accord with the ethic policies and Integrity standards of Nanyang Technological University and that the research data are presented honestly and without prejudice

6 Dec 2019

Date

Assoc. Prof. E.C.Leong

Authorship Attribution Statement

This thesis contains material from two conference papers and two manuscripts submitted to journals and currently under review where I was either the first or second author. Unless otherwise referenced, this thesis has been developed with the sole assistance of my supervisor who contributed ideas on the presentation of the thesis and analysis of the data. My supervisor has also contributed in way of proof-reading the work herein.

The material from my papers is distributed as follows in the thesis:

Chapter 4 contains material from the papers:

Leong, E.-C., Kizza, R. & Rahardjo, H. Measurement of soil suction using moist filter paper. E3S Web of Conferences, 2016. EDP Sciences, 10012.

Kizza, R & Leong, E.C. Suction measurements using initially dry and initially wet filter papers. Manuscript submitted to Geotechnical and Testing Journal. Under Review.

Chapter 6 contains material from the papers:

Kizza ,R., Leong, E.C & Rahardjo,H. Matric suction and shear strength of dynamically compacted soils. In Unsaturated soils: Research and Applications 2014. Taylor and Francis Group.

Kizza, R & Leong, E.C. Unconfined Strength and Tensile Strength of Compacted soils. Manuscript submitted to Canadian Geotechnical Journal. Under Review.

Material presented in chapters 5 and 7 is yet to be developed into publishable material.

5th December 2019

Kizza Richard

Acknowledgements

I extend my deepest gratitude to my supervisor Associate Professor Leong EngChoon first for accepting me as student in his research team, secondly for the excellent guidance received from him during my PhD studies and for his extreme patience with me and the willingness to address all my knowledge gaps.
My deep appreciation is also extended to Professor Harianto Rahardjo for all the assistance and encouragement extended to me. Your words of wisdom are always memorable.

I am also grateful to the Geotechnical Engineering Laboratory staff: Mr HengHiang Kim Vincent, Mr Tan Hiap Guan Eugene, Ms Susie Lim-Ding, and Mr Koh Sun Weng Andy for all the assistance they extended to me during my experimental work. Special thanks to Mr. Phua formerly of the Construction workshop for always being ready to help with the fabrications of the different equipment and apparatus necessary for the studies.

I am equally grateful to the administrative staff of CEE: Ms Ng Soo Ching , Ms Ng Hui Leng and Ms. Jamillah Bte Sa'adon for always being ready to assist with all manner of administrative issues.

Special thanks to the many friends just to mention a few: Dr. Huang Wengui (Winston), Mr. Sam Bulolo, Dr. Martin Wijaya, Dr. Alfrendo Satyanaga, Dr. Zhai Qai, Dr. Zhuoyuan, Mr. Ashraf Mohammed Assewaff, Mr. Varun Maruvanchery, Mr. Zul, and all treasured friends I met in Singapore. Thank you for all the assistance in all the forms am sure you know.

To my family back home in Uganda: What can I say? Thank you for the support through the years. This began many years ago. Thank you indeed.

My PhD studies and subsistence were funded by the Singapore International Graduate Award (SINGA). The financial assistance from SINGA is gratefully acknowledged.

Last but not least, I extend my greatest gratitude to God the Almighty for bringing me this far

Summary

Although enormous strides have been made in terms of theoretical and experimental advancements of unsaturated soil mechanics, its application in engineering practice remains limited. Reasons for limited application include expensive equipment required to measure unsaturated soil properties, long durations to measure these properties, high level of expertise required and the lack of simple and accessible tools for the practicing engineer to obtain unsaturated soil properties especially for routine work.

This background motivated this PhD study with the main objective to evaluate and investigate simple, economical and accessible techniques of measuring unsaturated soil properties. Three properties were studied: suction, hydraulic and strength. These properties were evaluated using dynamically compacted residual soils. Four residual soils obtained from the two major geological formations of Singapore; Jurong Formation and Bukit Timah Granite were studied.

For suction measurements, the filter paper method was studied and measurements were compared with those from a chilled-mirror dewpoint technique. The study investigated the use of both initially dry and initially wet filter papers in an attempt to reduce equilibration time and eliminate the need for two calibration curves. The study found that the use of initially wet filter paper did not reduce equilibration time, equilibration time is dependent on the mode of contact and that the non-contact filter paper requires much longer time to equilibrate. For low suctions, the non-contact filter paper may not reach equilibrium within the common durations used in literature of 7, 15, 21 or 28 days. Although there is a tendency for an initially wet filter paper used in the non-contact mode to approach the matric suction calibration curve, it may not reach equilibrium at the matric suction calibration curve within a practical time frame. The contact filter paper which measures matric suction can reliably

measure suctions both in the low and high range while the non-contact is best suited for suctions in the high range preferable above 1000 kPa. The hysteretic behavior was investigated by comparing suction measurements from initially dry and initially wet filter papers. A hysteresis within the range 3-5% was observed. Using this hysteresis, existing calibration curves can be modified to read suction from initially wet filter papers. Generally, an initially dry filter paper is preferable to an initially wet filter paper for both contact modes because an initially dry filter paper requires a less strict protocol. Finally, the study compared variation in filter papers before and after use and found that the variations were minor to warrant use of sacrificial filter papers as recommended in ASTM D5298-16.

Hydraulic properties of compacted soils were studied using a mini-disk infiltrometer and the conventional flexible wall permeameter were compared. A good agreement was found between the two. Because, the interpretation of the mini-disk infiltrometer requires prior knowledge of van Genutchen SWCC equation parameters, different approaches of obtaining these parameters were studied. It was found that all the approaches yield saturated permeabilities within two orders from the saturated permeability measured from the flexible wall permeameter. This being within acceptable error margin means that the mini-disk infiltrometer can be applied reliably to measure near saturated permeabilities hence reducing testing time for field permeability measurements.

Lastly, using conventional strength tests like the Brazilian tensile strength test, unconfined compression test, unconsolidated undrained shear strength test and consolidated undrained test, strength of the compacted soils were investigated. Observations suggest that shear strength parameters of unsaturated soils may be estimated from an initial suction measurement and the saturated shear strength parameters. Bounds of shear strength using Bishop's χ factor was evaluated and it seems possible to obtain a lower bound that is appropriate for engineering practice.

Table of contents

List of Tables

List of Figures

List of symbols/Abbreviations

A	Cross sectional area of a soil specimen
a	Fredlund and Xing (1994) SWCC model fitting parameter
α	van Genuchten (1980) model fitting parameter
AEV	Air-entry value of soil
c'	Effective soil cohesion
CW	Constant water content test
E	Total energy
e	void ratio
e_{min}	Minimum void ratio
e_0	Initial void ratio
g	Gravitational acceleration
G_s	Specific gravity
γ_w	Specific weight of water
HAE	High Air Entry
HCT	High Capacity Tensiometer
h_w	Hydraulic head or total head
h_1	Head of water at t_1

h_2	Head of water at t_2
Δh_w	Hydraulic head difference
Mw	Mass of water a selected point
m	A fitting parameter related to residual water content
μ	Viscosity of a fluid
n	van Genuchten (1980) model fitting parameter
p	Pressure
Θ	Normalized volumetric water content
θ	volumetric water content
θ_s	Saturated volumetric
$RMSE$	Root mean square error
R	Universal gas constant
r	Distance from center of circular tube from concentric cylindrical surface
ρ_w	Density of water
ρ	Pore radius
S	Degree of saturation
Se	Effective degree of saturation
Sr	Residual degree of saturation

SWCC	Soil Water Characteristic Curve
SWCC-S	Soil Water Characteristic curve based on degree of saturation
SWCC-w	Soil Water Characteristic curve based on gravimetric water content
SWCC-θ	Soil Water Characteristic curve based on volumetric water content
T	Absolute temperature
Ts	Surface tension
t	Time
τ	Shear strength
u_a	Pore-air pressure
u_w	Pore-water pressure
$u_a - u_w$	Matric suction
$\bar{u}v$	Partial pressure of pore-water vapor
$\bar{u}v0$	Saturation pressure of water vapor over a flat surface of pure water at the same temperature
w	gravimetric water content
χ	Bishop's effective stress parameter
ρ_d	Dry density
ψ	Soil suction

ψr	Suction corresponding to residual water content
σ	Total normal stress
σ'	Effective normal stress
$\sigma - u_a$	Net normal stress

Chapter 1. Introduction

1.1 Background to the study

Although geotechnical engineering practice has registered enormous success over the decades with the application of saturated soil mechanics, it is increasingly becoming clear that unsaturated soil mechanics can explain several phenomena better such as rain-induced slope failures. Commonly, these slope instabilities occur during rainy seasons of the year and in unsaturated materials. These landslides result in loss of lives as well as destruction of property. It has been noted by several researchers (e.g. Toll et al. 1999, Rahardjo et al.,2009, 2013) that understanding the cause as well as design of remedial systems require sound knowledge of unsaturated soil mechanics.

Secondly, major geotechnical structures like dams, foundations are often located in the unsaturated zone which means that they are influenced by the negative pore-water pressures (Tarantino and El Mountassir, 2013). Therefore it is important to consider ground-atmosphere interactions that will influence their performance throughout their design life. More care is needed when these geotechnical structures are built in soils susceptible to collapse and swelling on wetting to avoid future remedial costs that may arise if ignored.

The adoption of unsaturated soil mechanics principles in the design of geotechnical structures may also avoid the problem of over design often encountered when full saturation of soils is assumed in designs (Tarantino and El Mountassir (2013). Despite these glaring demands for unsaturated soil mechanics, unsaturated soil mechanics largely remains in research institutions with little application in practice. The low application of unsaturated soil mechanics is largely due to excessive costs and time required to determine unsaturated soil properties such as soil suction, permeability and shear strength (Fredlund, 2000; Tarantino

and El Mountassir, 2013; Vanapalli, 1995; Oh, 2012).With these obstacles, the practical application of unsaturated soil mechanics principles remains low especially in developing economies. Ironically, these principles are most needed in the developing world which lies in the tropics where unsaturated soils are often encountered.

To incorporate unsaturated soil mechanics into routine engineering practice will require more accessible tests to measure the soil properties. In some cases, this entails improvements to the existing experimental protocols. In addition, there is a need to connect unsaturated soil mechanics empirically or analytically with the experiences already gained from saturated soil mechanics.

Therefore, this research attempts to study the performance and reliability of simple, economical experimental techniques and procedures with the major aim of extending unsaturated soil mechanics to engineering practice.

1.2 Objectives and Scope

The main objective of this study is to investigate and evaluate simple, affordable and yet reliable tests to determine unsaturated soil properties. The study is motivated by the need to make unsaturated soil mechanics more accessible to practicing engineers especially those in developing countries. The study focuses on:

Suction measurements:

Although the filter paper and chilled-mirror dewpoint techniques are already in use as suction measurement techniques, researchers have not agreed on a number of issues regarding their use. For the filter paper technique, a number of studies have been done and the method has been standardized (ASTM D5298-16). However, its acceptance by researchers and practitioners has remained low largely because of questions on reliability. Using dynamically

compacted soils, several aspects of the filter paper technique are studied. The main factors investigated are equilibration time, hysteresis of the filter paper, applicable calibration curve, and inherent variability of the filter papers. Initially wet filter paper was explored with the aim of establishing any advantages over the conventional initially dry filter paper. The chilled-mirror dewpoint technique was used to benchmark against filter paper measurements for high suctions. Many filter paper tests were performed. It is envisaged that the experience and discussions greatly improve the understanding of this valuable yet very accessible technique.

Hydraulic properties:

Permeability is an important parameter in modelling water flow through soils and is needed in several geotechnical engineering problems such as rain-induced landslides, seepage through dams, and design of waste management systems. However, most of the existing techniques for measuring permeability are laborious, time consuming and may not represent actual field conditions. This study has therefore explored the use of the mini-disk infiltrometer in the estimation of near-saturated permeabilities of soils. The disk infiltrometer has been reported as inexpensive, robust and gives fast measurements of permeability. Despite these attributes, the disk infiltrometer has not been widely adopted by the geotechnical engineering community. Most of the existing studies on the disk infiltrometer have been done by soil scientists and hydrologists. In this study, permeability measurements using a disk infiltrometer were done on compacted soils and compared with measurements from the flexible wall permeameter. The findings and discussions are presented in the thesis.

Shear strength measurements:

Shear strength of soil is very crucial in the design of any geotechnical structure. It is also necessary in back analyses of failed geotechnical structures and for designing remedial measures. However measuring unsaturated soil shear strength is not only laborious but takes a long time and requires expensive equipment and high level of expertise to interpret the test results.

Therefore the study also investigates the possibility of determining shear strength of unsaturated soils using conventional soil test equipment and constant water content (CW) tests. In the thesis, unconfined compressive strength tests, unconsolidated undrained tests as well as the consolidated undrained test for saturated soils are also examined to interpret a constant water content shear strength test. Shear strength and tensile strength of dried and as-compacted soil specimens were examined to investigate the effects of soil structure, soil suction and void ratio.

1.3 Thesis Outline and description of the report.

This report consists of eight chapters and appendices:

Chapter One outlines the background of the study, its significance, objectives and scope.

Chapter Two reviews the literature relevant to the study. The literature review highlights the current state of knowledge in terms of theoretical advancements as well as the experimental techniques relevant to the thesis. The key debates and points of contention are highlighted and finally, the gaps the study aims to fill are pointed out.

In Chapter Three, the soil materials and the test specimen preparation are presented. The experimental work including the tests, equipment and apparatus used are also presented. The

test procedures followed have been noted and where deviations from the standards have been made, this too has been highlighted.

Chapter Four presents the results and discussion on suction measurements and soil-water characteristic curves of the test specimens.

Chapter Five presents results and discussion of the hydraulic properties of compacted soils. Both infiltration studies and measurements of saturated permeabilities in a flexible wall permeameter are presented.

Chapter Six presents results and discussion of the unconfined compressive strength and tensile strength of compacted soils.

Chapter Seven presents the results and interpretation of constant water content tests done using the unconfined compressive strength tests, unconsolidated undrained strength tests and the consolidated undrained tests on saturated soil specimens

Chapter Eight presents the conclusions of this study as well as the recommendations for further work.

Appendices

Finally appendices containing data either secondary to the discussions in the thesis or primary data in excess of what could be presented in the main thesis.

Chapter 2. Literature Review

2.1 Introduction

This chapter presents a review of the literature related to the different aspects of the study. The chapter covers the basic concepts related to unsaturated soil mechanics, water retention behavior, soil suction measurements and control, hydraulic behavior and strength of unsaturated soils. The review includes both the governing theories and experimental techniques commonly used in measuring the various properties of unsaturated soils. The chapter concludes by justifying the need for the present study

2.2 Unsaturated soils and their prevalence

While the pore space of saturated soils is completely filled with a liquid (typically water), that of unsaturated soils is partly filled with water and air. The inclusion of air in the pores makes unsaturated soils a multi-phase porous system. The behavior of these soils is controlled by the mutual interaction between the two phases (air and water) with the solid component (Fredlund and Rahardjo, 1993; Laloui, 2013).The mechanisms of interaction in such a multi-phase system introduce several complexities in terms of material behavior, testing techniques and numerical modeling (El Mountassir, 2011).

Unsaturated soils are prevalent especially in the tropical region of the world. In these areas, the near ground surface is usually unsaturated, i.e. has negative pore-water pressures, due to climatic conditions,. The depth of the unsaturated zone varies according to the local climatic conditions, ranging from several metres deep in the arid regions to just a few metres in the temperate zone. Figure 2.1 shows a simplified hydrological cycle in nature illustrating the complex interactions between climate, atmosphere and the ground. It is shown how the ground loses water to the atmosphere through evaporation and evapotranspiration. These

processes (evaporation and evapotranspiration) result into an upward flux for soil moisture causing drying, desaturation and desiccation cracks in the soils. On the other hand, the soil is recharged during a precipitation, Hence, a downward flux of water which results into an increase in the soil's degree of saturation and increase in pore-water pressure.

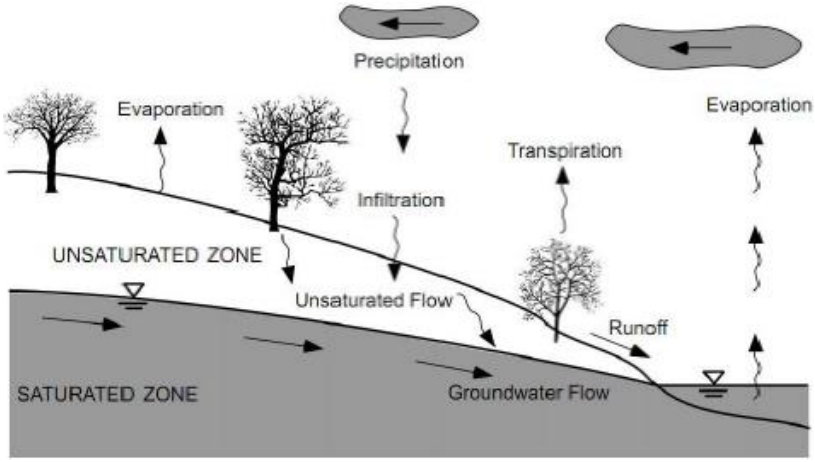

Figure 2.1: Interaction between unsaturated zone and the hydrological cycle (from Lu and Likos, 2004)

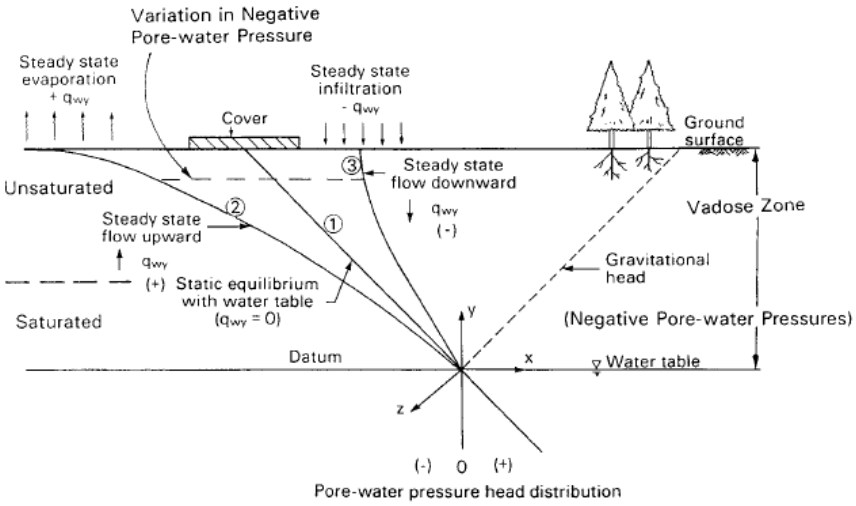

Figure 2.2: Illustration of flux processes in the unsaturated (vadose) zone (from Fredlund and Rahardjo, 1993)

Using lines 1, 2 and 3, Figure 2-2 illustrates the processes of static equilibrium, upward flux and downward flux, respectively, in the unsaturated (vadose) zone. Static equilibrium occurs when no net flux occurs across the unsaturated zone hence the hydrostatic line.

In addition to natural deposits, engineered soils such as compacted soils are also unsaturated. In fact, compacted soils are the only form of unsaturated soils that are encountered in classical soil mechanics. Compacted soils are commonly used in civil engineering works as fill material in embankments and dams, backfill behind retaining walls.

Gassy soils have also been reported as another possible form of unsaturated soils (Wheeler, 1988). Such soils result from biological activity when gases are released into the soil deposit or due to flow of gases into a deposit from a hydrocarbon reservoir (El Mountassir, 2011). These soils are usually found in deep offshore environments or in organic deposits with anaerobic activity taking place.

In this study, dynamically compacted soils are the main form of unsaturated soils studied.

2.3 Stress state variables for unsaturated soils

While there is general consensus regarding the stress state variable for saturated soils, there is still ongoing debate regarding the most suitable stress state variable(s) to describe unsaturated soils. The disagreement on the choice of stress state variable (s) is based on (Wijaya (2017):

- Capacity to evaluate both deformation and strength of the material without any difficulties.
- Appropriateness of including material properties as part of stress state variables. This arguably violates the principles of continuum mechanics
- The need to have continuity between saturated and unsaturated soil mechanics.
- The ease of measurement of the stress state variable both in the field and laboratory.

Owing to these disagreements, different researchers have suggested different stress state variables for unsaturated soils. The different approaches suggested can be categorized into three:

1. Single effective stress
2. Independent stress-state variables
3. Alternative /Modified stress variables(El Mountassir, 2011, Wijaya, 2017)

These approaches are briefly discussed below.

2.3.1 Single effective stress approach.

The effective stress approach proposed by Bishop (1959) is the commonest. Bishop (1959) proposed that effective stress in an unsaturated soil can be defined by combining two stress state variables i.e. net normal stress, $(\sigma_n\text{-}u_a)$ and matric suction, $(u_a\text{-}u_w)$ in addition to a material variable, χ . This formulation is reproduced in Equation 2.1.

$$\sigma' = (\sigma - u_a) + \chi(u_a - u_w) \qquad (2.1)$$

where u_a is pore-air pressure and u_w is the pore-water pressure. χ was assumed to take on values between 0 and 1

One noted advantage of the effective stress approach is that it follows directly from the classical soil mechanics formalism of effective stress.

While effective stress approach seems practically attractive, it has received a lot of criticisms from different researchers over the years, for example Burland (1965) argues that it is incorrect to combine both stress state variables $(\sigma_n\text{-}u_a)$ and $(u_a\text{-}u_w)$ into one equation. Morgenstern (1979) notes the non-unique behavior of the parameter, χ, when used in shear strength and volume change studies on the same soil material. In addition, according to

Morgenstern (1979), χ, being a material variable cannot be part of a stress state variable. Further, Morgenstern (1979) notes that the χ parameter can exceed one especially in the low suction which is incompatible with theoretical expectations. Bishop et al. (1960) and Jennings and Burland (1962) have further noted the difficulty in determining χ experimentally.

Despite these challenges, some proponents for the effective stress approach exist, for example Khalili and Khabbaz (1998) established an empirical relationship for χ with suction ratio $\frac{(u_a - u_w)}{(u_a - u_w)_b}$ given in Equation 2.2 for 14 soils at a coefficient of correlation of 0.94.

$$\chi = \begin{cases} \left[\frac{(u_a - u_w)}{(u_a - u_w)_b}\right]^{-0.55} & \text{for } (u_a - u_w) \geq (u_a - u_w)_b \\ 1 & \text{for } (u_a - u_w) \leq (u_a - u_w)_b \end{cases} \quad (2.2)$$

where $(u_a - u_w)_b$ = air entry value of the soil.

According to Khalili and Khabbaz (1998), Equation 2.2 is sufficient for practical purposes.

2.3.2 Independent stress state variable approach

The proponents of this approach arise owing to the difficulties of using the effective stress approach. In this approach, different combinations of stress state variables are used to describe the behavior of unsaturated soils. According to Fredlund and Morgenstern (1977), any two of three possible state variables: σ, u_w, u_a are sufficient in defining the stress state of unsaturated soils. This therefore leads to the following possible combinations of stress state variables:

1. (σ-u_a) and (u_a-u_w)
2. (σ-u_w) and (u_a-u_w)

3. $(\sigma-u_a)$ and $(\sigma-u_w)$

According to Fredlund et al. (2012), of the three combinations, the combination of net normal stress, $(\sigma-u_a)$ and matric suction, (u_a-u_w) has received the widest acceptance in describing behavior of unsaturated soils. This is because the pair allows for separation of the influences of total stress and pore-water pressure. In addition, since pore-air pressure is usually atmospheric, it makes practical advantage to have stress variables that are referenced to pore-air pressure (El Mountassir, 2011).

Some of the critics of this approach like Khalili and Khabbaz (1998) note that this approach requires extensive testing which is very time consuming. In addition the test equipment used to obtain the unsaturated soil properties is often very expensive and highly sophisticated. Khalili and Khabbaz (1998) further note that the highly non-linear relationship between $\phi^b$and soil suction limits the field application of the approach to only a small suction range often tested in the laboratory. Because of these limitations, Khalili and Khabbaz (1998) note that the method is not widely applied in practice.

2.3.3 Alternative /Modified stress variables approach

This approach combines both the effective stress approach and the independent stress approach. According to Wijaya (2017), this approach modifies the independent stress state variables with material properties hence generating modified stress state variables to describe the behavior of unsaturated soils

The proponents of this approach seek to investigate the independent contribution of degree of saturation and suction to the behavior of unsaturated soils. According to Wheeler et al. (2003), ignoring the independent influence of degree of saturation is not correct especially considering the hydraulic hysteresis of SWCC.

Wheeler et al. (2003) modified the work- conjugate stress variables of net stress, σ_v and suction, s suggested by Houlsby (1997) into two variables shown in Equation 2.3

$$\sigma_v^{"} = \sigma_v + sS_r \tag{2.3a}$$

$$s^* = ns \tag{2.3b}$$

where: $\sigma_v^{"}$ = average skeleton stress, s^* = modified suction, n = instantaneous porosity and S_r= degree of saturation.

Similarly, Alonso et al. (2013) suggested a constitutive stress, $\bar{\sigma}$, and effective suction, $\bar{s}$, to model the behavior of unsaturated soils. These stress variables are defined in Equation 2.4

$$\bar{\sigma} = \sigma - u_a + \bar{s} \tag{2.4a}$$

$$\bar{s} = sS_r^* \tag{2.4b}$$

where σ = total stress, u_a = pore-air pressure, s = matric suction, S_r^*= effective degree of saturation.

The effective degree of saturation has been defined by Romero and Vaunat (2000) and Tarantino and Tombolato (2005) in terms of a material variable, ξ_m as shown in Equation 2.5

$$\begin{aligned} S_r^* &= \frac{S_r - \xi_m}{1 - \xi_m} \text{ for } S_r > \xi_m \\ S_r^* &= 0 \qquad \text{for } S_r \le \xi_m \end{aligned} \tag{2.5}$$

where; Sr = degree of saturation

The material variable, ξ_m is defined as a ratio of microstructural void ratio, e_m to the total void ratio, e i.e. e_m/e

Gens et al. (2006) generalized the constitutive stress and modified suction as shown in Equation 2.6

$$(\sigma - u_a) + \mu_1(s,.....) \tag{2.6a}$$

$$\mu_2(s,.....) \tag{2.6b}$$

From Equation 2.6a, Gens et al. (2006) suggests three possible cases depending on the expression of μ_1 i.e

1. $\mu_1 = 0$; Equation 2.6a becomes the net normal stress
2. $\mu_1(s)$; Equation 2.6a is a function of suction and not degree of saturation
3. $\mu_1(s, S_r)$; Equation 2.6a is a function of both suction and degree of saturation which in turn is equivalent to the average skeleton stress given in Equation 2.3a

Similarly, different cases can be constructed out of Equation 2.6b

1. $\mu_2(s)$; if Equation 2.6b is a function of suction only, then it becomes matric suction only.
2. $\mu_2(n, s)$; if Equation 2.6b is a function of n and s, then it becomes modified suction as shown in Equation 2.3b
3. $\mu_2(s, S_r)$; if Equation 2.6b is a function of both suction and degree of saturation, it becomes effective suction as shown in Equation 2.4b

Usage of alternative stress state variables is receiving a lot of attention in the research community. One of its advantages is the ability to use conventional equipment in testing and also the fact that the testing is much less intensive compared to the independent stress state variable approach (Tarantino and El Mountassir, 2013).

2.4 Soil Suction

Soil suction is an important stress variable for unsaturated soils. There are two major components of soil suction (total suction) i.e., matric and osmotic suctions.

2.4.1 Definitions of suction

Aitchison (1964) defines the different components of soil suction as:

Matric suction or capillary component of free energy:

"In suction terms, it is the equivalent suction derived from the measurement of the partial pressure of the water vapour in equilibrium with the soil water, relative to the partial pressure of the water vapour in equilibrium with a solution identical in composition with the soil water."

Osmotic (or solute) component of free energy:

"In suction terms, it is the equivalent suction derived from the measurement of the partial pressure of the water vapour in equilibrium with a solution identical in composition with the soil-water, relative to the partial pressure of the water vapour in equilibrium with free pure water."

Total suction or free energy of soil-water

"In suction terms, it is the equivalent suction derived from the measurement of the partial pressure of the water vapour in equilibrium with the soil-water, relative to the partial pressure of water vapour in equilibrium with free pure water."

2.4.2 Matric suction

Matric suction is commonly expressed as the difference between pore-air and pore-water pressures (Fredlund and Rahardjo, 1993) as shown in Equation 2.7

$$(u_a - u_w) \tag{2.7}$$

According to El Mountassir (2011), matric suction is the affinity of the solid phase of soil for water which arises from the water retention mechanisms.

In granular materials where chemical interactions between solids and soil water hardly exist, capillary effects are the dominant contribution of matric suction. In clayey soils, capillary forces play a significant role in the low suction range (Tuller et al., 1999; Tuller and Or, 2005). In the higher suction range (low degrees of saturation), surface adsorptive forces dominate (Tuller et al., 1999; Tuller and Or, 2005).With surface adsorption, the water is held as films covering the solid particles. The thickness of the films depends on the surface adsorptive forces. Figure 2.3 presents a simplified schematic showing water films covering soil particles in a surface adsorption process.

Surface adsorption of the pore water is controlled by physico-chemical aspects which include; i) van der Waal's forces, ii) electrostatic forces and iii) hydration forces (Tuller et al., 1999; Tuller and Or, 2005; Tarantino, 2010)

The physico-chemical aspects responsible for the surface adsorptive forces are controlled by the mineralogy of the clay as well as the surface properties of the clay particles (Tuller et al., 1999; Tuller and Or, 2005)

Baker and Frydman (2009) note that in order to improve the constitutive models used for unsaturated soils, it is important to consider the contributions of both capillarity and surface adsorption to matric suction.

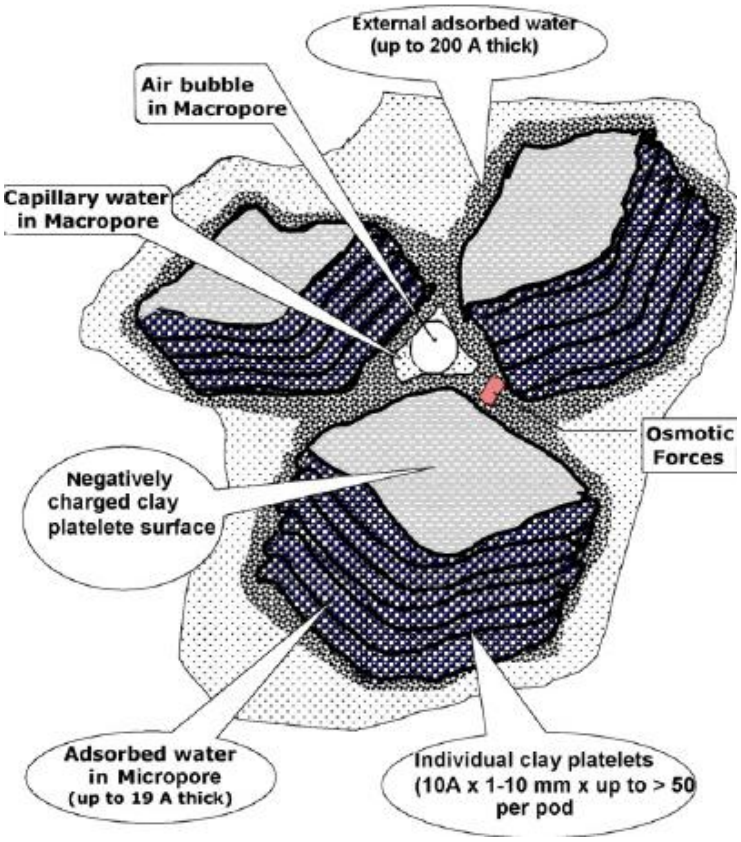

Figure 2.3: Schematic illustration of water adsorption on clay particle surafces (from Baker and Frydman, 2009)

2.4.3 Total suction

According to Tarantino (2010), water can be transferred from the soil via vapour when the partial water vapour pressure in equilibrium with soil pore water pressure gets lower than the water vapour pressure in equilibrium with pure free water. The depression of the soil water vapour pressure is due to two mechanisms: i) negative pressure of soil water and ii) solute concentration of soil water (Tarantino, 2010).

The Poynting effect explains that the pressure of the vapour in equilibrium with its own liquid reduces as the liquid pressure decreases where the decrease in the liquid pressure is generated by the solid phase (Tarantino, 2010). On the other hand, Raoult's law shows that the pressure of vapour in equilibrium with an aqueous solution decreases as the solute concentration increases. Therefore, total suction is generated by both the solid phase (matric

suction) and the solute concentration (osmotic or solute suction). Equation 2.8 shows the mathematical relationship between the three forms of suction

$$\psi = (u_a - u_w) + \pi \tag{2.8}$$

where: ψ = total suction, (u_a-u_w) = matric suction and π = osmotic suction

The thermodynamic relationship of the free energy of the soil water (total suction) and the relative humidity is expressed in Kelvin's law given in Equation 2.9.

$$\psi = \frac{RT}{M_w} \ln\left(\frac{P}{P_0}\right) \tag{2.9}$$

where: R = universal molar gas constant i.e., 8.31432J/(mol K), T = absolute temperature, M_w= molecular mass of water (kg/mol), $\frac{P}{P_0}$ = relative humidity of air in equilibrium with soil water.

For many applications in unsaturated soil mechanics, much focus is given to matric suction while ignoring osmotic suction partly because osmotic suction is a much smaller value compared to matric suction. In addition, for non-active soils, osmotic effects are likely to be negligible (Gens, 2010)

2.4.4 Suction control and measurements

In the practice of unsaturated soil mechanics, very often, there is need to either control or measure suction depending on the application. The different techniques used in the control and measurement of suction are briefly presented below.

2.4.4.1Techniques for controlling suction

a) Axis-translation technique

For unsaturated soils, it is typical that pore-air pressure is atmospheric i.e., $u_a = 0$ while the pore- water pressures are negative with respect to atmospheric pressure. Hilf (1956) proposed the axis- translation technique which translates the origin of reference for the pore-water pressure from standard atmospheric condition to the air pressure applied (Fredlund et al., 2012). Because of this translation, the problem of cavitation in laboratory test is avoided. Cavitation occurs when water is brought to a suction of -100kPa relative to the atmospheric pressure.

In a laboratory test employing this technique, the air pressure is applied inside an air-tight chamber and separation of the air phase from the water base is achieved using a water saturated disk of low porosity. This disk which is made of ceramic is often referred to as high air-entry value (HAEV) porous disk. The HAEV disks are often defined by their air-entry values (AEVs) or the air pressures that they are able to withstand before they start to desaturate. In the laboratory, typical HAEV disks have AEVs of 100, 500, and 1500kPa.

The reference pore-air pressure is elevated through an artificial increase while maintaining the pore-water pressure at some measurable reference value typically atmospheric (Delage et al., 2008; Lu and Likos, 2004).The matric suction $(u_a - u_w)$ can then be controlled over a wide range.

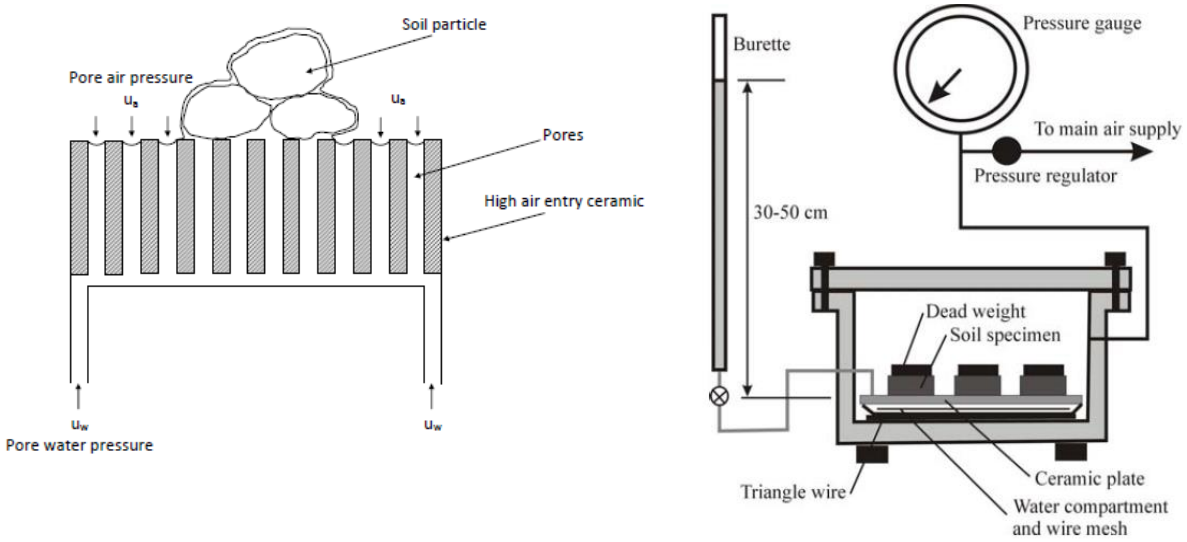

a) Principle of axis translation (after El Mountassir, 2011)

b) A typical pressure plate extractor applying axis-translation technique (after Samingan 2005)

Figure 2.4: Illustration of the axis-translation technique

The axis-translation technique has been criticized concerning the following aspects: i) it is not representative of field conditions where air pressure is under atmospheric condition; ii) there are some doubts in how the air pressurization process affects the water pressure when water is held by adsorption mechanisms; and finally iii) its application at nearly saturated states in the absence of a continuous gaseous phase is not straightforward (Delage et al., 2008); Baker and Frydman (2009).

The major experimental difficulties concerning the application of the axis-translation technique are associated with: i) the accumulation of diffused air beneath the HAEV disk, ii) the control of the relative humidity of the air chamber to minimize evaporation or condensation effects on the sample, iii) the application of the air pressurization process at elevated degrees of saturation, and iv) the estimation of the equalization time (Delage et al., 2008).

Despite these challenges, the axis-translation technique is the most commonly used technique of controlling suction. The technique is frequently used in determining the lower suction

range of the soil-water characteristic curve (usually less than 1500kPa). It has also been applied to several test apparatuses, for example Bishop and Donald (1961) designed the first suction-controlled triaxial apparatus using the axis-translation technique, Escario (1969) and Hoffmann et al. (2005) designed suction-controlled oedometers based on axis-translation technique to study swelling and expansive soils, respectively. Direct shear boxes with suction control using axis-translation technique have been developed by researchers such as Escario (1986) and Gan et al. (1988).In this thesis, the axis-translation technique has been applied to measure the SWCCs of the compacted soils.

b) Vapour equilibrium technique

In this technique, the relative humidity of a closed system (usually desiccators) is controlled using a chemical solution for example, a saline solution or an acid. When a soil specimen is placed in the desiccators as illustrated In Figure 2.5, water exchanges occur by vapour transfer between the pore water in the soil specimen and the aqueous solution until equilibrium is reached.

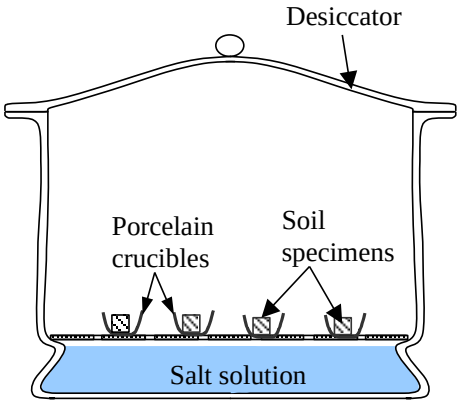

Figure 2.5: Vapor equilibrium technique (from Leong and Rahardjo, 2002)

According to Leong et al. (2002b) equilibration is in two stages; initially equilibrium has to be achieved between the suction source (chemical solution) and the environment (vapour space). This occurs through net water exchange between the liquid and vapour phases until

equilibrium is achieved (Blatz et al., 2008).The second stage involves equilibration between the soil specimen and the vapour space through an exchange of water.

The partial vapour pressure in the closed environment is directly related to the concentration of the aqueous solution. Both unsaturated and saturated salt solutions have been used by various researchers. However saturated solutions are usually preferred because the concentration of the solution remains almost constant despite the exchange of water between the soil specimens and the environment (Blatz et al., 2008; Young, 1967). Several works have published relative humidity levels generated by various salt solutions (Tang and Cui, 2005; Young, 1967). This technique is very easy to use and very high suctions in the range of 3-1000MPa can be reached (Pintado et al., 2009).

The vapour equilibrium technique has some setbacks which include:

- Long time for equilibrium as the equilibrium is a two-stage diffusion process.
- Strict control on temperature. Slight variations in temperature can cause dramatic changes in suction (Blatz et al., 2008). Blatz et al. (2008) suggests using water baths to minimize temperature variations.
- Not accurate at low suction levels (Agus and Schanz, 2005)
- Errors can be introduced during mixing of solution due to incomplete dissolution of solute, spillage of water, loss of water through evaporation and possible scale calibration errors (Blatz et al., 2008)

In this thesis, this technique has been used to attain high suctions in the test samples which will be discussed subsequently.

c) **Osmotic technique**

The osmotic technique was developed by biologists and was later adopted by soil scientists and then introduced to geotechnical engineering by Kassiff and Shalom (1971). In this technique the soil specimen is separated from an aqueous solution of large sized polyethyleneglycol (PEG) molecules by a semi-permeable membrane. Water transfer or exchange takes place across the semi-permeable membrane by the process of osmosis. The most commonly used semi-permeable membranes are cellulose membranes (Delage and Cui, 2008).Semi-permeable membranes are characterised by their molecular weight cut-off which is linked to the PEG molecules sizes (Delage et al., 2008). It is therefore important that the correct membrane is used for the PEG molecule size used in the experiments so that no exchange of PEG molecules takes place between the soil specimen and the aqueous solution. The water transfer takes place in liquid phase and ions can freely cross the semi-permeable membrane hence the osmotic technique controls matric suction of the soil and not osmotic suction (Blatz et al., 2008; Delage et al., 2008; Delage and Cui, 2008).Figure 2.6 illustrates how suction is imposed on a soil specimen using the osmotic technique.

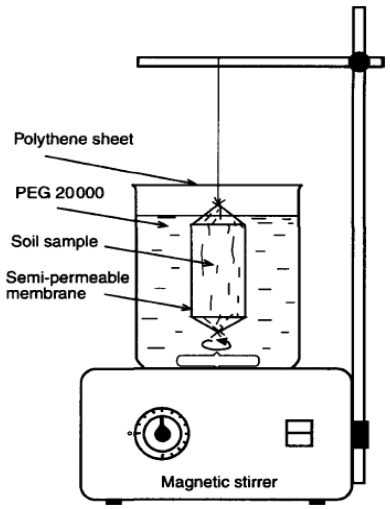

Figure 2.6: Application of the osmotic technique to impose suction on a soil sample (from Cui and Delage, 1996)

One advantage of the osmotic technique is that matric suction can be imposed on a soil sample without the need for applying an air pressure as in the case with the axis-translation technique (Delage and Cui, 2008; Delage et al., 2008). Avoidance of the air pressure has safety advantages but most importantly ensures that the samples are tested in conditions close to their natural conditions. Secondly, relatively high matric suctions (as high as 10MPa) (Delage et al., 2008) can be attained by the osmotic technique, which are not easily attained by the axis-translation technique. Matric suctions are adjusted by adjusting concentration of the PEG solution. The higher the concentration of the PEG solution, the higher will be the imposed matric suction. Because high suctions can be achieved in addition to the ability to apply a direct water potential to liquid water which is not the case in axis translation (Blatz et al., 2008), osmotic technique is suitable for high water content samples (Blatz et al., 2008).

The major setback of the osmotic technique is the durability of the membrane. The membrane is usually weak and very susceptible to microbial attack. In order to overcome the problem of microbial attack, a few drops of an antibiotic like penicillin into the aqueous solution are recommended (Delage et al., 2008). Some testing devices have been designed based on this technique, for example, Dineen and Burland (1995) designed an oedometer that is osmotically controlled and an osmotic direct shear box has been designed by Boso et al. (2005).

2.4.4.2 Suction measurement techniques

Several methods for suction measurement exist in the literature. Three common methods i.e., high capacity tensiometer, chilled mirror dewpoint technique and filter paper technique are presented below. Other methods are summarised in Table 2.1.

a) **High capacity tensiometer**

The high capacity tensiometer (HCT) is a direct method of measuring matric suction. Tensiometers measure matric suction by directly measuring negative pore-water pressure while pore air pressure is atmospheric. Tensiometers were for a long time limited to measure maximum suctions in the range 70-80kPa due to the limitation of cavitation. However following Ridley and Burland (1993)'s work, a tensiometer with capacity to measure suctions as high as 1500 kPa was invented hence the description high capacity tensiometer. Figure 2.7 shows a high capacity tensiometer.

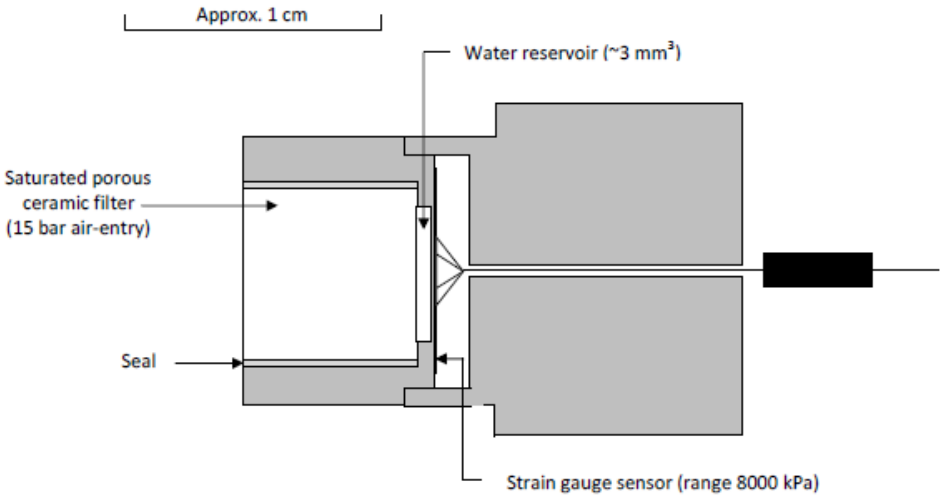

Figure 2.7: High Capacity tensiometer (after Ridley et.al, 2003)

A HCT typically consists of three components: i) high air entry value (HAEV) ceramic porous disk, ii) water reservoir/chamber, iii) strain/pressure gauge.

The HAEV ceramic disk acts as an interface between the negative water pressure in the soil and the measuring system (Fredlund et al., 2012). When the HAEV ceramic porous disk is in intimate contact with the pore water, exchange of water between the water reservoir and the soil occurs until equilibrium is reached. The strain gauge which is attached to the reservoir is designed to detect these movements (due to water exchange) hence determining the soil suction directly.

The main drawback of a HCT is cavitation. If cavitation occurs during the process of suction measurement, the measurement is disrupted and the system will need re-saturation. Therefore cavitation plays an important role in the design and operation of the HCT (Tarantino and Mongiovì, 2001). Some of the design considerations to limit cavitation include having a small water reservoir which reduces the chances of bubble formation in the reservoir, minimizing surface roughness/ imperfections on the ceramic disk in order to ensure good contact with the soil sample under test (Ridley et al., 2003).

Some of the precautions necessary when conducting suction measurements with a HCT include saturation of the ceramic porous disk and water reservoir prior to each testing, removal of air using a vacuum, ensuring good contact between the soil sample and the ceramic porous disk. Detailed procedures regarding operation of the HCT are presented in Tarantino and Mongiovì (2001), Tarantino and Mongiovi (2003), and Ridley et al. (2003).

Successes of the application of HCT in geotechnical testing have been variably reported, although majority are among the research community. Laboratory equipment have been designed to incorporate tensiometers for example: in oedometers (Wijaya, 2017), in direct shear testing (Caruso and Tarantino, 2004), triaxial testing (Marinho et al., 2016). Meilani et al. (2002) used mini-suction probes to successfully measure suctions up to 400kPa along the height of a test specimen during a triaxial test.

The main advantage of the tensiometer is the ability to measure suction directly in a short time. Being a direct method of suction measurement, it is suitable in validating indirect methods of suction measurement (Tarantino and Mongiovì, 2001).

b) Chilled mirror dew-point technique

This is an indirect suction measurement method that makes use of vapour pressure to determine total suction. The technique is useful for samples drier than the axis translation or ordinary tensiometric suction range (Campbell et al., 2007). ASTM D6836-16 recommends the technique for suctions higher than 1000kPa. In addition to capacity to measure high suctions, the technique takes a short time to attain equilibrium and hence total suction measurement (Gee et al., 1992; Leong et al., 2003).While measuring the total suction of compacted soils, Leong et al. (2003) noted that equilibrium was attained between a couple of minutes and 18 minutes. Agus and Schanz (2005) compared four methods for total suction measurement and noted that the chilled mirror hydrometer technique was the most accurate of them and recommended it as a bench mark against which other sensors can be assessed. The chilled-mirror dewpoint hygrometer is shown schematically in Figure 2.8.

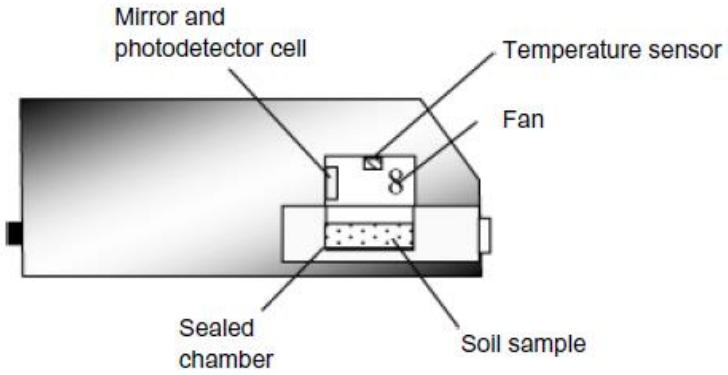

Figure 2.8: A schematic of the chilled-mirror dewpoint hygrometer (after Leong et al., 2003).

The chilled-mirror dewpoint hygrometer measures dew point and temperature of the headspace above the specimen. The specimen in a small plastic container (occupying half the container) is placed in a special closed chamber. The dew point is measured using a mirror which can detect the first appearance of condensation of water vapor. In order to maintain a constant thickness of the dew, the temperature of the mirror is precisely controlled by a thermoelectric cooler. A light beam directed onto the mirror is used to detect the first

appearance of water vapor condensation. A photo-detector cell is employed to measure the change in reflectance of the mirror caused by the condensed water vapor. The temperature of the specimen which is considered to be equal to the temperature of the vapor space is measured via an infrared thermocouple. The relative humidity or the water activity of the specimen is computed from the measured dew point and temperature. An internal fan is used to speed up equilibration time. The internal fan circulates the water vapor in the vapor space above the specimen. With the water activity or relative humidity and temperature of the vapor space above the soil specimen known, the total suction of the soil specimen is computed using Kelvin's Law given in Equation 2.9. Prior to usage, the chilled-mirror dewpoint hygrometer is calibrated using standard aqueous salt solutions whose relative humidity and hence total suctions are known.

In this thesis, the chilled-mirror dewpoint hygrometer was used to measure suctions both in the low and high ranges.

c) Filter paper technique

Usage of the filter paper technique as a soil suction measurement tool was first reported by Gardner (1937). Substantial studies have been made to improve understanding of this technique (Bulut et al., 2001; Bulut and Leong, 2008; Al-Khafaf and Hanks, 1974; Marinho and Oliveira, 2006; Marinho and da Silva Gomes, 2012; Haghighi et al., 2012; Bicalho et al., 2007; Bicalho et al., 2008; Likos and Lu, 2002). In addition, the technique has been standardized in ASTM D5298-16. Only ash-less filter papers are used for this technique (Bicalho et al., 2007). Despite the fact that several ash-less filter papers exist, the two commonly used filter papers for soil suction measurements are the *Whatman No. 42* and the *Schleicher and Schuell No. 589.*

In all the studies, it was generally agreed that this technique is economical, relatively simple to use, gives fairly reliable measurements, measures suctions over a wide range, and measures both matric and total suctions.

The different aspects of the technique are briefly presented below.

- ***Contact and Non-contact filter paper***

Several researchers (e.g., Swarbrick 1995; Leong et al. 2002b; Marinho and Oliveira 2006) have detailed the working principles of the filter paper technique. The filter paper method has also been standardized in ASTM D-5298-16.

The filter paper can be used in the contact or non-contact mode. If placed in direct contact with soil, moisture exchange between the filter paper and soil takes place through capillary flow and hence the contact filter paper measures matric suction. If the filter paper is not in contact with the soil but placed together in a sealed environment, moisture exchange between the filter paper and soil takes place through vapor flow and hence the non-contact filter paper measures total suction.

Once the filter paper is in equilibrium with the soil's suction, its weight is expected to remain constant. Suction can then be inferred from the water content of the filter paper using a calibration equation. Calibration involves establishing the moisture-suction relationship of the filter paper.

Several calibration curves for filter papers exist in the literature for example: Fawcett and Collis-George (1967), Hamblin (1981), Chandler and Gutierrez (1986), and Leong et al. (2002b).A detailed discussion of filter paper calibration procedures is presented by Leong et al. (2002b). The contact and non-contact filter paper are calibrated by allowing moisture

exchange with a system whose suction is known, through capillarity and vapour transfer, respectively. A typical calibration equation is bi-linear of the form shown in Equation 2.10

$$\log \psi = A + B \log w_f \qquad w_f < w_c$$
$$\log \psi = C + D \log w_f \qquad w_f \geq w_c \tag{2.10}$$

where ψ = suction, w_f = water content of filter paper, w_c = water content at which sensitivity if the filter paper changes, and A, B, C and D are calibration constants. Table 2.1 presents examples of calibration curves from the literature for both Whatman No.42 and Schleicher & Schuell No. 589 filter papers.

Marinho and Oliveira (2006) showed experimentally that the total suction calibration curve moves towards the matric suction calibration curve as equilibrium time increases. They argued that there should be only the matric suction calibration curve if sufficient time is allowed for equilibration in the non-contact filter paper method. However, Marinho and Oliveira (2006) conducted their tests on salt solutions whose suctions are known. This is different if suction measurements are made on the soil for two reasons:

i) The transfer mechanisms of water from soil to filter paper and from salt solution to filter paper is different.
ii) As the suction of the soil is unknown at the time of measurement, it is quite difficult to follow the recommendations of Marinho and Oliviera (2006).

This, therefore is a point of contention regarding the filter paper technique and this thesis attempts through experiments to further investigate the aspects of calibration curve as well as equilibration time.

- ***Hysteresis***

The moisture retention characteristics of a porous material have been observed to differ depending on whether the material is wetting or drying. This phenomenon is called hysteresis and applies to the filter paper as well. Previous studies (Fawcett and Collis-George 1967; Leong et al. 2002b; 2016) have demonstrated presence of the hysteretic behavior of filter paper. Al-Khafaf and Hanks (1974), Ridley (1995) and Swarbrick (1995) therefore recommend that the calibration process of filter papers should always take into account the hysteresis effect. Consequently, in the usage of the filter paper to evaluate suction, the appropriate calibration curve should be used to infer suction from the filter paper. Not much experimental data exists on the hysteretic behavior of the filter paper. This is partly because most experimenters use an initially dry filter paper and so the filter paper moves along the wetting path as it measures the soil suction. As part of this study, the hysteretic behavior of filter papers using both initially dry and initially wet filter papers was investigated.

- ***Inherent variability of the filter papers***

Filter papers are produced in batches. Some researchers e.g. Deka et al. (1995) recommend that each batch of filter papers should be calibrated for the entire range of suction they are to be used. This suggestion is not practical and hence Marinho and Oliveira (2006) have suggested a quick single point check for verification of the calibration curve to apply. Hamblin (1981) compared calibration data of Whatman No.42 papers calibrated two years apart in addition to data from Fawcett and Collis-George (1967), 14 years apart and found the data closely agreed. Leong et al. (2002b) have investigated quality of both the Whatman No.42 and the S &S 589 filter papers for the probable influence on the calibration of filter papers. Using their own data, in addition to published data, Leong et al. (2002b) concluded that the variation was minimal, and does not practically affect the calibration data. The

calibration data combined all lay in reasonably narrow band with more uniformity in the case of Whatman No.42 filter papers as shown in Figure 2.9 after Rahardjo and Leong (2006). Therefore unless extremely special situations arise, entire re-calibration of the filter papers may be practically unnecessary but rather may increase the time duration for the tests. It is important to ensure proper handling of the filter papers and provide sufficient equilibration time as suggested by Leong et al (2002b).

- ***Equilibration time***

Equilibration time is an important aspect for any suction measurement technique. Different studies have suggested that the equilibration time for filter papers is dependent on the mode of contact (contact or non-contact), the magnitude of suction being measured and the soil characteristics (Swarbrick, 1995; Marinho and Oliveira, 2006; Marinho and da Silva Gomes, 2011). ASTM D5298-16 recommends a minimum of seven days. As part of this study, the equilibration time was investigated and suggestions were made.

- ***Pre-treatment of the filter papers***

Different researchers (Gardner, 1937; McQueen and Miller, 1968; Al-Khafaf and Hanks, 1974) have suggested chemical pre-treatment of filter papers prior to usage. The main reason for pre-treating the filter papers is to avoid microbial attack of the filter papers during testing. In some cases for example Fawcett and Collis-George (1967), both chemical pre-treatment and oven-drying of the filter papers were done prior to the usage. ASTM D5298-16 suggests oven drying of filter papers prior to use. In addition, ASTM D5298-16 suggests usage of sacrificial filter papers in order to avoid microbial attack. Usage of sacrificial filter papers extends the equilibration time and needs to be studied. Hamblin (1981) and Chandler and Gutierrez (1986) reported that pre-treatment of filter papers is not necessary. Marinho and Oliveira (2006) note that pretreatment of the filter papers alters their absorption

characteristics and hence requires different calibration curves. In this study, the filter papers were not pre-treated and no sacrificial filter paper was used.

Table 2.1: Suction control and Suction measurement techniques (Ridley and Wray, 1996; Blatz et al, 2008; Bulut and Leong, 2008; Masrouri et al, 2008; Vanapalli et.al, 2008)

SC/SM*	Technique	Suction component	Suction range MPa	Approx. Equilibration time	Concerns
SC	Axis translation	Matric	0-1.5	days-weeks	Requires elevated air pressures, air diffusion through ceramic, saturation of ceramic is crucial, evaporation of soil sample.
SC	Vapour equilibrium	Total	3-1000	weeks –months	Long test durations, sensitive to temperature fluctuations, safety if acids are used
SC	Osmotic	Matric	0-10	days-weeks	Deterioration of membranes
SC	Centrifuge	Matric	0-0.08	days	Narrow suction range
SC	Hanging water column	Matric	0-0.12	hours	Narrow suction range
SM	Tensiometer	Matric	0-1.5	minutes-hours	Rigorous saturation required
SM	Chilled-mirror dewpoint	Total	1-60	10 minutes	Regular calibration, only a small amount of soil is tested
SM	Filter paper	Matric/Total	0.05-30	7 days-	A strict protocol, very dependent on workmanship skills
SM	Thermocouple psychrometer	Total	0.3-7	~1hr	Sensitive to ambient temperature changes
SM	Transistor psychrometer	Total	1-70	~1hr	Sensitive to ambient temperature, only a small soil specimen is tested
SM	Thermal conductivity sensor	Matric	0.001-1.5	hours-days	Different calibration for each sensor, Shows hysteresis on drying and wetting, contact between soil and sensor affects response
SM	Electrical conductivity sensor	Matric	0.05-1.5	6-50 hours	Not suitable in saline soils since gypsum block may get corroded, suffers from hysteresis

*SC = Suction control, SM = Suction measurement

Table 2.2: Calibration curves for Whatman No.42 and Schleicher & Schuell No.589 filter papers

Reference	Suction type Matric/Total	Unit	Suction equation
Whatman No.42 filter paper			
Hamblin (1981)	N/A	MPa	$\ln\psi = 2.397 - 3.683\ln w_f$
Chandler and Gutierrez (1986)	N/A	pF	$\psi = 5.85 - 0.0622,\ w_f > 47$
Greacen et al. (1987)	N/A	kPa	$\log\psi = 5.327 - 0.0780 w_f,\ w_f < 45.3$ $\log\psi = 2.413 - 0.0135 w_f,\ w_f > 45.3$
Leong et al. (2002)	Matric	kPa	$\log\psi = 2.909 - 0.0229 w_f,\ w_f \geq 47$ $\log\psi = 4.945 - 0.0673 w_f,\ w_f < 47$
Leong et al. (2002)	Total	kPa	$\log\psi = 8.778 - 0.222 w_f,\ w_f \geq 26$ $\log\psi = 5.31 - 0.0879 w_f,\ w_f < 26$
ASTM D-5298-16	N/A	kPa	$\log\psi = 5.327 - 0.0779\ w_f,\ w_f \leq 45.3$ $\log\psi = 2.412 - 0.0135 w_f,\ w_f > 45.3$
Schleicher and Schuell No. 589filter paper			
McQueen and Miller (1968)	N/A	kPa	$\log\psi = 5.238 - 0.0723\ w_f,\ w_f < 54$ $\log\psi = 1.8966 - 0.1025\ w_f,\ w_f > 54$
Al-Khafaf and Hanks (1974)	N/A	kPa	$\log\psi = 5.117 - 0.0337\ w_f,\ w_f < 83$ $\log\psi = 1.983 - 0.0090\ w_f,\ w_f > 83$
McKeen (1988)	N/A	kPa	$\log\psi = 4.9 - 0.0624\ w_f,\ w_f < 66$ $\log\psi = 1.25 - 0.0069\ w_f,\ w_f \geq 66$
Greacen et al. (1987)	N/A	kPa	$\log\psi = 5.058 - 0.0688\ w_f,\ w_f < 54$ $\log\psi = 1.882 - 0.0102\ w_f,\ w_f \geq 54$
Leong et al. (2002)	Matric	kPa	$\log\psi = 2.659 - 0.018\ w_f,\ w_f \geq 54$ $\log\psi = 5.438 - 0.069\ w_f,\ w_f < 54$
Leong et al. (2002)	Total	kPa	$\log\psi = 8.778 - 0.191\ w_f,\ w_f \geq 32$ $\log\psi = 5.26 - 0.0705\ w_f,\ w_f < 32$
ASTM D-5298-16	N/A	kPa	$\log\psi = 5.056 - 0.0688\ w_f,\ w_f \geq 54$ $\log\psi = 1.882 - 0.0102\ w_f,\ w_f < 54$

* w_f = filter paper moisture content in %, N/A: one curve for both total and matric suctions

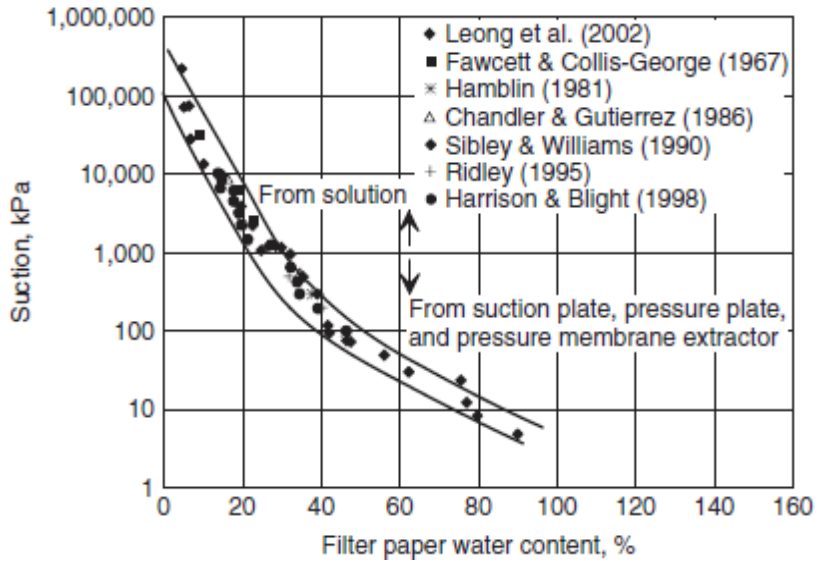

(a) Whatman No.42 filter papers

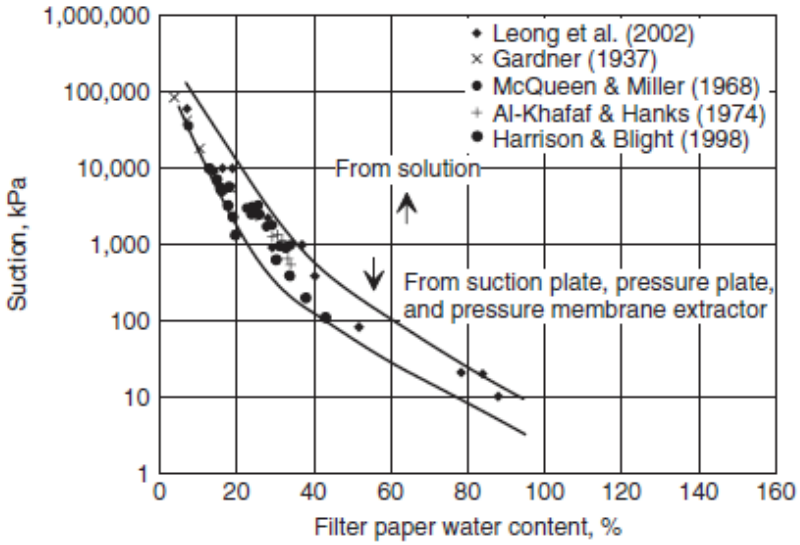

(b) Schleicher and Schuell No.589 filter papers

Figure 2.9: Calibration data for the filter papers from different researchers (from Rahardjo and Leong, 2006)

2.5 Soil-water characteristic curves

The soil-water characteristic curve (SWCC) is a graphical relationship between the amount of water in the soil and the soil suction (Fredlund and Rahardjo, 1993).The amount of water in the soil can quantified as either gravimetric water content (w), volumetric water content (θ_w) or degree of saturation (S). Hence, the SWCCs may be designated according to the form of water content used to describe it i.e. SWCC-w, SWCC-θ_w or SWCC-S.

Depending on the discipline, the soil-water characteristic curve takes on different names for example water retention curve, soil-moisture retention curve, soil-water release curve and soil-moisture characteristic curve. For civil engineering purposes, the term soil-water characteristic curve (SWCC) is recommended (Fredlund et al., 2002). Figure 2.10 shows a typical drying SWCC showing the different variables and zones.

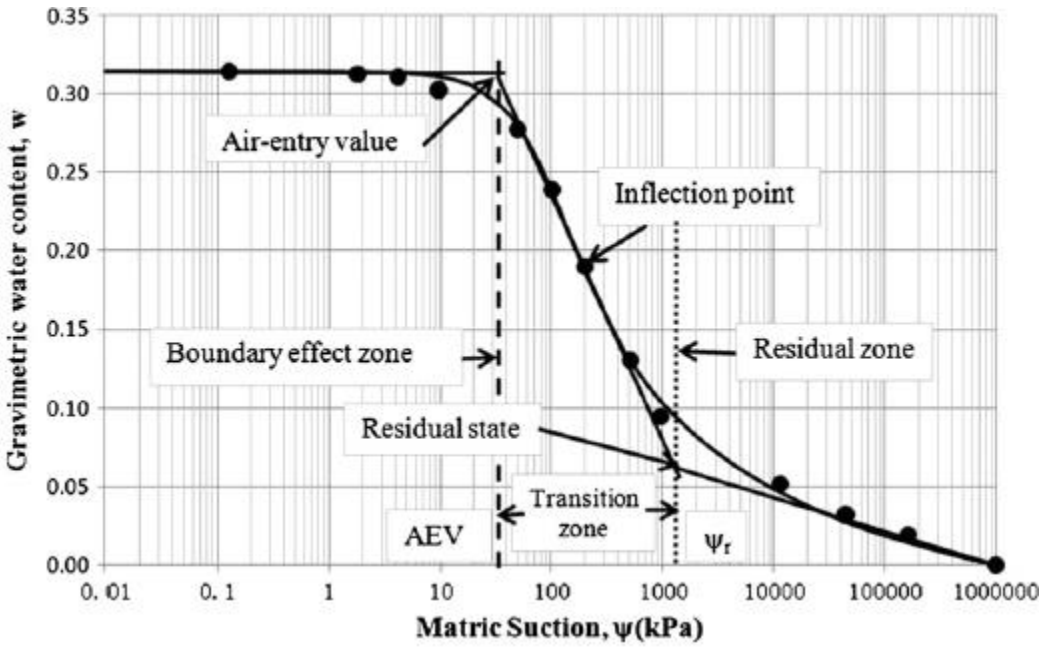

Figure 2.10: Drying SWCC showing the variables and the different zones(Fredlund, 2006)

Air entry value (AEV) is the matric suction at which air starts to enter the largest pores of the soil (Fredlund and Xing (1994). At this suction, the meniscus formed by the water surface tension in the largest pores is broken (Zhai and Rahardjo, 2012). Residual water content is the water content that requires a large suction to remove any additional water from the soil (Fredlund et al., 2012). The AEV and the residual water content are usually determined empirically by constructing a tangent through the point of inflection as shown in Figure 2.10 for a non-deforming soil; the point of intersection of this tangent and the horizontal tangent through the initial point is the AEV. In order to obtain the residual water content, a line extending from zero water content and 1GPa suction is drawn to intersect the tangent line through the point of inflection; the residual water content is the ordinate at the point of intersection of these two tangents as illustrated in Figure 2.10 (Vanapalli et al., 1998). Because the empirical approaches can be subjective when determining the SWCC variables, mathematical formulations have been suggested by Zhai and Rahardjo (2012).

The SWCC is very important in the implementation of unsaturated soil mechanics (Fredlund et al., 2002). The SWCC provides primary information for derivation of many unsaturated soil properties such as shear strength, permeability, pore size distribution either directly or indirectly.

In the laboratory, SWCC is measured by different methods for example hanging column, pressure extractor, chilled mirror hygrometer and centrifuge which have been standardized in ASTM D6836-16. Other techniques used are vapour equilibrium technique and filter paper technique which have been previously described. For most applications, only the drying SWCC is sufficient, however it is important to note that the SWCC is hysteretic i.e., the SWCC follows a different path during drying and during wetting processes of the soil. Figure 2.11 shows both the drying (desorption) curve and the wetting (absorption) curve of a silt soil.

Along the drying path, the suction is increasing hence leading to desorption, while wetting occurs under suction reduction hence leading to water absorption by the soil. The measurement of the wetting curve is quite cumbersome and more time consuming hence much less data exists for wetting SWCC compared to the drying SWCC, moreover drying SWCC seems sufficient in explaining or modeling majority of the phenomena in unsaturated soil.

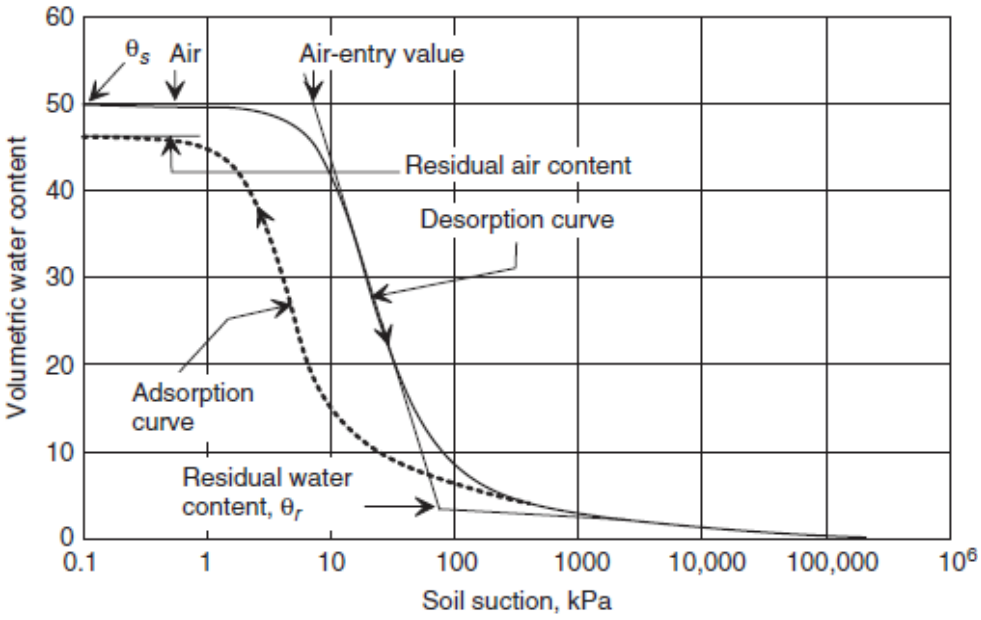

Figure 2.11: Typical SWCC for a silt soil (from Fredlund et al, 2012)

White et al. (1970) idealized the desorption curve of a porous material into four regions i.e., boundary effect zone, primary transition zone, secondary transition zone and residual desaturation zone. Vanapalli et al. (1996a) modified these regions into three as shown in Figure 2.10: boundary effect zone, transition zone (originally primary and secondary transition zones) and the residual zone. In the boundary effect zone, the pores are filled with water i.e., the water phase is continuous making the soil saturated. Therefore in the boundary effect zone, the effective stress, $(\sigma\text{-}u_w)$ is applicable as stress state variable. At the AEV, the soil starts to desaturate, making AEV the first most significant point on the SWCC (Vanapalli et al., 1996a).

Beyond the AEV, the soil desaturates and gets into the transition zone. Notably the water content of the soil reduces significantly with an increase in suction. In the transition zone, the water phase is no longer continuous. As suction increases, the residual water content is reached which marks the end of the transition zone and hence the soil is in the residual zone where a small change in soil water content requires substantially large increase in suction as illustrated in Figure 2.10.

2.5.1 Factors affecting the SWCC

SWCC is affected by different factors some of which include soil type, soil structure, method of specimen preparation for reconstituted soils, dry density, mineralogy, and stress history. Some of these factors are interlinked for example method of specimen preparation may be responsible for the soil structure. Some of these factors are discussed below.

2.5.1.1 Influence of soil type

The type of soil has a great influence on the type of SWCC. The soil type includes aspects of soil texture, plasticity, and gradation characteristics. Figure 2.12 shows the influence of texture on SWCC.

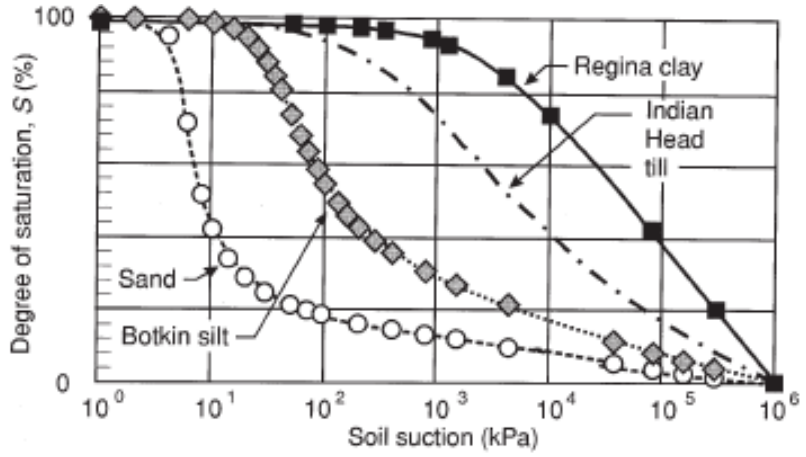

Figure 2.12: Influence of soil texture on SWCC (Vanapalli, 1994; Barbour, 1998)

Figure 2.12 shows variations in the SWCC slopes and AEV with fines content. The AEV generally reduces from Regina clay to sand. The slope of the SWCC in the transition zone is steepest in sand reducing toward Regina clay. These observations are largely due to the differences in pore sizes across the different soil textures. The shape of the SWCC for sand reveals a uniform pore size distribution which becomes gentler as clay content increases.

As discussed earlier, the water retention mechanisms in cohesive and cohesionless soils are different. In cohesive soils, both capillary and surface adhesion forces are present while in cohesionless soils, capillary forces are the most significant. This may explain why the sands and silts desaturate much faster than clays.

Marinho (2005) notes that the slope of the SWCC transition zone changes with liquid limit; for soils with liquid limits above 25%, the SWCC is a straight line between suctions of 100 and 10000kPa. Lu et al. (2007) studied the relationship between plasticity and water retention behavior and concluded that the higher the plasticity index, the higher the water retention capacity of the soil i.e., the lower the desaturation rate of the soil. This is not surprising since plasticity index is related to clay content.

Yang et al. (2004) and Gallage and Uchimura (2010) have studied the influence of grain size distributions on SWCCs of sandy soils and noted that:

- SWCCs have similar shapes with the grain size distribution curves.
- Coarse-grained soils generally have lower AEV, residual suction, water-entry suction and smaller hysteresis than fine-grained soils.
- The AEV, residual suction and hysteresis are inversely related to D_{10}.

- A soil with a uniform grain size distribution has a smaller hysteresis and a steeper drying SWCC than non-uniform grain size distributions.

Satyanaga et al. (2013) note that residual soils that have bimodal grain size distributions may possess bimodal SWCCs.

2.5.1.2 Influence of soil structure

The influence of soil structure on SWCC has been observed by some researchers. One way of studying soil structure is to evaluate the influence of moulding water content on the SWCC. Vanapalli (1994) and Vanapalli et al. (1999) evaluated the influence of moulding water content on SWCCs of compacted soils. Figure 2.13 shows SWCCs of compacted soils with different initial moulding water contents.

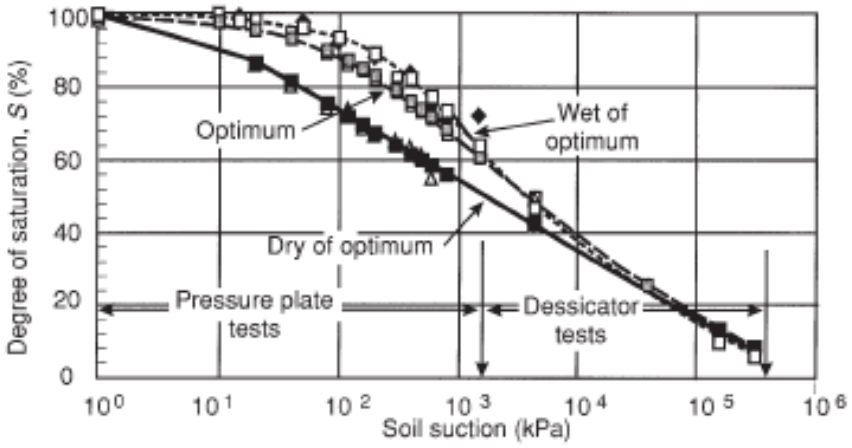

Figure 2.13: SWCCs for compacted soil at different initial moulding water contents (from Vanapalli, 1994)

Figure 2.13 shows that the sample compacted dry of optimum has the lowest AEV and consistently registers lower degree of saturation at a given suction followed by the sample compacted at optimum water content. The wet of optimum sample registers the highest suction for AEV and the slowest rate of desaturation. Vanapalli et al. (1999) generalized that the lower

the initial water content, the steeper is the slope of the SWCC i.e., the higher the rate of desaturation.

The samples compacted on the dry of optimum have a flocculated structure and thus the macrostructure governs the SWCC behavior. The macrostructure gives the dry of optimum compacted soils an open structure characterized with large interconnected pores (Vanapalli et al., 1996b) which allow for easy drainage on application of suction. In contrast, the soils compacted wet of optimum possess a dispersed structure with no interconnected pores. In these soils, the microstructure controls the SWCC behavior (Vanapalli et al., 1996b). The nature of the soil structure for soils compacted wet of optimum impedes drainage and as a result, the soils retain a higher quantity of water than the dry of optimum compacted samples at a given suction. At higher suctions, the influence of soil structure increasingly diminishes with the SWCCs merging in the residual zone.

2.5.1.3 Effect of initial density the SWCC

Different researchers have investigated the effect of initial density on the SWCCs of a given soil. The initial density affects the initial saturated gravimetric water content as shown in Figures 2.14. A decrease in the initial void ratio of a soil causes a decrease in the saturated gravimetric water content and thus affects the initial portion of the SWCC but as suction increases, the SWCCs merge into a single curve at high suctions (Wijaya, 2017). This observation is a unique advantage of the SWCC-w and has been taken advantage of when modeling initial density effects on SWCCs of a soil for example, Salager et al. (2010), and Wijaya and Leong (2017).

2.5.1.4 Effect of stress history and methods of sample preparation

Soil specimens of the same soil but subjected to different stress histories will show different SWCCs (Fredlund, 2002). Figure 2.15 shows SWCCs of soil specimens from the same soil but

subjected to different stress histories and preparation techniques. The four specimens have significantly different saturated gravimetric water contents which has a relationship with the saturated void ratios. The initially slurried specimen shows the highest rate of desaturation and the smallest AEV of the four specimens. The compacted specimen has the smallest saturated gravimetric water content which reflects the smallest saturated void ratio. The slurried specimens' SWCCs merge into a single curve implying that the only difference between the two specimens is the initial density (one is pre-consolidated).

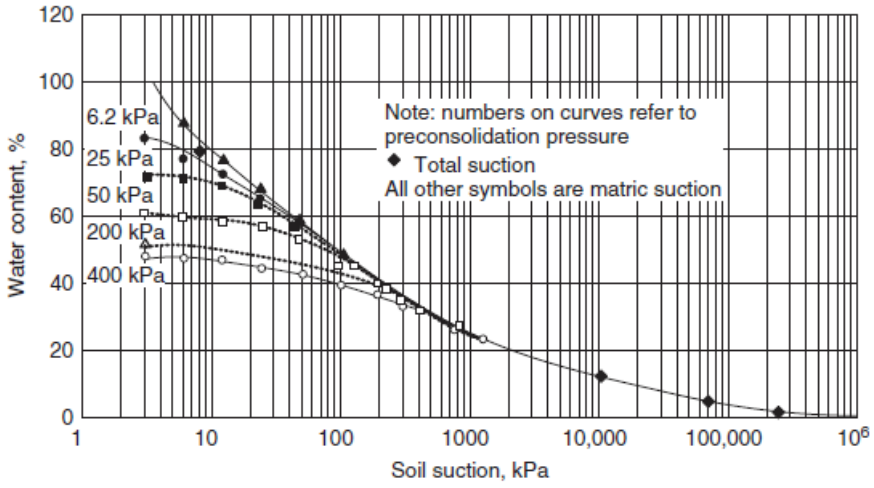

(a)

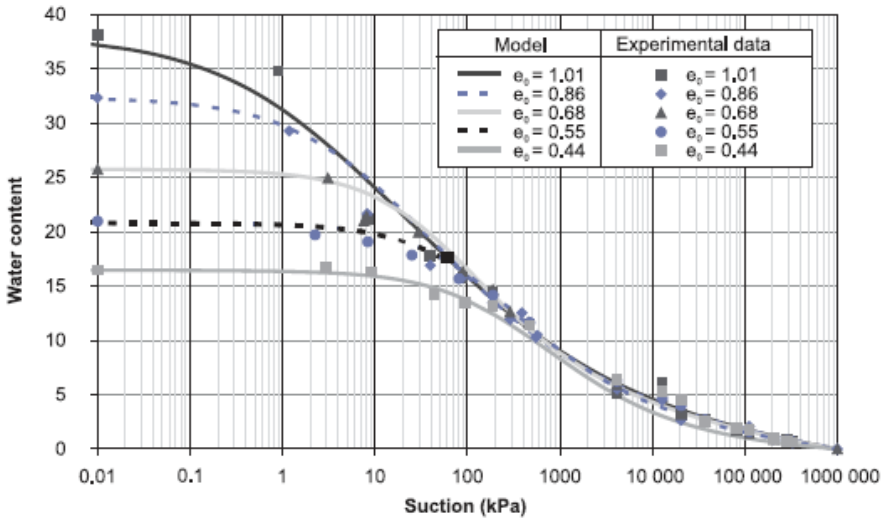

(b)

Figure 2.14: Effect of initial density on SWCC of a soil: a) pre-consolidated Regina clay (Fredlund, 1967), and b) compacted clayey silty sand (Salager et al., 2010)

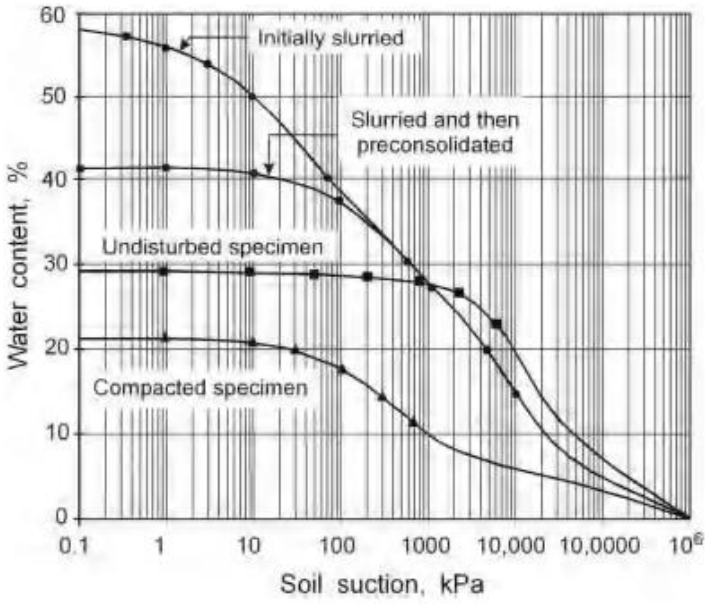

Figure 2.15: Effect of stress history and methods of specimen preparation on the SWCC (Fredlund, 2002)

2.5.2 Equations for soil-water characteristic curves

Several closed-form empirical equations have been proposed to fit laboratory determined SWCCs. Generally, all the equations fit the measured SWCC data using a least square regression analysis. Leong and Rahardjo (1997b) suggested that most of the SWCC equations can be derived from a generic equation given in Equation 2.11.

$$a_1\Theta^{b_1} + a_2\exp\left(a_3\Theta^{b_1}\right) = a_4\psi^{b_2} + a_5\exp\left(a_6\psi^{b_2}\right) + a_7 \qquad (2.11)$$

where: a_1, a_2, a_3, a_4, a_5, a_6, a_7, b_1 and b_2 are constant, ψ = suction, Θ = normalized volumetric water content i.e $(\theta_w-\theta_r)/(\theta_s-\theta_r)$; θ_w = volumetric water content, θ_s = saturated volumetric water content, θ_r = residual volumetric water contents.

Four common SWCC equations are briefly discussed below.

2.5.2.1 Gardner (1958)

Gardner (1958)'s equation is reported as the earliest of the SWCC equations. It is a continuous equation which was originally formulated to model permeability of unsaturated soils but has been adapted to model SWCC (Sillers et al., 2001). This equation, reproduced as Equation 2.12 has two fitting parameters: a which is related to the inverse of AEV and n which is related to the pore size distribution (Gardner, 1958).

$$\theta_w = \theta_r + \frac{\theta_s - \theta_r}{1 + a\psi^n} \tag{2.12}$$

2.5.2.2 Brooks and Corey (1964)

Brooks and Corey (1964)'s equation reproduced as Equation 2.13, assumes a constant water content for suctions less than AEV. Beyond the AEV, the material desaturates exponentially. The equation has two fitting parameters: a which is related to the AEV and λ which is related to the pore size distribution and is referred to as the pore size distribution index.

$$\begin{aligned} \theta_w &= \theta_s && \text{for } \psi < a \\ \theta_w &= \theta_s \left(\frac{\psi}{a}\right)^{-\lambda} && \text{for } \psi > a \end{aligned} \tag{2.13}$$

The larger the value of λ, the more uniform the pore size distribution is, which implies a steeper SWCC in the transition zone (Sillers et al., 2001). One criticism for the Brooks and Corey (1964)'s equation is its inability to provide a continuous function for the SWCC. Sillers et al. (2001) note that the discontinuity in the function at the suction value equal to a may cause instability during numerical modeling of unsaturated soil behavior. The Brooks and Corey (1964) equation is more suitable for coarse-grained soils.

2.5.2.3 van Genuchten (1980)

van Genuchten (1980) proposed a closed-form, smooth, three-parameter SWCC equation reproduced in Equation 2.14.

$$\theta_w = \theta_r + (\theta_s - \theta_r)\left[\frac{1}{1+(\alpha\psi)^n}\right]^m \quad (2.14)$$

where; α, n, m are fitting parameters.

van Genuchten (1980)'s equation herein referred to as VG model, allows for greater flexibility than the previous models hence successfully fits SWCC data for a wide range of soils. The fitting parameters have physical meaning; $\alpha\left(\text{kPa}^{-1}\right)$ is related to the inverse of the AEV, n is related to the pore size distribution of the soil and m is related to the overall symmetry of the SWCC (Sillers et al., 2001).

The parameter, m is very often constrained as either; $m = 1 - \frac{1}{n}$ or $m = 1 - \frac{1}{2n}$ which reduces the flexibility of the model but significantly simplifies it (Lu and Likos, 2004).

In this thesis, whenever the VG model has been used, it has been regarded as four-parameter model with residual volumetric water content θ_r also regarded as a fitting parameter as suggested by Leong and Rahardjo (1997b) and the constraint on parameter m has been considered as; $m = 1 - \frac{1}{n}$.

2.5.2.4 Fredlund and Xing (1994)

Fredlund and Xing (1994) suggest a continuous, closed-form three-parameter model similar to the VG model shown in Equation 2.15. In this thesis, the model will be referred to as FX model.

$$\theta_w = C(\psi)\left[\frac{1}{\left[\ln\left[e+\left(\frac{\psi}{a}\right)^n\right]\right]^m}\right] \quad (2.15)$$

where $C(\psi)$ is a correction factor that ensures the SWCC goes to suction of 1GPa at zero water content, a is a fitting parameter associated with the AEV, n is a fitting parameter associated with the rate of desaturation of the soil past the AEV, m is a fitting parameter associated with the residual water content, and e is natural number i.e., 2.71828..

The correction factor $C(\psi)$ as suggested by Fredlund and Xing (1994) is given in Equation 2.16

$$C(\psi) = \left[1 - \frac{\ln\left(1+\frac{\psi}{\psi_r}\right)}{\ln\left(1+\frac{10^6}{\psi_r}\right)}\right] \quad (2.16)$$

where ψ_r = residual suction.

Leong and Rahardjo (1997b) found best fits were obtained with the FX model were obtained when the correction factor, $C(\psi)$ is set to unity i.e 1 and this has been adopted in this thesis.

Further Leong and Rahardjo (1997b) found that the FX model gave the best fit to the SWCC data of a wide range of soils compared to the other models studied. Another noted advantage of the FX model is the ability to converge much faster compared to the VG model (Leong and Rahardjo, 1997b; Sillers et al., 2001).

2.6 Permeability

Darcy (1856) was the first to quantify flow of water through porous media. Having measured flow rates of water through saturated sand filters, Darcy (1856), discovered that the volume rate of flow, Q is directly proportional to the cross section area, A, of the porous medium and the hydraulic head difference between the inlet and outlet of water, Δh_w, and inversely proportional to the length, L, of the medium. This relationship is summarized in Equation 2.17.

$$Q \alpha \frac{A \Delta h_w}{L} \tag{2.17}$$

The term $\Delta h_w/L$ in Equation 2.17 is referred to as the hydraulic gradient (i) which is responsible for driving the flow i.e., the driving potential. If the volume flow rate were considered per unit cross sectional area, A, per unit time, t, and the proportionality constant, k, introduced, the flux, q, can be computed as shown in Equation 2.18

$$q = \frac{Q}{At} = k \frac{\Delta h_w}{L} \tag{2.18}$$

The proportionality constant, k, is referred to as the permeability or the hydraulic conductivity of the material.

2.6.1 Saturated permeability

As noted from Darcy's work, the driving potential for flow through saturated soils is the hydraulic gradient i i.e., whenever there is a hydraulic gradient, flow will occur. Saturated soils have their void filled with water and as a result their permeabilities are considered constant (Marshall et al., 1996). Several empirical formulations have been suggested relating saturated permeability of soils to different soil properties. Explicitly or implicitly, these formulations relate

saturated permeability to the void ratio, grain size characteristics and some other soil properties such as soil structure, .

Milan and Andjelko (1992) generalized the empirical formulations for saturated permeability, k, of soils as given in Equation 2.19.

$$k = \frac{g}{\nu}.C.f(n).d_e \qquad (2.19)$$

where g is acceleration due to gravity, ν is kinematic viscosity, C is sorting coefficient, f(n) is a function of porosity, d_e is effective grain diameter, ν is dynamic viscosity (μ)/fluid density (ρ).

Some of the commonest empirical formulations for permeability are:

- Hazen (1892)

Hazen (1892) suggested an empirical relationship predicting permeability, k (cm/s), of saturated sands. Following the generalization form given in Equation 2.19, Hazen's formulation is presented in Equation 2.20.

$$k = \frac{g}{\nu}.6\times10^{-4}\left[1+10(n-0.26)\right].D_{10}^2 \qquad (2.20)$$

Hazen's formulation is commonly presented simply as shown in Equation 2.21

$$k = C_H.D_{10}^2 \qquad (2.21)$$

where: C_H = Hazen's empirical coefficient and D_{10}= particle size for which 10% of the soil is finer.

Although Hazen developed the formulation for sands ($0.01cm<D_{10}<0.3cm$), it has been widely applied to in situ soils as well other soils which are not sands. Because of this, Carrier III (2003) notes that Hazen's empirical coefficient, C_H ranges from 1 to 1000 according to published data despite the fact that the coefficient usually takes on a value of 100. Hazen's formulation represents average situations and should be carefully applied to soils outside the range Hazen studied (Taylor (1948).

- Terzaghi (1925)

Terzaghi (1925) suggested a formulation for saturated soils given in Equation 2.22.

$$k = \frac{g}{\nu}.C_t\left[\frac{n-0.13}{\sqrt[3]{1-n}}\right].^2 D_{10}^2 \qquad (2.22)$$

where C_t= sorting coefficient; $61x10^{-3}<C_t<107x10^{-3}$

Terzaghi's formulaltion is suited for large-grained sands (Cheng and Chen, 2007). Odong (2007) studied permeabilities of unconsolidated aquifer materials, comparing different empirical formulations based on grain size and concluded that Terzaghi (2007) grossly underestimated the permeabilities and recommended that the formulation be restricted to large grain sands.

- Kozeny-Carman

The Kozeny-Carman (K-C) equation was first suggested by Kozeny (1927) and later modified by Carman (1956). The K-C equation is one of the most widely accepted empirical formulation for estimating permeability of saturated soils (Chapuis and Aubertin, 2003; Odong, 2007; Chapuis, 2012). Although there are several forms of the K-C equation, it can be generalized as shown in Equation 2.23

$$k = \frac{g}{\nu}.8\times10^{-3}\left[\frac{n^3}{(1-n)^2}\right].D_{10}^2 \qquad (2.23)$$

While most literature states that the K-C equation is best suited for sands, Chapuis and Aubertin (2003) demonstrates that the equation can in fact be applied in predicting fairly accurately, the saturated permeability of a wide range of soils.

2.6.2Unsaturated permeability

Despite contentions that previously surrounded the driving potential of flow in unsaturated soils, Fredlund et al. (2012) has demonstrated that hydraulic gradient is the only driving potential for flow in unsaturated soils similar to saturated soils.

Since the pore space in unsaturated soils consists of air and water phases, the permeability of unsaturated soils is not only a function of void ratio but also the quantity of water in the pore space (Fredlund and Rahardjo,1993). Therefore, since the quantity of water will vary, the permeability of unsaturated soils is not constant but rather a function of water content or suction of the soil. Although the permeability of unsaturated soils is not a constant, Darcy's law can still be applied to flow in unsaturated soils (Buckingham, 1907; Richards, 1931; Childs and Collis-George, 1950).

2.6.2.1 Relationship between unsaturated permeability and volume-mass relations of soils

LLoret and Alonso (1980) and Fredlund (1981) state that the coefficient of permeability, k_w is a function of any two of three volume-mass properties:

$$k_w = k_w\,(S,e)$$

$$k_w = k_w\,(e, w)$$

$$k_w = k_w (w, S)$$

where: S= degree of saturation, e = void ration and w = gravimetric water content.

For unsaturated soils, the coefficient of permeability is affected by combined of changes of void ratio and degree of saturation or water content (Fredlund et al., 2012). Some examples of relationships between permeability, void ratio and degree of saturation of unsaturated soils are listed in Table 2.3.

2.6.2.2 Permeability functions

Owing to the difficulties in direct measurement of unsaturated permeability such as cost, duration of tests, and experimental difficulties (Leong and Rahardjo, 1997a; Fredlund et al., 2012), indirect methods have been found useful. The indirect methods estimate permeability functions by either directly or indirectly relating to the features of the SWCC (Fredlund et al., 2012).

Leong and Rahardjo (1997a) categorise models for estimating permeability functions in indirect methods into three in order of increasing rigor: empirical, macroscopic and statistical models.

Table 2.3 Relationships of unsaturated permeability with void ratio and degree of saturation

Reference	Formulation	Notes
Mitchell et al. (1966)	$k_w = C\frac{e^3}{1+e}S^3$	C = constant, e = void ratio, S= degree of saturation.
LLoret and Alonso (1980)	$k_w = k_s(S, e_0)10^{C_1(e-e_0)}$	C_1=constant, k_s=saturated permeability, e_0= initial void ratio
Chang (1976), Chang and Duncan (1983)	$k_w = k_s\left(\frac{e^3(1+e_0)}{e_0^3(1+e)}\right)S_e^m$	S_e=effective degree of saturation, m=flexible constant

a) Empirical models

Leong and Rahardjo (1997a) present a detailed review of empirical models. Fredlund et al. (2012) note that empirical models are constructed by recognizing the relationship between the SWCC and the permeability function. These models therefore take on a similar shape as the SWCC. Leong and Rahardjo (1997a) generalized most empirical models in the literature in the form shown in Equation 2.24.

$$k_r = \Theta^p \qquad (2.24)$$

where: k_r = relative permeability given as ratio of water permeability (k_w) to the saturated permeability (k_s), Θ = normalized volumetric water content = $(\theta_w-\theta_r)/(\theta_s-\theta_r)$ where the subscripts r and s refer to residual and saturated state water contents, respectively.

Considering Equation 2.23, if the normalized volumetric water content, Θ, is expressed as function of matric suction, typical of the SWCC, then the k_r can directly be related to matric suction as demonstrated by Leong and Rahardjo (1997a). The successful usage of the empirical models requires sufficient permeability measurements so that fitting parameters are easily optimized (Leong and Rahardjo, 1997a).

b) Macroscopic models

Macroscopic models aim at constructing analytical permeability functions (Mualem, 1986). Mualem (1986) enlists the underlying assumptions for these models. The primary assumption is the similarity between laminar flow at microscopic level and the macroscopic flow through a porous media (soil). With this assumption, flow is then modeled as simple laminar flow system, interrelating macroscopic variables such as average flow velocity, hydraulic gradient, permeability and hydraulic radius (Mualem, 1986; Leong and Rahardjo, 1997a). With a direct analogy made between these macroscopic variables and the corresponding variables in the soil-water-air system, together with simplifying assumptions, Leong and Rahardjo (1997a) generalized macroscopic models using a power function form given in Equation 2.25

$$k_r = S_e^{\delta} \tag{2.25}$$

where S_e = effective degree of saturation and δ = constant which varies with different researchers.

According to Mualem (1986), the macroscopic models have a theoretical basis unlike empirical models, are easy to use and do not require many experimental data points for calibration. However, Childs and Collis-George (1950) note that these models neglect pore size distribution.

c) Statistical models

According to Mualem (1986), statistical models aim at deriving the coefficient of permeability from the SWCC. The assumptions underlying the statistical models are (Mualem (1986):

- The porous medium is regarded as a set of interconnected pores, randomly distributed in the sample. The characteristics of the pores are described by a statistical function, f(r).
- The Hagen-Poiseuille equation is considered valid at the microscopic level i.e., at the unit pore level.
- The SWCC is considered analogous to the pore-size distribution function

Three statistical models are reviewed below.

Childs and Collis-George (1950) proposed a statistical model based on a random variation of pore sizes. This model was improved by Marshall (1958) and finally modified by Kunze et al. (1968). This model was generalized by Agus et al. (2003) as given by Equation 2.26

$$k_r(\theta_w) = \Theta^x \left[\frac{\int_0^{\theta_w} \frac{(\theta_w - \xi)}{\psi^y} d\xi}{\int_0^{\theta_s} \frac{(\theta_w - \xi)}{\psi^y} d\xi} \right]^z \qquad (2.26)$$

where: Θ= normalized volumetric water content, ψ = suction, ξ = dummy variable

For the original model suggested by Childs and Collis-George (1950),x =0, y=2, and z=1 in Equation 2.26.Agus et al. (2003) observed that the model gives better estimates for permeability functions of clays and sands when x = 0, y = 0, and z = 2 compared to the original model.

Burdine (1953) proposed another statistical model that takes into account tortuosity given in Equation 2.27.

$$k_r(\theta_w) = \Theta^2 \left[\frac{\int_0^{\theta_w} \frac{d\theta_w}{\psi^2}}{\int_0^{\theta_s} \frac{d\theta_w}{\psi^2}} \right] \tag{2.27}$$

Mualem (1976) modified Childs and Collis-George (1950)'s model giving Equation 2.28.

$$k_r(\theta_w) = \Theta^{0.5} \left[\frac{\int_0^{\theta_w} \frac{d\theta_w}{\psi}}{\int_0^{\theta_s} \frac{d\theta_w}{\psi}} \right]^2 \tag{2.28}$$

Agus et al. (2003) generalized Equations 2.27 and 2.28 into Equation 2.29

$$k_r(\theta_w) = \Theta^x \left[\frac{\int_0^{\theta_w} \frac{d\theta_w}{\psi^y}}{\int_0^{\theta_s} \frac{d\theta_w}{\psi^y}} \right]^z \tag{2.29}$$

According to Fredlund and Rahardjo (1993), the computation procedures are implemented by dividing the SWCC into several equal increments of volumetric water contents as illustrated in Figure 2.16. The relative permeability k_{ri} at specific volumetric water content θ_{wi} is then computed by summing suctions corresponding to volumetric water contents at and below the specific volumetric water content.

The permeability function is calculated using Equation 2.30 which is a modification of Kunze et al. (1968)'s equation with pressure head replaced with matric suction ($u_a - u_w$) (Fredlund and Rahardjo, 1993)

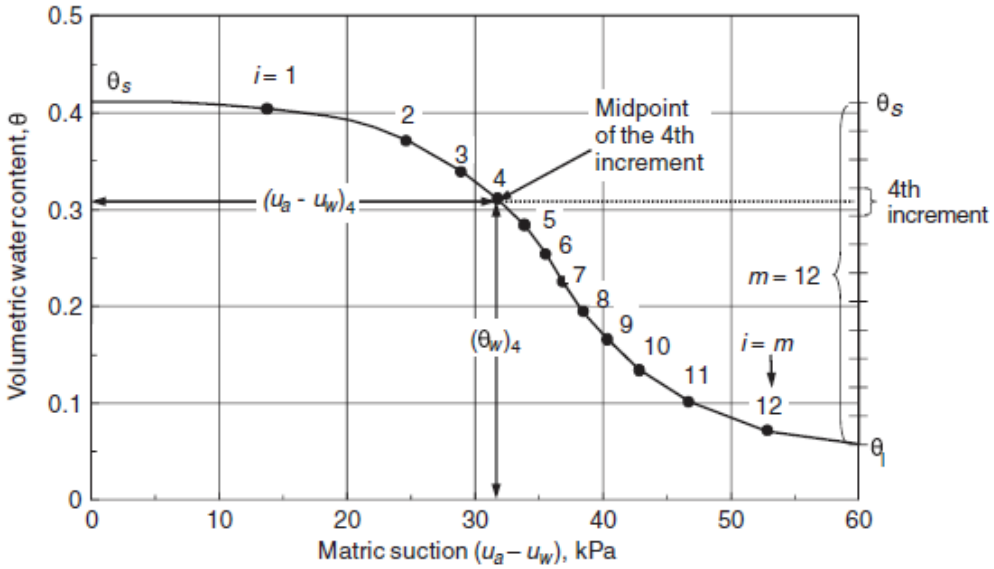

Figure 2.16: Calculation of the permeability function from the SWCC (from Marshall, 1958; Kunze et al, 1968)

$$k_w(\theta)_i = k_s \sum_{j=i}^{m} \left\{ (2j+1-2i)(u_a - u_w)_j^{-2} \right\} \qquad (2.30)$$

where: $k_w(\theta)_i$ = calculated coefficient of permeability for a specified volumetric water content, θ_i corresponding to the ith interval, k_s = measured saturated permeability, i = interval number that increases with decreasing water content, and j = counter from i to m.

2.6.3 Laboratory measurement of permeability

2.6.3.1 Saturated permeability

Two methods are usually used to measure saturated permeability in the laboratory i.e., the constant head and falling head techniques. In the constant head method, the hydraulic gradient is maintained constant in the test and the inflow or outflow volume rate of water is measured. The saturated permeability, k_s, is then measured according to Darcy's law using Equation 2.31

$$k_s = \frac{QL}{\Delta h_w A t} \tag{2.31}$$

where: Q = inflow/outflow rate of volume flow, L = length of soil specimen, Δh_w = hydraulic head difference, A = cross section area of the soil specimen, and t = time.

In the falling head method, the hydraulic gradient changes with time but the principle of continuity of flow is observed. Therefore k_s is computed using Darcy's law with Equation 2.32.

$$k_s = \frac{aL}{At} \ln\left(\frac{h_1}{h_2}\right) \tag{2.32}$$

where a = cross section area of the water reservoir, A = cross section area of the soil specimen, L = length of soil specimen, h_1 = hydraulic head at time t_1, h_2 = hydraulic head at time t_2, and t = time

These techniques can be applied to both the flexible and rigid wall permeameters that are commonly used to measure permeability in the laboratory. These techniques have been standardized in ASTM D5084-16a which details the procedure for measuring saturated permeability of soils using the flexible wall permeameter and ASTM D5856-15 which details the procedure to follow for the rigid wall permeameter.

The rigid wall permeameter, also called a fixed wall or a compaction mould permeameter (ASTM D5856-15), is largely used on compacted soils. Daniel et al. (1985) notes that the fixed wall permeameter is an affordable equipment however very often experiences side-wall leakage which leads to over estimation of permeability. In the same work, Daniel et al. (1985) describes the different modifications of the fixed wall permeameter together with their applicability, advantages and disadvantages. The flexible-wall permeameter is usually constructed out of a

triaxial or modified triaxial system (Daniel et al., 1984, Daniel et al., 1985). Although more costly and complicated to construct, the flexible-wall permeameter has numerous advantages over the fixed-wall permeameter. According to Daniel et al. (1985), the flexible wall permeameter is best suited for soils with irregular sides (such as natural soils, compacted soils with large particle sizes and clods), has no problem of side-wall leakage, saturation of samples can be enhanced by application of back pressure, permeability studies can be conducted at desired effective stress level and unsaturated permeability can easily be associated with the stress state variables (Samingan et al., 2003). Owing to its advantages, this study used the flexible-wall permeameter to determine the saturated permeability of the compacted soil.

2.6.3.2 Unsaturated permeability

Unsaturated permeability can be determined directly in the laboratory using either steady or unsteady methods. Measuring the unsaturated permeability of a soil requires a HAEV ceramic disk to separate the air and water phases. In order to minimize head loss across the HAEV disk, ASTM D7664-10 recommends the saturated permeability of the HAEV ceramic disk must be at least two orders of magnitude higher than the saturated permeability of the soil specimen to be measured.

One disadvantage of steady methods is that they require long duration and accurate volume determination (Klute, 1965; Klute, 1972; Olson and Daniel, 1981). Examples of equipment that have been designed to measure unsaturated permeability using steady state methods include: Klute (1965), Barden and Pavlakis (1971), and Huang et al. (1998).

Unsteady-state methods are attractive because they take a shorter time to conduct. These methods include instantaneous profile method (Richards and Weeks, 1953; Meerdink et al.,

1996; Krisdani et al., 2009), single or multi step outflow method (Gardner, 1956; Šimůnek et al., 1998; To-Viet et al., 2013), absorption method (Bruce and Klute, 1956) and sorptivity (Klute and Dirksen, 1986). However, the analysis to obtain the unsaturated permeability is more complex and both pore-water pressure and water content measurements are required.

2.6.4 Field measurements of permeability in the vadose zone

For laboratory techniques to be gainful, the samples must be carefully selected so that field conditions are represented as closely as possible. This may be quite difficult especially for coarse-grained soils. Secondly, in order to cater for the spatial variability, a large scale sampling exercise must be done which is very often hindered by resources. Due to these setbacks, field tests can be very useful and more representative. Some examples of field permeability tests in the vadose zone are briefly discussed below.

2.6.4.1 Constant head well permeameter

The constant head well permeameter sometimes referred to as a borehole permeameter is used to measure field-saturated permeameter. The permeability is measured around a well, augered in the unsaturated zone (Reynolds and Elrick, 2002). In addition to permeability, other measurements can be obtained such as matric flux potential, macroscopic capillary length parameter and the wetting front pressure head (Reynolds and Elrick, 2002).This method is based on a three dimensional quasi-steady state flow analysis.

According to Reynolds and Elrick (2002), the test may be carried out at a single or multiple heads i.e., the borehole may be ponded at different heads in order to establish the desired hydraulic parameters.

Several designs of the permeameter exist. Figure 2.17a shows an example of a schematic of the constant head well permeameter. Figure 2.17b shows the schematic diagram of the borehole simulating the flow domain. In order to minimize the effects of smearing, a sharp auger is used, augering is not done in wet soils especially clays and excess pressure on the auger is avoided. Smearing of the borehole influences the infiltration characteristics hence affecting the measured permeability (Reynolds and Elrick, 2002).

The permeameter is set up in the borehole and stabilized using a tripod stand as shown in Figure 2.17. Backfill material is necessary to avoid collapse of the borehole during testing when dealing with collapsible ground. In addition, Reynolds and Elrick (2002), notes that backfill material can minimize siltation of the well and ensures faster and uniform bubbling of the air tube especially when dealing with low permeability materials. Once the permeameter is filled with water, the air tube is lifted in order to attain the target head, H, in the borehole. The discharge, Q, is monitored until it attains a steady state. Elrick and Reynolds (1992) proposed a formula to estimate field saturated permeability, K_s for a steady state discharge, Q_s under a single steady state head, given in Equation 2.33.

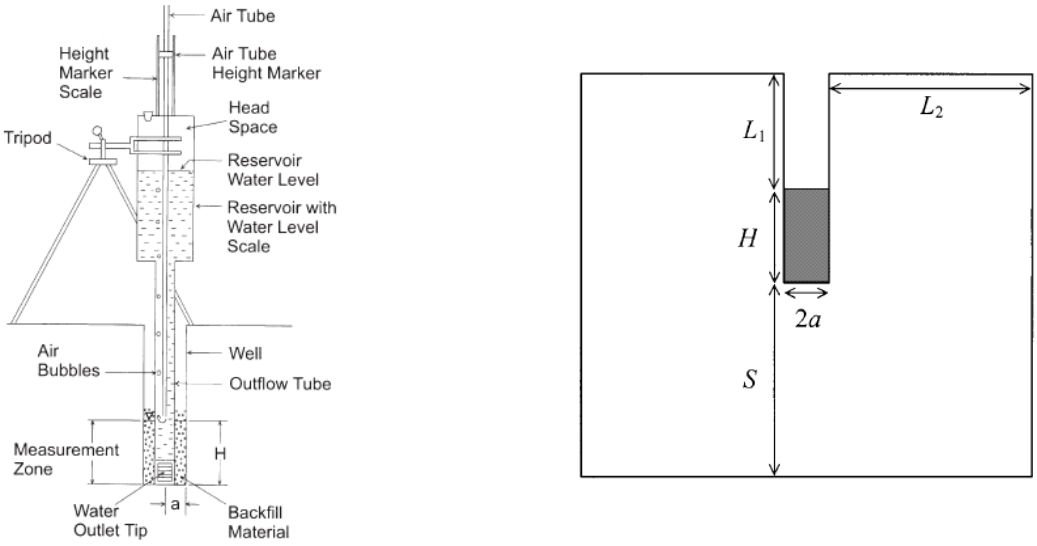

a) **b)**

Figure 2.17: Schematic representation of a) the constant head well permeameter(Reynolds and Elrick, 2002), and b) the simulation domain(Hayashi and Quinton, 2004)

$$K_s = Q_s\left(\frac{2\pi\pi^2}{C} + \frac{2\pi\pi}{\alpha C} + \pi a^2\right)^{-1} \tag{2.33}$$

where H = steady state depth of water in the well, C= dimensionless shape factor, α=parameter associated with effects of capillarity under steady state conditions, and a = radius of the well.

The underlying assumptions when applying this technique are: the soil is homogenous, isotropic and wetting of the soil is uniform

In order to minimize the boundary influence, Reynolds and Elrick (1987) suggested that boundaries should be located at a distance of at least 10H. Reynolds and Elrick (2002) presents formulations for estimating hydraulic parameters of the soil using multiple heads.

Daniel (1989) notes that the method is relatively affordable, easy to install, quite fast and takes into consideration unsaturated behavior. However, the method essentially measures horizontal

coefficient of permeability and is not suited for soils of low permeability; lower than 10^{-7} m/s (Daniel, 1989).

2.6.4.2 Ring infiltrometers

These infiltrometers consist of thin-walled, open-ended metallic or plastic cylinders with a sharp cutting edge at the bottom used for cutting into the ground with minimal disturbance during installation. Different arrangements of cylinders exist but some of the commonest are the single ring and double ring infiltrometers.

The single ring infiltrometer consists of a single cylinder while the double-ring infiltrometer consists of an inner measuring cylinder installed concentrically inside a wider buffer cylinder (Reynolds et al., 2002a). Once driven into the ground, the cylinders are ponded with water to a depth, H, as shown in Figure 2.18. These infiltrometers are usually used to determine the infiltration rate and the field saturated permeability.

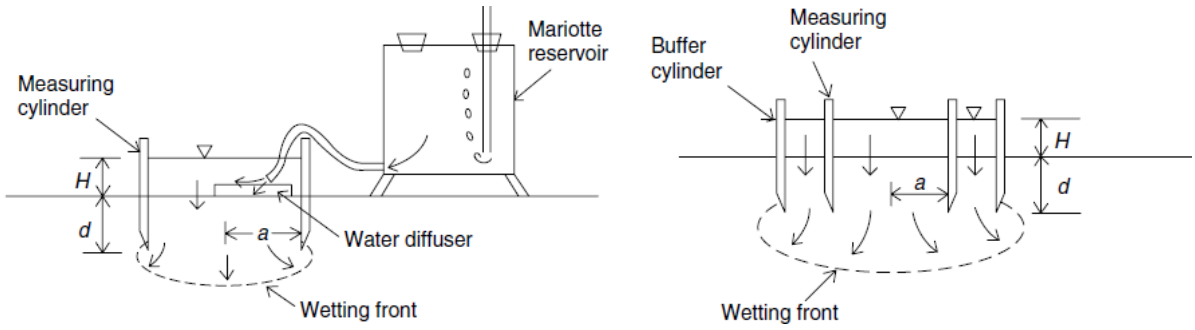

a) b)

Figure 2.18: Cross sections of a) Single ring infiltrometer, b) Double (concentric) ring infiltromer(Reynolds et al., 2002b)

It is important to maintain a constant ponding depth H which may be done manually by refilling to the required mark especially for cases of low infiltration rates. Alternatively, a reservoir is availed to ensure a constant H is maintained (Reynolds et al., 2002b) during infiltration. Infiltration rates are monitored until a steady state discharge is attained. According to Reynolds

et al. (2002b), the time required to attain steady state conditions depends on the soil texture, soil structure, depth of ponding (H), depth of embedment of the cylinders (d) and the radius of the cylinders (a)

Elrick and Reynolds (1990) suggested a formulation for computing the field saturated hydraulic conductivity, K_s from a ring infiltrometer at quasi-steady state conditions given in Equation 2.34

$$K_s = \frac{Q_s / \pi a^2}{\frac{H}{C_1 d + C_2 a} + \frac{1}{\alpha(C_1 d + C_2 a)} + 1} \tag{2.34}$$

where Q_s= steady state discharge, a= radius of the ring, H= steady state depth of ponded water in the ring, d= depth of ring embedded into the ground, α= macroscopic capillarity length while C_1 and C_2 are dimensionless constants.

Ring infiltrometers have great advantages for example affordability, ease of installation, capacity to give good estimate of vertical hydraulic conductivity due to the rings that restrict lateral spread. Despite these advantages, this technique has some major setbacks. The need to attain steady state infiltration may lead to long durations of time ranging from a few minutes to days depending on the size of cylinders, soil structure and texture (Scotter et al., 1982; Daniel, 1989). Daniel (1989) notes the need to correct for evaporative losses and difficulty to set up on a sloping ground unless a bench is established. It is important to also note that as the cylinders are driven into the ground, the soil may be disturbed hence influencing the subsequent measurements.

2.6.4.3 Tension or disk infiltrometers

These devices are usually used to determine field near-saturation permeability and sorptivity. A tension infiltrometer consists of an infiltrometer plate which may be a membrane or a hydrophilic porous disk (Reynolds, 2008). The disk/membrane is connected to a water reservoir which supplies it with water and a bubble tower that is used to control the suction head on the disk/membrane.

When placed on an unsaturated porous medium, the capillarity in the disk/membrane draws water out of the reservoir into the porous medium hence infiltration into the porous medium at the set suction head (Reynolds, 2008).

Since disk infiltrometers supply only a small tension at the soil surface, the effects of macropores on the infiltration are eliminated thus ensuring that only infiltration properties of the soil matrix are determined (Clothier and White, 1981). According to Clothier and White (1981), macropores have little influence during a natural rainfall infiltration and infiltration is controlled by the soil matrix. White and Sully (1987) further note that in order to reasonably offset the influence of macropores, the diameter of the disk should be at least equal to the macroscopic capillary length of the soil.

Techniques of obtaining hydraulic properties of the soil from disk infiltrometers can be categorized into steady state flow and transient flow. Wooding (1968) showed that the steady state flow rate, Q_o, of water from a surface disk of radius, r, containing water at a matric suction head, ψ_o is given by Equation 2.35

$$Q_O = \pi r^2 k_O + 4r\psi_o \qquad (2.35)$$

The characteristics of transient flow from disk infiltrometers are approximated by the first two terms of Philip (1957)'s expansion of the infiltration equation as given in Equation 2.36.

$$I = C_1 t^{\frac{1}{2}} + C_2 t \tag{2.36}$$

where I is the cumulative infiltration at a matric suction head, C_1 ($ms^{-1/2}$) and C_2 (ms^{-1}) are the parameters related to soil sorptivity, S and hydraulic conductivity, K, respectively.

Haverkamp et al. (1994) suggested a solution to Equation 2.36 which relates sorptivity S and permeability, k as given in Equation 2.37.

$$\begin{aligned} C_1 &= S \\ C_2 &= \frac{2-\beta}{3} K + \frac{\gamma S^2}{r\left(\theta_o - \theta_i\right)} \end{aligned} \tag{2.37}$$

where γ is proportionality constant in the range 0.6 -0.8, β is a coefficient lying between 0 and 1, r is the radius of the disk, θ_o is the final water content and θ_i is water content corresponding to the matric suction head imposed on the disk. Parameters C_1 and C_2 are obtained by curve fitting Equation 2.36 to the infiltration data. Once C_1 and C_2 are known, k and S can be computed.

Zhang (1997) suggested simple linear solutions to Equation 2.36 given in Equation 2.38.

$$\begin{aligned} C_1(h) &= A_1 S(h) \\ C_2(h) &= A_2 K(h) \end{aligned} \tag{2.38}$$

where A_1 and A_2 are dimensionless coefficients and h is the pressure head at which the mini-disk infiltrometer is set. Based on results of numerical experiments, Zhang (1997) suggested empirical relationships for calculating A_1 and A_2 given in Equation 2.39 and 2.40, respectively.

$$A_1 = \frac{1.4b^{0.5}\left(\theta_h - \theta_i\right)^{0.25}\exp\left[3\left(n-1.9\right)\alpha h\right]}{\left(\alpha\, r\right)^{0.15}} \tag{2.39}$$

$$A_2 = \frac{11.65\left(n^{0.1}-1\right)\exp\left[2.92\left(n-1.9\right)\alpha h\right]}{\left(\alpha\, r\right)^{0.91}} \qquad n \geq 1.9$$

$$A_2 = \frac{11.65(n^{0.1}-1)\exp\left[7.5(n\text{-}1.9)\,\alpha h\right]}{\left(\alpha\, r\right)^{0.91}} \qquad n < 1.9 \tag{2.40}$$

For n<1.35, Dohnal et al. (2010) suggested a modification to Equation 2.40 given in Equation 2.41.

$$A_2 = \frac{11.65(n^{0.82}-1)\exp\left[34.65(n\text{-}1.19)\,\alpha h\right]}{\left(\alpha\, r_0\right)^{0.6}} \qquad n < 1.35 \tag{2.41}$$

where: θ_h = volumetric water content corresponding to the applied disk matric suction head h (< 0), θ_i = initial volumetric water content, n and $\alpha(m^{-1})$ = VG SWCC fitting parameters, r = the disk radius and b = 0.55.

The VG SWCC-Θ model used in the computation is plotted in terms of the pressure head, h as shown in Equation 2.42.

$$\theta(h) = \theta_r + \left(\theta_s - \theta_r\right)\left[1 + \left|\alpha h\right|^n\right]^{-m}$$
$$\text{where} \quad m = 1 - \frac{1}{n}\,, \; n > 1 \tag{2.42}$$

Carsel and Parrish (1988) conducted several water retention experiments on different soil textural classes and developed average values for VG model parameters; n, α, θ_s and θ_r. Table 2.4 summarizes the findings of Carsel and Parrish (1988).

The n and α in Table 2.4 are very often used to solve Equation 2.40. This makes determination of the permeability very fast especially in the absence of time and facilities to measure the SWCC of the soil. However, it is important to check how reliable the permeability measurements obtained using Table 2.4 are compared to those obtained using the actual SWCC. This aspect was investigated in this thesis.

A mini-disk infiltrometer which is used in this study is one type of tension infiltrometer. Extra advantages of the mini-disk infiltrometer is its portability, ease of use, and fast measurements in the field.

Table 2.4 VG model calibration parameters for 12 soils (Carsel and Parrish, 1988)

Textural class	α (cm^{-1})	n	θ_s	θ_r
Sand	0.145	2.68	0.43	0.045
Loamy sand	0.124	2.28	0.41	0.057
Sandy Loamy	0.075	1.89	0.41	0.065
Loam	0.036	1.56	0.43	0.078
Silt	0.016	1.37	0.46	0.034
Silt Loam	0.020	1.41	0.45	0.067
Sandy Clay Loam	0.059	1.48	0.39	0.100
Clay Loam	0.019	1.31	0.41	0.095
Silty Clay Loam	0.010	1.23	0.43	0.089
Sandy Clay	0.027	1.23	0.38	0.100
Silty Clay	0.005	1.09	0.36	0.07
Clay	0.008	1.09	0.38	0.068

2.7 Shear strength of unsaturated soils

Shear strength behaviour of unsaturated soils is of great concern in engineering practice because unsaturated soils are very often encountered in practice. Over the years, the research community has contributed enormously towards understanding shear strength behavior of unsaturated soils.

Despite this effort, adoption by practitioners remains low owing to several factors some of which include: complexity of the science, expensive equipment, and test duration. Yet, unsaturated soil mechanics is needed to analyse rain-induced slope failures and seepage flow through dams, design remedial measures for failed slopes and waste containment system, and other problems in the vadose zone. In this thesis, the aspects of interest on shear strength of unsaturated soils are the shear strength equations and the testing procedures available. The literature review will be restricted to these two aspects.

2.7.1 Shear strength equations of unsaturated soils

Shear strength equations for unsaturated soils are commonly categorized based on the stress state variables criteria. Following subsection 2.3, the shear strength equations will be classified into two major categories: (i) equations based on a single stress state variable, and (ii) equations based on independent stress state variables.

2.7.1.1 Single stress state variable approach

a) Effective stress approach

The effective stress approach proposed by Bishop (1959) is the commonest in this category. Bishop (1959) proposed that effective stress in an unsaturated soil can be defined by combining two stress state variables i.e. net normal stress, $(\sigma_n - u_a)$ and matric suction, $(u_a - u_w)$ in addition to a material variable, χ . This formulation was reproduced in Equation 2.1.

One noted advantage of the effective stress approach is that it follows directly from the classical soil mechanics formalism of effective stress approach and is usually applied with the conventional Mohr-Coloumb (M-C) failure criterion. Therefore Equation 2.1, substituted into the

conventional M-C failure criterion given in Equation 2.43 yields Equation 2.44. Equation 2.44 is the shear strength formulation for unsaturated soils as suggested by Bishop et al. (1960).

$$\tau_f = c' + (\sigma_n - u_w)_f \tan\varphi' \quad (2.43)$$

$$\tau_f = c' + [(\sigma_n - u_a) + \chi(u_a - u_w)]\tan\varphi' \quad (2.44)$$

where τ_f = shear strength on the failure plane, c' = the effective cohesion and φ' = the friction angle.

The criticisms of the single effective stress approach have been stated in section 2.3.1. Owing to the elegance and simplicity of Equation 2.44, several researchers have attempted to either re-define parameter χ or to suggest ways of determining χ.

Khalili and Khabbaz (1998) studied 14 soils and established an empirical relationship for χ with suction ratio given in Equation 2.2. Other formulations in terms of degree of saturation or volumetric water content have been suggested by Vanapalli and Fredlund (2000) as re-stated in Equations 2.45 and 2.46.

$$\chi = S^{\kappa} = \left(\frac{\theta_w}{\theta_s}\right)^{\kappa} \quad (2.45)$$

$$\chi = \frac{S - S_r}{1 - S_r} = \frac{\theta_w - \theta_r}{\theta_s - \theta_r} \quad (2.46)$$

where S = degree of saturation, S_r = the residual degree of saturation, θ_w = the volumetric water content, θ_s = the saturated volumetric water content, θ_r = the residual volumetric water content and κ = fitting parameter which is optimized to obtain good fit between measured and predicted values.

Following Bishop (1959)'s formulation, other researchers have suggested shear strength equations based on a single stress variable. Three common ones are presented below:

a. **Greacen (1960)**

Greacen (1960) proposed Equation 2.47.

$$\tau_f = [\sigma_n + (u_a - u_w)]\tan\varphi'(1 - n_a) \qquad (2.47)$$

where n_a is the fraction of the voids filled with air.

Equation 2.47 assumes that suction in the soil water for an unsaturated soil supplies an additional isotropic stress on the internal area of contact hence increasing the soil's potential to resist shear. This implies that that increase in strength of an unsaturated soil is proportional to both an increment in applied normal stress and matric suction present in the soil again implying a single stress variable as suggested by Bishop (1959). Therefore, the limitations in Equation 2.44 also apply to Equation 2.47.

b. Lamborn (1986)

Extending micromechanics model by applying the principle of irreversible thermodynamics to a composite volume, Lamborn (1986) suggested Equation 2.48 to evaluate shear strength of unsaturated soils.

$$\tau_f = c' + (\sigma_n - u_a)\tan\varphi' + (u_a - u_w)\theta_w \tan\varphi' \qquad (2.48)$$

where: θ_w= volumetric water content.

Equation 2.48 is based on a single stress state variable in which shear strength in an unsaturated soil varies with the volumetric water content. According to Vanapalli (1994), this is only logical

if the desaturation process can be linked to the contribution that volumetric water content makes on shear strength.

c. Öberg and Sällfors (1997)

Öberg and Sällfors (1997) proposed Equation 2.49 to predict shear strength of unsaturated silts and sands based on the SWCC.

$$\tau_f = c' + [\sigma - Su_w - (1-S)u_a]\tan\varphi' \qquad (2.49)$$

where S = degree of saturation.

As determining χ to degree of saturation through the fraction of pore that are occupied by water i.e. $\frac{A_w}{A_{tot}}$. Therefore if the soil's SWCC is established, the shear strength of the soil can be determined for various degrees of saturation if the internal friction angle, ϕ' is known.

Despite the fact that there is no unique relationship between $\chi\left(=\frac{A_w}{A_{tot}}\right)$ and S, Equation 2.49 has been found to give satisfactory results in engineering practice (Öberg and Sällfors, 1997).

Vanapalli and Fredlund (2000) found that Equation 2.49 did not give good predictions of shear strength in relation to measured data irrespective of the suction range. However, Vanapalli and Fredlund (2000) tested the equation only on clayey material which may have affected its performance.

2.7.1.2 The independent stress state variable approach

Fredlund et al. (1978) proposed the concept of two independent stress state variables using multiphase continuum mechanics. This theory extends the Mohr-Coloumb failure envelope to a 3D planar surface. The formulation is re-stated in Equation 2.50

$$\tau_f = c' + (\sigma_n - u_a)_f \tan\phi' + (u_a - u_w)_f \tan\phi^b \quad (2.50)$$

where c' = the effective cohesion on the failure plane, $(\sigma_n\text{-}u_a)_f$ = the net normal stress at the failure on the failure plane at failure, $(u_a\text{-}u_w)_f$ = matric suction on the failure plane at failure, ϕ' = internal friction angle associated with the net normal stress $(\sigma_n\text{-}u_a)_f$, and ϕ^b = angle indicating the rate of increase of shear strength with matric suction, $(u_a\text{-}u_w)$.

Figure 2.19 illustrates the planar surface generated using Equation 2.50. The Mohr-circles are constructed in the 3-D space.

Equation 2.50 can be re-written as

$$\tau_f = C + (\sigma_n - u_a)_f \tan\phi' \quad (2.51)$$

where:

$$C = c' + (u_a - u_w)\tan\phi^b \quad (2.52)$$

Equation 2.52 is the equation of line of intercept of the extended M-C envelope with the matric suction axis as shown in Figure 2.19.

With Equation 2.51, the extended M-C envelope can be reduced to a 2-D τ-$(\sigma\text{-}u_a)$ plot in which the intercept on the τ axis is C as given in Equation 2.52.In this case, C is referred to as the total cohesion. Lu and Likos (2004) define the term $(u_a - u_w)\tan\phi^b$ as capillary cohesion, c''.

While Fredlund et al. (1978) assumed a constant value of ϕ^b for the entire range of soil matric range, later studies have demonstrated that ϕ^b varies with suction.

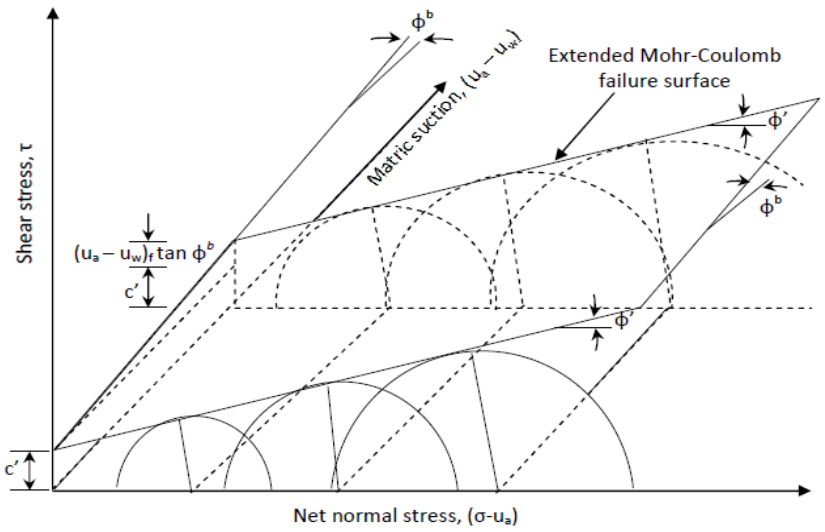

Figure 2.19: Extended Mohr-Coulomb failure envelope (from Fredlund and Rahardjo, 1993)

Shen and Yu (1996) proposed two hyperbolic equations for describing the shear strength of unsaturated soils shown in Equations 2.53 and 2.54.

$$\tau_f = c' + (\sigma_n - u_a)\tan\varphi' + (u_a - u_w)\left[\frac{1}{1 + (u_a - u_w)d}\right]\tan\varphi' \qquad (2.53)$$

$$\tau_f = c' + (\sigma_n - u_a)\tan\varphi' + (u_a - u_w)\left[\frac{1}{\cot\alpha + \frac{(u_a - u_w)}{\beta_1}}\right]\tan\varphi' \qquad (2.54)$$

where: d = fitting parameter, α= initial angle of shear strength with respect to shear strength, and

β= matric suction contribution to shear strength at peak value of shear strength.

Vanapalli et al. (1996a) proposed two formulations to capture the non-linearity of the extended M-C shear strength envelope shown as Equations 2.55 and 2.56.

$$\tau_f = c' + (\sigma_n - u_a)_f \tan\varphi' + (u_a - u_w)_f S^{\kappa} \tan\varphi' \quad (2.55)$$

$$\tau_f = c' + (\sigma_n - u_a)_f \tan\varphi' + (u_a - u_w)_f \frac{S - S_r}{1 - S_r} \tan\varphi' \quad (2.56)$$

where S = degree of saturation, S_r = residual degree of saturation, and κ = fitting parameter.

The formulations in Equations 15 and 16 can also be expressed in terms of volumetric or gravimetric water contents.

Garven and Vanapalli (2006b) found that the fitting parameter κ is closely related to the plasticity index, PI, of the soil as shown in Equation 2.57.

$$\kappa = -0.0016PI^2 + 0.0975PI + 1 \quad (2.57)$$

One advantage of formulations in Equations 2.55 and 2.56 is the ease of use with a SWCC of the soil. According to Garven and Vanapalli (2006a), commonly used shear strength equations consist of two parts: one part is the shear strength of the soil under saturated condition and the other part is the contribution to shear strength by the matric suction as shown by Equation 2.58.

$$\tau = \tau_{sat} + \tau_m \quad (2.58)$$

where: τ = total shear strength, τ_{sat} = shear strength of the soil under saturated conditions and τ_m = contribution to shear strength of matric suction. This observation can clearly be associated to

all the formulations presented above. Further Equation 2.58 can be further expressed as shown in Equation 2.59

$$\tau = c' + (\sigma_n - u_a)\tan\varphi' + \alpha\tan\varphi'(u_a - u_w) \quad (2.59)$$

where α is a function that varies depending on the formulation, $\tau_{sat} = c' + (\sigma_n - u_a)\tan\varphi'$ and $\tau_m = \alpha(u_a - u_w)\tan\varphi'$.

Equation 2.59 can be closely linked to Equation 2.44 and with such an attempt, the parameter, α can be severally defined. This has been demonstrated by Leong (2019) and partly shown in Table 2.5.

What is clear from Table 2.5 is the non-unique definition of χ as stated by different researchers. However, Table 2.5 also reveals an endeavour to reconcile the different shear strength equations and a successful reconciliation will greatly enhance application of unsaturated soil mechanics in practice.

Table 2.5: A comparison of selected shear strength equations to a generalised form (adopted from Leong 2019)

Reference formulation	Reference Equation in this thesis	α
Bishop et al. (1960)	2.44	χ
Fredlund et al. (1978)	2.50	$\frac{\tan\varphi^{b}}{\tan\varphi'}$
Lamborn (1986)	2.48	θ_{w}
Öberg and Sällfors (1997)	2.49	S
Vanapalli et al. (1996a)	2.55 and 2.56	S^{κ} or $\frac{S-S_{r}}{1-S_{r}}$
Khalili and Khabbaz (1998)	2.2	$\left[\frac{(u_{a}-u_{w})}{(u_{a}-u_{w})_{b}}\right]^{-0.55}$

2.7.1.3 Shear strength equations formulated from alternative stress variables

Tarantino and El Mountassir (2013) classified the shear strength approaches for unsaturated soils presented in the literature into two broad categories:

Category one: Those that assume that the contribution of partial saturation to shear strength is only through suction. Tarantino and El Mountassir (2013) further generalised such formulations as stated in Equation 2.60.

$$\tau = \sigma_{n}\tan\phi'+\Delta\tau(s) \text{ or } q = Mp + \Delta q(s) \qquad (2.60)$$

where $\Delta\tau$ = contribution of partial saturation to shear strength, s = soil suction, p = mean total stress, M = slope of saturated critical state line, and Δq = contribution to partial saturation to the deviator stress at ultimate state.

Under this category, the common formulations are those by Bishop (1960), Fredlund et al. (1978) and Khalili and Khabbaz (1998)

Category two: Those that assume that the contribution of partial saturation to shear strength is independently controlled by suction and degree of saturation. Tarantino and El Mountassir (2013) generalised such formulations as stated in Equation 2.61

$$\tau = \sigma_n \tan\phi' + \Delta\tau(s, S_\alpha) \text{ or } q = Mp + \Delta q(s, S_\alpha) \quad (2.61)$$

where S_α = degree of saturation

Under this category, the common formulations are those by Vanapalli et al. (1996a), Öberg and Sällfors (1997), and Tarantino and Tombolato (2005).

Category two are shear strength equations formulated using alternative or mixed variables discussed in section 2.3.3.

In category two, Tarantino and El Mountassir (2013) introduces the concept of effective suction which is suction weighted by effective degree of saturation. Effective degree of saturation is the degree of saturation of macropores (Tarantino and Tombolato, 2005; Tarantino, 2009). The formulation for effective degree of saturation S_{rm} is given in Equation 2.62

$$S_{rm} = \frac{e_w - e_{wm}}{e - e_{wm}} \quad (2.62)$$

where e = void ratio, e_w = water ratio i.e wGs and e_{wm} = microstructural water ratio associated with adsorbed water. Effective degree of saturation is used on the basis that only capillary water contained in the macropores contributes to the shear strength of the soil.

Utilization of category two equations as stated in section 2.3.3 accounts for aspects such as void ratio and hysteresis. Furthermore, Tarantino and El Mountassir (2013) demonstrated that this conceptualization of shear strength can reduce the rigor of testing since it can easily be adopted with conventional equipment in order to interpret simple tests such as the constant water content test.

It is interesting to note overlapping of concepts for example, while Öberg and Sällfors (1997)'s formulation given in Equation 2.49 can be idealized as an equation constructed using a single effective stress variable, it can still be categorized as one with mixed stress variables. This is also true for Vanapalli et al. (1996a)'s formulations. It is these agreements and controversies that hinder the application of unsaturated soil mechanics. More research is required to reach consensus.

2.7.2 Shear strength testing for unsaturated soils

Existing literature enlists two major tests to obtain shear strength parameters of unsaturated soils; the consolidated drained (CD) test and the constant water content (CW) test. The CD tests commonly reported in literature (Ho and Fredlund, 1982; Rahardjo et al., 1995; Rahardjo et al., 2004) used the axis-translation technique (ATT) as suggested by Hilf (1956) to maintain a constant suction during consolidation and shearing phases. In the CD test, both the air and water phases are drain during the test. The test is performed at a slow rate to ensure no pore-water pressure build up occurs in the specimen during shearing. The CD test has been noted to have

several setbacks which includes the long duration of the test, highly sophisticated and costly equipment and ATT may not necessarily reflect the real soil behavior in nature and practice.

Thu et al. (2006), Marinho et al. (2016), de Oliveira et al. (2016), note that the CW test can address some of the concerns of the CD test. Thu et al. (2006) and de Oliveira et al. (2016) note that construction of engineering structures using compacted cohesive soils is best represented using a CW test given that the soils have low permeability and the construction is usually done very fast thus not allowing drainage of the water phase, although the air phase is usually drained or is at atmospheric state. This is simulated in the CW test when the air phase of the soil specimen is allowed to drain while the water phase is in an undrained state.

Traditionally, the CW test is performed using the ATT which ensures that suctions higher than 100kPa are attained. The ATT imposes a constant air pressure onto the soil specimen while changes in pore-water pressure and soil suction are monitored (Rahardjo et al., 2004, Thu et al., 2006, Jotisankasa et al., 2009). In all these studies, the soil specimen is pre-saturated in the triaxial cell and consolidated at a given confining pressure. At the end of consolidation phase, the soil specimen is allowed to equilibrate at a selected matric suction using ATT prior to shearing. During shearing phase, the air pressure, u_a, is maintained while the pore-water pressure, u_w, in the soil specimen is monitored using pore-water pressure probes.

de Oliveira et al. (2016) and Marinho et al. (2016) suggested more accessible procedures for the CW test by eliminating the need for the ATT. In these procedures, the CW test is done on the as-compacted soil specimens with matric suctions monitored using a high capacity tensiometer (HCT) at the base of the specimen. The challenge with these tests was ensuring matric suction equalization in the soil specimen. The confining pressure is applied and matric suction monitored

with the HCT until it becomes stable under the confining pressure. The shearing phase of the test was done in load steps, ensuring matric suction equalization with each load step before the next until the specimen failed. These procedures are promising in making unsaturated soil mechanics more accessible to practicing engineers. In fact, Marinho et al. (2016), demonstrated that if a CW test is done well and matric suctions accurately determined, there may be no practical need for determining the conventional saturated parameters i.e., ϕ' and c'. These can be inferred from the 3D shear strength envelope.

However some drawbacks noted are: the cost and availability of HCT, the difficulty in saturating the HCT especially where the AEV of the ceramic disk is high, the likelihood of cavitation of the HCT system, and the difficulty to measure shear strength of dry soils with very high matric suctions. This study therefore attempts to measure shear strength of as-compacted soils with varying degrees of saturation using simple conventional tests. The main aim is to investigate the possibilities of interpreting unsaturated shear strength parameters within a short time duration using conventional equipment.

2.8 Concluding remarks

The chapter has given a brief overview of the fundamental concepts of unsaturated soil mechanics which are: the stress state variables, measurement and control of suction, the SWCC, hydraulic properties, and shear strength. Enormous strides in the development of the theory and appropriate test procedures have been noted. However, despite these strides, application of unsaturated soil mechanics in routine engineering practice is still limited.Some of the noted issues of interest to this thesis are:

1) The need to agree on stress state variables well suited for applications of unsaturated soil mechanics is still important. Despite great contributions, the research community lacks unanimity on this issue. This in turn affects equipment design and test protocols.
2) Suction control methods are an important part of applying unsaturated soil mechanics. The axis translation technique which is the commonest has drawn a lot of debate in recent years regarding its suitability in representing natural conditions.
3) Suction measurement techniques have developed over the years. The commonest ones have been presented in the chapter. Of interest to this thesis is the filter paper and the chilled-mirror dewpoint techniques. The advantages and drawbacks of these techniques have been presented. However, it is the position of this thesis that these techniques be further studied to clarify on issues like: equilibrium time, hysteresis, variability of filter papers and practical aspects surrounding their application.
4) Great advancements have been made in the theory and measurement of the SWCC. The SWCC as discussed in the chapter is key in implementation of unsaturated soil mechanics. The noted challenges from literature largely are duration of testing. Also more test data is still needed to validate the numerous models and observations that have been made over the years. This thesis has measured SWCCs for dynamically compacted soils and attempted to explain the different observations and where necessary validated existing theory.
5) A lot of work has been done regarding permeability including formulation of governing theory, measurement techniques and estimation. However there is still great need to develop fast and reliable methods for measuring permeability. The saturated permeability measurements in particular are an important measurement since from it permeability

functions for unsaturated soils can be estimated. Therefore, the thesis explores the application of a mini-disk infiltrometer in estimating saturated permeabilities. The disk infiltrometer is affordable, fast and therefore if found reliable, this will greatly improve the measurement of permeability.

6) Shear strength is a key property of soils. The common practice in unsaturated soil mechanics is to use suction-controlled tests that apply the axis translation technique. The drawback of these tests are the long test duration, cost of equipment and high level of expertise required. The thesis therefore attempts to explore possibility of measuring unsaturated shear strength using simple CW tests in which conventional tests and equipment are used. This, if found plausible will be useful in bridging saturated and unsaturated soil mechanics.

Chapter 3. Research Programme

3.1 Introduction

This chapter describes the soils for the experimental programme of this research project, together with the basic properties of the soils. The procedures used for making the soil specimens for the subsequent experiments are also presented. Finally, the apparatus, experimental set-ups and testing procedures employed in the research are described.

3.2 Soils and basic properties

The soils used in this research project were residual soils obtained from the Jurong Formation (JF) and the Bukit Timah Granite (BT) of Singapore. Owing to the variability in soil properties in the two formations (Leong et al., 2002a; Rahardjo et al., 2012), two soils at different locations were obtained for each formation. All soils were sampled in disturbed form. The materials are designated as BT1 and BT2 for soil materials from the Bukit Timah Granite and JF1 and JF2 for soil materials from the Jurong Formation. The Bukit Timah Granite is mainly an acidic igneous rock system while the Jurong Formation is predominantly a folded sedimentary rock system (Leong et al., 2002a). The upper layers of these formations were weathered into residual soils of varying thickness. Generally, the weathering depths in JF are greater than that in the BT. Table 3.1 shows the basic soil properties while Figure 3.1 shows the grain size distribution of the soils. Using Equation 3.1 as suggested by Fredlund (2000), Rahardjo et al. (2012) suggested lower and upper envelope bounds to grain size distributions (GSD) as well as typical GSDs for soils from the three major geological formations (Jurong Formation, Bukit Timah Granite and Old Alluvium) of Singapore.

$$P = \left[\frac{100}{\ln\left[\exp(1)+\left(\frac{a_{gr}}{d}\right)^{n_{gr}}\right]^{m_{gr}}}\right]\left[1-\left(\frac{\ln\left(1+\frac{d_r}{d}\right)}{\ln\left(1+\frac{d_r}{d_m}\right)}\right)^{7}\right] \quad (3.1)$$

where P = Percent passing, d = particle diameter (mm), a_{gr} = the point of inflection in the equation, n_{gr} = a parameter related to the steepest slope, m_{gr} = a parameter related to shape of the grain size curve as it approaches the fine-grained region, d_r = parameter related to the particle size in the fine-grained region and is referred to as the residual particle size and d_m = minimum diameter.

Table 3.1: Basic properties of soils studied

Property	Soil materials				Test procedure/reference
	BT1	BT2	JF1	JF2	
Specific gravity, Gs	2.63	2.63	2.70	2.71	ASTM D854-14
Atterberg limits:					ASTM D4318-17
Liquid limit (w_L)%	58	53	46	43	
Plastic limit (w_P),%	31	28	24	24	
Plasticity index	27	25	22	19	
Gradation characteristics:					ASTM D6913-17, D7928-17
d_{10}(mm)	0.0014	0.0016	-	-	
d_{30} (mm)	0.0023	0.0032	0.0060	0.0020	
d_{50} (mm)	0.0050	0.019	0.8000	0.0200	
d_{60} (mm)	0.0090	0.1600	1.9000	0.0800	
% <0.002mm	25	18	23	30	
USCS classification	MH	MH	CL	CL	ASTM D2487-17

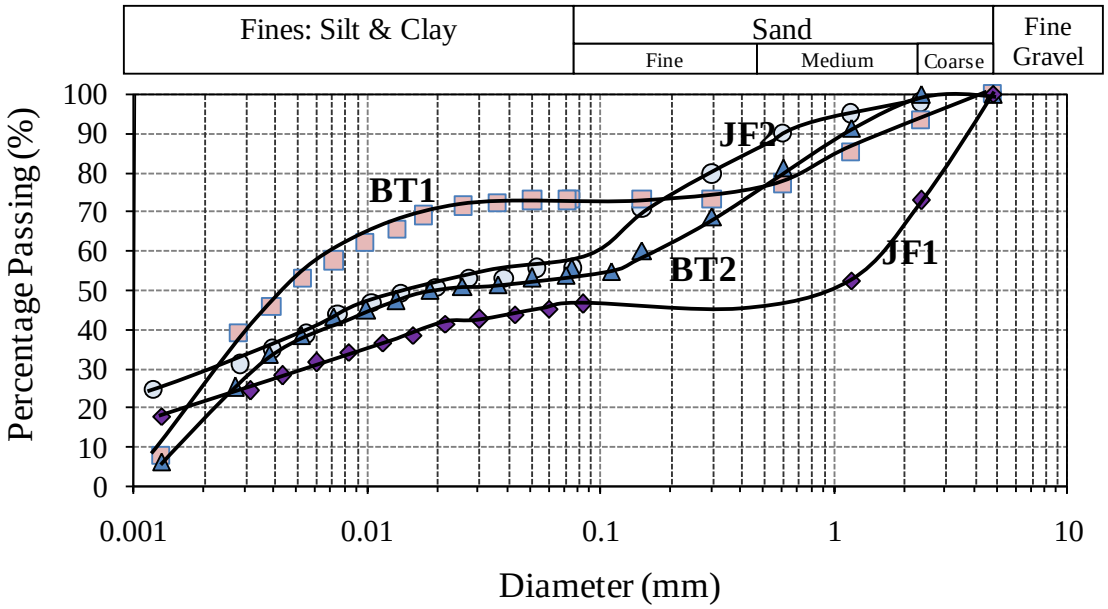

Figure 3.1: Grain size distributions for the studied soils

The parameters using Equation 3.1 to describe the upper, typical and lower envelope bounds for the GSDs of BT and JF soils as given by Rahardjo et al. (2012) are summarized in Table 3.2. An attempt has been made to compare the GSDs obtained in this study with these envelope bounds as shown in Figure 3.2. As Equation 3.1 is an empirical curve fitting equation, a_{gr}, m_{gr}, n_{gr} are values based on best fit of the grain size distribution curve.

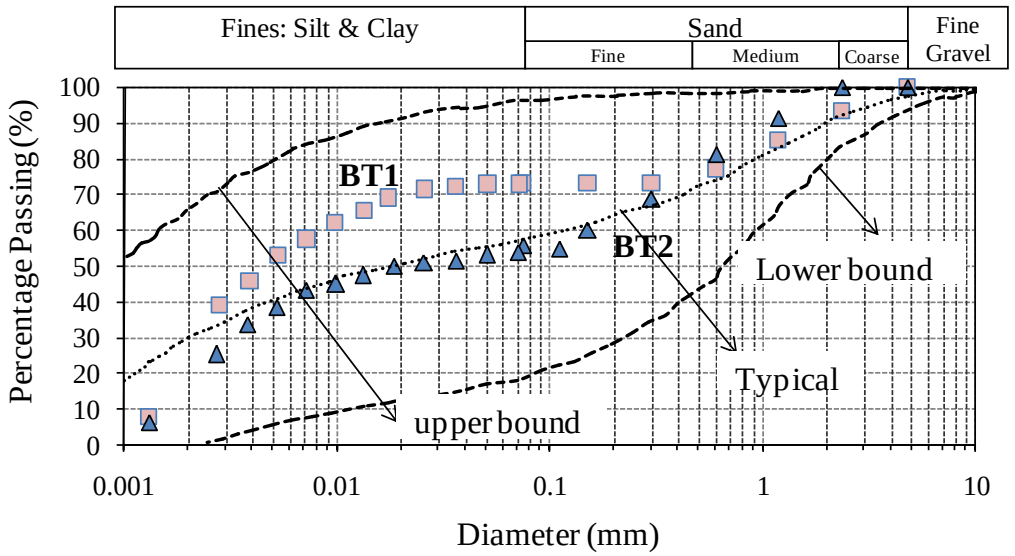

(a)

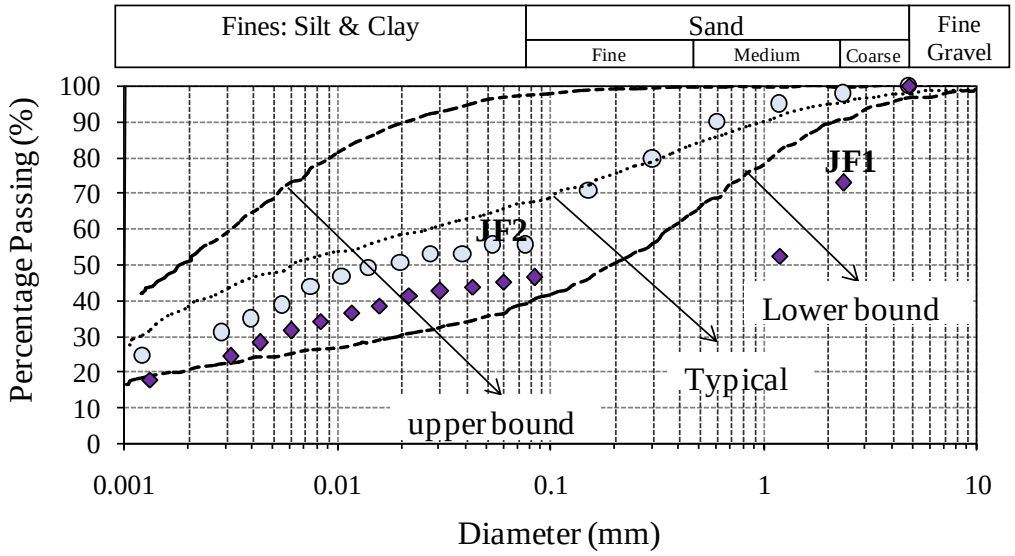

(b)

Figure 3.2: Grain size distributions: a) BT and b) JF soils in comparison with the upper and lower bound GSDs and typical GSD.

Table 3.2: Parameters defining the GSD envelopes for BT and JF formations (from Rahardjo et al., 2012)

Formation	GSD bound envelopes	a_{gr}	n_{gr}	m_{gr}	d_r (mm)	d_m(mm)
BT	Lower	1.68	1.66	0.98	20	0.002
	Typical	2.56	1.94	0.28	20	0.0005
	Upper	0.0001	0.58	5.85	9.57	0.0001
JF	Lower	1.25	1.38	0.7	0.010	0.0005
	Typical	1.23	1.13	0.35	5.00	0.0004
	Upper	0.006	1.06	1.13	0.00001	0.001

Figure 3.2 indicates that the GSDs of the soils used in this study are within the upper and lower GSD bounds suggested by Rahardjo et al. (2012) except for JF1 showing the higher variability of soils in the Jurong Formation compared to Bukit Timah Granite.

3.3 Compaction behavior and preparation of test specimens

3.3.1 Justification for use of compacted materials

Compaction is a densification process of soils by application of a mechanical energy. According to Tarantino and De Col (2008), the compaction process may be regarded as a fabrication process for soils where the soils undergo stress and phase changes. In this study, stress or phase evolution during compaction was not studied.

The test specimens used in this study were all dynamically compacted residual soils. The reason for using compacted soils in this study is two-fold. First, they are widely used in many civil engineering projects including dams, embankments, back fills and pavements. In fact, compacted

soils are the only soil in classical soil mechanics treated as unsaturated consisting of three phases: solid, water and air. Therefore, compacted soils are of great interest in engineering practice. Second, natural soils have inherent variability which makes systematic study of engineering properties difficult. Hence, reconstituted soils such as compacted soils provide more identical specimens to enable a systematic study to be carried out.

In addition, studies on compacted soils have demonstrated differences in soil structure on the dry of optimum and wet of optimum. These observations were first made by Lambe (1958) and have been validated over the years with more advanced testing techniques like the scanning electron microscopy (SEM) and mercury intrusion porosimetry (MIP) tests. Figure 3.3 shows an idealised compaction curve as well as Lambe (1958)'s classification of soil structure resulting from compaction. Dry of optimum fine-grained soils possess a flocculated fabric while on the wet of optimum, they are dispersed. With an increase in compactive effort, the soils become more dispersed despite the moulding water content (Holtz and Kovacs, 1981).

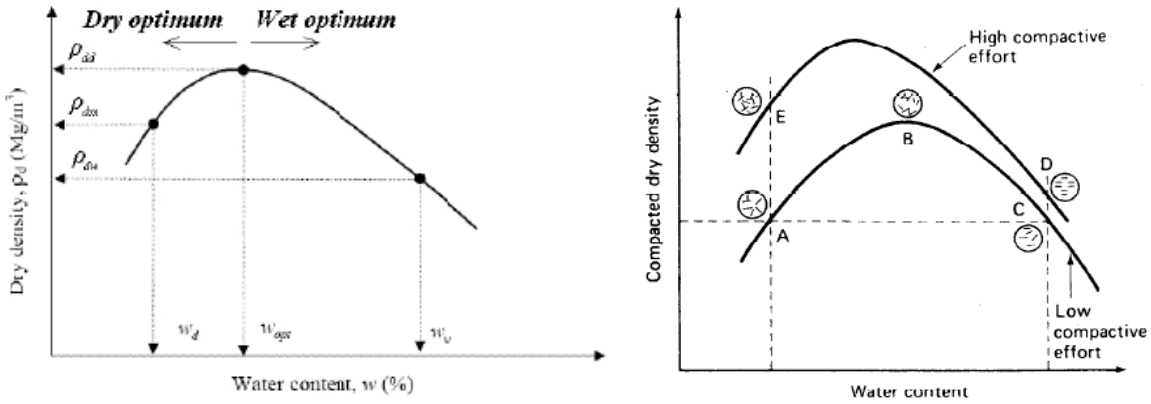

(a) (b)

Figure 3.3: Moisture-density relationships: a) Typical compaction curve, b) Effect of compaction on soil structure (Lambe, 1958)

Many studies have observed aggregation of the compacted soil most pronounced on the dry of optimum side (Delage et al., 1996; Cuisinier and Laloui, 2004; Frydman and Baker, 2009; Monroy et al., 2009) and that these structures have large influences on mechanical and hydraulic behaviour of the soils. Furthermore, studies on pore size distributions have concluded that at the dry of optimum and optimum water contents, soils may possess a dual-porosity or double structure while soils on the wet of optimum possess a unimodal pore size distribution (Ahmed et al., 1974; Delage et al., 1996).

Therefore, in addition to studying unsaturated soil behavior, compacted soils make it possible to study the influences of structure on the mechanical and hydraulic behaviour of soils.

3.3.2 Preparation of test specimens

Prior to compaction, the residual soils were air dried, disaggregated and thoroughly mixed to form homogenous soil samples. The homogenous soil was then sieved through the ASTM sieve No. 4 (4.75mm).

In all cases, the soil materials passing sieve No. 4 were thoroughly hand-mixed with distilled water at targeted water contents. After thorough mixing with distilled water, the soils were sealed in ziplock plastic bags and stored in a high humidity chamber for at least 120 hours to allow for moisture equilibration.

The soil materials were then compacted using standard and modified Proctor energies in accordance to ASTM D698-12 and ASTM D1557-12, respectively, to obtain the moisture-density relationships for the soil materials at the two energy levels. Figure 3.4 shows the moisture-density relationships for each of the four soils (BT1, BT2, JF1 and JF2).Table 3.3 summarises the compaction characteristics of the different materials

Table 3.3: Compaction properties of soils studied

	Soil materials			
Property	BT1	BT2	JF1	JF2
Standard Proctor test				
Optimum moisture content, %	16	19	18	16
Maximum dry density, Mg/m^3	1.69	1.71	1.65	1.76
Modified Proctor test				
Optimum moisture content, %	13	13	15	13.5
Maximum dry density, Mg/m^3	1.86	1.88	1.83	1.94

Most of the tests done in this study are for cylindrical specimens of about 50mm diameter and 100 mm height. In order to obtain such test specimens, samples compacted in the standard mould need to be trimmed. Trimming of compacted samples would not only be very cumbersome and time consuming but more importantly, it would be very difficult to obtain good quality test specimens especially on the dry side of optimum. Therefore, a two-part split cylindrical plastic mould (internal diameter = 52mm, height = 102mm) was fabricated so that the test specimens of the correct diameter are compacted directly. To ensure easy extraction of the compacted specimen from the split mould, each half of the mould has holes of 1mm diameter drilled in a grid fashion to allow escape of trapped air during compaction as well as to reduce the side friction.

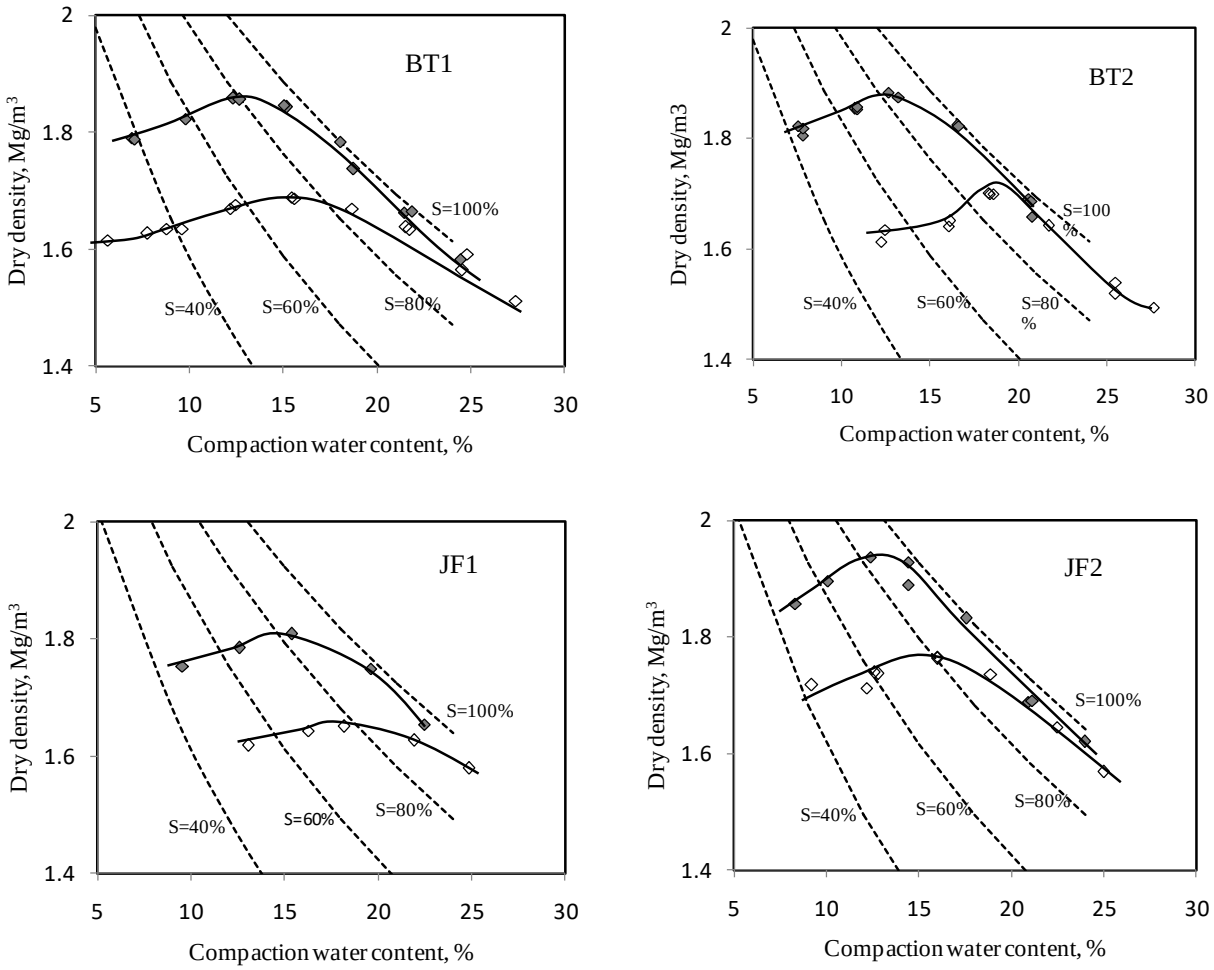

Figure 3.4: Moisture-density relationships for the soils studied at both standard and modified Proctor energies

In order to compact the test specimen in the plastic mould, a frame was set up using slotted angle bars fastened with nuts and bolts as shown in Figure 3.5. The frame was equipped with a pulley system where a nylon rope was used to lift a drop mass. The drop mass weighed 4.5 kg and has dimensions of 75mm diameter and 150mm in height. The drop mass has a central hole (diameter 26.5mm that slides along a 26 mm external diameter PVC tube. The PVC tube as shown in Figure 3.3 is fitted onto a spindle on top of a solid cylindrical steel bar, diameter 51.6mm. The solid bar rests on top of the soil in the mould and hence transfers the impact energy to the soil. The PVC tube guide ensures that the drop mass falls centrally on the solid cylindrical steel bar which then transfers the impact energy to the soil material in the plastic mould.

Using Equation 3.2, the height of drop of the drop mass was calibrated to deliver standard and modified Proctor energies (ASTM standard and modified Proctor energies are 600 and 2700kN-m/m^{3,} respectively) to the soil specimen. For the standard Proctor energy, the drop mass was dropped through a height, h = 200mm and the soil was compacted in three layers while for the modified Proctor energy, the drop mass was dropped through a height, h = 450mm, and the soil was compacted in five layers. For both compaction energies, each layer in the plastic mould was subjected to six blows. Table 3.4 shows a comparison of the ASTM compaction procedures and those followed in this thesis

Table 3.4 Comparison between the ASTM and thesis procedures of compaction

Item compared	ASTM Procedure		Thesis procedure	
	Standard Proctor	Modified Proctor	Standard Proctor	Modified Proctor
Mould dimension (mm)	Ht =116.4 Dia =101.6		Ht = 102 Dia = 52	
Rammer weight (kg)	2.5	4.5	4.5	4.5
Rammer drop height (mm)	305	457.2	200	450
Rammer diameter (mm)	50.8	50.8	75	75
Compaction layers	3	5	3	5
Blows per layer	25	25	6	6

The six blows per layer of compaction in the smaller PVC mould was based on equivalent energy compaction with the compaction in the standard compaction moulds. As number of blows is discrete, adjustment of the drop height was made as well as number of blows to account for the friction to try to achieve the same dry density for the moisture content on the compaction curve. It was assumed that maintaining equivalent energy input and dry density, the strength and soil structure obtained for the standard and PVC mould soil specimens will be similar.

Before each compaction, the two halves of the plastic mould were fastened with hose clips and the internal walls of the mould were lubricated with a thin layer of hydraulic oil of medium viscosity to minimize friction. During compaction, each layer was scarified using a fork before placing another layer to allow for bonding between the layers.

Figure 3.6 shows typical compaction specimens used in the study, the smaller specimen was obtained using the PVC (plastic) mould as described above and the larger specimen was obtained using the standard ASTM mould.

$$\text{compactive effort} = \frac{\left(\begin{matrix}\text{mass of}\\ \text{rammer}\end{matrix}\right)\times\left(\begin{matrix}\text{drop - height}\\ \text{of rammer}\end{matrix}\right)\times\left(\begin{matrix}\text{number of}\\ \text{blows per layer}\end{matrix}\right)\times\left(\begin{matrix}\text{number of}\\ \text{layers}\end{matrix}\right)\times g}{\text{mould volume}} \qquad (3.2)$$

(a) Photo

(b) Compaction accessories

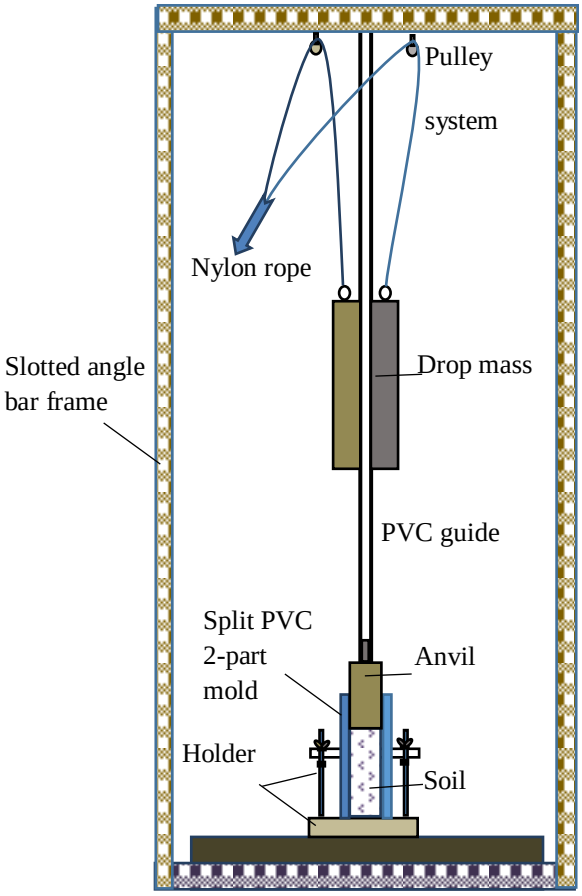

(c) Schematic drawing

Figure 3.5: Compaction set-up to prepare soil specimens in the PVC mould

The energy input per unit volume of soil is the same for both the standard ASTM procedure and the PVC mould procedure adopted in this thesis. In the standard procedures, the 25 blows of compaction hammer is not directed at only one spot on the top of the sample as it is in the case of the compaction in the smaller PVC mould. However, the soil sample in the PVC mould experiences more side friction compared to the soil sample in the standard mould. This made it difficult to match the dry density on the compaction curve. It is expected that there will be some difference in the soil structure but the general characteristics of the compacted samples in the

PVC mould and standard mould will be largely the same. When referring to dry of optimum, optimum and wet of optimum, the optimum moisture content as obtained from the standard mould is used in this thesis.

Figure 3.6: Typical compaction specimens, left specimen obtained using the PVC mould and the right specimen using the ASTM standard compaction mould

3.3.3 Nomenclature of the test specimens

As mentioned previously, four soils (two each from BT and JF) were studied. Specimens were prepared using two different compaction moulds, the standard ASTM mould and the PVC plastic mould. Additionally, test specimens were compacted at two energy levels, standard and modified Proctor, and various moulding water contents.

Given these variables, it was important to develop a nomenclature for the test specimens for ease of reference. The nomenclature adopted is in the form AAx-BBB-CCyy where AA refers to the formation from which the soil was obtained (BT or JF), x refers to soil 1 or soil 2 from each formation, BBB refers to compaction energy (STD for standard or MDF for modified), CC refers to the compaction mold used (ASTM mold or PL plastic mold) and yy refers to the compaction water content in % go the nearest whole number.

For example:

A soil 1 (x = 1) from Bukit Timah (AA = BT) compacted at standard Proctor energy (BBB = STD) using the standard ASTM mould (CC = ASTM) at a water content of 10% (y = 10) is designated as : BT1-STD-ASTM10 and if it was compacted at modified energy it is: BT1-MDF-ASTM10. If the mould was PVC plastic mold, the designation would be BT1-STD-PL10 and BT1-MDF-PL10.

Table 3.5 further illustrates the nomenclature adopted for the test samples (in the as-compacted state) for this study.

Table 3.5: A guide to the nomenclature adopted for the different test specimens

Geological Formation	**Compaction effort**	**Compaction mould**	**Compaction water content, %**
BT1, BT2, JF1 or JF2	STD= Standard Proctor MDF= Modified Proctor	ASTM = Standard compaction mould recommended by ASTM PL= plastic PVC mould fabricated in this study	e.g 10, 14 et.c

The subsections that follow present the different tests done on in this study. Detailed procedures are presented for the experiments including the rationale where applicable.

3.4 Suction measurements

Two major techniques of suction measurement were employed in the study, filter paper technique and chilled mirror dew-point technique. The adopted procedures are described below.

3.4.1 Filter paper technique

The filter papers used in this study were Whatman No. 42, ashless type, diameter 42.5mm. Whatman filter papers were preferred to other brands of ashless filter papers because they are thicker, have smaller pore sizes (Chandler and Gutierrez, 1986) and can measure suction over a wide range (Sibley and Williams, 1990).In this study, both contact and non-contact filter paper methods were used to measure the matric and total suctions, respectively. Both initially dry and initially wet Whatman No.42 filter papers of 42.5mm diameter were used.

In this thesis, the following notations have been adopted to identify the filter paper condition: ID-C-FP for initially dry contact filter paper, ID-NC-FP for initially dry non-contact filter paper, IW-C-FP for initially wet contact filter paper, and IW-NCFP for initially wet non-contact filter paper.

3.4.1.1 Initially dry filter papers

Initially dry filter papers were used as obtained directly from their boxes without any pre-treatment. The average initial water content of Whatman No. 42 filter papers was found by oven drying 48 pieces of the filter paper and found to be 6.6% with a standard deviation of 0.8%. Marinho and Oliveira (2006) reported an average initial water content of about 6% for Whatman No. 42 filter paper.

3.4.1.2 Initially wet filter papers

Most of the literature reported the use of initially dry filter paper to measure soil suction. The procedures suggested in ASTM D5298-16 are for an initially dry filter paper, in fact ASTM D5298-16 suggests oven-drying the filter paper prior to its use. A few researchers (e.g Muñoz-Castelblanco et al., 2010; Acikel et al., 2015; Leong et al., 2016) have examined the use of an initially wet filter paper to examine its possible advantages over initially dry filter paper. These studies indicate good potential for the use of initially wet filter paper for suction measurement. The inclusion of the initially wet filter paper in the test programme of this study followed the hypothesis that an initially wet filter paper reduces the equilibrium time, hence would reach equilibrium faster than an initially dry filter paper. Therefore, this thesis presents the test results of suction measurements using both initially dry and initially wet Whatman No. 42 filter papers. More than 1700 pieces of filter papers were used. The performances of initially dry and initially wet filter papers are assessed and are compared for the measurement of both matric and total suctions. In addition, equilibrium time, hysteresis and other factors influencing the measurement are evaluated.

Two methods were adopted in the preparation of the initially wet filter papers. In Method 1, the filter papers were initially soaked in distilled water for about 45 minutes and then left to dry over a saturated sodium chloride (NaCl) solution in an airtight desiccator for two hours. The room temperature varied between 24 and 26^{o}C, hence the relative humidity in the desiccators was expected to be about 76% (Young, 1967).

In Method 2, the filter papers were initially soaked in distilled water for about 45 minutes and then left to dry to water contents of between 40 and 70%over saturated NaCl solution in an airtight desiccator. This range of water content covers the region between the total suction and matric suction calibration curves of the Whatman No. 42filter paper.

For both Methods 1 and 2, the suction measured by the initially wet filter paper was compared to the suction measured by an initially dry filter paper. In Method 1, only specimens compacted in the standard mould were used as suction sources for the filter paper while in Method 2, specimens compacted in the plastic mould were used.

Filter paper handling and soil specimen preparation

In all cases, the filter papers, were handled using a clean pair of tweezers with gloved hands to ensure no contamination of the filter papers (Bulut et al., 2001). Airtight containers, internal diameter of 85 mm and height of 70 mm, were used to contain the soil specimen for equilibration with the filter paper. Regardless of the type of mould used, soil specimens were carefully trimmed from the compacted samples such that they occupied at least 75% of the volume of the airtight containers. Trimming the plastic mould compacted samples was easier than trimming the standard mold compacted samples. The cylindrical specimens were sliced at mid-height and a contact filter paper was sandwiched between the two halved specimens (Figure 3.7a). The soil specimen was then wrapped in three layers of cling film leaving only the top surface exposed when placed into the airtight container (Figure 3.7b). A PVC ring (diameter 40 mm and thickness 5 mm) was placed on top of the soil specimen onto which a piece of non-contact filter paper was placed (Figure 3.7b). The airtight container was then sealed and kept in a Styrofoam box (Figure 3.7c) where the filter paper was left to equilibrate with the soil specimen for different durations ranging from 7 to 60 days.

Determination of soil suction from the filter paper water content

At the end of each duration, the contact and non-contact filter papers were retrieved and their water contents were determined (Bulut et al., 2001).Prior to removing a filter paper, the mass of

a clean ziplock plastic bag was determined on a sensitive electronic balance (of accuracy 0.00001g) as shown in Figure 3.8 (a) and was recorded as M_1.The ziplock bag was cleared of any trapped air on a clean flat surface. With the mass of the ziplock bag known, the filter paper was transferred as fast as possible (less than 5 second) into the ziplock bag. The weight of the ziplock bag and filter paper together was determined as shown in Figure 3.8 (c) and recorded as M_2. In all cases the filter paper was handled using a clean pair of tweezers. The ziplock bags were handled using gloved hands to ensure no sweat or dirt was added to the ziplock bag. For the case of the contact filter paper (sandwiched), the filter paper was quickly removed, cleared of any loose soil particles using a clear soft brush as shown in Figure 3.8 (b) and then transferred into the ziplock bag for weighing.

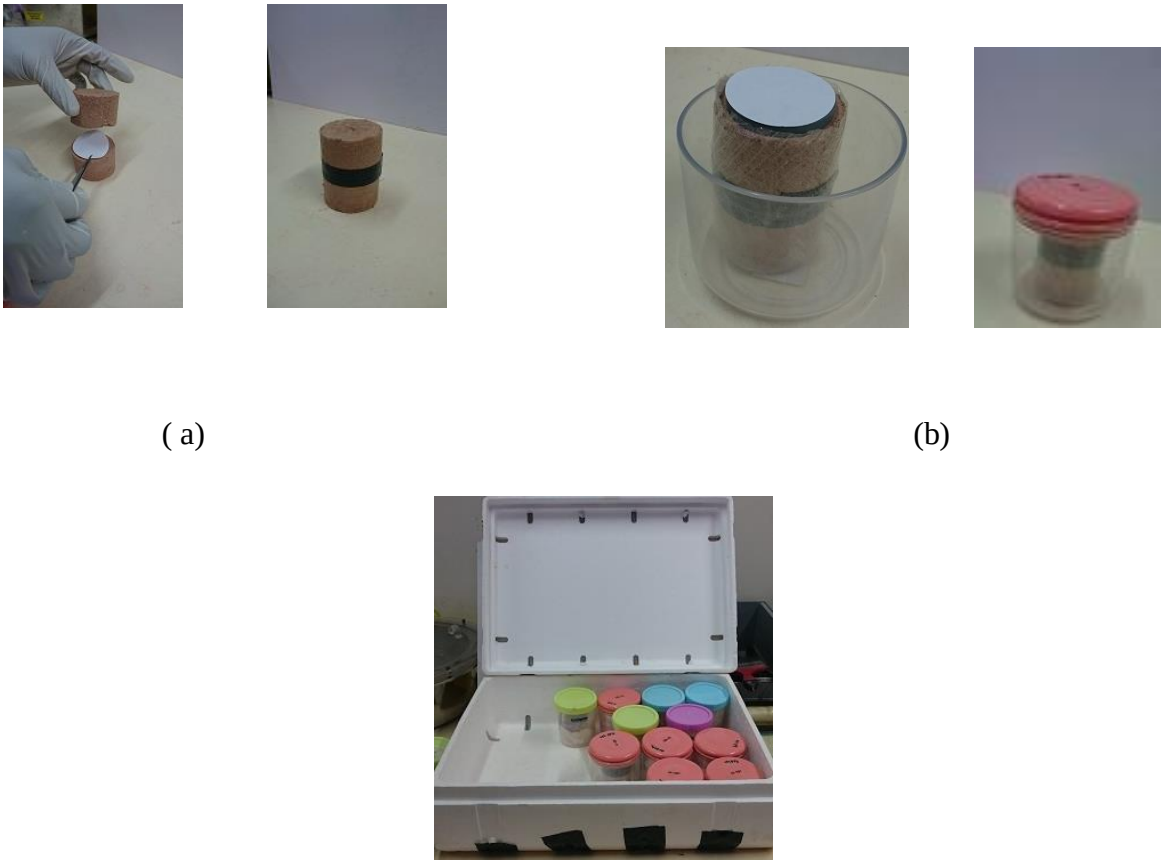

(a) (b)

(c)

Figure 3.7: Preparation of soil specimen for suction measurement using filter paper technique

The weighed filter paper was then transferred to a crucible (Figure 3.8d) and placed in the oven to dry (Figure 3.8e). In all cases, the label of the porcelain bowl was recorded against the soil specimen identity as well as the type of suction being tested (contact filter paper for matric and non-contact for total suction).In all cases, the crucibles were left half open while in the oven to allow the filter paper to dry.

(a)

(b)

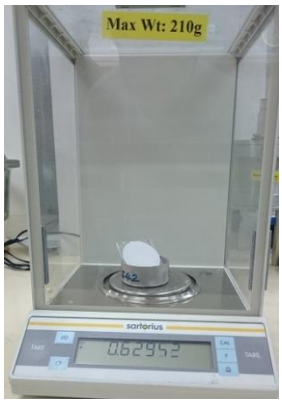

(c)

(d)

(e)

Figure 3.8: Filter paper handling post equilibration.

At the end of the drying, the cover of the crucible was then fully replaced and allowed to stay in the oven for about three minutes to allow for thermal equilibrium. The crucible containing the filter paper was then removed from the oven and placed in a desiccator to cool.

The filter paper was re-weighed. As before, the weight of the ziplock bag was determined on an electronic balance and recorded as M_3. The oven-dried filter paper was then transferred to the pre-weighed ziplock bag using tweezers and gloved hands and the weight of both the ziplock bag and filter paper was determined and recorded as M_4. In cases where ziplock bags were re-used, they were always re-weighed to re-establish their weights. Ziplock bags were never re-used if their weights between consecutive measurements differed by more than 0.00005g. For non-

contact filter papers, this was usually after three times of use while for contact filter papers, it was once or maximum twice, largely dependent on the level of contamination.

The filter paper water, w_f, content in all cases was computed as using Equation 3.3.

$$w_f = \frac{(M_2 - M_1) - (M_4 - M_3)}{M_4 - M_3} \times 100\% \quad (3.3)$$

With the filter paper water content obtained, soil suction was obtained using Whatman No.42 filter paper calibration equations by Leong et al. (2002b)given in Equations 3.4 and 3.5.

Matric suction

$$\begin{aligned} \log \psi &= 2.909 - 0.0229 w_f, \quad w_f \geq 47 \\ \log \psi &= 4.945 - 0.0673 w_f, \quad w_f < 47 \end{aligned} \quad (3.4)$$

Total suction

$$\begin{aligned} \log \psi &= 8.778 - 0.222 w_f, \quad w_f \geq 26 \\ \log \psi &= 5.31 - 0.0879 w_f, \quad w_f < 26 \end{aligned} \quad (3.5)$$

In addition the moisture content of the soil sample was also determined according to ASTM D2216-10 and hence the computed suction is matched with the soil moisture content.

3.4.2 Chilled mirror dew-point technique

In addition to using the filter papers, independent suction measurements were done on selected soil specimens using the chilled mirror dew-point (CMDP) technique following procedures suggested by Leong et al. (2003). Agus and Schanz (2005) evaluated four methods commonly used in the measurement of total suction and found the CMDP technique is the most reliable if used under a strict protocol. They suggest CMDP as a benchmark for assessing other techniques. The WP4C dew-point hygrometer from Decagon Devices set in precision mode was used. The device was switched on for at least 30 minutes prior to use to allow it to warm up and the sample cups were always ensured to be cleaned. Test specimens were trimmed from the larger compacted samples and placed in the sample cups. It was ensured that the quantity of the test

specimen does not exceed the marked-off height which is approximately mid-height of the testing cup. The specimens were immediately placed in the drawer of the chilled mirror device as shown in Figure 3.9 until equilibrium was achieved.

In order to reduce hysteretic effects often observed at low suction levels, time was allowed in between measurements especially for those specimens with large suction differences. At each compaction water content, at least three suction readings were taken. As expected, there was a close agreement in readings for the high suction compared to lower suction.

For verification, the calibration of the WP4C was regularly checked using concentrated solutions of both sodium chloride and potassium sulfate to ensure that it gave the correct suction reading. The WP4C is able to provide the suction of the soil directly. Under the precision mode, equilibrium was attained in about 10 to 15 minutes for each soil specimen with the longer equilibrium duration at low suction levels.

Figure 3.9: Mounting a test specimen with the chilled mirror hygrometer

3.5 Soil-water characteristics curves

The soil water characteristic curves of the test specimens were established using both the pressure plate extractor and the chilled-mirror dew-point apparatus. Methods C and D specified in ASTM D6836-16 were followed. For suctions up to and including 1000kPa, a pressure plate apparatus with a 15-bar HAEV ceramic plate cell was used. For suctions higher than 1000kPa, the chilled-mirror dew-point technique was used.

3.5.1 Pressure plate tests

The pressure plate system consists of a pressure chamber which contains a saturated HAEV ceramic disk. Beneath the ceramic disk is attached a neoprene rubber sheet which provides a hydraulic continuity between the saturated ceramic disk and a water burette outside the air-pressure chamber (Leong and Rahardjo, 2002) as shown in Figure 3.10.

The test specimens for the SWCC test using pressure plate were pre-saturated. The specimens compacted in the plastic mould were saturated following the procedure suggested by Samingan (2001). In this procedure, the compacted specimens were allowed to absorb water freely with close monitoring of their masses to ensure saturation. In order to limit lateral swell the samples were wrapped in four layers of plastic film. Whatman No. 54 filter papers were placed on both the top and bottom of the specimens to protect the specimens from erosion by the water. The specimens were then placed on wetted cotton wool in a plastic box. The specimens absorbed water from the wetted cotton wool. At the end of the saturation, the saturated samples were trimmed to obtain the test specimens. For the pressure plate test, cylindrical specimens of 50 mm diameter and 30 mm height were used.

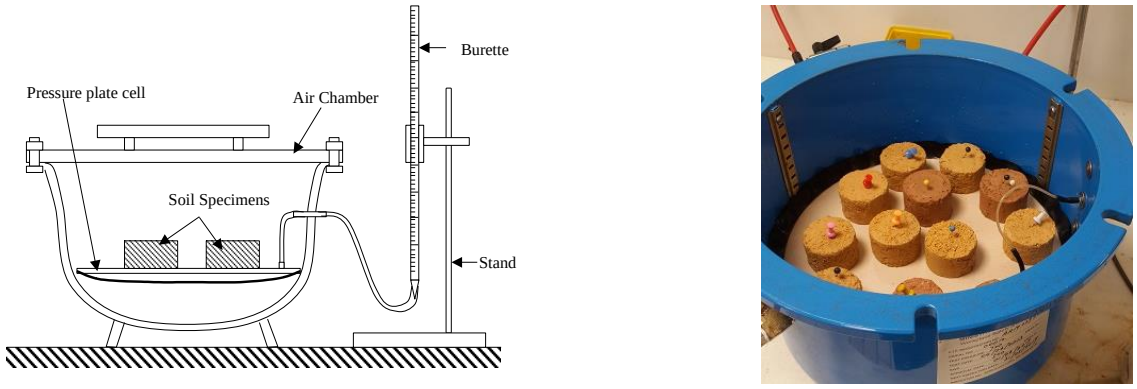

(a) Schematic b) Picture

Figure 3.10: Pressure plate system

For the specimens compacted in the standard mould, the specimens for SWCC test were those obtained from the flexible wall permeameter test as will be discussed later.

The dimensions and weight of saturated soil specimens were determined and then placed onto the saturated ceramic disk. The test suction levels in the pressure plate were increased incrementally from 10 to 1000kPa in pressure steps as recommended in ASTM D6836-16. The weights of the soil specimens were monitored daily. Equilibrium at a given suction level was attained when there was negligible change in the weight of the specimen. At equilibrium, the dimensions of the specimen were noted as well. Suction level was then increased to the next suction by adjustment of the air pressure. Finally, the water content of the soil specimen at equilibrium with each matric suction level was established in order to construct its SWCC.

3.5.2 Chilled mirror dew-point test

For suctions higher than 1000kPa, the chilled-mirror dew-point technique following Leong et al. (2003) was used. For this test, a cylindrical disk specimen of diameter 35mm and thickness 5mm was cookie-cut from the sample at the end of the saturation process using a PVC ring with a sharpened edge and placed in sample cups used for the chilled-mirror dew-point test.

These samples were dried in air-tight desiccators with saturated sodium chloride solution at the base of the desiccators. The room temperature varied between 24 and 26^{o}C, hence the relative humidity generated in the air-tight desiccators was expected to be approximately 76% (Young, 1967). The weights of the sample cups with the soil were monitored periodically as the soil dries. At the same time, the soil's suction was measured using the WP4C dewpoint hygrometer set in the precision mode. The drying continued until no further change in weight could be observed meaning the soil had reached equilibrium with the saturated salt solution. The sample cups with

the soil were then transferred to the open environment of the laboratory to allow for further drying until no further weight change could be recorded, each time measuring the suction of the test specimen using the WP4C.

As mentioned earlier, the WP4C measures the suction directly the Kelvin equation re-stated as Equation 3.6.

$$\psi = -\frac{RT}{v_{w0}\omega_v}\ln(R_h) \tag{3.6}$$

where ψ = total suction (kPa), R = universal gas constant (8.314232 J/mol K), T = absolute temperature (K), v_{w0} = specific volume of water, ω_v = molecular mass of water vapour (18.016 kg/kmol) and R_h = relative humidity.

Similar to the pressure plate test, the specimen's water contents at equilibrium with the measured suctions were established and combined with those from the pressure plate test to obtain a complete SWCC for each soil specimen.

3.6 Hydraulic properties of compacted soils

Two sets of experiments were performed in order to study the hydraulic properties of compacted soils, infiltration test using a mini-disk infiltrometer and measurement of saturated permeability using the flexible wall permeameter (FWP).

3.6.1 Infiltration test using a mini-disk infiltrometer

The mini-disk infiltrometer used in this study (Decagon Devices, 2014) can be adjusted from -0.5 to -7cm of pressure head**.** In this study, the infiltration tests were done on compacted soils in the laboratory by placing the infiltrometer on top of the compacted soil as extruded from the

ASTM standard compaction mould. Only samples compacted in the ASTM standard compaction mould were used for these tests.

Prior to extruding the compacted soil sample from the mould, the surface was leveled and scarified; leveled to ensure that the infiltrometer sits on a flat surface and scarified to ensure intimate contact between the infiltrometer disk and the soil water. Figure 3.11 shows the set up in the laboratory. The infiltrometer was supported in position using a retort stand as shown in Figure 3.11.

Figure 3.11: Infiltration test using a mini-disk infiltrometer

In order to preserve the soil moisture during the infiltration, the compacted soil was wrapped in three layers of plastic cling film and finally with two layers of aluminum foil. Aluminum foil is not included in Figure 3.11 in order to show the test specimen. The test specimens studied are discussed in Chapter 5. Infiltration studies were done at three suction heads,1, 2 and 5cm. For each suction head, a fresh sample was used. Therefore, for each selected compaction water

content, three specimens were compacted ensuring that they are identical in terms of water content and dry density. The water content variation was controlled to be within ±0.2%. Only specimens meeting these criteria were used for the tests.

3.6.2 Falling head flexible-wall permeameter

At the end of the infiltration test, one of the three specimens for each compaction water content was trimmed to obtain a specimen of diameter 50mm and height 40 mm. The soil specimen was then transferred into a flexible-wall permeameter and a falling-head test was conducted with water flow upwards from the base of the soil specimen. This ensured that the air in the soil voids was flushed out by upward displacement since air is less dense than water. Figure 3.12 shows the experimental set up.

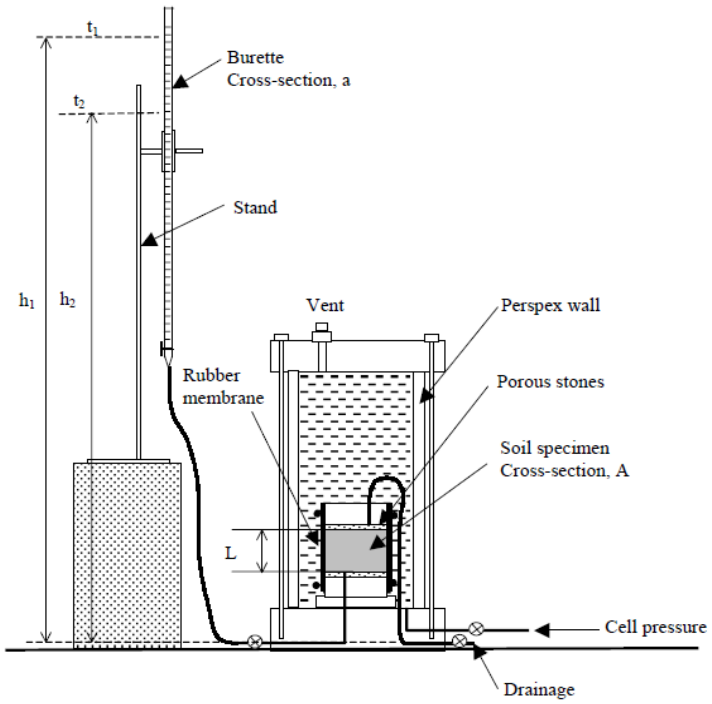

Schematic (after Samingan, 2001)

Figure 3.12: Flexible wall permeameter set up

In the permeameter, a de-aired porous stone was placed on the base pedestal, on top of which a filter paper (Whatman No.54) dipped in water (the permeant liquid) was placed. The soil specimen was placed on the filter paper. Similarly, another filter paper was placed on top of the soil specimen followed by another de-aired porous stone. A top cap (with drainage lines initially disconnected) was placed on to the top porous stone.

After placement of the top cap, a latex membrane was placed on to the soil specimen using a membrane stretcher. During placement of the membrane, it was ensured that the membrane extended from the bottom of the base pedestal to the top cap. The membrane was held in place by two O-rings; one placed on the base pedestal and the other on to the top cap. It was important that the membrane was firmly stretched so that no water flow occurs between the sides of the specimen and the membrane which would lead to an over estimation of the permeability. Any length of the membrane that extends above the top cap was rolled off and drainage lines connected to the top cap.

The cell wall was then replaced and the cell was filled with water. A nominal confining pressure of 10kPa was applied to support the specimen. Finally, the base of the specimen was connected to water line supplied from a burette as shown in Figure 3.12.

The water levels on the graduated burette were monitored at regular time intervals. For each specimen, several runs of the test were done. For each run, the burette was re-filled and hydraulic head drops, h, was monitored with time. This continued until a steady state was attained. Steady state was evaluated using Equation 3.7.

$$\log h = \log h_0 - \frac{Akt}{2.303aL} \qquad (3.7)$$

where h is the hydraulic head at time t while h_0 is the original hydraulic head (t=0). All hydraulic heads were referred to the tail water set at the base of the specimen.

Equation 3.7 is linear with a negative slope = $\frac{Ak}{2.303aL}$. With several runs done, a constant k_s was assumed to have been attained as the slopes of Equation 3.7 for the consecutive runs became very close or a constant value.

The saturated permeability, k_s, was obtained from the steady state slope, m_{st} as shown in Equation 3.8

$$k_s = \frac{2.303aL * m_{st}}{A} \tag{3.8}$$

For all the tests, the filter papers were cut to a diameter of 50mm which was equal to the diameter of the test specimen. The use of the filter papers was to ensure that the porous stones were not clogged by soil particles during the test. Prior to the test, the porous stones were soaked in water and placed in a vacuum desiccator for 24 hours to ensure they were de-aired. De-airing the porous stones ensured the stones were fully saturated.

3.7 Strength tests

Four strength tests were done on the compacted soils. Three were done on the as-compacted soil specimens and one test was done on the saturated test specimens in order to obtain the saturated shear strength parameters, the friction angle and the cohesion. Only specimens compacted in the plastic mould were tested for strength. The strength tests used in this study are described below.

3.7.1 Unconfined compression test

Given that the unsaturated soils often occur at shallow depths from the surface with very small confinement, unconfined compressive (UC) strength is useful in studying shear strength behavior of soils. Two series of experiments were conducted for the UC test. The first series involved the as-compacted soils at various water contents on both the standard and modified Proctor curves. The water contents selected for each soil are detailed in Chapter 6. In the first test series, the compacted soils were sheared immediately after compaction to obtain the as-compacted unconfined compressive strength.

The second test series was done on BT1, BT2 and JF2 as described in Chapter 6. This series of experiments involved soils compacted at wet of optimum on both the standard and modified Proctor curves. The test specimens were then dried in desiccators with saturated sodium chloride (NaCl) solution at the base of the desiccators. The saturated NaCl solution provides a constant relative humidity of about 76% (Young, 1967) to dry the test specimens. The test specimens were laid lengthwise over the saturated NaCl solution to minimize moisture gradients that may develop if placed upright and hence ensure more uniform drying of the test specimens. The weights of the specimens were monitored regularly. Specimens that attained the targeted weight (and hence moisture content) were wrapped in cling film and thereafter kept in a temperature-controlled humidity chamber to allow for moisture equalization in the test sample for about 10 days as recommended by Mendes (2011). The specimens were then sheared according to ASTM D2166-16 to obtain the unconfined compressive strength q_u. Prior to shearing, the dimensions of the specimens were measured for density, shear strength and volumetric shrinkage computations. After shearing, the moisture content of the test specimen were determined. It should be noted that all the UC tests were performed at atmospheric pressure i.e. $u_a=0$

Assuming $\sigma_x = \sigma_z = 0$, the unconfined compressive strength, σ_y was computed using Equation 3.9

$$\sigma_y = \frac{P}{A} \tag{3.9}$$

where P = peak load, and A= cross sectional area of the specimen.

3.7.2 Brazilian tensile strength test

Similar to the UCS test, the Brazilian tensile strength (BTS) test was also done in two test series. Similar moisture contents and densities as used for the UCS tests were used. To obtain BTS test specimens, samples compacted in the plastic mold were sawn using BuehlerIsoMet™ 4000 precision saw into cylindrical disk specimens of 30mm thick and 52mm diameter. Although the precision saw can minimize sample deformation and have low kerf loss, the compacted samples were wrapped in two layers of cling film followed by a single layer of masking tape along the sample height to prevent moisture loss and to limit surface cracking during sawing. Figure 3.13 shows a sample prepared for sawing. Three specimens were obtained from each compacted sample. The ASTM D3967-16 which is for rock core specimens was used as a guide for the BTS test. The thickness to diameter (t/d) ratio of the test specimens was maintained as close to 0.6as possible, within the recommended range of 0.2 to 0.75 in ASTM D3967-16.The test specimens for the BTS were loaded using two specially fabricated curved bearing blocks as recommended in ASTM D3967-16 to reduce contact stresses on the specimens during the test. The radii of contact arc with the test specimen was 10^o while the width of contact with the specimen was 30mm. During testing, the bearing blocks were attached to the loading platens of the UCS testing machines using magnets embedded into the base of the bearing block as shown in Figure 3.14.

Figure 3.13: Compacted sample prepared for sawing to obtain BTS test specimens

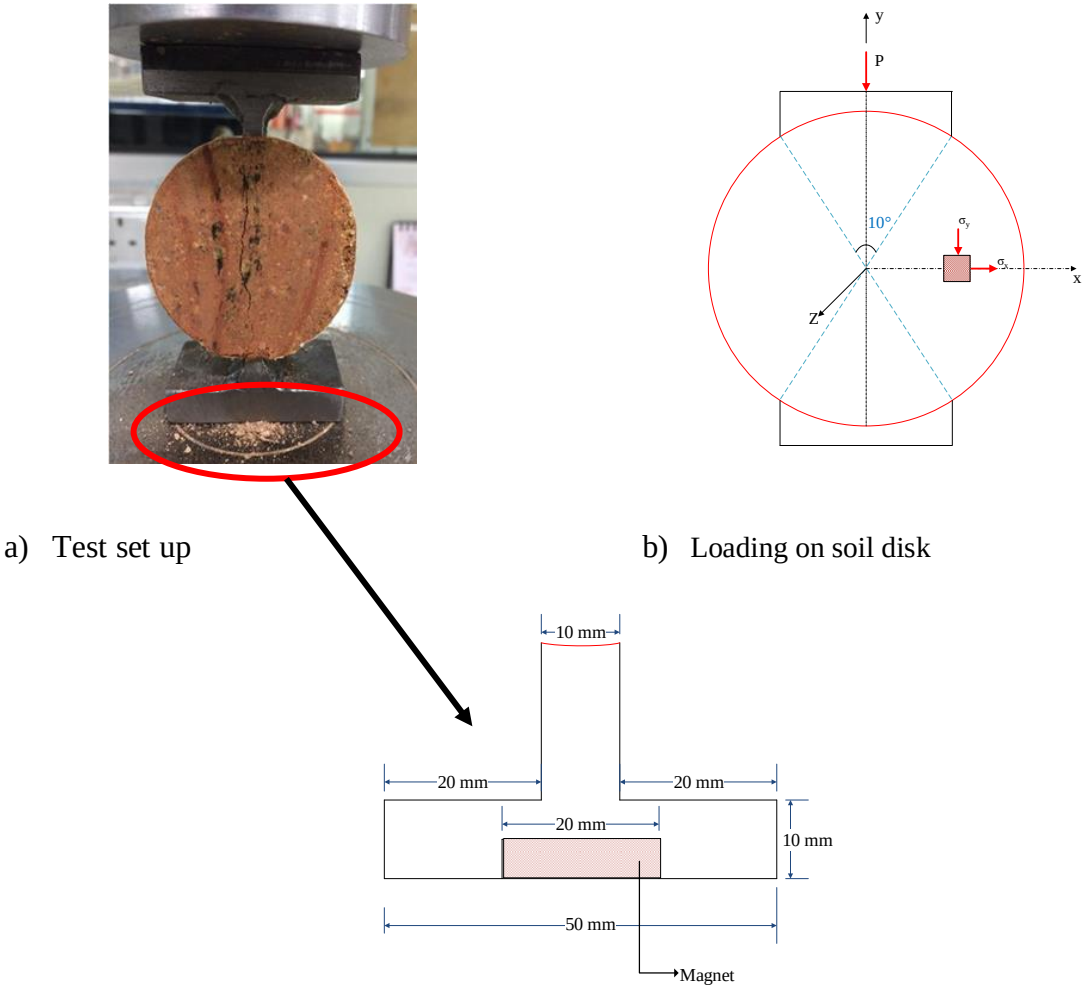

a) Test set up

b) Loading on soil disk

c) Curved bearing block

Figure 3.14: Test set-up and curved block for Brazilian tensile test

The BTS test was conducted at a loading rate of 0.5mm/min as recommended by Akin and Likos (2017) and all test specimens failed within 1 to 10 minutes (ASTM D3967-16).Assuming plane stress state at the centre of the BTS specimen, a closed-form elastic solution for the stress state in a BTS specimen at failure (Frydman, 1964, Akin and Likos, 2017) is given by Equations (3.10)

$$\sigma_x = \sigma_t = -\frac{2P}{\pi td} \tag{3.10a}$$

$$\sigma_y = -3.1\sigma_x = -\frac{6.2P}{\pi td} \tag{3.10b}$$

$$\sigma_z = 0 \tag{3.10c}$$

where P= peak compressive load at failure, d = average diameter of the soil specimen, t = average thickness of the specimen, σ_x = the tensile strength of the specimen, and σ_y, σ_z are normal stresses in the y and z directions, respectively.

3.7.3 Unconsolidated undrained test

The Unconsolidated undrained (UU) test was performed only on the as –compacted soil samples (test series 1). The test was done in accordance to ASTM D2850-15. Unlike the unconfined compression test described above, in this test soil specimens were subjected to a confining pressure. Three confining pressures were used 70kPa, 150kPa, 300, and 600kPa, elected with an aim to cover a wide range of confinement and hence investigate the soil response over the range. The UU test was conducted with air phase drained at atmospheric pressure and water phase undrained hence the test was a constant water (CW) test. Allowing for air drainage but not water drainage means the sample volume changes which simulates typical construction practices in which compacted layers are usually loaded fast enough not allowing water drainage however air will drain. The shearing was done at a rate of 1.57mm/min. The test was stopped when either a distinct shear plane was observable or substantial vertical deformation had been observed for wet

samples or at high confinement pressures. The extent of deformation allowed was also governed by the load ring capacity.

At the end of the test, the soil specimen was removed from the chamber and its moisture content determined in accordance with ASTM D2216-10.Data processing followed ASTM D2850-15 with membrane corrections performed as well as the area corrections.

3.7.4 Consolidated undrained test for saturated soils

In order to obtain the effective strength parameters i.e. φ' and c', consolidated undrained (CU) tests with pore-water pressure measurements were performed on the as-compacted soil specimens. The CU tests were performed in accordance to ASTM D4767-11. Because of the time duration required for saturation and also due to the high variability of dynamically compacted soils, the CU test was performed using the multistage technique closely following recommendations of Head (1998). According to Head (1998), the multistage testing is suitable for soils with low sensitivity, stable structure and those that fail at low strain levels all of which are largely satisfied by the soil specimens in this study.

Saturation of the soil specimens was done by applying back pressure and cell pressure while measuring the pore-water pressures developing in the samples in order to calculate Skempton B-parameter. In order to hasten the saturation, the samples were pre-saturated in a desiccator with application of a very small vacuum to ensure as much air as possible is displaced from the soil sample before being set up in the triaxial system. In addition, the porous stones were de-aired in a vacuum desiccator to ensure they were saturated. Drainage lines of the triaxial system were flushed by applying a water pressure of about 50kPa to eliminate all the entrapped air.

The samples were again saturated in the triaxial cell and considered to be saturated when the B-parameter was at least 0.96 (Head 1998). Multistage testing was done in three stages at effective confining pressures: 80, 150 and 300kPa, respectively. At each stage, the specimens were consolidated at the effective confining pressure before shearing. Volume of water expelled from the specimens during consolidation was noted using a burette and used in volume, area and length corrections at each stage. ASTM D4767-11 suggests a procedure for computing a shearing rate using consolidation data of the specimen. After doing some trials on a couple of test specimens, a shearing rate of 0.01mm/min was adopted. The same shearing rate was used for all the stages of the multistage technique. For the first and second stages, it was ensured that the axial strain never exceeded 6 and 2%, respectively, after which the sample was unloaded very fast. In the third stage, the specimen was sheared to failure. Failure was considered to have occurred when deviator stress began dropping. For samples that had no definite failure, deviator stress at 20% was considered as failure load.

The data processing followed ASTM D4767-11 as well as Head (1998). All appropriate area and membrane corrections were done.

Chapter 4. Soil Suction measurements and Soil-Water Characteristic Curves

4.1 Introduction

Suction measurement is important in evaluating and understanding the engineering behavior of unsaturated soils. This chapter presents and discusses experimental results from suction measurements made on the as-compacted soils as well SWCCs of the compacted soils. The main technique for suction measurement is the filter paper (FP) technique. More suction measurements were made using the chilled mirror dew-point (CMDP) technique for the purpose of comparison as recommended by Agus and Schanz (2005).The soil-water characteristic curve (SWCC) as discussed in Chapter 2 is key to the implementation of unsaturated soil mechanics. The SWCC shows the variation of soil water content with suction for a given soil. Because different compaction water contents result in different soil structures and hence different soils, influences of compaction on SWCCs are studied. Finally, a comparison between suction measurements derived from the SWCC and those obtained from suction measurements with the FP is made.

4.2 Suction measurements using the filter paper method

Suction measurement methods still face several challenges such as cost, measurement range, equilibrium time and reliability. Among the indirect suction measurement methods, the filter paper method offers many advantages as discussed in Chapter 2. However, despite its advantages, the filter paper technique has several shortcomings such as inherent variability, low sensitivity at low suctions, long equilibrium time, and reliability of results.

In this thesis, an attempt is made to study the following aspects:

1. Equilibration time of the filter paper
2. Influence of initial moisture state of the filter paper on the suction measurement
3. Hysteresis of the filter paper
4. Suction measurements- matric and total suction
5. Inherent variability of the filter paper.

As already emphasized earlier, the suction measurements were done on the as-compacted soils. Specimens compacted using the standard ASTM mould and the plastic mould were used for suction measurement. Figure 4.1 shows the moisture-density relationships for the soils.

It should be noted from Figure 4.1 that only BT1, BT2 and JF2 soils were largely used in the study of suction measurements. Only few measurements were made on JF1 soil whose results will be used in Chapter 7. Also notable in Figure 4.1 is the comparison between specimens compacted in the standard ASTM mould and those compacted in the plastic mould. The dry densities attained using the plastic mould for BT2 and JF2 soils and some points for BT1soil are lower than those attained using the standard mold. This was largely due to greater side-wall friction in the plastic mould.

4.2.1 Equilibration time for filter papers

The effect of equilibration time on filter paper water content was done for both the initially dry and initially wet filter papers in contact and non-contact with BT1 and JF2 soil specimens compacted using the standard and modified Proctor efforts. Figures 4.2 and 4.3 show the comparison for BT1 soil specimens while Figures 4.4 and 4.5 show the equivalent plots for JF2 soil specimens.

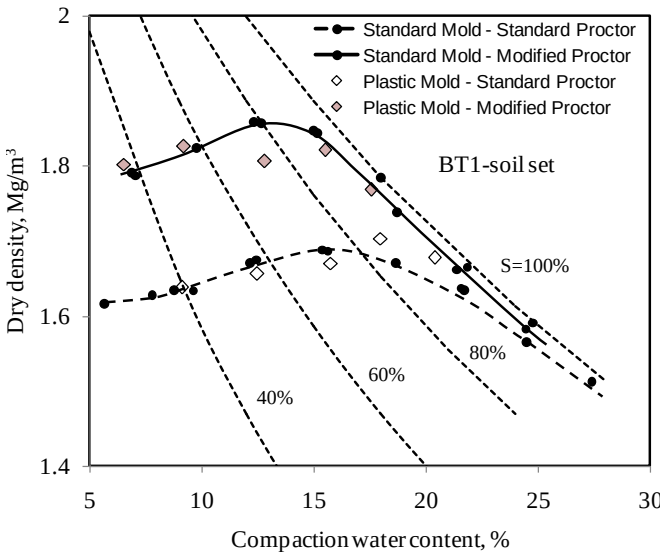

(a) BT1

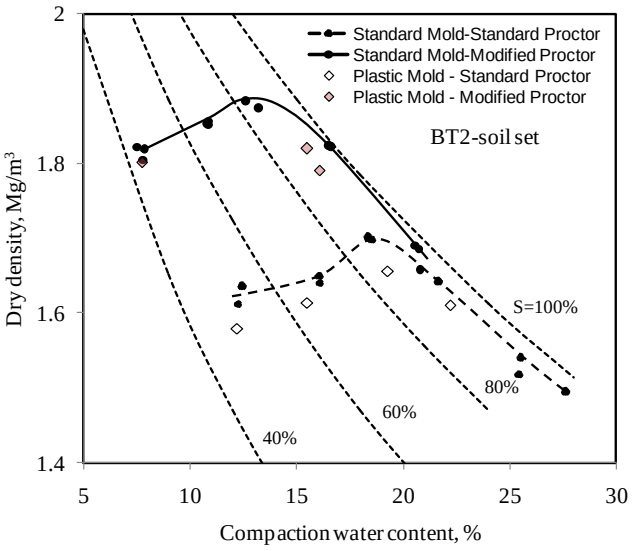

(b) BT2

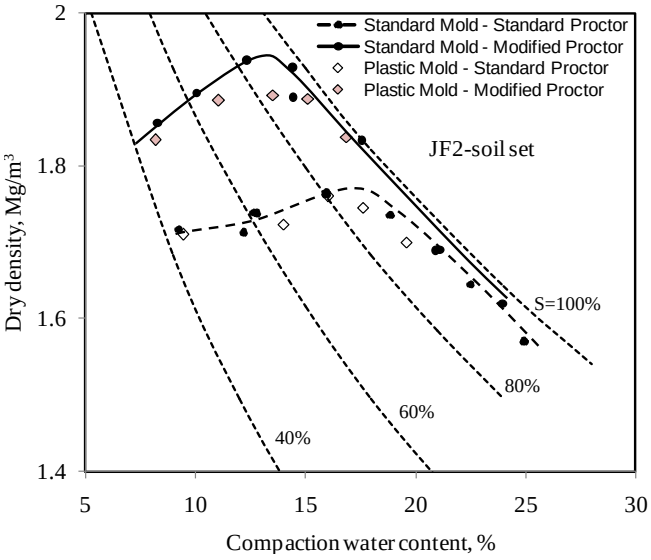

(c) JF2

Figure 4.1: Moisture-density relationships for the study materials used in suction measurements

In Figures 4.2 to 4.5, the equilibration time was from 7 to 28 days and the initially wet filter papers were prepared using Method 1 as described in Chapter 3. Figures 4.2 to 4.5 show that the equilibrium water content of the filter papers increases as the water content of the compacted soils increases from dry of optimum to wet of optimum. Figures 4.2 to 4.5 generally show that

the initially dry filter papers exhibit less scatter than the initially wet filter papers for both the contact and non-contact methods. For soil samples compacted at optimum and dry of optimum water contents, an equilibration time of 7days seems adequate for initially dry filter papers regardless of contact condition. This suggests that it is easier for an initially dry filter paper to wet rather than for an initially wet filter paper to dry. In addition, the higher the suction, the lower the equilibration time required by the filter paper, confirming the observation of Marinho and Oliveira (2006).

For soil specimens compacted on the wet side of optimum, the scatter in the filter paper water contents for both the initially dry and initially wet filter papers increase with increasing compaction water content. The non-contact filter papers sometimes failed to show equilibrium indicating that the filter paper failed to give any reliable suction measurements at such water contents. The initially wet filter paper shows less scatter when used in contact mode compared to when used in non-contact mode.

The results of the second series of compacted soil specimens (compacted in plastic mould) are shown in Appendix A1. The equilibration time used in the second series of compacted soil specimens ranges from 7 to 60 days and the initially wet filter papers were prepared using Method 2 as described in Chapter 3. Less scatter was observed for the initially wet filter paper indicating that the fluctuations are due to the preparation of the initially wet filter paper using Method 1. As a further check, 12 filter papers randomly picked from the same box of Whatman No. 42 filter papers were soaked in distilled water for 1 hour and thereafter allowed to dry in an airtight desiccator over a saturated NaCl solution. Their weights were taken at 4, 8 and 24 hours, after which the water content of the filter papers were determined. Figure 4.6 shows the drying pattern of the filter papers. Although the water contents of the filter papers seem to converge at

24 hours, the scatter in the water contents between 0 and 8 hours reveals wide differences in drying behavior. These differences in drying of the individual filter papers may partly explain the scatter observed with the initially wet filter paper prepared using Method 1 especially when used in the non-contact mode. Generally, the initially wet filter paper requires stricter control of its initial moisture content and selection of equilibration time especially when used in non-contact mode to measure total suction.

Leong et al. (2002b) note that equilibration for the non-contact filter paper method is a two-stage process; first, equilibration between the soil and the environment (air-space), and second, the equilibration between the environment and the filter paper. Therefore, the initially wet filter paper is expected to undergo either wetting or drying depending on the suction it is measuring. In addition, it is expected that initially wet filter paper having water content corresponding to the suction of the soil would equilibrate faster. Hence, the initially wet filter paper when measuring the low suction of soils compacted wet of optimum is expected to achieve equilibrium much quicker especially for total suction compared to initially dry filter paper. However, the experimental results do not show this benefit.

The performance of the initially wet filter paper seems to be affected by factors not observed in initially dry filter papers. When the size of the air space above the soil in the container is large, it may expectedly lead to longer equilibration time and when it is too small, the initially wet filter paper may fail to achieve equilibrium moisture with the air space. Another possible factor affecting the initially wet filter paper is the possible modification of the filter paper structure when wetted thus altering its surface adsorption properties and introducing more variability in the filter paper.

4.2.2 Initial moisture condition of filter paper

As stated in Chapter 3, the most commonly used filter paper method is to use initially dry filter paper directly from its box. ASTM D5298-16 recommends oven drying the filter papers before use to ensure zero initial moisture content. Although this may eliminate variability in the initial water content, it may alter the filter paper characteristics and hence affect its other properties such as absorption as noted by Marinho and Oliveira (2006). To avoid contamination and possible attack by microorganisms, ASTM D5298-16 further recommends the filter paper to be sandwiched between two other filter papers to measure the matric suction of the soil and to use two filter papers for the total suction. However, using more than one piece of filter paper may require longer equilibrium time and may result in measuring higher suction especially when used to measure suctions of drier soil specimens (Leong et al., 2002b).

Marinho and Oliveira (2006)'s suggestion to use a single calibration curve for the filter paper is problematic for non-contact filter paper in the low suction range. Marinho and da Silva Gomes (2011) found that suction measurement and equilibration time using the filter paper are influenced by particle size distribution of the soil, rugosity of the soil, hydraulic properties of the soil, moisture content of the soil and the contact level between soil and filter paper. The smaller the level of contact, the longer the required equilibration time. Hence, equilibrium may never be achieved within a practical time frame for the non-contact filter paper.

Figure 4.7 shows the comparison of the 28-days ID-C-FP and ID-NC-FP water contents for compacted BT1,BT2 and JF2 soils while Figure 4.8 shows the comparison of the 28-days IW-C-FP and IW-NC-FP water contents for compacted BT1, BT2 and JF2 soils.

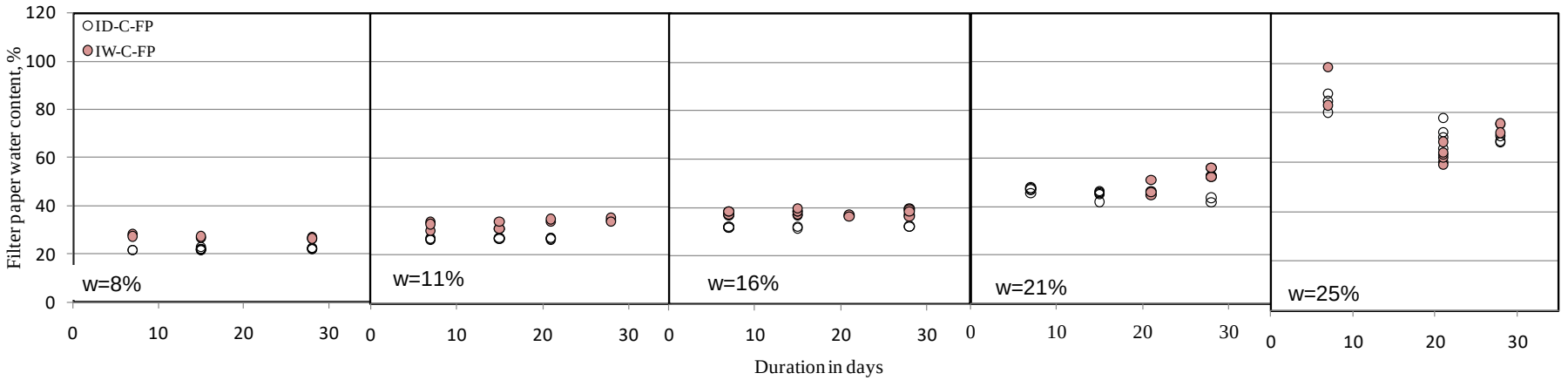

a) Contact Filter paper

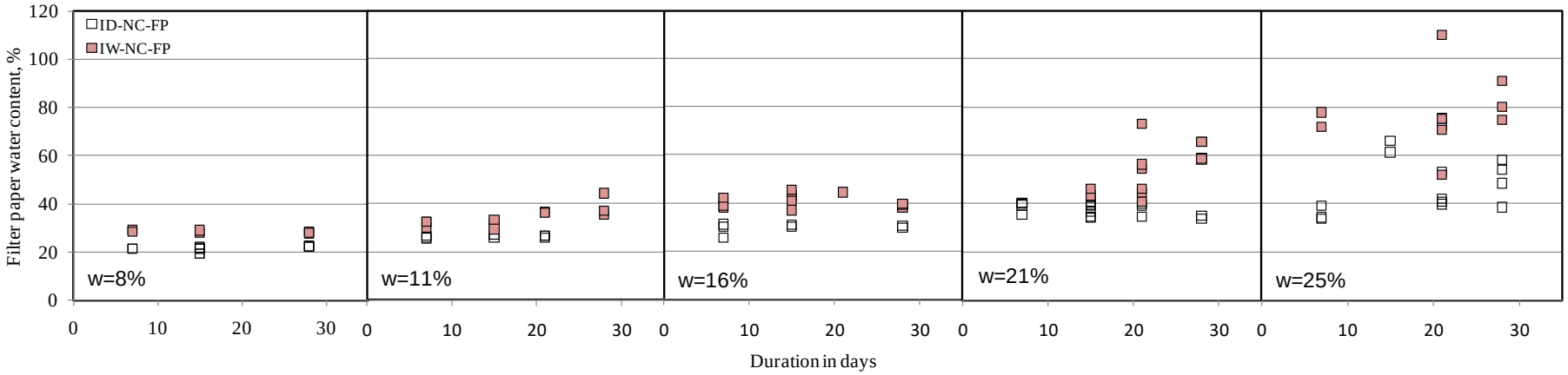

b) Non-contact Filter paper

Figure 4.2: Effect of equilibrium time on filter paper water content for standard Proctor compacted BT1 soils- Standard mold and Method 1

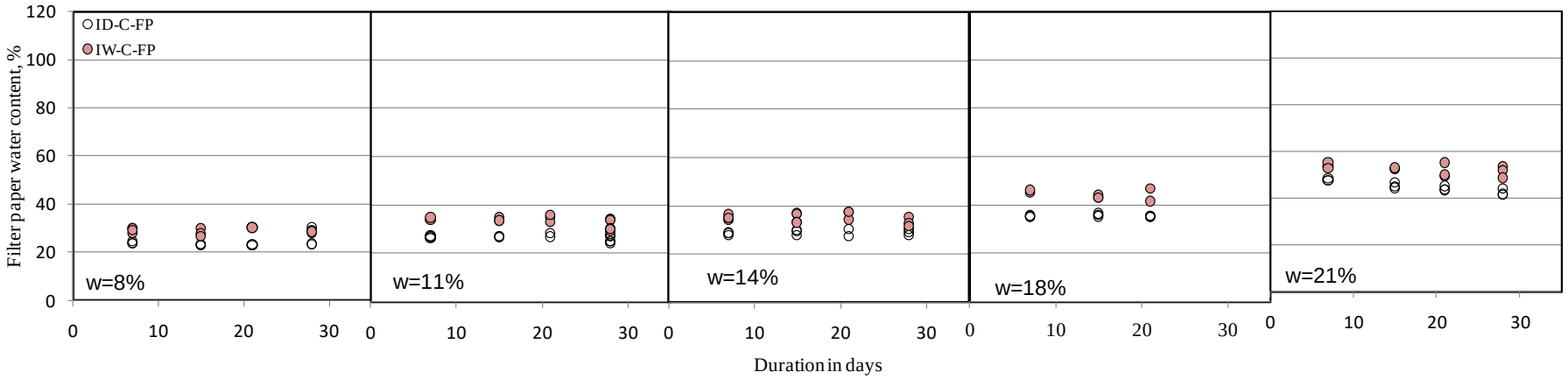

a) Contact Filter paper

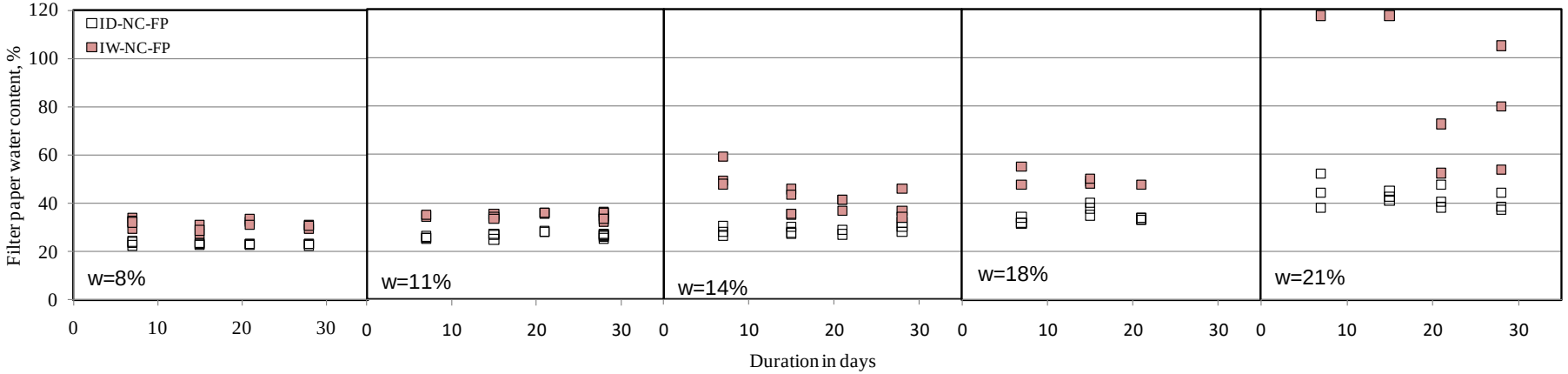

b) Non-contact Filter paper

Figure 4.3: Effect of equilibrium time on filter paper water content for modified Proctor compacted BT1 soils- Standard mold and Method 1

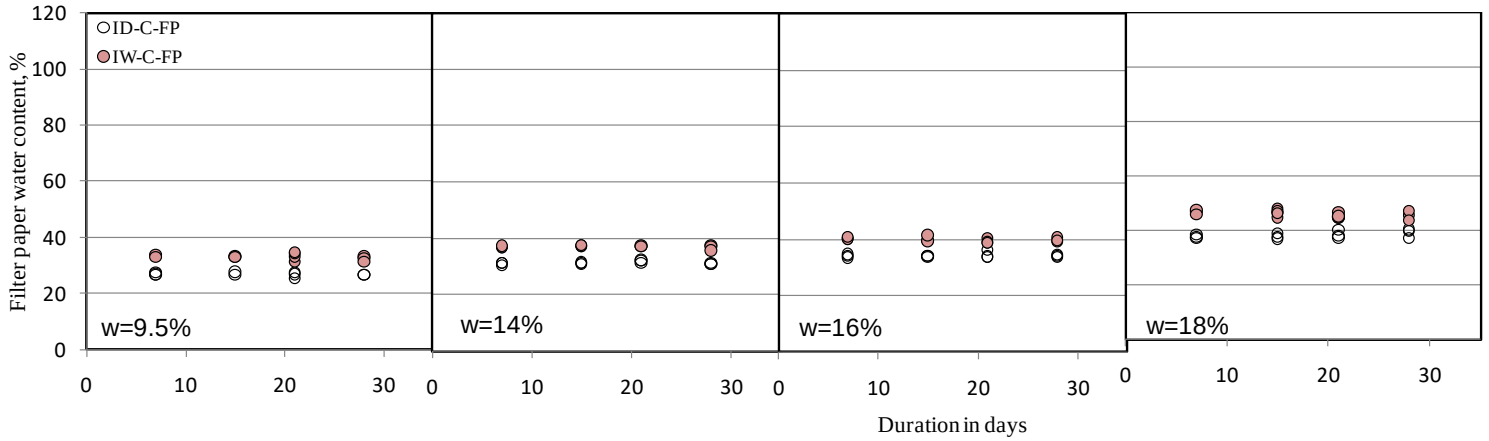

a) Contact Filter paper

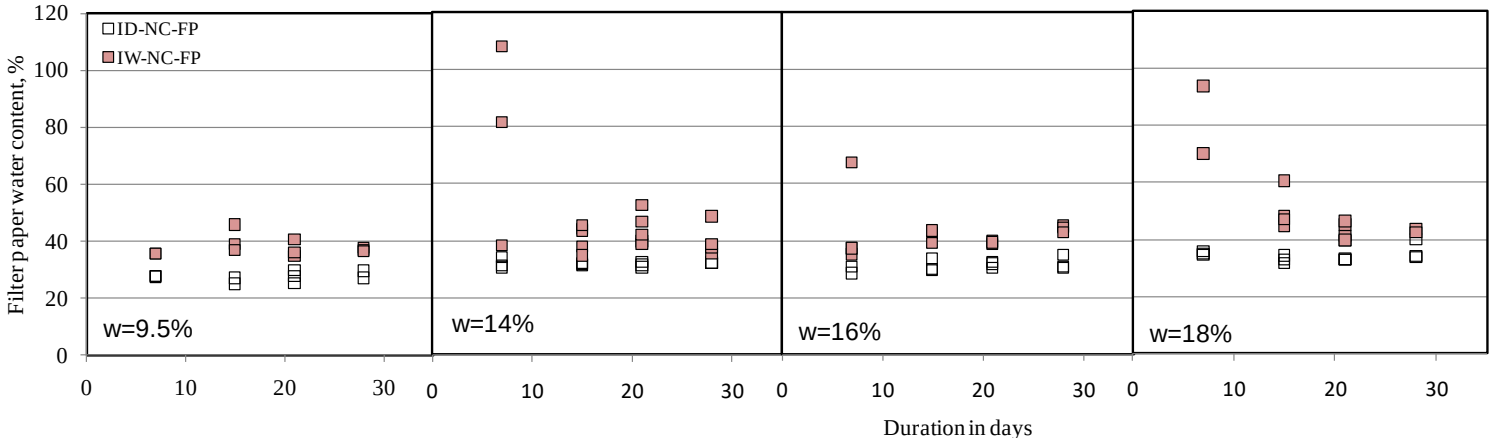

b) Non-contact Filter paper

Figure 4.4: Effect of equilibrium time on filter paper water content for standard Proctor compacted JF2 soils- Standard mold and Method 1

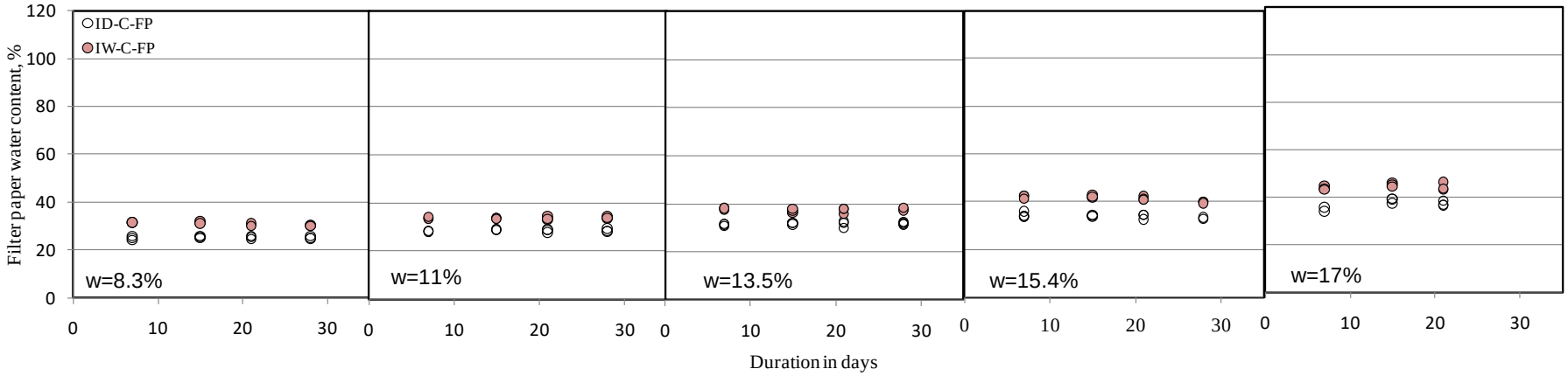

a) Contact Filter paper

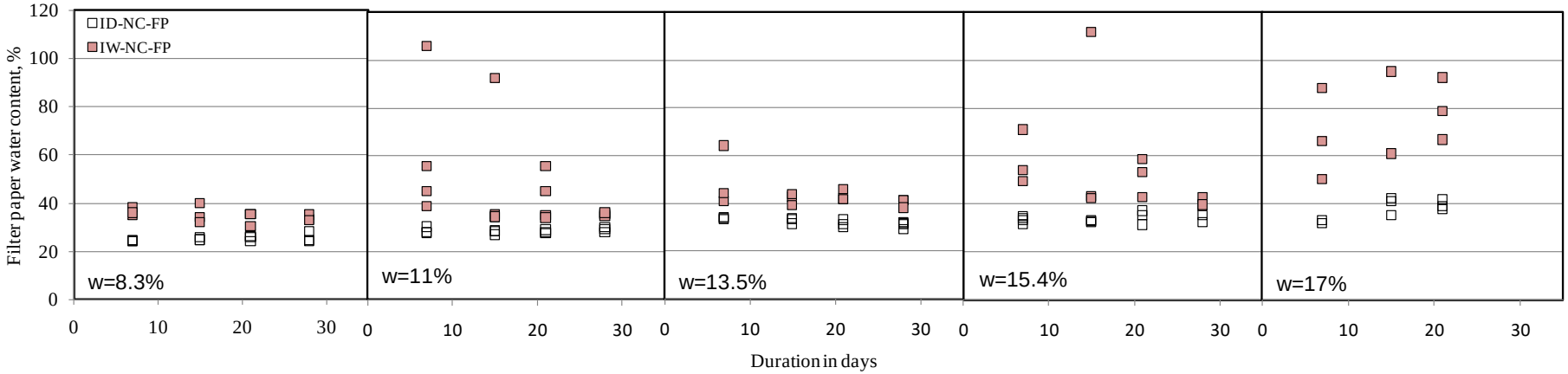

b) Non-contact Filter paper

Figure 4.5: Effect of equilibrium time on filter paper water content for modified Proctor compacted JF2 soils- Standard mold and Method 1

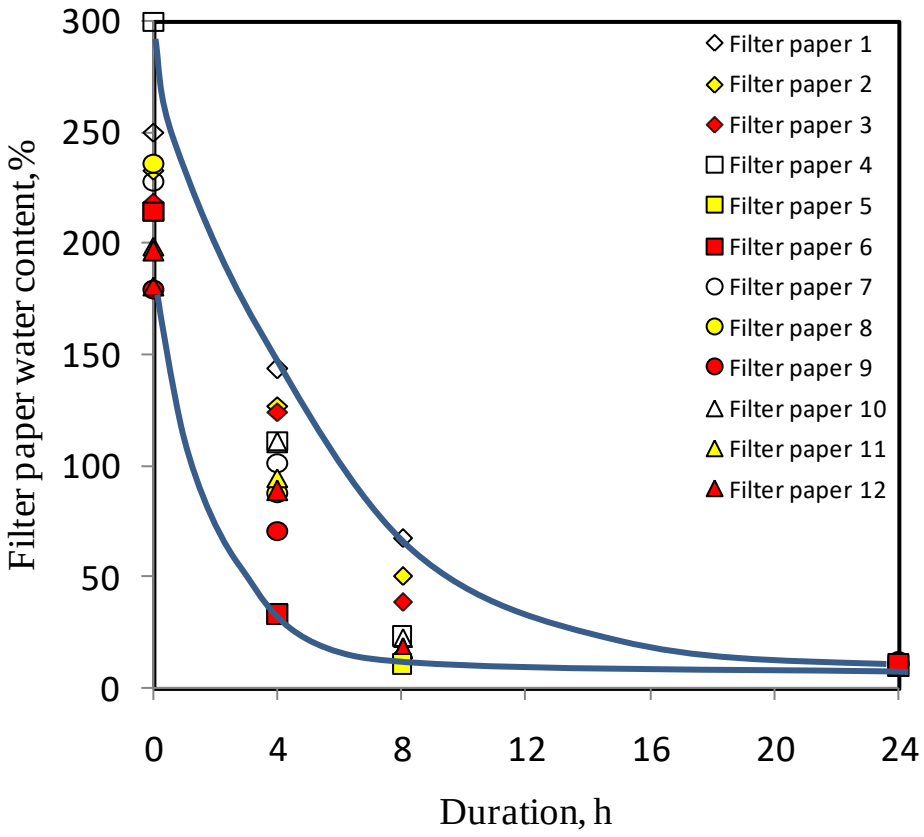

Figure 4.6: Drying pattern of 12 initially wet filter papers

Better agreement of contact and non- contact filter paper water contents is observed for the initially dry filter papers compared to initially wet filter papers. Deviations between the contact and non-contact filter papers' water contents occur when the water contents exceed 47% which coincides with the water content break in Equation 3.4. It is most likely that the non-contact filter paper did not have sufficient time to reach equilibrium within 28 days. Further evidence is shown by the ID-NC-FP water content being lower than the ID-C-FP water content, and the IW-NC-FP water content being higher than the IW-C-FP water content.

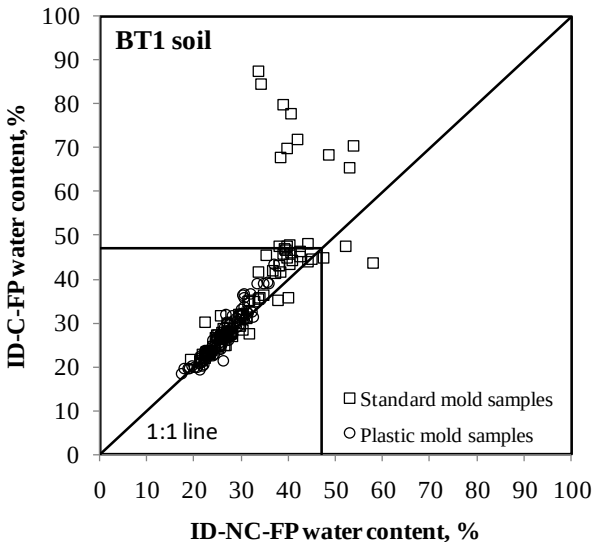

a) BT1

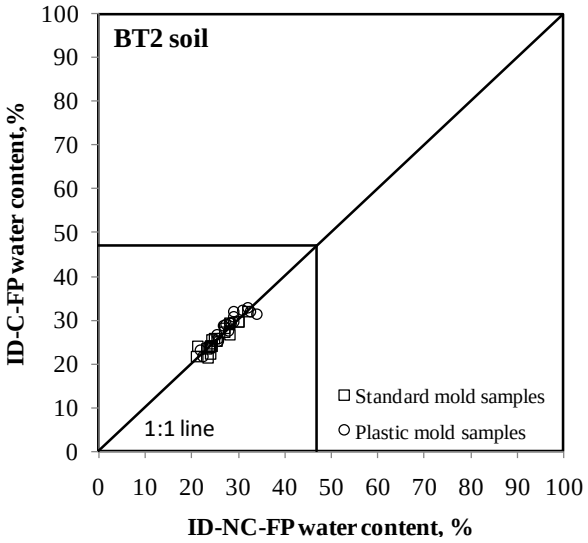

b) BT2

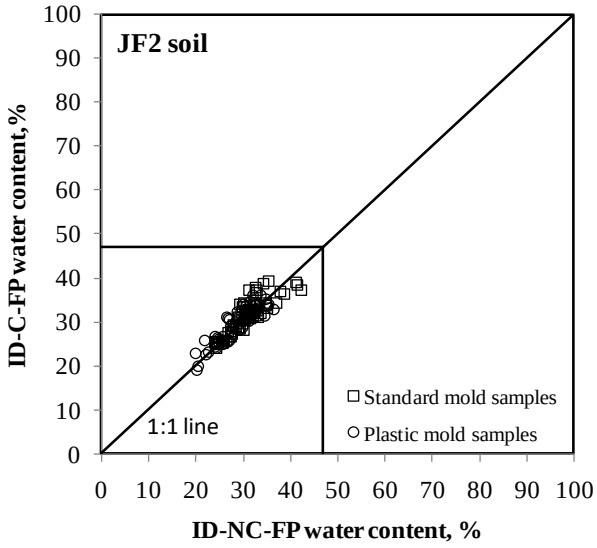

c) JF2

Figure 4.7: Comparison of contact and non-contact initially dry filter papers

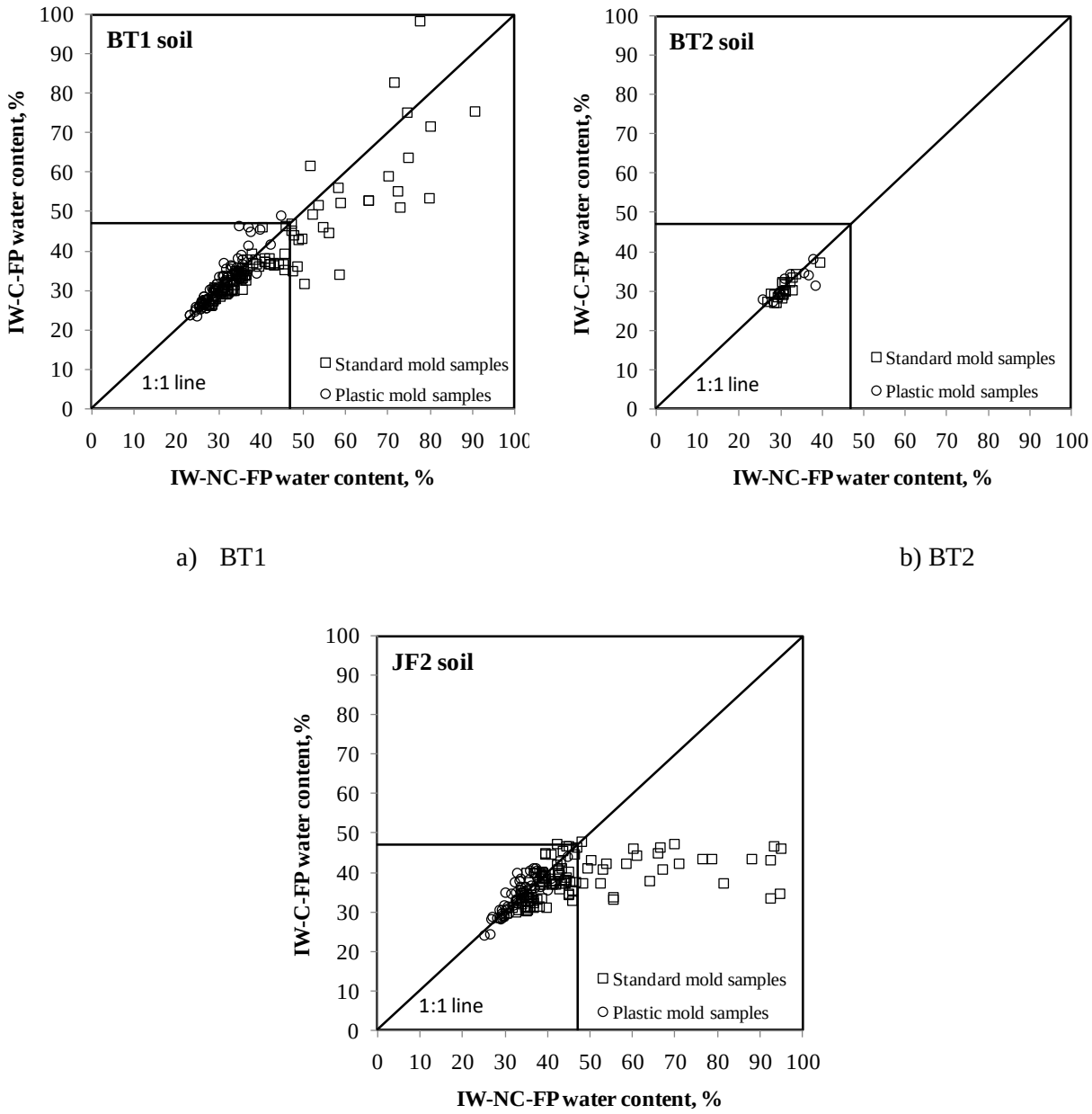

a) BT1

b) BT2

c) JF2

Figure 4.8:Comparison of contact and non-contact initially wet filter papers

4.2.3 Hysteresis

Figure 4.9 shows the hysteresis between the initially dry and initially wet filter papers in contact and non-contact modes for the BT1, BT2 and JF2 soils. The initially wet filter papers data shown

in Figure 4.9 were prepared using Method 2 and the equilibration time for all the filter papers was at least 28 days. Equivalent data for Method 1 are shown in Appendix A2.

Figure 4.9 shows that the hysteresis between the initially dry and initially wet filter papers is less than 5% as observed by Leong et al. (2002b). The hysteresis in the non-contact filter papers for soil BT1 and JF2 in Method 1 is higher than 5% (see Appendix A2). This is because there was less control on the initial water content of the filter paper in Method 1 and in addition, maximum equilibration time was 28 days. Therefore, the higher hysteresis may be due to insufficient equilibration time for the initially wet filter paper. The non-contact filter paper for BT2 was allowed longer duration time (up to 60 days) hence the smaller hysteresis between the initially dry and initially wet filter papers.

Because of the hysteresis between the initially dry and initially wet filter papers, calibration equation such as Equation 3.4 established using initially dry filter papers will underestimate the suction of the soil if used on initially wet filter papers. To account for hysteresis, the water contents in Equation 3.4 can be offset by -4% for initially wet filter papers as shown in Equation 4.1.

$$\begin{aligned} \log\psi &= 2.909 - 0.0229(w_f - 4) \quad (w_f - 4) \geq 47\% \\ \log\psi &= 4.945 - 0.0673(w_f - 4) \quad (w_f - 4) < 47\% \end{aligned} \qquad 4.1$$

4.2.4 Suction measurements

The suction of the as-compacted soil specimen was measured using both contact and non-contact filter papers. The ID-C-FP measures the matric suction of the soil specimens according to Equation 3.4. The matric suctions of the as-compacted soil specimens are plotted against the ID-NC-FP and the IW-NC-FP water contents for the same soil specimen in Figure 4.10. The initially

wet filter paper was prepared using Method 2 and equilibration time for all the filter papers was more than 28 days.

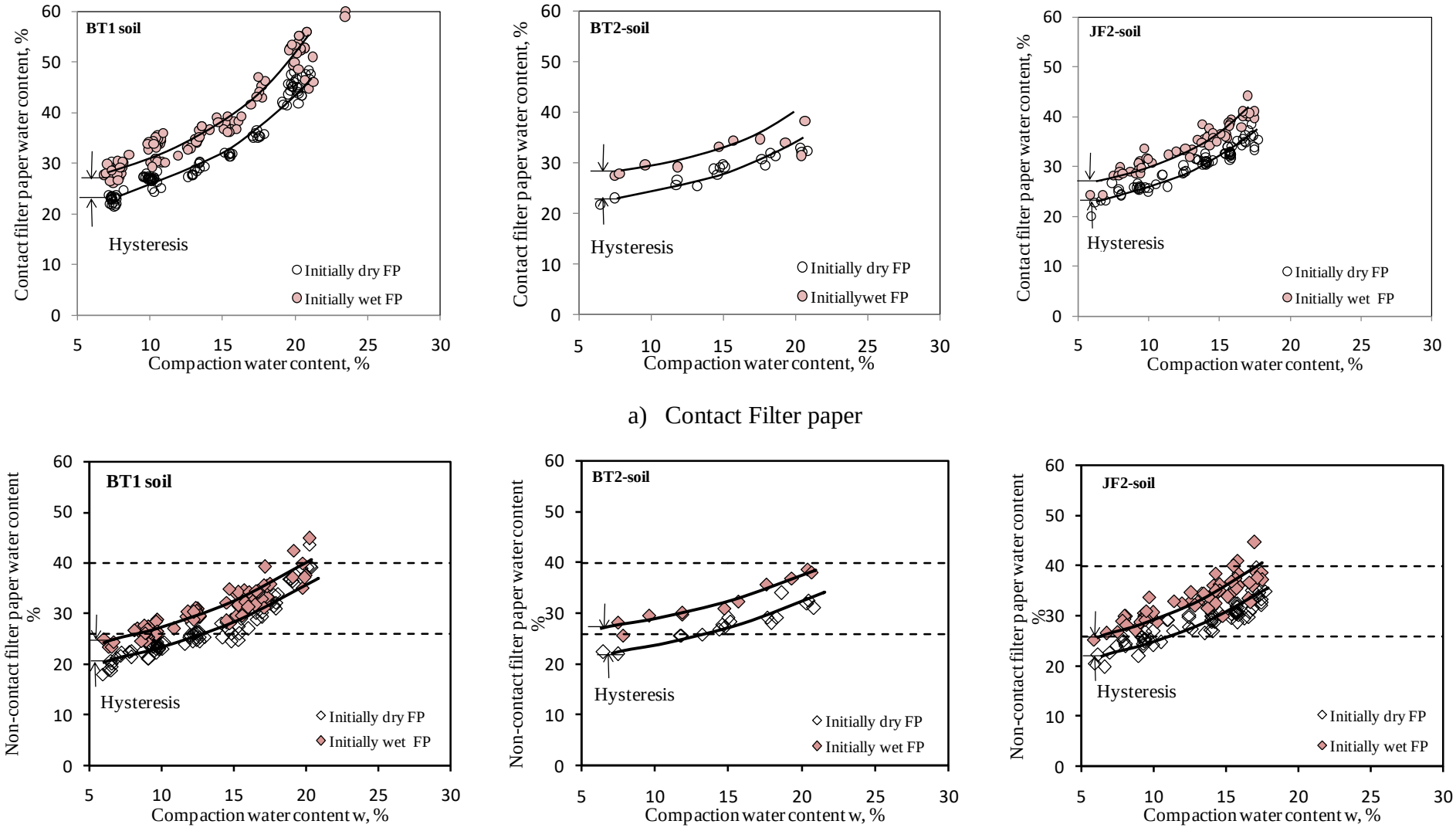

Figure 4.9: Hysteresis between initially dry and initially wet filter papers in contact and non-contact modes

Best-fit lines were determined and the equations are shown in Figure 4.10 together with the coefficient of determination R^2. In addition, Equations 3.4 and 4.1 for filter paper water content less than 47% are also plotted in Figure 4.10 for comparison. Good agreement can be found between the best-fit lines, and Equations 3.4 and 4.1, with the BT soil data showing better agreement than the JF soil data. This indicates that the ID-NC-FP and IW-NC-FP can be interpreted using the matric suction calibration curve equations, Equations 3.4 and 4.1, respectively, for filter paper water content less than 47%.

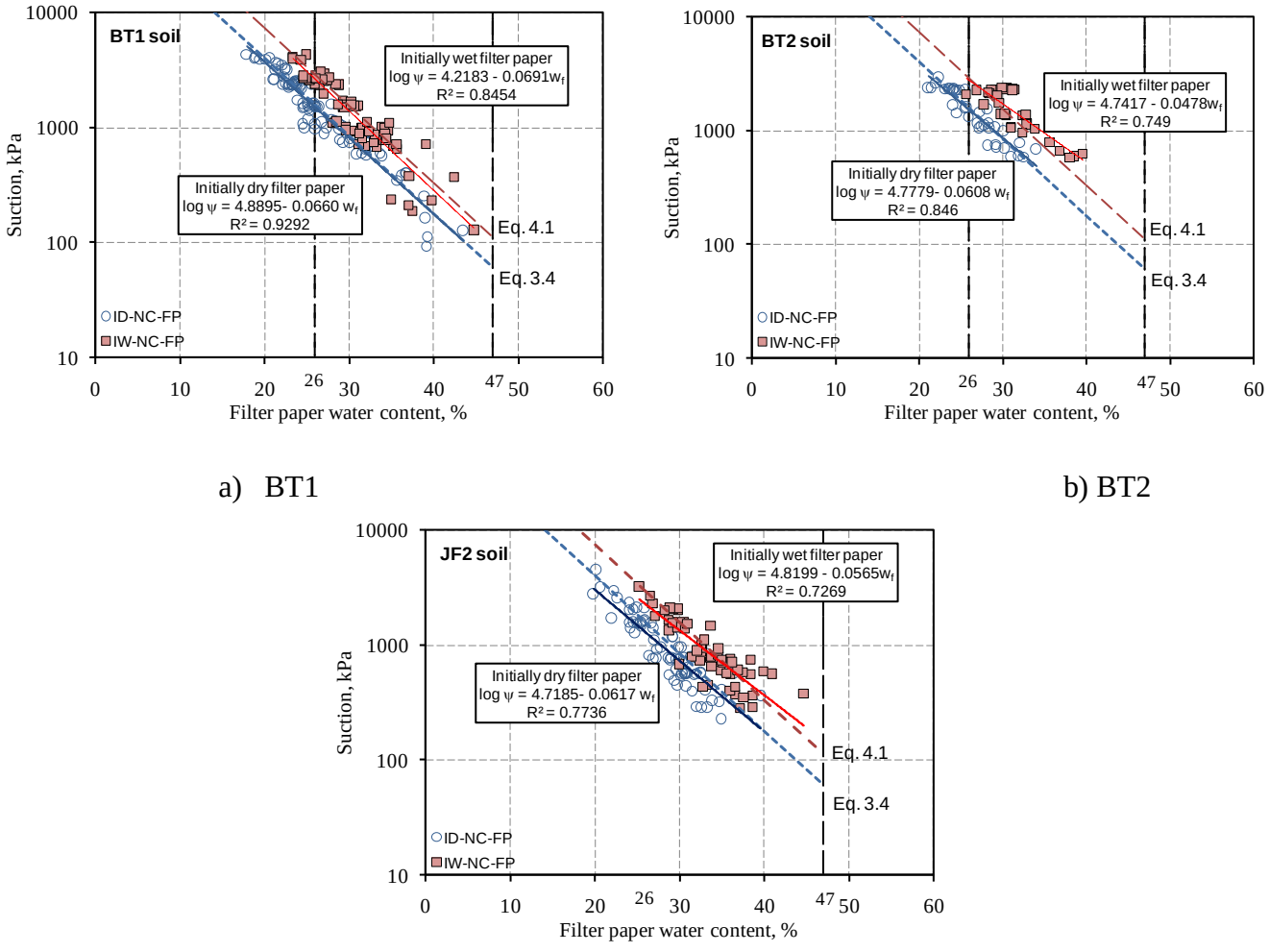

a) BT1 b) BT2

b) JF2

Figure 4.10: Suction calibration curves for initially dry and initially wet filter paper in non contact mode

The ID-NC-FP data in Figure 4.10 is re-plotted in Figure 4.11 together with the calibration data from Likos (2000) and Samingan (2005) for total suction. The calibration curves from Leong et al. (2002b) given by Equations 3.4 and 3.5 are also plotted in Figure 4.11. For Equation 3.5, Leong et al. (2002b) equilibrated Whatman No.42 filter papers over various concentrations of different salt solutions for 14 days. Likos (2000) equilibrated Whatman No.42 filter papers over various concentrations of NaCl and KCl solutions and saturated solutions of LiCl.H20, $MgCl_2.H_20$, $NaNO_2$ and $(NH4).H_2PO_4$ for seven days. Samingan (2005) equilibrated Whatman No.42 filter papers over various concentrations of NaCl solutions for suctions above 2000 kPa for five weeks. Figure 4.11 shows that the data merges at suctions above 10000 kPa.

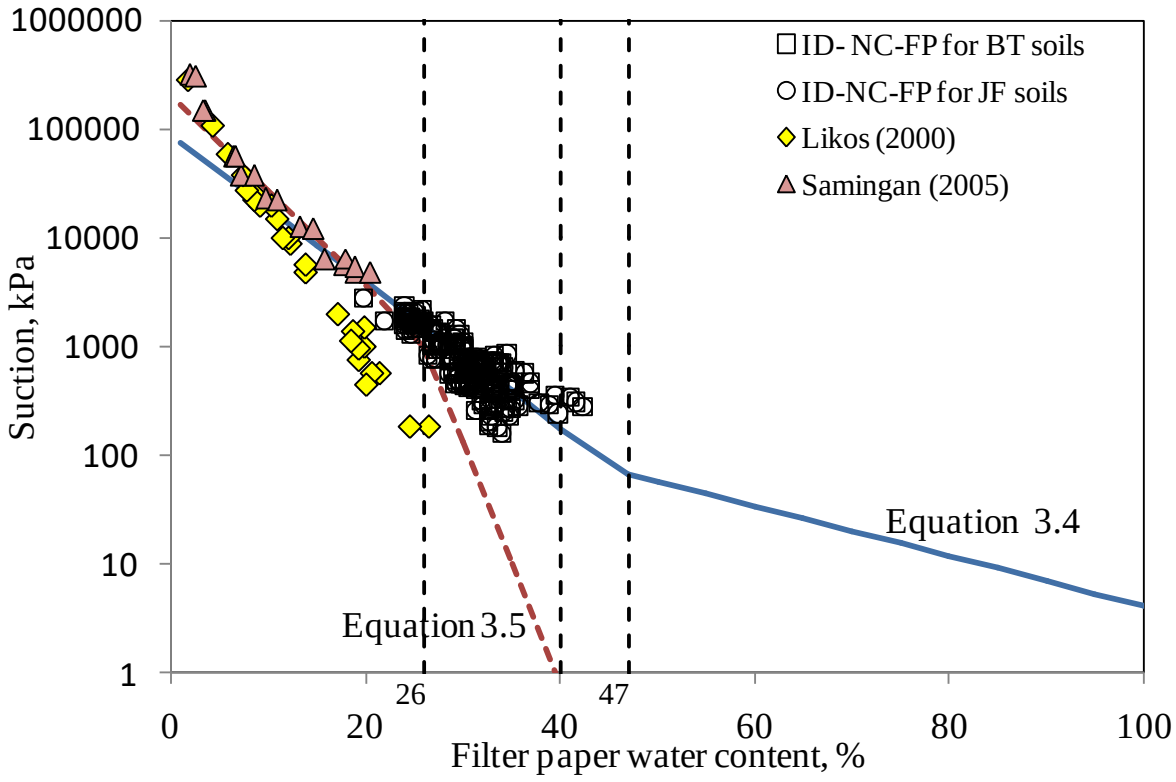

Figure 4.11: Comparison of initially dry non-contact filter paper measurement of suction with other researchers

For suctions less than 10000 kPa, Likos (2000)'s data starts to diverge from the rest probably due to insufficient equilibration time. Most of the ID-NC-FP data from the present study seems to straddle between the calibration curves given by Equations 3.4 and 3.5 indicating that equilibration time of 28 to 60 days may not be sufficient for some of the ID-NC-FP. This suggests Marinho and Oliveira (2006) is correct in explaining equilibration time being the cause of the difference between the total and matric suction calibration curves but it is difficult to use the matric suction calibration curve for the non-contact filter paper as equilibrium may not be achieved within a reasonable time. This suggests that the non-contact filter paper is only suitable for use in the high suction range. The present data indicates that the suction range for non-contact filter paper should be above 1000 kPa.

Total suction of the soil specimens were also measured independently using the CMDP technique. The total suction measured by WP4C, ID-NC-FP and ID-C-FP are plotted against compaction water content in Figure 4.12.

The ID-NC-FP was interpreted using both Equations 3.4 and 3.5. The ID-C-FP was interpreted using Equation 3.4. Generally, there is good agreement for suctions above 1000 kPa. Below 1000 kPa suction, the suction given by the WP4C lies in between the suctions given by Equations 3.4 and 3.5 for the ID-NC-FP. The suctions given by Equation 3.4 for ID-NC-FP are higher than the suctions given by WP4C and can be attributed to insufficient equilibrium time. The large divergence of the suctions given by Equation 3.5 for the ID-NC-FP and the suctions given by WP4C is due to Equation 3.5 diverging from Equation 3.4 below 1000 kPa. Although ASTM D6836-16 does not recommend the CMDP technique to measure suctions below 1000 kPa, there

seems to be good agreement between the suctions given by Equation 3.4 for the ID-C-FP and the suctions given by WP4C for suctions below 1000 kPa.

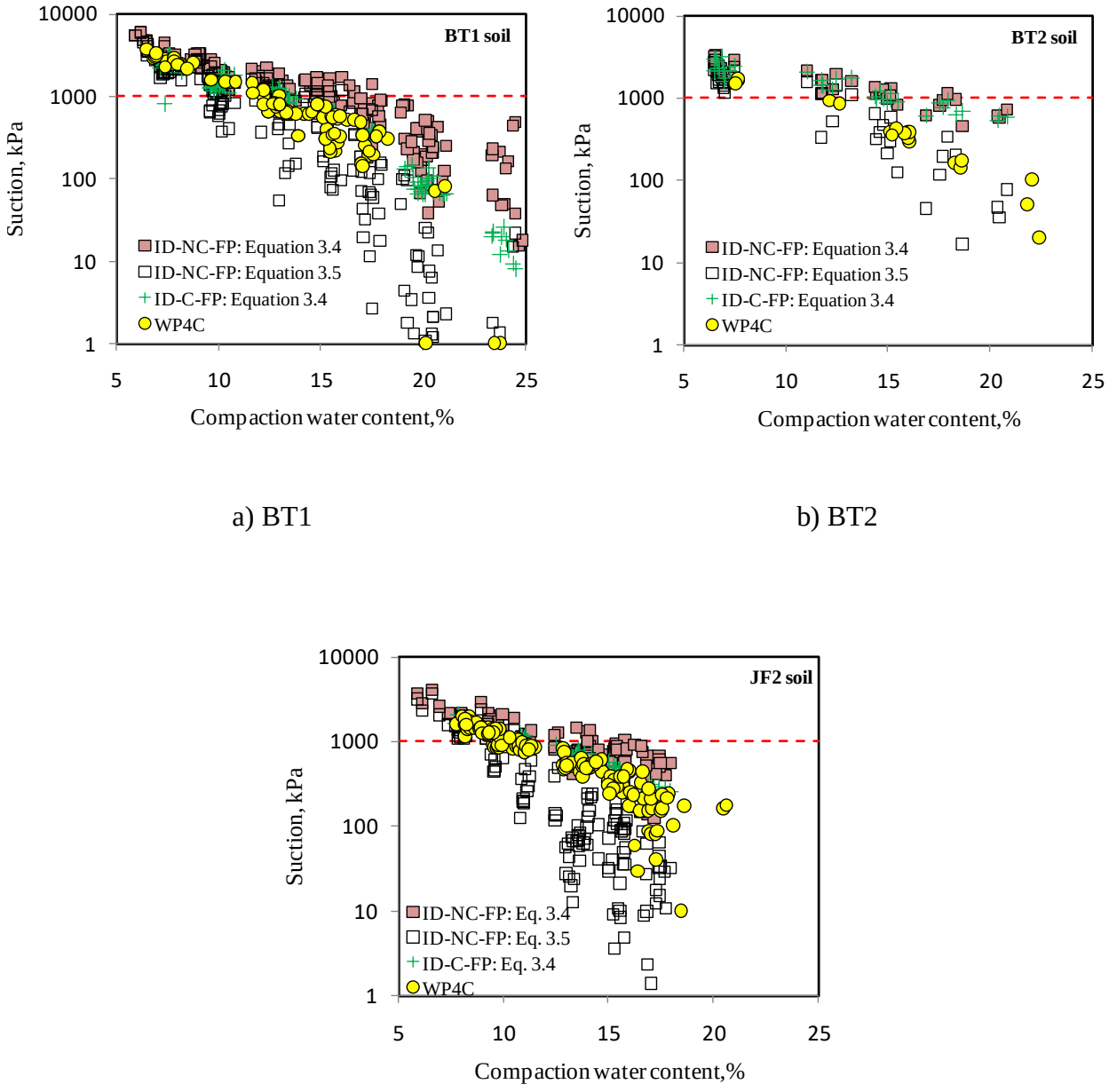

a) BT1

b) BT2

c) JF2

Figure 4.12: Comparison of suction measurements by initially dry non-contact filter paper and chilled mirror dewpoint technique

4.2.5 Variability of filter papers

Deka et al. (1995) and Marinho and Oliveira (2006) investigated the inherent variability of the Whatman No.42 filter papers and noted that different batches of filter papers may have different characteristics causing differences in the calibration curves between batches. Bulut and Wray (2005) also suggested a change in absorption characteristics of the Whatman No. 42 filterpaper under the application of a pressure.

The variability of Whatman No. 42 filter papers in terms of weight after oven drying was examined for 48 unused filter papers and 1716 used filter papers. The used filter papers were separated into those used in contact (844 filter papers) and non-contact (872 filter papers) modes. According to the manufacturer's specifications, the Whatman No. 42 filter paper weighs 100g/m^2. Hence, for a filter paper that is 42.5 mm in diameter, the mean weight is expected to be 0.142g. Accounting for the initial moisture content (6.6%) of the filter paper, the expected mean weight is 0.133g. The weight distributions of the used and unused filter papers shown in Figure 4.13 have a normal distribution. The unused filter papers have a narrower weight distribution from 0.13 to 0.14g with peak at 0.135g. The used filter papers have a wider weight distribution with the non-contact filter papers showing a weight distribution from 0.115 to 0.145g with a peak at 0.13g and the contact filter papers showing a weight distribution from 0.11 to 0.15g with a peak at 0.135g.

Hence, some permanent changes occurred in the filter paper after use and the change is slightly more for the contact filter paper. There is little evidence that the contact filter paper becomes contaminated during use hence the use of sacrificial filter papers recommended by ASTM D5298-16 seems unnecessary.

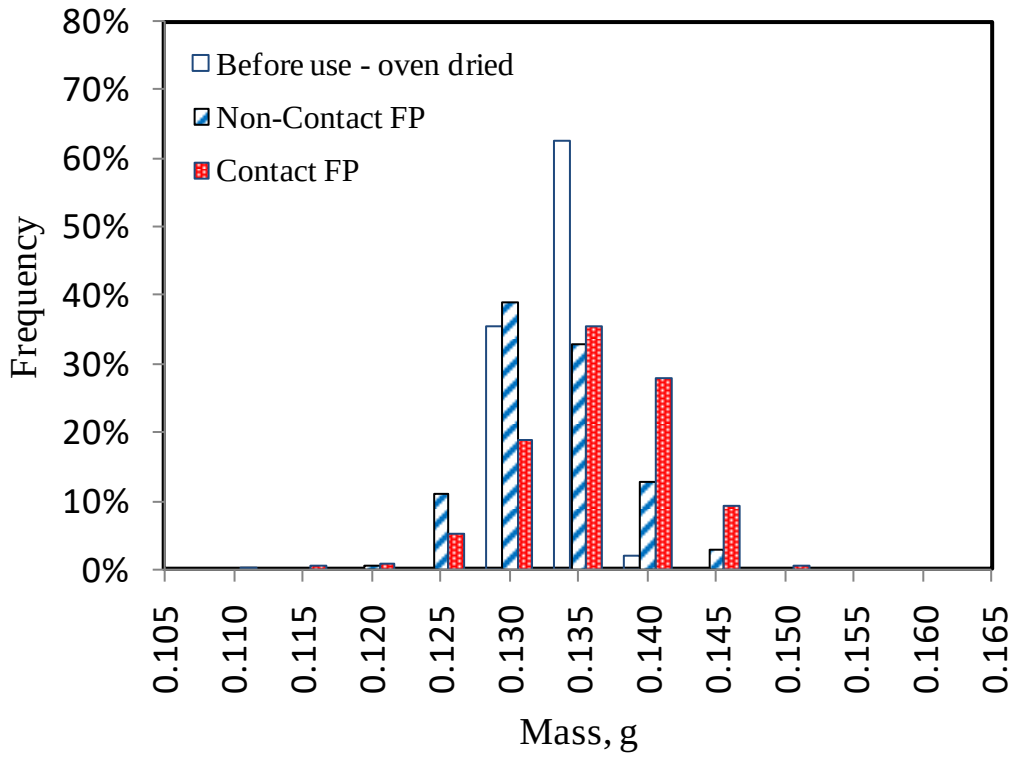

Figure 4.13: Weight distribution of dried filter papers before and after use

4.2.6 Summary

In this study, the efficacy of using initially dry and initially wet Whatman No. 42 filter papers for suction measurement of dynamically compacted soils was evaluated using more than 1700 pieces of filter papers. Suction measurements were performed on soils compacted at various water contents using both the standard and modified Proctor efforts. The initially wet filter papers were prepared using two methods. Important conclusions from this study are:

1) It is easier to handle initially dry filter papers compared to initially wet filter papers. When filter papers are wetted, there is a likelihood of altering their characteristics and hence affecting their performance in suction measurement.
2) When using initially wet filter paper, pre-wetting to a specific moisture content (Method 2) will give better outcome than not controlling its moisture content.

3) An initially wet filter paper may require even longer equilibrium time compared to an initially dry filter paper. When used in the non-contact mode, the equilibrium time depends on the air space above the soil specimen, the suction of the soil and the initial moisture condition of the filter paper.
4) Hysteresis between initially dry and initially wet filter paper can be accounted for by applying an offset on the water content in the initially dry filter paper calibration curve. The study showed that the offset is about -4% for the Whatman No. 42 filter paper.
5) Comparison of the weight distributions of used and unused filter papers show that the used filter papers have a slightly wider weight distribution than the unused filter papers. There is negligible difference in weight distributions between the contact and non-contact filter papers indicating that contamination of filter paper is not an issue and hence, there may not be a need to use sacrificial filter papers in the contact method to prevent contamination of the filter paper.
6) Good agreement was found between the suctions measured using the WP4C and the initially dry contact filter paper.
7) For both initially dry and initial wet filter papers, the contact mode gives more reliable suction measurement than the non-contact mode.
8) The non-contact filter paper is suitable only for the high suction range, above 1000 kPa whereas the contact filter paper is suitable for both the high and low suction ranges.

4.3 Soil-water characteristic curves of compacted soils

Soil-water characteristics curves (SWCC) of compacted soils have been studied by other researchers. Factors influencing the SWCC studied includes:

1) Initial compaction water content e.g.Vanapalli et al. (1999).

2) Initial dry density e.g. Salager et al. (2010), Zhou et al. (2012), Mirzaii and Yasrobi (2012), and Wijaya and Leong (2017).

3) Influence of stress history e.g. Vanapalli et al. (1999) and Marinho (2005).

These factors are further explored in this study. Both the SWCC-w and SWCC-S for the soil specimens were studied. Only the drying SWCCs have been studied in this thesis. The as-compacted characteristics of the soil specimens are presented in Tables 4.1 to 4.4.

Table 4.1: Average properties for BT1 specimens measured for SWCC

BT1- soil			dry densities, Mg/m^3	
BT1-PL/ASTM	Compacted at	w%	PL specimen	ASTM specimen
STD10	dry of optimum	10	1.64	1.64
STD13	dry of optimum	13	1.66	1.68
STD16	optimum	16	1.68	1.69
STD18	wet of optimum	18	1.69	1.67
STD20	wet of optimum	20	1.66	1.64
MDF7	dry of optimum	7	1.80	1.79
MDF10	dry of optimum	10	1.83	1.83
MDF13	optimum	13	1.83	1.86
MDF16	wet of optimum	16	1.81	1.82
MDF18	wet of optimum	18	1.77	1.78

Table 4.2: Average properties for BT2 specimens measured for SWCC

BT2-PL/ASTM	Compacted at	w%	dry densities, Mg/m^3 PL specimen	ASTM specimen
STD13	dry of optimum	13	1.58	1.63
STD16	dry of optimum	16	1.63	1.65
STD19.5	wet of optimum	19.5	1.68	1.70
STD22	wet of optimum	22	1.61	1.63
MDF8	dry of optimum	8	1.78	1.83
MDF11	dry of optimum	11	-	1.86
MDF13	optimum	13	-	1.88
MDF15	wet of optimum	15	1.84	1.86
MDF16	wet of optimum	16	1.82	1.83

Table 4.3: Average properties of JF1 specimens measured for SWCC

JF1-PL	Compacted at	w%	dry density, Mg/m^3
STD13	dry of optimum	13	1.59
STD18	optimum	18	1.63
STD22	wet of optimum	22	1.63
MDF9	dry of optimum	9	1.74
MDF15	optimum	15	1.78
MDF19.5	wet of optimum	19.5	1.74

Table 4.4: Average properties for JF2 specimens measured for SWCC

JF2-PL/ASTM	Compacted at	w%	dry densities, Mg/m^3 PL specimen	ASTM specimen
STD10	dry of optimum	10	1.71	1.70
STD14	dry of optimum	14	1.73	1.76
STD16	optimum	16	1.76	1.77
STD18	wet of optimum	18	1.75	1.75
STD20	wet of optimum	20	1.71	1.69
MDF8	dry of optimum	8	1.83	1.86
MDF11	dry of optimum	11	1.86	1.91
MDF13.5	optimum	13.5	1.88	1.94
MDF15	wet of optimum	15.2	1.84	1.90
MDF18/17	wet of optimum	18/17*	1.80	1.84

The PL specimen was at w=18% while the ASTM specimen was at w =17%

Tables 4.1 to 4.4 indicate properties for both specimens compacted in the plastic mould (PL specimen) and those compacted in the ASTM mould (ASTM specimen). JF1 soil was only compacted in the plastic mould hence only PL specimens.

4.3.1 SWCC-w

As noted in Chapter 2, the quantity of water in the soil with suction is best represented using a SWCC. The water content can be represented as either gravimetric water content (w), volumetric water content (θ_w) or degree of saturation (S). Because of this, the resulting SWCC can be designated based on the type of water content used to represent it i.e., SWCC-w for gravimetric water content, SWCC-θ_W for volumetric water content and SWCC-S for degree of saturation (Wijaya and Leong, 2017).

In this subsection, different features of the SWCC-w are studied. Because the SWCC-w is obtained using mass properties, it is easier to compute and more reliable compared to SWCC-θ_W and SWCC-S that depend on volumetric properties. Volumetric properties of soil such as void ratio are difficult to obtain accurately. In fact, the SWCC-w may be regarded as the primary SWCC from which SWCC-θ_W and SWCC-S are derived as discussed in Chapter 2. Figure 4.14 shows the SWCC-w of BT1 and BT2 soil specimens compacted in the standard mould at both standard and modified Proctor energies respectively. Similarly in Figure 4.15, SWCC-w of JF1 and BT2 soils compacted in the plastic mould are shown. The SWCC-w plots for other soils are given in Appendices A3 and A4.

.

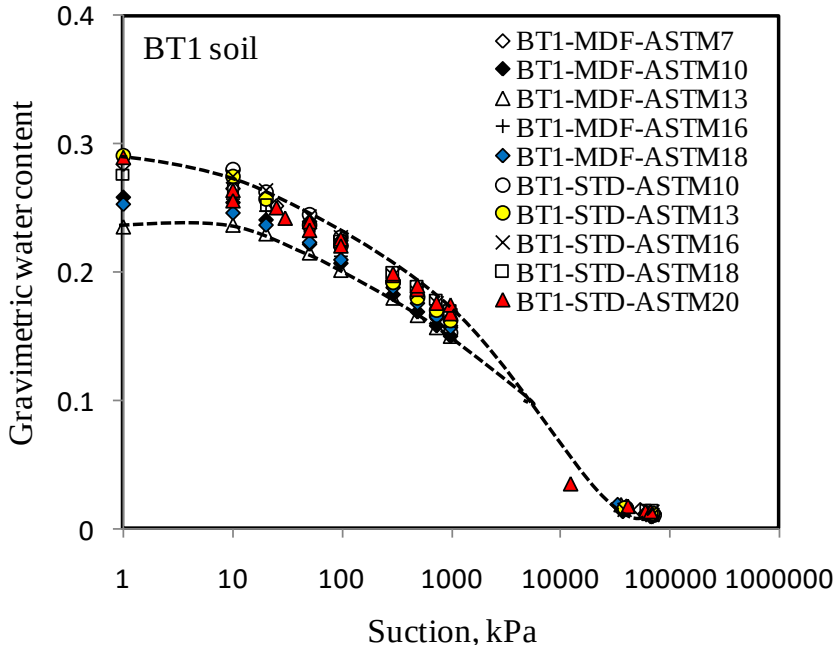

(a) BT1

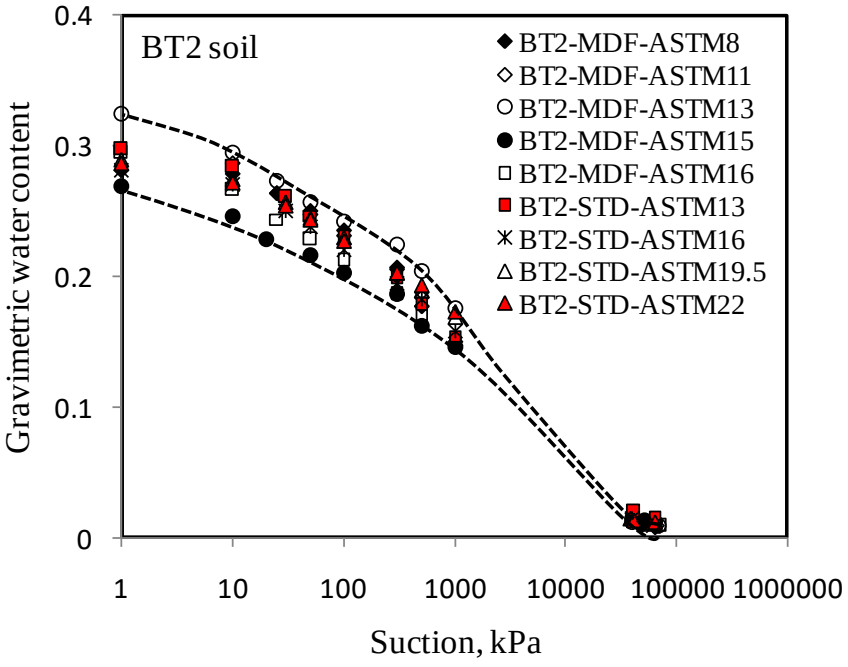

(b) BT2

Figure 4.14: SWCC-w for samples compacted in the standard mould

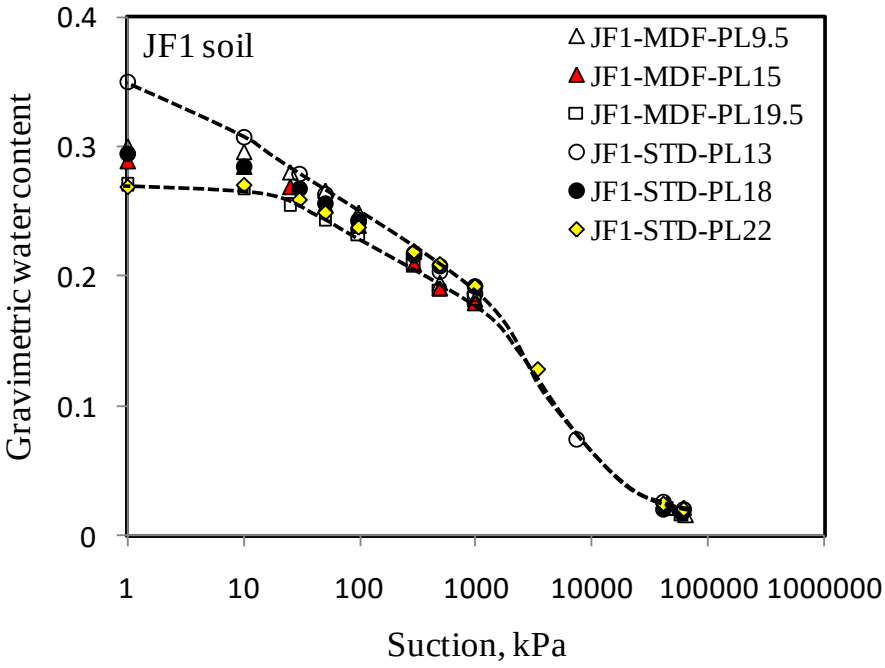

(a) JF1

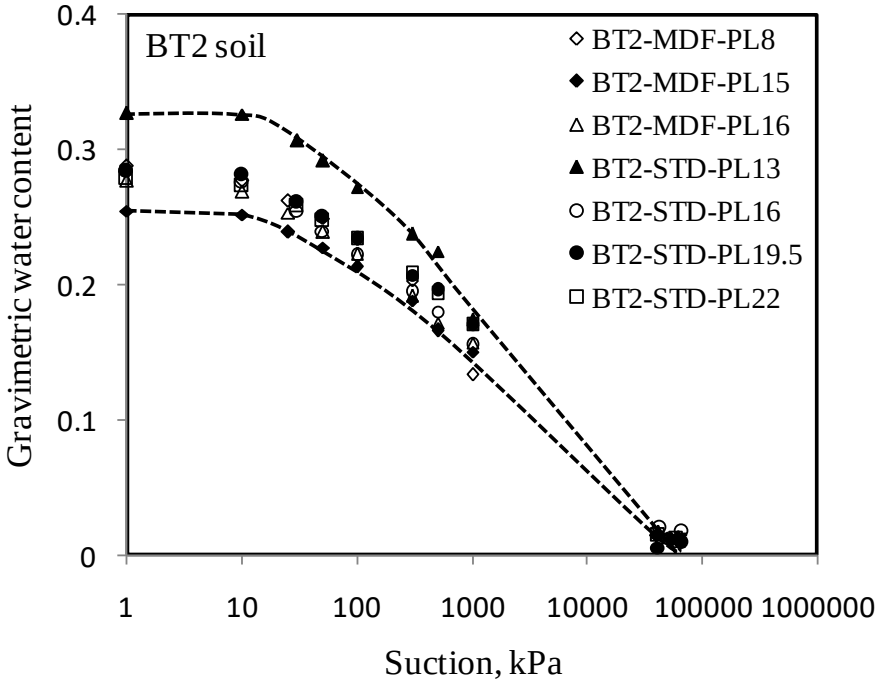

(b) BT2

Figure 4.15: SWCC-w for specimens compacted in the plastic mould

Wijaya and Leong (2017) note that density can be modeled as either saturated water content w_{sat}, void ratio e, or relative density. In Figures 4.14 and 4.15, as well as figures in Appendices A3

and, the effect of density is represented by saturated gravimetric water content, w_{sat}. It is observed that initially the SWCCs show clear differences owing to differences in w_{sat}, however as suction increases, the SWCCs converge or near converge into a single curve which Wijaya and Leong (2017) refers to as the virgin drying line.

The soil specimens compacted at standard Proctor effort using the standard ASTM mould generally show a narrower band in their SWCCs compared to those compacted at modified Proctor effort (Appendix A3). This indicates that the soil specimens compacted at standard Proctor effort have a more uniform pore size distribution although it is expected that soil specimens compacted at a higher compaction effort should have a more uniform pore size distribution. However, the soil specimens compacted in the plastic mould behaved as expected (Appendix A4).

It is difficult to control the initial dry density of the compacted soil specimens precisely. The error will show up in the initial part of the SWCC-w through w_{sat}. Apart from BT2 soil specimens, most of the SWCC-w tend to converge into one curve beyond a suction of 1000 kPa. The SWCC-w of BT2 soil specimens whether compacted in the standard mould or plastic mould tend to converge much slower than the rest of the soil sets.

The SWCC-w can also be represented as plots of normalised gravimetric water content against soil suction. The gravimetric water content is normalised by dividing gravimetric water content with the saturated gravimetric water content i.e., w/w_{sat}. For soils with negligible volume change during drying, normalised gravimetric water content is equivalent to degree of saturation (Fredlund et al., 2012). For illustration, Figure 4.16 shows normalized SWCC-w for BT1 and JF2 soil specimens compacted in the standard mould at both standard and modified Proctor

efforts. Complete plots are shown in Appendix A5, including those of BT2 soil specimens compacted in the standard mould and all specimens compacted in the plastic mould.

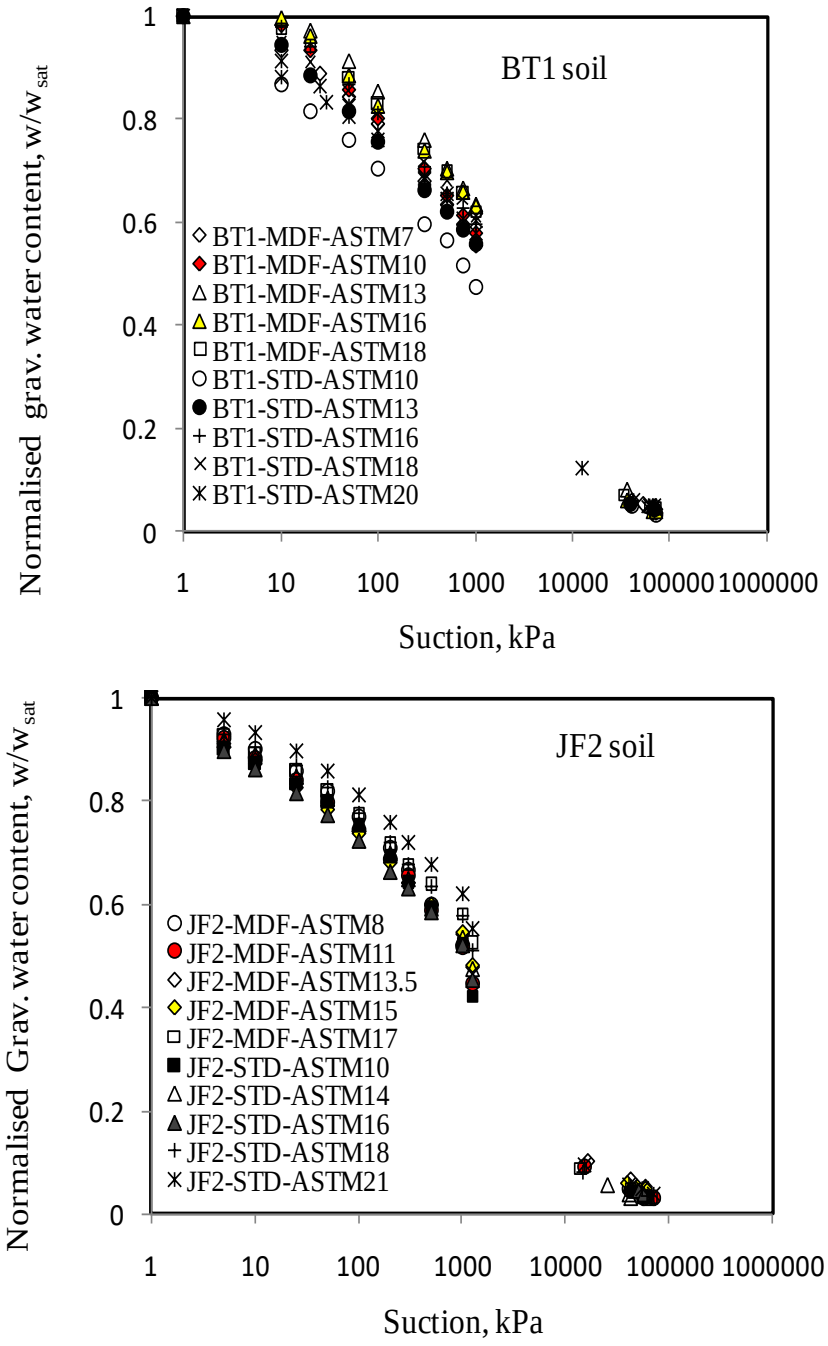

Figure 4.16: SWCC-w plotted in terms of normalised gravimetric water contents for soil specimens compacted in the standard mould

From Figure 4.16 and Appendix A5 it is generally observed that SWCCs of specimens compacted at modified Proctor effort have gentler slopes than those at standard Proctor effort. Specimens compacted at the same compaction effort show that SWCC-w of specimens compacted wet of optimum have gentler slopes than those compacted dry of optimum.

The slope of the SWCC-w is a reflection of the soil structure. Samples compacted wet of optimum have a dispersed uniform structure and their SWCCs are generally controlled by the microstructure (Vanapalli et al., 1999). In addition, specimens compacted at modified Proctor effort have more oriented (dispersed) structures than those compacted at standard Proctor effort (Holtz and Kovacs, 1981).The dispersed/ oriented structure implies a pore network that is disconnected and more uniform, hence a more gradual desaturation process reflected through the gentle slope of the SWCCs.

4.3.2 SWCC-S

The SWCC-S is the only SWCC that should be used to determine the air entry value (AEV) of a soil that undergoes volume changes on drying (Fredlund et al., 2012). In order to establish SWCC-S, volume measurements of the soil are required hence very often the SWCC-S is derived from SWCC-w using a soil shrinkage curve (Wijaya and Leong, 2017). The shrinkage curve represents the volume changes of the soil as it dries and is very often plotted as a relationship between void ratio and gravimetric water content. In this study, volume measurements of the specimens were taken as they dried during the SWCC tests in order to determine their shrinkage curves. Figure 4.17 shows typical shrinkage curves for specimens compacted at optimum water content for the BT1 and JF2 soils. The data was fitted using

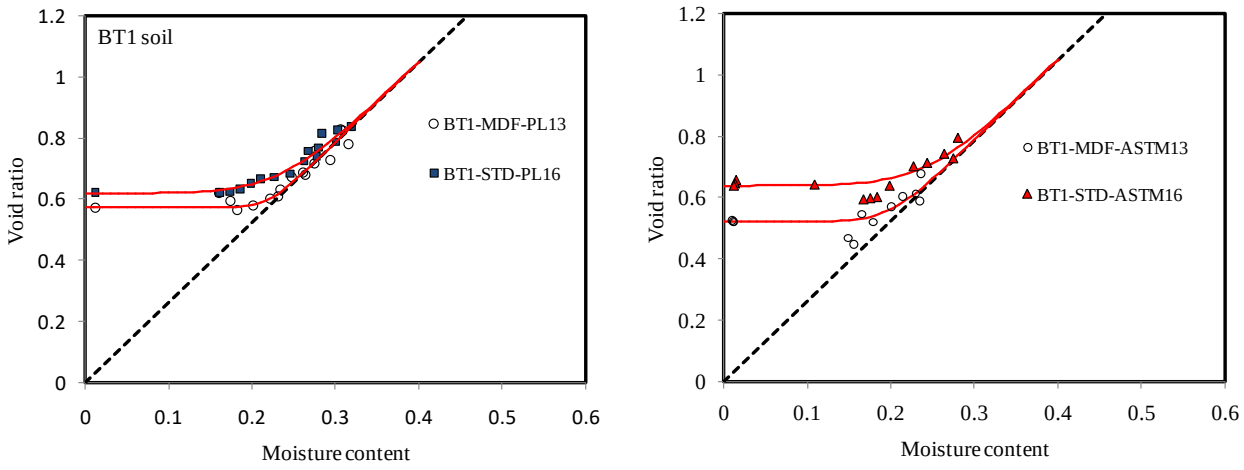

a) BT1

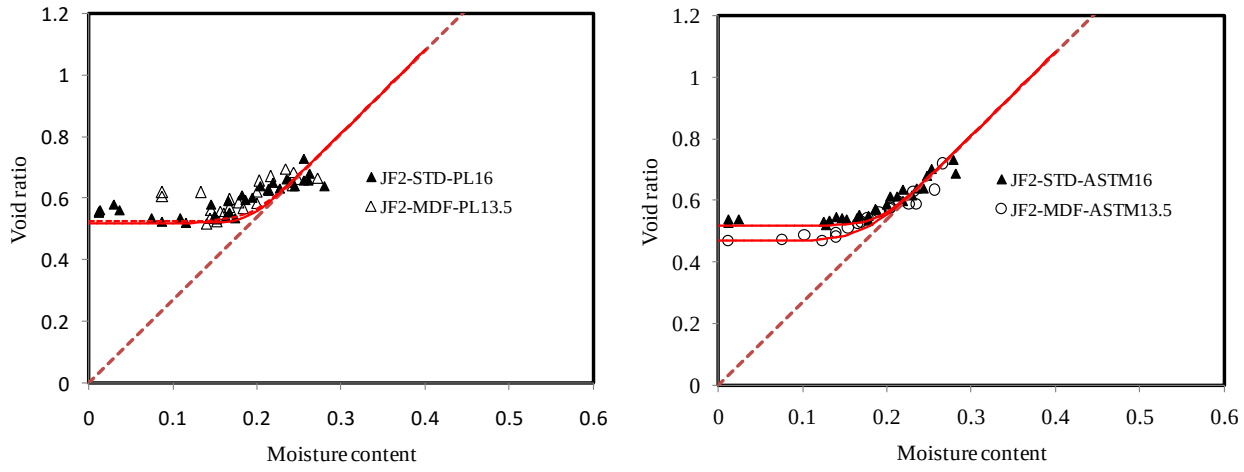

b) JF2

Figure 4.17: Typical shrinkage curves

Leong and Wijaya (2015)'s universal shrinkage equation. It is observed that the samples compacted at modified Proctor have a smaller e_{min} compared to those compacted at standard Proctor.

4.3.2.1 Effect of compaction water content on SWCC-S

As discussed in Chapter 3, compaction water content influences the soil structure with specimens compacted dry of optimum reportedly showing a flocculated soil structure which is further characterized by a dual porosity (Sridharan et al., 1971; Ahmed et al., 1974; Delage et al., 1996). The wet of optimum compacted specimens on the other hand are characterized by a dispersed structure and a unimodal pore size distribution.

Figure 4.18 and 4.19 show typical SWCC-S for JF2 soil specimens compacted in the plastic and the standard moulds, respectively. The SWCC-S data in Figures 4.18 and 4.19 were curve fitted with Fredlund and Xing (1994) equation. This equation was recommended by Leong and Rahardjo (1997b) as the best of all the SWCC equations commonly used in curve fitting unimodal SWCC data. From Figures 4.18 and 4.19, the wet of optimum specimens have higher AEVs, followed by the specimens compacted at optimum water content and finally the dry of optimum specimens. According to Vanapalli et al. (1999), specimens compacted at dry of optimum have less resistance to de-saturation owing to large voids between the clods which constitute the macrostructure. The macrostructure controls the initial de-saturation process for the specimens compacted dry of optimum (Vanapalli et al., 1999; Marinho, 2005) which facilitates de-saturation at low suction levels. On the other hand, specimens compacted wet of optimum have a pore network that is not interconnected resulting from a dispersed structure. This ensures higher water storage capacity for soils compacted wet of optimum and greater resistance to de-saturation hence the need for higher suctions for de-saturation to commence (Vanapalli et al., 1999).

Figure 4.18 also shows that beyond the AEV, the wet of optimum specimens compacted in the plastic mould de-saturate faster than the specimens compacted at optimum and dry of optimum

water contents. This is reflected by a steeper slope in the SWCC-S. Hence, the slope of the SWCC-S reflects the pore size distribution of the specimen where a steeper slope represents a more uniform pore size distribution. Figure 4.22 shows variation of AEV with dry density of the compacted specimens for BT1 and BT2 both sets compacted using the standard ASTM mould. The specimens compacted wet of optimum show higher AEV than those dry of optimum for the reasons presented above. The specimens at the optimum density seem to lie in between. Similar observations have been reported by Vanapalli et.al, (1999). Although it is expected that the AEVs of wet of optimum specimens are supposed to be less sensitive to dry density than those on the dry of optimum, both BT1 and BT2 show almost similar sensitivities

4.3.2.2 Effect of compaction effort on SWCC-S

Figures 4.20 and 4.21 presents the SWCC-S of BT1 soil specimens compacted in the plastic and standard moulds, respectively. The SWCC-S have been categorized according to initial compaction water content of the soil specimens i.e., either wet of optimum or dry of optimum. The SWCC-S for specimens compacted at standard and modified Proctor efforts are combined in each set.

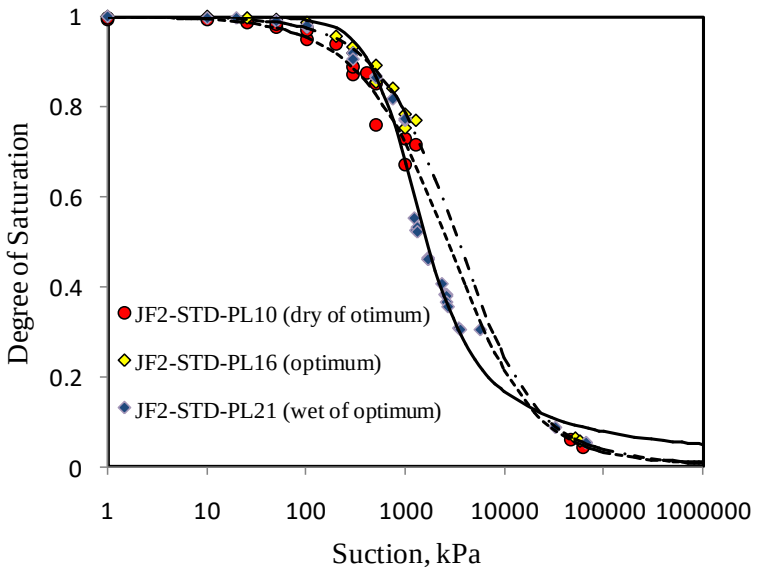

a) Specimens compacted at standard Proctor effort

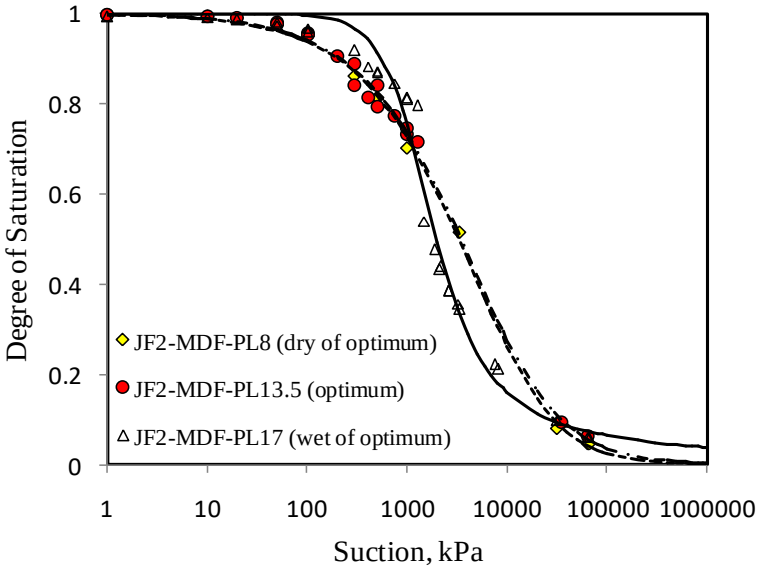

b) Specimens compacted at modified Proctor effort

LEGEND:

FX model-fitted to wet of optimum SWCC data

FX model fitted to dry of optimum SWCC data

FX model fitted to optimum SWCC data

Figure 4.18:SWCC-S for JF2 soil specimens compacted at standard and modified Proctor efforts in the plastic mould

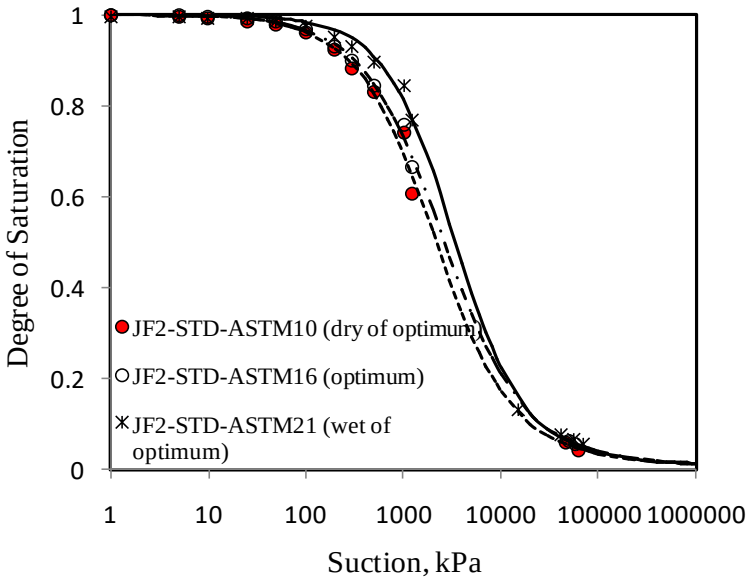

a) Specimens compacted at standard Proctor effort

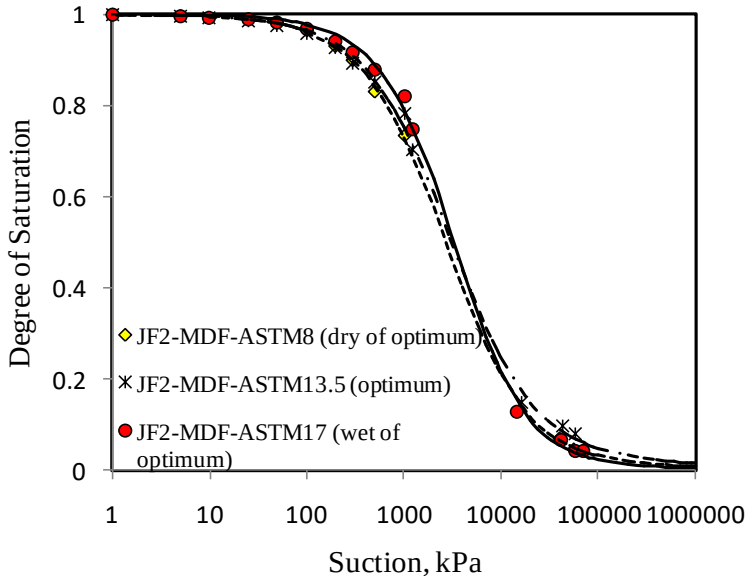

b) Specimens compacted at modified Proctor effort

Figure 4.19: SWCC-S for JF2 soil specimens compacted at standard and modified Proctor efforts in the standard mould

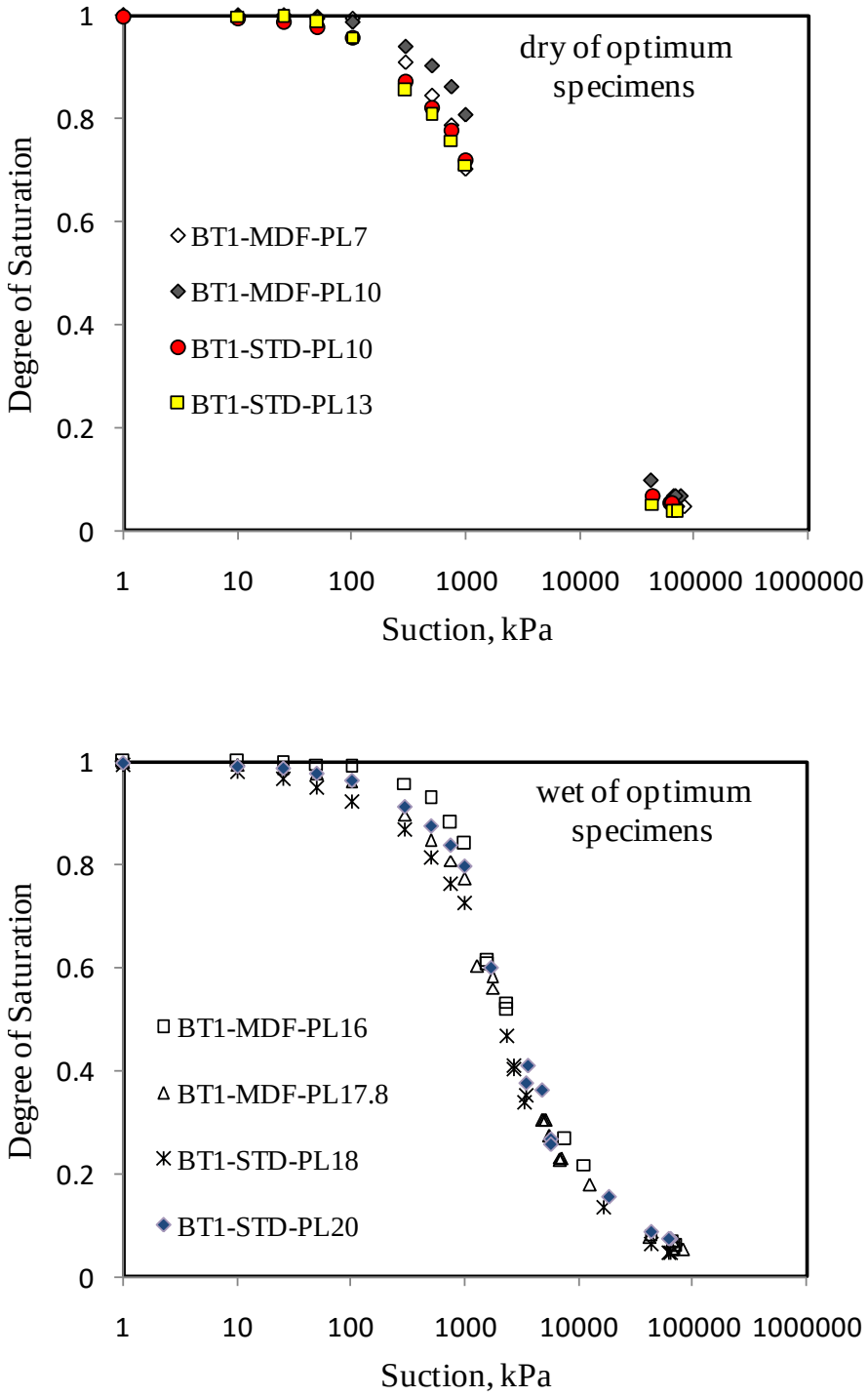

Figure 4.20: SWCC-S for BT1 soil specimens compacted dry and wet of optimum in the plastic mould at standard and modified Proctor efforts

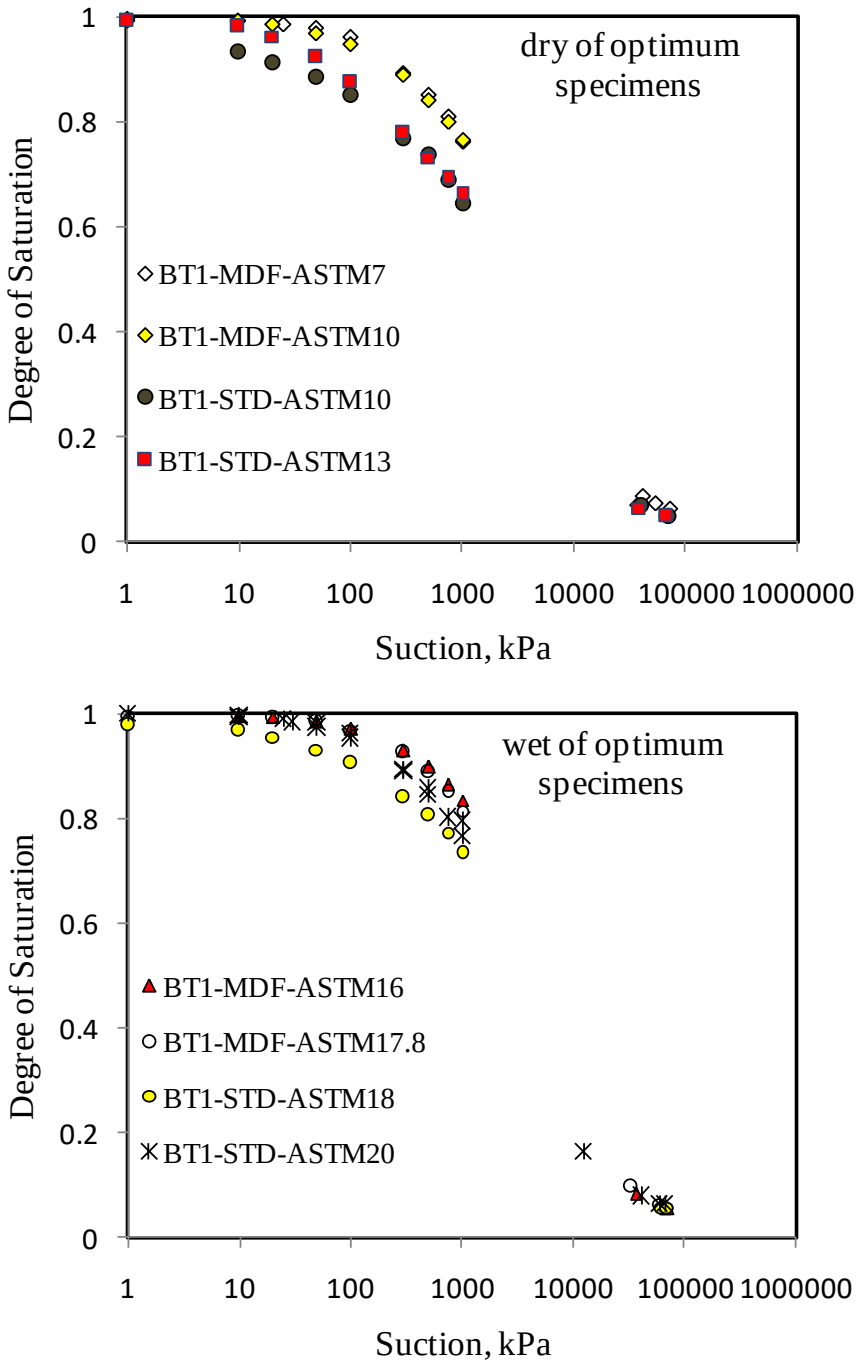

Figure 4.21: SWCC-S for BT1 soil specimens compacted dry and wet of optimum in the standard mould at standard and modified Proctor efforts

For specimens compacted dry and wet of optimum, the AEV increases with compaction effort (Figures 4.20 and 4.21). The SWCC-S for specimens compacted wet of optimum display a

narrower band than those compacted dry of optimum. This implies that specimens compacted wet of optimum are less sensitive to stress history. A similar observation was made by Vanapalli et al. (1999).

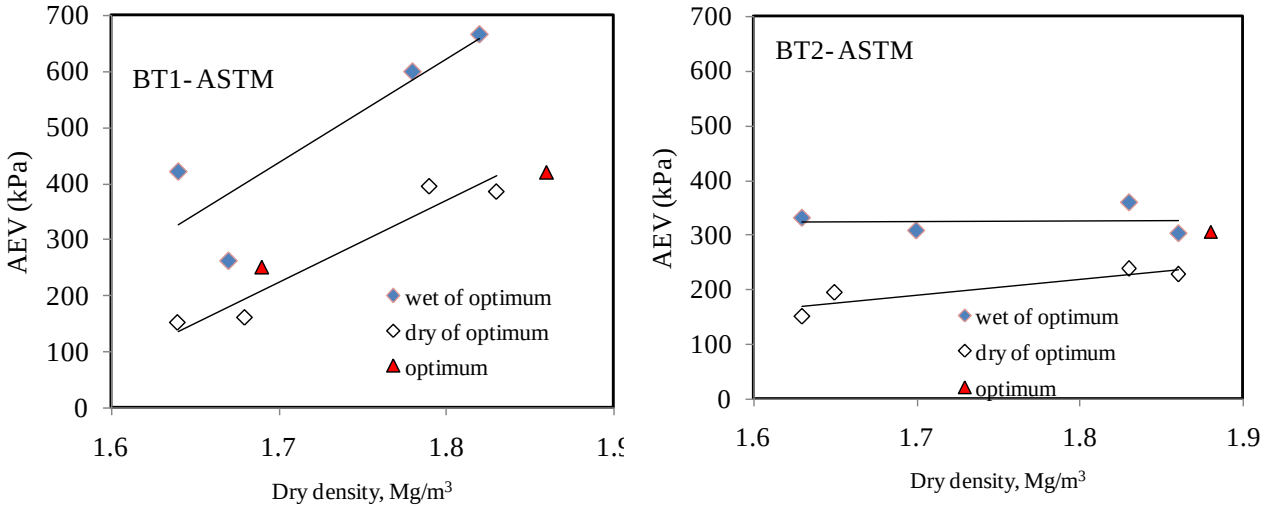

a) BT1 b) BT2

Figure 4.22: Variation of AEV with dry density

4.3.3 Comparison of SWCCs with previous studies

Agus et al. (2001) made an extensive study on the SWCCs of residual soils from Singapore two main geological formations i.e., Bukit Timah Granite and the Jurong Formation. The SWCCs were for natural soils obtained from various depths of the formations. The SWCC measurements were plotted in terms of normalized volumetric water contents, θ_w/θ_s and the data was fitted with Fredlund and Xing (1994) equation reproduced in the Equation 4.2. Agus et al. (2001) suggested lower and upper bounds as well as the average for the SWCC data of the two formations. The fitting parameters suggested by Agus et al. (2001) are given in Table 4.5.The SWCC data measured in this study was compared with the bounds suggested in Table 4.5 and the comparison is shown in Figure 4.23.

$$\theta_w = \frac{\theta_s}{\left[\ln\left(e + \left(\frac{\psi}{a}\right)^n\right)\right]^m} \qquad 4.2$$

where θ_w = volumetric water content, θ_s = saturated volumetric water content, ψ = suction, e = natural logarithmic constant and a, n and m are fitting parameters.

Table 4.5: SWCC fitting parameters for Singapore residual soils (after Agus et.al 2001)

Geological Formation	Fitting parameters	Lower bound	Average	Upper bound
Bukit Timah Granite	a(kPa)	32	36	159
	n	0.525	0.565	0.792
	m	2.243	1.147	0.704
Jurong Formation	a(kPa)	1185	299	432
	n	0.448	0.554	0.93
	m	5.387	1.869	1.004

From Figure 4.23, it is observed that the capillary zones of SWCC data from the present study are generally biased towards the upper bound while the residual zone is biased to the lower bound. This is attributed to the fact that the present study dealt with compacted soils with different pore size distributions from the natural soils that Agus et al (2001) studied. From Figure 4.23, the pore size distribution for natural residual soils is wider than for those for compacted soils.

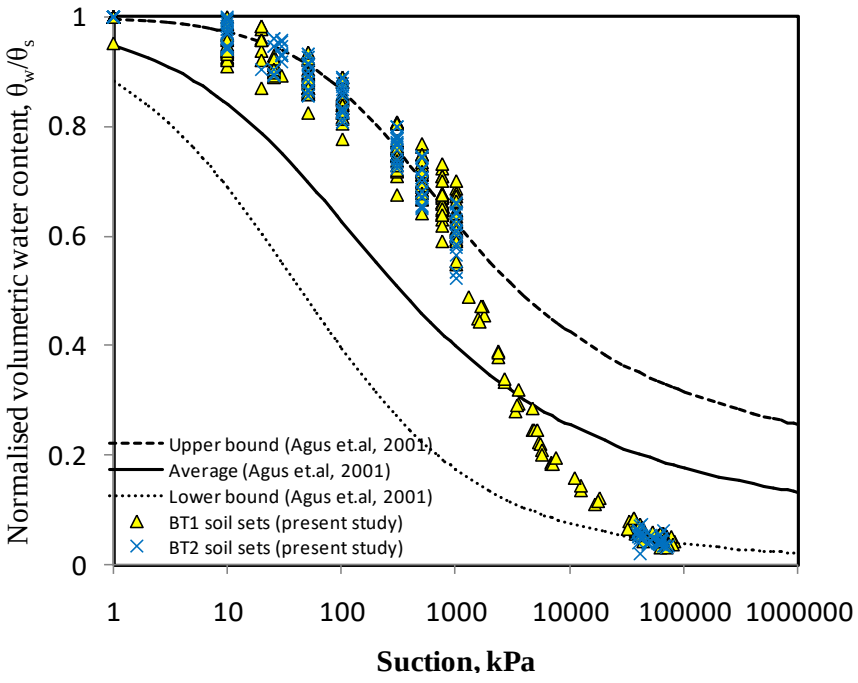

a) Bukit Timah Granite

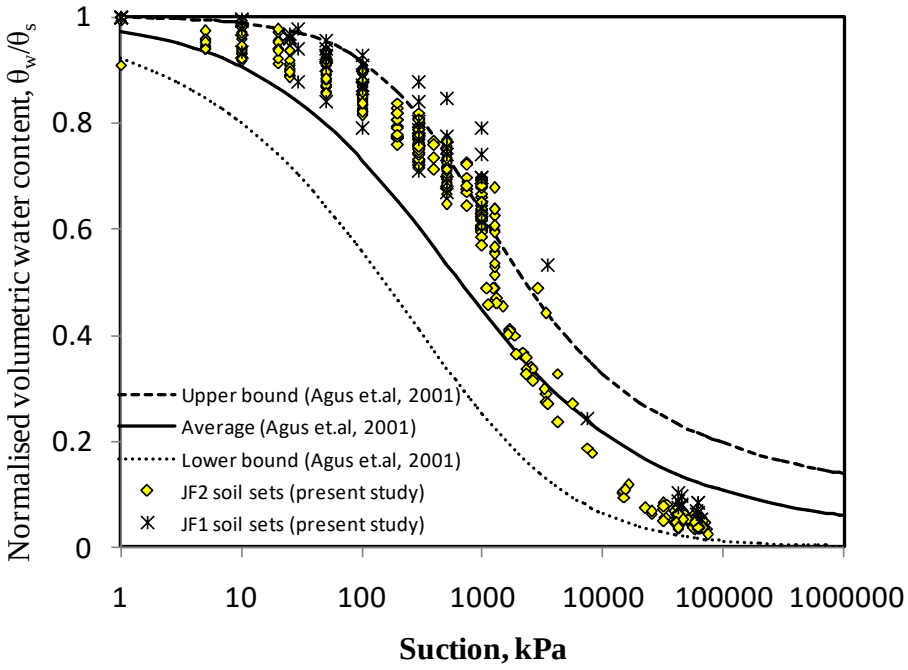

b) Jurong Formation

Figure 4.23: Comparison of SWCC data with SWCC envelopes suggested by Agus et al. (2001)

4.4 Comparison of suctions from filter paper method and SWCC

This section presents the suctions of the as-compacted soil specimens measured using the filter paper technique as well as the suctions estimated from the SWCC of the same compacted soils. The comparison is shown in Figure 4.24.

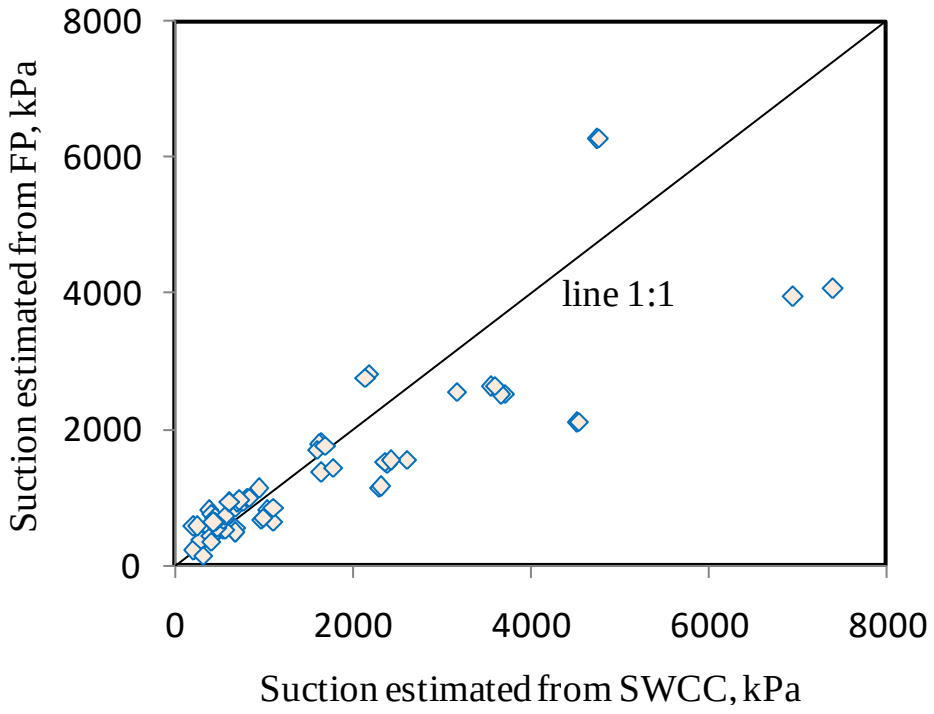

Figure 4.24: Comparison of suctions measured using filter paper technique and suctions estimated from the SWCC

It should be emphasized that the filter paper method measured the suctions of as-compacted soils and each specimen compacted at a particular water content is considered to be a "different soil" as discussed in Chapter 3. Each of the compacted soil specimens has a different SWCC.

From Figure 4.24, it is observed that suctions from the filter paper method compares very well with suctions estimated from the SWCCs in the lower suction range, especially below 1000 kPa. In the high suction range, suctions from the SWCC are higher than those from the filter paper

method. In the low suction range, the water phase in the soil specimen is continuous and hence it is easier to measure matric suction more accurately using the contact filter paper.

The present study did not have many SWCC measurements above 1000kPa which may have influenced the bias in the data shown in Figure 4.24.

4.5 Concluding remarks

This chapter presented two main issues: suction measurements using the filter paper method and SWCCs. As earlier emphasized, the suction measurements using the filter paper were done on as-compacted soil specimens and each specimen compacted at a particular water content and compaction effort should be regarded as a "different" soil with its own SWCC.

The main findings in this chapter are summarized below:

1) The filter paper technique is still a very valuable technique in suction measurement if a strict protocol is observed because the filter paper method can measure a wide range of suctions and is affordable. The initially dry filter paper is preferred to the initially wet filter paper. It is easier to handle initially dry filter papers compared to initially wet filter papers. When filter papers are wetted, there is a likelihood of altering their characteristics and hence affecting their performance in suction measurement. When using initially wet filter paper, pre-wetting to a specific moisture content (Method 2) will give better outcome than not controlling its moisture content.
2) An initially wet filter paper may require even longer equilibrium time compared to an initially dry filter paper. When used in the non-contact mode, the equilibrium time depends on the air space above the soil specimen, the suction of the soil and the initial

moisture condition of the filter paper. The hypothesis that an initially wet filter paper may reduce equilibration time was not supported by study.

3) Hysteresis between initially dry and initially wet filter paper can be accounted for by applying an offset on the water content in the initially dry filter paper calibration curve. The study showed that the offset is about -4% for the Whatman No. 42 filter paper.
4) Comparison of the weight distributions of used and unused filter papers show that the used filter papers have a slightly wider weight distribution than the unused filter papers. There is negligible difference in weight distributions between the contact and non-contact filter papers indicating that contamination of filter paper is not an issue and hence, there may not be a need to use sacrificial filter papers in the contact method to prevent contamination of the filter paper.
5) For both initially dry and initial wet filter papers, the contact mode gives more reliable suction measurement than the non-contact mode. Good agreement was found between the suctions measured using the WP4C and the initially dry contact filter paper. The non-contact filter paper is suitable only for the high suction range, above 1000 kPa whereas the contact filter paper is suitable for both the high and low suction ranges.
6) The study agrees with previous studies that 1000 kPa is an appropriate boundary between the low and high suction ranges for practical applications. It is recommended that the contact filter paper is best suited for the low suction range while the non-contact filter paper is best suited for the high suction range. This observation has been corroborated by equilibration durations for the two modes of contact.
7) The effects of compaction water content, compaction effort and initial dry density on the SWCCs were investigated and findings largely agree with previous studies. The

advantages of SWCC-w in examining influences of initial dry density on the SWCC previously observed by different researchers have been corroborated in this study.

8) A comparison between suction measurements using the filter paper technique on the as-compacted water soil specimens has been made with suction readings from the SWCCs of the different specimens. Good agreement is observed in the low suction range. The comparison in the higher suction range needs further study.

Chapter 5. Hydraulic properties of compacted soils

5.1 Introduction

For unsaturated soils, the permeability is a function of soil water content or suction and requires long test durations and sophisticated equipment to determine. Because of this, indirect methods to estimate the permeability function, k_w, of the unsaturated soil using the coefficient of saturated permeability, k_s coefficient and the SWCC as discussed in Chapter 2 were used. While this substantially reduces testing time, the determination of k_s and SWCC needs to be reliable, affordable and if possible done in a short time. In the laboratory, k_s is usually obtained using either flexible or fixed-wall permeameters described in Daniel et al. (1985),Benson and Daniel (1990), ASTM D5856-15, and ASTM D5084-16a. In Chapter 2, advantages and limitations of these permeameters have been presented. In this study, the flexible wall permeameter was used to measure k_s of the compacted soils as described in Chapter 3.

Limitations notwithstanding, in situ measurements of permeability are desired over laboratory measurements because they are more representative of the soil conditions since sampling is very likely to disturb the soil and only a small sample is tested in the laboratory. In this study, an attempt is made to measure k_s of compacted residual soils using a mini-disk infiltrometer. The operation and advantages of a mini-disk infiltrometer have been discussed in Chapter 2. The measurements from the mini-disk infiltrometer are compared with those obtained from a falling head flexible-wall permeameter. The main purpose of the study is to evaluate the reliability of the mini-disk infiltrometer in obtaining acceptable values of k_s. The k_s measurements from the flexible-wall permeameter are considered to be the reference for the measurements from the mini-disk infiltrometer.

5.2 Soils studied

Three soils were studied for this part of the thesis i.e., BT1, BT2 and JF2. The moisture-density relationships for the study soils are shown in Figure 5.1 together with the test points that were selected for the study of hydraulic properties.

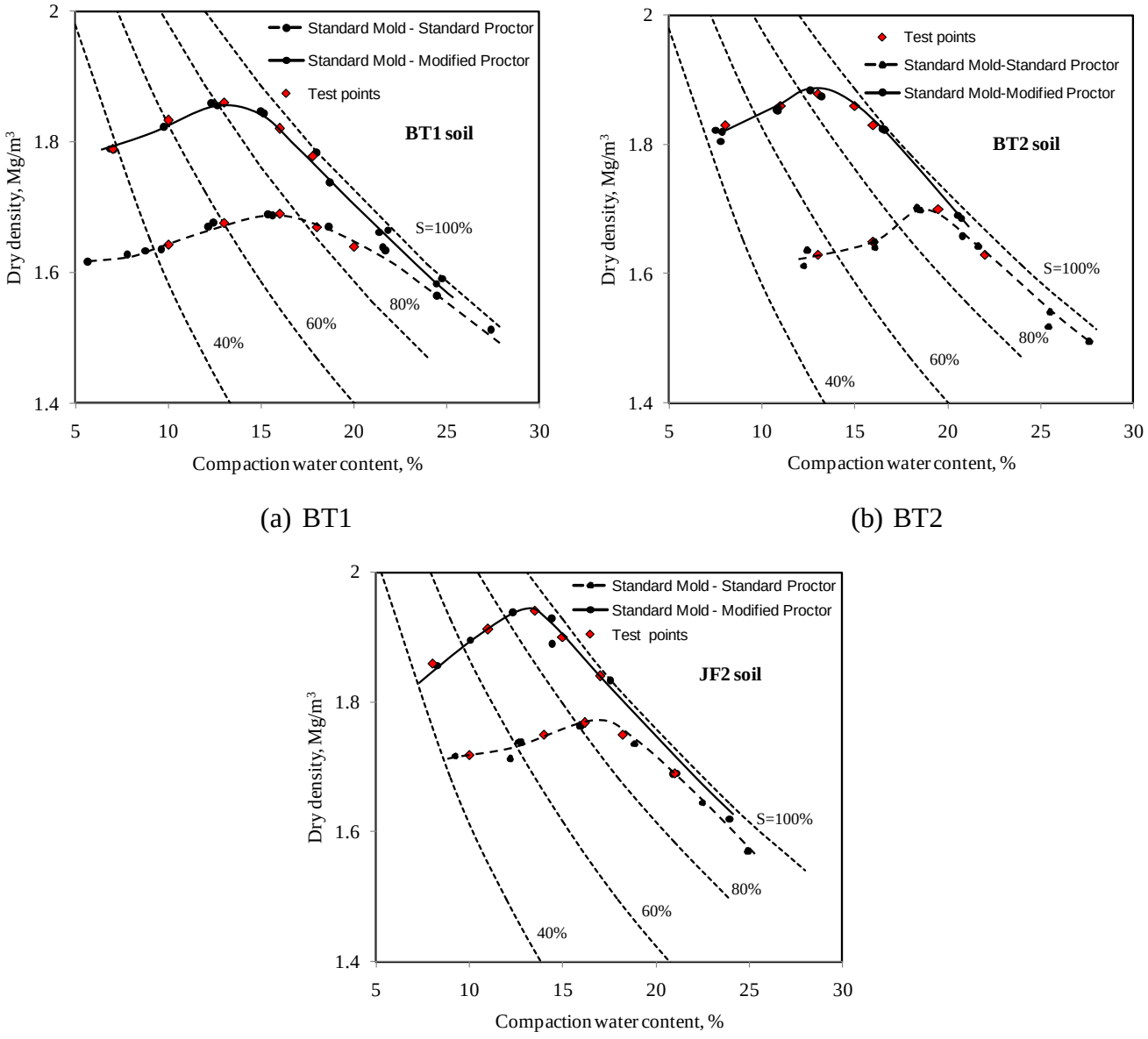

Figure 5.1: Moisture-density relationships for the soil studied together with the specific test points

Tables 5.1 , 5.2 and 5.3 show the notations of the test specimens together with their compaction water contents (w%), dry densities (ρ_d), degree of saturation (S) and the as-compacted suction values obtained from the filter paper method as described in Chapter 4. Only specimens compacted in the standard mould were used in the study of hydraulic properties of compacted soils as explained in Chapter 3.

Table 5.1: Properties of BT1 soil specimens whose hydraulic properties were studied

Notation BT1-	Compacted at	w%	ρ_d (Mg/m^3)	S	Suction (kPa)
STD-ASTM10	dry of optimum	10	1.64	0.44	1426
STD-ASTM13	dry of optimum	13	1.68	0.60	634
STD-ASTM16	optimum	16	1.69	0.76	282
STD-ASTM18	wet of optimum	18	1.67	0.82	152
STD-ASTM20	wet of optimum	20	1.64	0.87	88
MDF-ASTM7	dry of optimum	7	1.79	0.39	3450
MDF-ASTM10	dry of optimum	10	1.83	0.60	1630
MDF-ASTM13	optimum	13	1.86	0.83	770
MDF-ASTM16	wet of optimum	16	1.82	0.95	364
MDF-ASTM18	wet of optimum	18	1.78	0.98	232

Table 5.2: Properties of BT2 soil specimens whose hydraulic properties were studied

Notation BT2-	Compacted at	w%	ρ_d (Mg/m^3)	S	Suction (kPa)
STD-ASTM13	dry of optimum	13	1.63	0.56	848
STD-ASTM16	dry of optimum	16	1.65	0.71	345
STD-ASTM19.5	optimum	19.5	1.70	0.94	121
STD-ASTM22	wet of optimum	22	1.63	0.94	57
MDF-ASTM8	dry of optimum	8	1.83	0.48	1579
MDF-ASTM11	dry of optimum	11	1.86	0.70	920
MDF-ASTM13	optimum	13	1.88	0.86	642
MDF-ASTM15	wet of optimum	15	1.86	0.95	473
MDF-ASTM16	wet of optimum	16	1.83	0.96	374

Table 5.3: Properties of JF2 soil specimens whose hydraulic properties were studied

Notation JF2-	Compacted at	w%	ρ_d (Mg/m^3)	S	Suction (kPa)
STD-ASTM10	dry of optimum	10	1.70	0.46	1066
STD-ASTM14	dry of optimum	14	1.76	0.70	392
STD-ASTM16	optimum	16	1.77	0.81	238
STD-ASTM18	wet of optimum	18	1.75	0.89	144
STD-ASTM21	wet of optimum	21	1.69	0.94	75
MDF-ASTM8	dry of optimum	8	1.86	0.47	1555
MDF-ASTM11	dry of optimum	11	1.91	0.71	970
MDF-ASTM13.5	optimum	13.5	1.94	0.92	545
MDF-ASTM15	wet of optimum	15	1.90	0.95	272
MDF-ASTM17	wet of optimum	17	1.84	0.97	67

5.3 Saturated Permeability

The procedure to measure saturated permeabilities of soil specimens using the flexible wall permeameter has been described in Chapter 3. One challenge that is encountered during the determination of saturated permeability in the flexible wall permeameter is the difficulty to saturate the specimens fully prior to measuring their permeabilities. This has been listed as common Mistake 2 by Chapuis (2017). In this study, as discussed in Chapter 3, it was desired to supply as little confinement to the specimen as possible in attempt to represent a surface soil with close to zero confinement. In order to ensure specimens were saturated, upward flow was used in the falling-head test. As already discussed in Chapter 3, several runs of upward flow falling head test were made for each specimen. For each run, the burette was refilled with water and the timer re-set. A k_s value was calculated for each run using Equation 5.1.The measurement was repeated until the k_s values were near constant or constant with subsequent runs. Consequently, either the constant k_s value or average of the near constant k_s value was recorded as the saturated permeability of the specimen. Appendix B1 shows the plots for the different runs for each specimen as well as the variation of k_s with the run number.

At the end of each test, the dimensions and weight of the specimens were re-measured and moisture contents determined in order to establish the degree of saturation at the end of the test. All samples registered degrees of saturation in the range of 98 to 115%. The upper value of the degree of saturation is outside the expectation of ASTM D5084-16a which envisages a range of 95 to 105%. The discrepancy is attributed to measurement errors in the volume.

$$\log h_t = \log h_0 - \frac{Akt}{2.303aL} \tag{5.1}$$

where h_t is the hydraulic head at time t while h_0 is the original hydraulic head (t=0). All hydraulic heads are referenced to the tail water as datum.

5.3.1 Variation of k_s with compaction water content

Figure 5.2 shows the variation of k_s with compaction water content. It is generally observed that the saturated permeability reduces with increase in compaction water content irrespective of the compactive effort (Bjerrum and Huder, 1957; Lambe, 1958; Mitchell et al., 1966). For this study, the permeability decreases by an order from the dry to wet of optimum for BT soils but JF2 soils tend to have the same order of permeability from the dry to wet of optimum. The decrease in permeability with increase in compaction water content is attributed to the difference in soil structure between the dry and wet of optimum. On the dry of optimum, the soil has a more random and open (flocculated) structure hence presence of large voids that allow for higher permeation of the water. On the wet of optimum, the soil has a parallel (dispersed) structure which impedes flow hence lower permeability. Leong and Rahardjo (2002) performed similar tests on compacted soils from the Jurong Formation of Singapore and obtained similar results to those reported for the JF2 soils.

With different compaction effort, the specimens compacted at standard Proctor effort generally have higher permeability than those compacted at modified Proctor effort owing to smaller pore sizes of the soil specimens compacted at modified Proctor effort.

5.3.2 Variation of k_s with void ratio

Figure 5.3 shows plots of k_s versus void ratio for both the dry and wet of optimum specimens. It is observed that the relationship between k_s and void ratio differs for samples compacted dry and wet of optimum. Leong and Rahardjo (2002) have attributed this behavior to the differences in pore size distribution on the dry and wet of optimum.

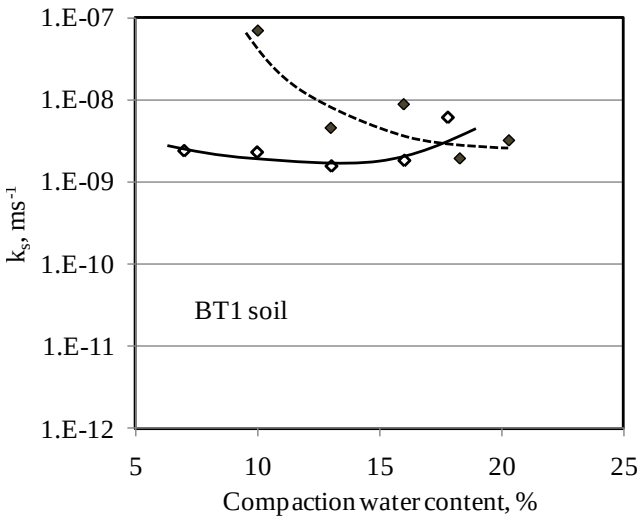

(a) BT1

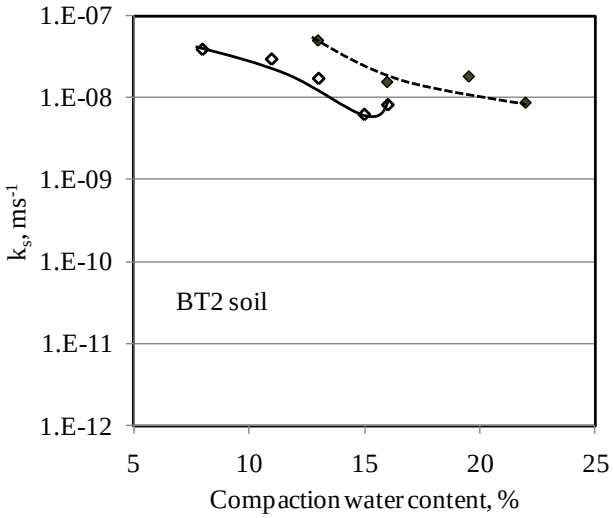

(b) BT2

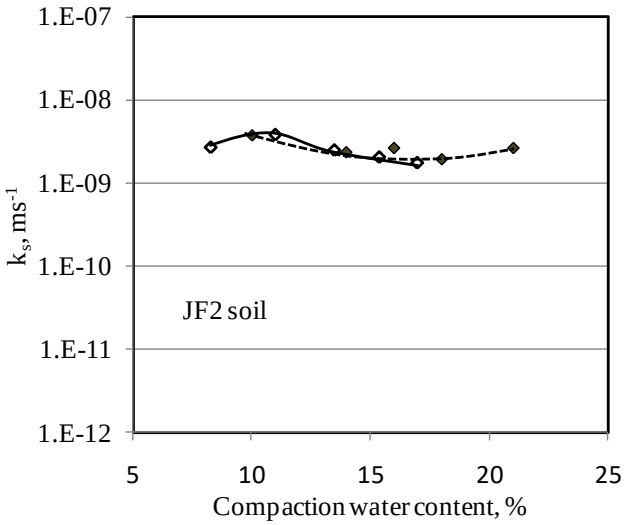

(c) JF2

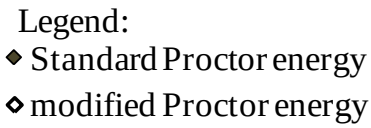

Figure 5.2: Variation of k_s with compaction water content

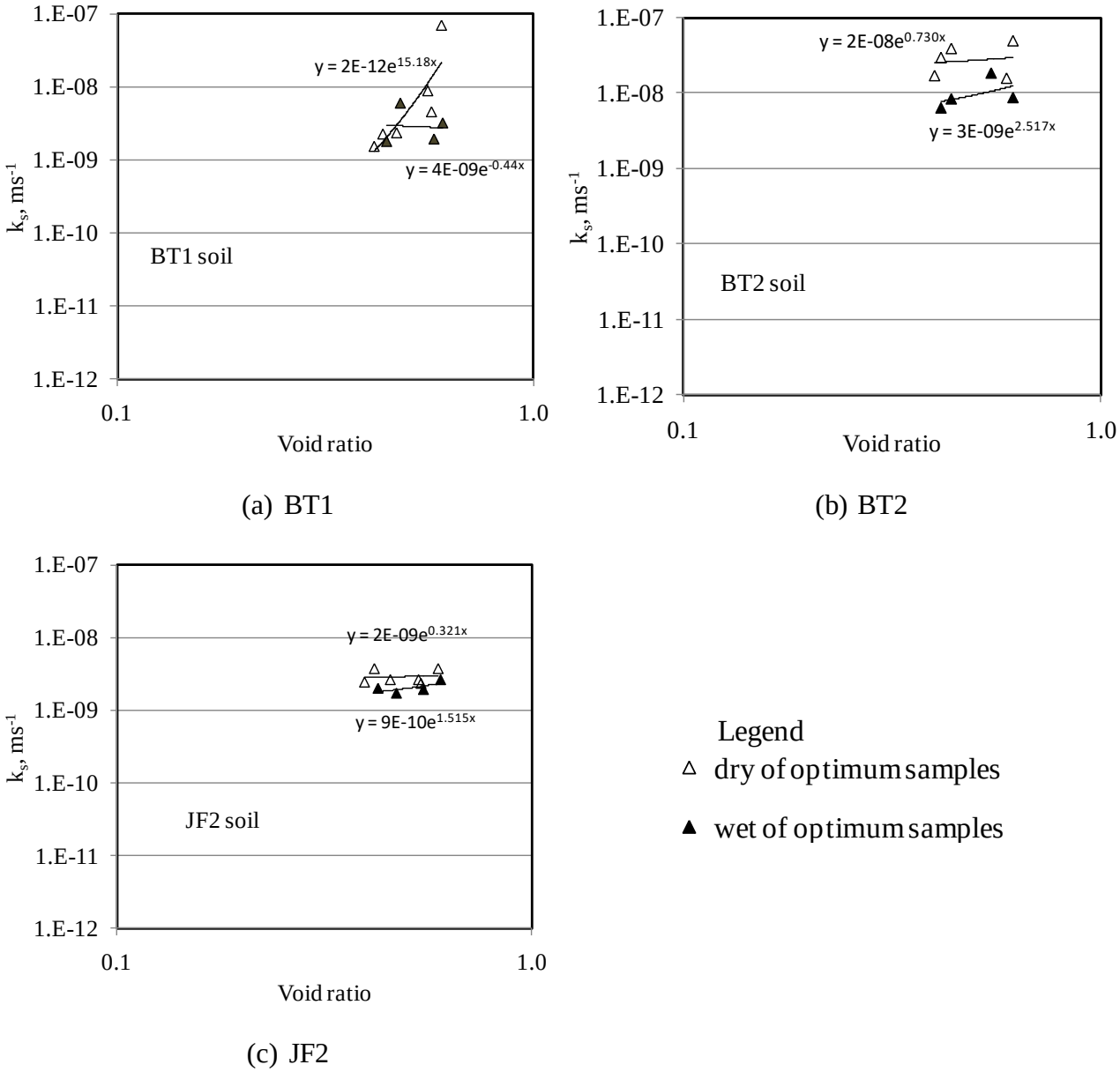

Figure 5.3: Variation of ks with void ratio

5.4 Infiltration tests using a mini-disk infiltrometer.

5.4.1 Infiltration rates

As discussed in Chapter 2, in order to estimate the near saturation permeability using a mini-disk infiltrometer, the cumulative infiltration from the infiltrometer test was fitted with Philip (1957)

two-parameter equation given in Equation 2.36 in Chapter 2. Some of the plots of cumulative infiltration versus square root of time for three suction heads studied (1, 2 and 5cm) are presented in Figures 5.4 and 5.5 for BT2 and JF2 soils. More of such plots are given in Appendix B2. The fitted equations to the measured cumulative infiltration in Figures 5.4 and 5.5 as well as plots in Appendix B2 are all second order quadratic functions. The equations are presented in Appendix B3. Also included in the Tables in Appendix B3, are the R^2 values to indicate the goodness of fit to the measured data. The R^2 values are all above 0.98 indicating very good fits.

In this study, solutions of Equation 2.36 suggested by Zhang (1997) were used to study the measured data. As shown in Equation 2.38, these solutions solve for sorptivity using constant C_1 and permeability using C_2. As this study focuses on permeability, only the solution associated with permeability i.e one using C_2 will be considered. The solution linked to permeability is reproduced in Equation 5.2.

$$C_2(h) = A_2 K(h) \tag{5.2}$$

where A_2 is a dimensionless coefficient, h is the suction head of the test, K(h) is the permeability which is a function of the suction head

As discussed in Chapter 2, Zhang (1997) suggested empirical relationships for coefficient A_2 given Equation 2.40.

For n<1.35, Dohnal et al. (2010), suggested a modification to Equation 2.40, which given in Equation 2.41.

5.4.1.1 Effect of suction head on infiltration

As discussed earlier, three suction heads: 1, 2 and 5 cm were used in the study. Generally the infiltration is fastest at 1 cm and slowest at 5 cm irrespective of the compaction effort used as shown in Figures 5.4 and 5.5 as well as Appendix B2. The rate of infiltration depends on the difference between the suction at the disk and the suction at the soil surface. At h= -1 cm, the hydraulic head difference is largest hence the highest infiltration rate.

Because the suction heads are really small and close, the infiltration rates at the three suction heads can be very close. BT2 soils generally recorded the highest infiltration rates and JF2 the slowest. Since BT is a granite derivative and JF, generally a clay, this observation is not surprising.

5.4.1.2 Effect of compaction water content on infiltration

The effect of compaction water content on infiltration can be observed in Figures 5.3 and 5.4 as well as Appendix B2. In Figures 5.4 and 5.5, the specimens are identified as either being on the dry of optimum or wet of optimum for BT2 and JF2 soils. It is observed that the infiltration rates are much higher for specimens on the dry optimum. The dry of optimum specimens have higher suctions than the wet of optimum specimens as shown in Tables 5.1, 5.2 and 5.3. This implies that the hydraulic head difference between the dry of optimum specimens and the suction imposed at the infiltrometer disk is always highest for dry of optimum specimens hence higher rate of flow into the specimens.

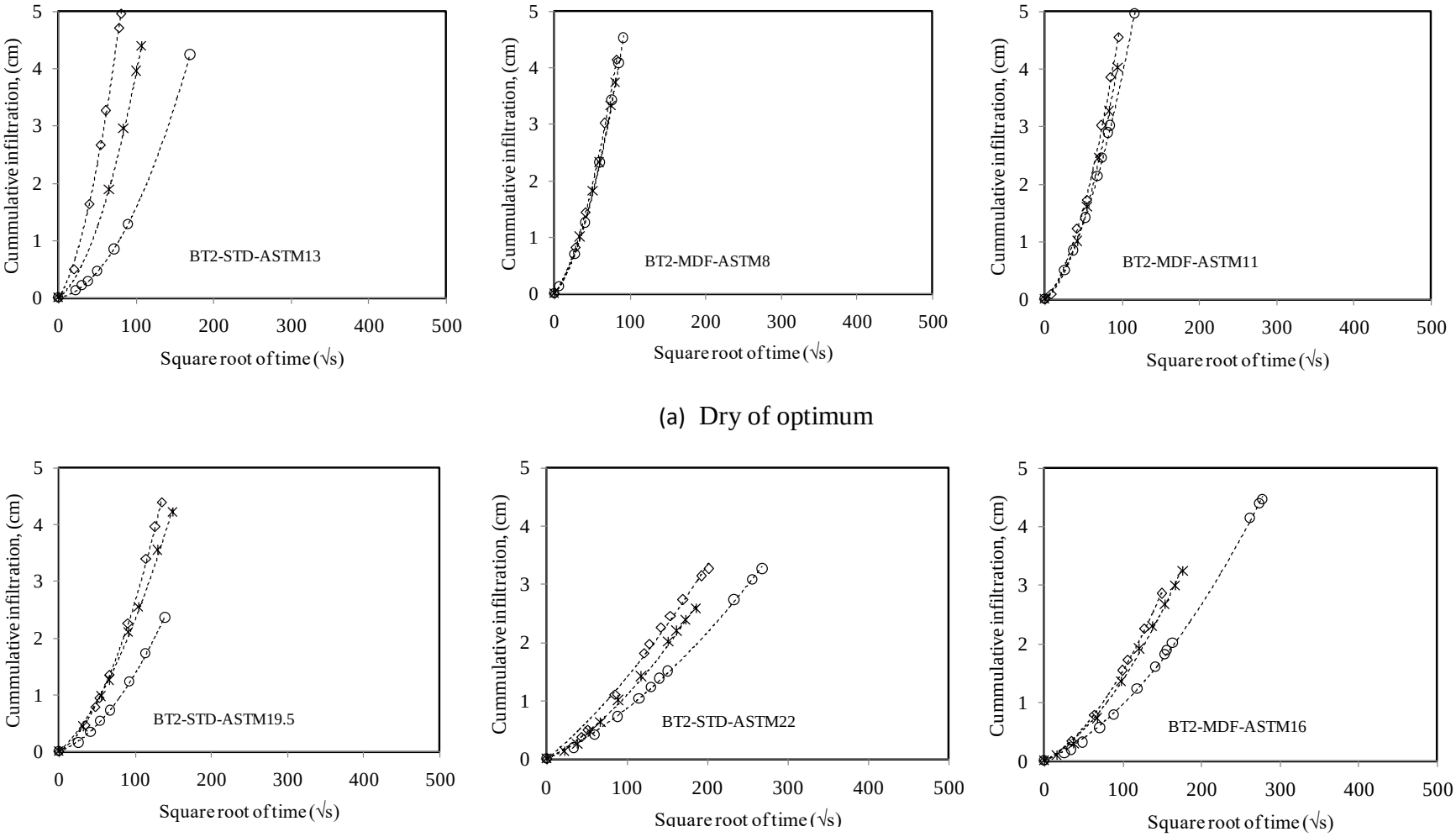

Figure 5.4: Cumulative infiltration vs square root time at three suction heads for selected BT2 soil specimens

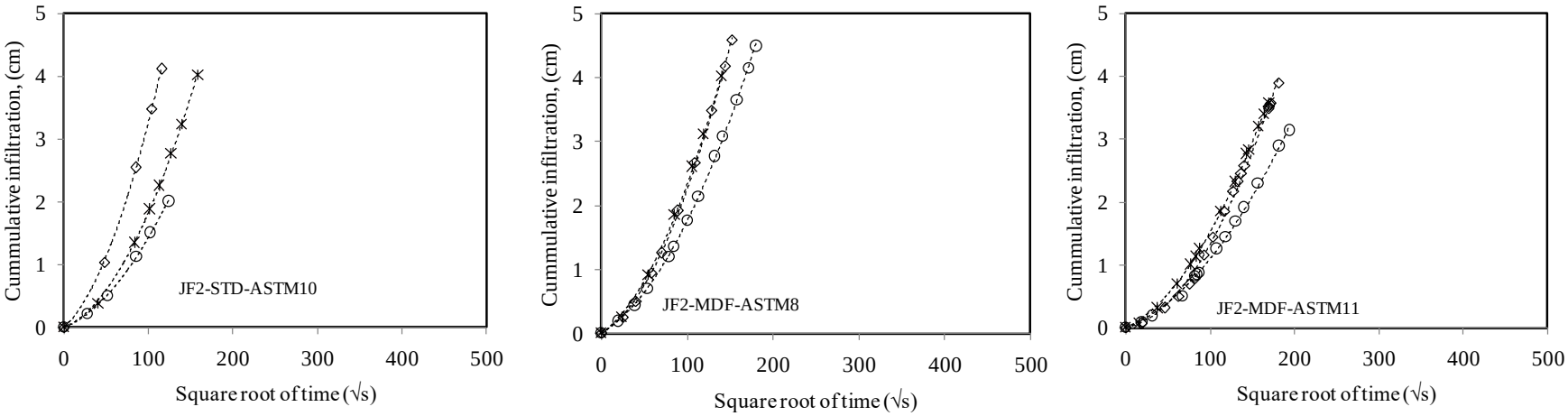

(a) Dry of optimum

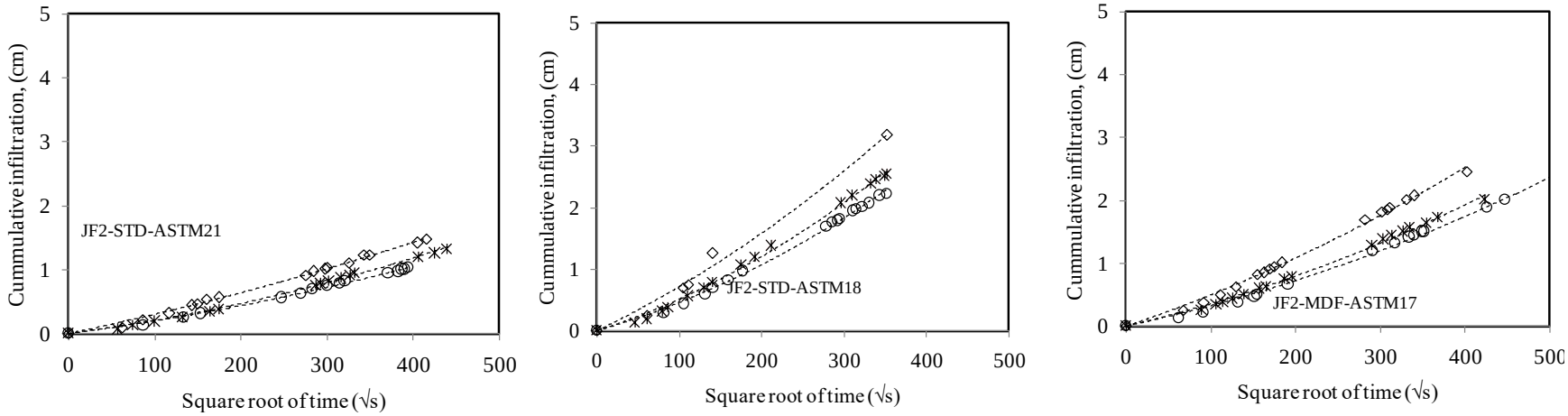

(b) Wet of optimum

Figure 5.5: Cumulative infiltration vs square root time at three suction heads for selected JF2 soil specimens

In addition to suction, two other factors were examined, soil structure and void ratio. As the compaction water content increases, the soil structure varies from a flocculated system to a dispersed system. The dispersed soil structure reduces the available void space for water infiltration leading to long duration of ponding on the soil surface. The flocculated structure typical of dry of optimum specimens has been described to have a dual porosity structure (Ahmed et al., 1974; Delage et al., 1996).It would therefore be expected that the macropores between the clods on the dry of optimum provide preferential paths for infiltration. However, Clothier and White (1981) note that since disk infiltrometers supply only a small tension at the soil surface, the effects of macropores on the infiltration are eliminated thus ensuring that infiltration is only influenced by the properties of the soil matrix. With the elimination of macroporosity, the remaining influencing factors to infiltration are microstruture and soil suction. Mitchell (1976) defines microstructure as the elementary particle association within the soil while macrostructure refers to the arrangement of the soil aggregates.

A further study on the influence of compaction water content is shown in Figures 5.6 and 5.7 and Appendix B4A in which the infiltration rates are studied for different compaction water contents at given suction heads for both specimens compacted at both standard and modified Proctor efforts . Plots for BT1 soil specimens are shown in Figure 5.6 while Figure 5.7 shows plots for JF2 soil specimens. The plots for BT2 soil specimens are shown in Appendix B4A. It is observed that for all the three suction heads, infiltration reduces with increase in compaction water content irrespective of the compaction effort.

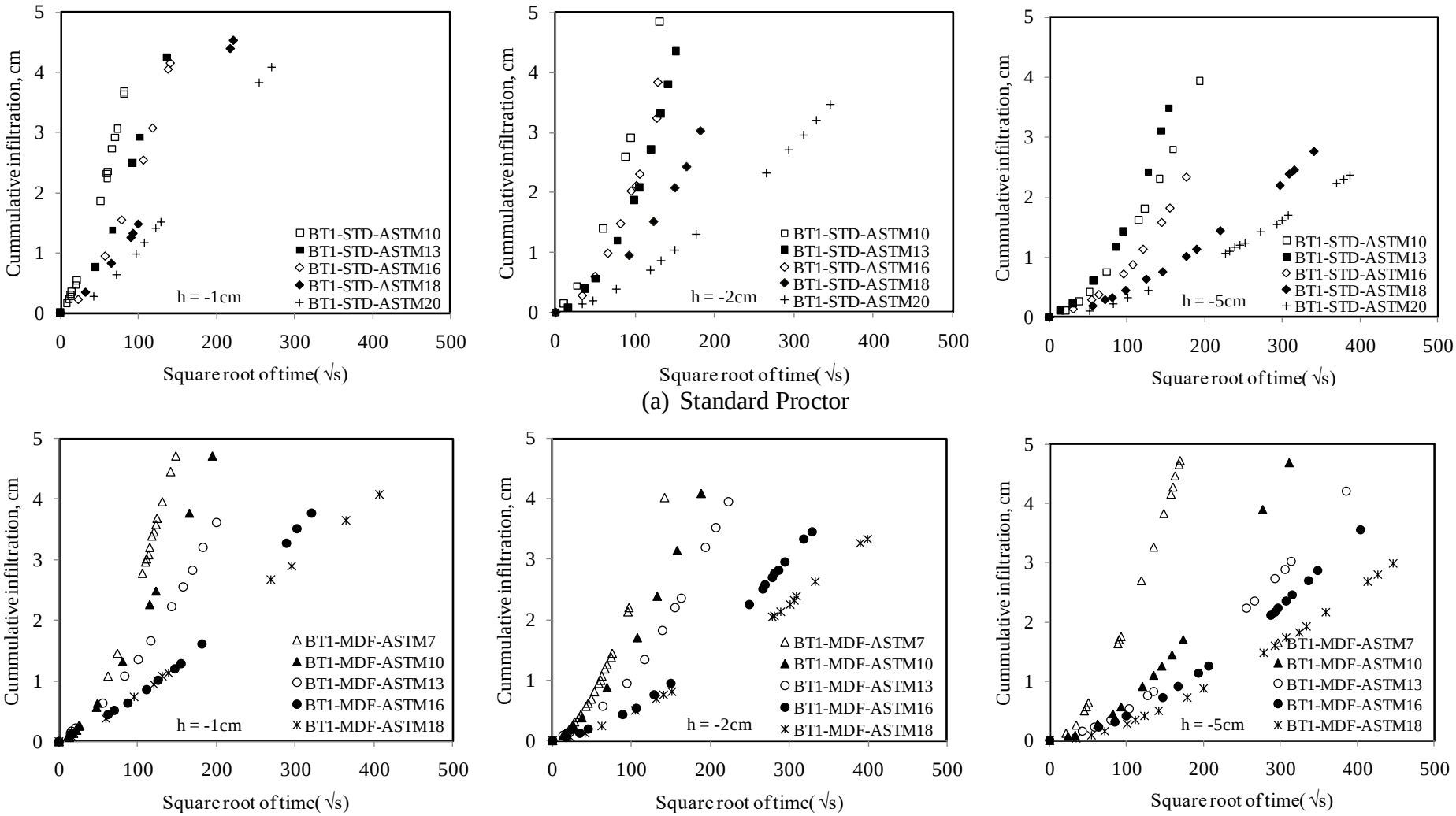

Figure 5.6: Comparison of infiltration rates for different compaction water contents at given suction heads for BT1 soils compacted at standard and modified Proctor efforts

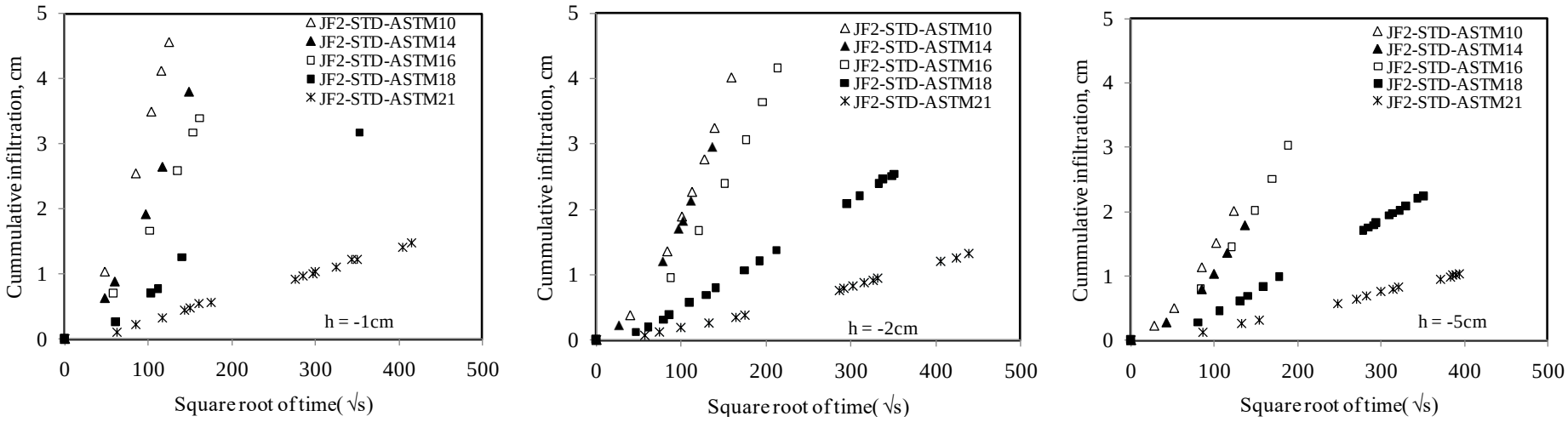

(a) Standard Proctor

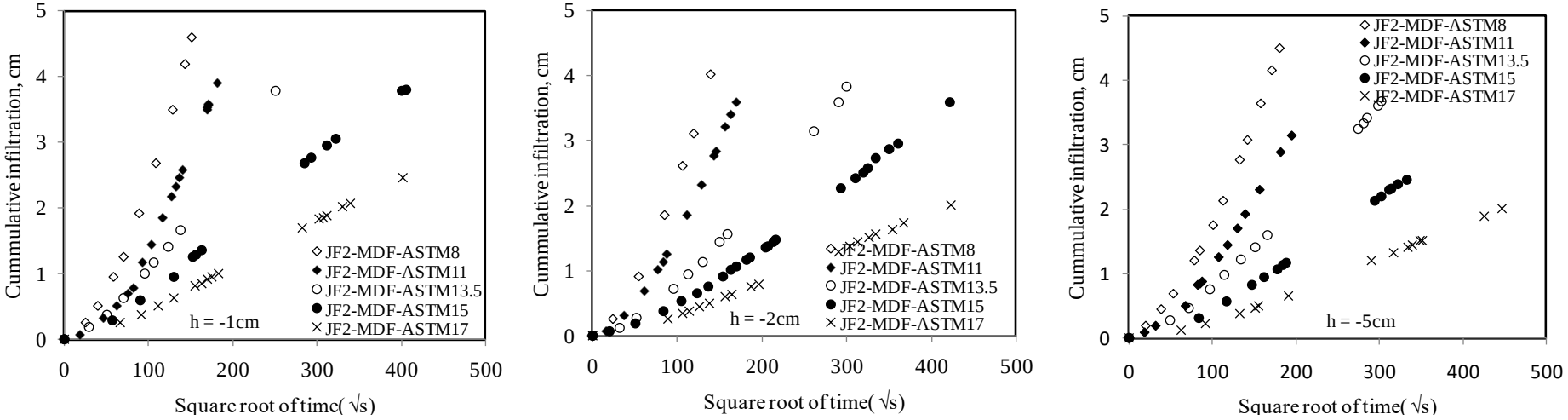

(b) Modified Proctor

Figure 5.7: Comparison of infiltration rates for different compaction water contents at given suction heads for JF2 soils compacted at standard and modified Proctor efforts.

5.4.1.3 Effect of compaction effort on infiltration

In order to examine the influence of compaction effort on the infiltration, data at the different suction heads are plotted for specimens compacted at the standard and modified Proctor efforts as shown in Figure 5.8 and Appendix B4B. Similarly, three factors are at play; the soil suction, soil structure and void ratio. The influence of compaction effort is not distinct. Figure 5.8 and plots in Appendix B4B show clusters for specimens compacted dry of optimum and wet of optimum irrespective of compaction effort. This indicates that suction overrides void ratio in influencing infiltration into the compacted specimens. The specimens compacted dry of optimum have higher infiltration rates than those specimens compacted on the wet of optimum.

The influence of void ratio is more glaring by comparing the infiltration of the three soils. The clayey JF2 soil specimens (CL) have the lowest infiltration rates because of the greater tendency to pack more densely at the same compaction effort. The coarser BT2 has the highest infiltration rate.

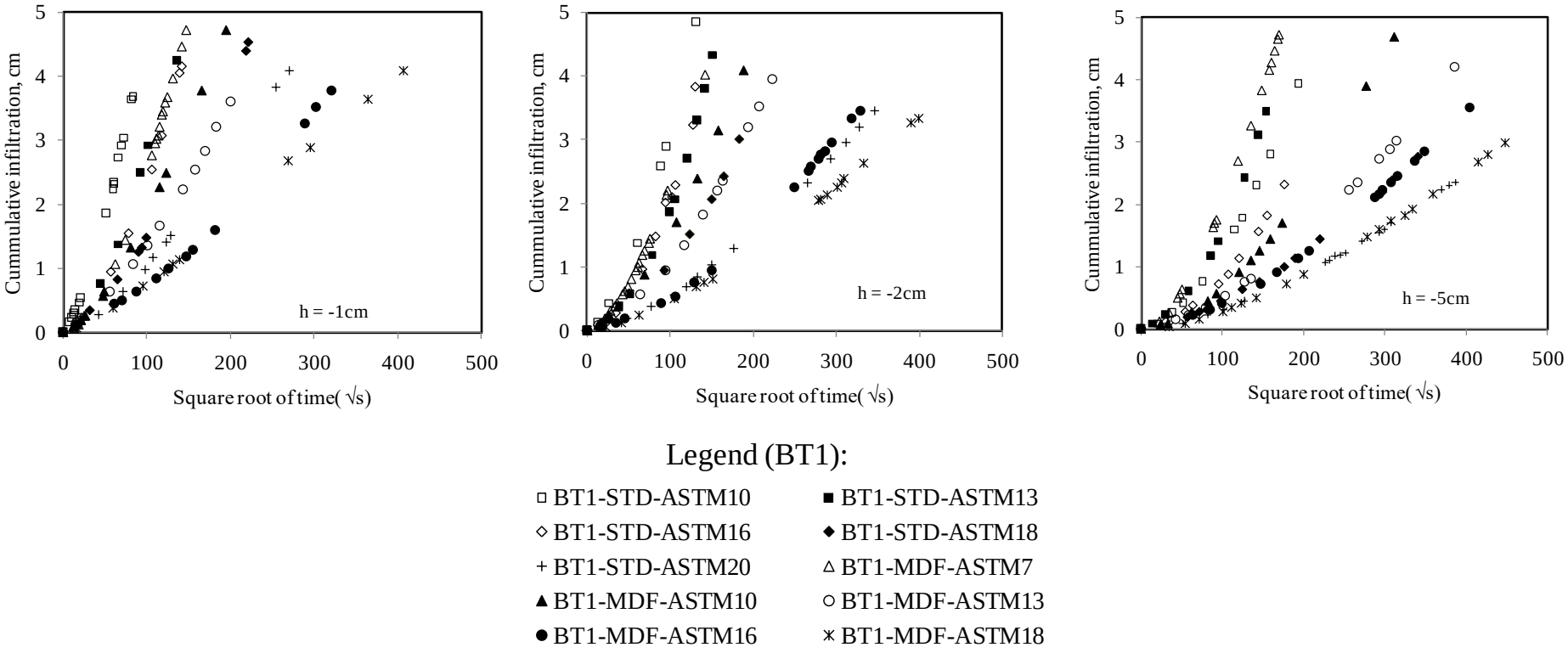

Figure 5.8: Comparison of infiltration rates for different water compaction water contents at given suction heads for both standard and modified Proctor energies for BT1 soil specimens

5.4.2 Estimation of near saturated permeability using infiltration measurements

5.4.2.1 Case studies for parameter A_2

Parameter A_2 in Equation 5.2 can be evaluated using different methods as discussed in Chapter 2, four cases have been evaluated as stated below:

Case 1: The VG SWCC parameters n and α used in the computation of A_2 in Equation 2.40 were obtained by curve fitting the SWCC of the specimen using the VG SWCC equation as shown in Equation 2.42. For cases where n<1.35, Equation 2.41 suggested by Dohnal et al. (2010) was used in the computation of A_2

Case 2: A_2 is evaluated using n and α values suggested by Carsel and Parrish (1988) for different soil textural classes given in Table 2.4 in Chapter 2.

Case 3: A_2 is evaluated with a modification in Carsel and Parrish (1988)'s α parameter. The α parameter suggested by Carsel and Parrish (1988) was reduced by a factor of 100. The justification for this reduction is discussed in section 5.4.2.2.

Case 4: If n<1.35 according to Carsel and Parrish (1988), Equation 2.41 as suggested by Dohnal et al. (2010) was used to evaluate A_2. This case is motivated by the fact that Dohnal et al. (2010) correction was later than Carsel and Parrish (1988).

In order to use Carsel and Parrish (1988) values of n and α, the study materials had to be classified according to the United States Department of Agriculture (USDA) soil textural triangle. Soils BT1 and JF2 were classified as clay loam while soil BT2 was classified as loam. Therefore with this textural classification, it is possible to apply n and α suggested by Carsel and

Parrish (1988) in Table 2.4. According to Carsel and Parrish (1988), loam has n>1.35 hence Case 4 is not applicable to soil BT2.

Appendix B5 gives a summary of the A_2 values evaluated for the different cases at the different suction heads.

Table 5.4: Summary of C_2 coefficientsfor the different soil specimens at the different suction heads

BT1 soil sets	Suction head, cm		
	-1	-2	-5
	C_2 (ms^{-1})	C_2 (ms^{-1})	C_2 (ms^{-1})
STD-ASTM10	3.E-04	2.E-04	9.E-05
STD-ASTM13	1.E-04	2.E-04	1.E-04
STD-ASTM16	2.E-04	2.E-04	7.E-05
STD-ASTM18	5.E-05	7.E-05	2.E-05
STD-ASTM20	3.E-05	2.E-05	1.E-05
MDF-ASTM7	2.E-04	1.E-04	1.E-04
MDF-ASTM10	7.E-05	8.E-05	4.E-05
MDF-ASTM13	5.E-05	6.E-05	2.E-05
MDF-ASTM16	2.E-05	2.E-05	1.E-05
MDF-ASTM18	7.E-06	1.E-05	1.E-05

BT2 soil sets	Suction head, cm		
	-1	-2	-5
	C_2 (ms^{-1})	C_2 (ms^{-1})	C_2 (ms^{-1})
STD-ASTM13	5.E-06	3.E-06	1.E-06
STD-ASTM16	3.E-06	3.E-06	2.E-06
STD-ASTM19.5	2.E-06	1.E-06	9.E-07
STD-ASTM22	3.E-07	4.E-07	2.E-07
MDF-ASTM8	4.E-06	4.E-06	4.E-06
MDF-ASTM11	4.E-06	4.E-06	2.E-06
MDF-ASTM13	2.E-06	2.E-06	2.E-06
MDF-ASTM15	9.E-08	1.E-07	1.E-07
MDF-ASTM16	8.E-07	6.E-07	3.E-07

JF2 soil sets	Suction head, cm		
	-1	-2	-5
	C_2 (ms^{-1})	C_2 (ms^{-1})	C_2 (ms^{-1})
STD-ASTM10	2.E-04	1.E-04	9.E-05
STD-ASTM14	1.E-04	1.E-04	7.E-05
STD-ASTM16	8.E-05	6.E-05	6.E-05
STD-ASTM18	5.E-06	6.E-06	6.E-06
STD-ASTM21	1.E-06	2.E-06	2.E-06
MDF-ASTM8	1.E-04	1.E-04	1.E-04
MDF-ASTM11	1.E-04	1.E-04	7.E-05
MDF-ASTM13.5	3.E-05	2.E-05	2.E-05
MDF-ASTM15	6.E-06	1.E-05	1.E-05
MDF-ASTM17	3.E-06	3.E-06	3.E-06

With the A_2 values obtained for the different cases, permeability values were computed using the C_2 coefficients at the different suction heads. The C_2 values are summarized in the sub-tables given as Table 5.4. The derived permeabilities for all the study cases are summarized in Appendix B6.

5.4.2.2Soil water characteristic curves (SWCC)

Soil water characteristic curves as determined in the laboratory were fitted with the VG model in Equation 2.42 to obtain the parameters n and α used for the computation of A_2 in Case 1. Unlike the usual practice of plotting the volumetric water content data against suction, the volumetric water contents were plotted against absolute suction heads (m). In order to convert the measured suctions to corresponding pressure heads, the suctions were divided by the unit weight of water, $9.81kN/m^3$. The SWCCs for cases 1, 2 and 3 are plotted. Typical plots are shown in Figure 5.9 and the rest are presented in Appendix B7.

The VG parameters for case 1 are also given in Appendix B7 including the sum of squared errors (SSE). For cases 2 and 3, the VG SWCC equation was fitted to the measured SWCC data using parameters suggested by Carsel and Parrish (1988) as given in Table 2.4. As mentioned earlier BT1 and JF2 are classified as clay loam while BT2 is a loam according to the USDA classification. In order to improve the fit, the α value suggested by Carsel and Parrish (1988) was divided by 100 hence the study Case 3 as stated above. Observing plots in Figure 5.9 and those in Appendix B7, case 1 gives the best fit to the measured SWCC data and case 2 gives the poorest fit. There is an observed improvement in the fit in case 3 implying that the α parameter suggested by Carsel and Parrish (1988) is generally large for the compacted materials studied. This is not surprising since Carsel and Parrish (1988) developed their parameters using natural soils which can be substantially different from the compacted soils.

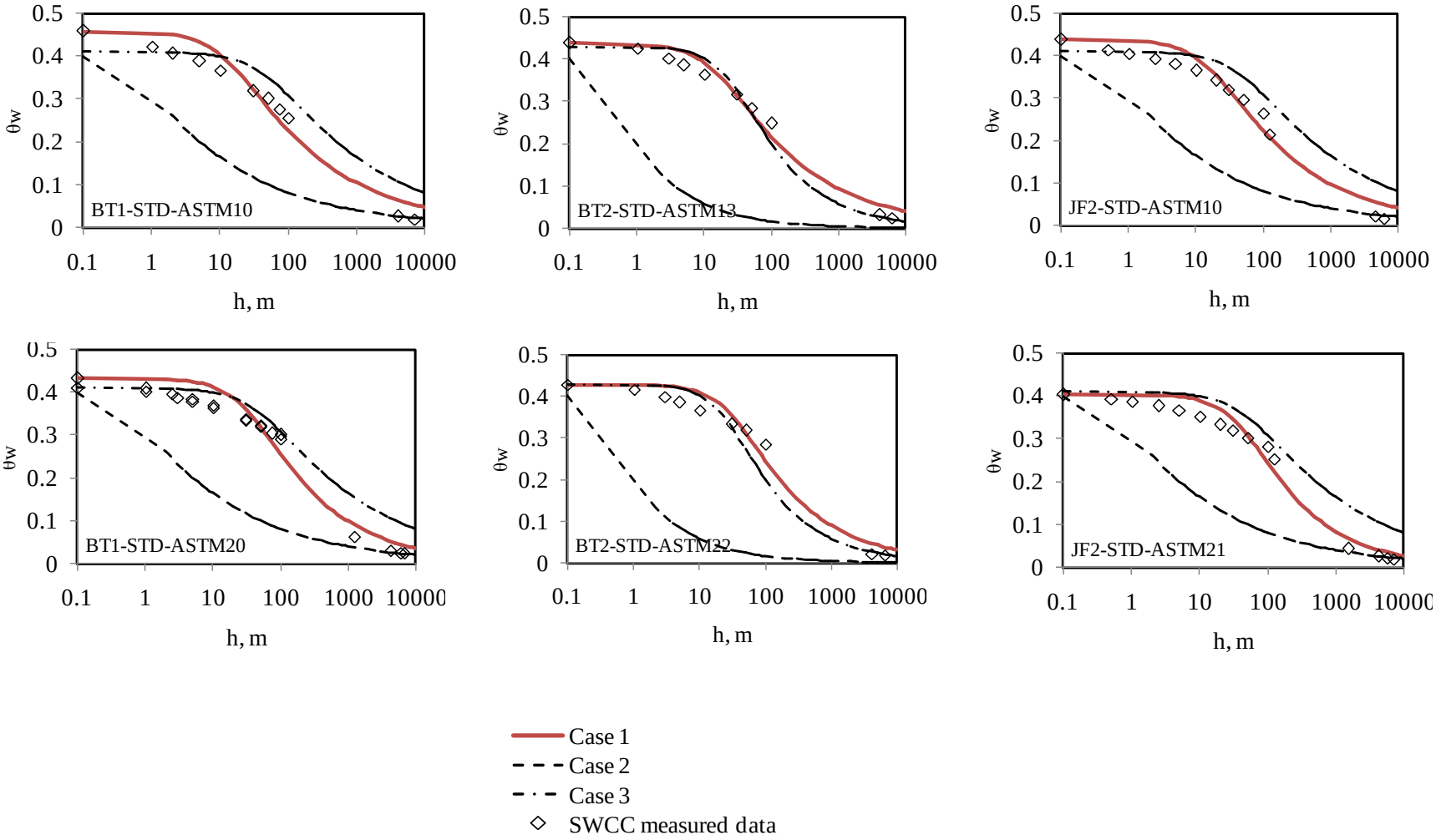

Figure 5.9: Typical SWCC plots for the Cases 1, 2 and 3

5.4.2.3 Comparison of permeabilities obtained from the falling head permeability test and mini-disk infiltrometer

The saturated permeability as measured by the flexible wall permeameter was compared with the near-saturated permeabilities measured using the mini-disk infiltrometer for Cases 1, 2, 3 and 4.The plots in Figure 5.10 show typical comparisons for selected BT2 and JF2 soil specimens. Other soil sets are presented in Appendix B8. The saturated permeability obtained from the falling head permeability test is plotted at suction head h=0 while the other permeabilties are plotted against the corresponding suction heads imposed on the disk during the test i.e., 1, 2, and 5 cm. Since the suction heads used in the study are small, very close to the saturated state (h=0), it is expected that the permeability values obtained using the infiltrometer should approximate the saturated permeability of the soil. To check the comparison, the permeabilities at suction heads 1, 2 and 5 cm for the different study cases were fitted with a straight line as shown in Figure 5.10 and Appendix B8. The intercepts of the straight lines on the vertical axis where h = 0 cm were read off as the estimation for saturated permeability for the different cases.

The estimated permeability k_{est} was normalized by the corresponding saturated permeability k_{sat} of the specimens. The ratio of k_{est}/ k_{sat} is plotted against compaction water contents as shown in Figures 5.11, 5.12 and 5.13 for BT1, BT2 and JF2 soils, respectively. It is observed that k_{est} for cases 1 and 3 compare best with the saturated permeability especially for soils compacted dry of optimum. Case 2 generally performs the worst indicating that the parameters suggested by Carisel and Parrish (1988) may not be suitable for compacted soils. This is shown by Case 3 where k_{est} substantially improves when the α value suggested by Carsel and Parrish (1988) is reduced by 100.

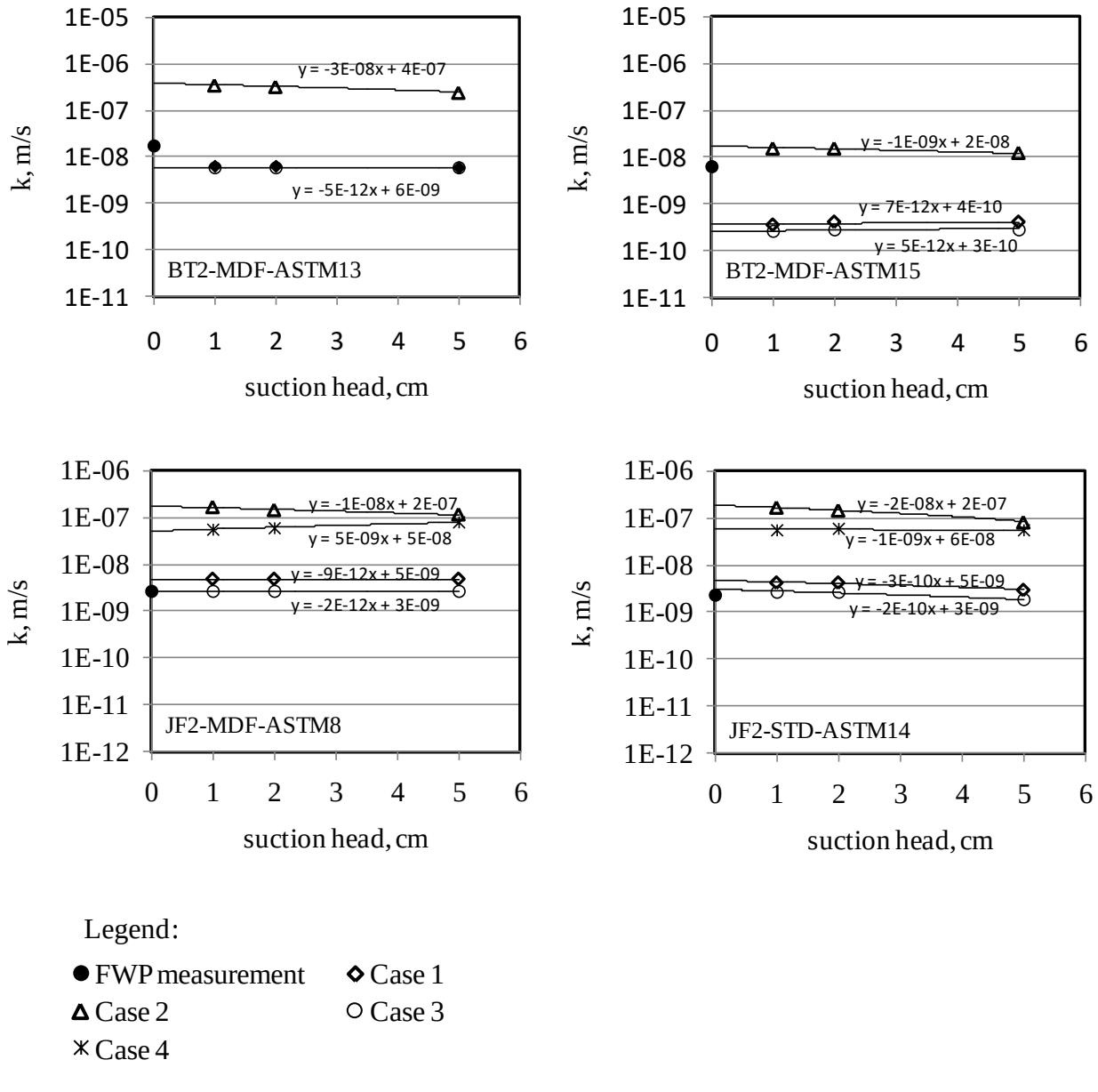

Figure 5.10: Comparison of permeabilities from FWP and the different study case

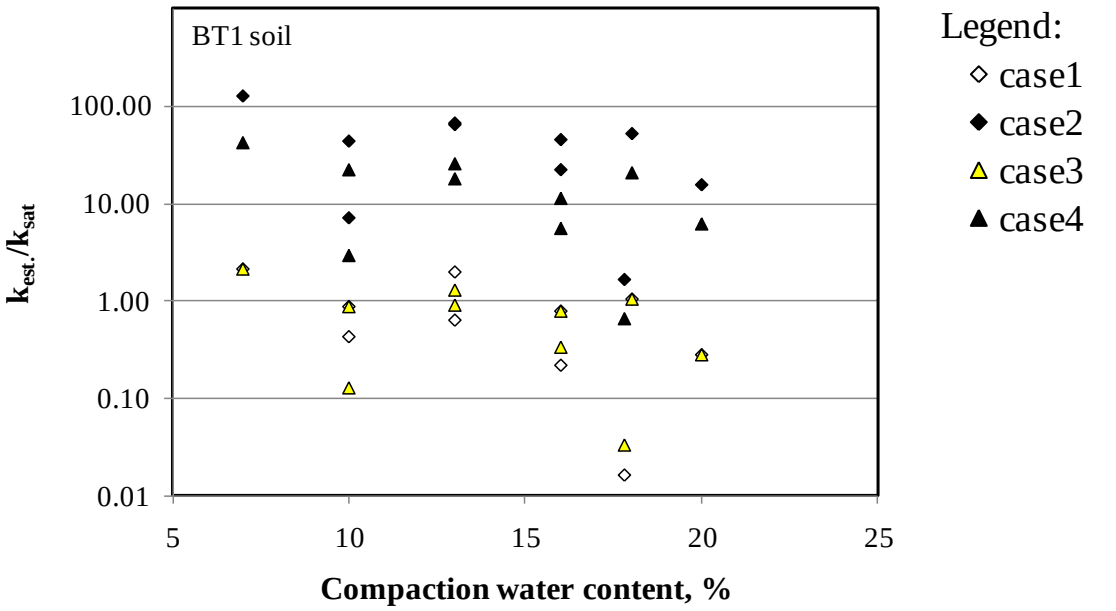

Figure 5.11: Comparison of saturated and estimated permeabilities for different cases for BT1 soil

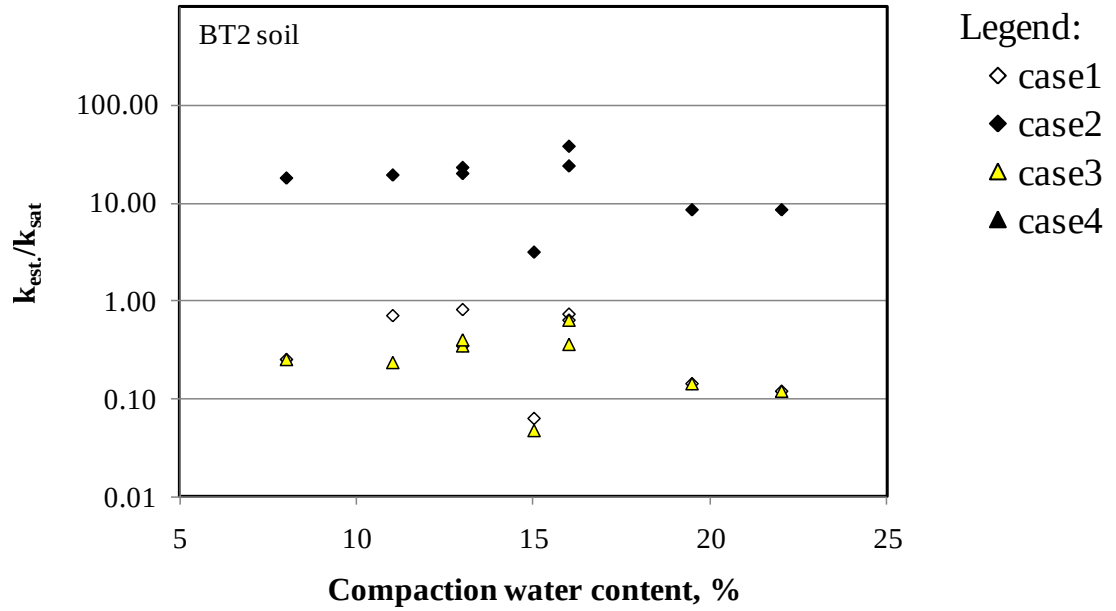

Figure 5.12: Comparison of saturated and estimated permeabilities for different cases for BT2 soil

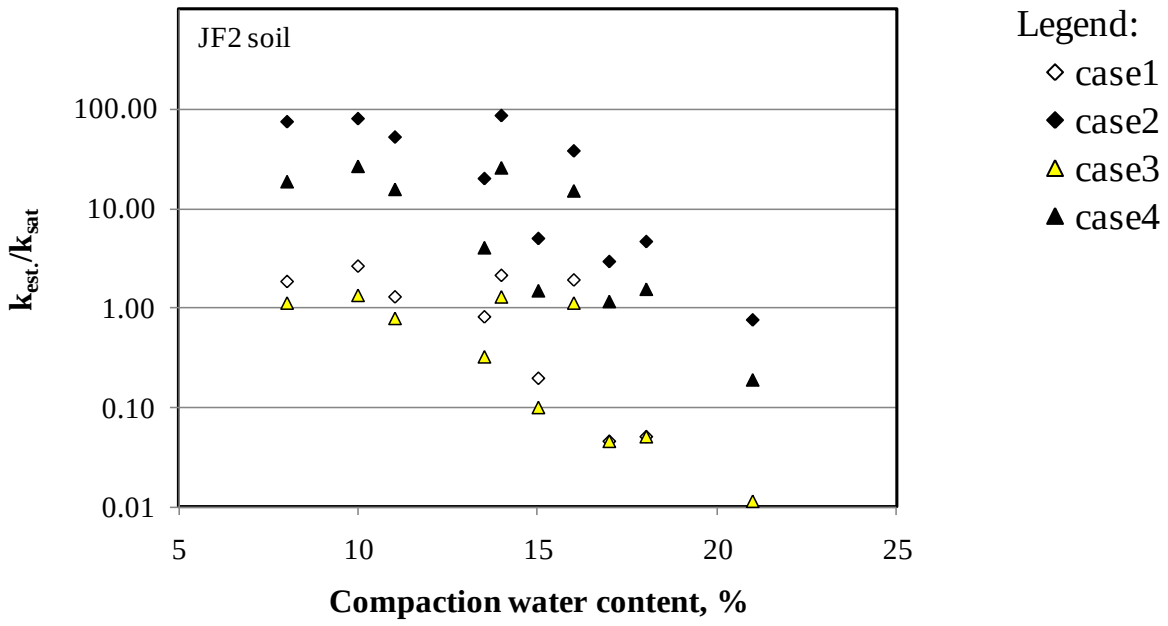

Figure 5.13: Comparison of saturated and estimated permeabilities for different cases for JF2 soil

Dohnal et al. (2010)'s correction applied in Case 4 improves the estimate of permeability using Carsel and Parrish (1988) parameters but only dismally. Infact the permeabilities remain at the same order. The estimates for cases 1 and 3 get worse as compaction water contents increases implying that the mini-disk infiltrometer is best suited for dry soils with rapid infiltration. In summary, all the estimates of permeability are within two orders of the saturated permeability which suggests acceptability of the disk infiltrometer test for estimating near saturated permeabilities of the compacted soils.

5.5 Statistical permeability model

As stated above, measurements of unsaturated permeability are quite tedious, time consuming, require expensive equipment and high level of expertise. It was against this background that indirect methods were formulated. One such method is the statistical model. As noted earlier, the statistical permeability model is quite rigorous and hence most reliable of all permeability

models (Leong and Rahardjo, 1997a). With a saturated permeability value, k_s, the permeability function can be estimated using a statistical model (Fredlund et al., 2012). In this work, since k_s (m/s) values have been determined from the flexible wall permeameter, an attempt was made to compute the permeability function for the different soil specimens in order to evaluate the various influences on the permeability function.

Figure 5.14 and 5.15 show the variation of relative permeability k_r with suction for the different soil specimens studied. At a given suction, the wet of optimum specimens have a higher k_r value than the dry of optimum specimens, a reflection of the structural differences as well as pore size distribution. Given the dispersed structure typical of wet of optimum specimens, desaturation is much slower and consequently the continuity of the water phase is retained much longer hence a higher k_r value. Also notable is that the permeability functions have a narrower band for specimens compacted at modified Proctor effort, a reflection of a more uniform pore size distribution and a more related structure. Mitchell et al. (1966) note that increased compaction effort leads to a more dispersed structure.

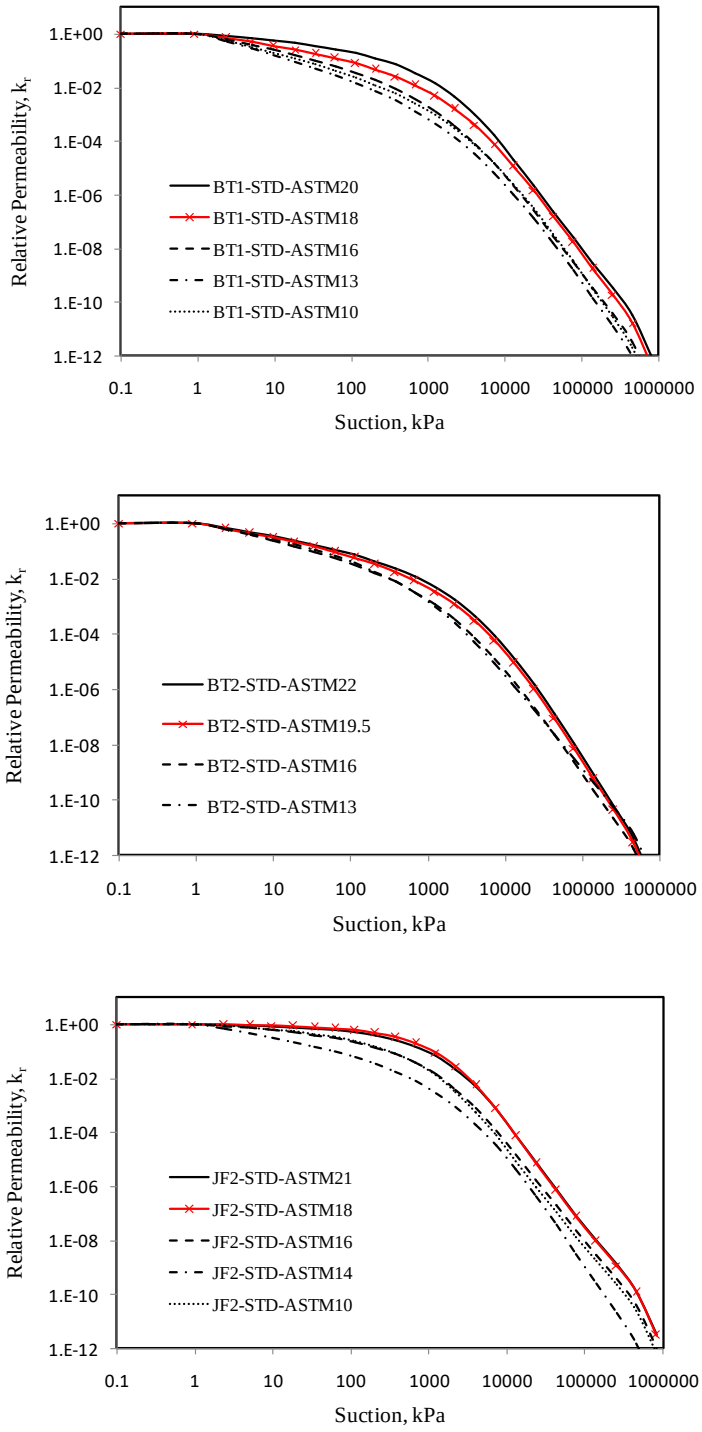

Figure 5.14: Variation of k_r with suction for soil specimens compacted at standard Proctor effort

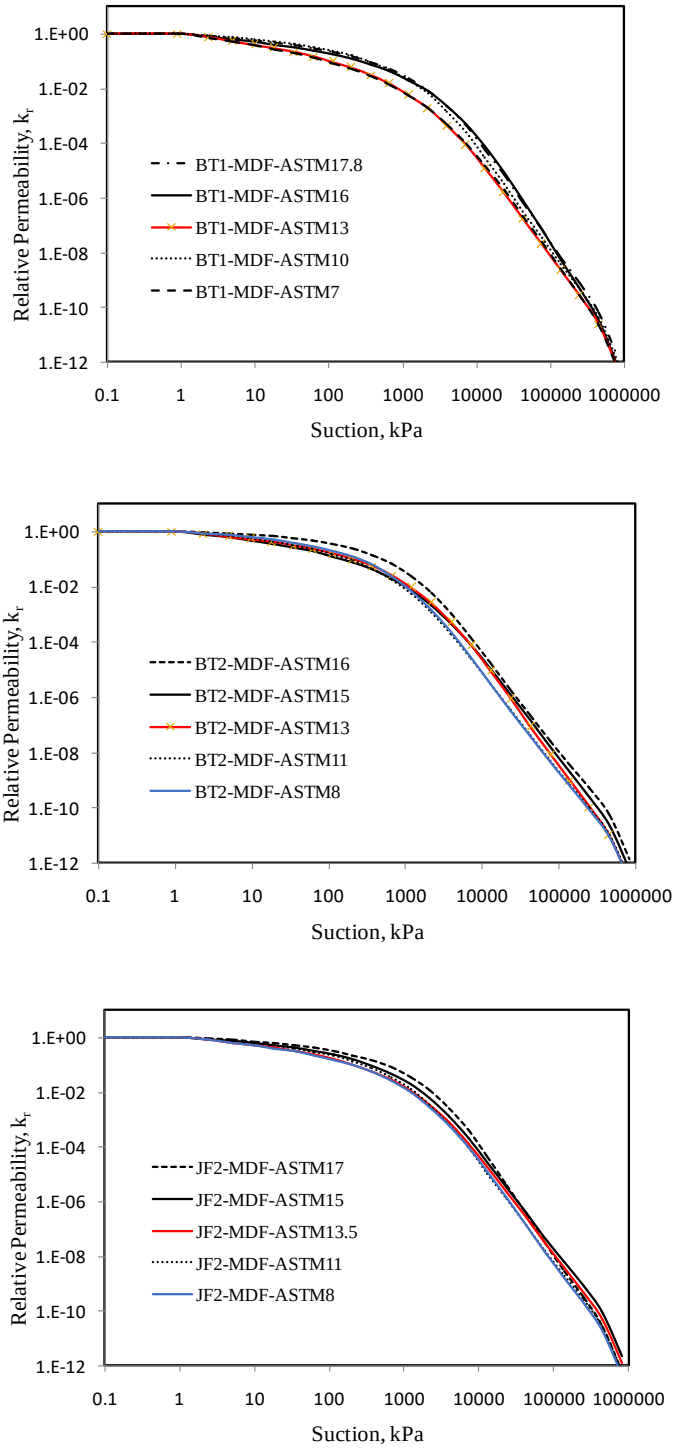

Figure 5.15: Variation of k_r with suction for soil specimens compacted at modified Proctor effort

5.6 Concluding remarks

The main aim of the chapter was to investigate the suitability of a mini-disk infiltrometer in measuring near-saturated permeabilities of soils. Three soils have been studied i.e., BT1, BT2 and JF2 compacted at both standard and modified Proctor efforts. Typical compacted specimens at different compaction water contents and different compaction efforts were selected for discussion in the chapter. Infiltration tests using a mini-disk infiltrometer were done on these specimens at suction heads of 1, 2 and 5 cm. In addition, the saturated permeability of each specimen was measured using a flexible wall permeameter. The saturated permeability from the flexible wall permeameter was used as a reference for the permeabilities measured from the mini-disk infiltrometer tests. Permeabilities from the mini-disk infiltrometer were studied using four cases and it was found that cases 1 and 3 gave the best estimates of near-saturated permeabilities from the mini-disk infiltrometer. However, all permeability estimates from the different cases were within two orders of difference from the saturated permeability. Considering that error in each type of permeability test is one order, it is not surprising when comparing the two different permeability measurements that the error can be up to two orders. This therefore indicates that the mini-disk infiltrometer can be very valuable in obtaining quick estimates of saturated permeabilities of soils.

More studies are recommended for wet soils to investigate possibilities of obtaining more reliable permeabilities of such soils using a mini-disk infiltrometer.

Chapter 6. Unconfined Compressive Strength and Tensile Strength of compacted soils

6.1 Introduction

Experimental studies (Cuisinier and Laloui, 2004, Koliji et al., 2006, Tarantino, 2011) have demonstrated that the structure of compacted soils evolves with changing mechanical or hydraulic regimes that the soils are subjected. It is also well documented that changes in climatic conditions affect the matric suction of unsaturated soils; decreasing during wetting and increasing during drying. With changes in both the structure and the matric suction of the soil, it is expected that strength, compressibility, and hydraulic conductivity of the soil will be affected.

Tensile strength determination is also increasingly becoming useful in studying effects of matric suction on the effects on the mechanical behavior of unsaturated soils and this can substantially reduce the testing time typical of suction-controlled tests (Akin and Likos, 2017). Piratheepan et al. (2012) have suggested a criterion of determining cohesion and internal friction angle for stabilized materials from unconfined compressive strength (UCS) and Brazilian tensile strength (BTS). This is useful because the UCS and BTS tests are easy to do, affordable and can be done in a really short time.

This chapter investigates the influence of matric suction, soil structure, and void ratio on the UCS and BTS of compacted soils using two test series. The first test series investigates the strength of the as-compacted soil specimens while the second test series studies the strength evolution of soil specimens compacted wet of optimum as it dries towards the dry of optimum water content as stated in Chapter 3. Through an evaluation of the changes in UCS and BTS, the

contribution of soil structure and matric suction are qualitatively assessed and discussed. Also, two tensile strength models are evaluated using the test results.

6.2 Test Series 1 - As-compacted soil specimens

As stated earlier, test series 1 involved testing as-compacted soil specimens. In this subsection, the test results of these specimens are presented and discussed. Figures 6.1 and 6.2, show test series 1 specimens on the standard Proctor (sP) and modified Proctor (mP) compaction curves.

Compacting of BT2 soil into the plastic mould was extremely difficult on the dry of optimum. Very often the specimen got stuck in the mould and split diametrically on opening the split mould. This may be attributed to the high sand content in the Bukit Timah Granite that generated tremendous friction between the plastic mould and the soil. Because of this difficulty, it proved difficult to compact specimens on the dry of optimum of the modified Proctor (mP) compaction curve as shown in Figure 6.1(b).

Tables 6.1, 6.2, 6.3 and 6.4 show the average water content and dry density of the specimens tested for test series 1 of each soil.

6.2.1 Stress- strain plots for UCS test

Figure 6.3 shows the stress-strain plots from UCS test for specimens compacted at both standard and modified Proctor efforts. In Figure 6.3, BT1 and JF2 are presented for illustration. Similar plots for BT2 and JF1 are presented in Appendix C1.

Irrespective of the compaction effort, the dry of optimum specimens show stiffer response during shearing. Figure 6.3 and Appendix C1 also show the axial strain at failure increases with compaction water content hence the specimens compacted on the dry of optimum show more brittle failure compared to specimens on the wet of optimum which are more ductile.

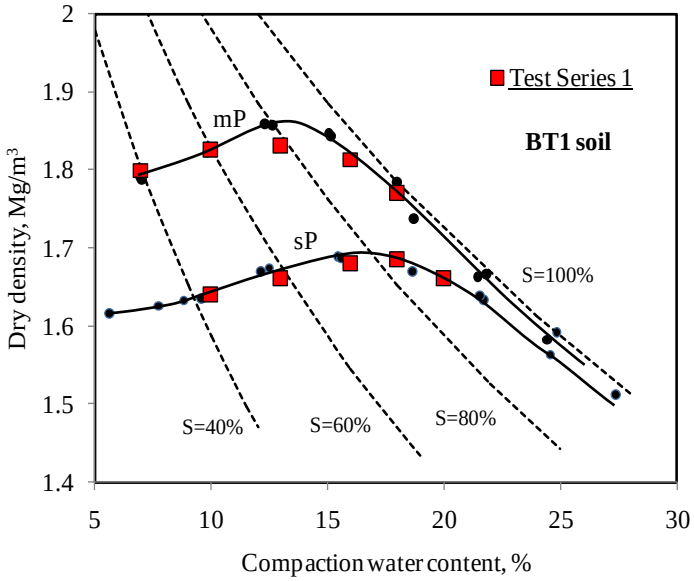

(a) BT1 soil

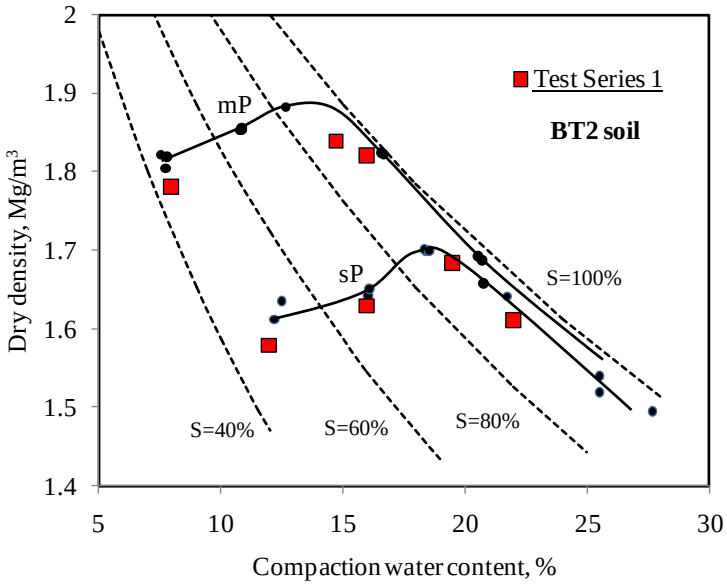

(b) BT2 soil

Figure 6.1: BT1 Test series 1 specimens

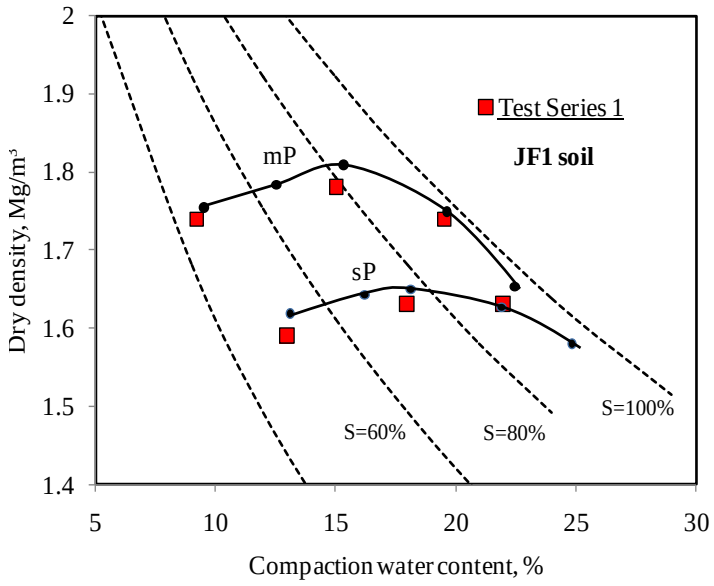

(a) JF1

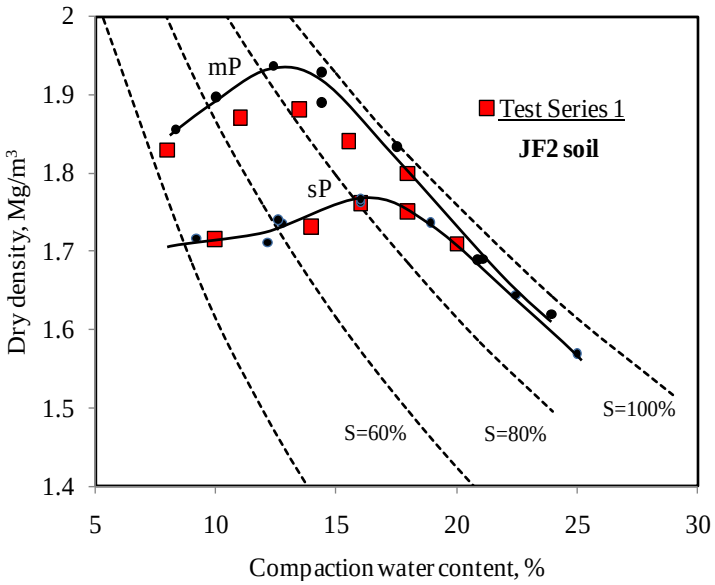

(b) JF2

Figure 6.2: JF Test series 1specimens

Table 6.1: Properties of BT1 test specimens

Notation BT1-	Compacted at	w%	ρ_d(Mg/m^3)
STD-PL10	dry of optimum	10	1.64
STD-PL13	dry of optimum	13	1.66
STD-PL16	optimum	16	1.68
STD-PL18	wet of optimum	18	1.69
STD-PL20	wet of optimum	20	1.66
MDF-PL7	dry of optimum	7	1.80
MDF-PL10	dry of optimum	10	1.83
MDF-PL13	optimum	13	1.83
MDF-PL16	wet of optimum	16	1.81
MDF-PL18	wet of optimum	18	1.77

Table 6.2: Properties of BT2 test specimens

Notation BT2-	Compacted at	w%	ρ_d(Mg/m^3)
STD-PL12	dry of optimum	12.0	1.58
STD-PL16	dry of optimum	16.0	1.63
STD-PL19.5	wet optimum	19.5	1.68
STD-PL22	wet of optimum	22.0	1.61
MDF-PL8	dry of optimum	8.0	1.78
MDF-PL15	wet of optimum	15.0	1.84
MDF-PL16	wet of optimum	16.0	1.82

Table 6.3: Properties of JF1 test specimens

Notation JF1-	Compacted at	w%	ρ_d(Mg/m^3)
STD-PL13	dry of optimum	13.0	1.59
STD-PL18	optimum	18.0	1.63
STD-PL22	wet optimum	22.0	1.63
MDF-PL9	dry of optimum	9.2	1.74
MDF-PL15	optimum	15.0	1.78
MDF-PL19.5	wet of optimum	19.5	1.74

Table 6.4: Properties of JF2 test specimens

Notation JF2-	Compacted at	w%	ρ_d(Mg/m^3)
STD-PL10	dry of optimum	10.0	1.71
STD-PL14	dry of optimum	14.0	1.73
STD-PL16	optimum	16.0	1.76
STD-PL18	wet of optimum	18.0	1.75
STD-PL20	wet of optimum	20.0	1.71
MDF-PL8	dry of optimum	8.0	1.83
MDF-PL11	dry of optimum	11.0	1.86
MDF-PL13.5	optimum	13.5	1.88
MDF-PL15.5	wet of optimum	15.5	1.84
MDF-PL17	wet of optimum	17.6	1.80

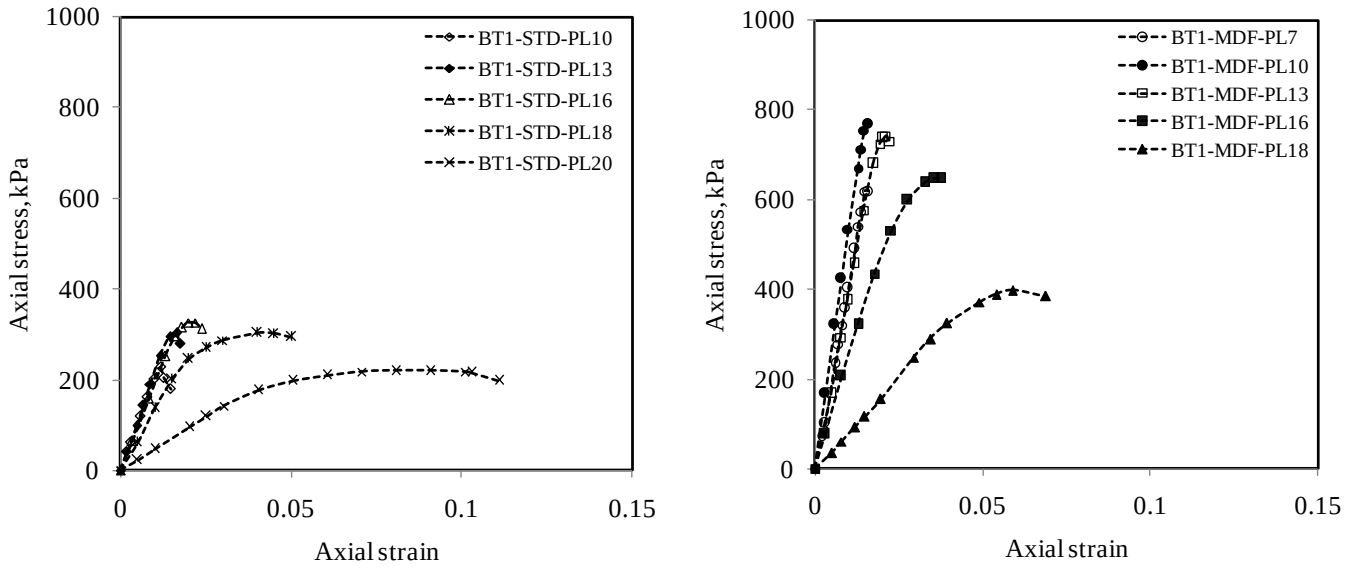

(a) BT1

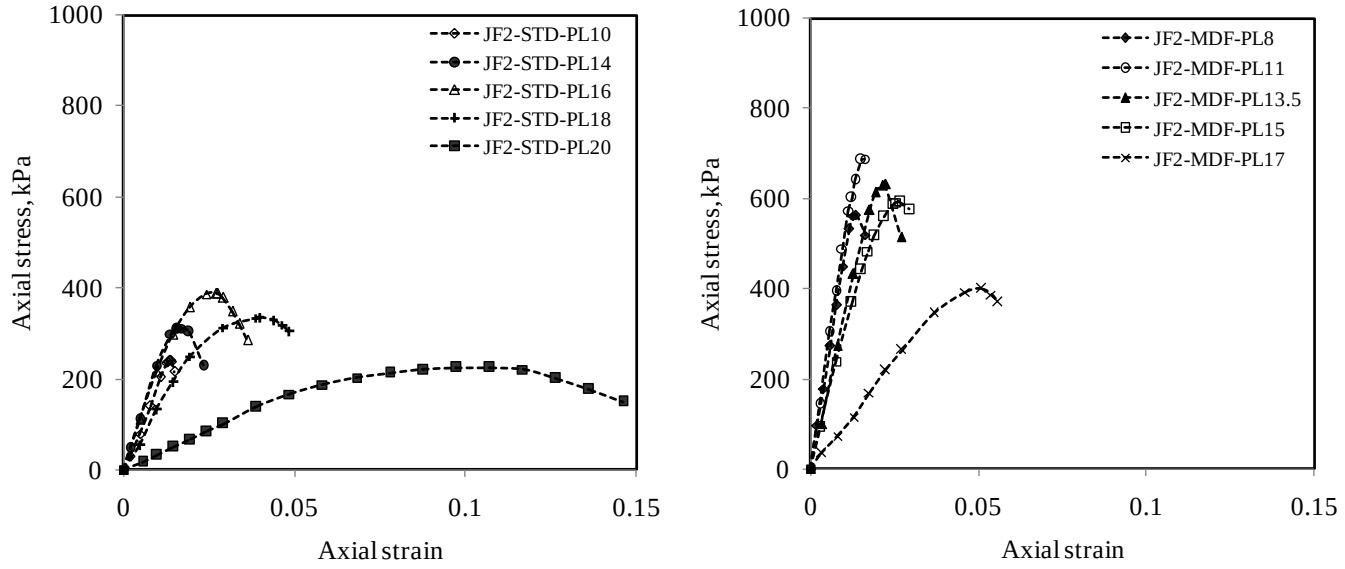

(b) JF2

Figure 6.3: Stress-strain plots from UCS test for BT1 and JF2 soil specimens compacted at both standard and modified Proctor efforts

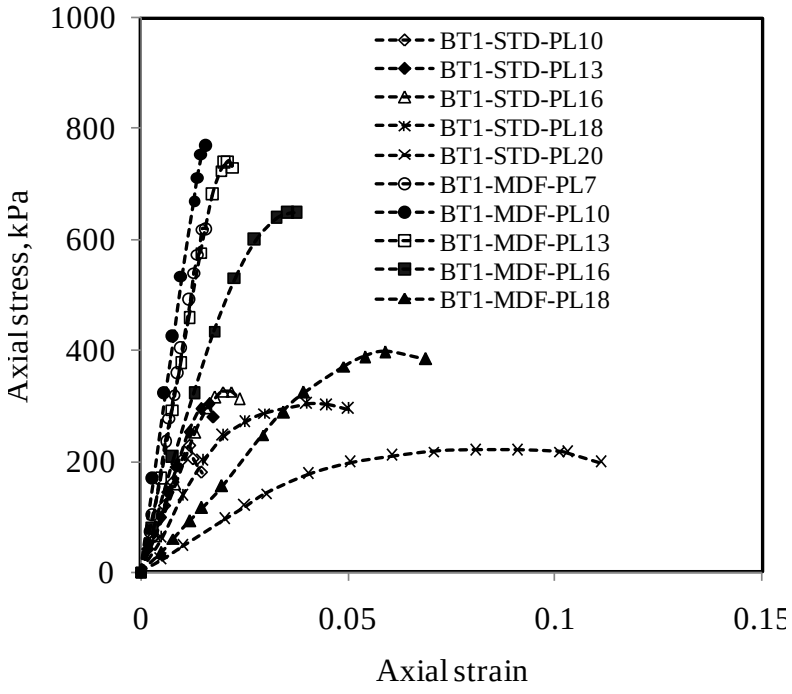

(a) BT1

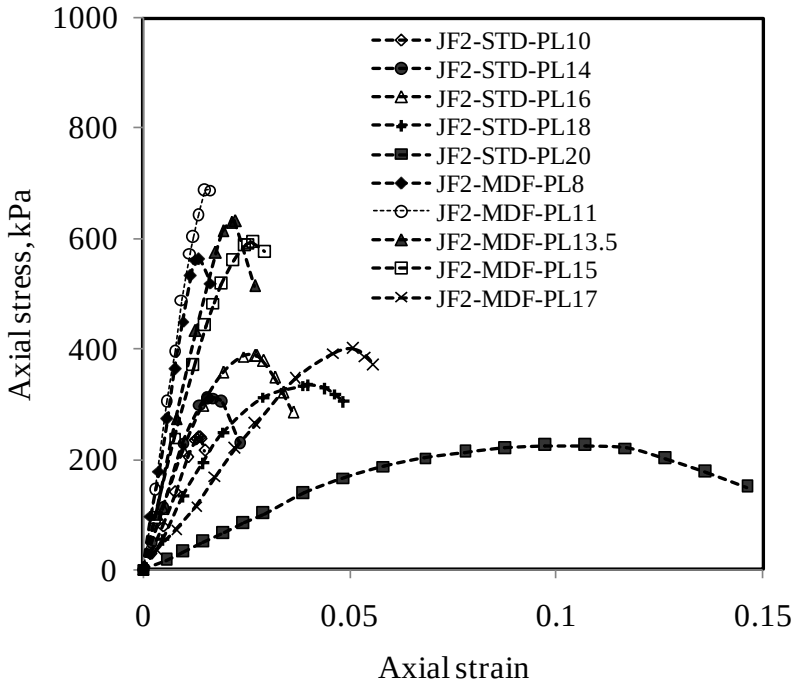

(b) JF2

Figure 6.4: Stress-strain plots from UCS test for both standard and modified Proctor compacted soils

The peak strengths are generally higher on the dry of optimum compared to the wet of optimum specimens. This is due to structural difference and matric suction between specimens on the dry of optimum and wet of optimum. This is further discussed in the subsequent subsections. In Figure 6.4 and Appendix C2, the stress-strain plots for specimens compacted at standard and modified Proctor efforts for the same soil are combined. From Figure 6.4 and Appendix C2, it is observed that an increase in compaction effort results in higher peak strengths, stiffer stress-strain behavior, and more brittle failure depicted by the smaller axial strains at failure. In the following subsection, a further discussion on peak strengths is presented.

6.2.2 Unconfined compressive strength and Brazilian tensile strength

Figure 6.5 shows the variation of UCS, q_u and BTS, σ_t with compaction water content for the Test series 1 (as-compacted test specimens). From Figure 6.5, it is observed that generally, both q_u and σ_t show the same trends as the compaction curves, increasing with water content on the dry side of optimum to a peak value and then reducing with increasing water content. The peaks of q_u and σ_t generally occur at the optimum water content except for the q_u of modified Proctor compacted samples. This is observed for both BT1 and JF2 soils where the peak q_u occurs at less than the optimum water content. This suggests that both void ratio and compaction water content influence q_u and σ_t. It has generally been documented that UCS of unsaturated soils is influenced by both the void ratio and suction (Marinho and Oliveira; 2012, Kato et al., 2005)

The σ_t data shows more scatter than the q_u data, reflecting greater variability in the smaller size BTS test specimens. For soils that were dynamically compacted in layers as in this study, inhomogeneity of the test specimen may influence σ_t depending on the position of the sample layer from which the test specimen was prepared, i.e., whether it is top, middle or bottom layer of the sample. Heibrock et al. (2005) attributes this to structural differences induced by the

compaction process along the sample height. However, in this study no distinct trend was observed among specimens compacted at the same compaction energy as shown in Figures 6.6 suggesting that the compacted sample was relatively homogeneous.

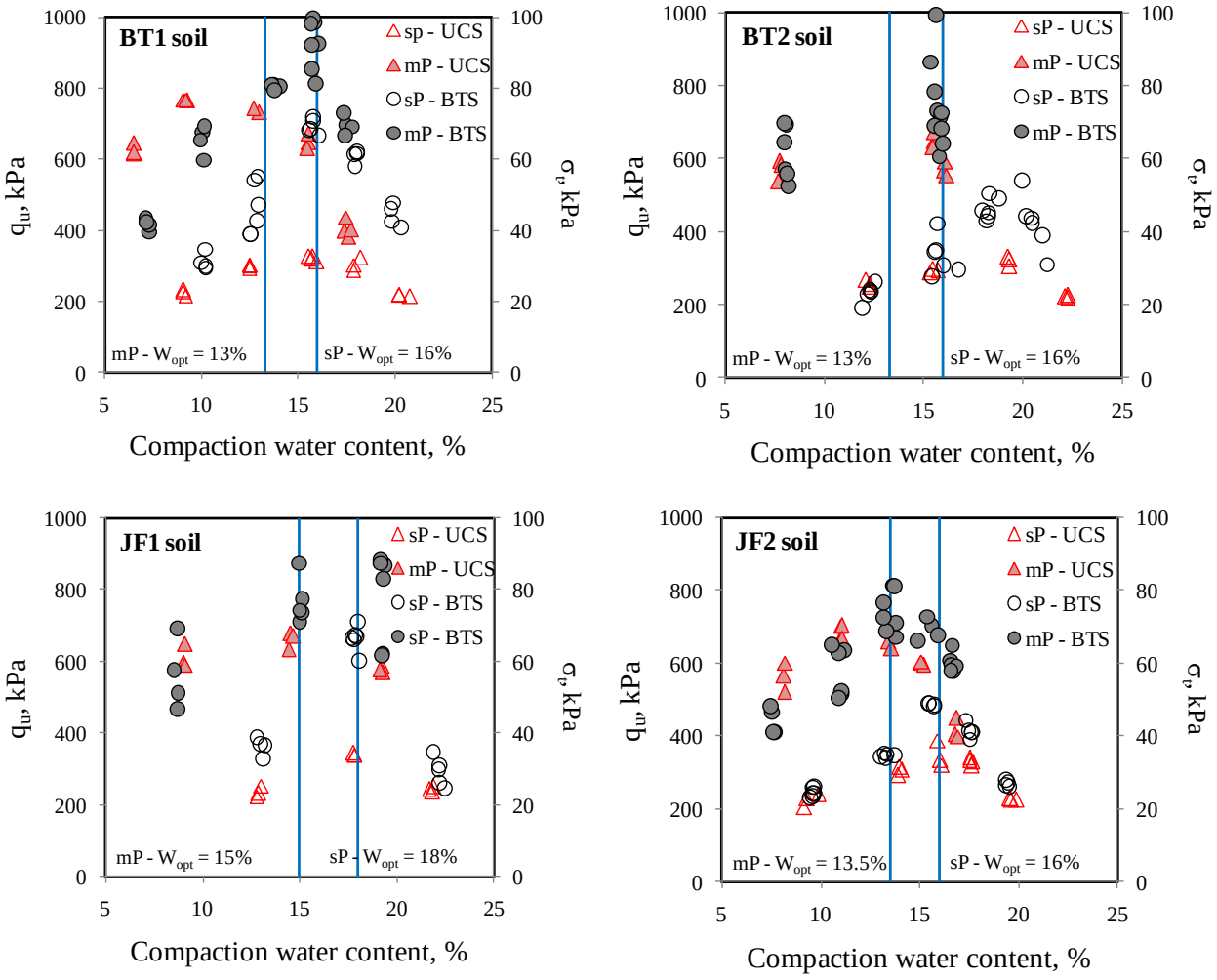

Figure 6.5: UCS and BTS with compaction water content-Test series 1

Figure 6.7 shows variation of matric suction with compaction water content. Matric suction generally decreases with increase in compaction water content, independent of compaction effort. A similar trend has been observed by other researchers such as Fleureau et al. (2002), Leong et al. (2003) and Li et al. (2017). The relationship in Figure 6.7 is bi-linear with the break

point occurring around the optimum water content. This observation can be explained by soil fabric. Compaction on the dry side of optimum largely compresses the inter-aggregate voids. According to Fleureau et al. (2002) and Li et al. (2017), the intra-aggregate voids that contain the capillary water that influences matric suction, are hardly compressed by the compaction process on the dry side of optimum. Therefore, an increase in compaction effort will result in more compression of the inter-aggregate voids hence yielding a denser material but with negligible effect on matric suction as observed in Figure 6.7. The increase in density explains why specimens compacted at modified Proctor effort on the dry of optimum have higher UCS compared to those compacted at standard Proctor effort despite almost having the same matric suction.

As the compaction water content increases towards the wet of optimum, the fabric becomes more dispersed and the compaction effort can substantially compress the inter-aggregate voids hence affecting the matric suction more. The change in matric suction with respect to moulding water content on the dry side of optimum is less than on the wet side of optimum. Fleureau et al. (2002) and Li et al. (2017) have defined the slopes of both lines as suction capacity C given in Equation 6.1:

$$\log \psi = -C.w + z \qquad (6.1)$$

where ψ is suction, w is compaction water content and z is a constant. A summary of C and z together with the coefficient of determination, R^2 is shown in Table 6.5.

The low values of R^2 for BT2 standard Proctor compacted specimens on the dry of optimum and BT2 modified Proctor compacted specimens may be attributed to insufficient tests. A better fit is expected if the number of test increases.

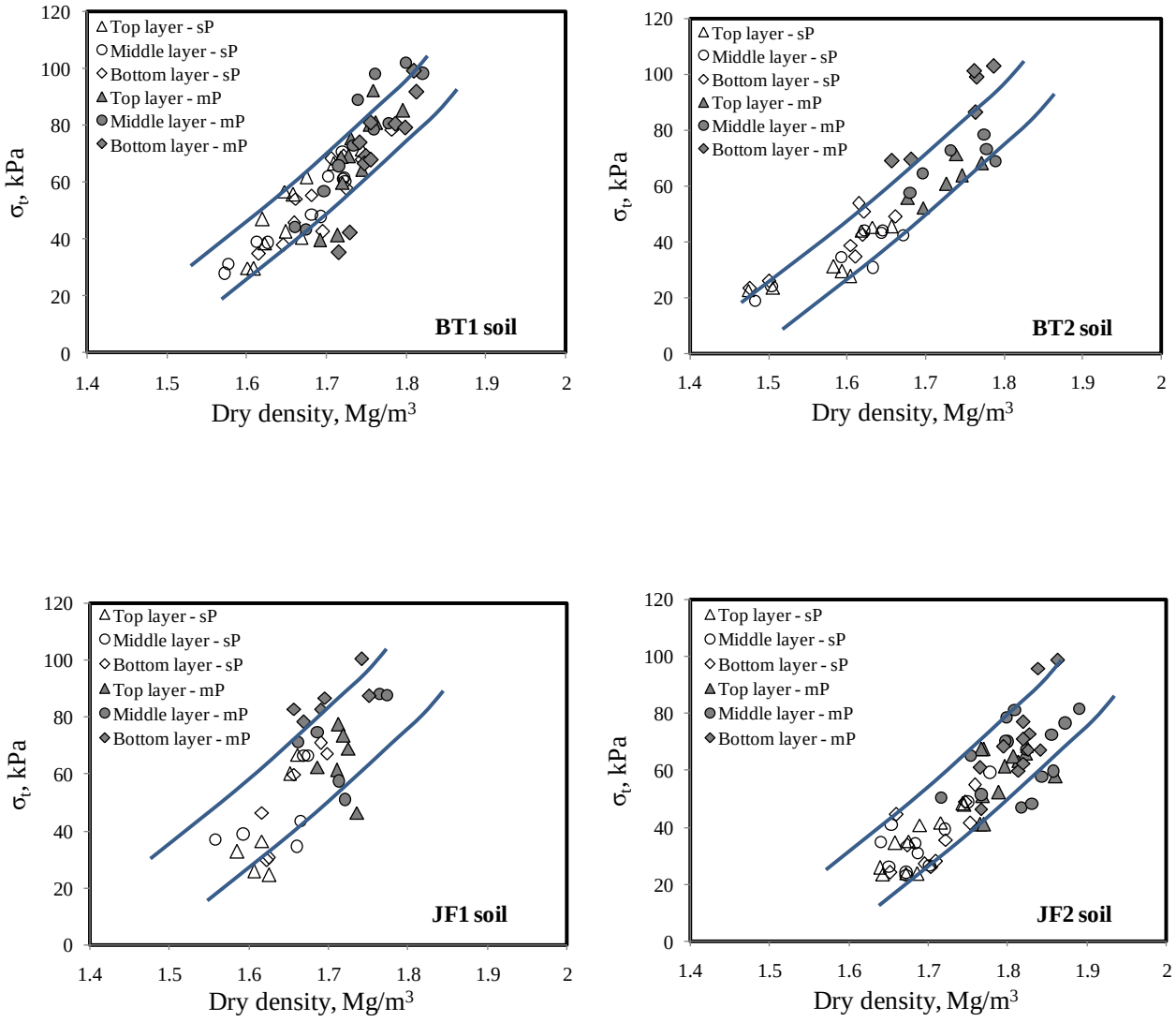

Figure 6.6: Variability of the BTS for disk specimens taken from different compaction layers with dry density-Test series 1

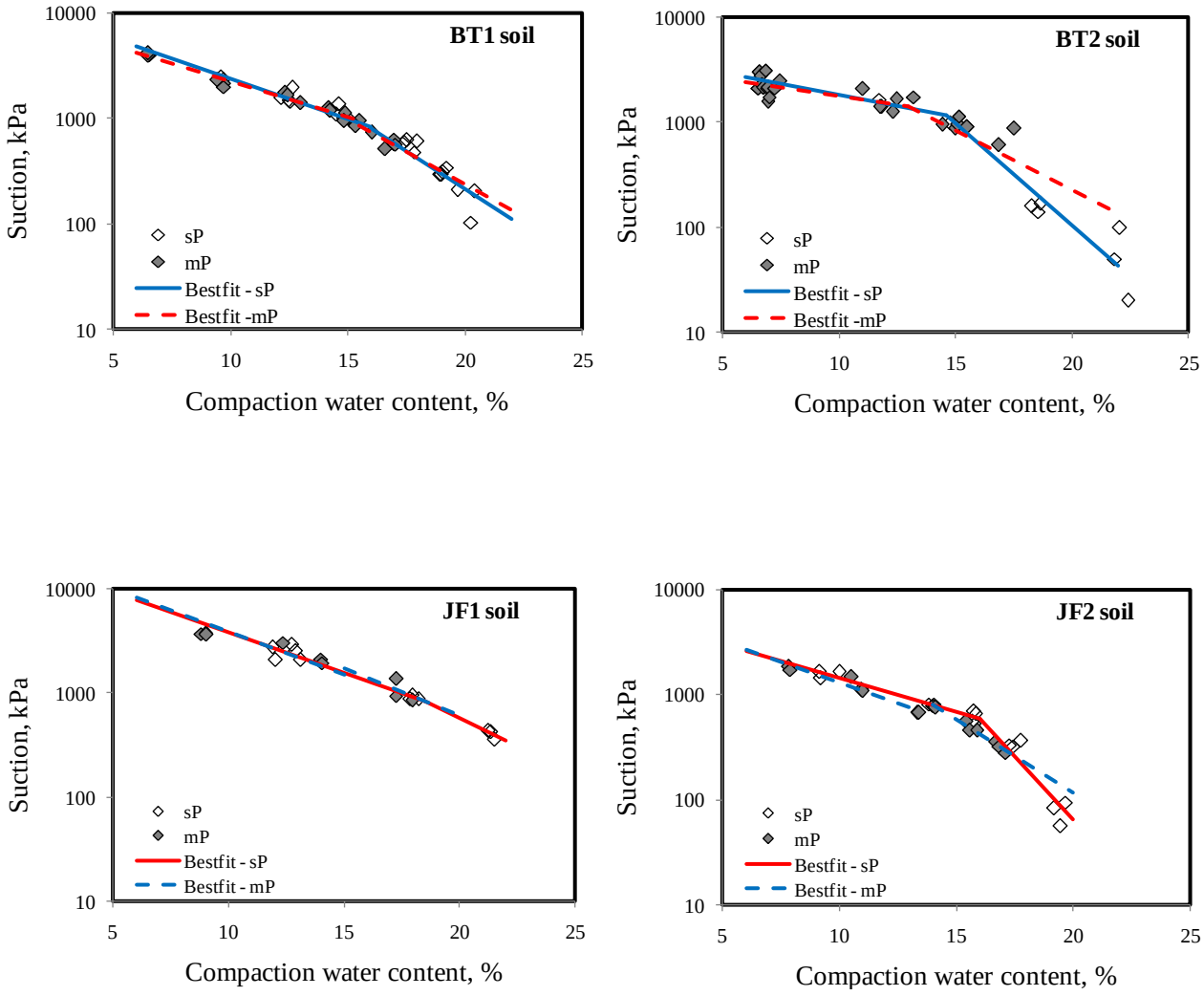

Figure 6.7: Variation of suction with compaction water content

Table 6.5: Relationship of suction with compaction water content

Soil	Standard Proctor					
	Dry of optimum			Wet of optimum		
	C	Z	R^2	C	z	R^2
BT1	0.077	4.157	0.895	0.145	5.235	0.892
BT2	0.042	3.678	0.677	0.194	5.891	0.889
JF1	0.078	4.371	0.915	0.108	4.921	0.985
JF2	0.065	3.807	0.949	0.240	6.603	0.915
Soil	Modified Proctor					
	Dry of optimum			Wet of optimum		
	C	Z	R^2	C	z	R^2
BT1	0.067	4.027	0.972	0.123	4.837	0.936
BT2	0.032	3.580	0.447	0.073	4.107	0.593
JF1	0.084	4.425	0.911	0.090	4.590	0.924
JF2	0.077	3.890	0.938	0.141	4.884	0.999

6.3 Test Series 2 -Pre-dried specimens compacted wet of optimum

In order to examine further the influence of matric suction and soil fabric on soil strength, test series 2 was conducted. Test series 2, comprises sample sets A to I, compacted wet of optimum using the plastic mould. Each sample set consists of more than 10 specimens. As described in Chapter 3, the specimens were then dried in airtight desiccators containing saturated NaCl solutions to selected water contents before testing. On attaining the desired water content, the UCS, q_u and BTS, σ_t of the specimens were determined.

Figures 6.8, 6.9 and 6.10 show the test series 2 specimens on the compaction curves for BT1, BT2 and JF2 soils, respectively. The soil sets are labelled A-I. The average properties of the soil sets are given in Table 6.6.

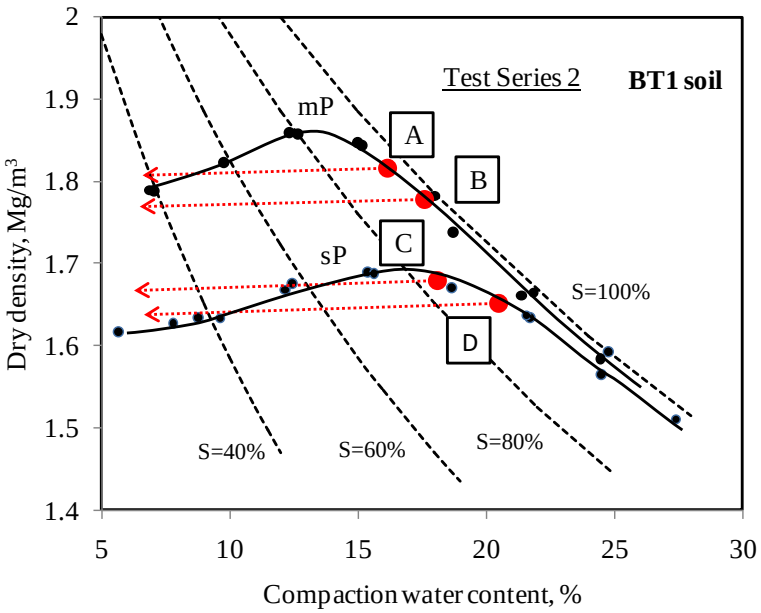

Figure 6.8: BT1 test series 2 specimens

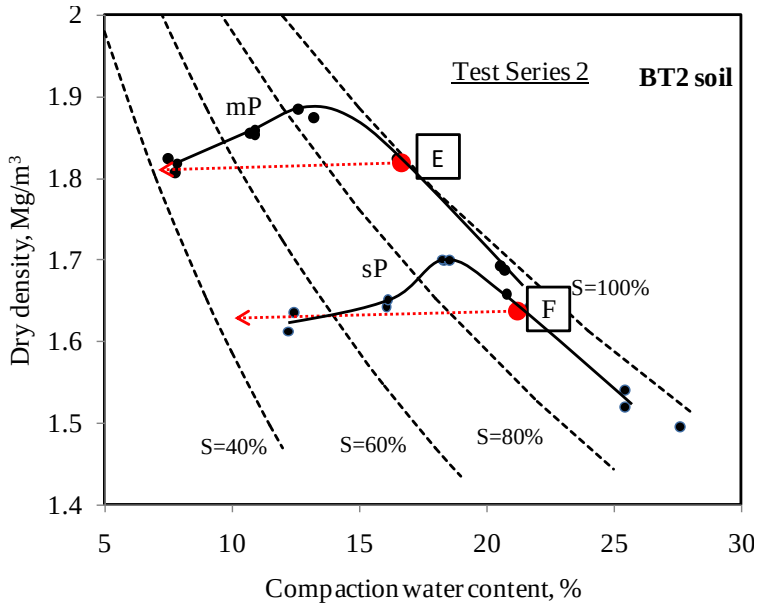

Figure 6.9: BT2 test series 2 specimens

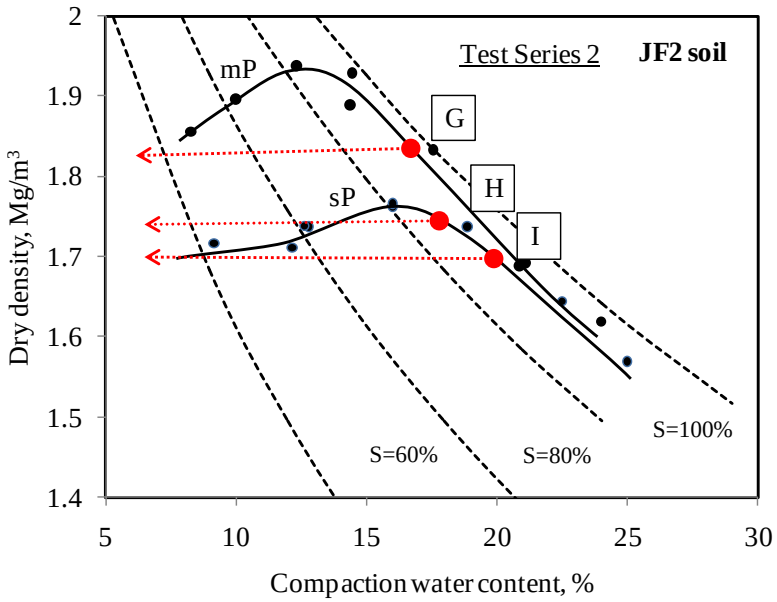

Figure 6.10: JF2 test series 2 specimens

Table 6.6: Average properties of sample sets A to I in Test series 2

Soil	Sample set	Average w (%)	Average ρ_d (Mg/m^3)	Proctor effort
BT1	A	16.0	1.82	Modified
	B	17.5	1.77	Modified
	C	18.0	1.70	Standard
	D	20.2	1.67	Standard
BT2	E	16.0	1.82	Modified
	F	22.2	1.61	Standard
JF2	G	17.0	1.84	Modified
	H	18.0	1.75	Standard
	I	20.0	1.70	Standard

6.3.1 Stress- strain plots for UCS test

Stress – strain plots for sample sets A to C for test series 2 are presented in Figure 6.11. Similar plots for sample sets D to I are presented in Appendix C3. The stress-strain plots for each sample set are separated into two plots for clarity as shown in Figure 6.11.

As the specimens dry, their stiffness and strength increase while their axial strain at failure reduces i.e. becoming more brittle. A point is reached when the specimens display no more increase in stiffness and the increase in strength is negligible as shown in the second plot of stress-strain curves for each of the sample sets in Figure 6.11 and Appendix C3. Because no substantial increase in stiffness was observed, the stress-strain curves are represented by an average curve.

Figure 6.12 and Appendix C4 show the UCS, q_u and BTS, σ_t plotted together with the SWCC and shrinkage curve data of the soil specimens. The shrinkage curve data consists of the volume measurements of the SWCC, UCS and BTS specimens. It is observed that the shrinkage curve data from the SWCC specimens which were pre-saturated generally have slightly higher void ratios at similar water content when compared to the UCS and BTS specimens. This can be attributed to swelling of the SWCC specimens due to saturation. The SWCC data was fitted with Fredlund and Xing (1994) SWCC equation using correction factor as unity following recommendation of Leong and Rahardjo (1997b). The shrinkage curve data was fitted using Leong and Wijaya (2015)'s universal shrinkage equation.

For all the nine sample sets A to I, drying of the soil specimens from the wet of optimum to dry of optimum showed an increase in both q_u and σ_t with more remarkable increases noted in q_u. The strength values are observed to increase up to a certain limit and then generally becoming constant despite further drying or increase in soil suction. Some slight drop in strength at extremely low water contents were observed especially with σ_t which can be attributed to formation of internal micro-fissures common at low water contents in clayey and silty materials (Sun and Cui, 2017).

The degrees of saturation at which q_u and σ_t ceased to increase vary between 82 and 85%, and between 95 and 97%, respectively, for all the sample sets. Locating these degrees of saturation on the shrinkage curves indicates that they correspond approximately to the curvature of the shrinkage curve. As the soils dry, their volume decreases and suction increases. These factors collectively influence the soil strength. However, the contribution of suction becomes increasingly minimal past the air-entry value (AEV) of the soil since the water phase becomes increasingly discontinuous in the soil system. On the other hand, the void ratio may continue to reduce due to shrinkage contributing to the increase in soil strength. When the shrinkage limit is reached, the strength ceases to increase and becomes constant. Any variation from the constant value can be attributed to experimental errors.

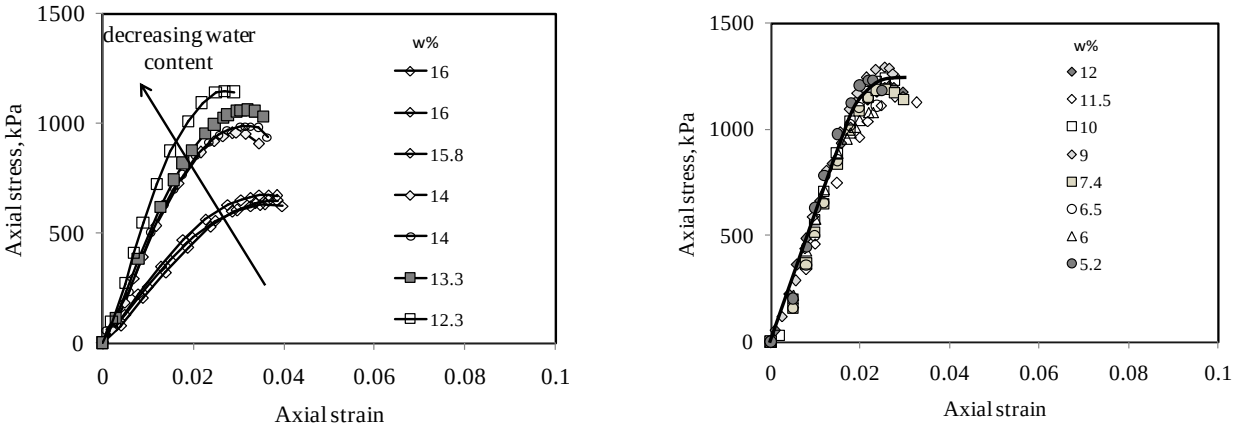

(a) Sample set A

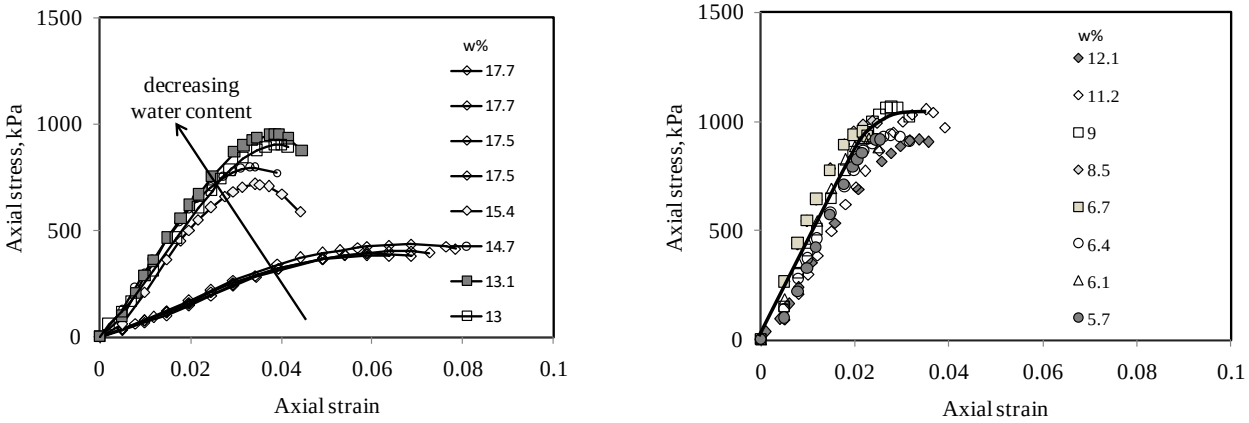

(b) Sample set B

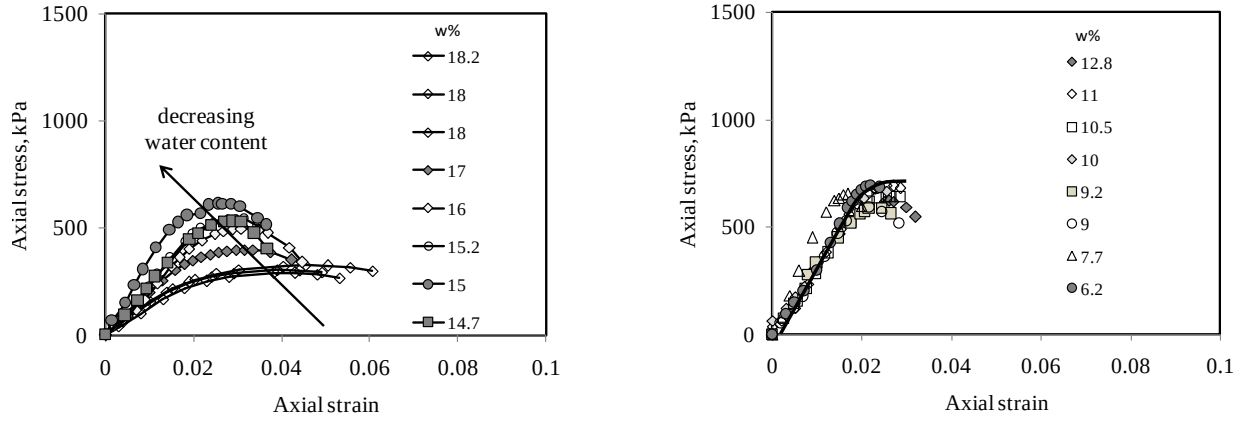

(c) Sample set C

Figure 6.11: Stress-strain plots for sample sets A, B and C-Test series

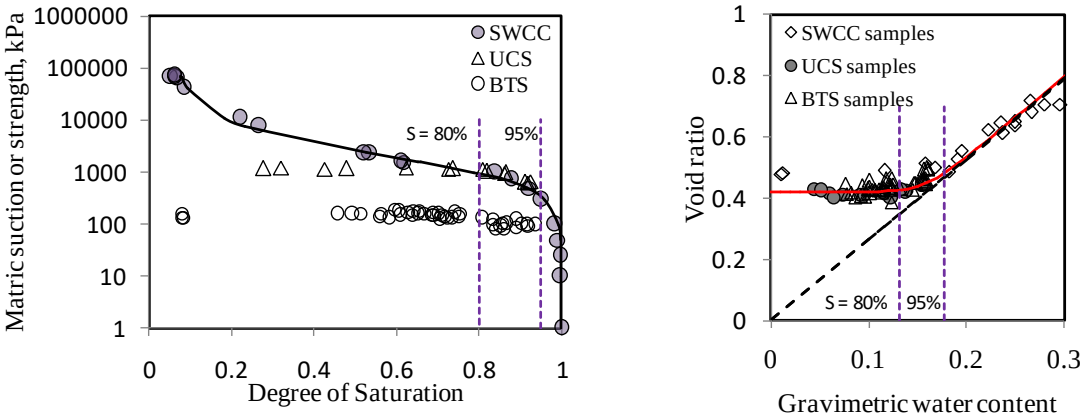

a) Sample set A

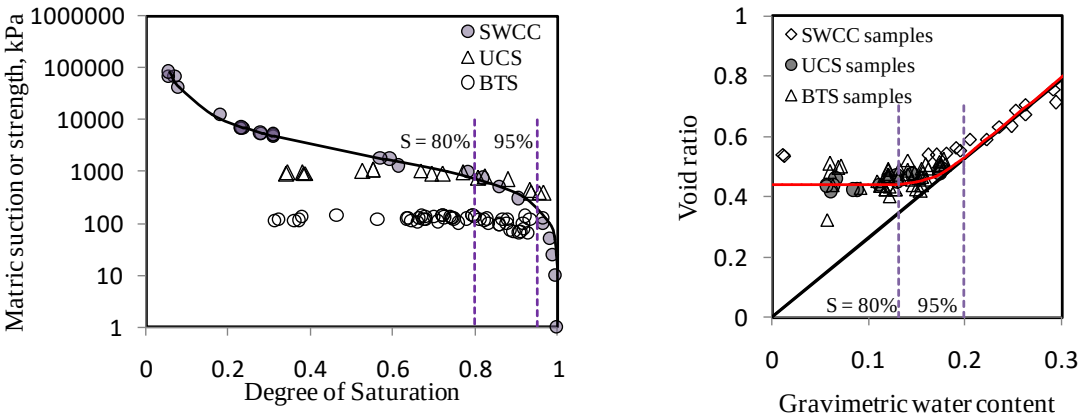

(b) Sample set B

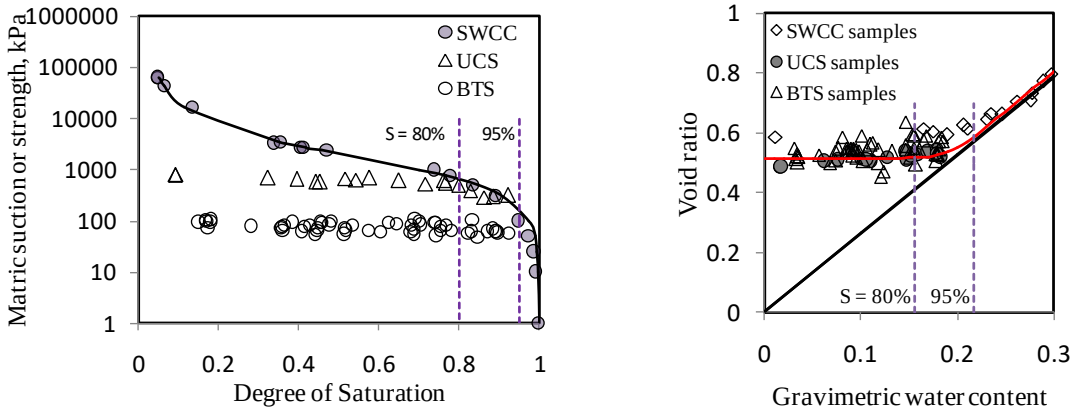

(c) Sample set C

Figure 6.12: Variation of UCS and BTS with degree of saturation and SWCC for sample sets A to C- Test series 2

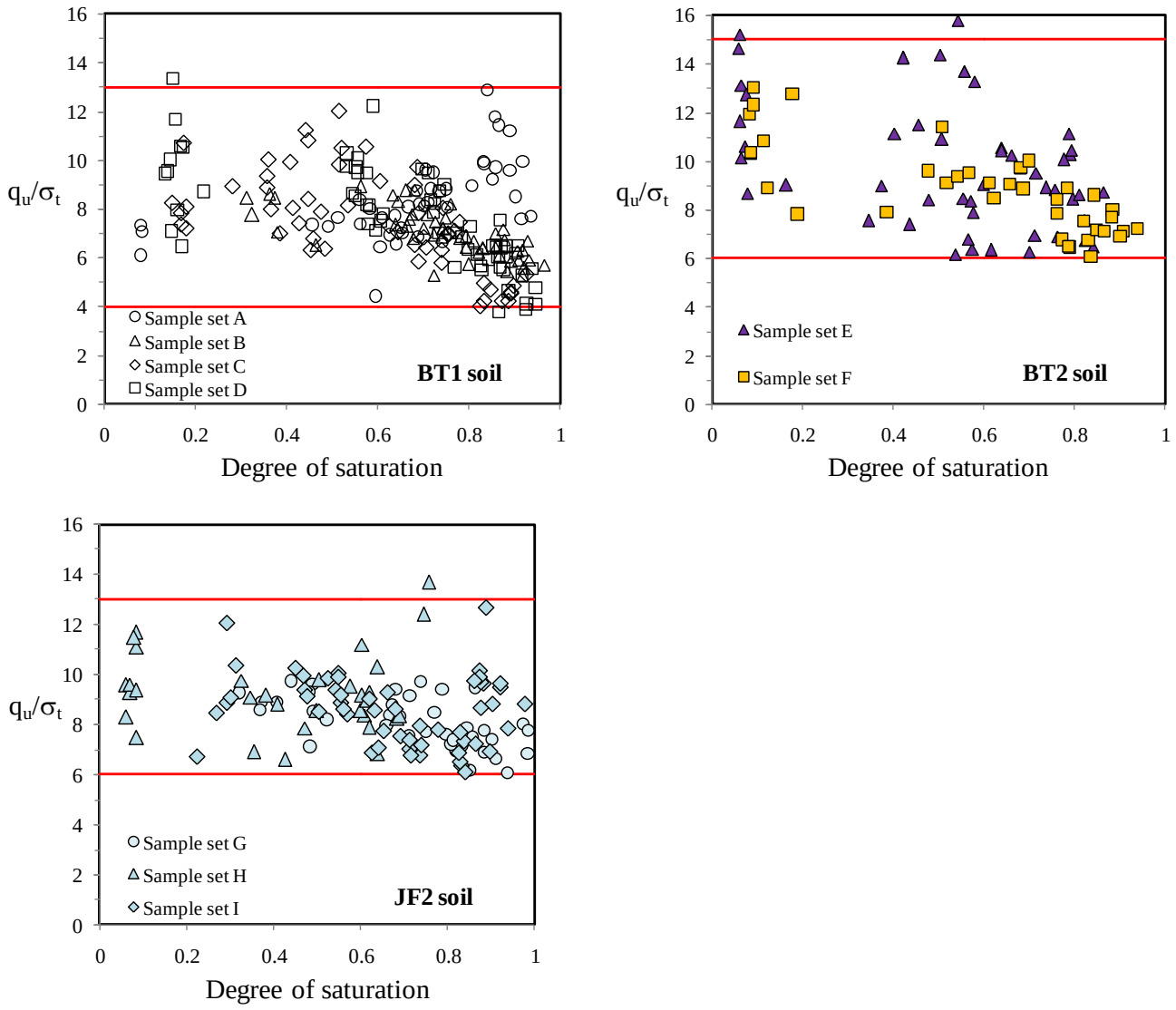

Figure 6.13: Variation of q_u/σ_t with degree of saturation for sample sets A to I- Test series 2

Figure 6.13 shows the ratio of q_u/σ_t with degree of saturation. For BT1 soils, the q_u/σ_t ratio varies between 4 and 13, whereas for BT2 soil ,the q_u/σ_t ratio varies between 6 and 15 and for JF2 soils, the q_u/σ_t ratio varies between 6 and 13. In all three cases the ratio is within the range of 4 to 16 observed by others. Narain and Rawat (1970) reported a q_u/σ_t ratio between 6 and 12 for compacted soils, Das et al. (1995) reported a q_u/σ_t ratio of 10 for soils compacted at the optimum

water content while Tamrakar et al. (2007) reported a q_u/σ_t ratio between 4 and 16 for unsaturated soils.

6.4 Tensile strength models

Several models have been proposed to estimate tensile strength of soils. Yin and Vanapalli (2018) have summarized some of these models. Two tensile strength models by Lu et al. (2009) and Yin and Vanapalli (2018) are evaluated using the data from this study. Although these models are developed largely for sands, they have been reviewed and evaluated with the data obtained in this thesis as they both used unsaturated soil concepts similar to the thesis.

6.4.1 Lu etal. (2009) tensile strength model

Lu et al. (2009) proposed a model to estimate σ_t of unsaturated cohesionless soils by making use of suction stress (Equation 6.2), internal friction angle ϕ_t and parameters α and n of VG SWCC equation. The tensile strength σ_t is given by Equation 6.3.The suction stress σ^s and the tensile strength σ_t in Equations 6.2 and 6.3, respectively are presented, in terms of degree of saturation, S.

$$\sigma^s = u_w \quad \text{for } (u_a - u_w) \le 0$$
$$\sigma^s = -\frac{S_e}{\alpha}\left(S_e^{n/(1-n)} - 1\right)^{1/n} \quad \text{for } (u_a - u_w) \ge 0 \tag{6.2}$$

$$\sigma_t = 2\tan\phi_t \tan\left[\frac{\pi}{4} - \frac{\phi_t}{2}\right]\frac{S_e}{\alpha}\left[S_e^{n/(1-n)} - 1\right]^{1/n} \tag{6.3}$$

$$S_e = \frac{S - S_r}{1 - S_r} \tag{6.4}$$

where u_a = pore air pressure, u_w = pore water pressure, S_e = effective degree of saturation, and S_r = residual saturation.

Lu et.al (2009) suggest that ϕ_t can be obtained using a non-linear Mohr-Coulomb envelope in the low stress zone. Therefore, ϕ_t was estimated using q_u and σ_t in this study. The slope of the tangent to the Mohr circles from the UCS and BTS tests as shown in Figure 6.14 was used to estimate ϕ_t.

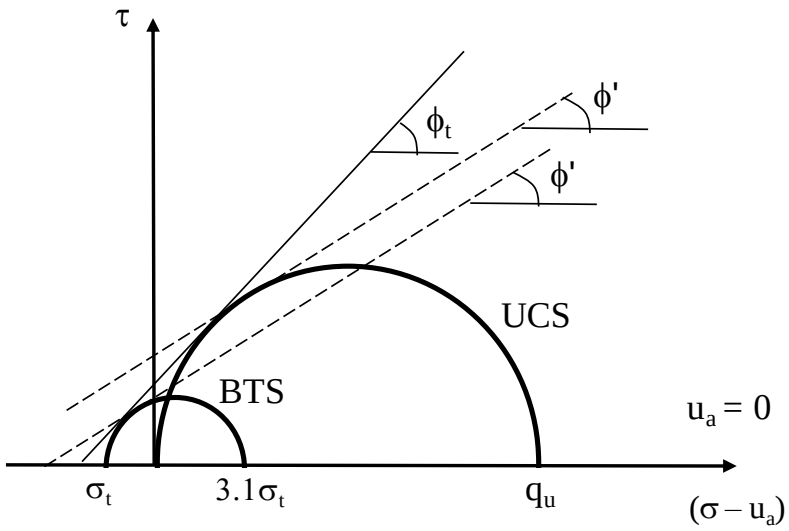

Figure 6.14: Determination of ϕ_t from UCS and BTS

Plots of these Mohr circles were constructed at different S as the soil dries and hence, a variation of ϕ_t with S can be obtained as shown in Figure 6.15 for the soil sets A-I. The ϕ_t in Figure 6.15 is denoted as ϕ_{t_exp}.

The effective shear strength parameters ϕ' and c' from consolidated undrained triaxial tests for saturated soil specimens of each sample set conducted in accordance to ASTM D4767-11 are also indicated in Table 6.7.

Based on Figure 6.15, ϕ_{t_exp} is not constant but varies with degree of saturation. However, in the application of Equation 6.3, only a single value of ϕ_t is admissible. Hence, the sensitivity of ϕ_t is

investigated. A number of cases were evaluated. However, only four significant cases are presented below:

Case 1: All parameters are as evaluated from experimental data, i.e.α and n of the VG equation from curve fitting the SWCC data while $\phi_t = \phi'$.

Case 2: Values of α and n of the VG equation from Case 1 are doubled while ϕ_t is set to the lowest value of ϕ_{t_exp} and ϕ'.

Case 3: Values of α and n of the VG equation from Case 1 are doubled while ϕ_t is set to the highest value of ϕ_{t_exp} and ϕ'.

Case 4: Values of α and n of the VG equation from Case 1 are doubled while $\phi_t = \phi'$.

To evaluate the performance of Lu et al. (2009) tensile strength model against the experimental data, the root mean square error (RMSE) is computed. The RMSE is defined in Equation 6.5.

$$RMSE = \sqrt{\frac{\sum_{i=1}^{n}\left(X_{obs,i} - X_{model,i}\right)^2}{n}} \tag{6.5}$$

where $X_{obs,i}$ = observed/measured value, $X_{model,i}$ = model value as predicted at same conditions as observed value, n = number of data points

Table 6.7: Shear strength and SWCC equations parameters for sample sets A-I

Sample set	From CU tests with pore-water pressure measurements		$\phi_{t\_exp}(^o)$	Fredlund and Xing (1994) SWCC equation's parameters			van Genuchten (1980) SWCC equation's parameters	
	ϕ' (^{o})	c' (kPa)		a (kPa)	n	m	α (kPa^{-1})	n
A	26.0	16	16.0 - 40.0	1477	1.577	1.425	0.0010	1.6493
B	27.5	16	15.0 – 40.0	1506	1.278	1.737	0.0011	1.7150
C	27.5	4	28.6 - 45.0	1477	1.247	1.916	0.0013	1.6839
D	27.5	3	15.0 – 40.0	1439	1.541	1.446	0.0010	1.6751
E	30.0	12	45.0-52.0	2000	0.986	2.347	0.0016	1.5727
F	32.0	0	20.0-45.0	4556	0.860	3.329	0.0027	1.4765
G	30.0	10	40.0 – 48.0	1128	1.95	1.256	0.0010	1.9491
H	30.0	5	27.0 – 47.0	1339	1.248	1.839	0.0013	1.6711
I	30.0	10	37.0 – 48.0	1029	1.313	1.593	0.0014	1.7366

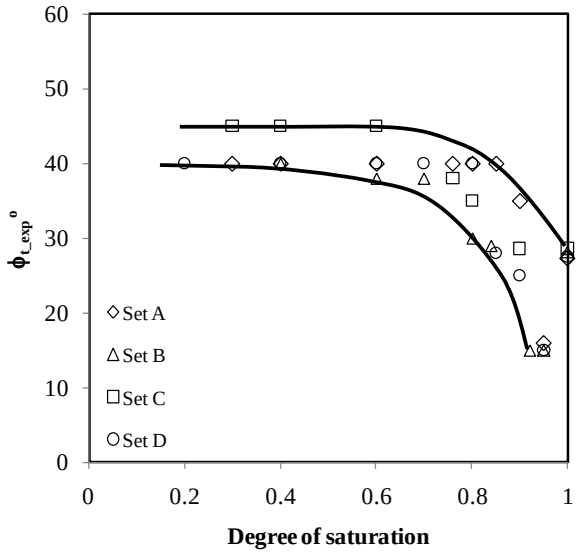

BT1 soil sets

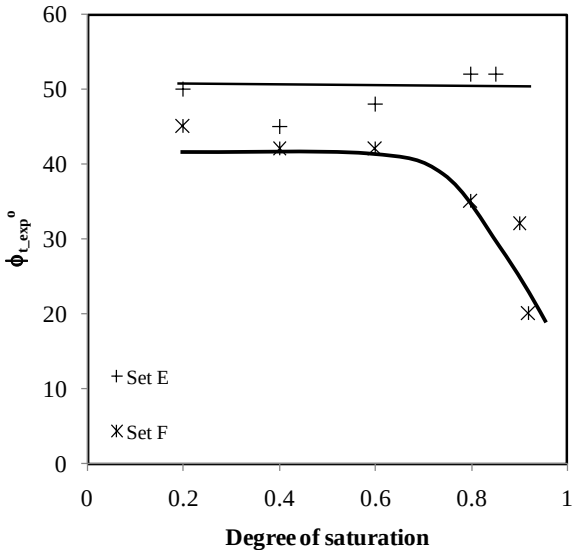

BT2 soil sets

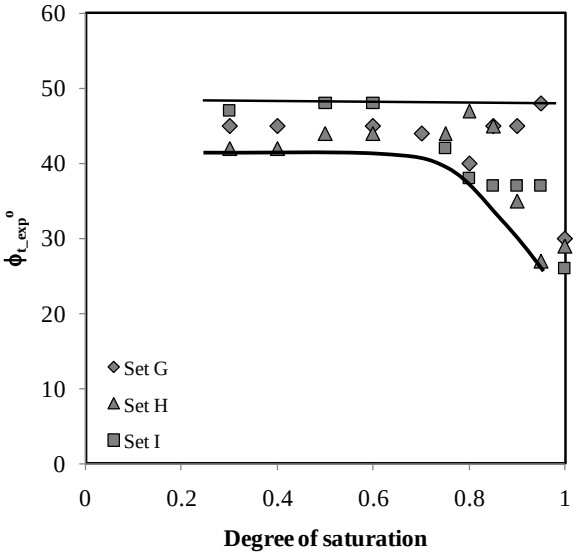

JF2 soil sets

Figure 6.15: Variation with degree of saturation for sample sets A to G - Test series 2

Figure 6.16 shows the four cases where tensile strength is plotted against degree of saturation for all the sample sets, A, B, C, D, G,H and I. In Figure 6.16, the SWCC is also plotted. Lu et al.

(2009) termed the tensile strength versus degree of saturation curve as tensile strength characteristic curve (TSCC).Table 6.8 summarises the RMSE. Generally, Case 2 gives the best estimation while Case 1 gives the worst estimation of the tensile strength data for all the sample sets. Cases 2 and 4 coincide when $\phi_t = \phi'$, as observed for sample sets C, E, G and I. The values of α and n of the VG equation seem too low to fit the tensile strength data. Doubling of these values yields better predictions for the model as observed in Cases 2, 3 and 4. Lu et.al. (2009) tensile strength model was developed for sand materials where α and n are larger than the α and n for sample sets A to G. The difference amongst Cases 2, 3 and 4 is the value of ϕ_t. Interestingly, Case 2 with the lowest value of ϕ_t gives the best estimation of tensile strength. The values of ϕ_t used in Lu et al. (2009) for different sand materials range from 48^o to 55^o, much higher than the range of ϕ_t found in this study.

6.4.2 Yin and Vanapalli (2018) tensile strength model

Yin and Vanapalli (2018) extended Lu et.al. (2009) model and the new model is expected to be more versatile. Besides the SWCC and internal friction angle ϕ_t, Yin and Vanapalli (2018) model requires information on the particle size distribution of the soil and void ratio. The model is a summation of the contributions to tensile strength of matric suction and water bridges making it a two-term model. This model assumes that the TSCC can have a double peak, at the degrees of saturation corresponding to the AEV and at the residual suction. Yin and Vanapalli (2018) model is given in Equation 6.6.

$$\sigma_t = 2\tan\phi_t \tan\left[\frac{\pi}{4} - \frac{\phi_t}{2}\right]\left[S_e^k\left(u_w - u_a\right) + T_s.a_{aw}\right] \qquad (6.6)$$

where k is a flexibility parameter to give a peak in the TSCC at the AEV, T_s is the surface tension of water at a given temperature of the fluid in the pores and a_{aw} is the specific air-water interface area per pore volume.

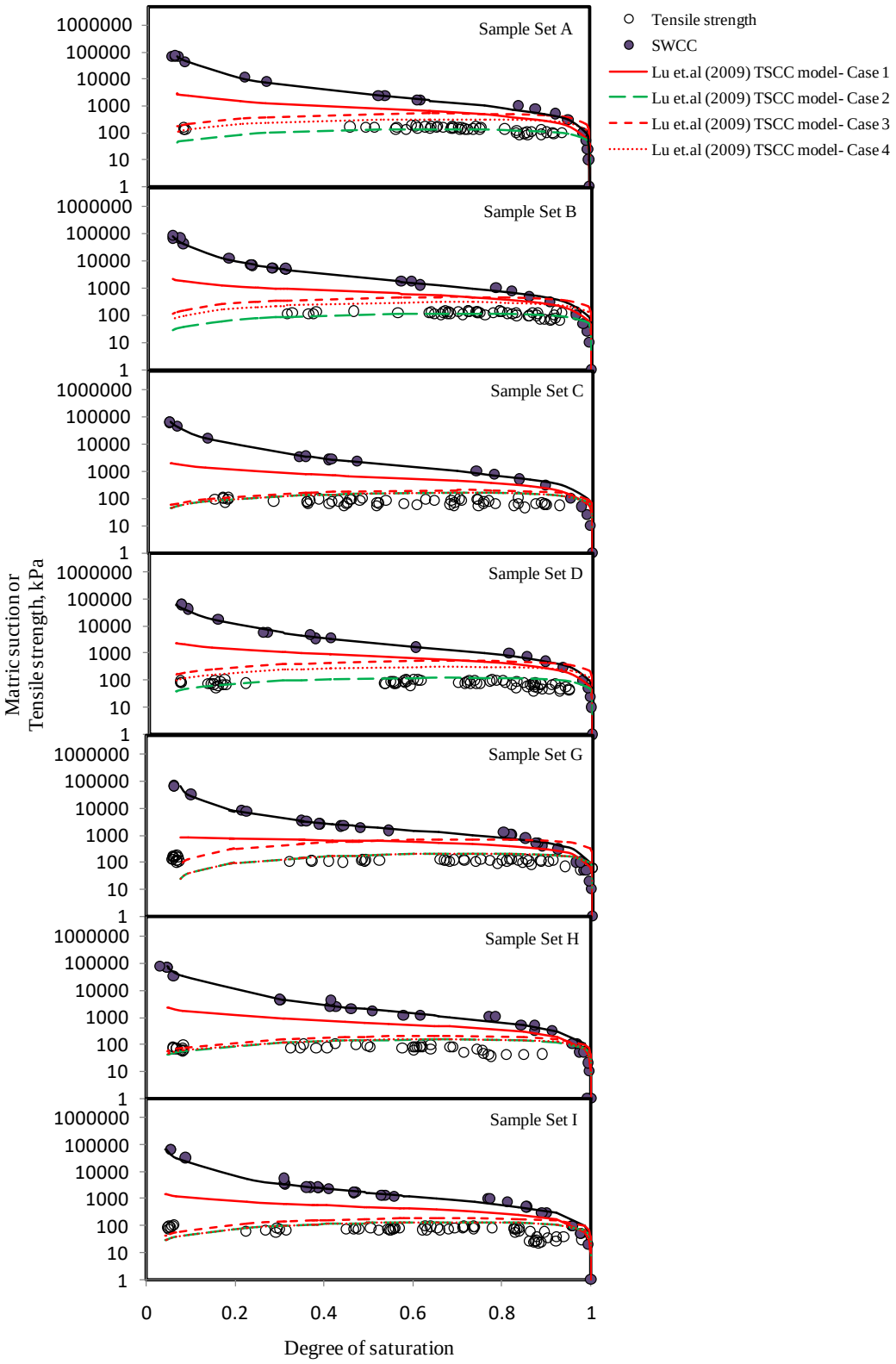

Figure 6.16: Evaluation of Lu et.al (2009) tensile strength model

Table 6.8: Summary of RMSE for Lu et.al (2009) tensile strength model

Sample set	Case 1	Case 2	Case 3	Case 4
A	721.8	33.7	93.6	54.3
B	382.2	20.6	93.8	57.9
C	576.8	72.9	111.8	72.9
D	835.8	40.6	134.2	95.1
E	1445.0	39.5	70.9	39.5
F	1494.7	8.0	32.4	18.6
G	476.7	92.3	127.8	92.3
H	918.4	64.7	106.3	70.0
I	504.2	60.8	105.0	60.8

Yin and Vanapalli (2018) suggest that a_{aw} is related to void ratio e, mean particle size d_{50} and two parameters η_s and λ_s, as shown in Equation 6.7.

$$a_{aw} = \eta_s \frac{\pi}{e d_{50}} S_e^{\lambda_s} \left(1 - S_e\right) \tag{6.7}$$

The parameter λ_s, shown in Equation 6.8, is to ensure that the second peak of the TSCC occurs at the residual degree of saturation, S_r.

$$\lambda_s = \frac{S_r}{1 - S_r} \tag{6.8}$$

Therefore with λ_s related to S_r, Yin and Vanapalli (2018) model has two major fitting parameters: k and η_s. The parameters k and η_s are related to the coefficient of uniformity, C_u through Equations 6.9 and 6.10, respectively.

$$k = \frac{1}{(n-1)} \frac{1}{1-\left[(0.85 \pm 0.15) S_c\right]^{n/n-1}} \quad \text{for } C_u \le 6$$
$$k = \frac{1}{(n-1)} \frac{1}{1-\left[(0.45 \pm 0.15) S_c\right]^{n/n-1}} \quad \text{for } C_u > 6 \qquad (6.9a)$$

where S_0= degree of saturation corresponding to first peak of the tensile strength model and S_c = capillary degree of saturation corresponding to the AEV are related as follows:

$$\frac{S_0}{S_c} = (0.85 \pm 0.15) \text{ for } C_u \le 6$$
$$\frac{S_0}{S_c} = (0.45 \pm 0.15) \text{ for } C_u > 6 \qquad (6.9b)$$

$$\eta_s = 0.73 C_u \qquad (6.10)$$

The tensile strength of sample sets A to G do not show any peaks. Similar to the Lu et.al (2009) tensile strength model, Yin and Vanapalli (2018) model did not fit the experimental data well and hence, a sensitivity analysis was conducted on the parameters in the model. Although many cases were evaluated, only four significant cases are presented below:

Case 1: The parameters k and η_s are computed using Equations 6.9 and 6.10, respectively, while $\phi_t = \phi'$.

Case 2: ϕ_t is equal to the lowest value of ϕ_{t_exp} and ϕ' while other parameters are same as in Case1

Case 3: Parameter k is set to 1.5 times the value computed in Case 1, leaving the rest of the parameters same as Case 1.

Case 4: Parameters k is set to 1.5 times the value in Case 1 while ϕ_t is equal to the lowest value of ϕ_{t_exp} and ϕ', leaving all the other parameters same as Case 1.

The void ratio e in Equation 6.7 is taken to be e_{min} from the shrinkage curve (Leong and Wijaya (2015). For computation of k in Case 1, the ratio S_0/S_c was set at 0.9 and 0.6 for BT and JF soils, respectively, within the range of values given by Equation 6.9b. The shear strength and SWCC equations parameters are summarized in Table 6.7.

Figure 6.17 shows the four cases where tensile strength is plotted against degree of saturation for the sample sets A, B, C, D, G,H and I. In Figure 6.17, the SWCC is also plotted. Table 6.9 summarizes the parameters and the RMSE values for all the sample sets. Case 4 gives the lowest RMSE for all the sample sets as parameter k was best fitted. For all sample sets, Case 1 gives the worst estimation (highest RMSE) of the tensile strength. Generally, the fit is poorer near saturation for all the sample sets. Comparing Cases 1 and 2 shows that ϕ_t affects the tensile strength slightly with the higher ϕ_t giving a slightly higher estimate of tensile strength. By comparing the RMSE values of all the sample sets for Cases 2, 3 and 4, it is observed that the effect of ϕ_t is minimal. Therefore, Yin and Vanapalli (2018) tensile strength model largely depends on the parameters k and η_s. Comparing the model fits for sample sets A-D (from Bukit Timah Granite) with sample sets G-I (from Jurong Formation), it is observed that parameter k has a greater effect on the model fit quality. Despite an increase in η_s for sample sets G-I, the quality of fit is poorer largely because of the low values of parameter k. A higher k implies a reduction in the value of parameter n in the VG equation associated with a soil having a wider

pore-size distribution. A large value of η_s like in the case of sample sets G-I suggests a large number of interparticle contacts, a complex soil structure and soil fabric both of which are typical of compacted soils.

Additionally, Yin and Vanapalli (2018) suggest that η_s represents the anisotropy of the tensile strength of the material and therefore a large η_s value points to increased anisotropy in the distribution of pore water, pore air and consequently the air-water interface as the soil dries up. Overall, the lowest ϕ_t give better agreement with the tensile strength data in all cases. Soil sample sets from the Bukit Timah Granite (A-D) generally show better fit than sample sets from the Jurong Formation (G-I). This is largely due to the larger k value computed for the sample sets A-D compared with that computed for sample sets G-I. A larger value of k is associated with coarse materials expected of A-D sample sets since they are derived from the Bukit Timah Granite. This is expected since the Yin and Vanapalli (2018) model was developed largely for coarse materials.

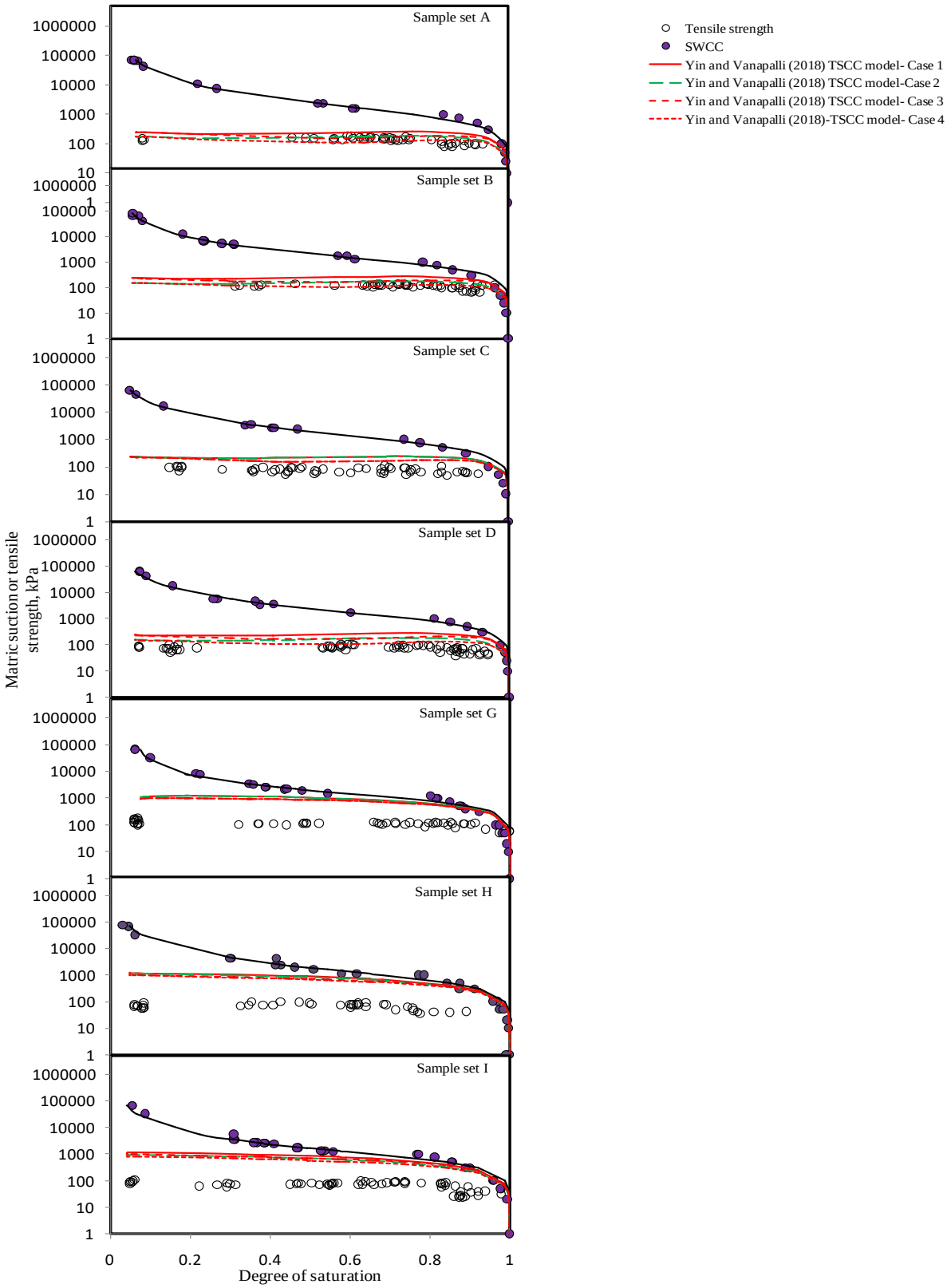

Figure 6.17: Evaluation of Yin and Vanapalli (2018) tensile strength model

Table 6.9: Parameters for Yin and Vanapalli (2018) tensile strength model for Cases 1 to 4

Sample set	Changed model parameters and RMSE	Case 1 $\phi_t = \phi'$	Case 2 ϕ_t = min (ϕ', ϕ_{t_exp})	Case 3 $\phi_t = \phi'$ (ϕ', ϕ_{t_exp})	Case 4 ϕ_t = min (ϕ', ϕ_{t_exp})	Other model parameters
A	η_s	4.38	4.38	4.38	4.38	e = 0.45
	k	4.04	4.04	6.07	6.07	d_{50} = 0.005 mm
	RMSE	114.25	47.09	58.91	39.11	S_c= 0.92 S_r = 0.0010
B	η_s	4.38	4.38	4.38	4.38	e = 0.48
	k	3.52	3.52	5.29	5.29	d_{50} = 0.005 mm
	RMSE	137.68	52.37	73.94	23.92	S_c= 0.90 S_r = 0.0140
C	η_s	4.38	4.38	4.38	4.38	e = 0.515
	k	3.61	3.61	5.42	5.42	d_{50} = 0.005 mm
	RMSE	148.63	148.63	92.37	92.37	S_c= 0.90 S_r = 0.0010
D	η_s	4.38	4.38	4.38	4.38	e = 0.49
	k	3.64	3.64	5.46	5.46	d_{50} = 0.005 mm
	RMSE	147.74	73.05	94.27	40.10	S_c= 0.90 S_r = 0.0010
	η_s	4.38	4.38	4.38	4.38	e = 0.48
E	k	4.32	4.32	6.48	6.48	d_{50}=0.02 mm
	RMSE	44.51	44.51	30.95	30.95	S_c =0.90 S_r=0.0010
	η_s	4.38	4.38	4.38	4.38	e = 0.57
F	k	2.46	2.46	3.70	3.70	d_{50}=0.02 mm
	RMSE	117.44	76.26	53.72	28.72	S_c= 0.90 Sr = 0.0010
G	η_s	73	73	73	73	e = 0.44
	k	1.49	1.49	2.24	2.24	d_{50} = 0.02 mm
	RMSE	707.99	707.99	608.17	608.17	S_c= 0.92 S_r = 0.0580
H	η_s	73	73	73	73	e = 0.44
	k	1.90	1.90	2.85	2.85	d_{50} = 0.02 mm
	RMSE	811.07	755.51	676.53	629.52	S_c= 0.90 S_r = 0.0001
I	η_s	73	73	73	73	e = 0.505
	k	1.77	1.77	2.66	2.66	d_{50} = 0.02 mm
	RMSE	657.04	524.89	552.22	439.15	S_c= 0.920 S_r = 0.0065

Hence, the empirical Equations 6.9 and 6.10 suggested by Yin and Vanapalli (2018) are not applicable for the soils tested in this study.

6.4.3 Summary

Two tensile strength models, Lu et al. (2009) and Yin and Vanapalli (2018), were evaluated against the experimental data in this study. Both models did not perform well using the parameters as proposed. Both models performed poorer with soil sample sets from the Jurong Formation (sample sets G-I) compared with those from the Bukit Timah Granite (sample sets A-D).

Case 2 provides the best estimation of tensile strength for the Lu et al. (2009) model while Case 4 provides the best estimation of tensile strength for the Yin and Vanapalli (2018) model. RMSE values suggest that Yin and Vanapalli (2018) model performs better than Lu et al. (2009) model for sample sets A-D while the Lu et.al (2009) model performs better for the sample sets G-I. However, it should be noted that the Lu et.al (2009) model performs better for JF soil sets (G-I) because the VG model parameters are doubled (Cases 2 to 4) suggesting more coarseness in the material compared to the original material (Case 1). This therefore suggests that the Yin and Vanapalli (2018) generally performs better than the Lu et.al (2009) model. However Lu et.al (2009) model requires much fewer parameters compared to the Yin and Vanapalli (2018) model, making it much easier to use.

The models performed better at the lowest ϕ_t for all degrees of saturation. This is at odd with the suggestion by Lu et al. (2009) who suggest that ϕ_t should be higher than ϕ'. However, Lu et al. (2009)'s tensile strength model was developed from experiments performed on sands. In Yin and Vanapalli (2018) tensile strength model, the effect of ϕ_t seems minimal.

Lu et al. (2009)'s tensile strength model is best suited for soils with n in VG equation greater than 2, i.e. coarse-grained materials, whereas the n obtained for the compacted soils in this study

are all less than 2. The empirical relations of k and η_s suggested by Yin and Vanapalli (2018) are inadequate for the compacted soils in this study.

6.5 Concluding remarks

This chapter has investigated the unconfined compressive strength and tensile strength of compacted soils. The effects of soil suction, structure and void ratio on the strength of compacted soils have been examined. Two tensile strength models were also evaluated using the experimental data in this study. The main findings are:

There is an interplay of matric suction, soil structure and void ratio influencing soil strength. The influence of matric suction on strength is minimal for dry soils. The contribution of matric suction to strength as a near saturated soil dries is significant up to the air-entry value, beyond which the contribution is negligible as the water phase becomes discontinuous.

The unconfined compressive strength and the Brazilian tensile strength with compaction water content have the same shape as the compaction curve.

The unconfined compressive strength data shows less scatter than the Brazilian tensile strength data possibly reflecting the greater variability of smaller specimens in the Brazilian tensile strength tests.

Although significant increase in the unconfined compressive strength is noted up to the AEV, strength increase continues up to the shrinkage limit, albeit at a decreased rate. Hence, shrinkage limit which indicates no further change in void ratio is an important water content in strength of unsaturated soils.

The ratio of unconfined compressive strength to Brazilian tensile strength (q_u/σ_t) lies within the range of 4 to 15.

The two tensile strength models evaluated were not able to capture the tensile strength of the compacted soils. Further research is needed to develop better tensile strength models that take into account the complex structures of compacted soils.

Chapter 7. Constant water content shear strength tests on compacted soils

7.1 Introduction

The common practice of determining shear strength parameters for unsaturated soils is through consolidated drained (CD) test performed with suction-controlled equipment, either the direct shear or the triaxial apparatus. These equipment have been reported by several researchers to be expensive and highly sophisticated hence requiring high level expertise to conduct the tests. In addition, the test duration is long and the suction range is limited by the HAEV ceramic disk.

The constant water content (CW) test addresses some of these concerns. As mentioned in Chapter 2, studies have noted that the CW test not only addresses some of the concerns of the CD test but may actually be more representative of some field stress paths. During a CW test, the air phase of the soil sample is allowed to drain while the water phase is undrained.

The CW test is usually performed using the axis translation technique (ATT). However recently some researchers such as de Oliveira et al. (2016) and Marinho et al. (2016) have suggested more accessible procedures for the CW test that eliminate the need for the ATT. In these procedures, the CW test is done on the as-compacted soil specimens with matric suctions monitored using a high capacity tensiometer (HCT) at the base of the specimen. While these tests substantially reduce testing time and specimens with high matric suctions can be tested, attaining equilibrium with HCT is sometimes challenging especially with dry soils (high matric suction). The problem of cavitation was presented in Chapter 2 .

In this study, an attempt is made to evaluate possibility of determining shear strength parameters of unsaturated soils using compacted soils and conventional soil tests namely, unconfined

compression (UC) test, undrained unconsolidated (UU) test and the consolidated undrained (CU). As discussed in Chapter 3, the UC and UU tests have been done on the as-compacted (unsaturated) specimens while the consolidated undrained (CU) tests have been done to obtain saturated shear strength parameters i.e., ϕ' and c'. Apart from measuring the matric suction of the as-compacted specimens, no matric suction measurement was done during the test.

The average properties of the test specimens used in this part of the study are the same as those used for test series 1 in Chapter 6 as given in Figures 6.1 and 6.2 and Tables 6.1 to 6.4.

7.2 Unconfined compression and unconsolidated undrained tests

As mentioned above, UC and UU tests were done on the as-compacted soil specimens. The observations for these specimens are presented below

7.2.1 Stress-strain behavior

7.2.1.1 Effect of net confining pressure

Figure 7.1 shows typical deviator stress versus axial strain plots of the as-compacted soil specimens for both the UC and UU tests. The UC tests were done in triplicate. Only selected plots of soil BT1 are shown in Figure 7.1, the other plots and those of other soil specimens are presented in Appendix D1. In Figure 7.1, each subplot is for a different compaction water content as indicated on the plot. For each compaction water content, shearing was done at five net confining pressures (σ-u_a) of 0, 70, 150, 300, 600 kPa. Net confining pressure (σ-u_a) = 0 refers to the unconfined compression (UC) test.

At a given compaction water content, an increase in (σ-u_a) shows an increase in ductility of the specimen i.e., the higher the confining pressure, the less distinct is the peak deviator stress. Thu

et al. (2006) attributes the increase in ductility to restrained dilation during shearing as a result of increase in confinement. When dilation is restrained, the peak stress is attained gradually instead of abruptly.

Figure 7.1 also shows that the axial strain at failure increases as net confining pressure increases. Specimens at low net confining pressure display behavior similar to overconsolidated clays which have brittle failure. This is particularly pronounced for specimens compacted dry of optimum and sheared at low net confining pressure. The stiffness and shear strength increase with increase in net confining pressure. There is more remarkable increase in shear strength for specimens compacted dry optimum compared to specimens compacted wet of optimum. On the wet of optimum, as net confining pressure increases, the specimens tend to get close to saturation hence increasing net confining pressure may not have great benefit on the shear strength.

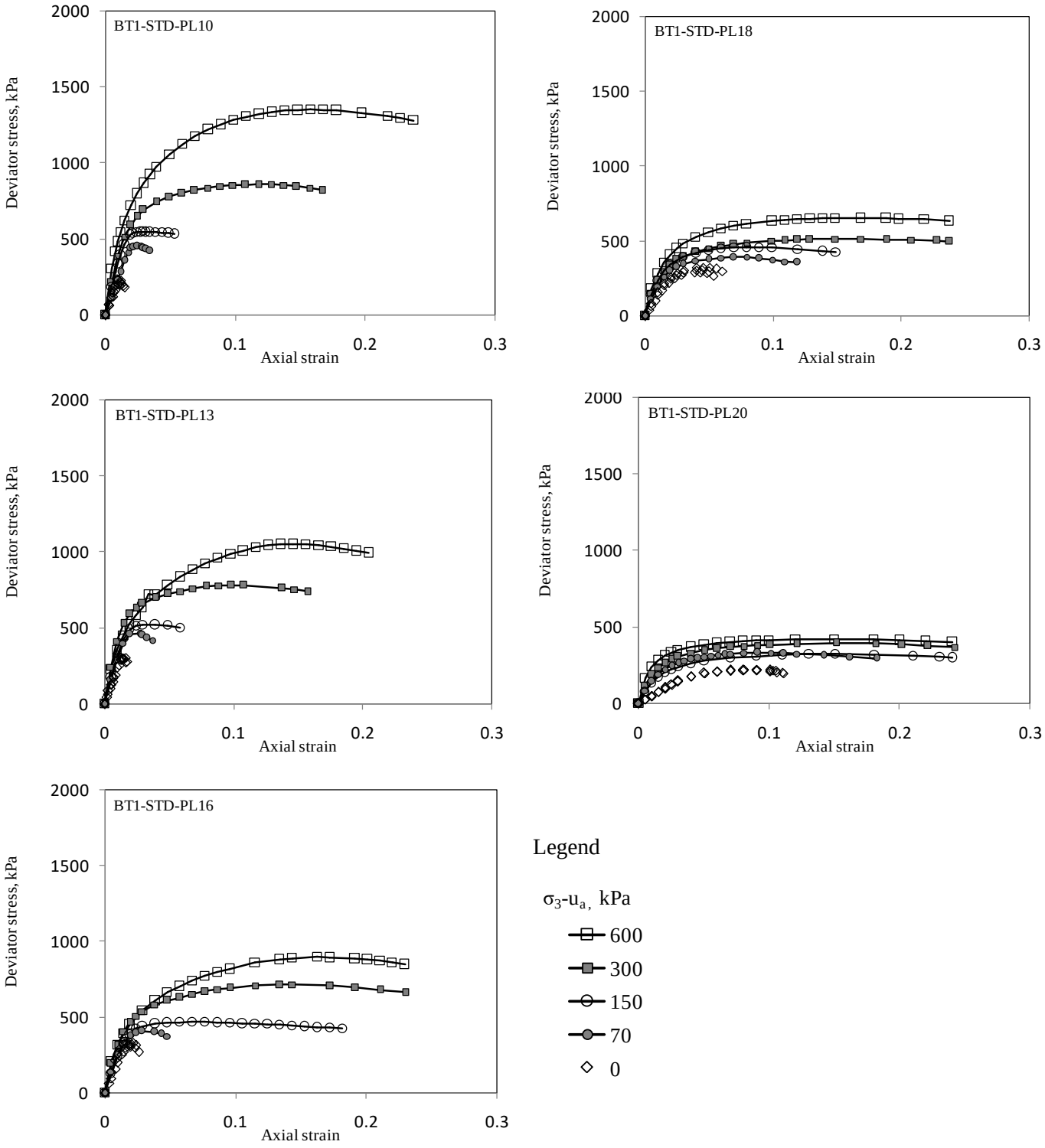

Figure 7.1: Deviator stress versus axial strain plots for UC and UU tests

Specimens compacted dry of optimum do not show remarkable change in initial stiffness despite increase in net confining pressure. The stress-strain curves tend to cluster together showing slight

increment in stiffness despite substantial increase in shear strength. Similar observations are seen for the other soil specimens presented in Appendix D1.

7.2.1.2 Effect of compaction water content

It has generally been accepted that different compaction water contents yield soils with different structures hence non-identical soils. Figure 7.2 shows the stress-strain curves for BT1 specimens compacted at different compaction water contents at various net confining pressure. The other plots and those of other soil specimens are presented in Appendix D2. Irrespective of compaction effort at the same confining pressure, the specimens become more brittle as compaction water content reduces i.e., soil specimens compacted dry of optimum tend to display high brittleness compared to those soil specimens compacted wet of optimum. The axial strain at failure became increasingly smaller with reduction in compaction water content. In fact, dry of optimum specimens in some cases display post-peak softening. This can be attributed to the high suctions of soil specimens compacted dry of optimum as well as an open structure of these soils. As Thu et al. (2006) observed, soils with high suctions exhibit overconsolidated behavior hence increasing the brittle behavior. The open structure plus a high likelihood of internal microstructures (Sun and Cui, 2017) also contribute to high brittleness. As the specimens get wetter, their structures become flocculated and they display plastic behavior more typical of normally consolidated clays.

At a given net confining pressure, peak shear strength increases with reduction in compaction water content. This is attributed to suction which increases with the compaction water content. It is interesting to note that for a given compaction effort and net confining pressure, suction seems to override the void ratio effect i.e., drier specimens display higher shear strength than wetter

ones irrespective of their initial void ratio. The stiffness of the specimen increases with reduction in compaction water content attributed to increase in suction.

Similar observations are seen for the other soil specimens presented in Appendix D2.

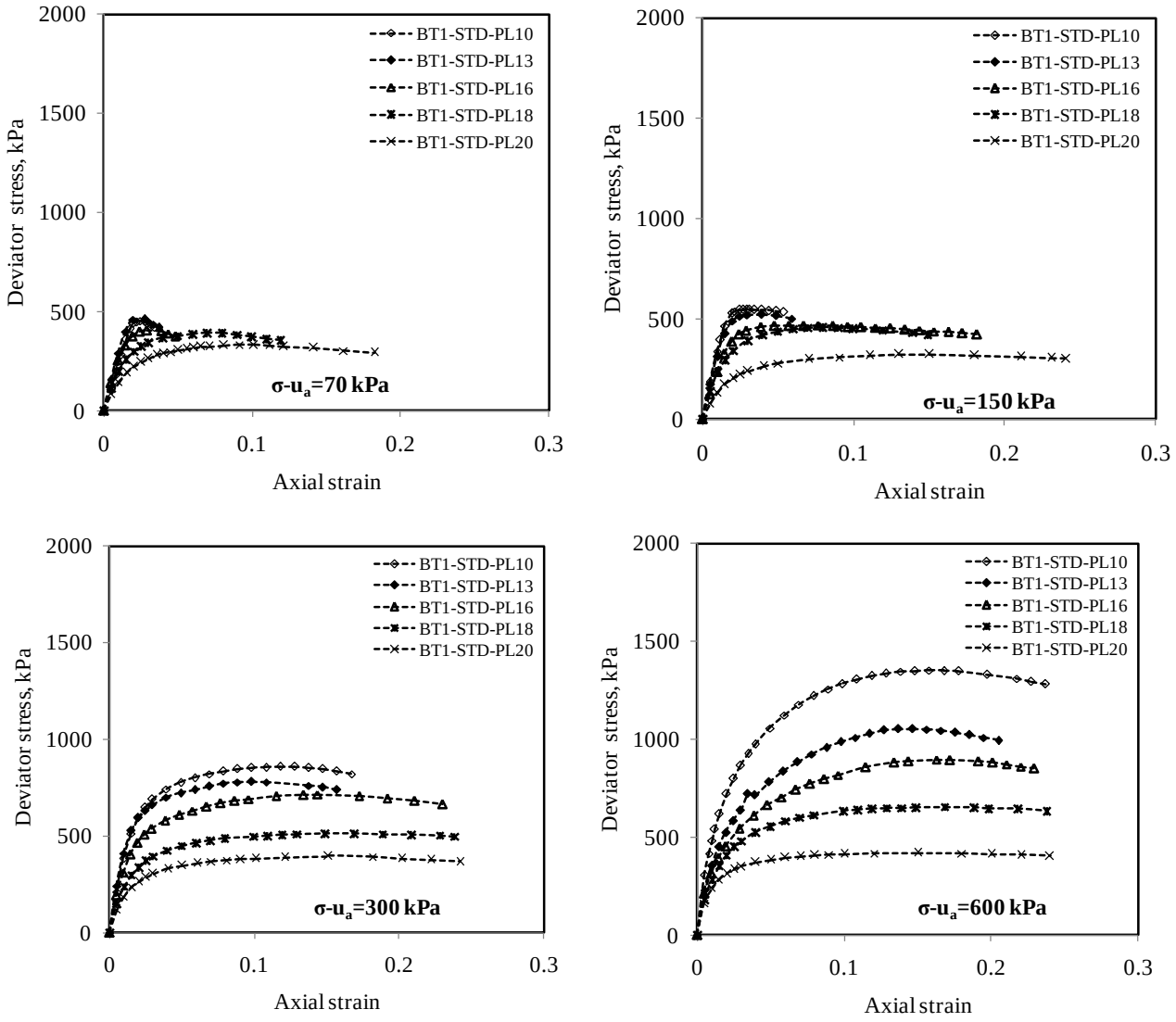

Figure 7.2: Effect of compaction water content on the stress-strain behaviour of compacted test specimens

7.2.1.3 Effect of compaction effort

As mentioned earlier, two compaction efforts were used in the study, standard and modified Proctor. The major influence of increasing compaction effort is the decrease in void ratio. Typical stress-stain plots are shown in Figure 7.3. The other plots can be found in Appendices D1 and D2.Figure 7.3 shows that increase in compaction effort generally increases the shear strength of the soil. At same net confining pressure, specimens compacted at modified Proctor effort are more brittle that those compacted at standard Proctor effort. Owing to their higher density (smaller void ratios), specimens compacted at modified Proctor effort show less effect with net confining pressure and hence are more likely to dilate during shear as compared to the specimens compacted at standard Proctor effort. Dilation will cause brittle failures and more post-peak softening. Post-peak softening behavior of dry of optimum specimens compacted at modified Proctor effort is more persistent than similar specimens compacted at standard Proctor effort. This can be clearly observed in Appendix D2 at net confining pressure of 600kPa. The post-peak softening behavior of specimens compacted at standard Proctor effort fades out with increasing net confining pressure.

Comparing specimens on same side of the optimum, specimens compacted at modified Proctor effort are generally stiffer than specimens compacted at standard Proctor effort at the same net confining pressure. This is partly due to smaller void ratios of the modified Proctor compacted specimens.

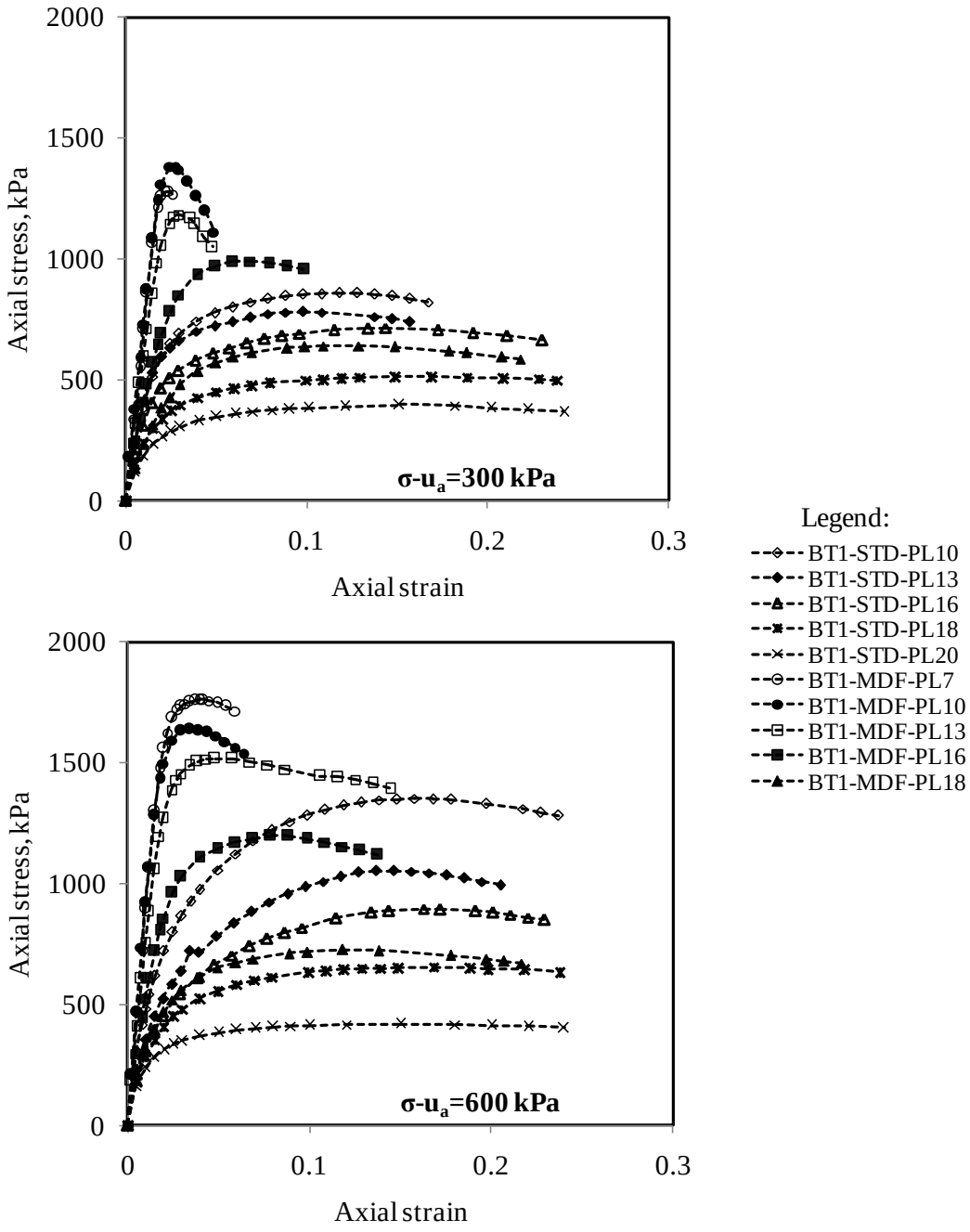

Figure 7.3: Influence of compaction effort on the stress-strain plots

7.2.2 Peak strength

As discussed above, the peak strength is influenced by compaction water content, net confining pressure as well as the compaction effort. Figure 7.4 shows typical plots of variation of peak unconfined compressive strength (q_u) with compaction water content, net confining pressure as well as compaction effort. The other plots are shown in Appendix D3. It is observed that at a given compaction water content, peak strength generally increases with increase in confining pressure. The increase is more pronounced with drier soils. As the compaction water content increases, there is increasingly less benefit because the soils are tending towards saturation hence a drop in suction. It is also interesting to note that the variation of unconfined compressive strength with compaction water content follows almost the same trend as the respective compaction curves at low net confining pressures. At high net confining pressures, the unconfined compressive strength decreases as compaction water content increases.

Figure 7.5 shows typical Mohr circles derived from the peak deviator stresses at the different net confining pressures. Peak deviator stresses for the UC and UU tests together with the failure axial strains are presented in Appendix D5. The plots in Figure 7.5 show behavior of the specimens compacted dry and wet of optimum. The specimens compacted dry of optimum show increase in strength with increasing confining pressure for the range of pressures studied. Therefore, undrained shear strength of unsaturated soils is a function of the confining pressure. The specimens on wet of optimum soon get to saturated state as confining pressure is increased. This is reflected by the Mohr circles negligibly increasing in size as confining pressure increases, a behavior typical of the $\varphi_u = 0$ concept observed in saturated soils. Under the $\varphi_u = 0$, a horizontal line can be drawn tangential to all the Mohr circles since any increment in confining pressure is

counteracted by an increase in pore water pressure hence resulting in no net increase in the shear strength. In addition to Figure 7.5, more plots are presented in Appendix D6.

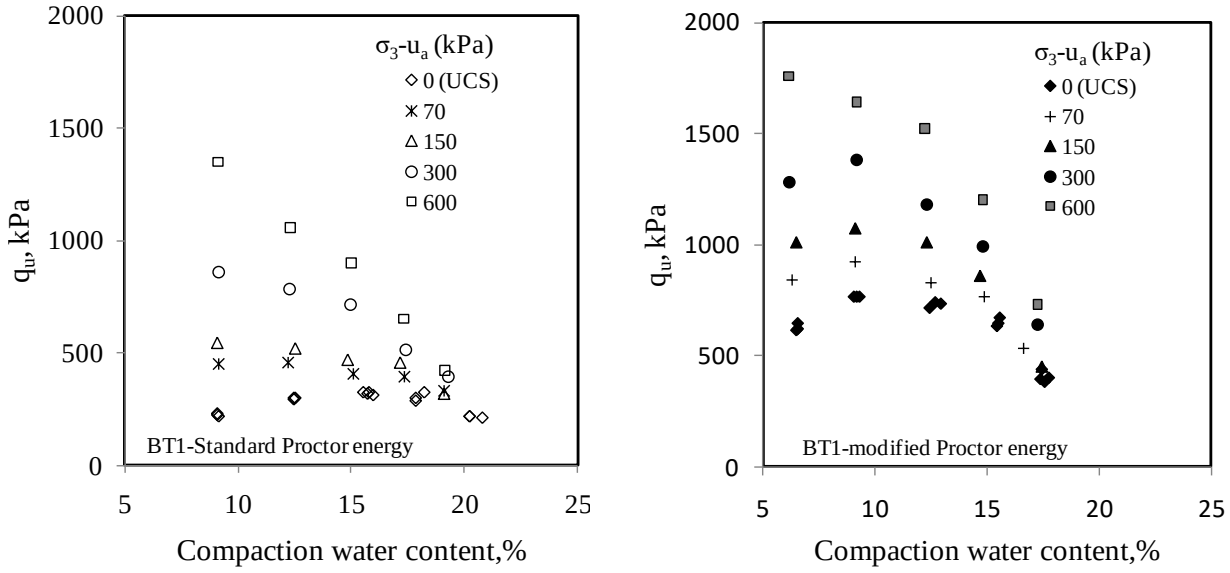

(a) BT1 soil

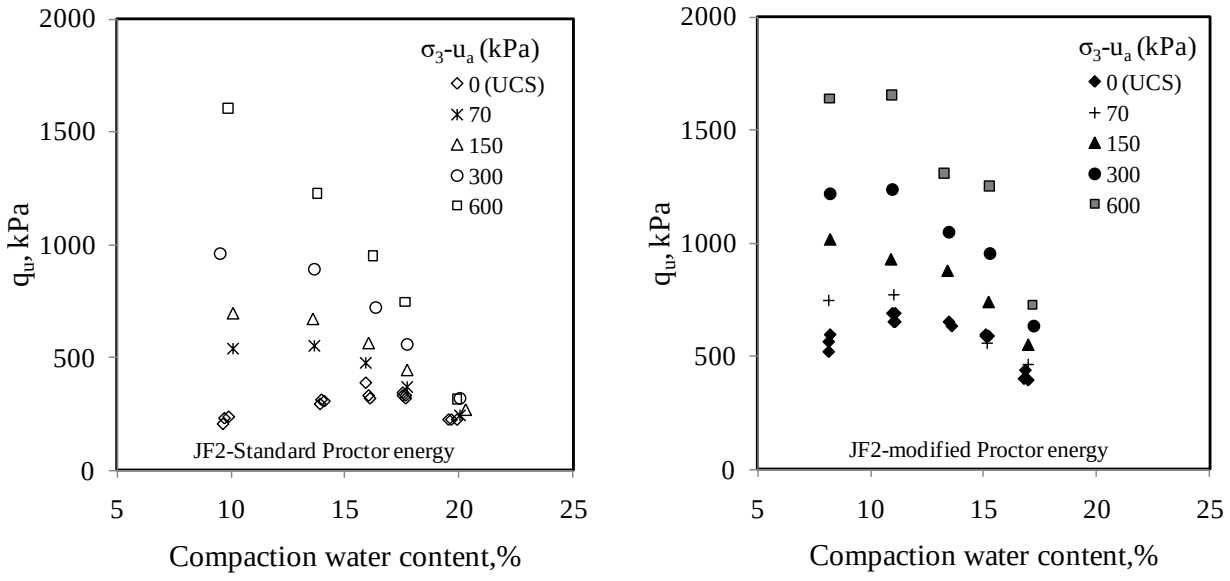

(b) JF2 soil

Figure 7.4:Peak strength variation with net confining pressure , compaction water content and compaction efforts

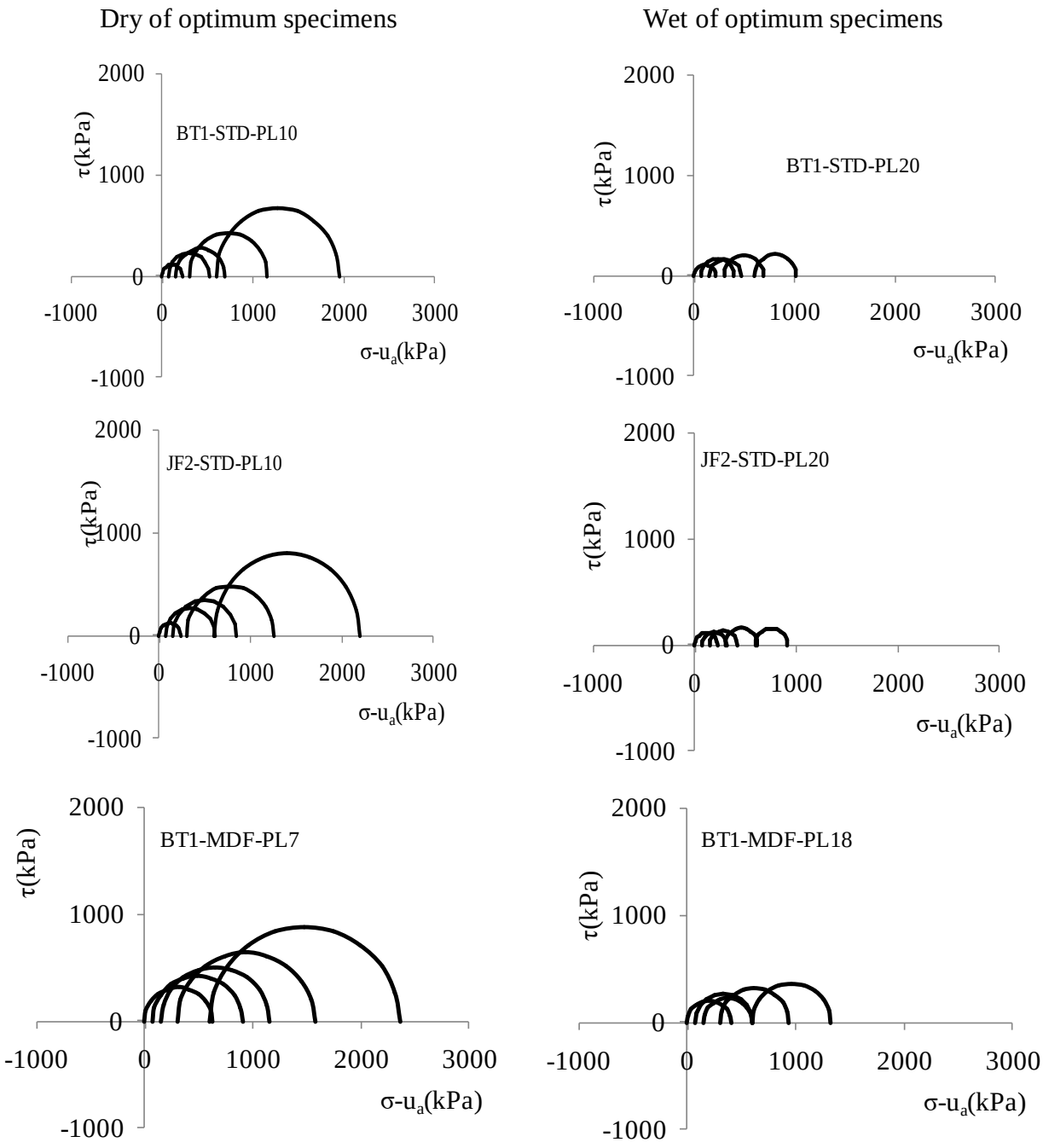

Figure 7.5: Typical Mohr circle plots for the UC and UU tests

7.3 Saturated shear strength parameters

As mentioned earlier, in order to interpret shear strength behavior of unsaturated soils, it is important to evaluate the saturated shear strength parameters of the soil i.e., ϕ' and c'. Unsaturated shear strength is a combination of the saturated shear strength and contribution to shear strength from matric suction. Following the idea that compaction water content affects the structure of the compacted soil, it was assumed that each compaction water content yielded a different soil and hence for each compaction water content, ϕ' and c' were determined using a CU test described in Chapter 3.Figure 7.6 shows such typical plots of deviator stress versus axial strain for the multi-stage testing including the derived Mohr-Coulomb envelopes. Appendix D4 shows a summary of CU test data including ϕ' and c' for all the compacted specimens.

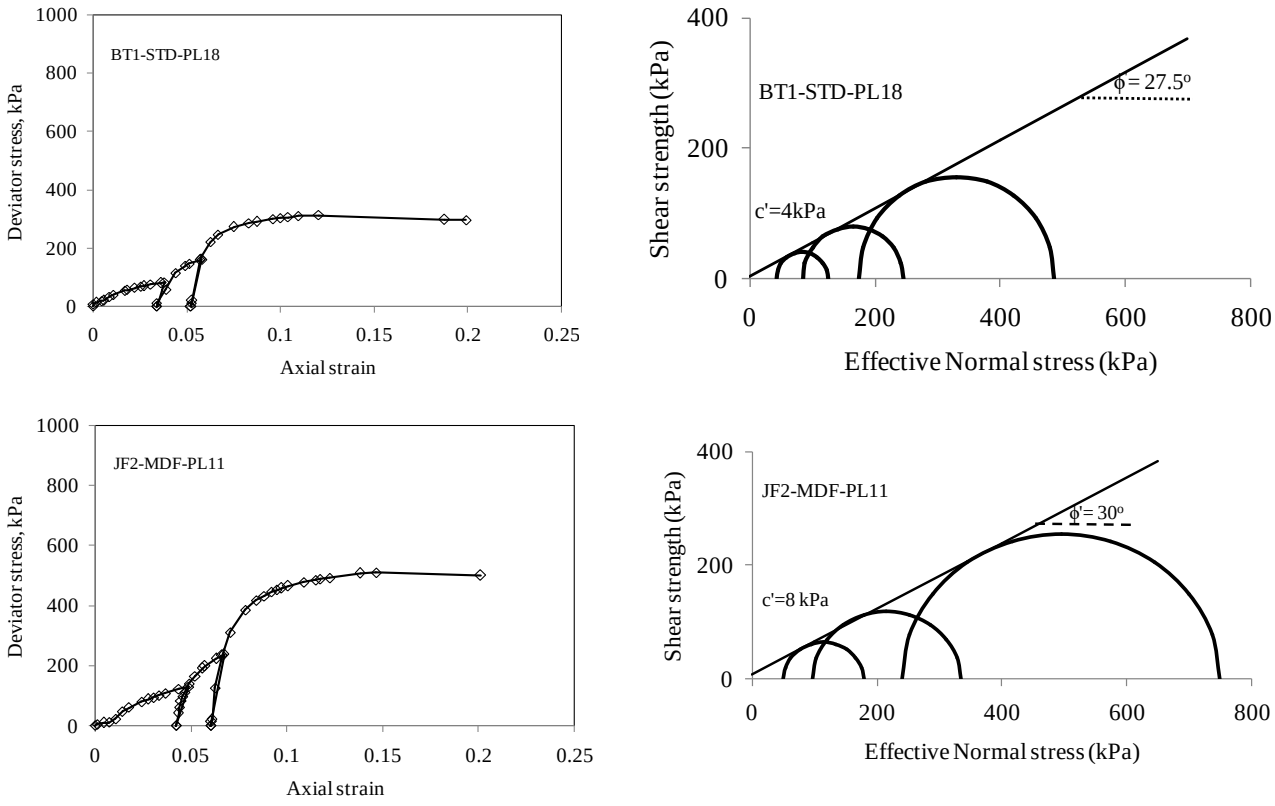

Figure 7.6: Typical stress-strain plots for the CU multi-stage test and the derived Mohr-Coulomb envelope

Figure 7.7 shows the variation of ϕ' with compaction water content and compaction dry density, while similar plots for c' are shown in Figure 7.8

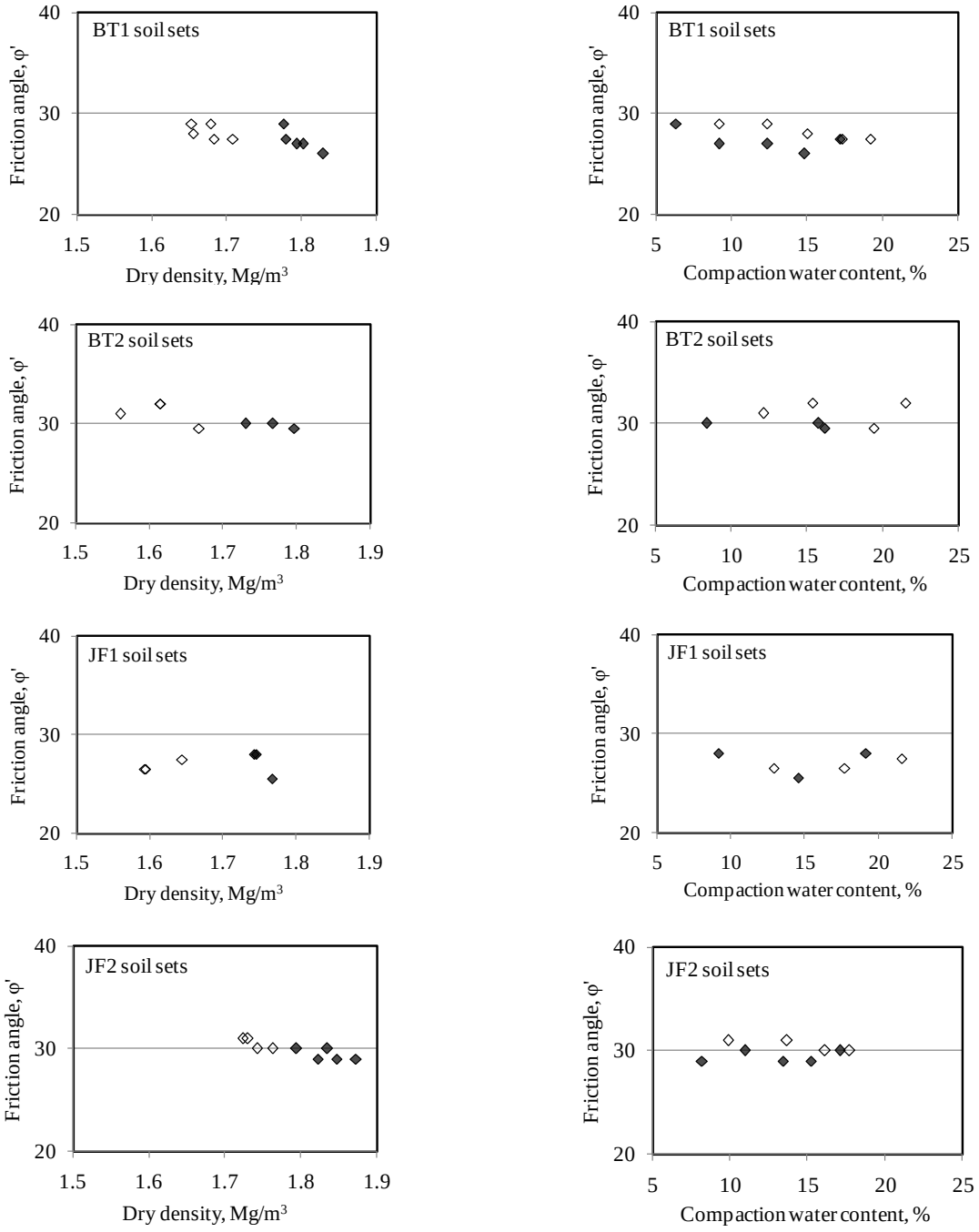

Figure 7.7:Variation of friction angle with dry density and compaction water content

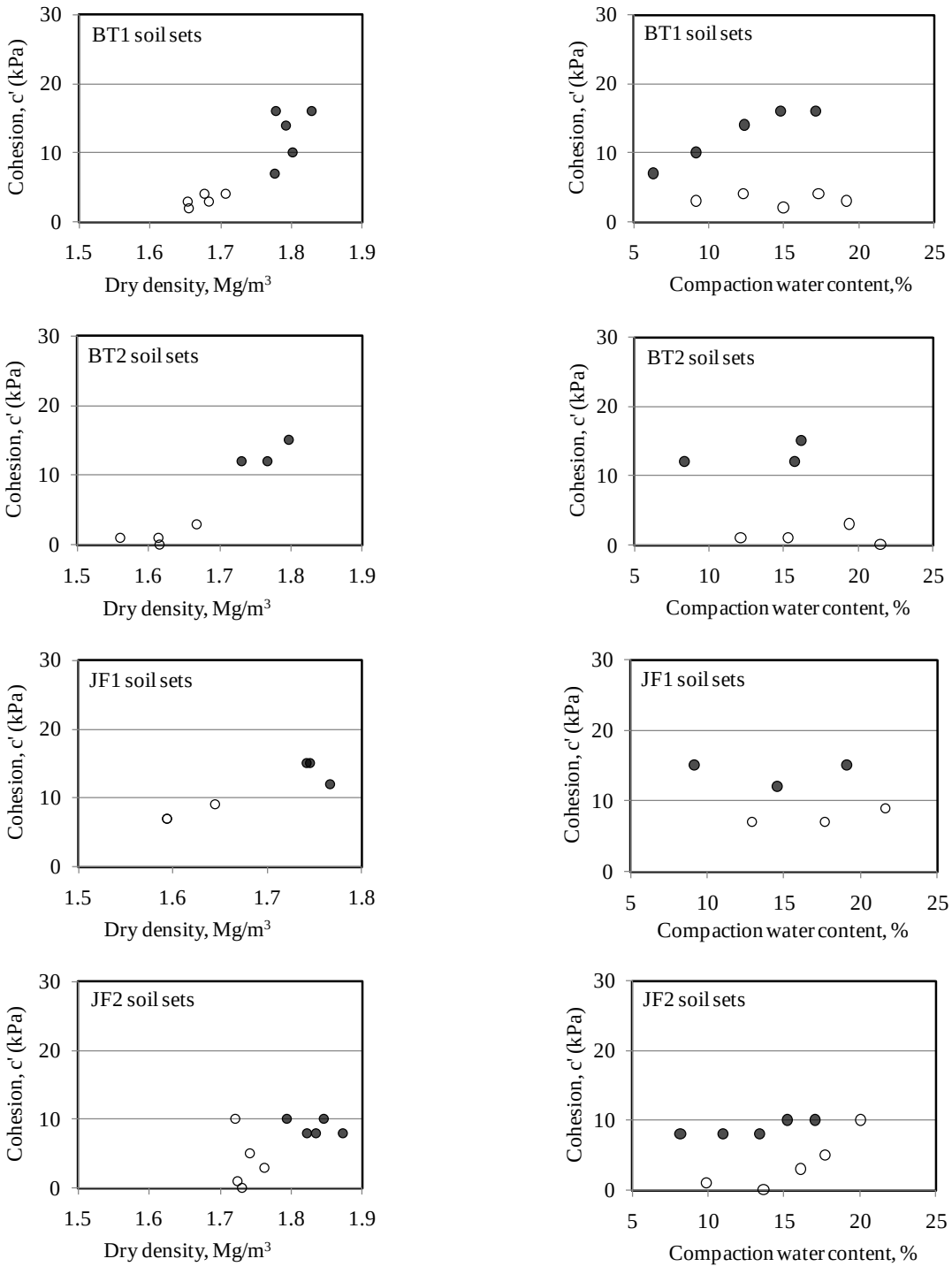

Figure 7.8: Variation of effective cohesion with dry density and compaction water content

From Figure 7.7 the dependency of ϕ' on dry density is not obvious. Intuitively, it is expected that ϕ' increases with dry density. Although soil structure may also affect ϕ' coupled with experimental errors, the variation of ϕ' over the range of dry density studied is small. A similar observation has been reported by Marinho et al. (2016). Also as mentioned in section 7.2.1.1, compacted soils tend to display over-consolidated (OC) behavior at low net confining pressure and normally consolidated (NC) behavior at high net confining pressure. This has great implication on the selection of effective confining pressures for the CU test yet very often the initial stress state of the specimens at the end of the compaction process is unknown. In this study, effective confining pressures of 80, 150 and 300 kPa were selected taking into account the limitations of the pressure equipment in the laboratory. Figure 7.9 illustrates the OC and NC behaviour largely observed with samples compacted dry of optimum. From Figure 7.9a it is observed that the soil specimen displays OC behavior for the first two Mohr circles and NC behavior for last Mohr-circle. These effects show the ambiguity in determining saturated shear strength behavior of compacted soils. In this study, this ambiguity was not explored in further details. In this study, given the small variation of ϕ' for the same soil compacted at different compaction water contents, an average ϕ' was adopted for each compaction effort for interpretation of c'. Figure 7.10 shows that when an average effective friction angle is used to interpret the results, more scatter is observed in the effective cohesion showing a conclusion that there is a greater uncertainty in the determination of c', a well known fact in geotechnical engineering. Table 7.1 presents the minimum, average and maximum ϕ' for each soil at the different compaction efforts. Also shown in Table 7.1 is the average ϕ' for the same soil regardless of compaction effort. Figure 7.10 shows the interpretation effective cohesion , c' using the average friction angle for each compaction effort. If the spread of the friction angles is

narrow, it is expected that adoption of an average value for friction reduces the scatter in the effective cohesion values. This is not easy to attain given the sensitivity of effective cohesion to friction angle as the M-C envelope is fitted to the Mohr circles. A slight change in the inclination of the envelope may affect the cohesion value substantially hence the greater variability in cohesion compared to friction.

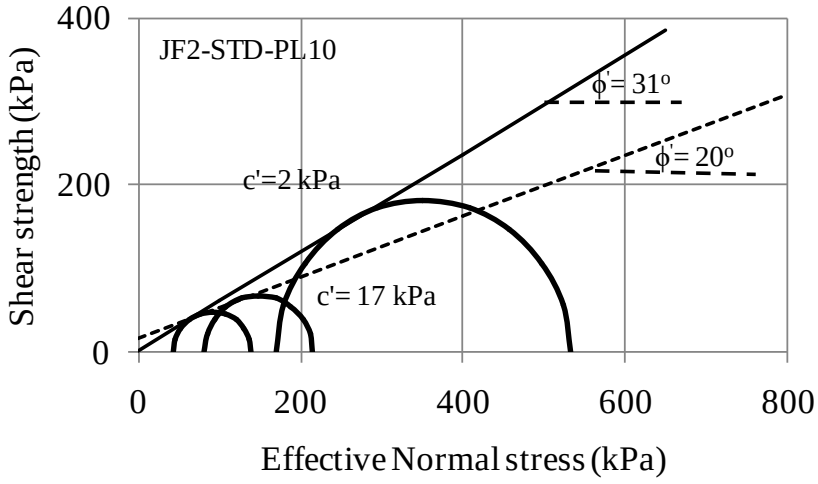

a)

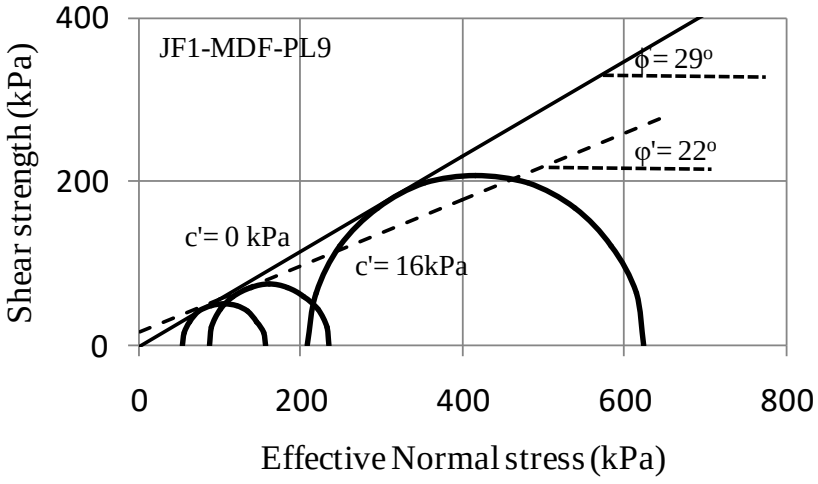

b)

Figure 7.9: Errors in determining shear strength parameters of compacted soils

Table 7.1: Variation of friction angles for the different soils

Soil	Compaction Proctor effort	Minimum φ'(°)	Average φ'(°)	Maximum φ'(°)	Overall average φ'(°)
BT1	Standard	27.5	28.5	30.6	27.9
	Modified	26.0	27.3	29.0	
BT2	Standard	29.5	31.1	32.0	30.6
	Modified	29.5	29.8	30.0	
JF1	Standard	26.5	26.8	27.5	27.0
	Modified	25.5	27.2	28.0	
JF2	Standard	30.0	30.5	31.0	29.9
	Modified	28.0	29.4	30.0	

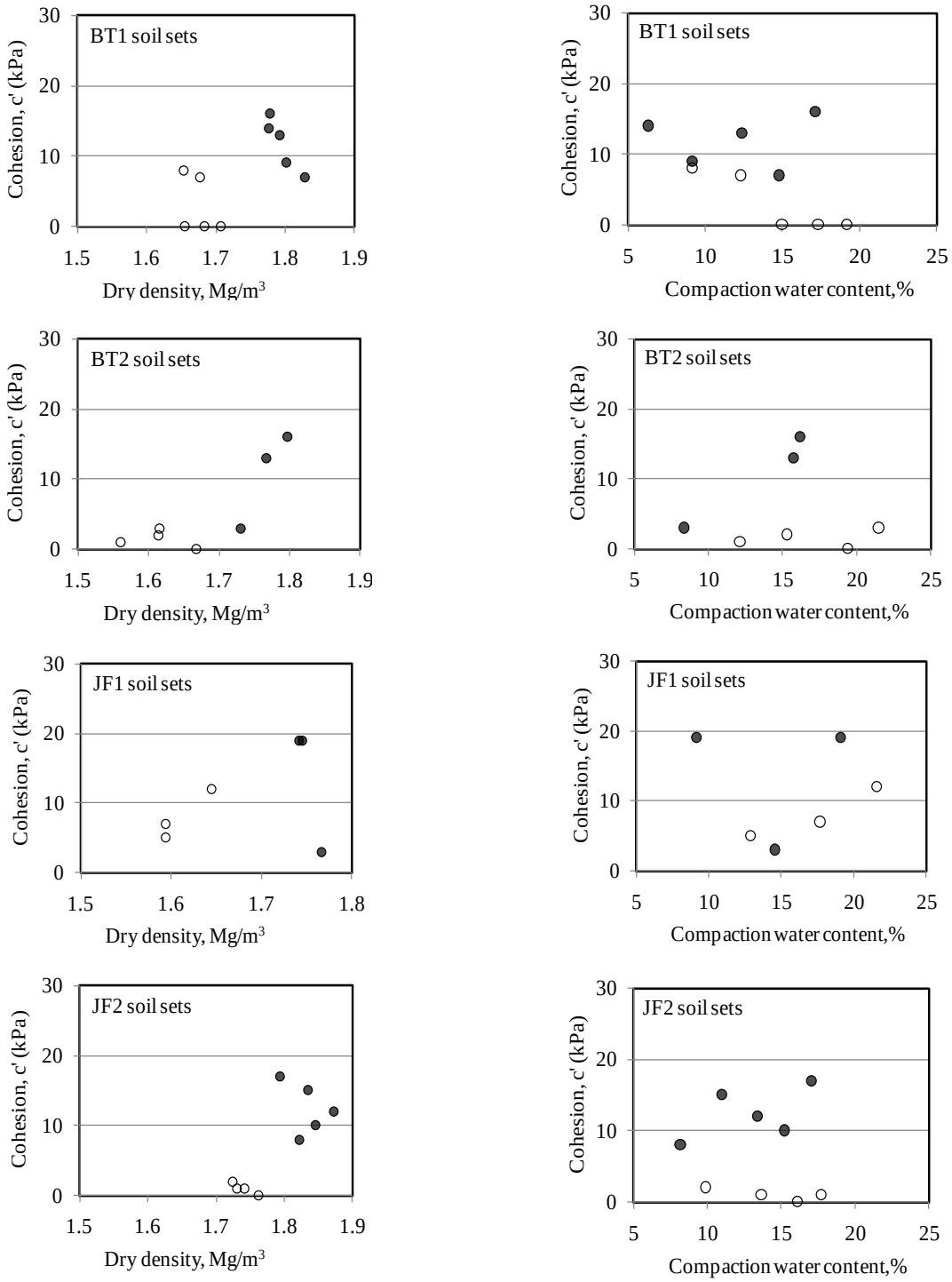

Figure 7.10: Effective cohesion using an average friction angle for each compaction effort

7.4 Proposed interpretation of the CW test

As discussed above, using peak deviator stresses in Appendix D5, Mohr circles were constructed as illustrated in Figure 7.5. An attempt is made to derive total cohesion from UC and UU tests conducted on the as-compacted soil specimens. Lines with slope of ϕ' are drawn tangentially to each Mohr circle as shown in Figure 7.11 for selected soil specimens. The rest of the plots are presented in Appendix D6. It is assumed that as the unsaturated soil specimen is compressed under the net confining pressure, its degree of saturation will increase resulting in a reduction of its matric suction. The reduction in matric suction will be reflected in the total cohesion, C given by the y-intercept of the line shown in Figure 7.11. The total cohesion, C is the sum of the effective cohesion, c' (from saturated tests, CU) and the shear strength contribution from matric suction at zero net normal stress.

Figure 7.12 shows the variation of total cohesion with net normal stress for BT1 soil specimens. It is observed that the total cohesion remains constant at low net normal stress and then decreases with increase in net normal stress. This indicates that the matric suction may remain the same as the as-compacted specimen at low net normal stress and decreases as net normal stress increases.

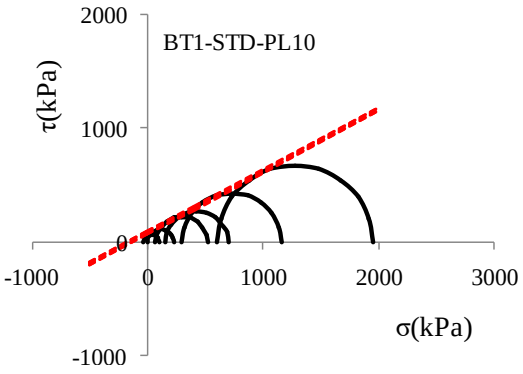

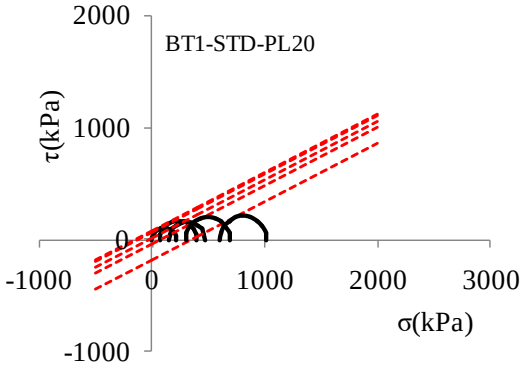

(a) BT1

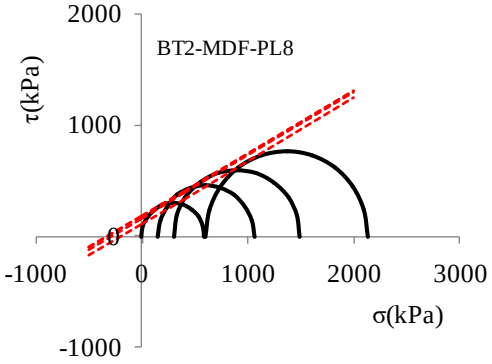

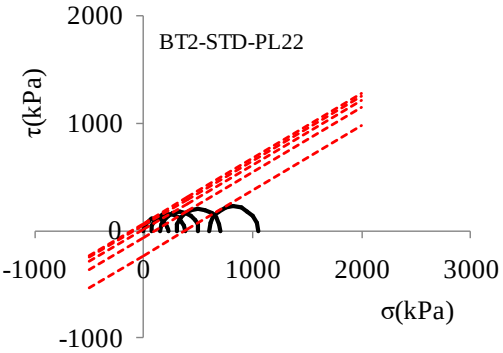

(b) BT2

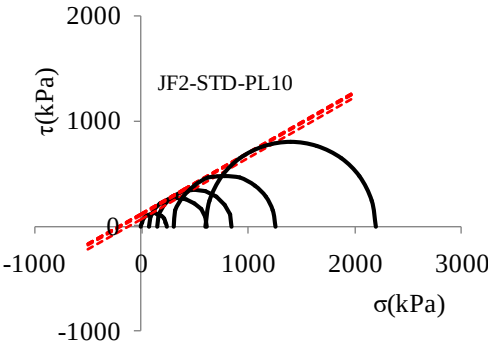

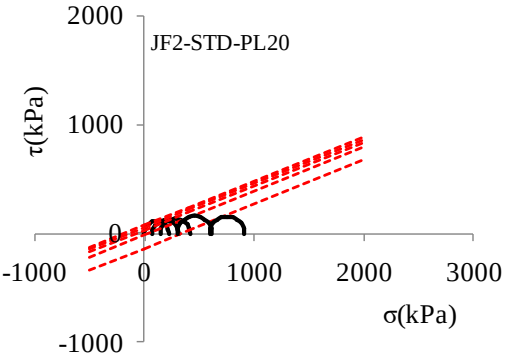

(c) JF2

Figure 7.11: Typical plots showing UU Mohr circles fitted with tangent lines at the respective effective friction angles

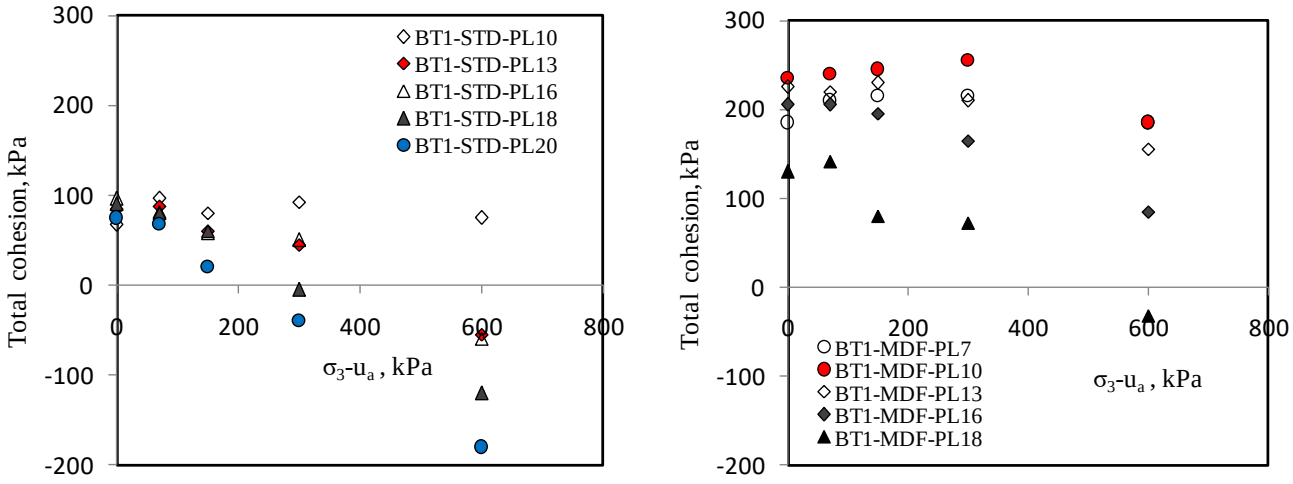

Figure 7.12: Variation of total cohesion with net confining pressure for BT1 soils compacted at standard and modified Proctor efforts

Figure 7.13 shows the Mohr circles of specimens compacted dry of optimum. A single tangent line is able to be drawn to all the Mohr circles revealing that specimens compacted dry of optimum did not experience a reduction in matric suction when net normal stress increases. This suggests that it may also be possible to obtain ϕ' for the specimen without conducting a CU test. Perhaps this is a similar observation that Marinho et al. (2016) made and concluded that with a well performed CW test, the CU test may not be necessary. This is an interesting observation especially for dry soils since they difficult to test using available methods whether ATT or HCT.

This observation is useful in interpreting CW tests. Validating it with more experimental data would be very gainful in the practice of unsaturated soil mechanics. Assuming this holds largely true for most soils including the materials studied in this thesis then the as-compacted suction would be sufficient in fully interpreting a UCS test.

Vanapalli (1994) notes that the unconfined compression (UC) test on a dry soil can be assumed to be conducted at constant suction. In this thesis, only the as-compacted suctions for the soil specimens were determined using the filter paper method as discussed in Chapter 4. Therefore with suction measurements, (u_a-u_w) is available and $\tan\phi^b$ which represents the rate of shear strength increase with (u_a-u_w) can be obtained from the total cohesion C given in Equation 2.52. From Equation 2.52, $\tan\varphi^b$ is evaluated as given in Equation 7.1

$$\tan\phi^b = (C-c')/(u_a-u_w) \qquad (7.1)$$

c' is the effective cohesion obtained from the CU test.

Using the UC test and UU test at the lowest net confining pressure ,$\tan\phi^b$ can be computed from C using with (u_a-u_w) and c' for all the as-compacted specimens. Plots of $\tan\phi^b/\tan\phi'$ versus degree of saturation are given in Figure 7.14.

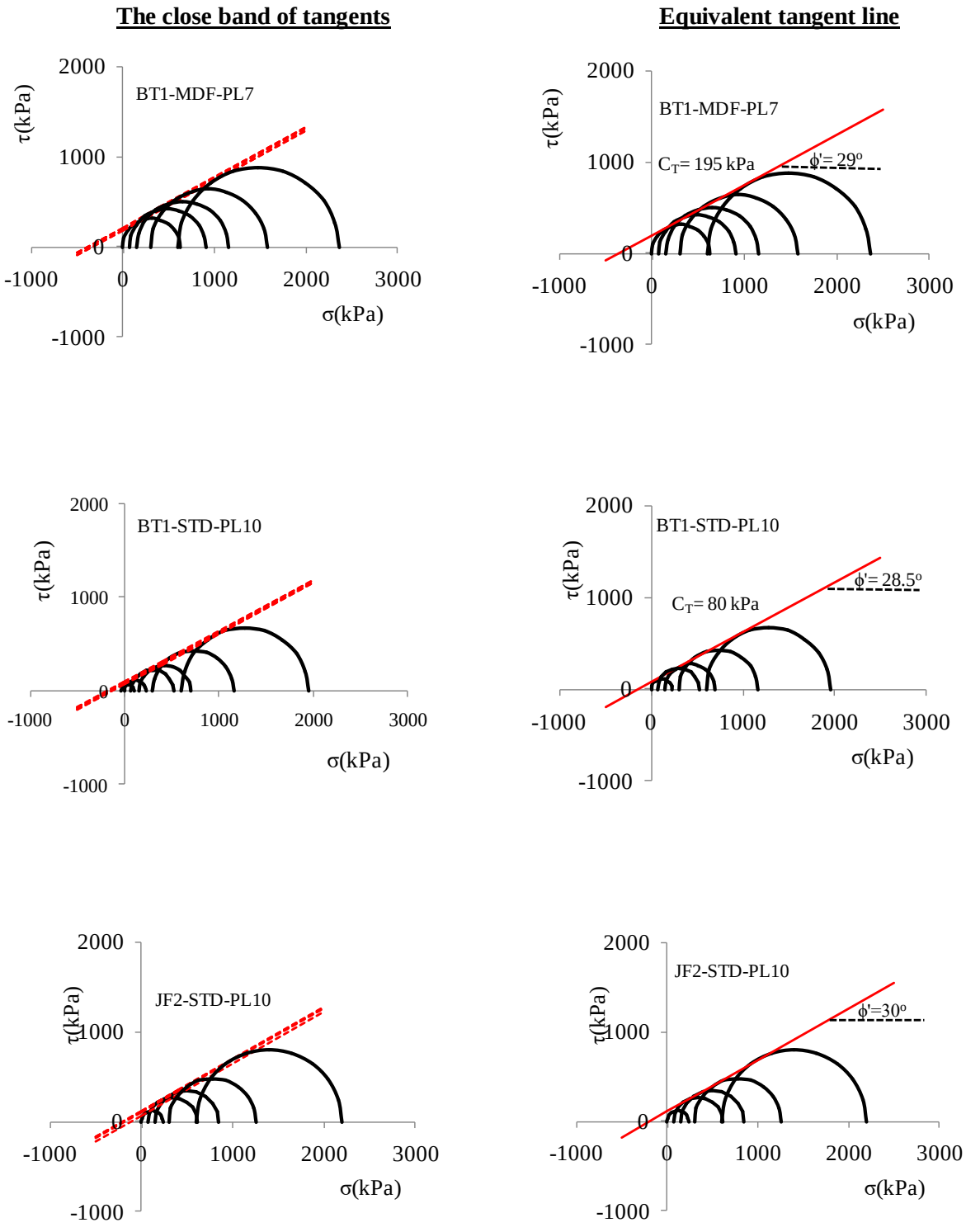

Figure 7.13: A single line for Mohr circles of specimens compacted dry of optimum

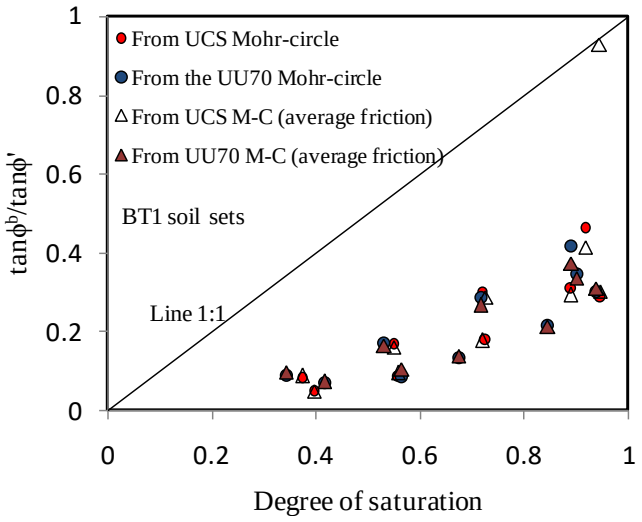

(a) BT1

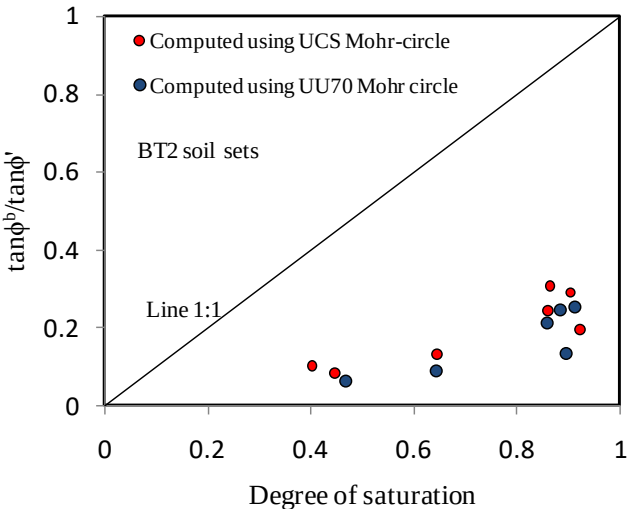

(b) BT2

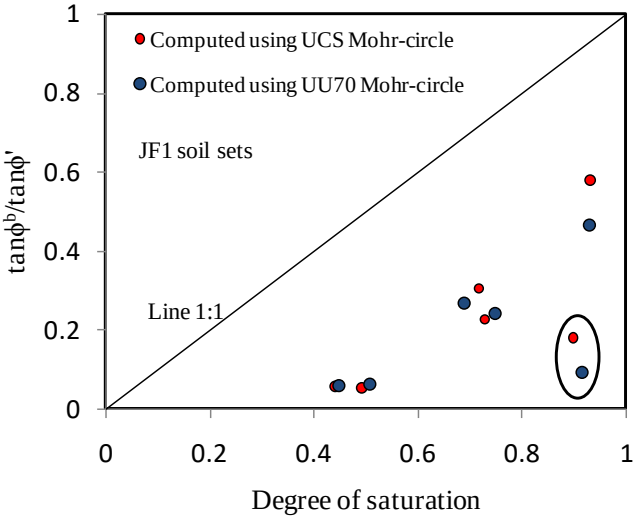

(c) JF1

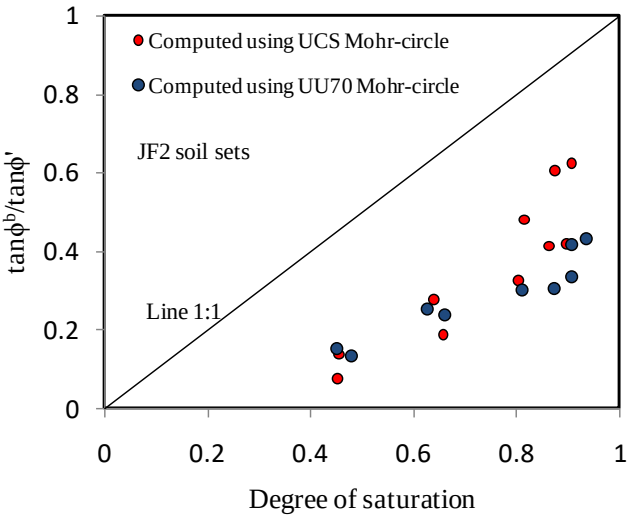

(d) JF2

Figure 7.14: Plots of tanφ^b/tanφ' versus degree of saturation for the as-compacted soil specimens

In Figure 7.14, tan ϕ^b/tan ϕ' ratios derived from fitting tangents to both the UC and UU at lowest net confining pressure of 70kPa (UU70) Mohr circles. The assumption for UU70 may not be correct for the wet of optimum specimens as can be seen for JF2 soil (Figure 7.14d).

For BT1 shown in Figure 7.14a, an attempt was made to include tan ϕ^b/tan ϕ' computed assuming an averageϕ' for all the specimens. As shown in Table 7.1, the overall average ϕ' for BT1 is 27.9^o. Figure 7.14a shows that apart from one point, all the other points seem to agree with those computed using the individual ϕ'. Also observed in Figure 7.14, is that normalization of tan ϕ^b with tan ϕ' may not eliminate the soil structure effect between the specimens. Figure 7.15 combines the tan ϕ^b/tan ϕ' of the as-compacted specimens in Figure 7.14 and those computed using test series 2 in Chapter 6. Similar to the as-compacted samples in Figure 7.14, normalization of tan ϕ^b with tan ϕ' in Figure 7.15 fails to eliminate the soil structure effects between the specimens. The specimens compacted at modified Proctor effort generally show higher tanϕ^b/tan ϕ' than those compacted at standard Proctor apart from JF2 where JF2-STD-PL20 shows higher ratios than JF-MDF-PL17. Also worth noting in Figure 7.15 is that the tan ϕ^b/tan ϕ' from as-compacted soil specimens are lower than those of the dried specimens. This may be important for design as it implies that tanϕ^b determined from as-compacted specimens is conservative compared to dried specimens. .

In Figure 7.16, χ is plotted against the suction ratio as suggested by Khalili and Khabbaz (1998). Khalili and Khabbaz (1998)'s equation for χ is given as Equation 2.2 in Chapter 2. As discussed in Chapter 2, Bishop's χ parameter can be defined in several manner. In trying to link Bishop (1959)'s effective stress concept with Fredlund and Morgenstern (1977)'s concept of independent stress state variables, $\chi$was shown to be tan ϕ^b/tan ϕ' as discussed in Chapter 2. Therefore,χ in Equation 2.2 can be substituted with tanϕ^b/tanϕ'.

While Khalili and Khabbaz (1998) suggested an exponent n= - 0.55 for best fit, in this study n=-0.55 forms the upper bound for BT1 while n=-0.9 forms the upper bound for BT2 and JF2 soil specimens and in all cases n=-1.8 gives the lower bound as shown in Figure 7.16.

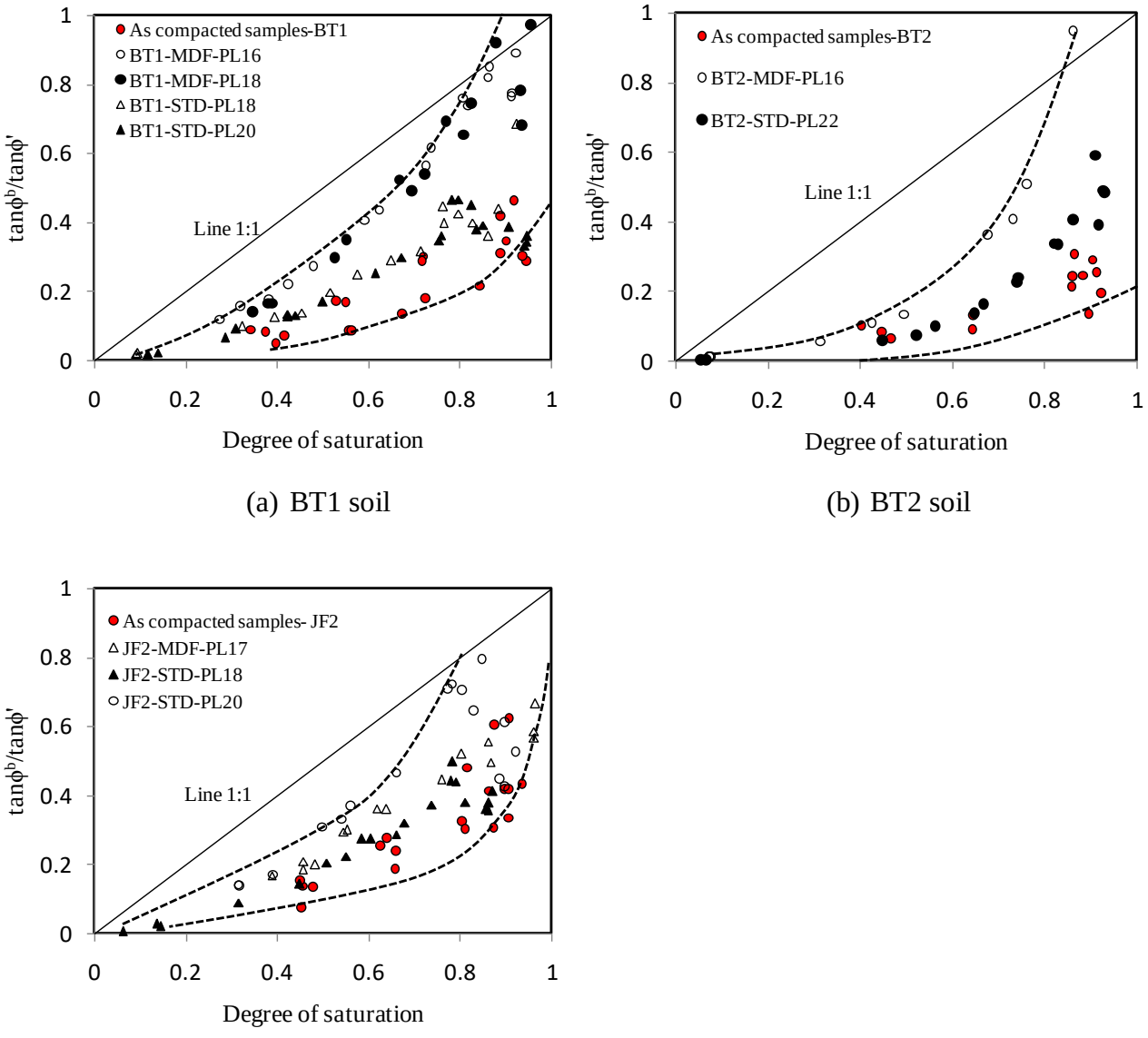

(a) BT1 soil

(b) BT2 soil

(c) JF2 soil

Figure 7.15: Plots of tanφ^b/tanφ' versus degree of saturation for the as-compacted and dried soil specimens

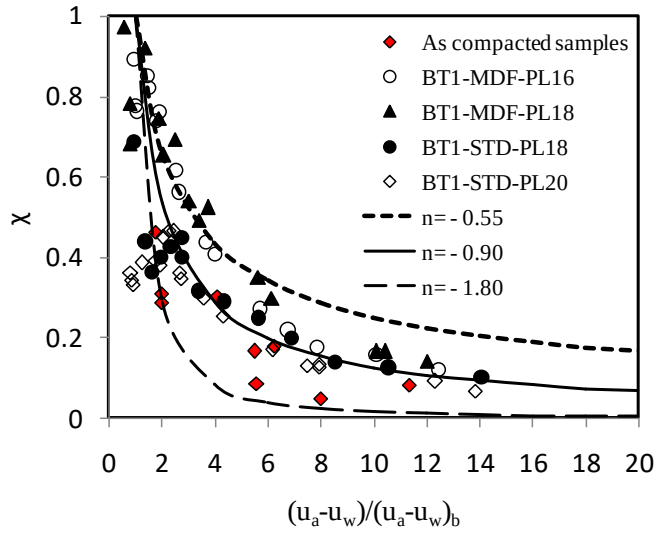

(a) BT1 soil

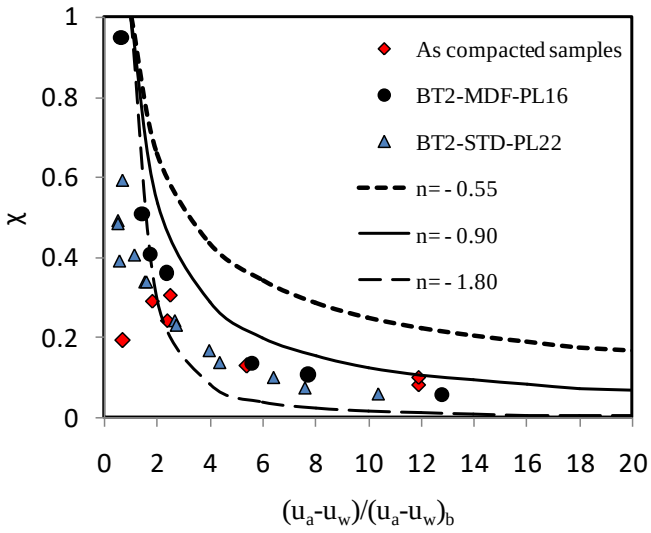

(b) BT2 soil

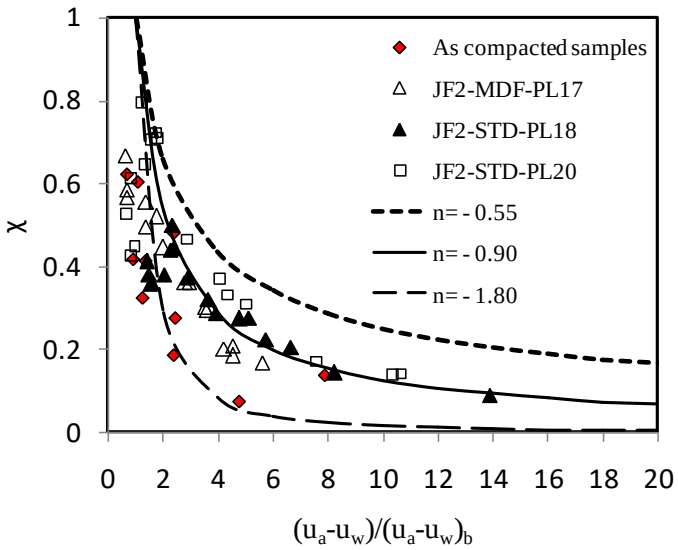

(c) JF2 soil

Figure 7.16: Variation of χ with suction ratio

7.5 Concluding remarks

This chapter has explored possibilities of applying conventional tests to obtain unsaturated shear strength parameters. Although the chapter has been largely exploratory, the following issues have been highlighted:

Stress history, suction, void ratio and structure have great influence on the shear strength behavior of unsaturated soils. The influence of strain rate was not investigated in this study. However, it is envisaged that strain rate has an important influence on the observations and needs to be studied.

In order to obtain meaningful saturated shear strength parameters from a CU test, it is important that stress history of the soil is understood. Compacted soils possess a stress history which is revealed by their stress-strain behavior.

In this study, variation of effective friction angle with dry density was not observed possibly due to experimental errors. However, the variation of effective friction angle over the range of dry density tested was small.

It seems possible to use UU test on unsaturated soils at low net confining stress to determine the effective friction angle hence, CU test for such soils may not be necessary. This needs more study.

The as-compacted soils provide lower values for $\tan\phi^b$ compared to dried soils and hence may provide conservative $\tan\phi^b$ for design. It would be interesting to investigate behavior of specimens tested as-compacted at a constant density with only variation in compaction water content. In this study both dry density and compaction water content varied.

One set back of the present study is that matric suction of the specimen was not monitored during shearing. Without matric suction measurements, observations into the soil behavior are limited and some assumptions are needed. However, this study presents a possible way of interpreting a CW shear test for unsaturated soil test which is fast and possibly applicable in practice. It is recommended that the observations be validated with suction monitoring during shearing.

8. Conclusion and Recommendations

This study explores simple, economical and accessible means of obtaining unsaturated soil properties with a motivation to apply unsaturated soil mechanics in practice. The main focus has been on determination of suction, permeability and shear strength of compacted soils. Below are the conclusion and recommendations for the study.

8.1 Conclusions

8.1.1 Suction measurements

The filter paper technique has been the main focus of suction measurement owing to its affordability, ease of use and capacity to measure a wide range of suction. Both the initially dry and initially wet filter papers were studied as possible suction sensors. The study concluded that:

Although not much field data exists on using filter paper technique, the technique is still very valuable for suction measurement especially if a strict protocol is observed. The initially dry filter paper was found to be preferable to the initially wet filter paper in terms of shorter equilibration time. The hypothesis that an initially wet filter paper may reduce equilibration time was not supported by experimental data

The study agrees with previous studies that 1000 kPa is an appropriate boundary between the low and high suction ranges for practical applications. The contact filter paper is best suited for low suction range while the non-contact one is best for the high suction range. This observation has been corroborated by equilibration durations for the two contact modes of measurement.

Comparing suction measurements using the filter paper method on the as-compacted soil specimens with suction readings from the SWCCs of the different specimens indicated good

agreement in the low suction range. The comparison in the higher suction range needs more scrutiny through more studies

Good agreement was found between the suctions measured using the WP4C and the initially dry contact filter paper. Since the WP4C is recommended as a benchmark for other techniques, this observation is very positive for the filter paper method.

Comparison of the weight distributions of used and unused filter papers show that the used filter papers have a slightly wider weight distribution than the unused filter papers. There is negligible difference in weight distributions between the contact and non-contact filter papers indicating that contamination of filter paper is not an issue and hence, there may not be a need to use sacrificial filter papers in the contact filter paper method to prevent contamination of the filter paper.

8.1.2 Permeability measurements

The suitability of a mini-disk infiltrometer in measuring near-saturated permeabilities of soils has been investigated using measurements from the flexible wall permeameter as the benchmark. It was observed that:

Structure and void ratio influence the permeability of soils.

Permeabilities from the mini-disk infiltrometer are reliable and can give fast indications of the surface infiltration characteristics of the ground. It is greatly preferred to obtain parameters from SWCC measurements to compute the permeability from the infiltrometer test results, however usage of empirical parameters has proved useful and can be relied on as first level estimate of permeability.

As the tension infiltrometers eliminate the effect of macroporosity, they are very valuable in studying rain infiltration which too is largely influenced by the soil matrix and not the macropores.

Better estimates of permeability are obtained for dry soils compared to wet soils. This further re-in forces the usefulness of a disk infiltrometer as a tool to measure permeability.

8.1.3 Unconfined compressive strength and tensile strength

Studies of the unconfined compressive strength and tensile strength of compacted soils revealed that:

There is an interplay of matric suction, soil structure and void ratio influencing soil strength. As soils dry, the influence of matric suction on strength becomes increasingly minimal past the air-entry value, the contribution is negligible as the water phase becomes increasingly gets discontinuous. This is valuable in designing shear strength experiments for unsaturated soils.

The unconfined compressive strength for a near saturated soil as it dries increases up to the shrinkage limit. Hence, shrinkage limit which indicates no further change in void ratio is an important water content in strength of unsaturated soils.

The ratio of unconfined compressive strength to Brazilian tensile strength (q_u/σ_t) lies within the range of 4 to 15.

The two tensile strength models evaluated were not able to capture the tensile strength of the compacted soils studied indicating complexity of the soil structure for compacted soils.

8.1.4 Constant water content tests

Possibilities of applying conventional tests to obtain unsaturated shear strength parameters have been explored. A conventional triaxial apparatus was used to conduct UC and UU tests for as-compacted soil specimens as well as the CU tests on the saturated soil specimens. The main findings are listed below.

Stress history, suction, void ratio and structure have great influence on the shear strength behavior of unsaturated and saturated soils. Compacted soils possess a stress history which needs to be studied to have a better understanding on their shear strength measurements.

By fitting tangent lines inclined at effective friction angle to the Mohr circles from UC and UU tests, shear strength of unsaturated soils can be obtained. This seems valuable especially for dry of optimum soils which behave like OC clays. The results indicate that it may even be possible to estimate the effective friction angle and hence conventional CU test may not be necessary for such soils. However, this needs further exploration.

The as-compacted soils provide the lower $\tan\phi^b$ values than the dried soils and hence are useful for determining design values necessary for conservative design in unsaturated soils.

8.2 Recommendations

Not all issues were satisfactorily studied in this thesis. The following recommendations are made for future study:

1) A lot of success has been recorded on the usage of filter paper method in laboratory measurements of soil suction. Few measurements exist on field soil samples thus limiting its application. In order to extend its use into practice, it is necessary to do more suction

measurements on field soil specimens using the filter paper method. Such experience will be valuable for practitioners.

2) The effect of the sacrificial filter paper recommended by ASTM D-5298-16 on equilibration time of filter papers needs to be further investigated as the current study shows that it is not needed.
3) Infiltrometers with larger disk diameters need to be studied further and their advantages over mini-disks in terms of reliability of results be further investigated.
4) More studies are needed on how to obtain reliable permeabilities for wet soils using mini-disk infiltromters considering spatial variability of soils.
5) In this thesis, infiltration studies were done on compacted soils. It would be interesting to investigate the reliability of Carsel and Parrish (1988) empirical parameters on natural soils and compare with actual SWCC measurements. If found reliable, the duration of permeability measurements with a disk infiltrometer would be further shortened for practice.
6) More studies of UCS and BTS are necessary to establish ways of obtaining reliable unsaturated shear strength parameters in a short time. Studies relating UCS and BTS have been done in stabilized materials but do not seem to align with unsaturated soil mechanics principles. This needs to be studied. Also, the linkage between BTS and the SWCC of soils needs more investigation especially for soils with complex structures such as compacted soils.
7) The tensile strength models evaluated in this study indicates that there is a need to develop a new model to estimate tensile strength of compacted soils.

8) Initial stress state of compacted soils needs to be established in order to gain more understanding of the shear strength tests of these soils.
9) The framework of the CW test presented in Chapter 7 is very promising and needs to be investigated further on different soils especially soils with high matric suctions. Measurements such as volume change during shear, suction changes during shearing are necessary to validate the observations and assumptions made. The influence of strain rate on the observations also needs to be studied.

References

ASTM D698-12. *Standard Test Methods for Laboratory Compaction Characteristics of Soil Using Standard Effort (12 400 ft-lbf/ft3 (600 kN-m/m3)), ASTM International.* West Conshohocken, PA 2012, www.astm.org.

ASTM D854-14. *Standard Test Methods for Specific Gravity of Soil Solids by Water Pycnometer, ASTM International.* West Conshohocken, PA 2014, www.astm.org.

ASTM D2166 / D2166M - 16. *Standard Test Method for Unconfined Compressive Strength of Cohesive Soil, ASTM International.* West Conshohocken, PA 2016, www.astm.org.

ASTM D2216-10. *Standard Test Methods for Laboratory Determination of Water (Moisture) Content of Soil and Rock by Mass.* West Conshohocken, PA 2010, www.astm.org.

ASTM D2487-17. *Standard Practice for Classification of Soils for Engineering Purposes (Unified Soil Classification System), ASTM International.* West Conshohocken, PA 2017, www.astm.org.

ASTM D2850-15. *Standard Test Method for Unconsolidated-Undrained Triaxial Compression Test on Cohesive Soils, ASTM International.* West Conshohocken, PA 2015, www.astm.org.

ASTM D3967 - 16. *Standard Test Method for Splitting Tensile Strength of Intact Rock Core Specimens, ASTM International.* West Conshohocken, PA 2016, www.astm.org.

ASTM D4318-17. *Standard Test Methods for Liquid Limit, Plastic Limit, and Plasticity Index of Soils, ASTM International* West Conshohocken, PA 2017, www.astm.org.

ASTM D4767-11. *Standard Test Method for Consolidated Undrained Triaxial Compression Test for Cohesive Soils.* West Conshohocken, PA 2011, www.astm.org.

ASTM D5084 − 16a. *Standard Test Methods for Measurement of Hydraulic Conductivity of Saturated Porous Materials Using a Flexible Wall Permeameter, ASTM International.* West Conshohocken, PA 2016, www.astm.org.

ASTM D5298-16. *Standard Method for Measurement of Soil Potential (Suction) Using Filter Paper, ASTM International.* West Conshohocken, PA 2016, www.astm.org.

ASTM D5856 − 15. *Standard Test Method for Measurement of Hydraulic Conductivity of Porous Material Using a Rigid-Wall, Compaction-Mold Permeameter, ASTM International.* West Conshohocken, PA 2015, www.astm.org.

ASTM D6836 - 16. *Standard Test Methods for Determination of the Soil Water Characteristic Curve for Desorption Using Hanging Column, Pressure Extractor, Chilled Mirror Hygrometer, or Centrifuge, ASTM International.* West Conshohocken, PA 2016, www.astm.org.

ASTM D6913/D6913M-17. *Standard Test Methods for Particle-Size Distribution (Gradation) of Soils Using Sieve Analysis.* West Conshohocken, PA 2017, www.astm.org.

ASTM D7664-10. *Standard Test Methods for Measurement of Hydraulic Conductivity of Unsaturated Soil, ASTM International.* West Conshohocken, PA 2010, www.astm.org.

ASTM D7928-17. *Standard Test Method for Particle-Size Distribution (Gradation) of Fine-Grained Soils Using the Sedimentation (Hydrometer) Analysis, ASTM International* West Conshohocken, PA 2017, www.astm.org.

Decagon Devices (2014). *Mini disk infi ltrometer: Model S, user's manual version 3.* Decagon Devices, Pullman, WA.

ACIKEL, A., SINGH, R., BOUAZZA, A., GATES, W. & ROWE, R. 2015. Applicability and accuracy of the initially dry and initially wet contact filter paper tests for matric suction measurement of geosynthetic clay liners. *Geotechnique: international journal of soil mechanics,* 65**,** 780-787.

AGUS, S., LEONG, E. & SCHANZ, T. 2003. Assessment of statistical models for indirect determination of permeability functions from soil–water characteristic curves. *Géotechnique,* 53**,** 279-282.

AGUS, S. S., LEONG, E. C. & RAHARDJO, H. 2001. Soil—water characteristic curves of Singapore residual soils. *Unsaturated soil concepts and their application in geotechnical practice.* Springer.
AGUS, S. S. & SCHANZ, T. 2005. Comparison of four methods for measuring total suction. *Vadose Zone Journal,* 4**,** 1087-1095.
AHMED, S., LOVELL, C. W. & DIAMOND, S. 1974. Pore sizes and strength of a compacted clay.
AITCHISON, G. D. 1964. Engineering concepts of moisture equilibria and moisture changes in soils. Statement of the Review Panel , In Moisture Equilibria and Moisture Changes in Soils Beneath Covered Areas. 7-21.
AKIN, I. D. & LIKOS, W. 2017. Brazilian Tensile Strength Testing of Compacted Clay. *Geotechnical Testing Journal,* 40**,** 608-617.
AL-KHAFAF, S. & HANKS, R. 1974. Evaluation of the filter paper method for estimating soil water potential. *Soil Science,* 117**,** 194-199.
ALONSO, E., PINYOL, N. & GENS, A. 2013. Compacted soil behaviour: initial state, structure and constitutive modelling. *Géotechnique,* 63**,** 463.
BAKER, R. & FRYDMAN, S. 2009. Unsaturated soil mechanics: Critical review of physical foundations. *Engineering Geology,* 106**,** 26-39.
BARBOUR, S. L. 1998. Nineteenth Canadian Geotechnical Colloquium: The soil-water characteristic curve: a historical perspective. *Canadian Geotechnical Journal,* 35**,** 873-894.
BARDEN, L. & PAVLAKIS, G. 1971. Air and water permeability of compacted unsaturated cohesive soil. *Journal of Soil Science,* 22**,** 302-318.
BENSON, C. & DANIEL, D. 1990. Influence of Clods on Hydraulic Conductivity of.
BICALHO, K. V., CORREIA, A. G., FERREIRA, S. R., FLEUREAU, J.-M. & MARINHO, F. A. 2007. Filter paper method of soil suction measurement.
BICALHO, K. V., MARINHO, F. A., CORREIA, A. G., FERREIRA, S. R. & FLEUREAU, J.-M. 2008. Effect of the filter paper calibration on the soil-water retention curve of an unsaturated compacted silt sand.
BISHOP, A., ALPAN, I. & BLIGHT, G. Factors controlling the shear strenth of partly saturated cohesive soil. ASCE Res. Conf. Shear Strength of Loheslve Soil. Univ. of Colordo, Boulder P, 1960.
BISHOP, A. W. 1959. The principle of effective stress. *Teknisk ukeblad,* 39**,** 859-863.
BISHOP, A. W. 1960. *The principles of effective stress*, Norges Geotekniske Institutt.
BISHOP, A. W. & DONALD, I. The experimental study of partly saturated soil in the triaxial apparatus. Proceedings of the 5th international conference on soil mechanics and foundation engineering, Paris, 1961. 13-21.
BJERRUM, L. & HUDER, J. Measurement of the permeability of compacted clays. Proceedings of the 4th international conference on soil mechanics and foundation engineering, London, 1957. 6-10.
BLATZ, J. A., CUI, Y.-J. & OLDECOP, L. 2008. Vapour equilibrium and osmotic technique for suction control. *Laboratory and Field Testing of Unsaturated Soils.* Springer.
BOSO, M., TARANTINO, A. & MONGIOVI, L. 2005. A direct shear box improved with the osmotic technique. *Proceedings of advanced experimental unsaturated soil mechanics, Trento***,** 85-91.
BROOKS, R. H. & COREY, A. T. 1964. Hydraulic properties of porous media. *Colorado State University, Hydrology Paper No.3,* 3**,** 27.
BRUCE, R. & KLUTE, A. 1956. The Measurement of Soil Moisture Diffusivity 1. *Soil Science Society of America Journal,* 20**,** 458-462.
BUCKINGHAM, E. 1907. Studies on the movement of soil moisture. *US Dept. Agic. Bur. Soils Bull.,* 38.
BULUT, R. & LEONG, E. C. 2008. Indirect measurement of suction. *Geotechnical and Geological Engineering,* 26**,** 633-644.
BULUT, R., LYTTON, R. L. & WRAY, W. K. Soil suction measurements by filter paper. Expansive clay soils and vegetative influence on shallow foundations, 2001. ASCE, 243-261.

BULUT, R. & WRAY, W. K. 2005. Free energy of water-suction-in filter papers. *ASTM geotechnical testing journal,* 28**,** 355-364.
BURDINE, N. 1953. Relative permeability calculations from pore size distribution data. *Journal of Petroleum Technology,* 5**,** 71-78.
BURLAND, J. 1965. Some Aspects of the Mechanical Behaviour of Party Saturated Soils. *Moisture equilibria and moisture changes in soils beneath covered areas***,** 270-278.
CAMPBELL, G. S., SMITH, D. M. & TEARE, B. L. 2007. Application of a dew point method to obtain the soil water characteristic. *Experimental Unsaturated Soil Mechanics.* Springer.
CARMAN, P. C. 1956. Flow of gases through porous media.
CARRIER III, W. D. 2003. Goodbye, hazen; hello, kozeny-carman. *Journal of geotechnical and geoenvironmental engineering,* 129**,** 1054-1056.
CARSEL, R. F. & PARRISH, R. S. 1988. Developing joint probability distributions of soil water retention characteristics. *Water resources research,* 24**,** 755-769.
CARUSO, M. & TARANTINO, A. 2004. A shearbox for testing unsaturated soils at medium to high degrees of saturation. *Géotechnique,* 54.
CHANDLER, R. & GUTIERREZ, C. 1986. The filter-paper method of suction measurement. *Géotechnique,* 36**,** 265-268.
CHANG, C. & DUNCAN, J. 1983. Consolidation analysis for partly saturated clay by using an elastic–plastic effective stress–strain model. *International Journal for Numerical and Analytical Methods in Geomechanics,* 7**,** 39-55.
CHANG, C. S. 1976. Analysis of consolidation of earth and rockfill dams. *Ph. D Thesis, University of California***,** 1-225.
CHAPUIS, R. 2017. Compacted Clay: Difficulties Obtaining Good Laboratory Permeability Tests. *Geotechnical Testing Journal,* 40**,** 185-198.
CHAPUIS, R. P. 2012. Predicting the saturated hydraulic conductivity of soils: a review. *Bulletin of engineering geology and the environment,* 71**,** 401-434.
CHAPUIS, R. P. & AUBERTIN, M. 2003. On the use of the Kozeny Carman equation to predict the hydraulic conductivity of soils. *Canadian Geotechnical Journal,* 40**,** 616-628.
CHENG, C. & CHEN, X. 2007. Evaluation of methods for determination of hydraulic properties in an aquifer–aquitard system hydrologically connected to a river. *Hydrogeology Journal,* 15**,** 669-678.
CHILDS, E. C. & COLLIS-GEORGE, N. 1950. The permeability of porous materials. *Proc. R. Soc. Lond. A,* 201**,** 392-405.
CLOTHIER, B. & WHITE, I. 1981. Measurement of Sorptivity and Soil Water Diffusivity in the Field 1. *Soil Science Society of America Journal,* 45**,** 241-245.
CUISINIER, O. & LALOUI, L. 2004. Fabric evolution during hydromechanical loading of a compacted silt. *International Journal for Numerical and Analytical Methods in Geomechanics,* 28**,** 483-499.
DANIEL, D. E. 1989. In situ hydraulic conductivity tests for compacted clay. *Journal of Geotechnical Engineering,* 115**,** 1205-1226.
DANIEL, D. E., ANDERSON, D. C. & BOYNTON, S. S. 1985. Fixed-wall versus flexible-wall permeameters. *Hydraulic barriers in soil and rock.* ASTM International.
DANIEL, D. E., TRAUTWEIN, S. J., BOYNTON, S. S. & FOREMAN, D. E. 1984. Permeability testing with flexible-wall permeameters. *Geotechnical Testing Journal,* 7**,** 113-122.
DARCY, H. 1856. Les fontaines publiques de la ville de Dijon, Victor Dalmont, Paris. *The Flow of Homogeneous Fluids Through Porous Media*.
DAS, B., YEN, S. & DASS, R. 1995. Brazilian tensile strength test of lightly cemented sand. *Canadian Geotechnical Journal,* 32**,** 166-171.

DE OLIVEIRA, O. M., LI, P., MARINHO, F. A. & VANAPALLI, S. K. 2016. Mechanical behaviour of a compacted residual soil of gneiss from Brazil under constant water content condition. *Indian Geotechnical Journal,* 46**,** 299-308.

DEKA, R., WAIRIU, M., MTAKWA, P., MULLINS, C., VEENENDAAL, E. & TOWNEND, J. 1995. Use and accuracy of the filter-paper technique for measurement of soil matric potential. *European Journal of Soil Science,* 46**,** 233-238.

DELAGE, P., AUDIGUIER, M., CUI, Y.-J. & HOWAT, M. D. 1996. Microstructure of a compacted silt. *Canadian Geotechnical Journal,* 33**,** 150-158.

DELAGE, P. & CUI, Y. J. 2008. An evaluation of the osmotic method of controlling suction∗. *Geomechanics and Geoengineering: An International Journal,* 3**,** 1-11.

DELAGE, P., ROMERO, E. & TARANTINO, A. Recent developments in the techniques of controlling and measuring suction in unsaturated soils. Keynote Lecture, Proc. 1st Eur. Conf. on Unsaturated Soils, 2008. 33-52.

DEVICES , DECAGON. Mini disk infiltrometer user's manual version 10 (Decagon Devices,Inc: Pullman, WA) 2013.

DINEEN, K. & BURLAND, J. A new approach to osmotically controlled oedometer testing. PROCEEDINGS OF THE FIRST INTERNATIONAL CONFERENCE ON UNSATURATED SOILS/UNSAT'95/PARIS/FRANCE/6-8 SEPTEMBER 1995. VOLUME 2, 1995.

DOHNAL, M., DUSEK, J. & VOGEL, T. 2010. Improving hydraulic conductivity estimates from minidisk infiltrometer measurements for soils with wide pore-size distributions. *Soil Science Society of America Journal,* 74**,** 804-811.

EL MOUNTASSIR, G. 2011. *Behaviour of a collapsible structured unsaturated fill material.* PhD thesis, University of Strathclyde.

ELRICK, D. & REYNOLDS, W. 1990. Ponded Infiltration from a Single Ring: I. Analysis of Steady Flow. *Soil Science Society of America Journal SSSJD 4,* 54.

ESCARIO, V. Swelling of soils in contact with water at a negative pressure. Proceedings of the 2nd international conference expansive clay soils, Texas A&M University, 1969. 207-217.

ESCARIO, V. 1986. The shear strength of partly saturated soils. *Geotech,* 36**,** 453-456.

FAWCETT, R. & COLLIS-GEORGE, N. 1967. A filter-paper method for determining the moisture characteristics of soil. *Australian Journal of Experimental Agriculture,* 7**,** 162-167.

FLEUREAU, J.-M., VERBRUGGE, J.-C., HUERGO, P. J., CORREIA, A. G. & KHEIRBEK-SAOUD, S. 2002. Aspects of the behaviour of compacted clayey soils on drying and wetting paths. *Canadian geotechnical journal,* 39**,** 1341-1357.

FREDLUND, MORGENSTERN & WIDGER 1978. The shear strength of unsaturated soils. *Canadian Geotechnical Journal,* 15**,** 313-321.

FREDLUND, D. Seepage in saturated soils. Panel Discussion: Ground water and seepage problems. Proc. 10 th Int. Conf. Soil Mech. Found. Eng. Estocolmo, Suecia, 1981. 629-641.

FREDLUND, D. Use of soil-water characteristic curves in the implementation of unsaturated soil mechanics. Proceedings of the 3rd International Conference on Unsaturated Soils, Recife, Brazil, 2002. 887-902.

FREDLUND, D. G. 1967. *Comparison of soil suction and one-dimensional consolidation characteristics of a highly plastic clay*, National Research Council Canada, Division of Building Research.

FREDLUND, D. G. 2000. The 1999 RM Hardy Lecture: The implementation of unsaturated soil mechanics into geotechnical engineering. *Canadian Geotechnical Journal,* 37**,** 963-986.

FREDLUND, D. G. 2006. Unsaturated soil mechanics in engineering practice. *Journal of geotechnical and geoenvironmental engineering,* 132**,** 286-321.

FREDLUND, D. G. & MORGENSTERN, N. R. 1977. Stress state variables for unsaturated soils. *Journal of Geotechnical and Geoenvironmental Engineering,* 103.

FREDLUND, D. G. & RAHARDJO, H. 1993. *Soil mechanics for unsaturated soils*, John Wiley & Sons.
FREDLUND, D. G., RAHARDJO, H. & FREDLUND, M. D. 2012. *Unsaturated soil mechanics in engineering practice*, John Wiley & Sons.
FREDLUND, D. G. & XING, A. 1994. Equations for the soil-water characteristic curve. *Canadian geotechnical journal,* 31**,** 521-532.
FREDLUND, M. D., WILSON, G. W. & FREDLUND, D. G. 2002. Use of the grain-size distribution for estimation of the soil-water characteristic curve. *Canadian Geotechnical Journal,* 39**,** 1103-1117.
FRYDMAN, S. 1964. Applicability of the Brazilian (indirect tension) test to soils.
FRYDMAN, S. & BAKER, R. 2009. Theoretical soil-water characteristic curves based on adsorption, cavitation, and a double porosity model. *International Journal of Geomechanics,* 9**,** 250-257.
GALLAGE, C. P. K. & UCHIMURA, T. 2010. Effects of dry density and grain size distribution on soil-water characteristic curves of sandy soils. *Soils and Foundations,* 50**,** 161-172.
GAN, J., FREDLUND, D. & RAHARDJO, H. 1988. Determination of the shear strength parameters of an unsaturated soil using the direct shear test. *Canadian Geotechnical Journal,* 25**,** 500-510.
GARDNER, R. 1937. A method of measuring the capillary tension of soil moisture over a wide moisture range. *Soil Science,* 43**,** 277-284.
GARDNER, W. 1956. Calculation of Capillary Conductivity from Pressure Plate Outflow Data 1. *Soil Science Society of America Journal,* 20**,** 317-320.
GARDNER, W. 1958. Some steady-state solutions of the unsaturated moisture flow equation with application to evaporation from a water table. *Soil science,* 85**,** 228-232.
GARVEN, E. & VANAPALLI, S. Evaluation of empirical procedures for predicting the shear strength of unsaturated soils. Unsaturated Soils 2006, 2006a. ASCE, 2570-2592.
GARVEN, E. & VANAPALLI, S. 2006b. Evaluation of empirical procedures for predicting the shear strength of unsaturated soils. *Unsaturated Soils 2006.*
GEE, G., CAMPBELL, M., CAMPBELL, G. & CAMPBELL, J. 1992. Rapid measurement of low soil water potentials using a water activity meter. *Soil Science Society of America Journal,* 56**,** 1068-1070.
GENS, A. 2010. Soil-environment interactions in geotechnical engineering. *Géotechnique,* 60**,** 3.
GENS, A., SÁNCHEZ, M. & SHENG, D. 2006. On constitutive modelling of unsaturated soils. *Acta Geotechnica,* 1**,** 137.
GREACEN, E. 1960. Water content and soil strength. *Journal of Soil Science,* 11**,** 313-333.
GREACEN, E., WALKER, G. & COOK, P. 1987. Evaluation of the filter paper method for measuring soil water suction.
HAGHIGHI, A., MEDERO, G. M., MARINHO, F. A., MERCIER, B. & WOODWARD, P. K. 2012. Temperature effects on suction measurement using the filter paper technique. *ASTM geotechnical testing journal,* 35**,** 83-90.
HAMBLIN, A. 1981. Filter-paper method for routine measurement of field water potential. *Journal of Hydrology,* 53**,** 355-360.
HAVERKAMP, R., ROSS, P., SMETTEM, K. & PARLANGE, J. 1994. Three-dimensional analysis of infiltration from the disc infiltrometer: 2. Physically based infiltration equation. *Water Resources Research,* 30**,** 2931-2935.
HAYASHI, M. & QUINTON, W. L. 2004. A constant-head well permeameter method for measuring field-saturated hydraulic conductivity above an impermeable layer. *Canadian journal of soil science,* 84**,** 255-264.
HAZEN, A. 1892. Some physical properties of sands and gravels: with special reference to their use in filtration, publisher not identified.
HEAD, K. H. 1998. *Manual of soil laboratory testing, Volume 3: Efffective stress tests. Ed. 2*, John Wiley and sons Ltd.

HEIBROCK, G., ZEH, R. & WITT, K. 2005. Tensile strength of compacted clays. *Unsaturated soils: Experimental studies.* Springer.
HILF, J. W. 1956. An investigation of pore water pressure in compacted cohesive soils.
HO, D. Y. & FREDLUND, D. G. 1982. A multistage triaxial test for unsaturated soils. *Geotechnical Testing Journal,* 5**,** 18-25.
HOFFMANN, C., ROMERO, E. & ALONSO, E. Combining different controlled-suction techniques to study expansive clays. Proceedings of the international symposium on advanced experimental unsaturated soils mechanics EXPERUS, Trento, Balkema, 2005. 61-67.
HOLTZ, R. D. & KOVACS, W. D. 1981. *An introduction to geotechnical engineering*.
HOULSBY, G. 1997. The work input to an unsaturated granular material. *Géotechnique,* 47**,** 193-6.
HUANG, S., FREDLUND, D. & BARBOUR, S. 1998. Measurement of the coefficient of permeability for a deformable unsaturated soil using a triaxial permeameter. *Canadian Geotechnical Journal,* 35**,** 426-432.
JENNINGS, J. & BURLAND, J. 1962. Limitations to the use of effective stresses in partly saturated soils. *Géotechnique,* 12**,** 125-144.
JOTISANKASA, A., COOP, M. & RIDLEY, A. 2009. The mechanical behaviour of an unsaturated compacted silty clay. *Géotechnique,* 59**,** 415-428.
KASSIFF, G. & SHALOM, A. B. 1971. Experimental relationship between swell pressure and suction. *Géotechnique,* 21**,** 245-255.
KATO, S., YOSHIMURA, Y. & FREDLUND, D. G. Role of matric suction in the interpretation of unconfined compression tests In Proceedings of the Fifty-Eighth Canadian Geotechnical Conference, 2005.
KHALILI, N. & KHABBAZ, M. 1998. A unique relationship of chi for the determination of the shear strength of unsaturated soils. *Geotechnique,* 48.
KLUTE, A. 1965. Laboratory measurement of hydraulic conductivity of unsaturated soil. *Methods of Soil Analysis. Part 1. Physical and Mineralogical Properties, Including Statistics of Measurement and Sampling***,** 253-261.
KLUTE, A. 1972. The determination of the hydraulic conductivity and diffusivity of unsaturated soils1. *Soil Science,* 113**,** 264-276.
KLUTE, A. & DIRKSEN, C. 1986. Hydraulic conductivity and diffusivity: Laboratory methods. *Methods of soil analysis: part 1—physical and mineralogical methods***,** 687-734.
KOLIJI, A., LALOUI, L., CUSINIER, O. & VULLIET, L. 2006. Suction induced effects on the fabric of a structured soil. *Transport in porous media,* 64**,** 261-278.
KOZENY, J. 1927. Uber kapillare leitung der wasser in boden. *Royal Academy of Science, Vienna, Proc. Class I,* 136**,** 271-306.
KRISDANI, H., RAHARDJO, H. & LEONG, E.-C. 2009. Use of instantaneous profile and statistical methods to determine permeability functions of unsaturated soils. *Canadian Geotechnical Journal,* 46**,** 869-874.
KUNZE, R., UEHARA, G. & GRAHAM, K. 1968. Factors Important in the Calculation of Hydraulic Conductivity 1. *Soil Science Society of America Journal,* 32**,** 760-765.
LALOUI, L. 2013. *Mechanics of unsaturated geomaterials*, John Wiley & Sons.
LAMBE, T. W. 1958. The engineering behavior of compacted clay. *Journal of the Soil Mechanics and Foundations Division,* 84**,** 1-35.
LAMBORN, M. J. 1986. *A micromechanical approach to modeling partly saturated soils.* Texas A&M University.
LEONG, E.-C., KIZZA, R. & RAHARDJO, H. Measurement of soil suction using moist filter paper. E3S Web of Conferences, 2016. EDP Sciences, 10012.
LEONG, E.-C., TRIPATHY, S. & RAHARDJO, H. 2003. Total suction measurement of unsaturated soils with a device using the chilled-mirror dew-point technique. *Geotechnique,* 53**,** 173-182.

LEONG, E. 2019. Stress State Variables for Unsaturated Soils—Consensus and Controversy. *Geotechnical Design and Practice.* Springer.
LEONG, E. & RAHARDJO, H. Soil-water characteristic curves of compacted residual soils. Unsaturated soils. Proceedings of the 3rd international conference on unsaturated soils (UNSAT 2002), Recife, Brazil, 2002. 271-276.
LEONG, E., RAHARDJO, H. & TANG, S. Characterisation and engineering properties of Singapore residual soils. Proceedings of the International Workshop on Characterisation and Engineering Properties of Natural Soils, Singapore, December, 2002a. 2-4.
LEONG, E. & WIJAYA, M. 2015. Universal soil shrinkage curve equation. *Geoderma,* 237**,** 78-87.
LEONG, E. C., HE, L. & RAHARDJO, H. 2002b. Factors affecting the filter paper method for total and matric suction measurements. *ASTM geotechnical testing journal,* 25**,** 322-333.
LEONG, E. C. & RAHARDJO, H. 1997a. Permeability functions for unsaturated soils. *Journal of Geotechnical and Geoenvironmental Engineering,* 123**,** 1118-1126.
LEONG, E. C. & RAHARDJO, H. 1997b. Review of soil-water characteristic curve equations. *Journal of geotechnical and geoenvironmental engineering,* 123**,** 1106-1117.
LI, Z.-S., FLEUREAU, J.-M. & TANG, L.-S. 2017. Aspects of compaction and drying–wetting curves of a subgrade clayey soil. *Géotechnique,* 67**,** 1120-1126.
LIKOS, W. J. 2000. *Total suction-moisture content characteristics for expansive soils.* Colorado School of Mines. Arthur Lakes Library.
LIKOS, W. J. & LU, N. 2002. Filter paper technique for measuring total soil suction. *Transportation Research Record: Journal of the Transportation Research Board,* 1786**,** 120-128.
LLORET, A. & ALONSO, E. 1980. Consolidation of unsaturated soils including swelling and collapse behaviour. *Géotechnique,* 30**,** 449-477.
LU, N., KIM, T.-H., STURE, S. & LIKOS, W. J. 2009. Tensile strength of unsaturated sand. *Journal of engineering mechanics,* 135**,** 1410-1419.
LU, N. & LIKOS, W. J. 2004. *Unsaturated soil mechanics*, Wiley.
LU, Y.-F., LUO, X.-Q., WU, Y.-C. & CUI, Y. Study of fundamental properties of soil–water characteristic curve. Proceedings of the 3rd Asian conference on unsaturated soils. Beijing: Science Press, 2007. 243-249.
MARINHO, F., AM , GONZALO CARNERO GUZMÁN, G. & DEL GAUDIO ORLANDO, P. 2016. Constant water content compression tests on unsaturated compacted soil with suction measurement using a HCT. *International Journal of Geomechanics,* 16**,** D4015008.
MARINHO, F. A. 2005. Nature of soil–water characteristic curve for plastic soils. *Journal of geotechnical and geoenvironmental engineering,* 131**,** 654-661.
MARINHO, F. A. & DA SILVA GOMES, J. E. 2011. The effect of contact on the filter paper method for measuring soil suction. *Geotechnical testing journal,* 35**,** 172-181.
MARINHO, F. A. & DA SILVA GOMES, J. E. 2012. The Effect of Contact on the Filter Paper Method for Measuring Soil Suction. *ASTM geotechnical testing journal,* 35**,** 172-181.
MARINHO, F. A. & OLIVEIRA, O. M. 2006. The filter paper method revisited. *ASTM geotechnical testing journal,* 29**,** 250-258.
MARINHO, F. A. & OLIVEIRA, O. M. 2012. Unconfined shear strength of compacted unsaturated plastic soils. *Proceedings of the Institution of Civil Engineers-Geotechnical engineering,* 165**,** 97-106.
MARSHALL, T. 1958. A relation between permeability and size distribution of pores. *Journal of Soil Science,* 9**,** 1-8.
MARSHALL, T. J., HOLMES, J. W. & ROSE, C. W. 1996. *Soil physics*, Cambridge University Press.
MASROURI, F., BICALHO, K. V. & KAWAI, K. 2008. Laboratory hydraulic testing in unsaturated soils. *Geotechnical and Geological Engineering,* 26**,** 691-704.

MCKEEN, R. Soil characterization using suction measurements. Proc., 25th Paving and Transportation Conf, 1988.
MCQUEEN, I. S. & MILLER, R. F. 1968. Calibration and evaluation of a wide-range gravimetric method for measuring moisture stress. *Soil Science,* 106**,** 225-231.
MEERDINK, J., BENSON, C. & KHIRE, M. 1996. Unsaturated hydraulic conductivity of two compacted barrier soils. *Journal of geotechnical engineering,* 122**,** 565-576.
MEILANI, I., RAHARDJO, H., LEONG, E.-C. & FREDLUND, D. G. 2002. Mini suction probe for matric suction measurements. *Canadian Geotechnical Journal,* 39**,** 1427-1432.
MENDES, J. 2011. *Assessment of the impact of climate change on an instrumented embankment: An unsaturated soil mechanics approach* PhD thesis, Durham University, Durham, U.K.
MILAN, V. & ANDJELKO, S. 1992. *Determination of hydraulic conductivity of porous media from grain-size composition*.
MIRZAII, A. & YASROBI, S. 2012. Influence of initial dry density on soil-water characteristics of two compacted soils. *Geotechnique Letters,* 2**,** 193-198.
MITCHELL, J. K. 1976. *Fundamental of Soil Behaviour*, John Wiley and Sons, New York.
MITCHELL, J. K., HOOPER, D. R. & CAMPANELLA, R. G. 1966. Permeability of compacted clay. *Journal of Soil Mechanics & Foundations Div,* 92.
MONROY, R., ZDRAVKOVIC, L. & RIDLEY, A. 2009. Evolution of microstructure in compacted London Clay during wetting and loading. *Géotechnique,* 60**,** 105-119.
MORGENSTERN, N. Properties of compacted soils. Contribution to panel discussion, Session IV, Proc., 6th Panamerican Conf. on Soil Mechanics and Foundation Engineering, 1979. 349-354.
MUALEM, Y. 1976. A new model for predicting the hydraulic conductivity of unsaturated porous media. *Water resources research,* 12**,** 513-522.
MUALEM, Y. 1986. Hydraulic conductivity of unsaturated soils: prediction and formulas. *Methods of Soil Analysis: Part 1—Physical and Mineralogical Methods***,** 799-823.
MUÑOZ-CASTELBLANCO, J., PEREIRA, J.-M., DELAGE, P. & CUI, Y.-J. Suction measurements on a natural unsaturated soil: A reappraisal of the filter paper method. Unsaturated Soils-Proc. Fifth Int. Conf. on Unsaturated Soils, 2010. 707-712.
NARAIN, J. & RAWAT, P. C. 1970. Tensile strength of compacted soils. *Journal of Soil Mechanics & Foundations Div*.
ÖBERG, A.-L. & SÄLLFORS, G. 1997. Determination of shear strength parameters of unsaturated silts and sands based on the water retention curve. *ASTM geotechnical testing journal,* 20**,** 40-48.
ODONG, J. 2007. Evaluation of empirical formulae for determination of hydraulic conductivity based on grain-size analysis. *Journal of American Science,* 3**,** 54-60.
OH, W. T. 2012. *Simple techniques for the implementation of the mechanics of unsaturated soils into engineering practice.* PhD, University of Ottawa.
OLSON, R. & DANIEL, D. 1981. Measurement of the hydraulic conductivity of fine-grained soils. *Permeability and groundwater contaminant transport.* ASTM International.
PHILIP, J. R. 1957. The theory of infiltration: 4. Sorptivity and algebraic infiltration equations. *Soil science,* 84**,** 257-264.
PINTADO, X., LLORET, A. & ROMERO, E. 2009. Assessment of the use of the vapour equilibrium technique in controlled-suction tests. *Canadian Geotechnical Journal,* 46**,** 411-423.
PIRATHEEPAN, J., GNANENDRAN, C. & ARULRAJAH, A. 2012. Determination of c and ϕ from IDT and unconfined compression testing and numerical analysis. *Journal of materials in civil engineering,* 24**,** 1153-1164.
RAHARDJO, H., HENG, O. B. & CHOON, L. E. 2004. Shear strength of a compacted residual soil from consolidated drained and constant water content triaxial tests. *Canadian Geotechnical Journal,* 41**,** 421-436.

RAHARDJO, H. & LEONG, E. 2006. Suction measurements. *Unsaturated Soils 2006.*
RAHARDJO, H., LIM, T., CHANG, M. & FREDLUND, D. 1995. Shear-strength characteristics of a residual soil. *Canadian Geotechnical Journal,* 32**,** 60-77.
RAHARDJO, H., REZAUR, R. & LEONG, E. Mechanism of rainfall-induced slope failures in tropical regions. The 1st Italian workshop on landslides, Napoli, Italy, 2009. 8-10.
RAHARDJO, H., SATYANAGA, A. & LEONG, E.-C. 2013. Effects of flux boundary conditions on pore-water pressure distribution in slope. *Engineering Geology,* 165**,** 133-142.
RAHARDJO, H., SATYANAGA, A., LEONG, E.-C., NG, Y. S. & PANG, H. T. C. 2012. Variability of residual soil properties. *Engineering geology,* 141**,** 124-140.
REYNOLDS, W. 2008. Unsaturated hydraulic properties: Field tension infiltrometer. *Soil sampling and methods of analysis***,** 54.
REYNOLDS, W. & ELRICK, D. 1987. A laboratory and numerical assessment of the Guelph permeameter method. *Soil Science,* 144**,** 282-299.
REYNOLDS, W. & ELRICK, D. 2002. b. Constant head well permeameter (vadose zone). p. 844–858. JH Dane and GC Topp (ed.) Methods of soil analysis. Part 4. Physical methods. SSSA Book Ser. 5. SSSA, Madison, WI. *Constant head well permeameter (vadose zone). p. 844–858. In JH Dane and GC Topp (ed.) Methods of soil analysis. Part 4. Physical methods. SSSA Book Ser. 5. SSSA, Madison, WI.***,** -.
REYNOLDS, W., ELRICK, D. & YOUNGS, E. 2002a. Ring or cylinder infiltrometers (vadose zone). p. 818–843. JH Dane and GC Topp (ed.) Methods of soil analysis. Part 4. Physical methods. SSSA Book Ser. 5. SSSA, Madison, WI. *Ring or cylinder infiltrometers (vadose zone). p. 818–826. In JH Dane and GC Topp (ed.) Methods of soil analysis. Part 4. Physical methods. SSSA Book Ser. 5. SSSA, Madison, WI.***,** -.
REYNOLDS, W., ELRICK, D. & YOUNGS, E. 2002b. Single-ring and double-or concentric-ring infiltrometers. p. 821–826. JH Dane and GC Topp (ed.) Methods of soil analysis: Part 4. Physical methods. SSSA Book Ser. 5. SSSA, Madison, WI. *Single-ring and double-or concentric-ring infiltrometers. p. 821–826. In JH Dane and GC Topp (ed.) Methods of soil analysis: Part 4. Physical methods. SSSA Book Ser. 5. SSSA, Madison, WI.***,** -.
RICHARDS, L. A. 1931. Capillary conduction of liquids through porous mediums. *physics,* 1**,** 318-333.
RICHARDS, S. J. & WEEKS, L. V. 1953. Capillary Conductivity Values from Moisture Yield and Tension Measurements on Soil Columns 1. *Soil Science Society of America Journal,* 17**,** 206-209.
RIDLEY, A. & BURLAND, J. 1993. A new instrument for the measurement of soil moisture suction. *Géotechnique,* 43.
RIDLEY, A., DINEEN, K., BURLAND, J. & VAUGHAN, P. 2003. Soil matrix suction: some examples of its measurement and application in geotechnical engineering. *Géotechnique,* 53**,** 241-253.
RIDLEY, A. & WRAY, W. Suction measurement: a review of current theory and practices. PROCEEDINGS OF THE FIRST INTERNATIONAL CONFERENCE ON UNSATURATED SOILS/UNSAT'95/PARIS/FRANCE/6-8 SEPTEMBER 1995. VOLUME 3, 1996.
RIDLEY, A. M. 1995. Discussion on “Laboratory Filter Paper Suction Measurements” by Sandra L. Houston, William N. Houston, and Anne-Marie Wagner. *Geotechnical Testing Journal,* 18**,** 391-396.
ROMERO, E. & VAUNAT, J. 2000. Retention curves of deformable clays. *Experimental evidence and theoretical approaches in unsaturated soils.* CRC Press.
SALAGER, S., EL YOUSSOUFI, M. S. & SAIX, C. 2010. Definition and experimental determination of a soil-water retention surface. *Canadian Geotechnical Journal,* 47**,** 609-622.
SAMINGAN, A. S. 2001. *Hydraulic properties of residual soils* Master thesis, Nanyang Technological University , Singapore.

SAMINGAN, A. S. 2005. *An experimental study on hydro-mechanical characteristics of compacted bentonite-sand mixtures.* PhD thesis., Bauhaus-University Weimar.
SAMINGAN, A. S., LEONG, E.-C. & RAHARDJO, H. 2003. A flexible wall permeameter for measurements of water and air coefficients of permeability of residual soils. *Canadian Geotechnical Journal,* 40**,** 559-574.
SATYANAGA, A., RAHARDJO, H., LEONG, E.-C. & WANG, J.-Y. 2013. Water characteristic curve of soil with bimodal grain-size distribution. *Computers and Geotechnics,* 48**,** 51-61.
SCOTTER, D., CLOTHIER, B. & HARPER, E. 1982. Measuring saturated hydraulic conductivity and sorptivity using twin rings. *Soil Research,* 20**,** 295-304.
SHEN, Z. & YU, S. The problems in the present studies on mechanics for unsaturated soils. Proceedings of the Symposium on Geotechnical Aspects of Regional Soils, 1996.
SIBLEY, J. W. & WILLIAMS, D. J. 1990. A new filter material for measuring soil suction. *Geotechnical Testing Journal,* 13**,** 381-384.
SILLERS, W. S., FREDLUND, D. G. & ZAKERZADEH, N. 2001. Mathematical attributes of some soil—water characteristic curve models. *Unsaturated soil concepts and their application in geotechnical practice.* Springer.
ŠIMŮNEK, J., ANGULO-JARAMILLO, R., SCHAAP, M. G., VANDERVAERE, J.-P. & VAN GENUCHTEN, M. T. 1998. Using an inverse method to estimate the hydraulic properties of crusted soils from tension-disc infiltrometer data. *Geoderma,* 86**,** 61-81.
SRIDHARAN, A., ALTSCHAEFFL, A. & DIAMOND, S. 1971. Pore size distribution studies. *Journal of the soil mechanics and foundations division,* 97**,** 771-787.
SUN, W.-J. & CUI, Y.-J. 2017. Investigating the microstructure changes for silty soil during drying. *Géotechnique,* 68**,** 370-373.
SWARBRICK, G. Measurement of soil suction using the filter paper method. PROCEEDINGS OF THE FIRST INTERNATIONAL CONFERENCE ON UNSATURATED SOILS/UNSAT'95/PARIS/FRANCE/6-8 SEPTEMBER 1995. VOLUME 2, 1995.
TAMRAKAR, S. B., MITACHI, T. & TOYOSAWA, Y. 2007. Factors Affecting Tensile Strength Measurement and Modified Tensile Strength Measuring Apparatus for Soil. *Experimental Unsaturated Soil Mechanics.* Springer.
TANG, A.-M. & CUI, Y.-J. 2005. Controlling suction by the vapour equilibrium technique at different temperatures and its application in determining the water retention properties of MX80 clay. *Canadian Geotechnical Journal,* 42**,** 287-296.
TARANTINO, A. 2009. A water retention model for deformable soils. *Géotechnique,* 59**,** 751-762.
TARANTINO, A. 2010. Basic concepts in the mechanics and hydraulics of unsaturated geomaterials. . *Mechanics of Unsaturated Geomaterials, Ed. Lyesse Laloui*.
TARANTINO, A. 2011. Unsaturated soils: compacted versus reconstituted states. *Unsaturated soils. Edited by EE Alonso and A. Gens. CRC Press, Barcelona, Spain***,** 113-136.
TARANTINO, A. & DE COL, E. 2008. Compaction behaviour of clay. *Géotechnique,* 58**,** 199-213.
TARANTINO, A. & EL MOUNTASSIR, G. 2013. Making unsaturated soil mechanics accessible for engineers: Preliminary hydraulic–mechanical characterisation & stability assessment. *Engineering Geology,* 165**,** 89-104.
TARANTINO, A. & MONGIOVI, L. 2003. CALIBRATOIN OF TENSIOMETER FOR DIRECT MEASUREMENT OF MATRIC SUCTION. *Géotechnique,* 53.
TARANTINO, A. & MONGIOVÌ, L. 2001. Experimental procedures and cavitation mechanisms in tensiometer measurements. *Unsaturated Soil Concepts and Their Application in Geotechnical Practice.* Springer.
TARANTINO, A. & TOMBOLATO, S. 2005. Coupling of hydraulic and mechanical behaviour in unsaturated compacted clay. *Géotechnique,* 55**,** 307-317.

TAYLOR, D. 1948. *Fundamentals of soil mechanics*, Chapman And Hall, Limited.; New York.
TERZAGHI, K. 1925. Erdbaumechanik auf bodenphysikalischer Grundlage.
THU, T. M., RAHARDJO, H. & LEONG, E.-C. 2006. Shear strength and pore-water pressure characteristics during constant water content triaxial tests. *Journal of Geotechnical and Geoenvironmental Engineering,* 132**,** 411-419.
TO-VIET, N., MIN, T.-K. & SHIN, H. 2013. Using inverse analysis to estimate hydraulic properties of unsaturated sand from one-dimensional outflow experiments. *Engineering Geology,* 164**,** 163-171.
TOLL, D., RAHARDJO, H. & LEONG, E. Landslides in Singapore. Proceedings of the 2nd International Conference on Landslides, Slope Stability and the Safety of Infra-Structures, Singapore, 1999. 27-28.
TULLER, M. & OR, D. 2005. Water films and scaling of soil characteristic curves at low water contents. *Water Resources Research,* 41.
TULLER, M., OR, D. & DUDLEY, L. M. 1999. Adsorption and capillary condensation in porous media: Liquid retention and interfacial configurations in angular pores. *Water Resources Research,* 35**,** 1949-1964.
VAN GENUCHTEN, M. T. 1980. A closed-form equation for predicting the hydraulic conductivity of unsaturated soils 1. *Soil science society of America journal,* 44**,** 892-898.
VANAPALLI, S. & FREDLUND, D. 2000. Comparison of different procedures to predict unsaturated soil shear strength. *Geotechnical Special Publication***,** 195-209.
VANAPALLI, S., FREDLUND, D. & PUFAHL, D. 1999. The influence of soil structure and stress history on the soil–water characteristics of a compacted till. *Geotechnique,* 49**,** 143-159.
VANAPALLI, S., FREDLUND, D., PUFAHL, D. & CLIFTON, A. 1996a. Model for the prediction of shear strength with respect to soil suction. *Canadian Geotechnical Journal,* 33**,** 379-392.
VANAPALLI, S., SILLERS, W. & FREDLUND, M. The meaning and relevance of residual state to unsaturated soils. 51st Canadian Geotechnical Conference, 1998. sn, 4-7.
VANAPALLI, S. K. 1994. *Simple test procedures and their interpretation in evaluating the shear strength of an unsaturated soil. .* PhD thesis, University of Saskatchewan, Saskatoon.
VANAPALLI, S. K. 1995. *Simple test procedures and their interpretation in evaluating the shear strength of an unsaturated soil*.
VANAPALLI, S. K., FREDLUND, D. G. & PUFAHL, D. E. 1996b. The relationship between the soil-water characteristic curve and the unsaturated shear strength of a compacted glacial till. *Geotechnical Testing Journal,* 19**,** 259-268.
VANAPALLI, S. K., NICOTERA, M. & SHARMA, R. S. 2008. Axis translation and negative water column techniques for suction control. *Laboratory and Field Testing of Unsaturated Soils.* Springer.
WHEELER, S. 1988. A conceptual model for soils containing large gas bubbles. *Geotechnique,* 38**,** 389-397.
WHEELER, S., SHARMA, R. & BUISSON, M. 2003. Coupling of hydraulic hysteresis and stress–strain behaviour in unsaturated soils. *Géotechnique,* 53**,** 41-54.
WHITE, I. & SULLY, M. 1987. Macroscopic and microscopic capillary length and time scales from field infiltration. *Water Resources Research,* 23**,** 1514-1522.
WHITE, N. F., DUKE, H. R., SUNADA, D. K. & COREY, A. T. 1970. Physics of desaturation in porous materials. *Journal of the Irrigation and Drainage Division,* 96**,** 165-191.
WIJAYA, M. 2017. *Compression, Shrinkage and Wetting-induced volume change of unsaturated soils.* PhD thesis, Nanyang Technological Unviversity.
WIJAYA, M. & LEONG, E. C. 2017. Modelling the effect of density on the unimodal soil-water characteristic curve. *Géotechnique,* 67**,** 637-645.

WOODING, R. 1968. Steady infiltration from a shallow circular pond. *Water resources research,* 4**,** 1259-1273.
YANG, H., RAHARDJO, H., LEONG, E.-C. & FREDLUND, D. G. 2004. Factors affecting drying and wetting soil-water characteristic curves of sandy soils. *Canadian Geotechnical Journal,* 41**,** 908-920.
YIN, P. & VANAPALLI, S. K. 2018. Model for predicting tensile strength of unsaturated cohesionless soils. *Canadian Geotechnical Journal,* 55**,** 1313-1333.
YOUNG, J. F. 1967. Humidity control in the laboratory using salt solutions—a review. *Journal of Applied Chemistry,* 17**,** 241-245.
ZHAI, Q. & RAHARDJO, H. 2012. Determination of soil–water characteristic curve variables. *Computers and Geotechnics,* 42**,** 37-43.
ZHANG, R. 1997. Determination of soil sorptivity and hydraulic conductivity from the disk infiltrometer. *Soil Science Society of America Journal,* 61**,** 1024-1030.
ZHOU, A., SHENG, D. & CARTER, J. P. 2012. Modelling the effect of initial density on soil-water characteristic curves. *Géotechnique,* 62**,** 669-680.

APPENDICES

Appendix A-Suction and SWCC data

Contains Appendices A1-A5 (referenced in Chapter 4)

Appendix A1

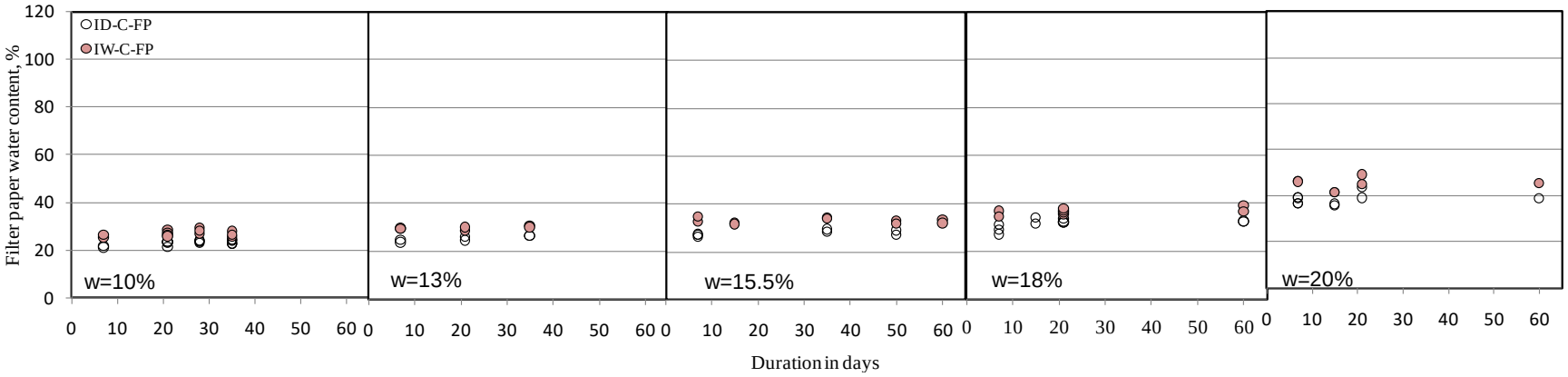

a) Contact filter paper

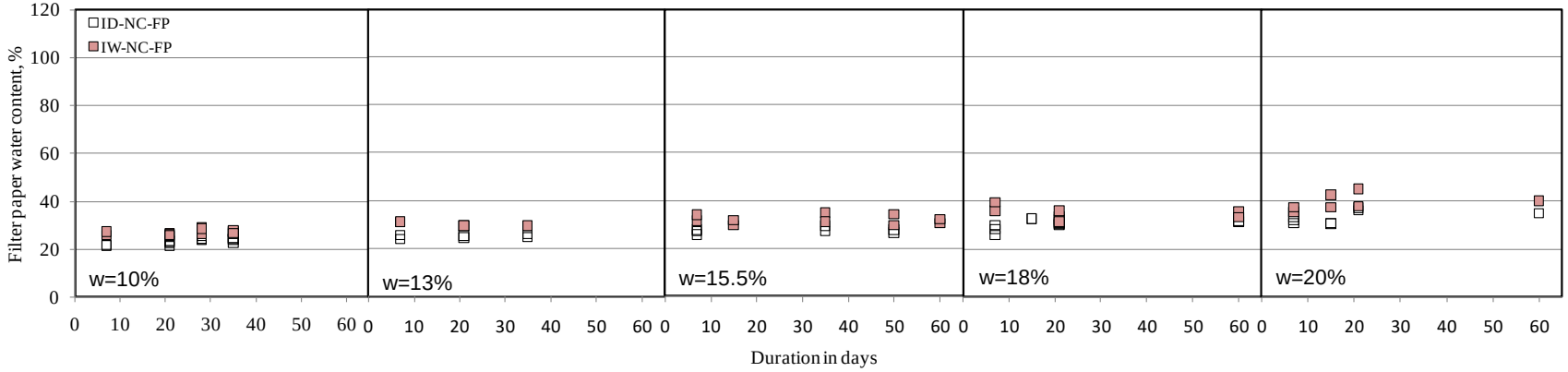

b) Non-contact filter paper

Figure A1-1: Effect of equilibrium time on filter paper water content for standard Proctor compacted BT1 soils – Plastic mold and Method 2

Appendix A1

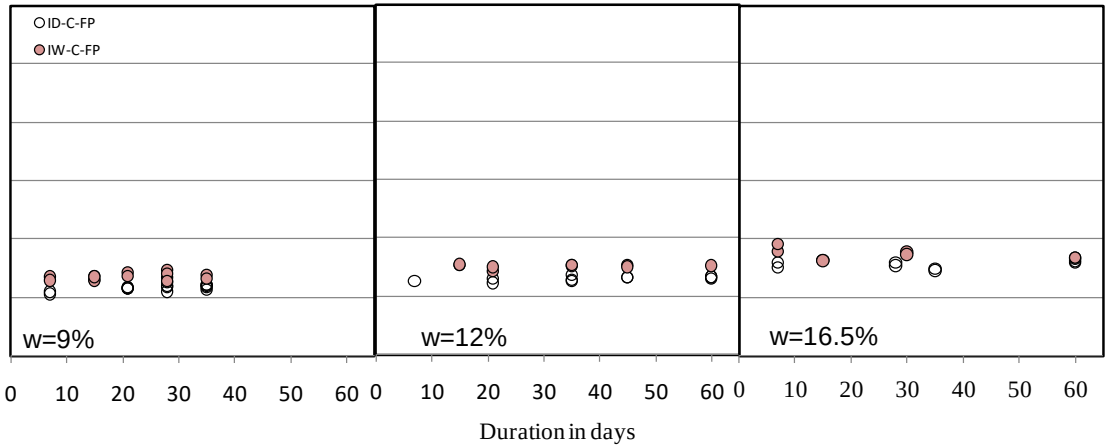

a) Contact filter paper

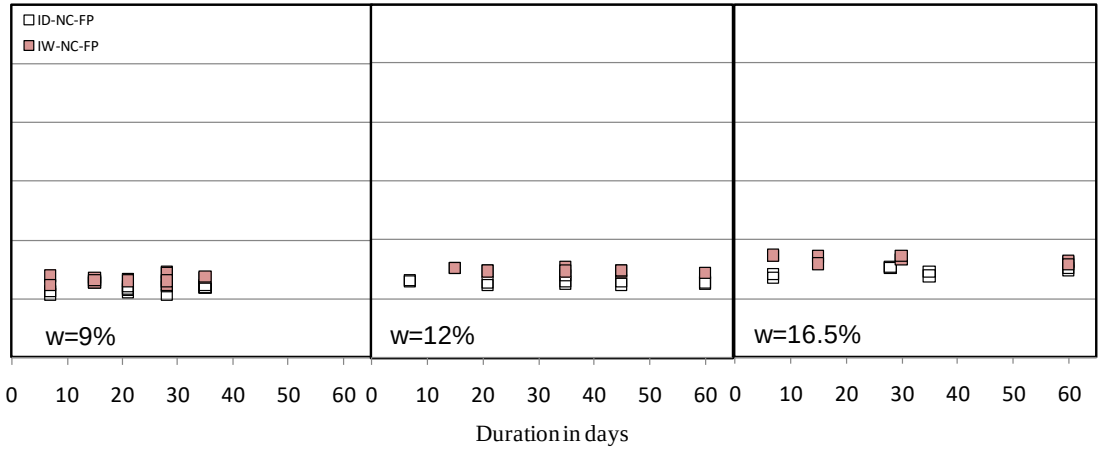

b) Non-contact filter paper

Figure A1-2: Effect of equilibrium time on filter paper water content for modified Proctor compacted BT1 soils – Plastic mold and Method 2

Appendix A1

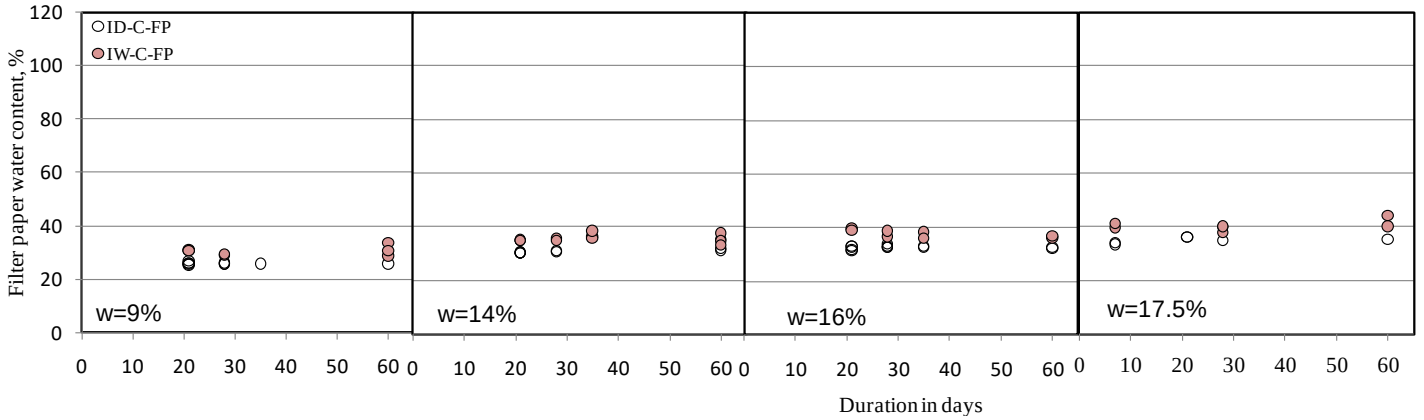

a) Contact filter paper

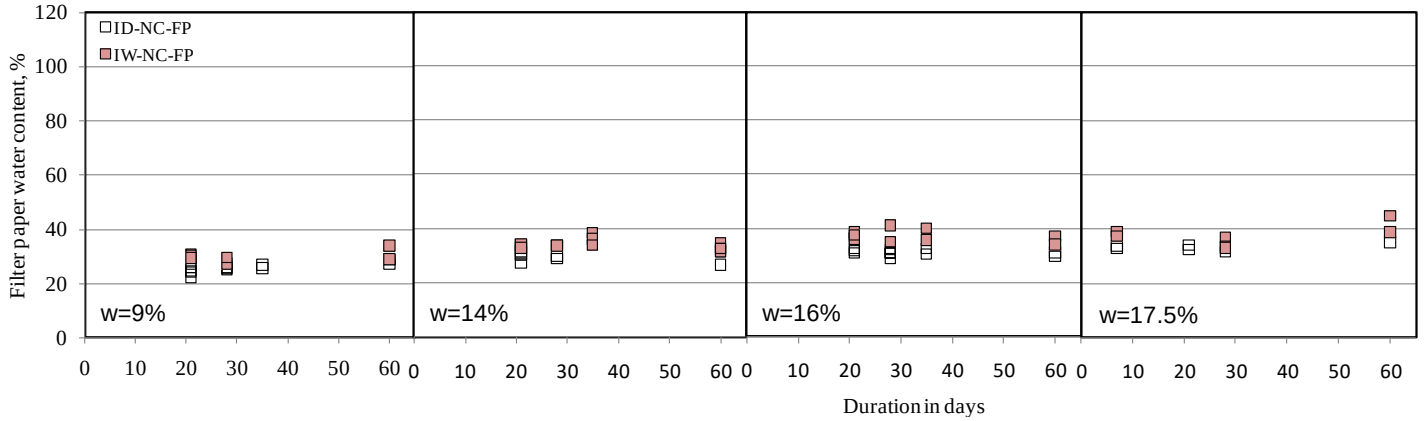

b) Non-contact filter paper

Figure A1-3: Effect of equilibrium time on filter paper water content for standard Proctor compacted JF2 soils – Plastic mold and Method 2

Appendix A1

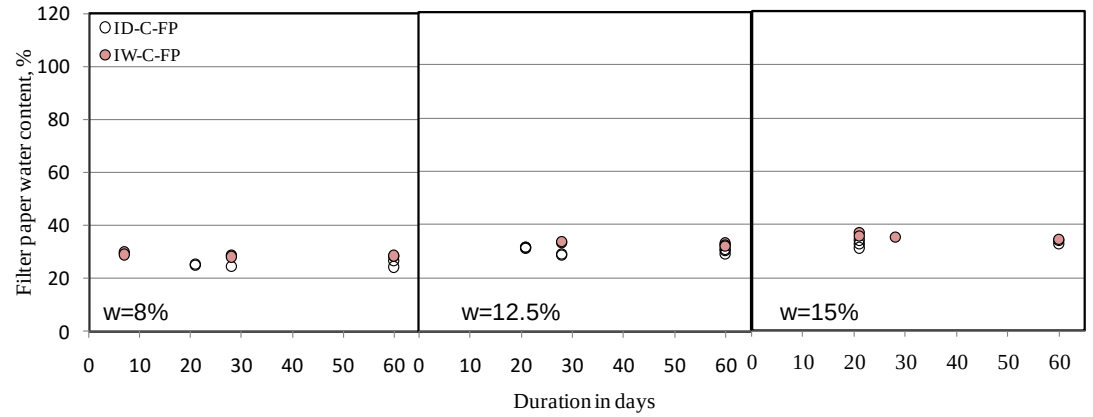

a) Contact filter paper

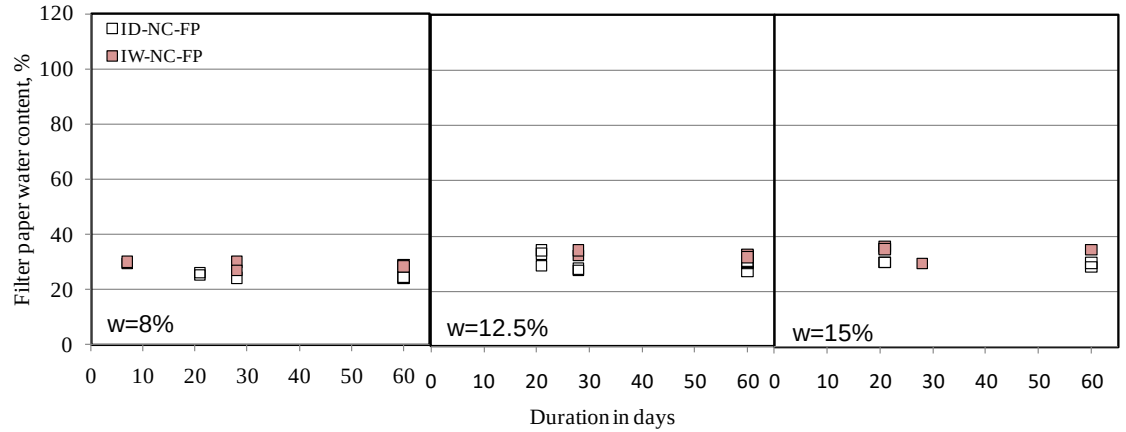

b) Non-contact filter paper

Figure A1-4: Effect of equilibrium time on filter paper water content for modified Proctor compacted JF2 soils – Plastic mold and Method 2

Appendix A2

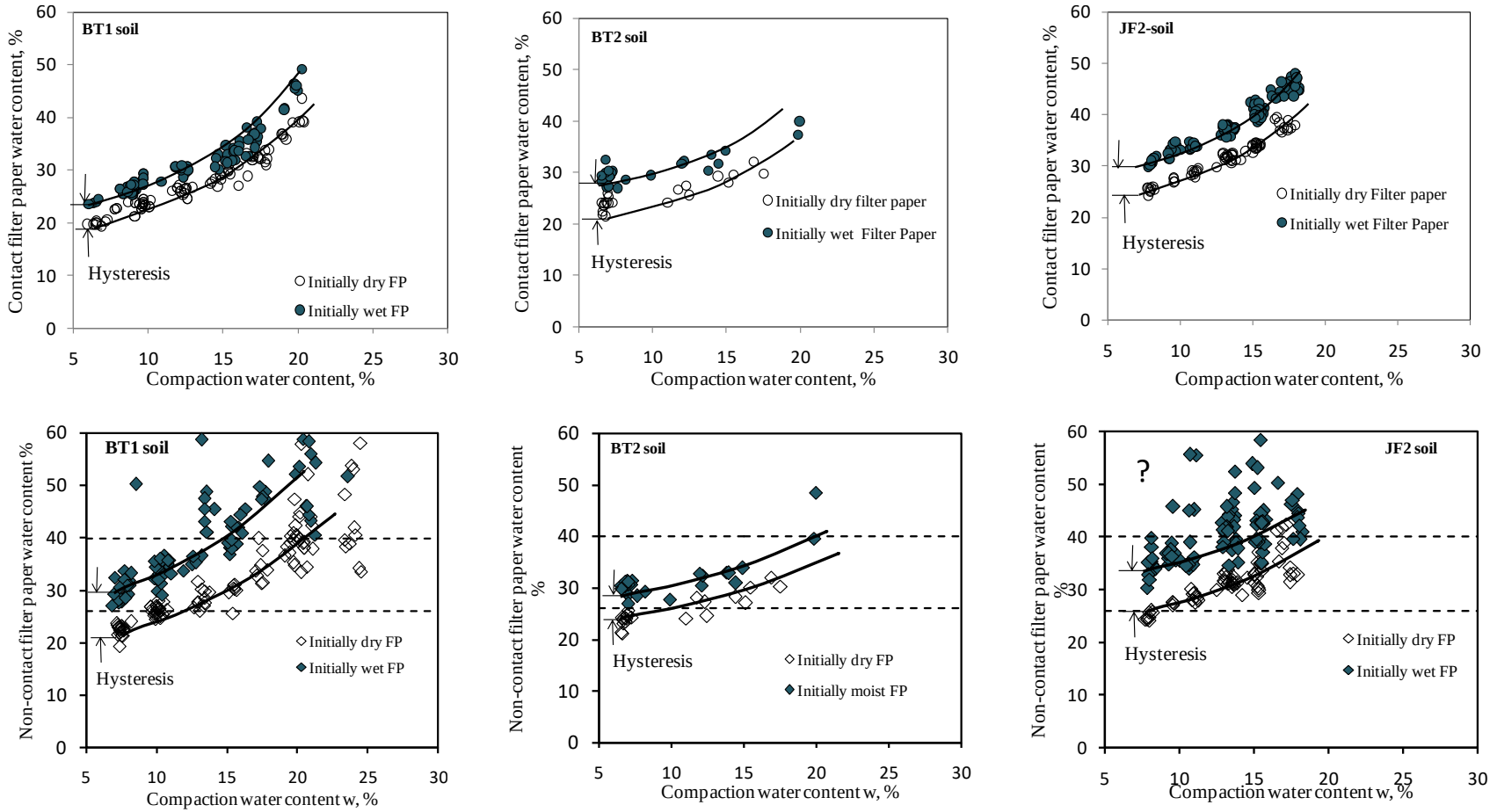

Figure A2-1Hysteresis between initially dry and initially wet filter papers in contact and non-contact modes- Method 1-Standard mold

Appendix A3

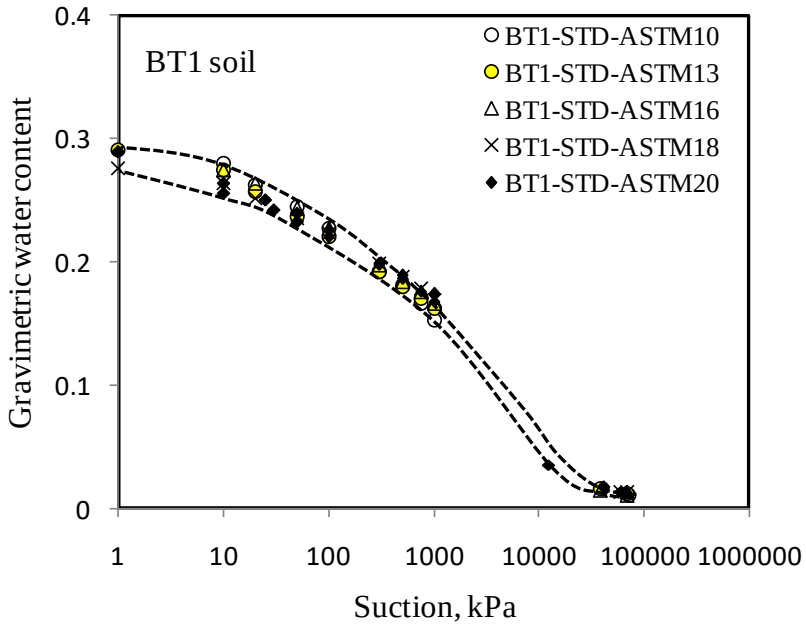

Figure A3-1: SWCC-w for BT1 standard Proctor specimens compacted in the standard mold.

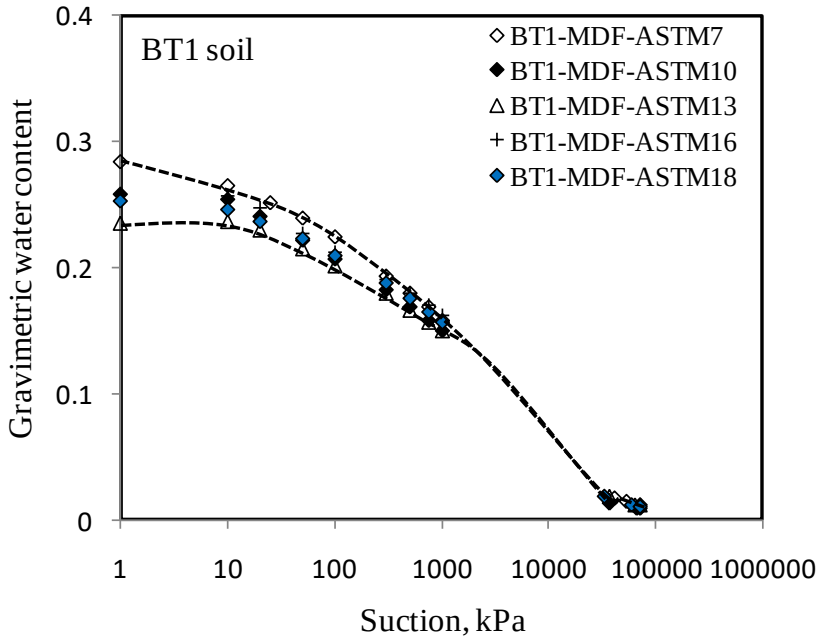

Figure A3-2: SWCC-w for BT1 modified Proctor specimens compacted in the standard mold.

Appendix A3

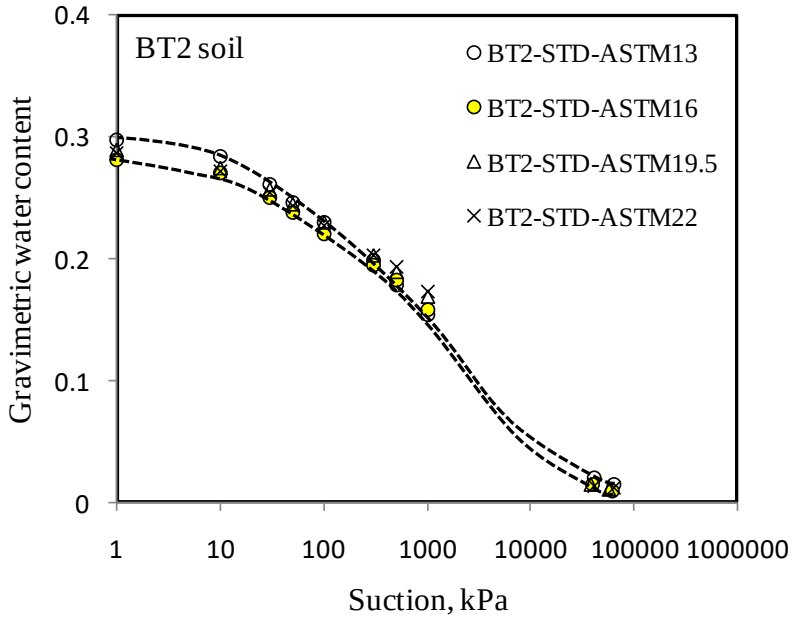

Figure A3-3: SWCC-w for BT2 standard Proctor specimens compacted in the standard mold.

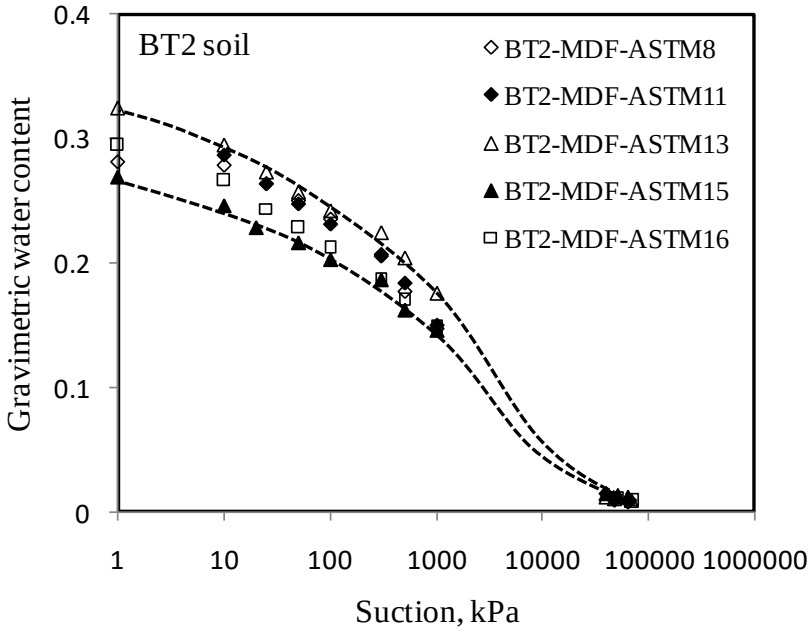

Figure A3-4: SWCC-w for BT2 modified Proctor specimens compacted in the standard mold.

Appendix A3

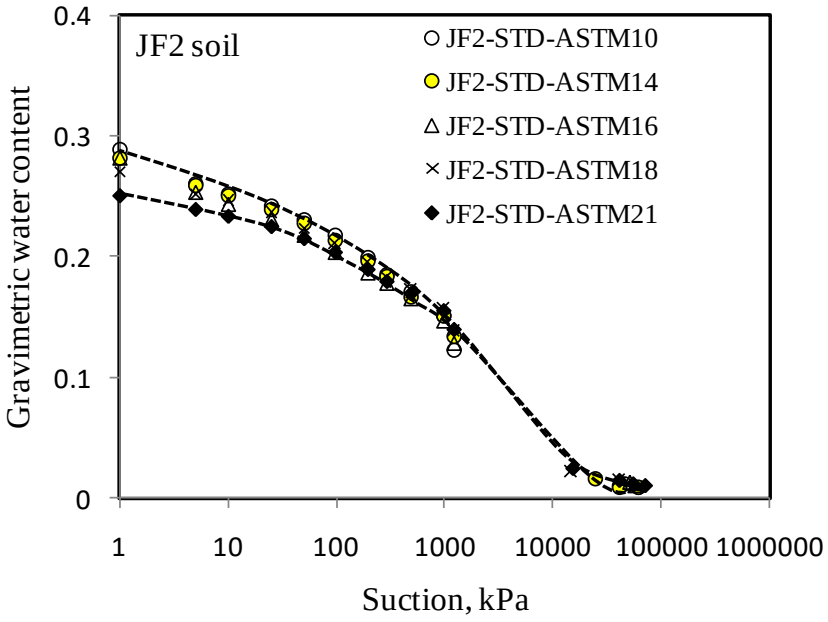

Figure A3-5: SWCC-w for JF2 standard Proctor specimens compacted in the standard mold.

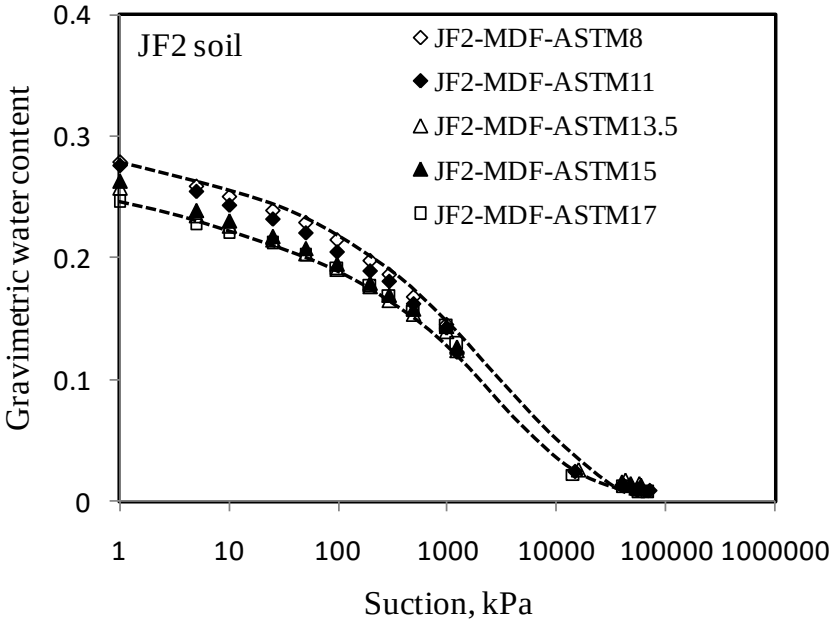

Figure A3-6: SWCC-w for JF2 modified Proctor specimens compacted in the standard mold.

Appendix A3

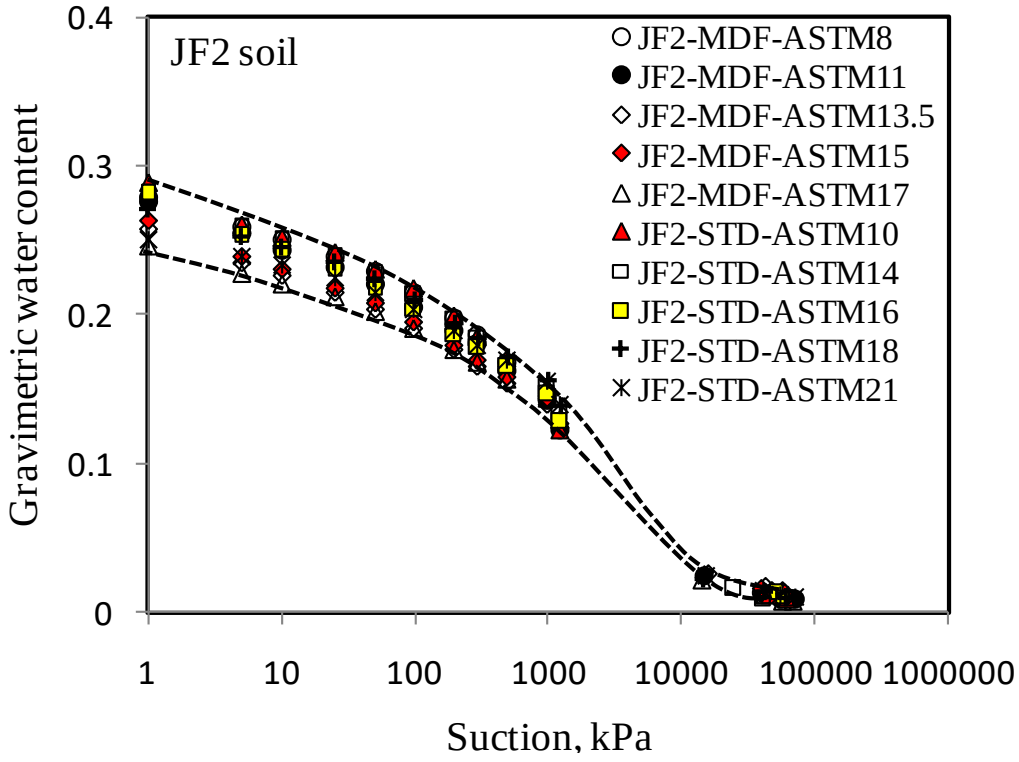

Figure A3-7: SWCC-w for JF2 standard and modified Proctor specimens compacted in the standard mold.

Appendix A4

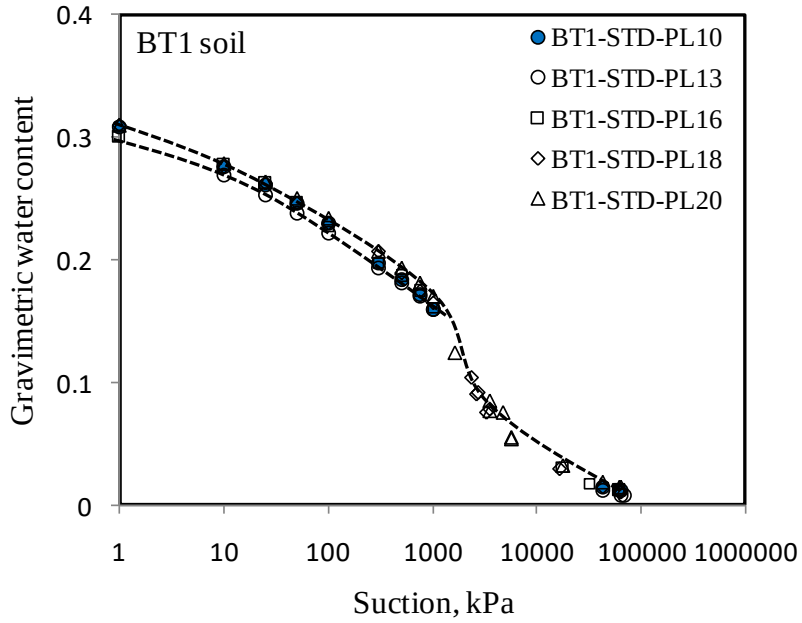

Figure A4-1-SWCC-w for BT1 standard Proctor samples compacted in plastic mold

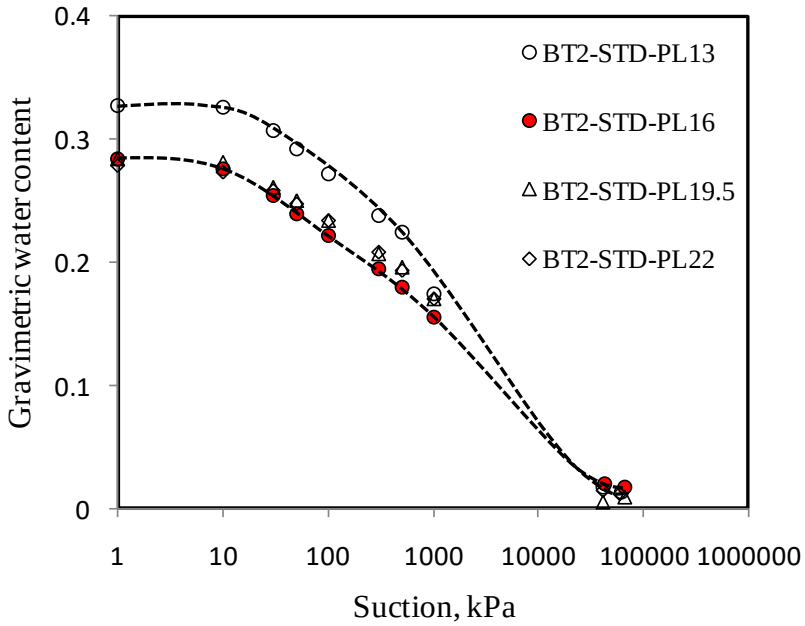

Figure A4-2-SWCC-w for BT2 standard Proctor samples compacted in plastic mold

Appendix A4

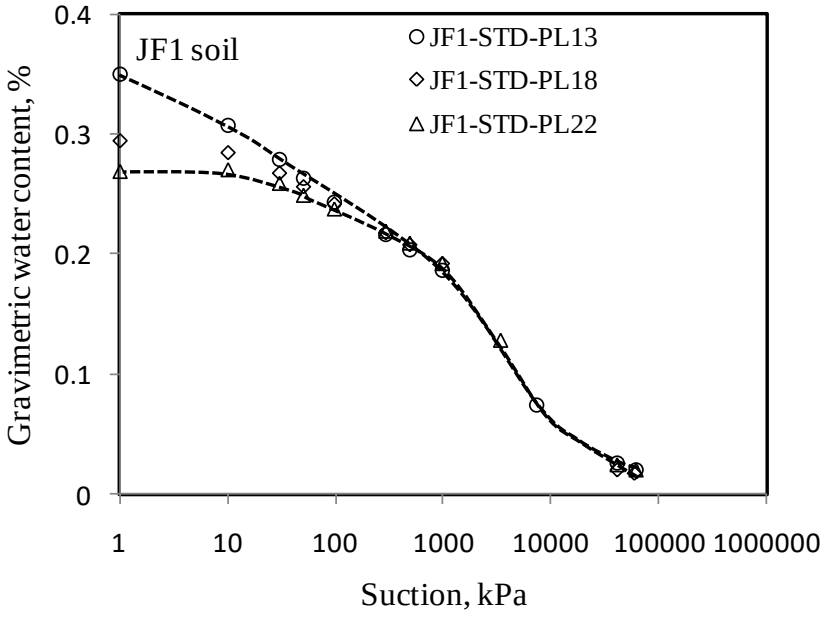

Figure A4-3-SWCC-w for JF1 standard Proctor samples compacted in plastic mol

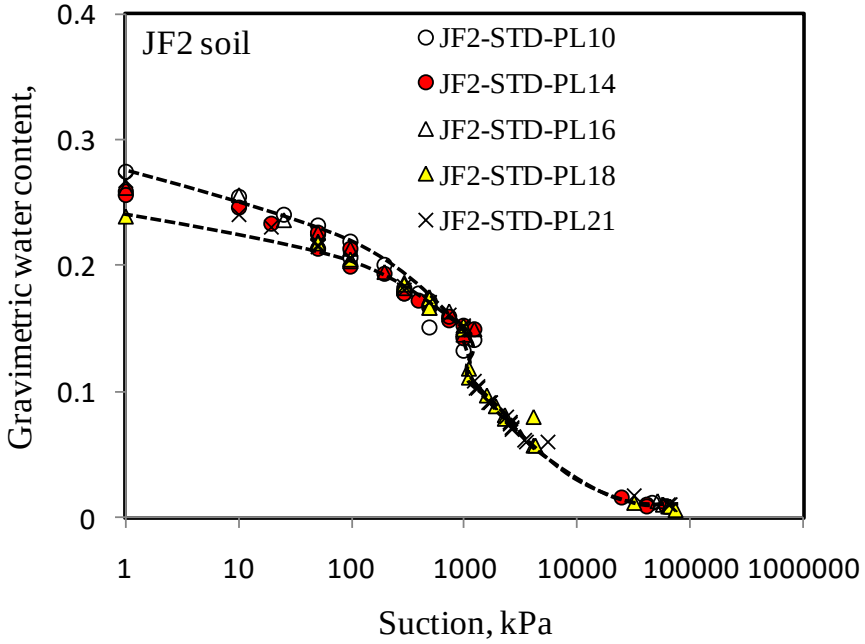

Figure A4-4-SWCC-w for JF2 standard Proctor samples compacted in plastic mold

Appendix A4

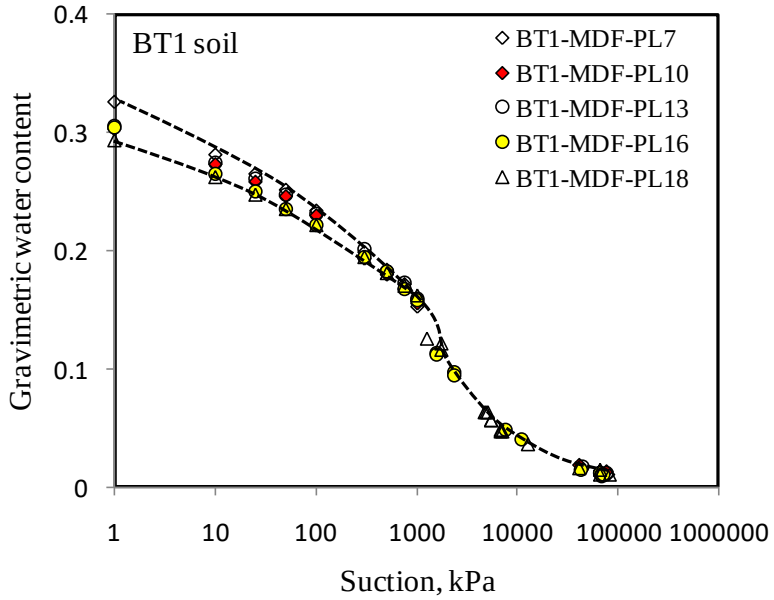

Figure A4-5-SWCC-w for BT1 modified Proctor samples compacted in plastic mold

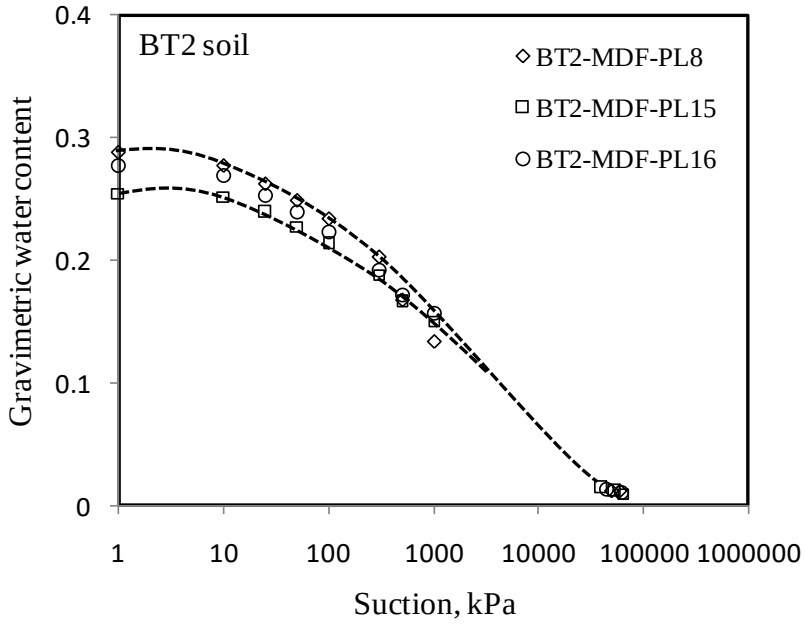

Figure A4-6-SWCC-w for BT2 modified Proctor samples compacted in plastic mold

Appendix A4

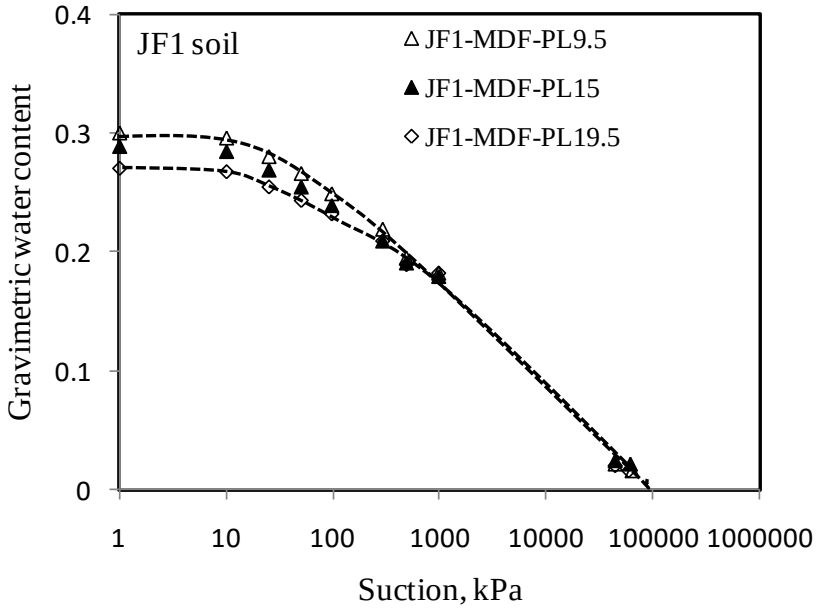

Figure A4-7-SWCC-w for JF1 modified Proctor samples compacted in plastic mold

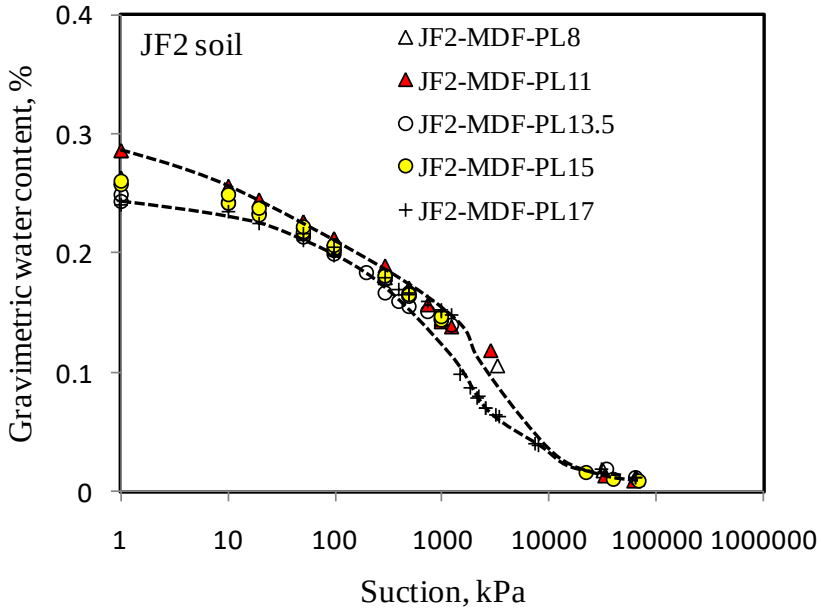

Figure A4-8-SWCC-w for JF2 modified Proctor samples compacted in plastic mold

Appendix A4

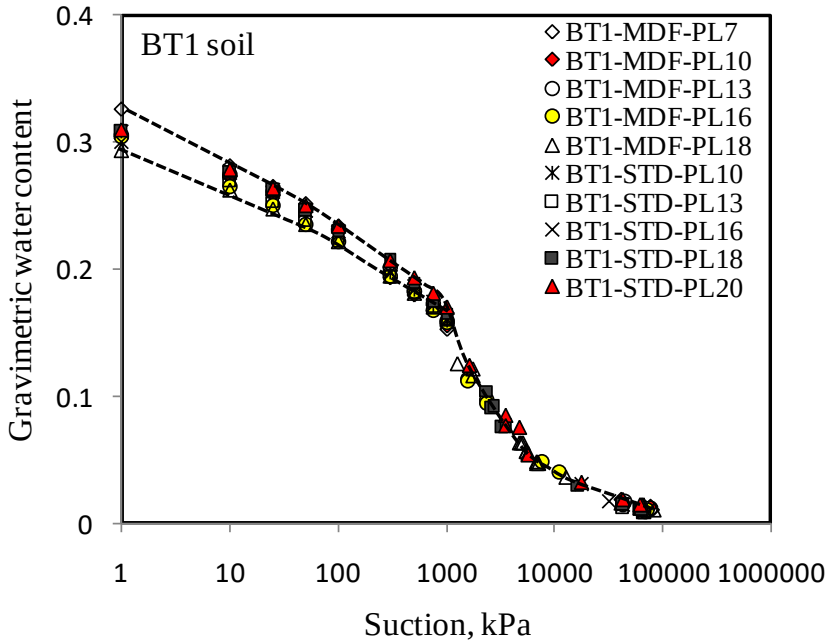

Figure A4-9-SWCC-w for BT1 standard and modified Proctor samples compacted in plastic mold

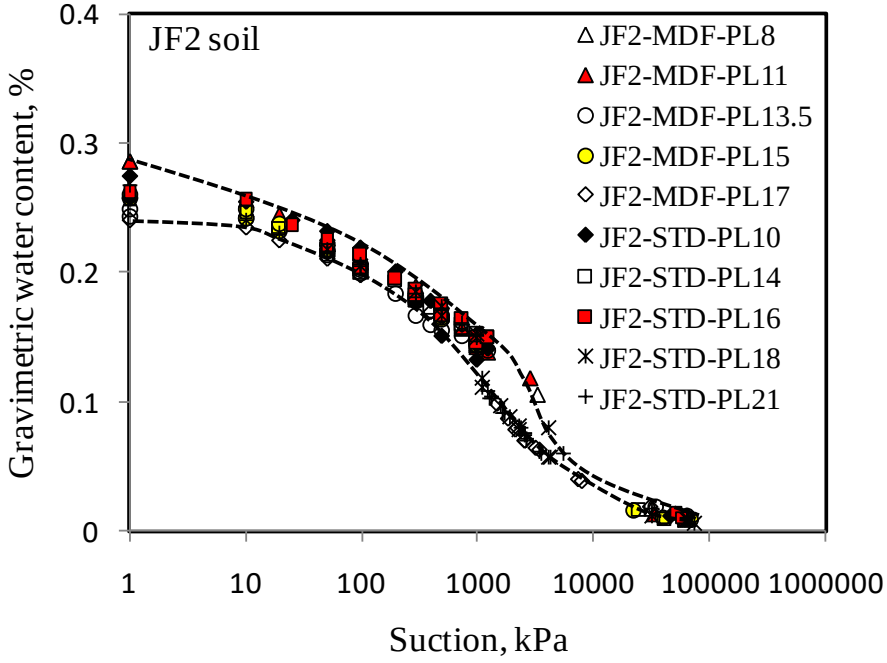

Figure A4-10-SWCC-w for JF2 standard and modified Proctor samples compacted in plastic mold

Appendix A5

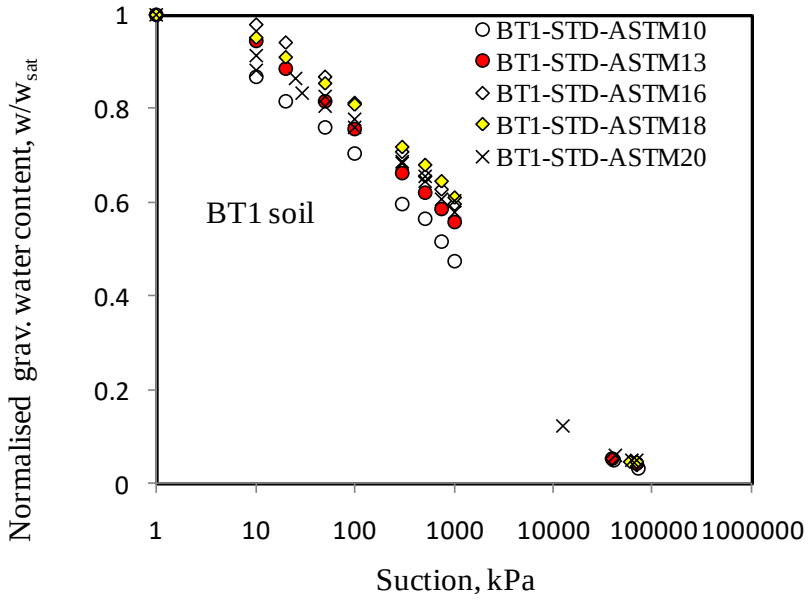

Figure A5-1: BT1 SWCCs plotted in terms of normalized gravimetric water contents for specimens compacted standard Proctor in the standard mold

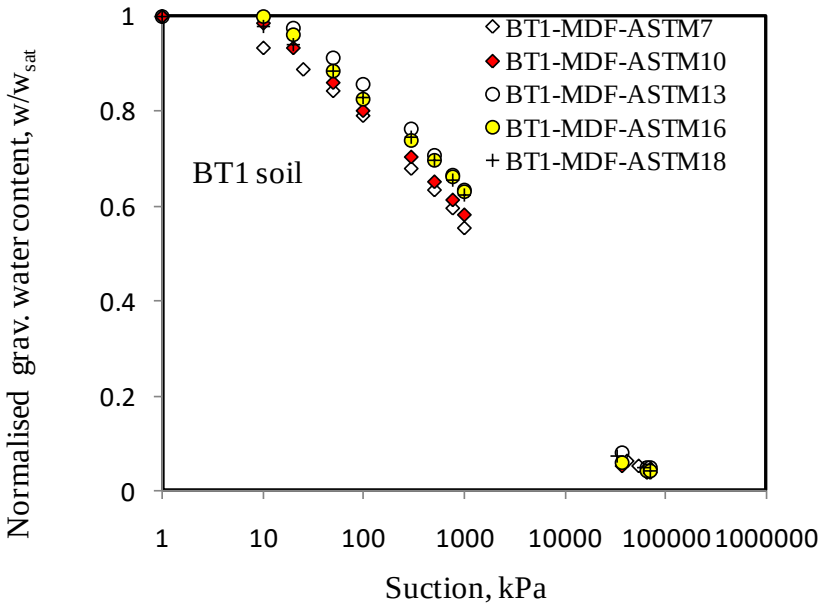

Figure A5-2: BT1 SWCCs plotted in terms of normalized gravimetric water contents for specimens compacted at modified Proctor in the standard mold

Appendix A5

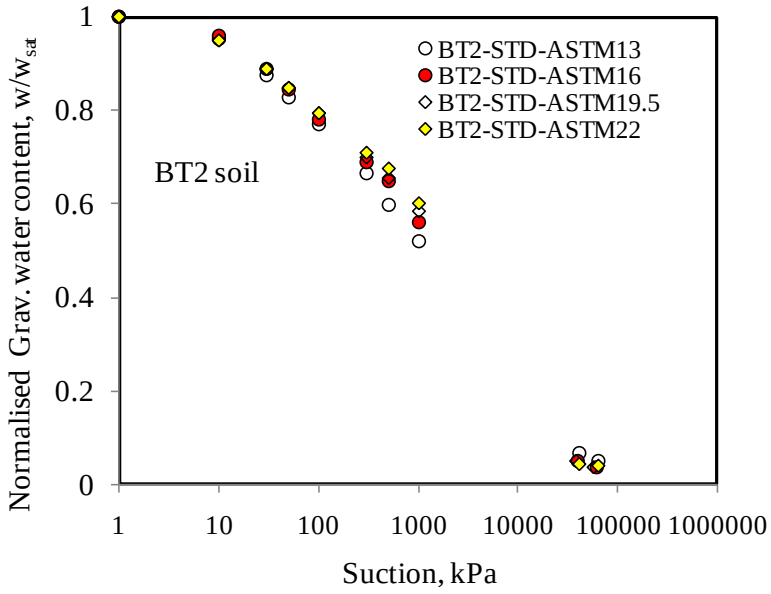

Figure A5-3: BT2 SWCCs plotted in terms of normalized gravimetric water contents for specimens compacted at standard Proctor in the standard mold

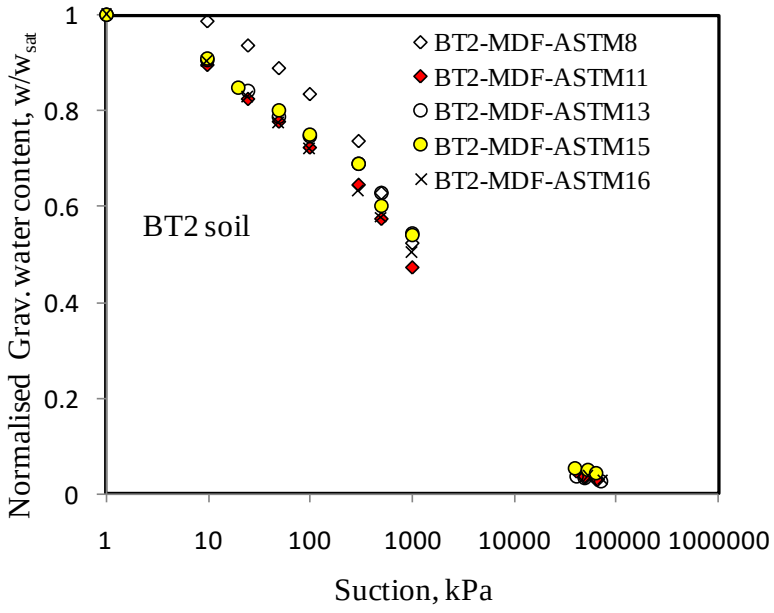

Figure A5-4: BT2 SWCCs plotted in terms of normalized gravimetric water contents for specimens compacted at modified Proctor in the standard mold

Appendix A5

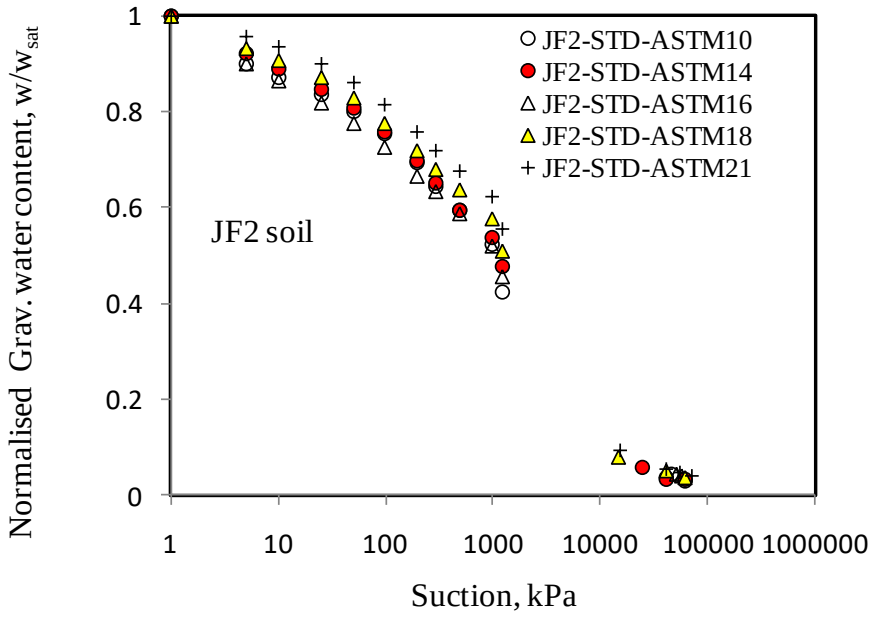

Figure A5-5: JF2 SWCCs plotted in terms of normalized gravimetric water contents for specimens compacted at standard Proctor in the standard mold

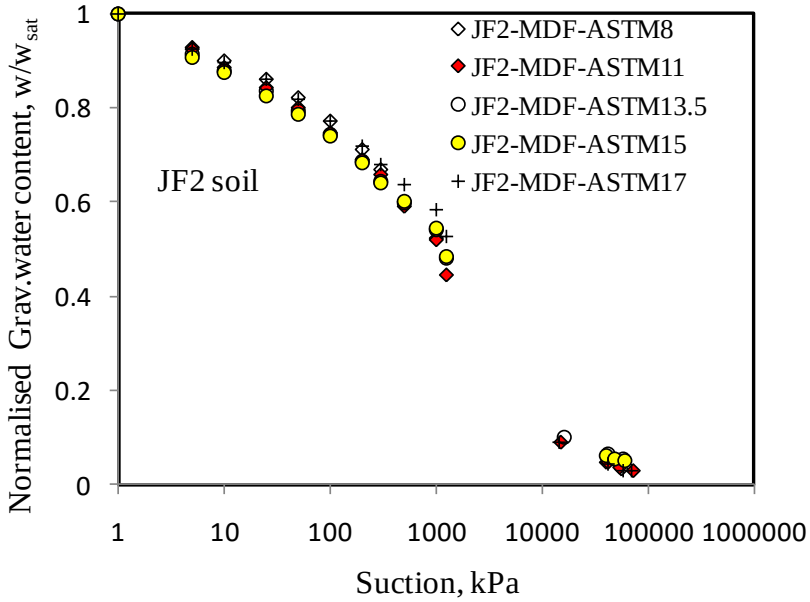

Figure A5-6: JF2 SWCCs plotted in terms of normalized gravimetric water contents for specimens compacted at standard Proctor in the standard mold

Appendix A5

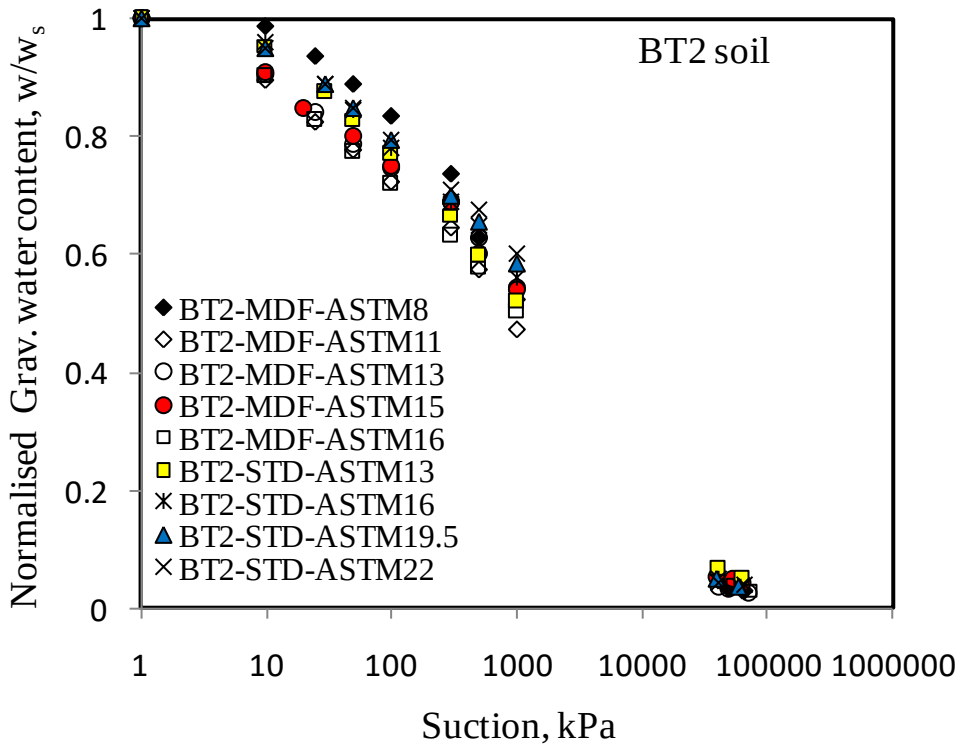

Figure A5-7: BT2 SWCCs plotted in terms of normalized gravimetric water contents for specimens compacted at both standard and modified Proctor in the standard mold

Appendix A5

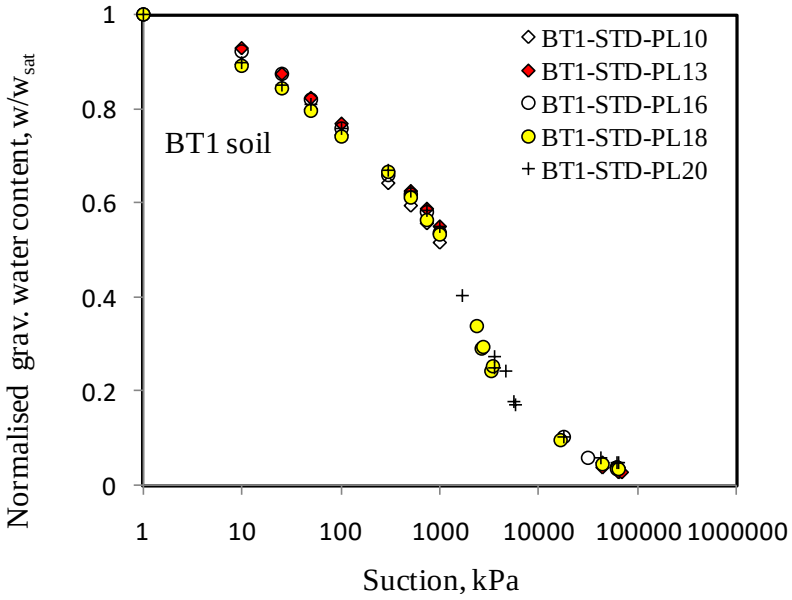

Figure A5-8: BT1 SWCCs plotted in terms of normalized gravimetric water contents for specimens compacted at standard Proctor in the plastic mold

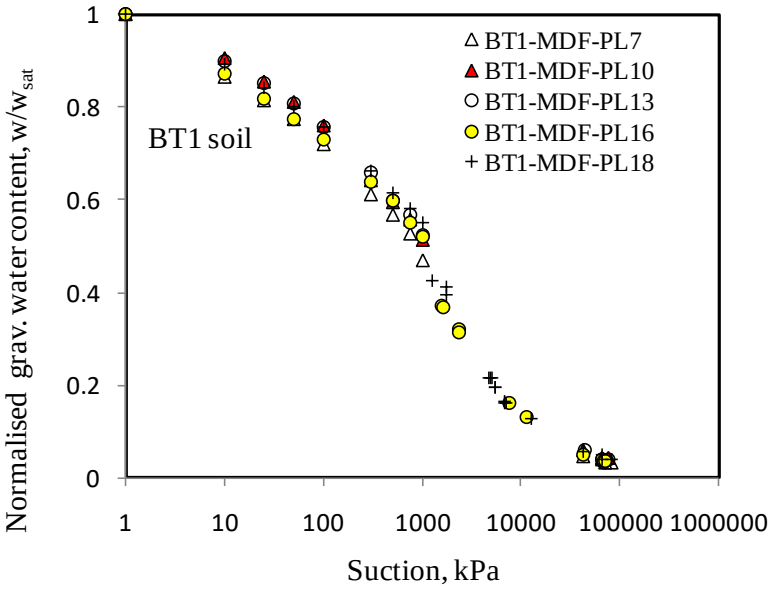

Figure A5-9: BT1 SWCCs plotted in terms of normalized gravimetric water contents for specimens compacted at modified Proctor in the plastic mold

Appendix A5

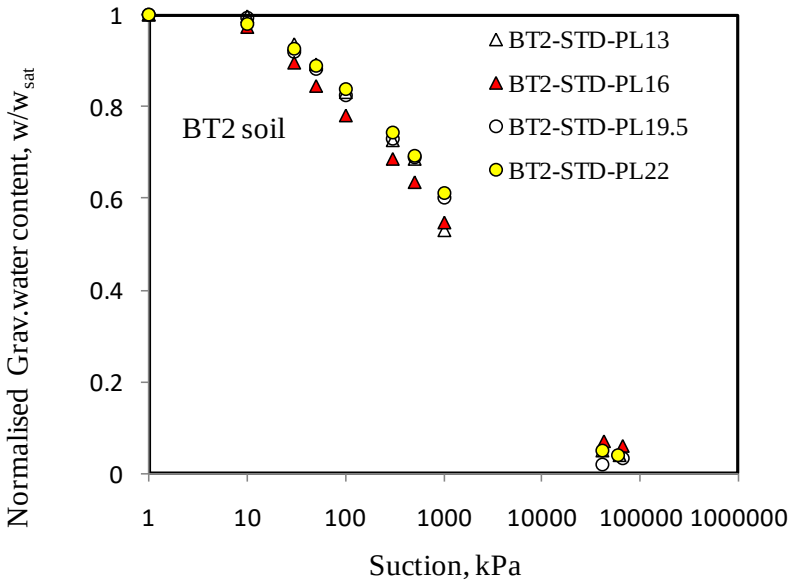

Figure A5-10: BT2 SWCCs plotted in terms of normalized gravimetric water contents for specimens compacted at standard Proctor in the plastic mold

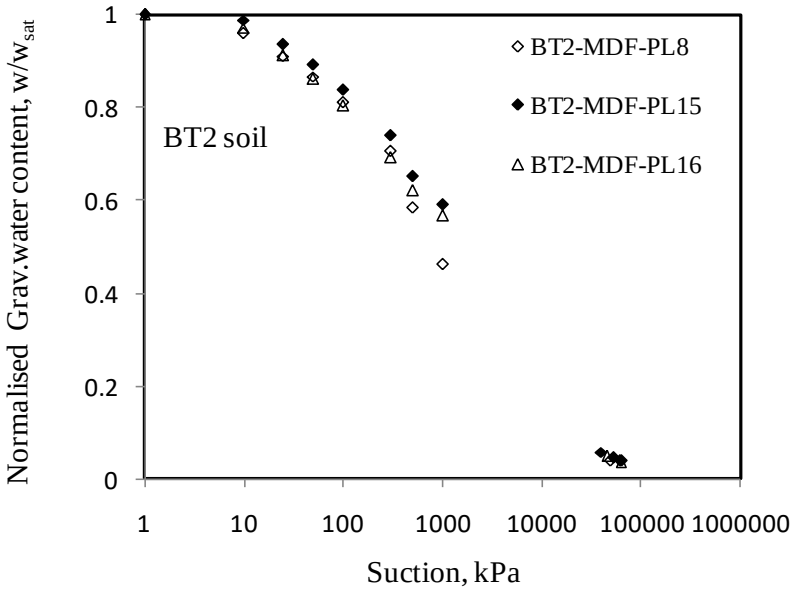

Figure A5-11: BT2 SWCCs plotted in terms of normalized gravimetric water contents for specimens compacted at modified Proctor in the plastic mold

Appendix A5

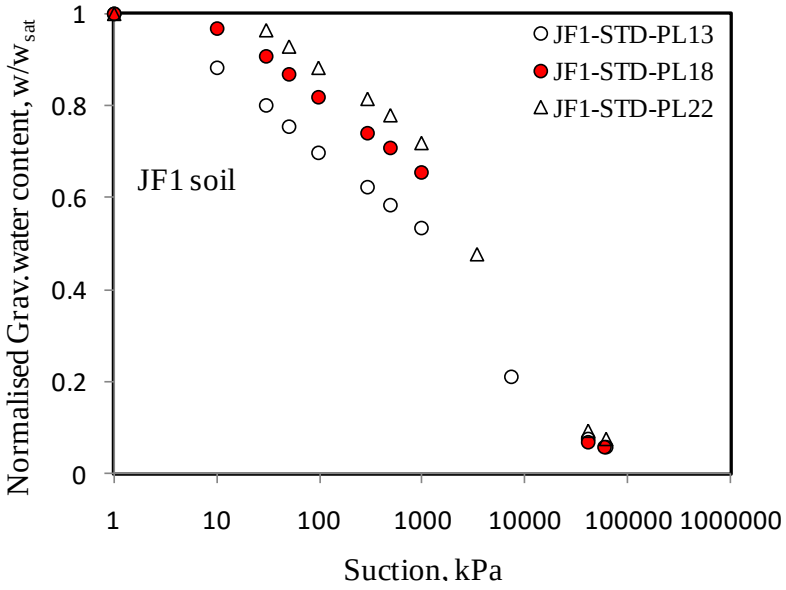

Figure A5-12: JF1 SWCCs plotted in terms of normalized gravimetric water contents for specimens compacted at standard Proctor in the plastic mold

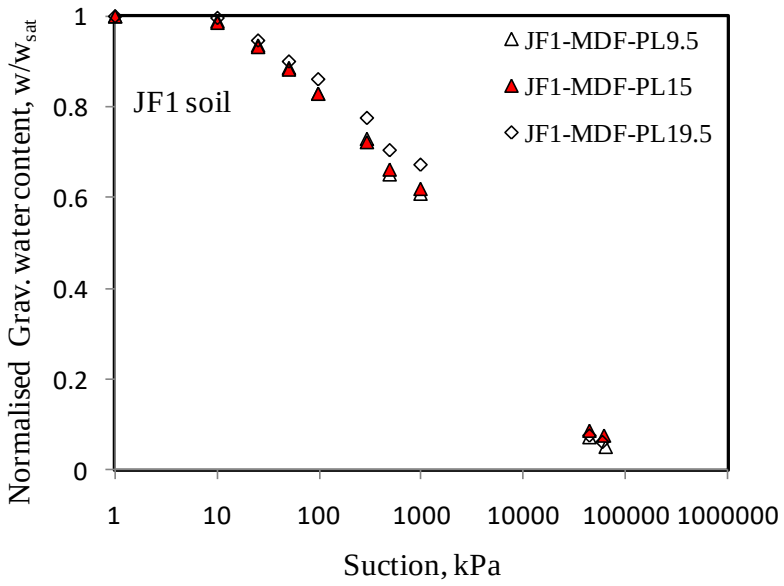

Figure A5-13: JF1 SWCCs plotted in terms of normalized gravimetric water contents for specimens compacted at modified Proctor in the plastic mold

Appendix A5

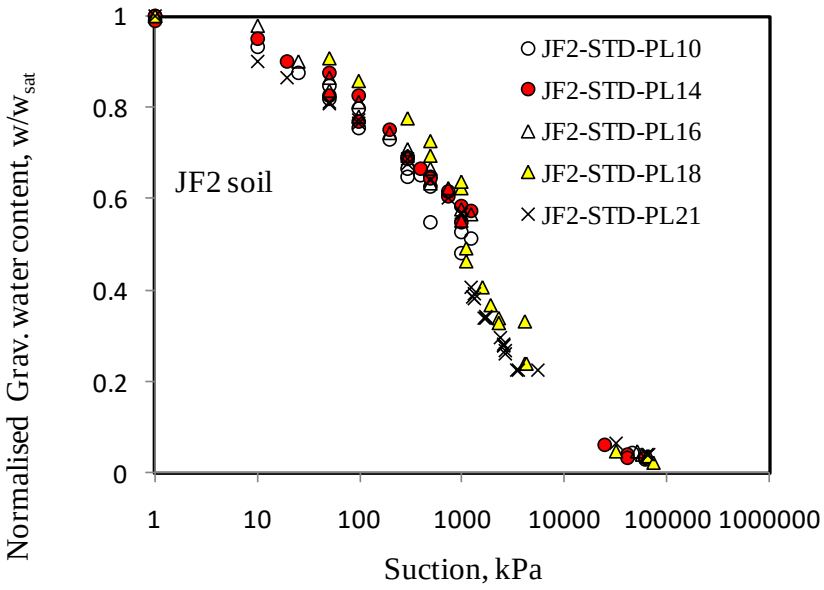

Figure A5-14: JF2 SWCCs plotted in terms of normalized gravimetric water contents for specimens compacted at standard Proctor in the plastic mold

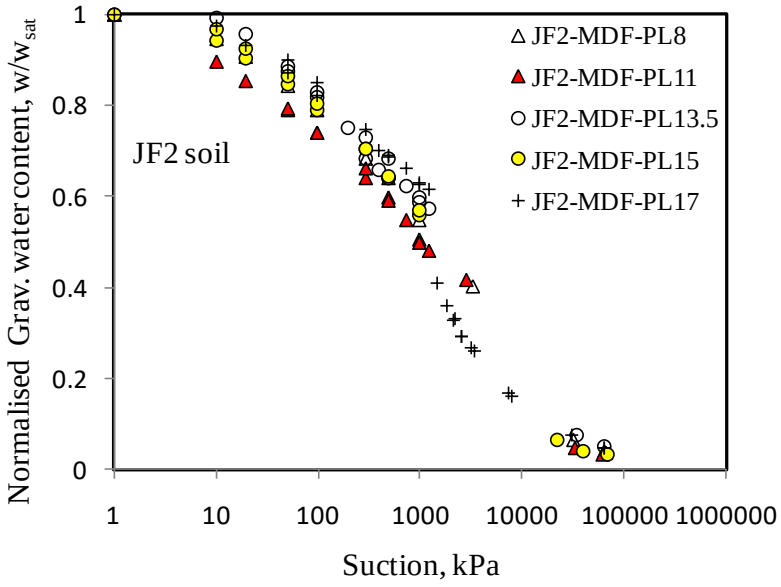

Figure A5-15: JF2 SWCCs plotted in terms of normalized gravimetric water contents for specimens compacted at modified Proctor in the plastic mold

Appendix A5

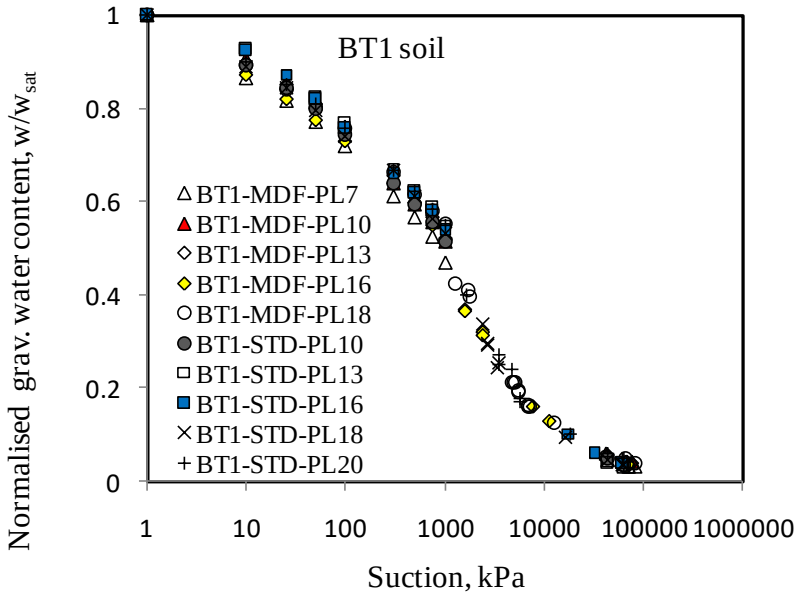

Figure A5-16: BT1 SWCCs plotted in terms of normalized gravimetric water contents for specimens compacted at both standard and modified Proctor in the plastic mold

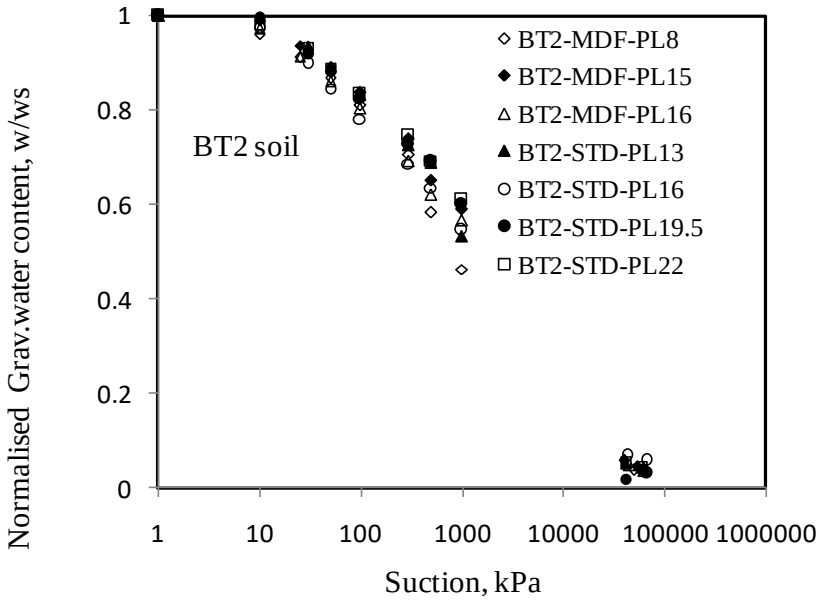

Figure A5-17: BT2 SWCCs plotted in terms of normalized gravimetric water contents for specimens compacted at both standard and modified Proctor in the plastic mold

Appendix A5

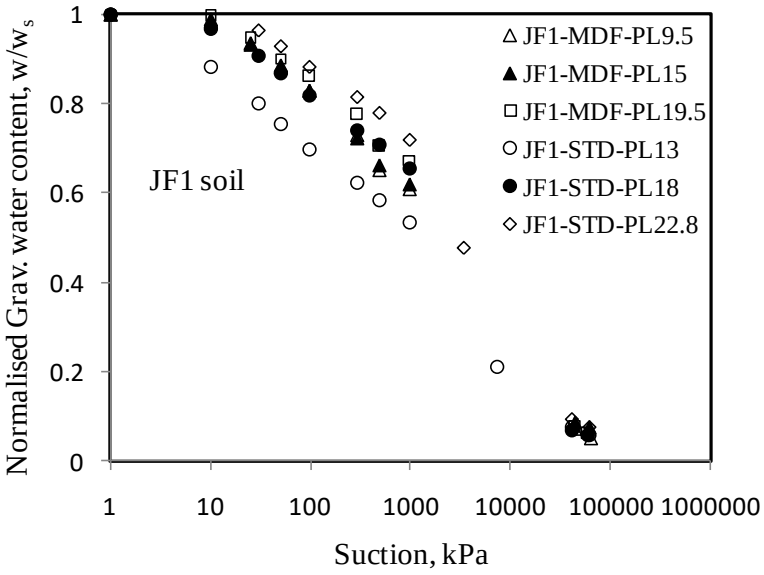

Figure A5-18: JF1 SWCCs plotted in terms of normalized gravimetric water contents for specimens compacted at both standard and modified Proctor in the plastic mold

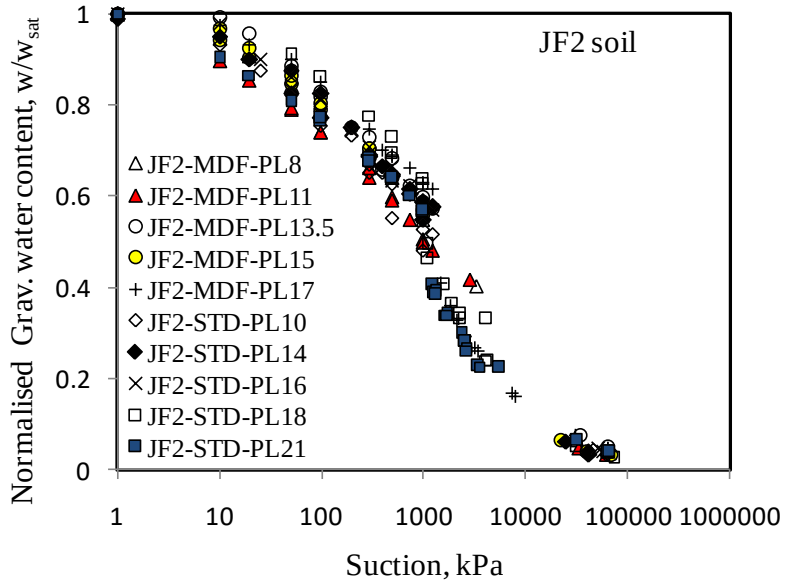

Figure A5-19: JF2 SWCCs plotted in terms of normalized gravimetric water contents for specimens compacted at both standard and modified Proctor in the plastic mold

Appendix B-Hydraulic properties

Contains Appendices B1-B8 (Referenced to in Chapter 5)

Appendix B1: Flexible wall permeameter- Experimental runs for the determination of k_s

APPENDIX B1- BT1 soil sets

Experimental runs

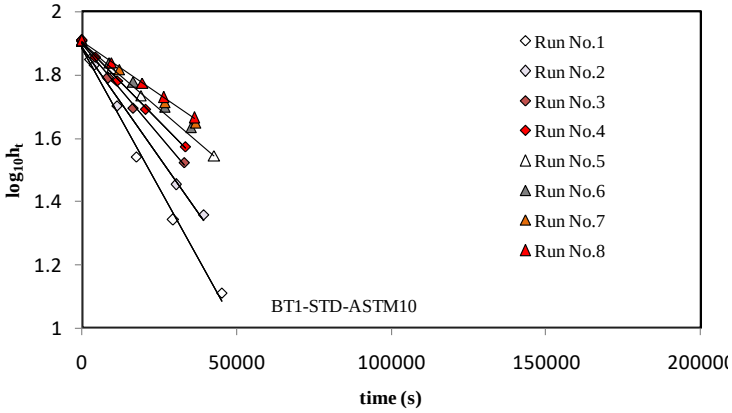

k_s-values with run numbers

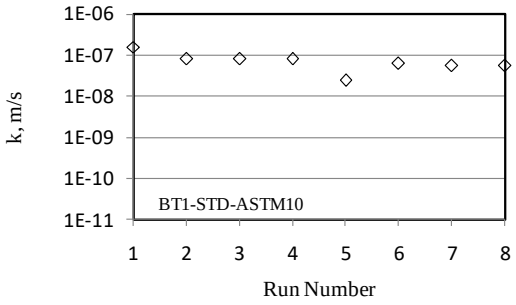

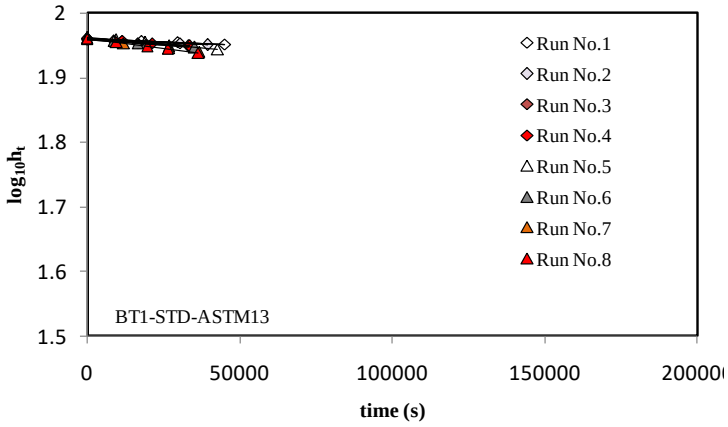

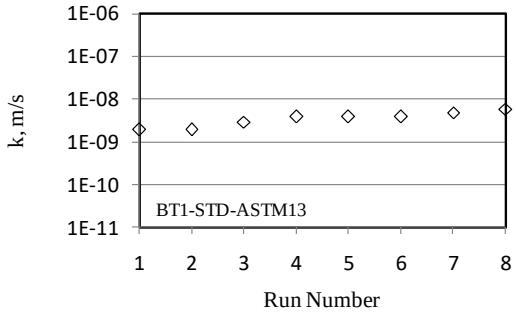

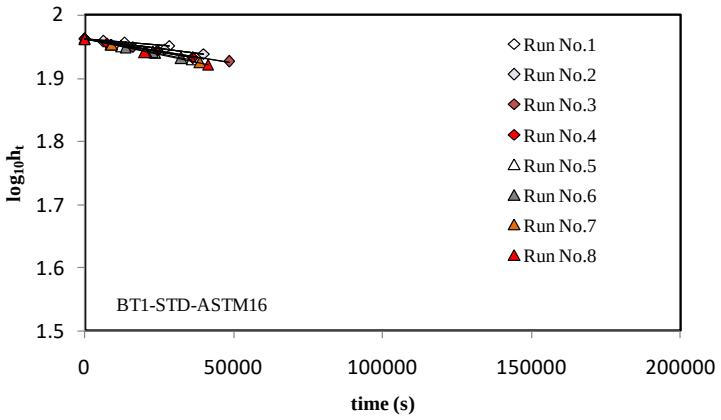
Run No.1
Run No.2
Run No.3
Run No.4
Run No.5
Run No.6
Run No.7
Run No.8
BT1-STD-ASTM16
log10ht
time (s)

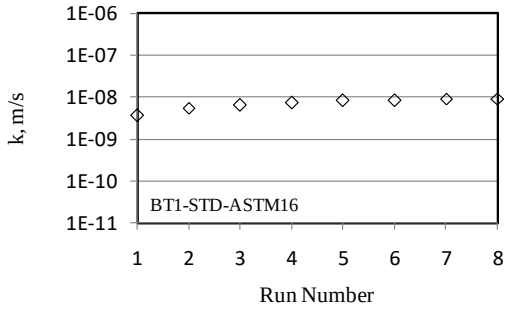
BT1-STD-ASTM16
k, m/s
Run Number

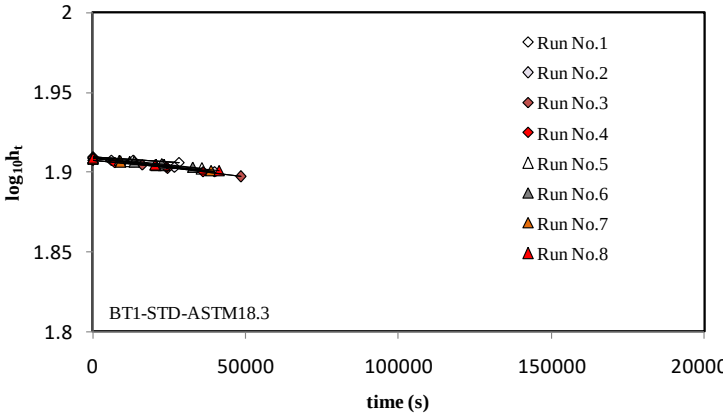
Run No.1
Run No.2
Run No.3
Run No.4
Run No.5
Run No.6
Run No.7
Run No.8
BT1-STD-ASTM18.3
log10ht
time (s)

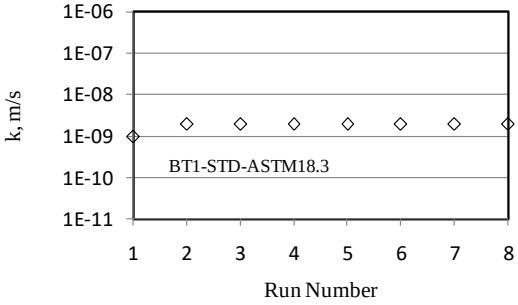
BT1-STD-ASTM18.3
k, m/s
Run Number

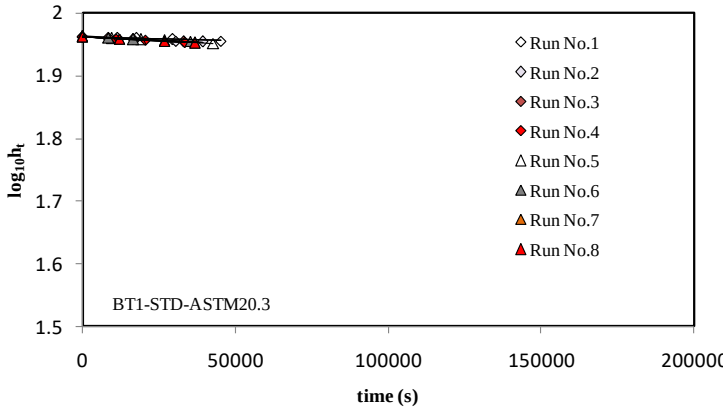
Run No.1
Run No.2
Run No.3
Run No.4
Run No.5
Run No.6
Run No.7
Run No.8
BT1-STD-ASTM20.3
log10ht
time (s)

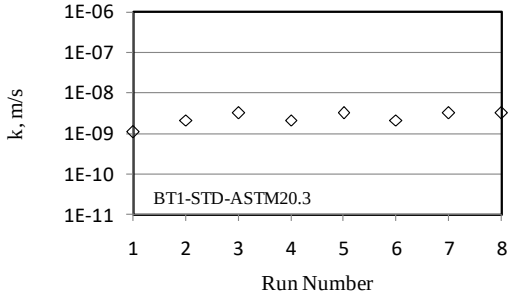
BT1-STD-ASTM20.3
k, m/s
Run Number

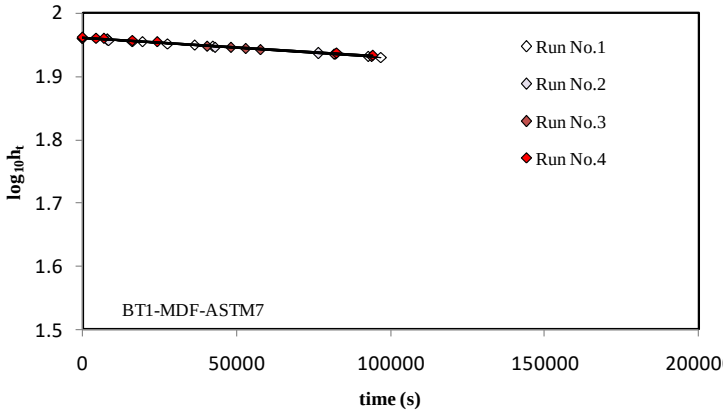
Run No.1
Run No.2
Run No.3
Run No.4
BT1-MDF-ASTM7
log10ht
time (s)

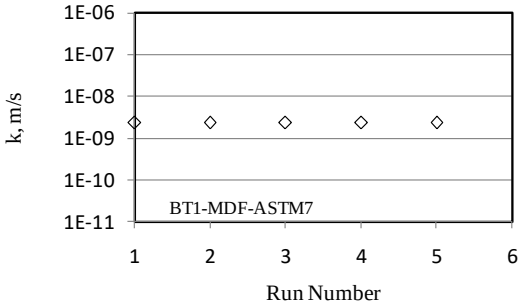
BT1-MDF-ASTM7
k, m/s
Run Number

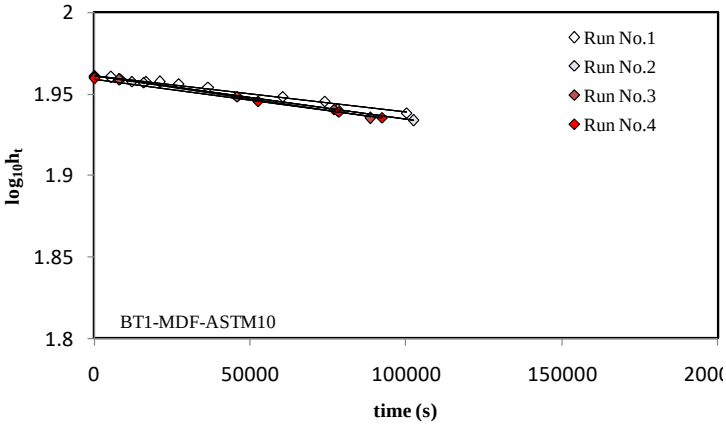
Run No.1
Run No.2
Run No.3
Run No.4
BT1-MDF-ASTM10
log10ht
time (s)

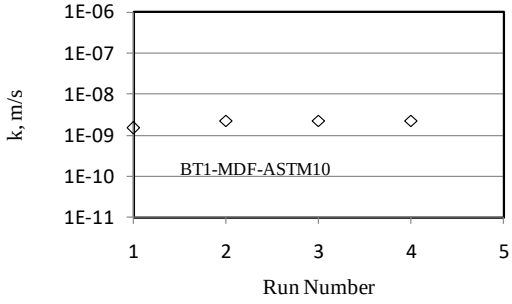
BT1-MDF-ASTM10
k, m/s
Run Number

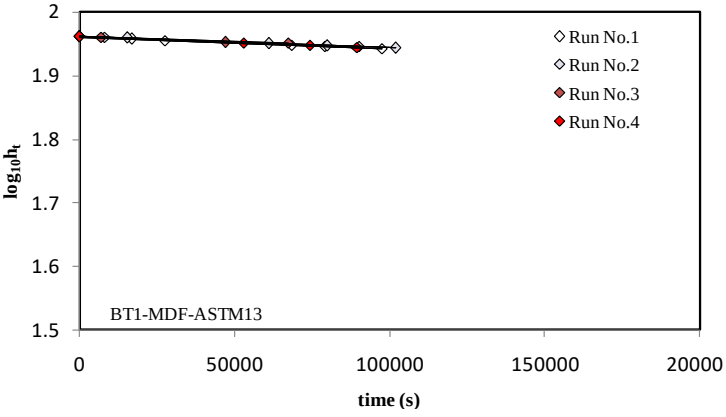
Run No.1
Run No.2
Run No.3
Run No.4
BT1-MDF-ASTM13
log10ht
time (s)

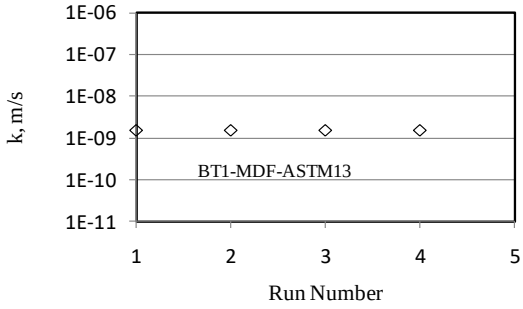
BT1-MDF-ASTM13
k, m/s
Run Number

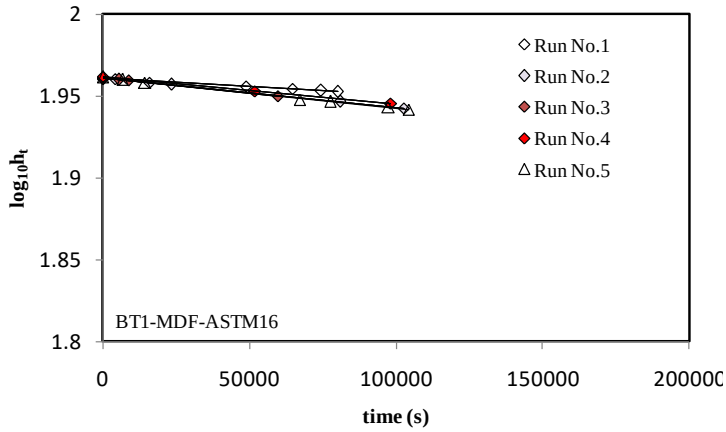

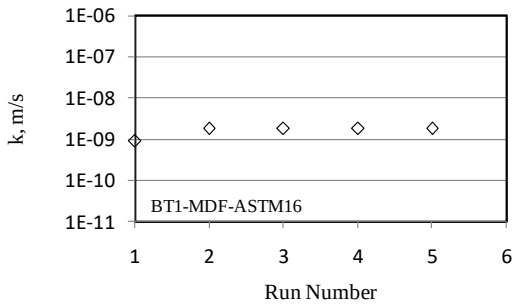

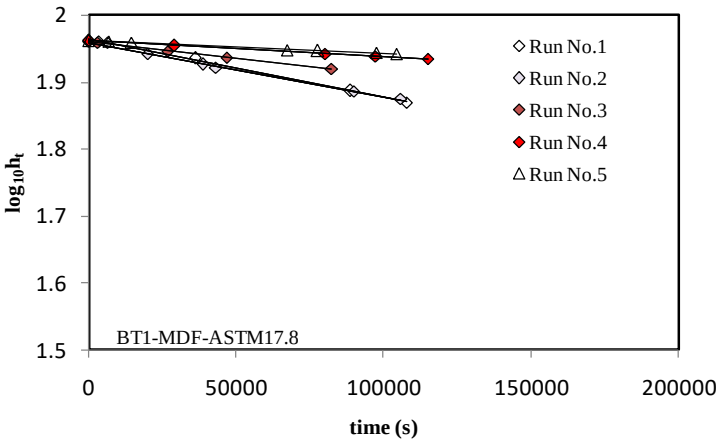

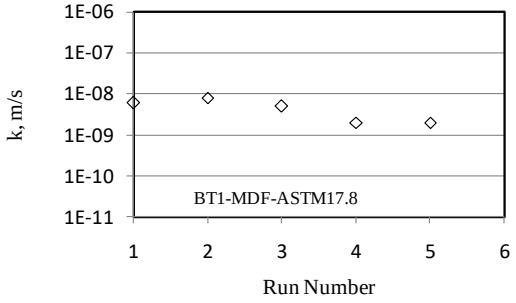

Appendix B1- BT2 soil sets

Experimental runs

k-values with run numbers

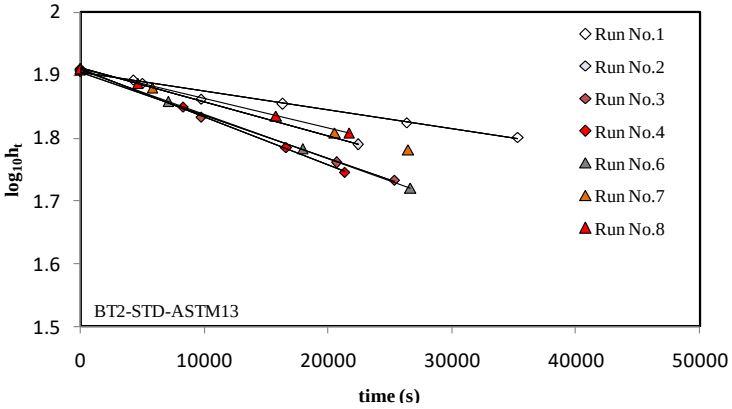

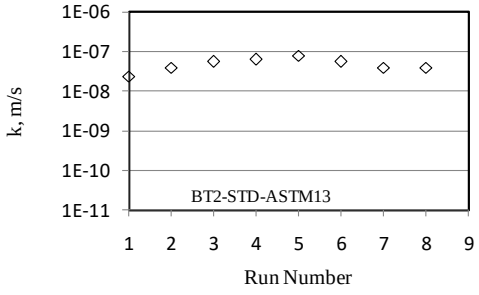

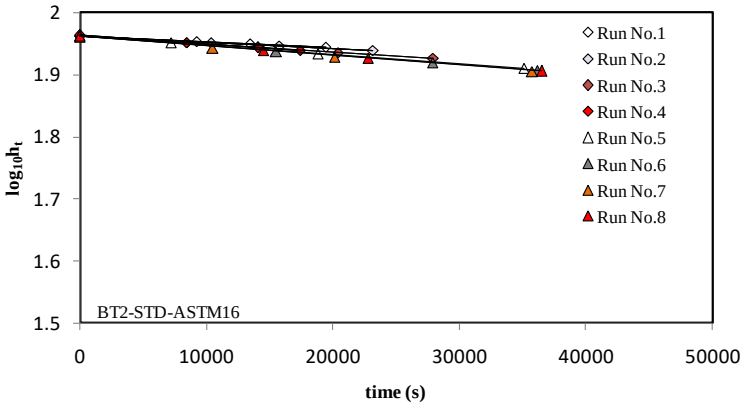
Run No.1
Run No.2
Run No.3
Run No.4
Run No.5
Run No.6
Run No.7
Run No.8
BT2-STD-ASTM16
log10ht
time (s)

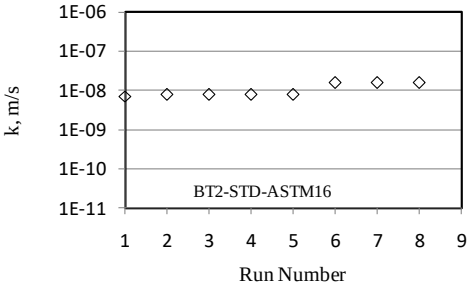
BT2-STD-ASTM16
k, m/s
Run Number

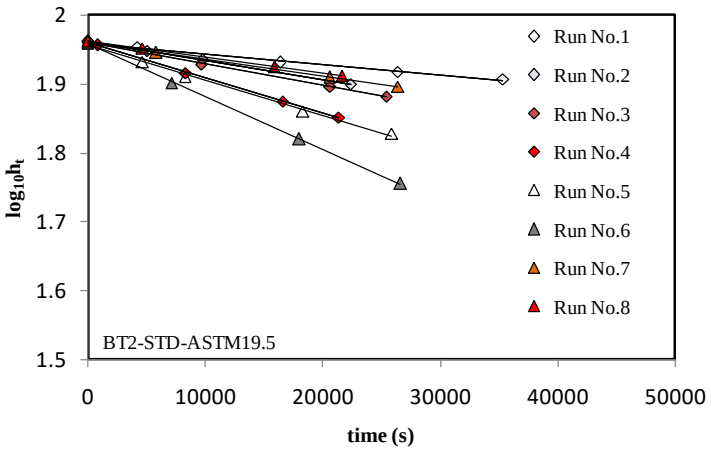
Run No.1
Run No.2
Run No.3
Run No.4
Run No.5
Run No.6
Run No.7
Run No.8
BT2-STD-ASTM19.5
log10ht
time (s)

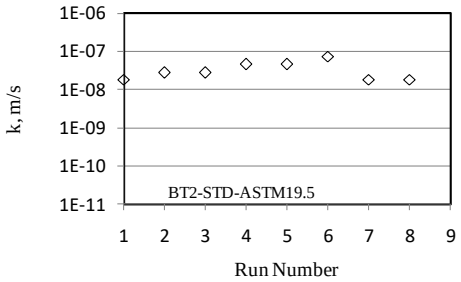
BT2-STD-ASTM19.5
k, m/s
Run Number

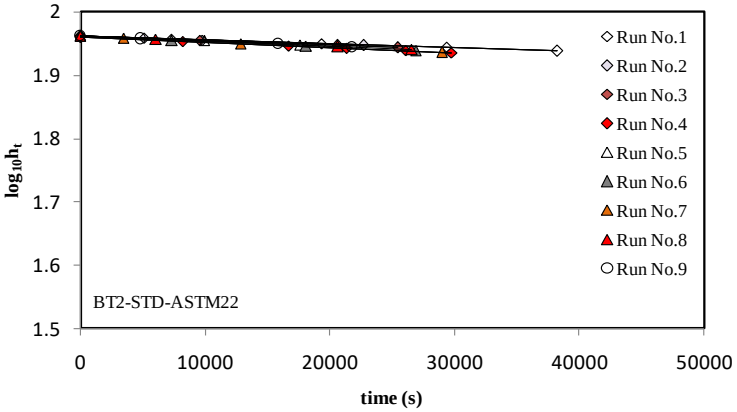
Run No.1
Run No.2
Run No.3
Run No.4
Run No.5
Run No.6
Run No.7
Run No.8
Run No.9
BT2-STD-ASTM22
log10ht
time (s)

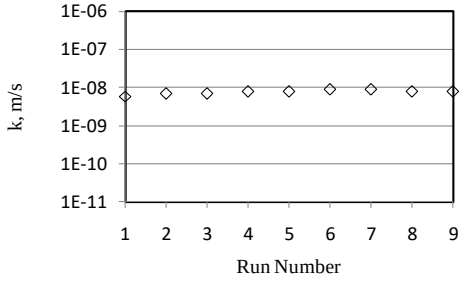
k, m/s
Run Number

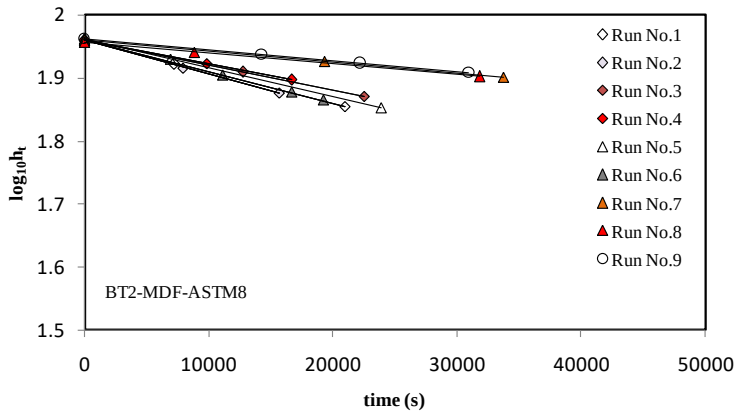
Run No.1
Run No.2
Run No.3
Run No.4
Run No.5
Run No.6
Run No.7
Run No.8
Run No.9
BT2-MDF-ASTM8
log10ht
time (s)

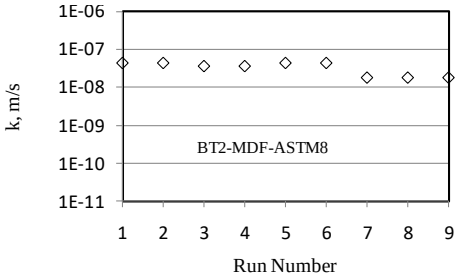
BT2-MDF-ASTM8
k, m/s
Run Number

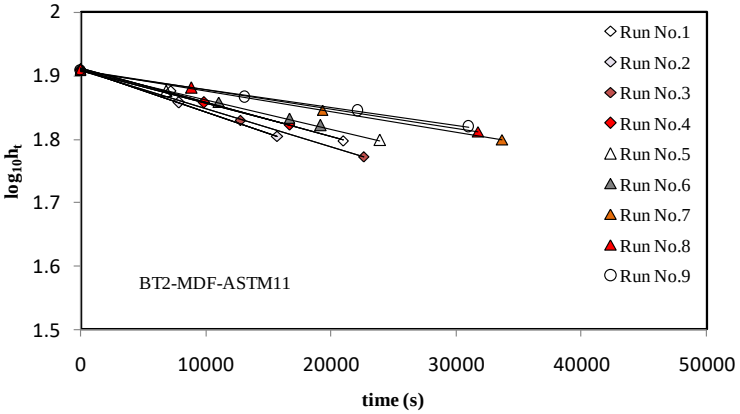
Run No.1
Run No.2
Run No.3
Run No.4
Run No.5
Run No.6
Run No.7
Run No.8
Run No.9
BT2-MDF-ASTM11
log10ht
time (s)

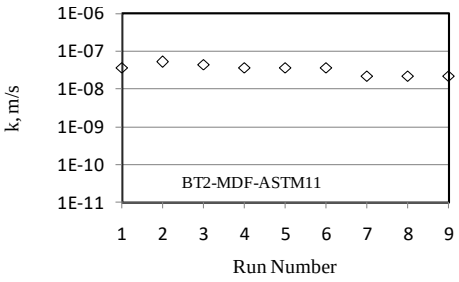
BT2-MDF-ASTM11
k, m/s
Run Number

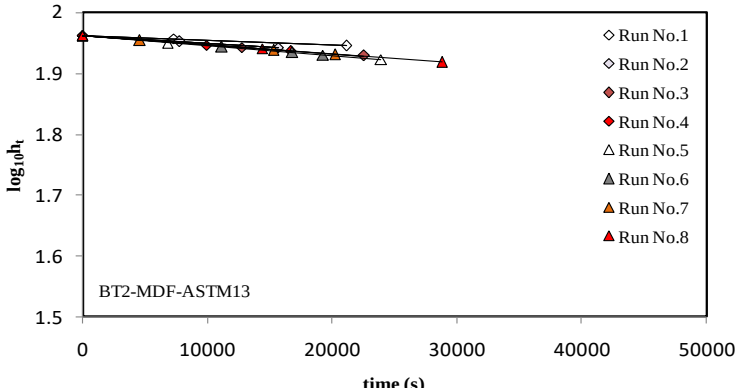
Run No.1
Run No.2
Run No.3
Run No.4
Run No.5
Run No.6
Run No.7
Run No.8
BT2-MDF-ASTM13
log10ht
time (s)

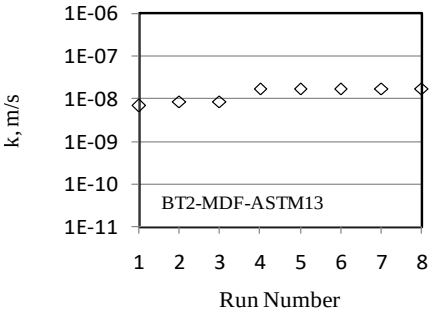
BT2-MDF-ASTM13
k, m/s
Run Number

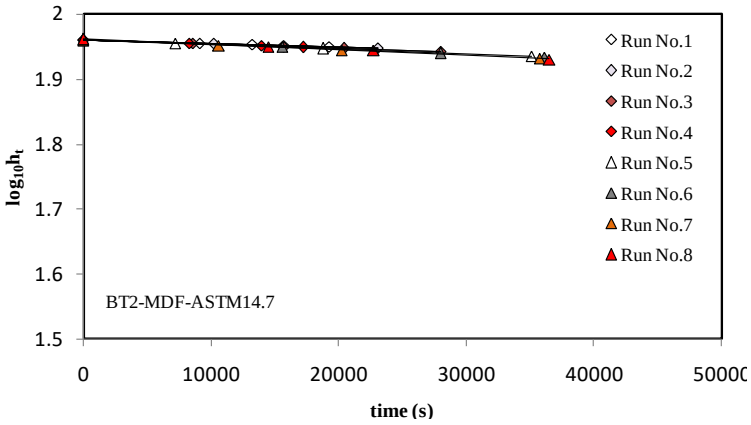

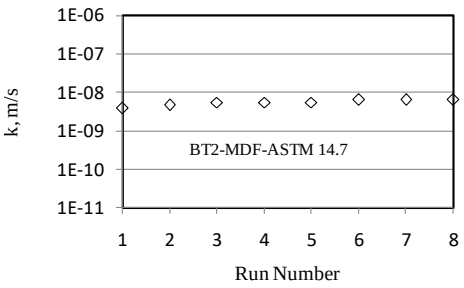

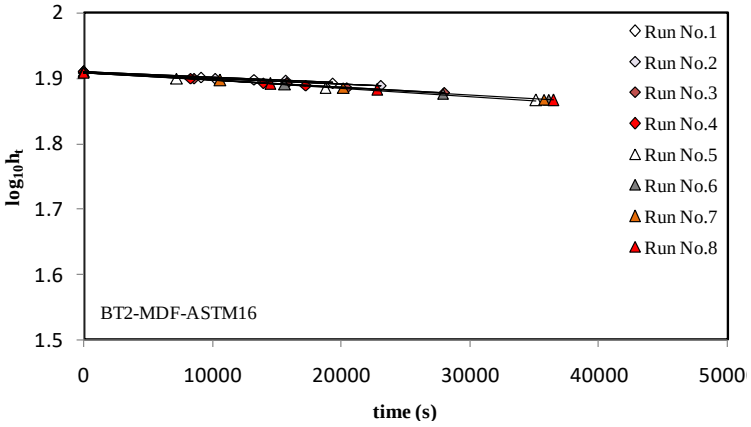

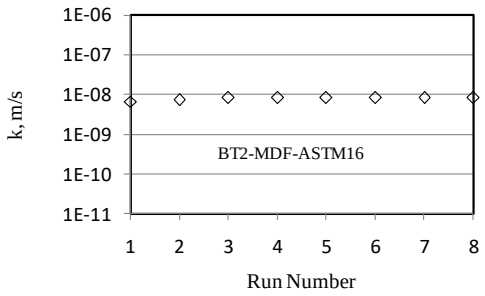

APPENDIX BT1- JF2 soil sets

Experimental runs

k-values with run numbers

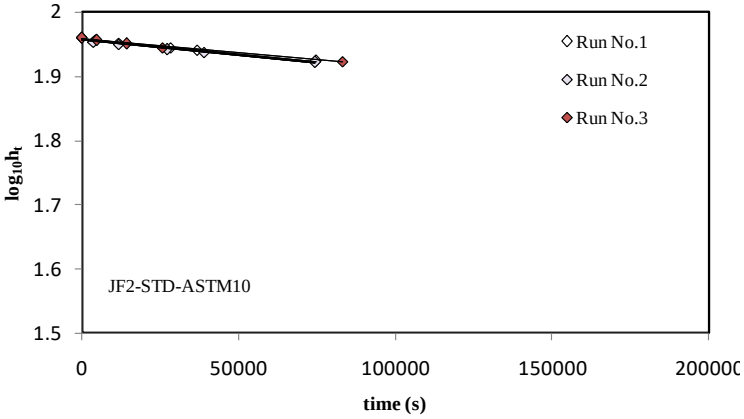

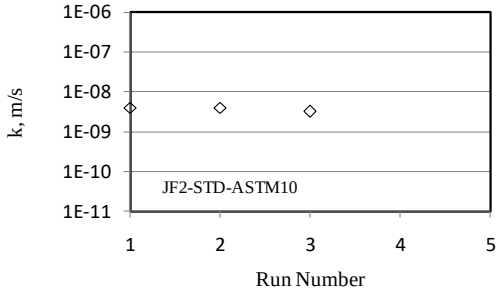

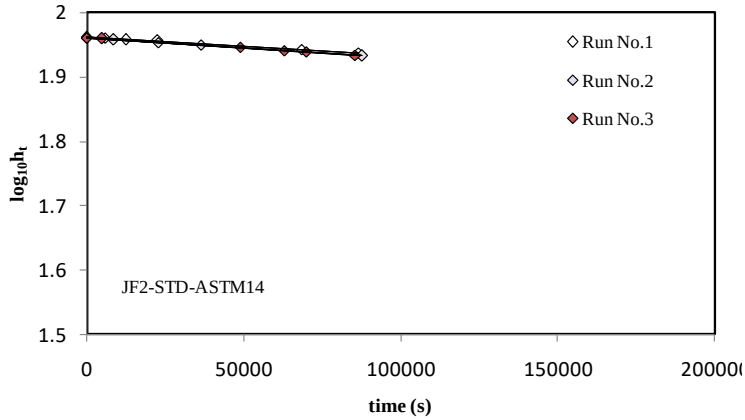
Run No.1
Run No.2
Run No.3
JF2-STD-ASTM14
log10ht
time (s)

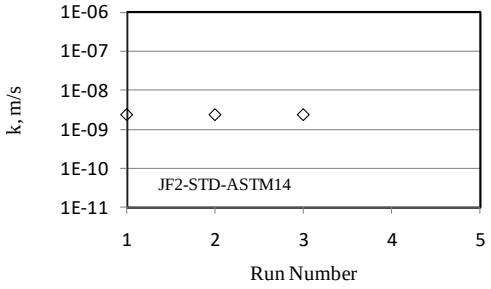
JF2-STD-ASTM14
k, m/s
Run Number

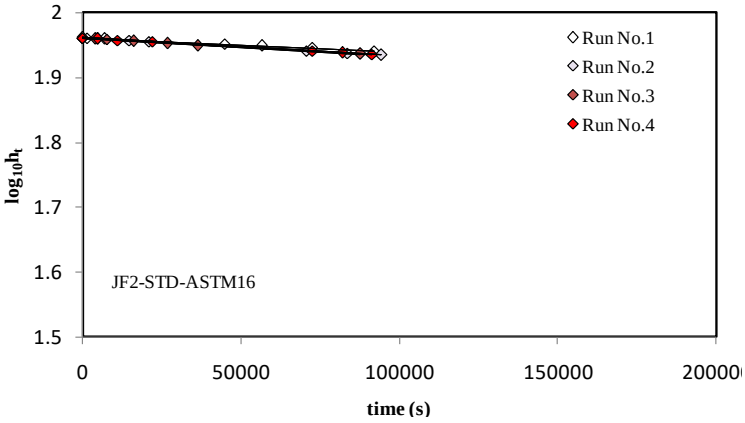
Run No.1
Run No.2
Run No.3
Run No.4
JF2-STD-ASTM16
log10ht
time (s)

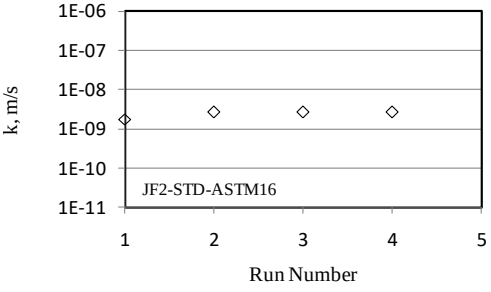
JF2-STD-ASTM16
k, m/s
Run Number

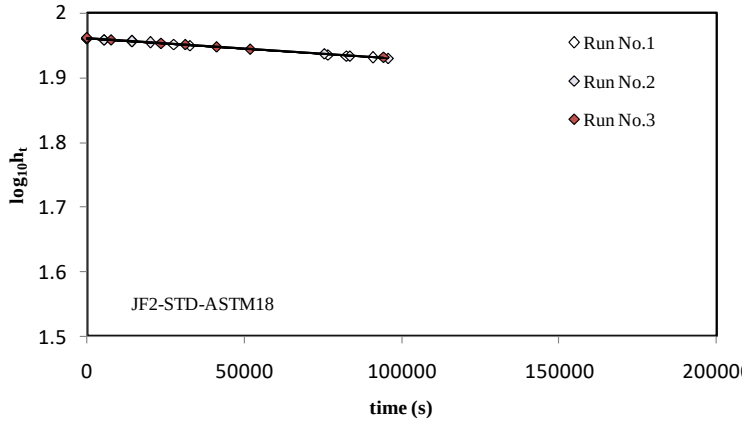
Run No.1
Run No.2
Run No.3
JF2-STD-ASTM18
log10ht
time (s)

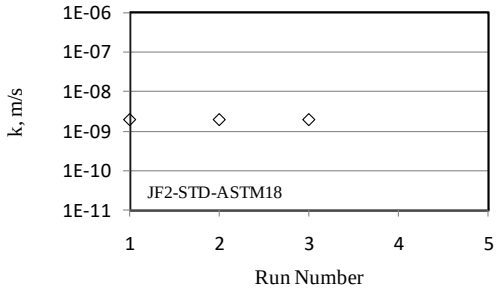
JF2-STD-ASTM18
k, m/s
Run Number

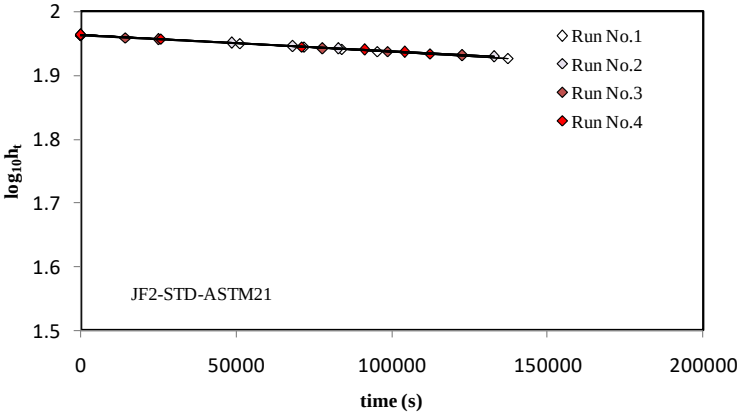
Run No.1
Run No.2
Run No.3
Run No.4
JF2-STD-ASTM21
log10ht
time (s)

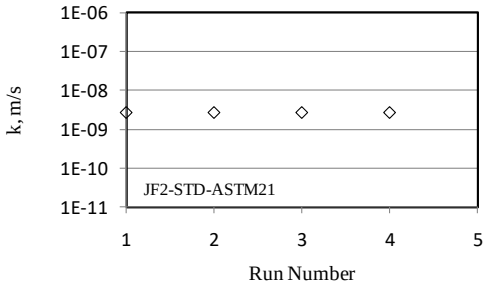
JF2-STD-ASTM21
k, m/s
Run Number

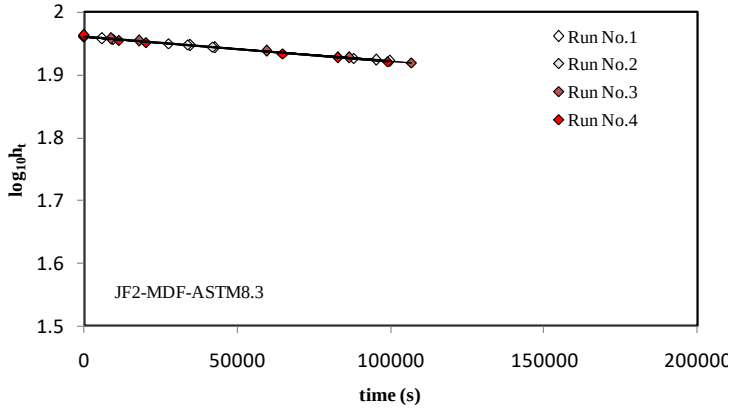
Run No.1
Run No.2
Run No.3
Run No.4
JF2-MDF-ASTM8.3
log10ht
time (s)

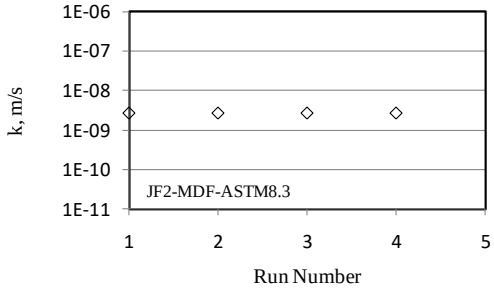
JF2-MDF-ASTM8.3
k, m/s
Run Number

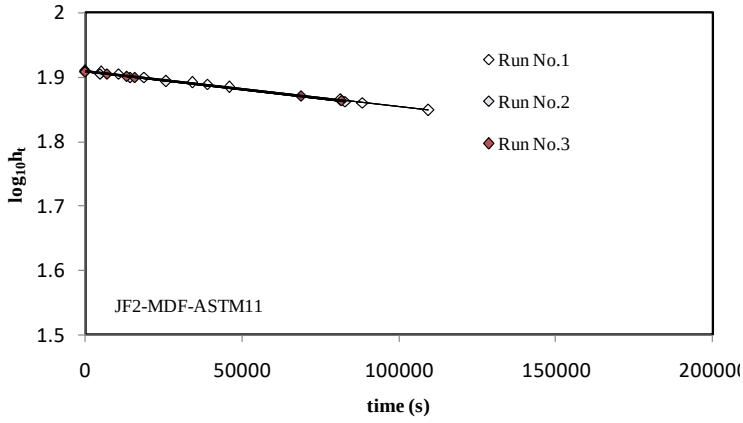
Run No.1
Run No.2
Run No.3
JF2-MDF-ASTM11
log10ht
time (s)

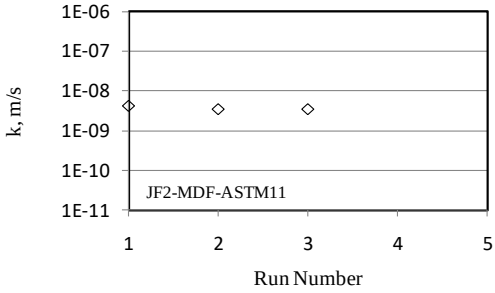
JF2-MDF-ASTM11
k, m/s
Run Number

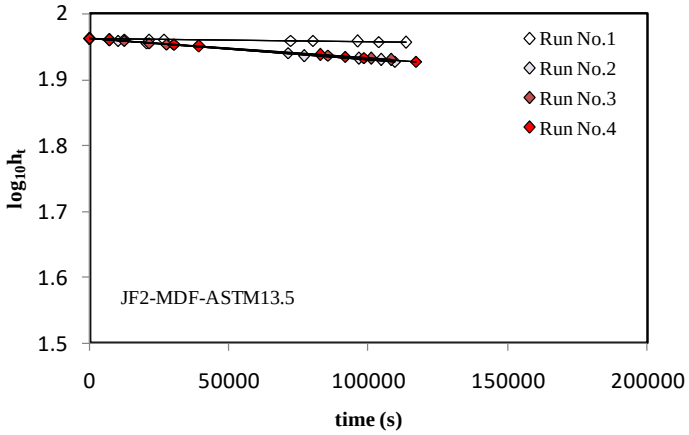
Run No.1
Run No.2
Run No.3
Run No.4
JF2-MDF-ASTM13.5
log10ht
time (s)

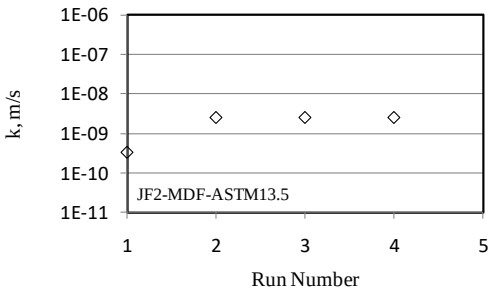
JF2-MDF-ASTM13.5
k, m/s
Run Number

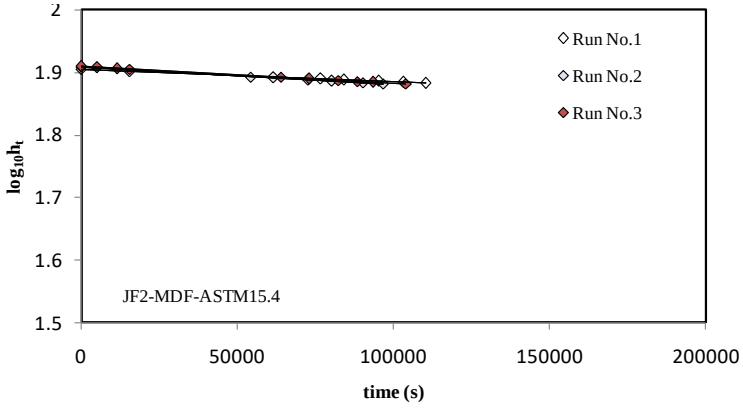
Run No.1
Run No.2
Run No.3
JF2-MDF-ASTM15.4
log10ht
time (s)

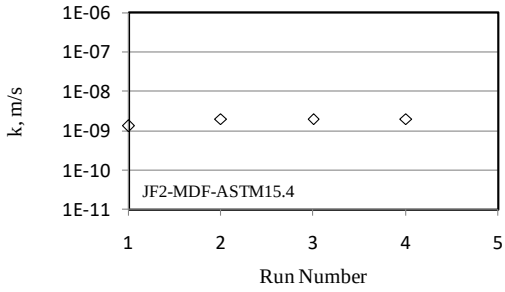
JF2-MDF-ASTM15.4
k, m/s
Run Number

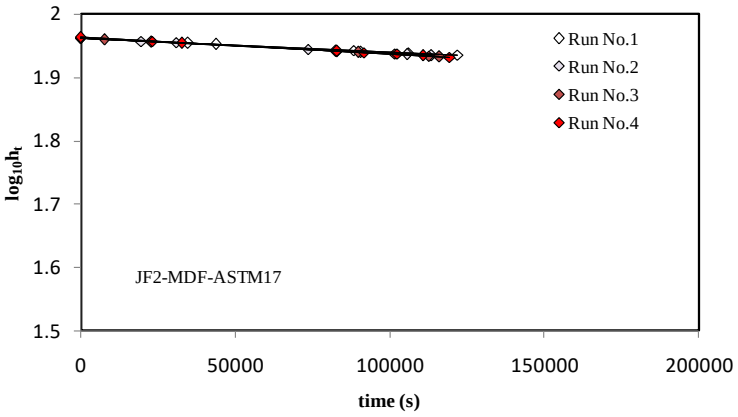
Run No.1
Run No.2
Run No.3
Run No.4
JF2-MDF-ASTM17
log10ht
time (s)

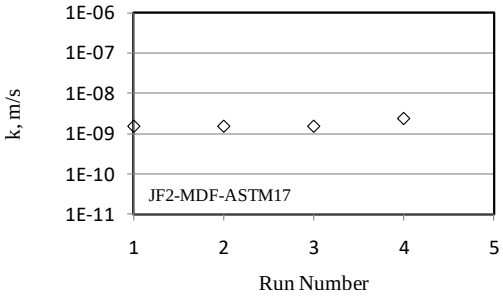
JF2-MDF-ASTM17
k, m/s
Run Number

APPENDIX B2- Infiltration- time plots using the mini-disk infiltrometer

Dry of optimum (BT1 soil)

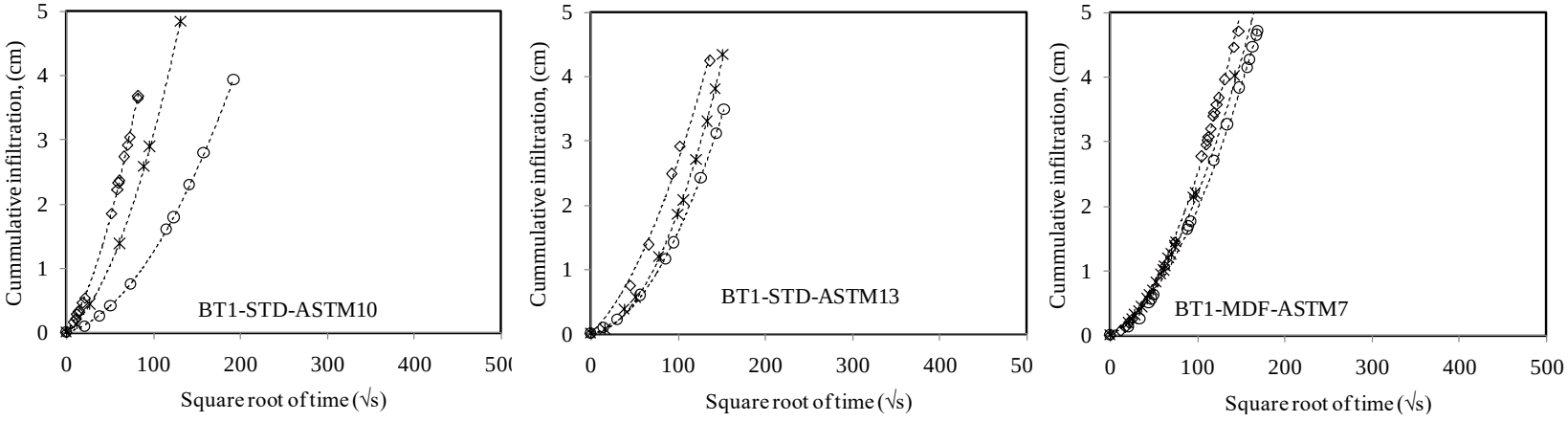

Wet of optimum (BT1 soil)

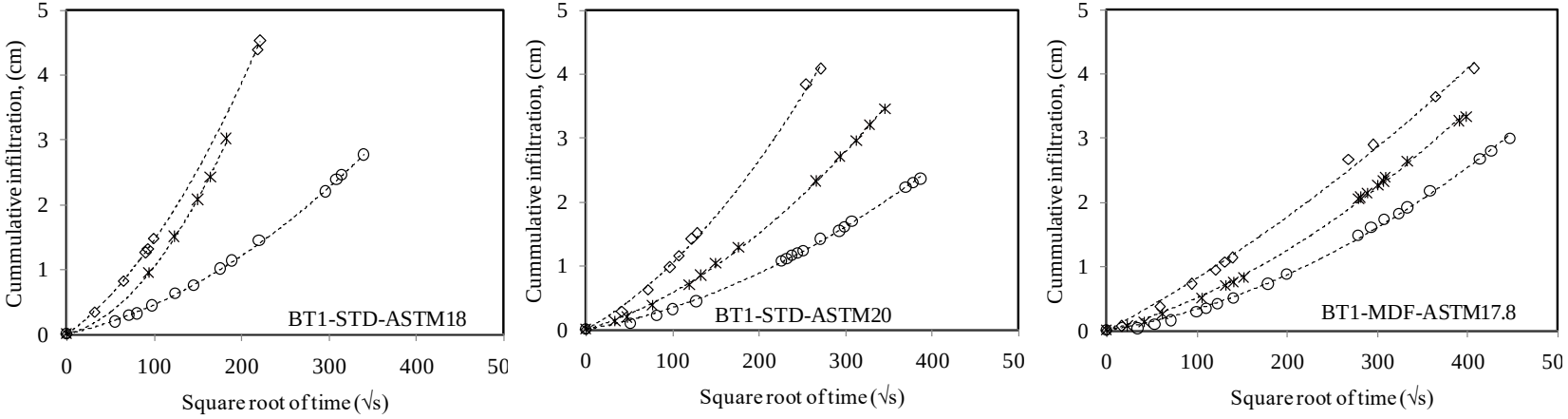

Figure B2-1: Infiltration-time plots for BT1 soil specimens

optimum

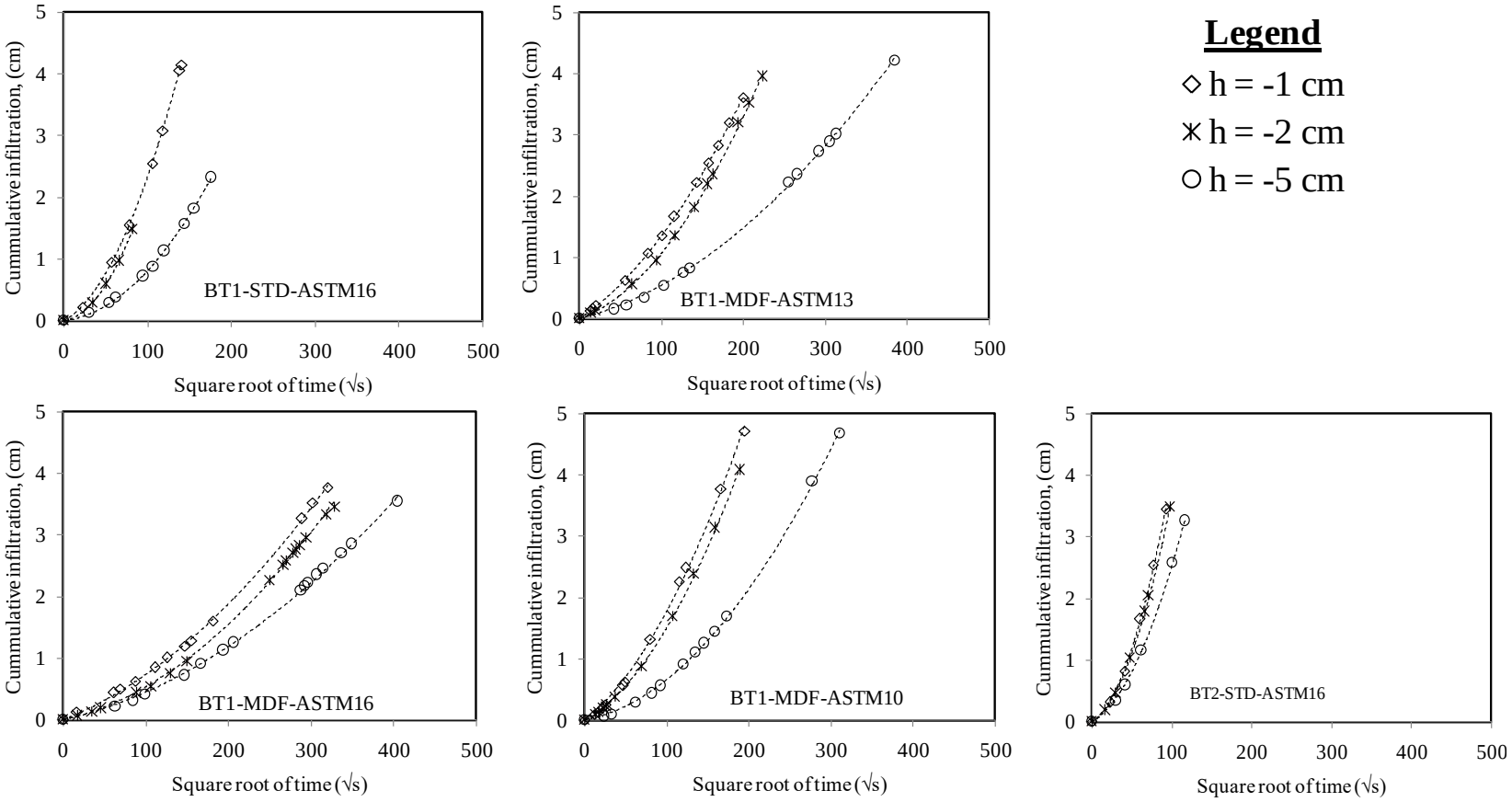

Figure B2-1: Infiltration-time plots for BT1 soil specimens

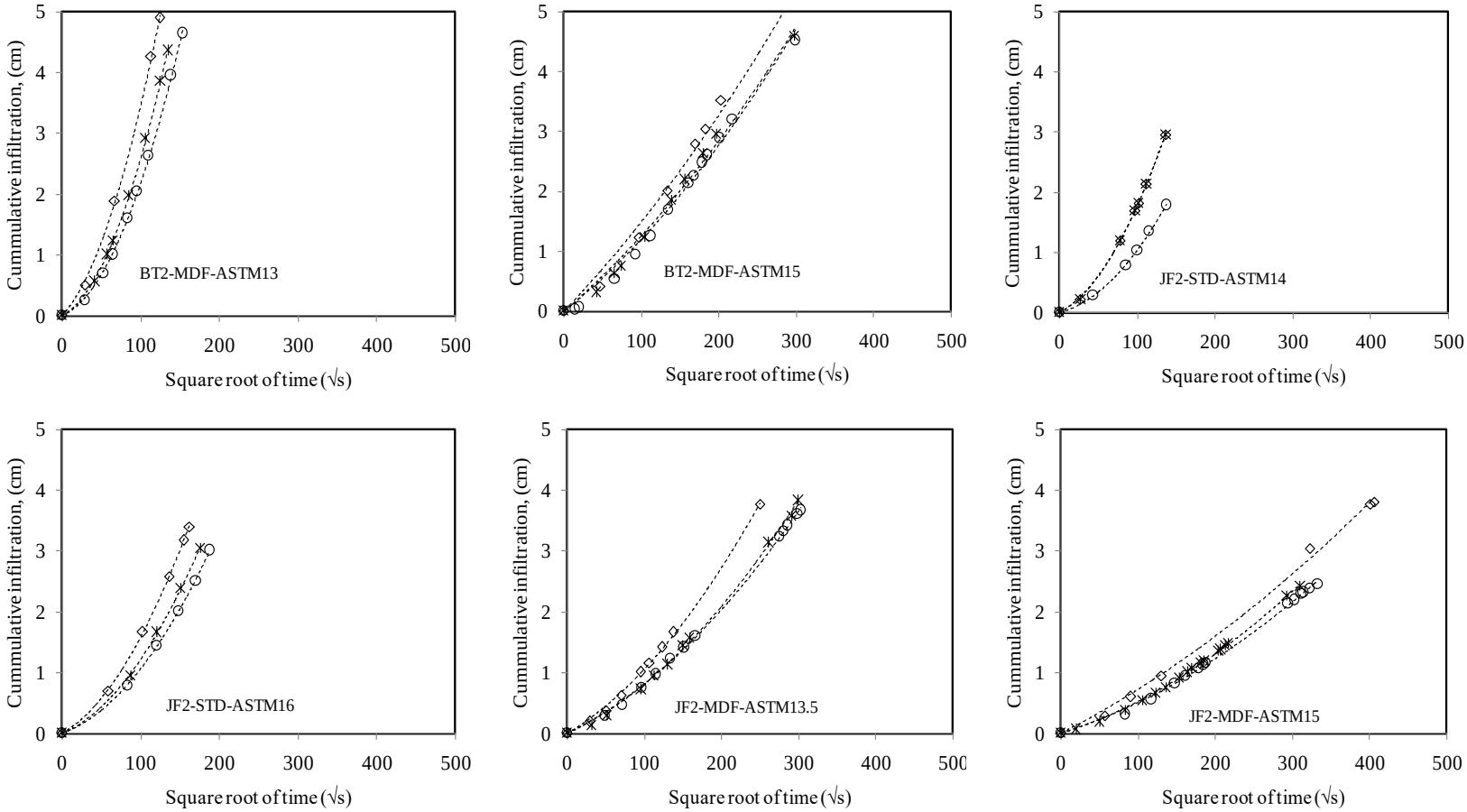

Figure B2-2: Infiltration-time plots for BT2 and JF2 soil specimens

APPENDIX B3: Infiltration equations for different soil sets at different suction pressure head

Appendix B3- Table B3-1: Infiltration equations with corresponding R^2 for BT1 soil specimens at the different suction heads

BT1 soil sets	Suction heads, cm		
	-1	-2	-5
STD-ASTM10	$y=3E-4x^2+0.0201x$, $R^2=0.999$	$y=2E-4x^2+0.0109x$, $R^2=0.999$	$y=9E-5x^2+0.0038x$, $R^2=1$
STD-ASTM13	y=1E-4x2+0.0133x, $R^2=0.995$	$y=2E-4x^2+0.0022x$, $R^2=0.999$	$y=1E-4x^2+0.0023x$, $R^2=1$
STD-ASTM16	$y=2E-4x^2+0.0074x$, $R^2=1$	$y=2E-4x^2+0.0016x$, $R^2=1$	$y=7E-05x^2+0.0015x$, $R^2=0.999$
STD-ASTM18	$y=5E-05x^2+0.0097x$, $R^2=1$	$y=7E-05x^2+0.0033x$, $R^2=0.999$	$y=2E-05x^2+0.003x$, $R^2=0.999$
STD-ASTM20	$y=3E-05x^2+0.0076x$, $R^2=.999$	$y=2E-05x^2+0.004x$, $R^2=0.999$	$y=1E-05x^2+0.002x$, $R^2=0.998$
MDF-ASTM7	$y=2E-4x^2+0.0008x$, $R^2=0.999$	$y=1E-4x^2+0.0087x$, $R^2=0.999$	$y=1E-4x^2+0.0073x$, $R^2=0.999$
MDF-ASTM10	$y=7E-5x^2+0.0105x$, $R^2=0.998$	$y=8E-5x^2+0.0076x$, $R^2=0.999$	$y=4E-5x^2+0.0023x$, $R^2=0.999$
MDF-ASTM13	$y=5E-5x^2+0.0089x$, $R^2=1$	$y=6E-5x^2+0.0049x$, $R^2=0.999$	$y=2E-5x^2+0.0035x$, $R^2=0.999$
MDF-ASTM16	$y=2E-05x^2+0.005x$, $R^2=0.999$	$y=2E-05x^2+0.003x$, $R^2=0.999$	$y=1E-05x^2+0.003x$, $R^2=0.999$
MDF-ASTM18	$y=7E-06x^2+0.0075x$, $R^2=0.997$	$y=1E-05x^2+0.003x$, $R^2=0.999$	$y=1E-05x^2+0.0023x$, $R^2=0.998$

Appendix B3- Table B3-2: Infiltration equations with corresponding R^2 for BT2 soil specimens at the different suction heads

BT2 soil sets	Suction heads, cm				
	-1		-2		-5
STD-ASTM13	$y=5E-4x^2+0.00213x$,	$R^2=0.999$	$y=3E-4x^2+0.0107x$,	$R^2=0.999$	$y=1E-4x^2+0.0025x$, $R^2=1$
STD-ASTM16	$y=3E-4x^2+0.0081x$,	$R^2=0.999$	$y=3E-4x^2+0.0083x$,	$R^2=0.999$	$y=2E-4x^2+0.0075x$, $R^2=0.999$
STD-ASTM19.5	$y=2E-4x^2+0.0082x$,	$R^2=0.999$	$y=1E-4x^2+0.0124x$,	$R^2=0.998$	$y=9E-05x^2+0.0051x$, $R^2=0.999$
STD-ASTM22	$y=3E-05x^2+0.0115x$,	$R^2=0.993$	$y=4E-05x^2+0.0073x$,	$R^2=0.997$	$y=2E-05x^2+0.007x$, $R^2=0.999$
MDF-ASTM8	$y=4E-4x^2+0.0193x$,	$R^2=0.999$	$y=4E-4x^2+0.0177x$,	$R^2=1$	$y=4E-4x^2+0.016x$, $R^2=0.999$
MDF-ASTM11	$y=4E-4x^2+0.0138x$,	$R^2=0.999$	$y=4E-4x^2+0.0097x$,	$R^2=0.999$	$y=2E-4x^2+0.0144x$, $R^2=0.999$
MDF-ASTM13	$y=2E-4x^2+0.0139x$,	$R^2=0.999$	$y=2E-4x^2+0.0066x$,	$R^2=0.999$	$y=2E-4x^2+0.0053x$, $R^2=0.999$
MDF-ASTM15	$y=9E-06x^2+0.013x$,	$R^2=0.990$	$y=1E-05x^2+0.010x$,	$R^2=0.991$	$y=1E-05x^2+0.010x$, $R^2=0.992$
MDF-ASTM16	$y=8E-05x^2+0.007x$	$R^2=0.999$	$y=6E-05x^2+0.007x$,	$R^2=0.997$	$y=3E-05x^2+0.006x$, R2= 0.999

Appendix B3- Table B3-3: Infiltration equations with corresponding R^2 for JF2 soil specimens at the different suction heads

JF2 soil sets	Suction heads, cm				
	-1		-2		-5
STD-ASTM10	$y=2E-4x^2+0.0142x$,	$R^2= 0.999$	$y=1E-4x^2+0.006x$,	$R^2= 1$	$y=9E-5x^2+0.005x$, $R^2= 0.999$
STD-ASTM14	y=1E-4x2+0.008x,	$R^2= 0.999$	$y=1E-4x^2+0.0066x$,	$R^2= 1$	$y=7E-5x^2+0.0034x$, $R^2= 1$
STD-ASTM16	$y=8E-5x^2+0.007x$,	$R^2= 0.999$	$y=6E-5x^2+0.006x$,	$R^2= 1$	$y=6E-05x^2+0.0046x$, $R^2= 1$
STD-ASTM18	$y=5E-06x^2+0.006x$,	$R^2= 0.988$	$y=6E-06x^2+0.004x$,	$R^2= 0.996$	$y=6E-06x^2+0.003x$, $R^2= 0.997$
STD-ASTM21	$y=1E-06x^2+0.002x$,	$R^2= 0.995$	$y=2E-06x^2+0.001x$,	$R^2= 0.996$	$y=2E-06x^2+0.001x$, $R^2= 0.996$
MDF-ASTM8	$y=1E-4x^2+0.0077x$,	$R^2= 1$	$y=1E-4x^2+0.0096x$,	$R^2=0.999$	$y=1E-4x^2+0.0072x$, $R^2= 1$
MDF-ASTM11	$y=1E-4x^2+0.0011x$,	$R^2= 0.997$	$y=1E-4x^2+0.0054x$,	$R^2= 0.999$	$y=7E-5x^2+0.0035x$, $R^2= 0.998$
MDF-ASTM13.5	$y=3E-5x^2+0.0075x$,	$R^2= 0.999$	$y=2E-5x^2+0.0058x$,	$R^2= 0.998$	$y=2E-5x^2+0.0061x$, $R^2= 0.999$
MDF-ASTM15	$y=3E-05x^2+0.0036x$,	$R^2= 0.998$	$y=1E-05x^2+0.004x$,	$R^2= 0.999$	$y=1E-05x^2+0.004x$, $R^2= 0.998$
MDF-ASTM17	$y=3E-06x^2+0.004x$,	$R^2= 0.996$	$y=3E-06x^2+0.003x$,	$R^2= 0.996$	$y=3E-06x^2+0.002x$, $R^2= 0.995$

APPENDIX B4A: Comparison of infiltration rates for different compaction water contents at given suction heads for both standard and modified Proctor energies for the BT1 soil

BT2 soils (Standard Proctor)

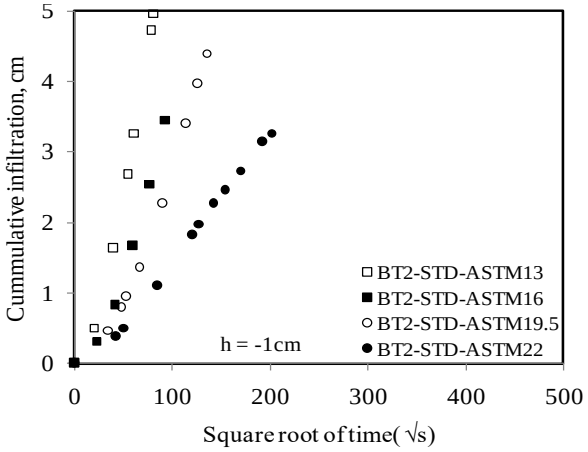

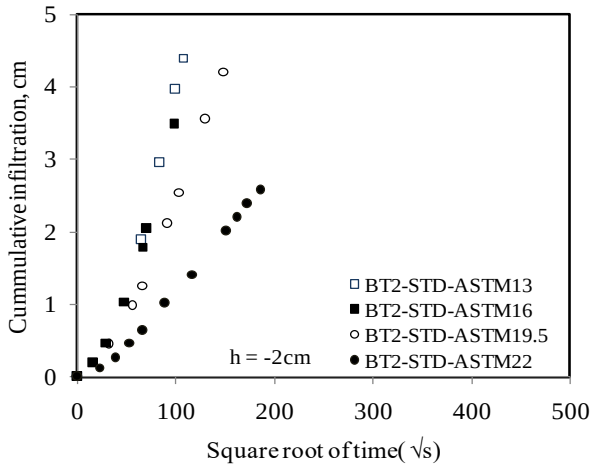

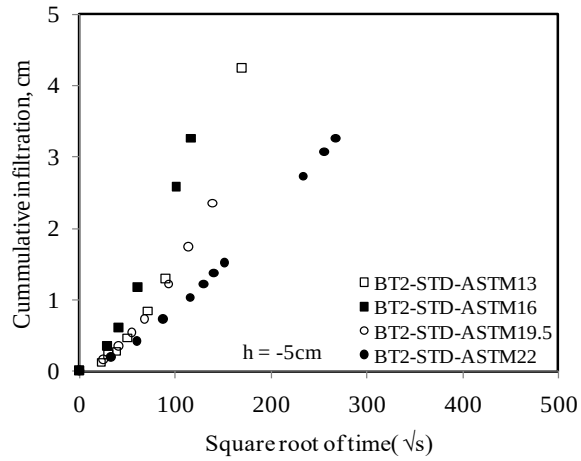

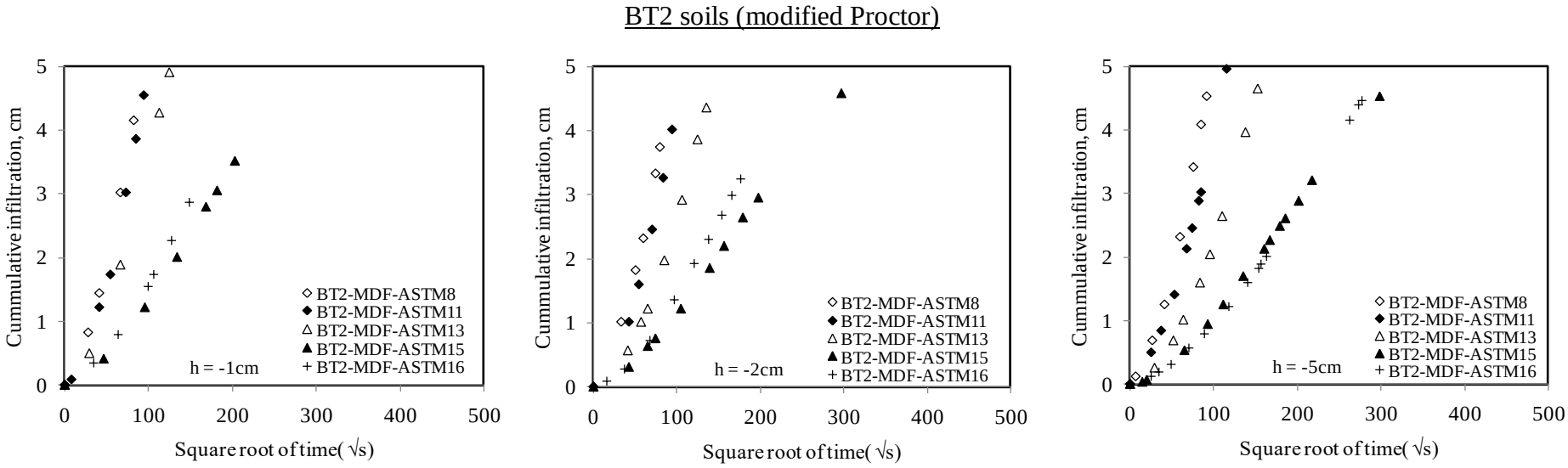

Figure B4-1: Comparison of infiltration rates for different compaction water contents at given suction heads for both standard and modified Proctor energies for the BT2 soil

APPENDIX B4B: Comparison of infiltration rates for different compaction water contents at given suction heads for both standard and modified Proctor energies

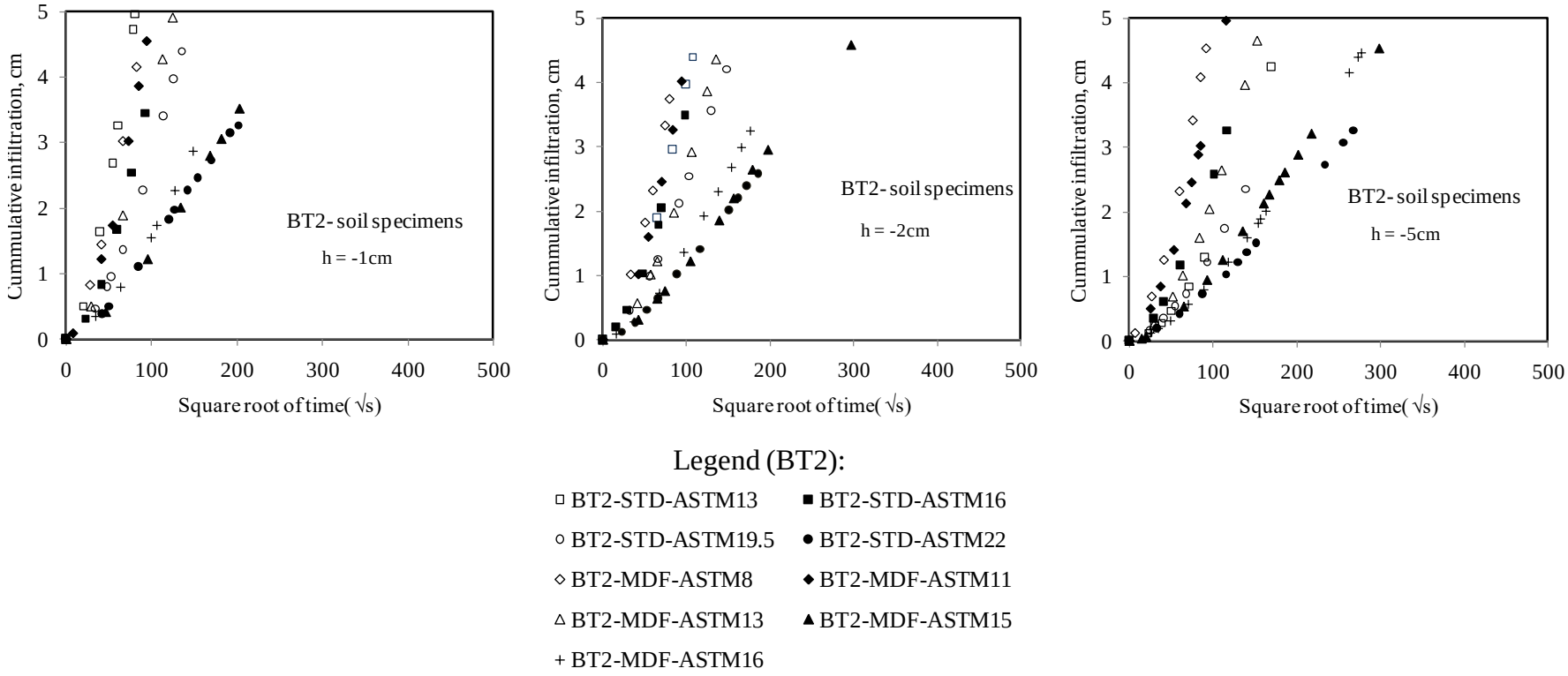

Figure B4-2: Comparison of infiltration rates for different compaction water contents at given suction heads for both standard and modified Proctor energies for the BT2 soil

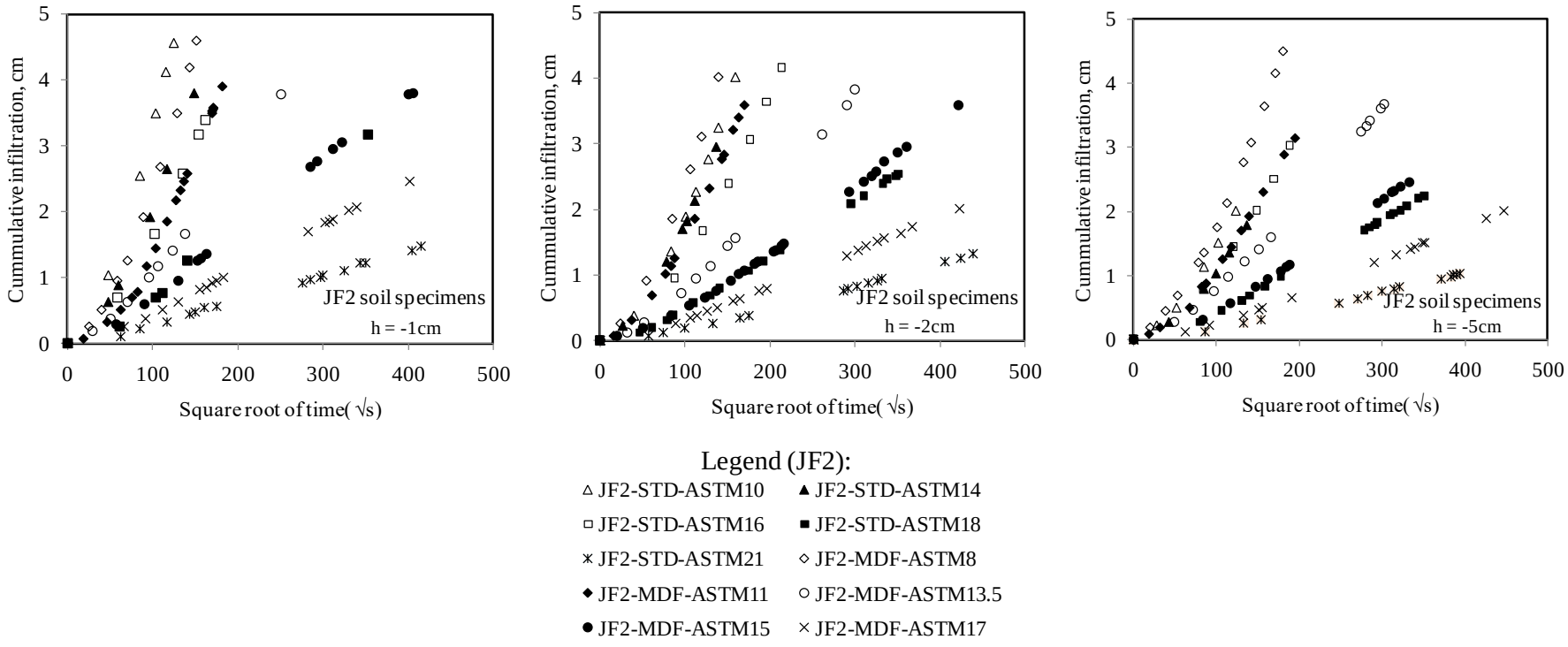

Figure B4-3: Comparison of infiltration rates for different compaction water contents at given suction heads for both standard and modified Proctor energies for the JF2 soil

APPENDIX B5: A_2 values for the different study cases for the different soil specimens

Table B5-1: A_2 values for the different study cases- BT1

A_2 (dimensionless)												
BT1 soil sets	Suction head, cm											
	-1				-2				-5			
	case 1	case 2	case 3	case 4	case 1	case 2	case 3	case 4	case 1	case 2	case 3	case 4
STD-ASTM10	123.39	6.11	371.38	17.69	123.75	6.64	371.70	16.34	124.86	8.55	372.64	12.89
STD-ASTM13	176.90	6.11	371.38	17.69	177.26	6.64	371.70	16.34	178.35	8.55	372.64	12.89
STD-ASTM16	389.65	6.11	371.38	17.69	389.99	6.64	371.70	16.34	391.00	8.55	372.64	12.89
STD-ASTM18	400.26	6.11	371.38	17.69	400.59	6.64	371.70	16.34	401.61	8.55	372.64	12.89
STD-ASTM20	363.08	6.11	371.38	17.69	363.42	6.64	371.70	16.34	364.44	8.55	372.64	12.89
MDF-ASTM7	375.44	6.11	371.38	17.69	375.78	6.64	371.70	16.34	376.80	8.55	372.64	12.89
MDF-ASTM10	460.78	6.11	371.38	17.69	461.10	6.64	371.70	16.34	462.07	8.55	372.64	12.89
MDF-ASTM13	600.95	6.11	371.38	17.69	601.26	6.64	371.70	16.34	602.19	8.55	372.64	12.89
MDF-ASTM16	641.30	6.11	371.38	17.69	641.60	6.64	371.70	16.34	642.50	8.55	372.64	12.89
MDF-ASTM18	580.24	6.11	371.38	17.69	580.55	6.64	371.70	16.34	581.48	8.55	372.64	12.89

Appendix B5

Table B5-2: A_2 values for the different study cases- BT2

A_2 (Dimensionless)									
BT2 soil sets	Suction head, cm								
	-1			-2			-5		
	case 1	case 2	case 3	case 1	case 2	case 3	case 1	case 2	case 3
STD-ASTM13	152.77	5.72	344.94	153.14	6.27	345.26	154.24	8.25	346.21
STD-ASTM16	231.39	5.72	344.94	231.75	6.27	345.26	232.82	8.25	346.21
STD-ASTM19.5	329.25	5.72	344.94	329.59	6.27	345.26	330.62	8.25	346.21
STD-ASTM22	368.85	5.72	344.94	369.19	6.27	345.26	370.21	8.25	346.21
MDF-ASTM8	356.19	5.72	344.94	356.52	6.27	345.26	357.52	8.25	346.21
MDF-ASTM11	182.25	5.72	344.94	182.62	6.27	345.26	183.72	8.25	346.21
MDF-ASTM13	330.24	5.72	344.94	330.58	6.27	345.26	331.60	8.25	346.21
MDF-ASTM15	243.30	5.72	344.94	243.66	6.27	345.26	244.73	8.25	346.21
MDF-ASTM16	148.85	5.72	344.94	149.22	6.27	345.26	150.32	8.25	346.21

Appendix B5

Table B5-2: A_2 values for the different study cases- JF2

A_2 (Dimensionless)												
JF2 soil sets	Suction head, cm											
	-1				-2				-5			
	case 1	case 2	case 3	case 4	case 1	case 2	case 3	case 4	case 1	case 2	case 3	case 4
STD-ASTM10	163.66	6.11	371.38	17.69	164.03	6.64	371.70	16.34	165.12	8.55	372.64	12.89
STD-ASTM14	233.91	6.11	371.38	17.69	234.27	6.64	371.70	16.34	235.34	8.55	372.64	12.89
STD-ASTM16	144.23	6.11	371.38	17.69	143.73	6.64	371.70	16.34	142.21	8.55	372.64	12.89
STD-ASTM18	345.77	6.11	371.38	17.69	346.11	6.64	371.70	16.34	347.14	8.55	372.64	12.89
STD-ASTM21	492.53	6.11	371.38	17.69	492.85	6.64	371.70	16.34	493.82	8.55	372.64	12.89
MDF-ASTM8	204.95	6.11	371.38	17.69	205.31	6.64	371.70	16.34	206.40	8.55	372.64	12.89
MDF-ASTM11	222.58	6.11	371.38	17.69	222.94	6.64	371.70	16.34	224.02	8.55	372.64	12.89
MDF-ASTM13.5	161.97	6.11	371.38	17.69	162.33	6.64	371.70	16.34	163.42	8.55	372.64	12.89
MDF-ASTM15	159.73	6.11	371.38	17.69	160.09	6.64	371.70	16.34	161.18	8.55	372.64	12.89
MDF-ASTM17	334.22	6.11	371.38	17.69	334.22	6.64	371.70	16.34	335.25	8.55	372.64	12.89

APPENDIX B6: Derived Permeabilities for the different study cases for the different soil specimens

Table B6-1:Derived Permeabilities for the different study cases- BT1

BT1 soil sets	k (m/s)											
	Suction head, cm											
	-1				-2				-5			
	case 1	case 2	case 3	case 4	case 1	case 2	case 3	case 4	case 1	case 2	case 3	case 4
STD-ASTM10	2.43E-08	4.91E-07	8.08E-09	1.70E-07	1.62E-08	3.01E-07	5.38E-09	1.22E-07	7.21E-09	1.05E-07	2.42E-09	6.98E-08
STD-ASTM13	5.65E-09	1.64E-07	2.69E-09	5.65E-08	1.13E-08	3.01E-07	5.38E-09	1.22E-07	5.61E-09	1.17E-07	2.68E-09	7.76E-08
STD-ASTM16	5.13E-09	3.27E-07	5.39E-09	1.13E-07	5.13E-09	3.01E-07	5.38E-09	1.22E-07	1.79E-09	8.19E-08	1.88E-09	5.43E-08
STD-ASTM18	1.25E-09	8.18E-08	1.35E-09	2.83E-08	1.75E-09	1.05E-07	1.88E-09	4.28E-08	4.98E-10	2.34E-08	5.37E-10	1.55E-08
STD-ASTM20	8.26E-10	4.91E-08	8.08E-10	1.70E-08	5.50E-10	3.01E-08	5.38E-10	1.22E-08	2.74E-10	1.17E-08	2.68E-10	7.76E-09
MDF-ASTM7	5.33E-09	3.27E-07	5.39E-09	1.13E-07	2.66E-09	1.51E-07	2.69E-09	6.12E-08	2.65E-09	1.17E-07	2.68E-09	7.76E-08
MDF-ASTM10	1.52E-09	1.15E-07	1.88E-09	3.96E-08	1.73E-09	1.20E-07	2.15E-09	4.90E-08	8.66E-10	4.68E-08	1.07E-09	3.10E-08
MDF-ASTM13	8.32E-10	8.18E-08	1.35E-09	2.83E-08	9.98E-10	9.04E-08	1.61E-09	3.67E-08	3.32E-10	2.34E-08	5.37E-10	1.55E-08
MDF-ASTM16	3.12E-10	3.27E-08	5.39E-10	1.13E-08	3.12E-10	3.01E-08	5.38E-10	1.22E-08	1.56E-10	1.17E-08	2.68E-10	7.76E-09
MDF-ASTM18	1.21E-10	1.15E-08	1.88E-10	3.96E-09	1.72E-10	1.51E-08	2.69E-10	6.12E-09	1.72E-10	1.17E-08	2.68E-10	7.76E-09

Table B6-2:Derived Permeabilities for the different study cases- BT2

k (m/s)									
BT2 soil sets	Suction head, cm								
	-1			-2			-5		
	case 1	case 2	case 3	case 1	case 2	case 3	case 1	case 2	case 3
STD-ASTM13	3.27E-08	8.74E-07	1.45E-08	1.96E-08	4.78E-07	8.69E-09	6.48E-09	1.21E-07	2.89E-09
STD-ASTM16	1.30E-08	5.24E-07	8.70E-09	1.29E-08	4.78E-07	8.69E-09	8.59E-09	2.42E-07	5.78E-09
STD-ASTM19.5	6.07E-09	3.50E-07	5.80E-09	3.03E-09	1.59E-07	2.90E-09	2.72E-09	1.09E-07	2.60E-09
STD-ASTM22	8.13E-10	5.24E-08	8.70E-10	1.08E-09	6.38E-08	1.16E-09	5.40E-10	2.42E-08	5.78E-10
MDF-ASTM8	1.12E-08	6.99E-07	1.16E-08	1.12E-08	6.38E-07	1.16E-08	1.12E-08	4.85E-07	1.16E-08
MDF-ASTM11	2.19E-08	6.99E-07	1.16E-08	2.19E-08	6.38E-07	1.16E-08	1.09E-08	2.42E-07	5.78E-09
MDF-ASTM13	6.06E-09	3.50E-07	5.80E-09	6.05E-09	3.19E-07	5.79E-09	6.03E-09	2.42E-07	5.78E-09
MDF-ASTM15	3.70E-10	1.57E-08	2.61E-10	4.10E-10	1.59E-08	2.90E-10	4.09E-10	1.21E-08	2.89E-10
MDF-ASTM16	5.37E-09	1.40E-07	2.32E-09	4.02E-09	9.57E-08	1.74E-09	2.00E-09	3.64E-08	8.67E-10

Table B6-3:Derived Permeabilities for the different study cases- JF2

k (m/s)												
JF2 soil sets	Suction head, cm											
	-1				-2				-5			
	case 1	case 2	case 3	case 4	case 1	case 2	case 3	case 4	case 1	case 2	case 3	case 4
STD-ASTM10	1.22E-08	3.27E-07	5.39E-09	1.13E-07	6.10E-09	1.51E-07	2.69E-09	6.12E-08	5.45E-09	1.05E-07	2.42E-09	6.98E-08
STD-ASTM14	4.28E-09	1.64E-07	2.69E-09	5.65E-08	4.27E-09	1.51E-07	2.69E-09	6.12E-08	2.97E-09	8.19E-08	1.88E-09	5.43E-08
STD-ASTM16	5.55E-09	1.31E-07	2.94E-09	4.52E-08	4.17E-09	9.04E-08	2.21E-09	3.67E-08	4.22E-09	7.02E-08	2.21E-09	4.65E-08
STD-ASTM18	1.45E-10	8.18E-09	1.35E-10	2.83E-09	1.73E-10	9.04E-09	1.61E-10	3.67E-09	1.73E-10	7.02E-09	1.61E-10	4.65E-09
STD-ASTM21	2.03E-11	1.64E-09	2.69E-11	5.65E-10	4.06E-11	3.01E-09	5.38E-11	1.22E-09	4.05E-11	2.34E-09	5.37E-11	1.55E-09
MDF-ASTM8	4.88E-09	1.64E-07	2.69E-09	5.65E-08	4.87E-09	1.51E-07	2.69E-09	6.12E-08	4.85E-09	1.17E-07	2.68E-09	7.76E-08
MDF-ASTM11	4.49E-09	1.64E-07	2.69E-09	5.65E-08	4.49E-09	1.51E-07	2.69E-09	6.12E-08	3.12E-09	8.19E-08	1.88E-09	5.43E-08
MDF-ASTM13.5	1.85E-09	4.91E-08	8.08E-10	1.70E-08	1.23E-09	3.01E-08	5.38E-10	1.22E-08	1.22E-09	2.34E-08	5.37E-10	1.55E-08
MDF-ASTM15	3.76E-10	9.82E-09	1.62E-10	3.39E-09	6.25E-10	1.51E-08	2.69E-10	6.12E-09	6.20E-10	1.17E-08	2.68E-10	7.76E-09
MDF-ASTM17	8.99E-11	4.91E-09	8.08E-11	1.70E-09	8.98E-11	4.52E-09	8.07E-11	1.70E-09	8.95E-11	3.51E-09	8.05E-11	2.33E-09

APPENDIX B7- SWCCs fitted with Cases 1, 2 and 3

SWCCs for BT1 soil sets

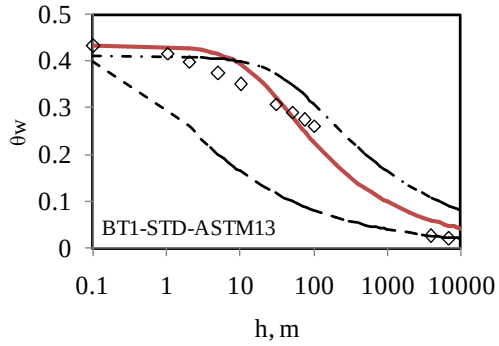

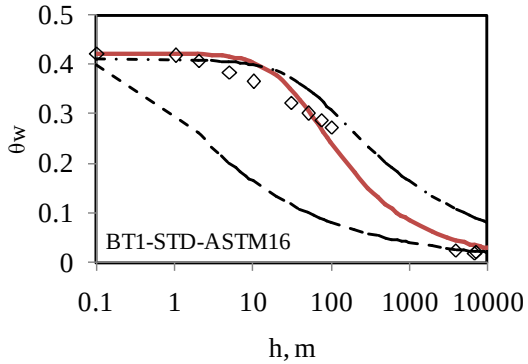

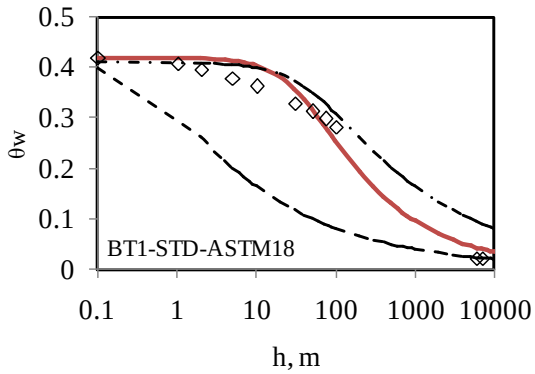

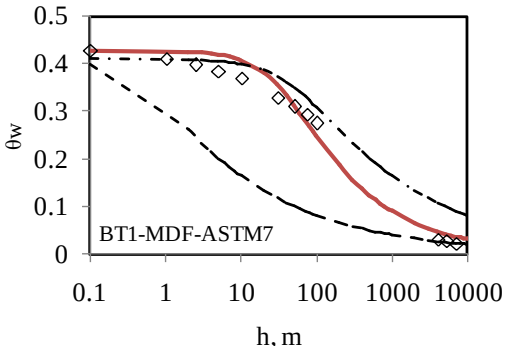

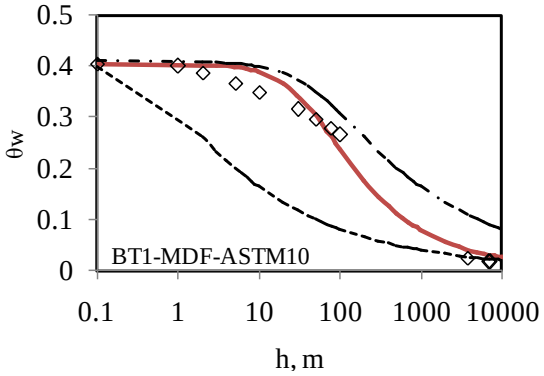

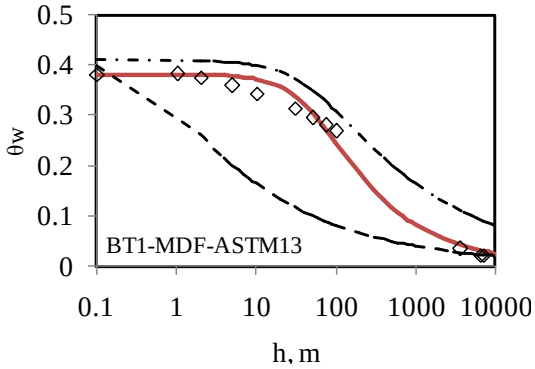

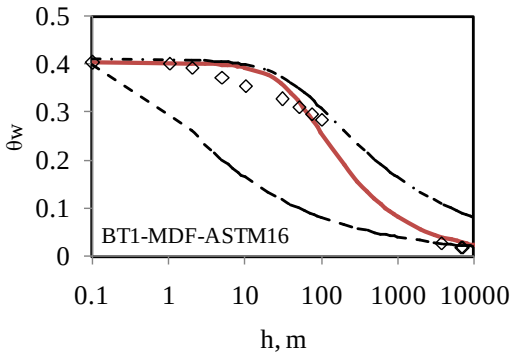

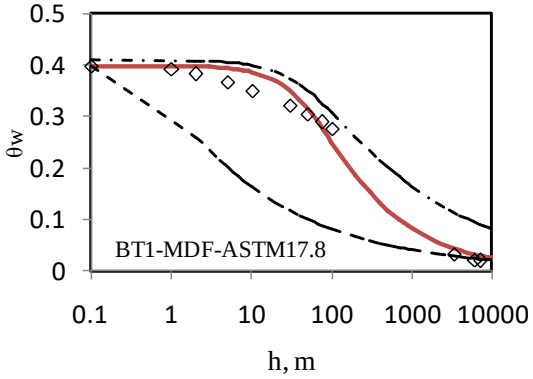

Legend:
- Data fitted using Case 1
- Data Fitted using Case 2
- Data fitted using Case 3
- ◇ SWCC measured data

SWCCs for BT2 soil sets

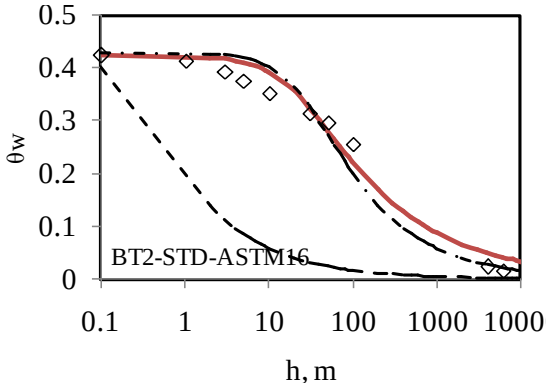

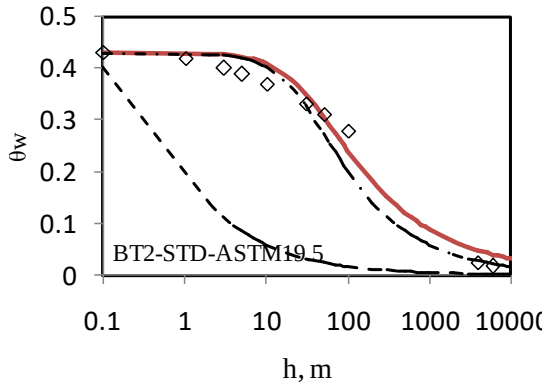

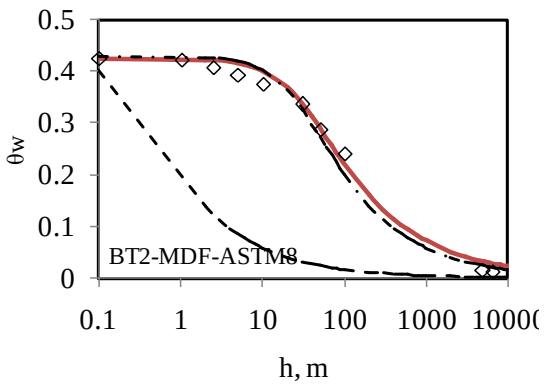

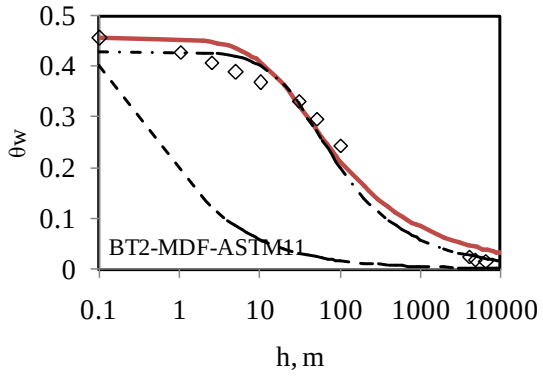
0.5
0.4
0.3
0.2
0.1
0
θw
BT2-MDF-ASTM11
0.1
1
10
100
1000
10000
h, m

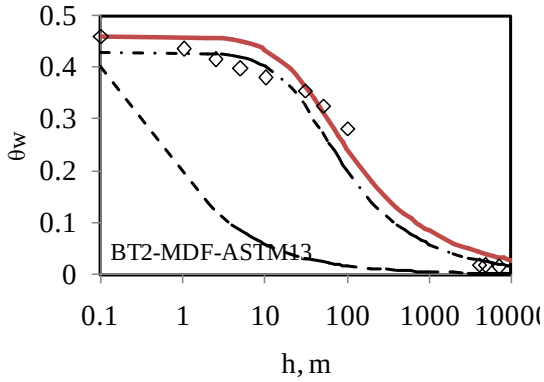
0.5
0.4
0.3
0.2
0.1
0
θw
BT2-MDF-ASTM13
0.1
1
10
100
1000
h, m

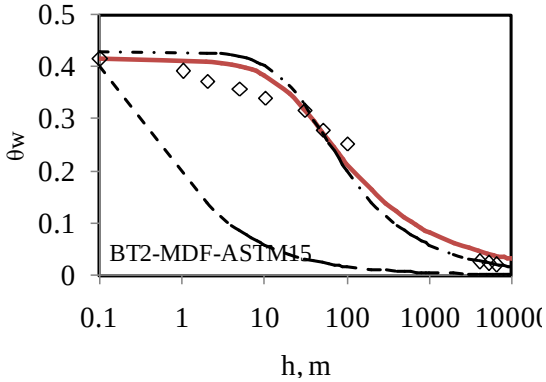
0.5
0.4
0.3
0.2
0.1
0
θw
BT2-MDF-ASTM15
0.1
1
10
100
1000
h, m

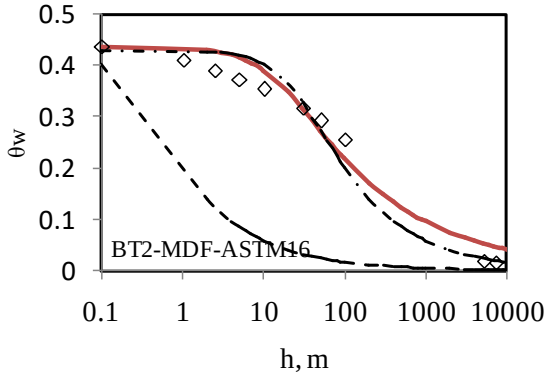
0.5
0.4
0.3
0.2
0.1
0
θw
BT2-MDF-ASTM16
0.1
1
10
100
1000
10000
h, m

SWCCs for JF2 soil sets

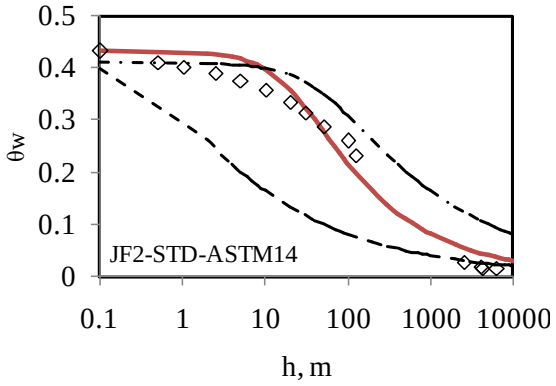

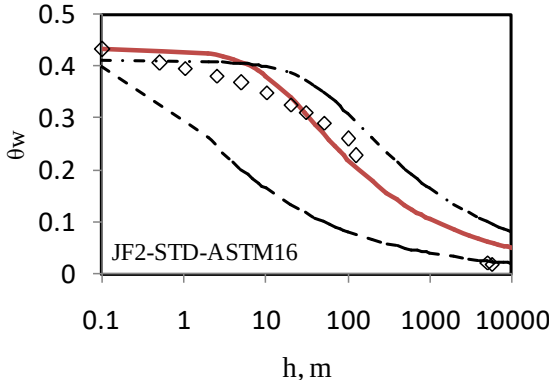

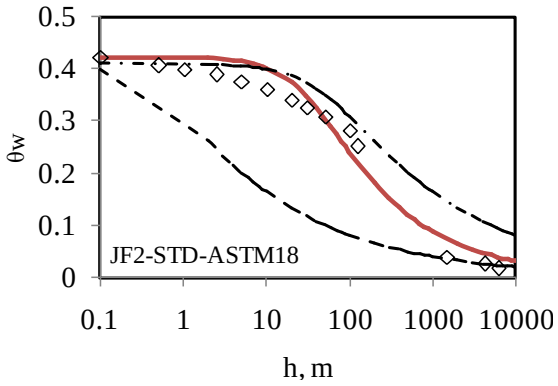

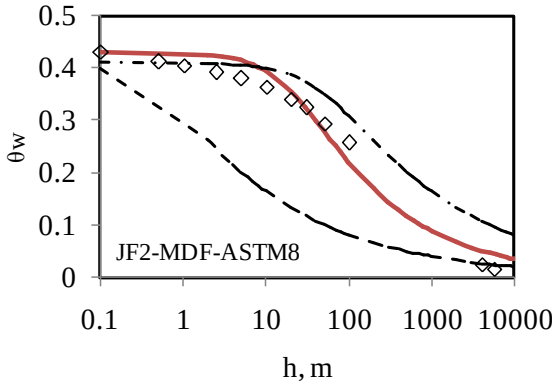

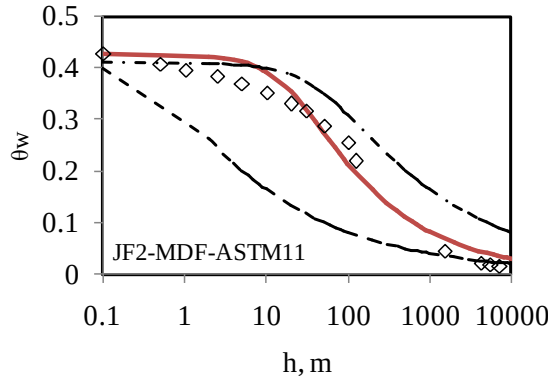

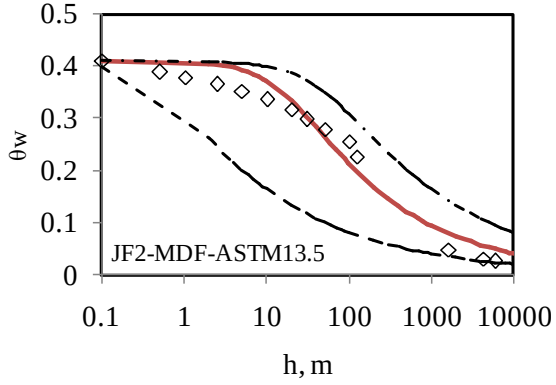

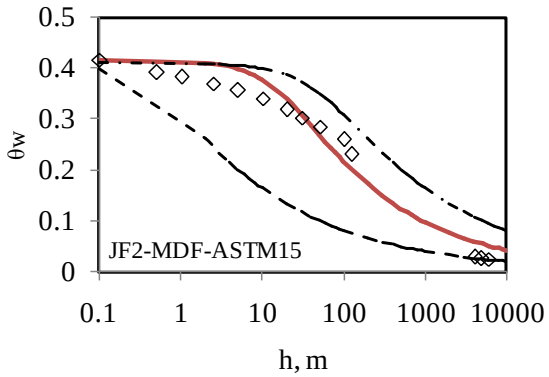
0.5
0.4
0.3
0.2
0.1
0
θw
JF2-MDF-ASTM15
0.1
1
10
100
1000
10000
h, m

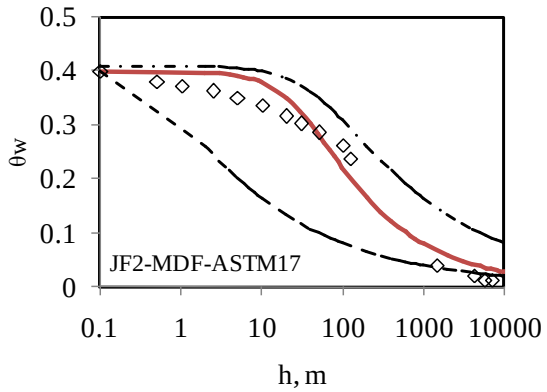
0.5
0.4
0.3
0.2
0.1
0
θw
JF2-MDF-ASTM17
0.1
1
10
100
1000
10000
h, m

APPENDIX B7: V-G fitting parameters for the SWCC test data (Case 1)

BT1-soil sets	n	α	Θ_s	Θ_r	SSE
STD-ASTM10	1.478	0.028	0.414	0.001	0.0049
STD-ASTM13	1.475	0.026	0.399	0.001	0.0051
STD-ASTM16	1.545	0.020	0.400	0.001	0.0037
STD-ASTM18	1.546	0.016	0.392	0.001	0.0031
STD-ASTM20	1.585	0.014	0.392	0.001	0.0063
MDF-ASTM7	1.545	0.018	0.398	0.001	0.0029
MDF-ASTM10	1.581	0.017	0.381	0.001	0.0031
MDF-ASTM13	1.566	0.015	0.368	0.001	0.0019
MDF-ASTM16	1.614	0.014	0.384	0.001	0.0029
MDF-ASTM18	1.595	0.014	0.377	0.001	0.0024

BT2-soil sets	n	α	Θ_s	Θ_r	SSE
STD-ASTM13	1.443	0.036	0.413	0.001	0.0028
STD-ASTM16	1.514	0.025	0.396	0.001	0.0037
STD-ASTM19.5	1.555	0.019	0.403	0.001	0.0034
STD-ASTM22	1.576	0.017	0.399	0.001	0.0035
MDF-ASTM8	1.563	0.025	0.410	0.001	0.0014
MDF-ASTM11	1.543	0.027	0.416	0.001	0.0040
MDF-ASTM13	1.622	0.017	0.419	0.001	0.0044
MDF-ASTM15	1.536	0.022	0.379	0.001	0.0035
MDF-ASTM16	1.496	0.026	0.398	0.001	0.0043

JF2-soil sets	n	α	Θ_s	Θ_r	SSE
STD-ASTM10	1.487	0.027	0.402	0.001	0.0044
STD-ASTM14	1.558	0.022	0.393	0.001	0.0062
STD-ASTM16	1.449	0.028	0.391	0.001	0.0056
STD-ASTM18	1.610	0.015	0.387	0.001	0.0053
STD-ASTM21	1.631	0.013	0.374	0.001	0.0043
MDF-ASTM8	1.499	0.026	0.400	0.000	0.0034
MDF-ASTM11	1.523	0.024	0.391	0.001	0.0048
MDF-ASTM13.5	1.478	0.024	0.372	0.001	0.0052
MDF-ASTM15	1.481	0.023	0.376	0.001	0.0056
MDF-ASTM17	1.627	0.014	0.361	0.001	0.0055

APPENDIX B8- Comparison of permeabilities from FWP and the different study cases using the mini-disk infiltrometer

BT1 soil sets

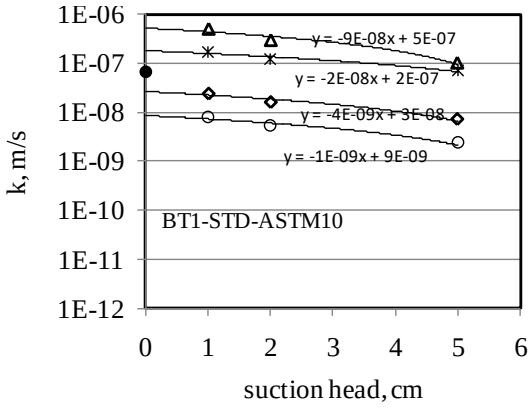

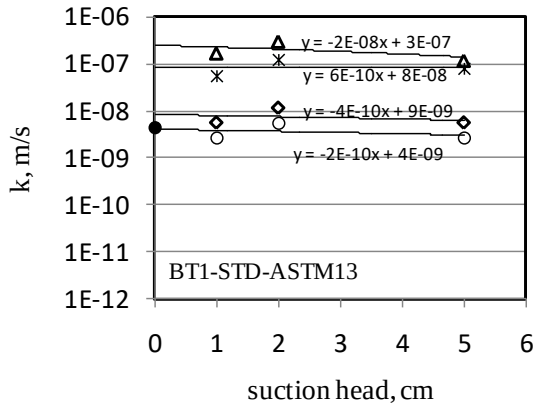

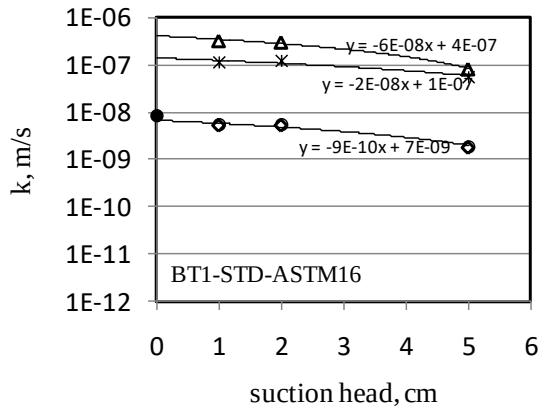

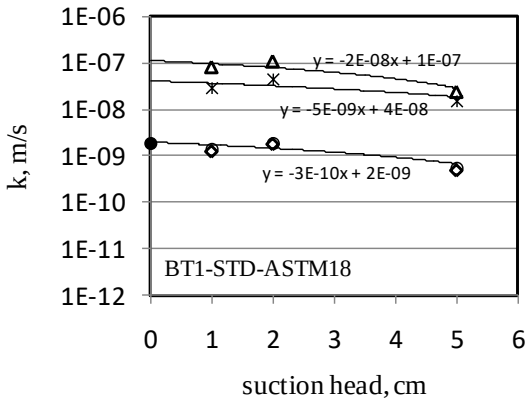

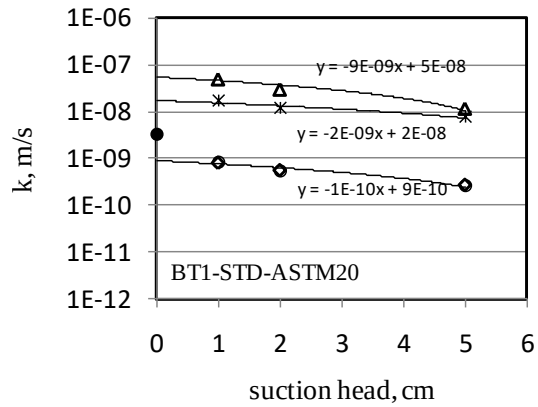

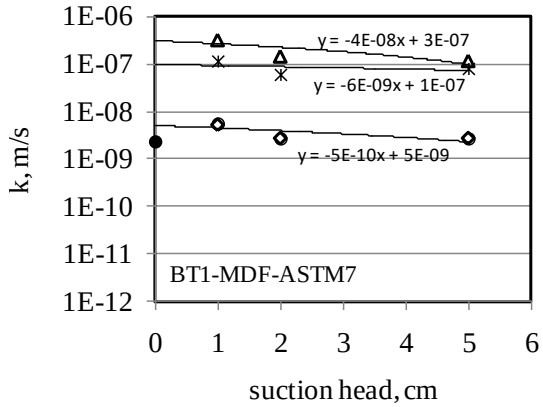

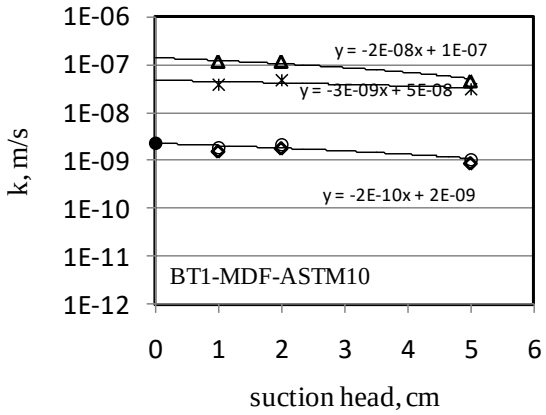

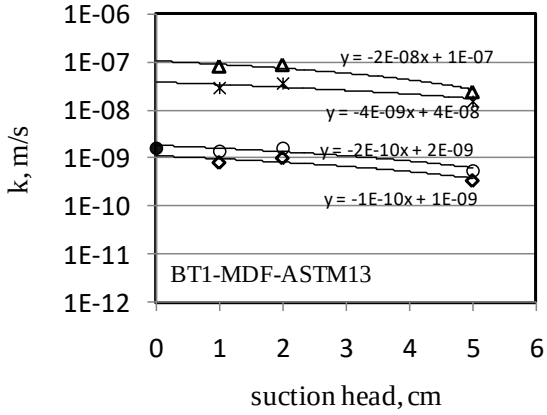

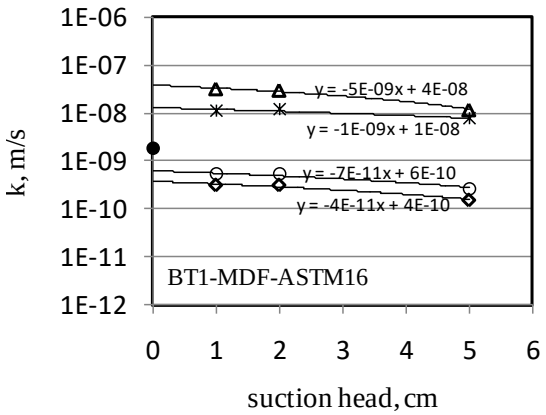

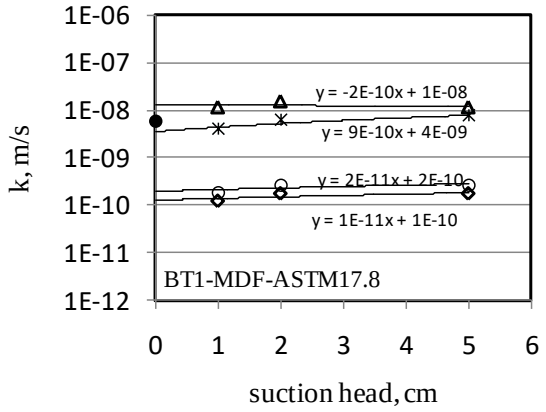

Legend:

- ● FWP measurement
- ◇ Case 1
- △ Case 2
- ○ Case 3
- ✳ Case 4

BT2 sets

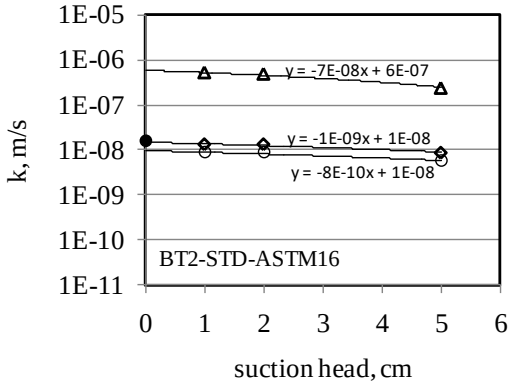
1E-05
1E-06
1E-07
1E-08
1E-09
1E-10
1E-11
k, m/s
y = -7E-08x + 6E-07
y = -1E-09x + 1E-08
y = -8E-10x + 1E-08
BT2-STD-ASTM16
0 1 2 3 4 5 6
suction head, cm

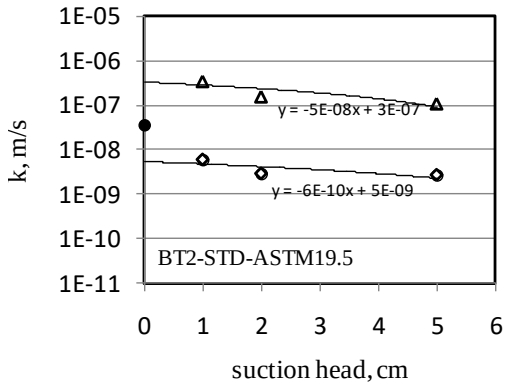
1E-05
1E-06
1E-07
1E-08
1E-09
1E-10
1E-11
k, m/s
y = -5E-08x + 3E-07
y = -6E-10x + 5E-09
BT2-STD-ASTM19.5
0 1 2 3 4 5 6
suction head, cm

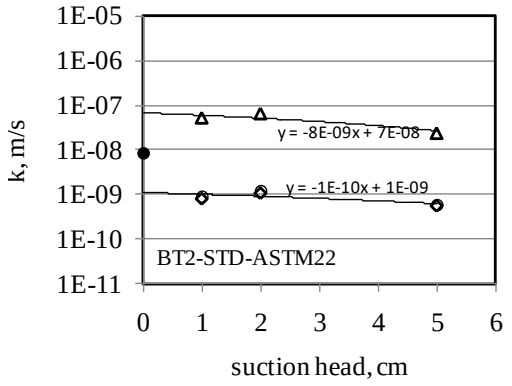
1E-05
1E-06
1E-07
1E-08
1E-09
1E-10
1E-11
k, m/s
y = -8E-09x + 7E-08
y = -1E-10x + 1E-09
BT2-STD-ASTM22
0 1 2 3 4 5 6
suction head, cm

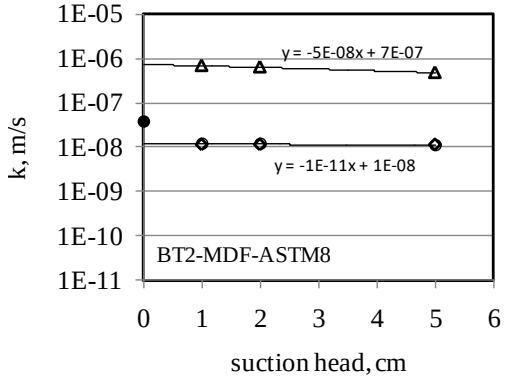
1E-05
1E-06
1E-07
1E-08
1E-09
1E-10
1E-11
k, m/s
y = -5E-08x + 7E-07
y = -1E-11x + 1E-08
BT2-MDF-ASTM8
0 1 2 3 4 5 6
suction head, cm

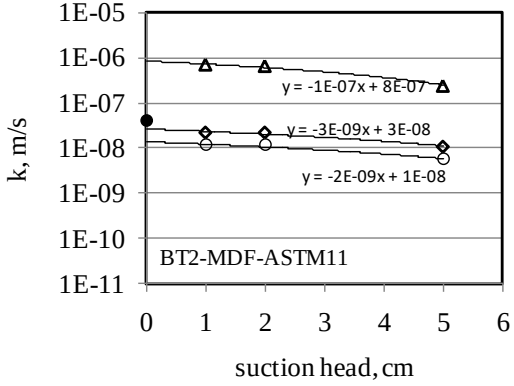
1E-05
1E-06
1E-07
1E-08
1E-09
1E-10
1E-11
k, m/s
y = -1E-07x + 8E-07
y = -3E-09x + 3E-08
y = -2E-09x + 1E-08
BT2-MDF-ASTM11
0 1 2 3 4 5 6
suction head, cm

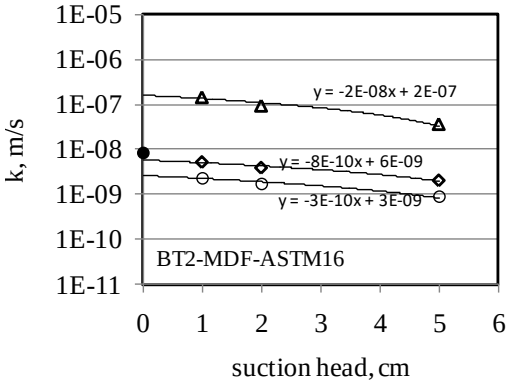
1E-05
1E-06
1E-07
1E-08
1E-09
1E-10
1E-11
k, m/s
y = -2E-08x + 2E-07
y = -8E-10x + 6E-09
y = -3E-10x + 3E-09
BT2-MDF-ASTM16
0 1 2 3 4 5 6
suction head, cm

JF2 soil sets

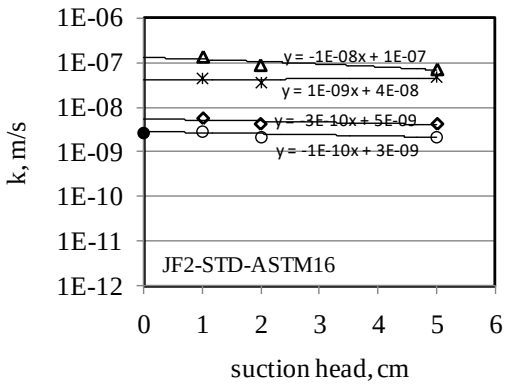

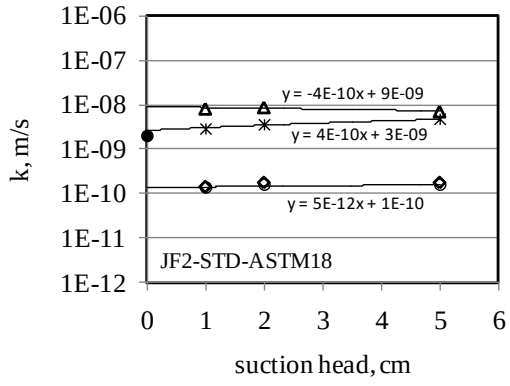

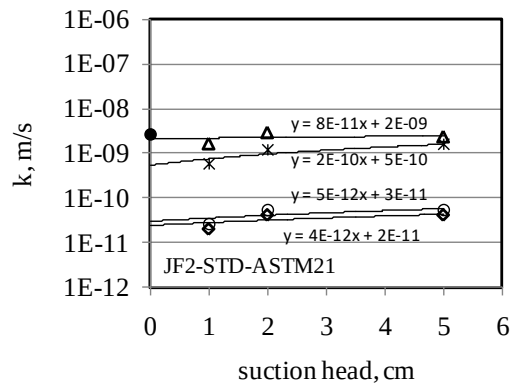

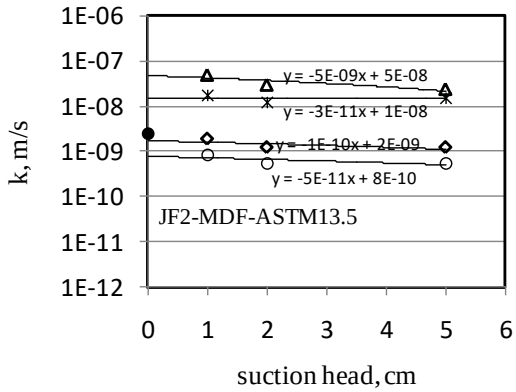

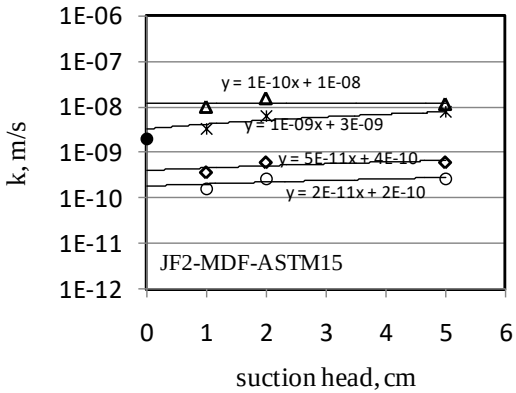

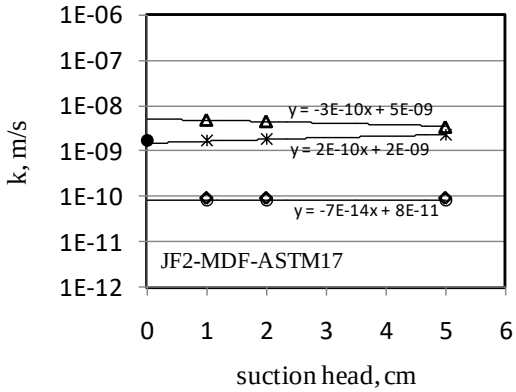

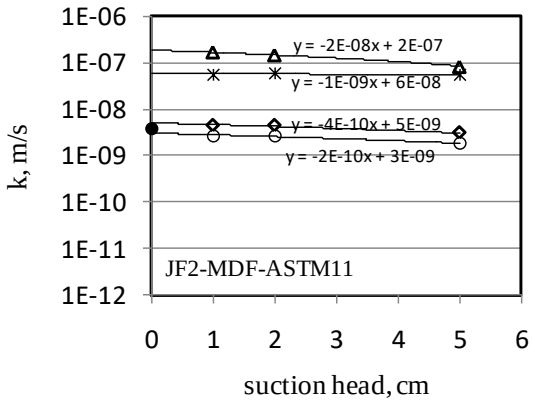
1E-06
1E-07
1E-08
1E-09
1E-10
1E-11
1E-12
k, m/s
y = -2E-08x + 2E-07
y = -1E-09x + 6E-08
y = -4E-10x + 5E-09
y = -2E-10x + 3E-09
JF2-MDF-ASTM11
0
1
2
3
4
5
6
suction head, cm

Appendix C- UC and BTS data

Contains Appendices C1-C4 (Referenced to in Chapter 6)

APPENDIX C1- Stress-strain plots for BT2 and JF1 soil- Test series 1

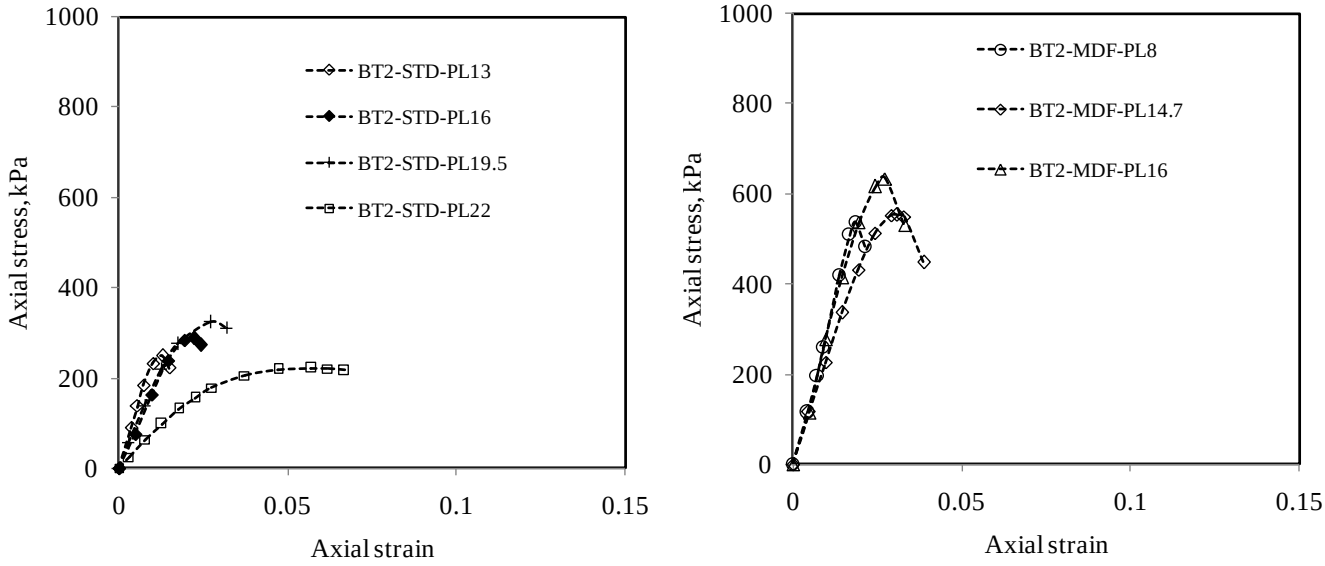

a) BT2 soil

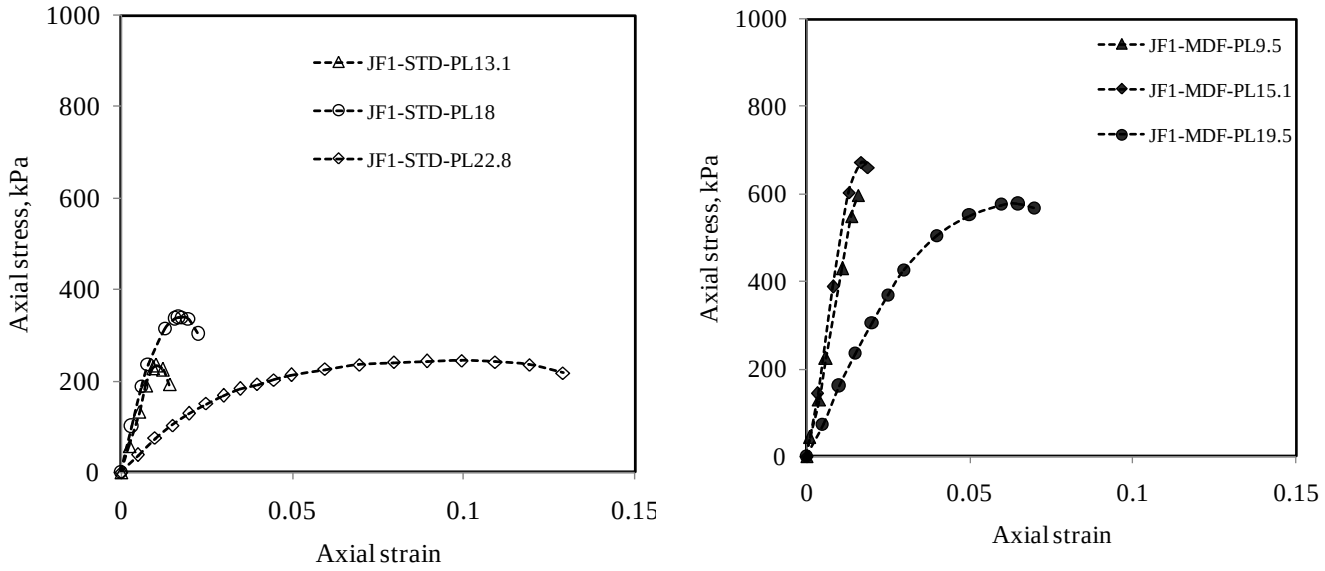

b) JF1 soil

Figure C1-1: Stress-strain plots for BT2 and JF1 soil- Test series 1

APPENDIX C2- Stress-strain plots for BT2 and JF1 soil (effect of compaction energy)- Test series 1

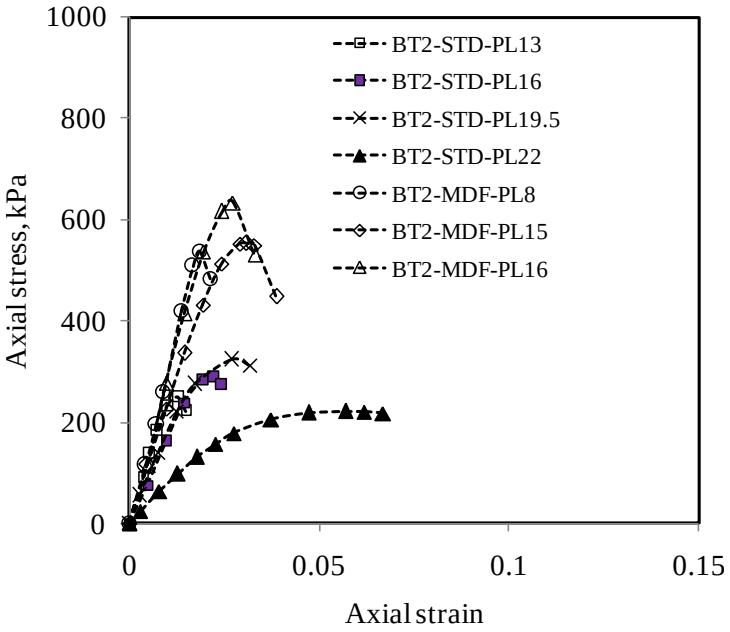

a) BT2

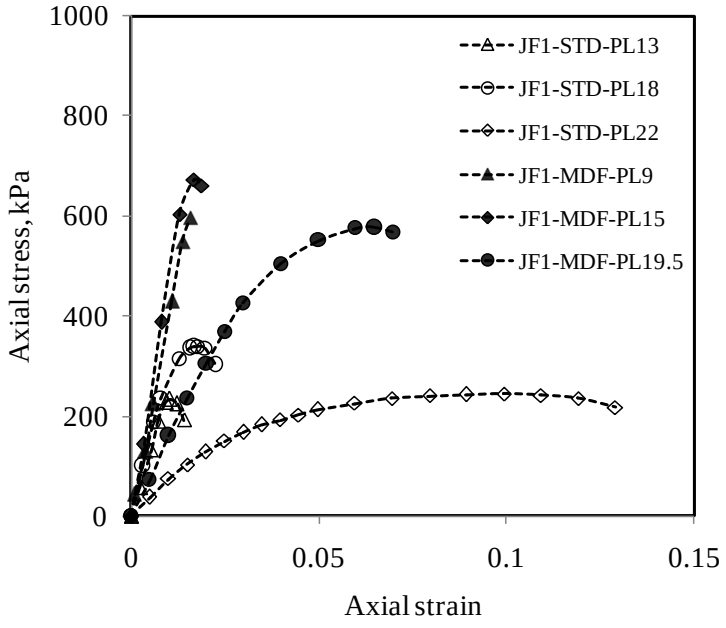

b) JF1

Figure C2-1: Stress-strain plots from UCS test for both standard and modified Proctor compacted soils for BT2 and JF1 (Test series 1)

APPENDIX C3- Stress-strain plots sample sets D to I- Test series 2

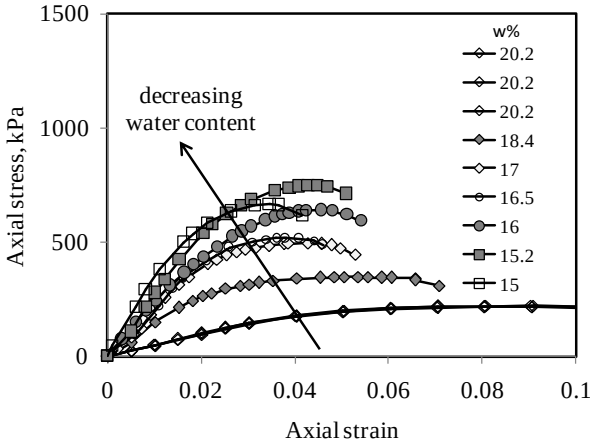

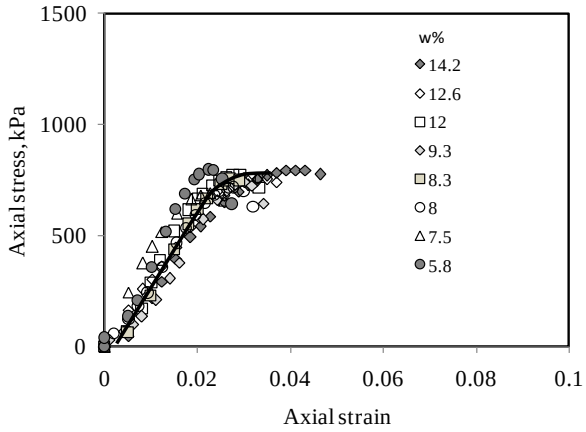

Sample set D

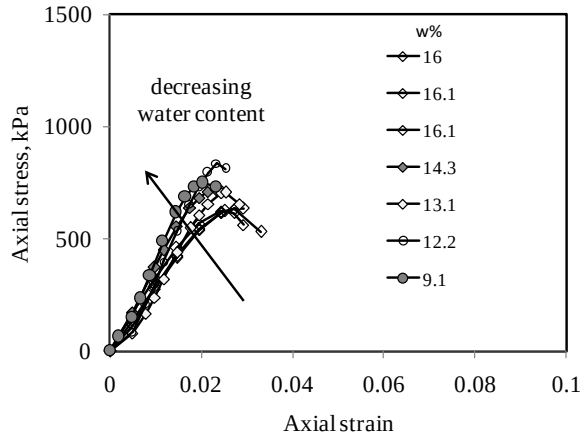

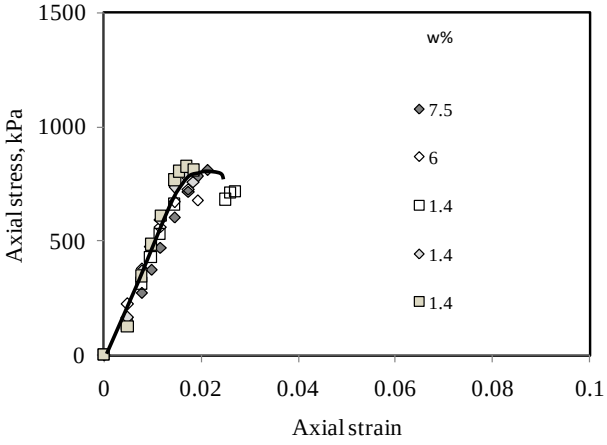

Sample set E

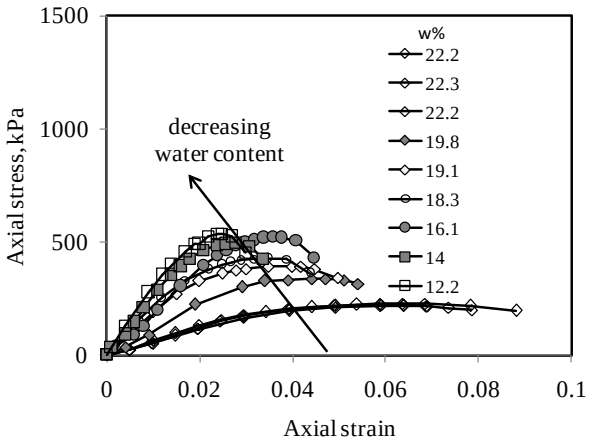

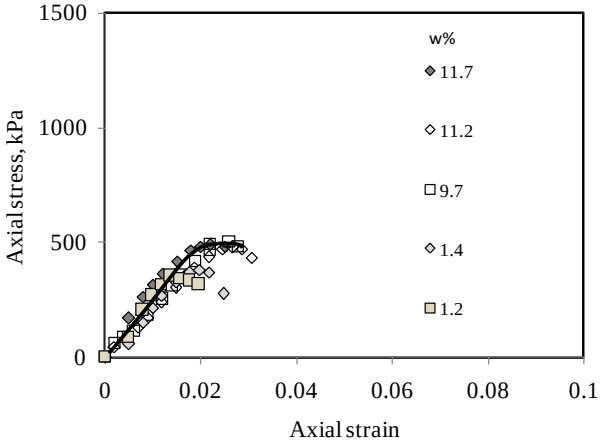

Sample set F

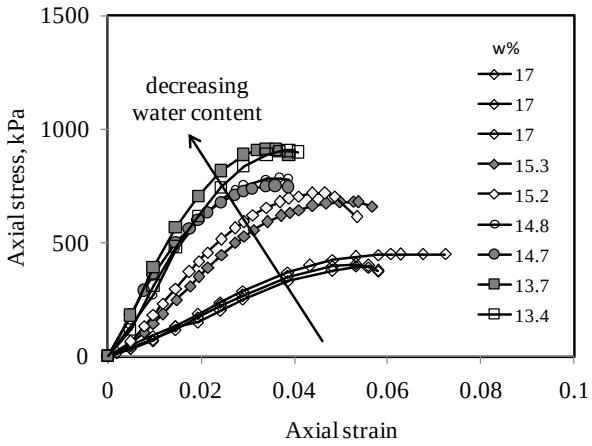

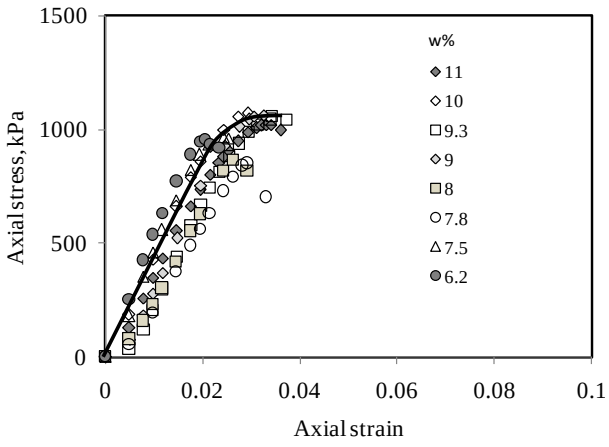

Sample set G

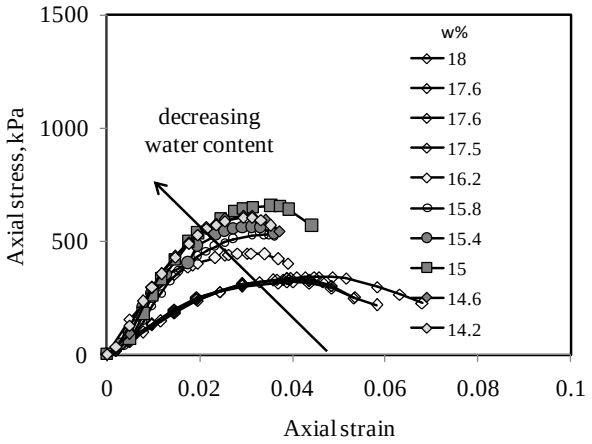

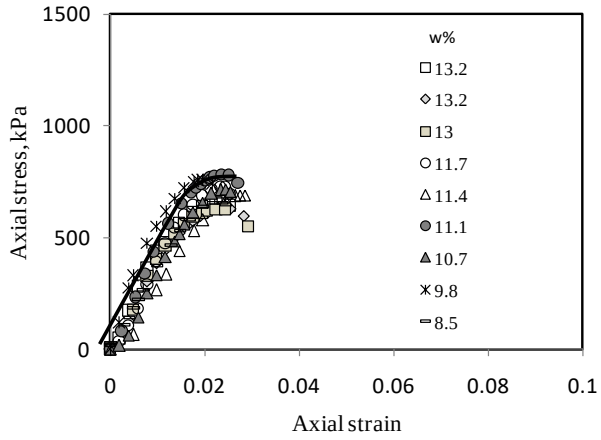

Sample set H

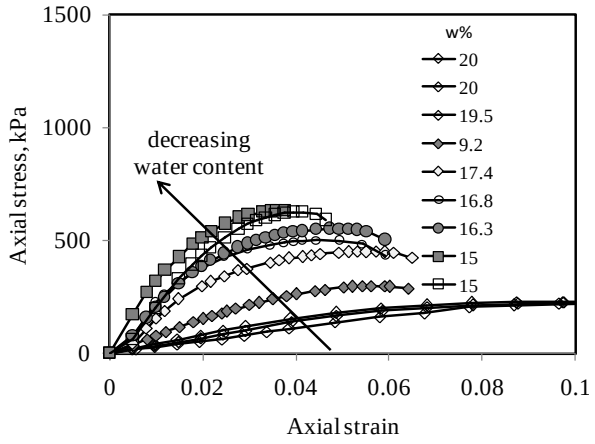

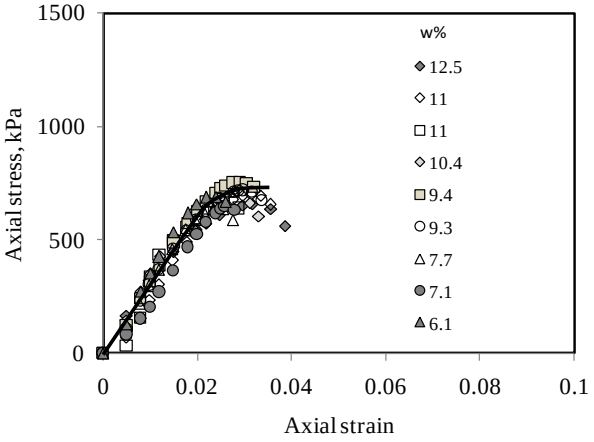

Sample set I

APPENDIX C4- Variation of UCS and BTS with degree of saturation and SWCC for sample sets D to I – Test series 2

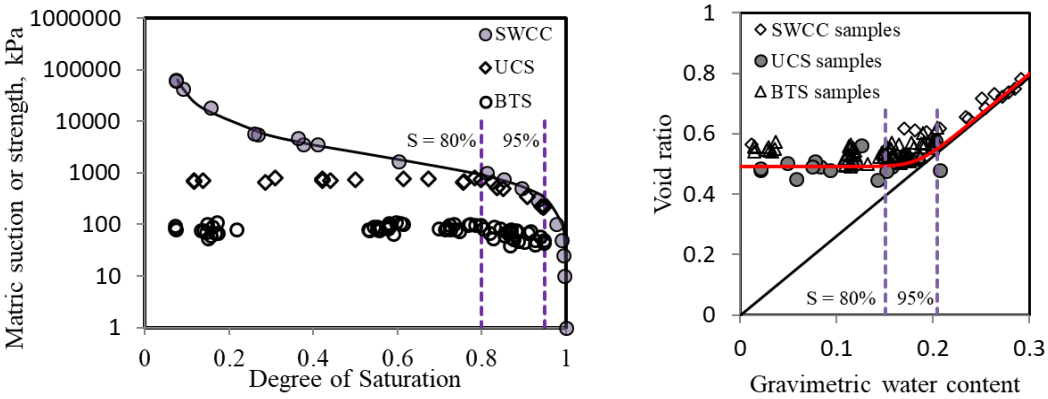

a) Sample set D

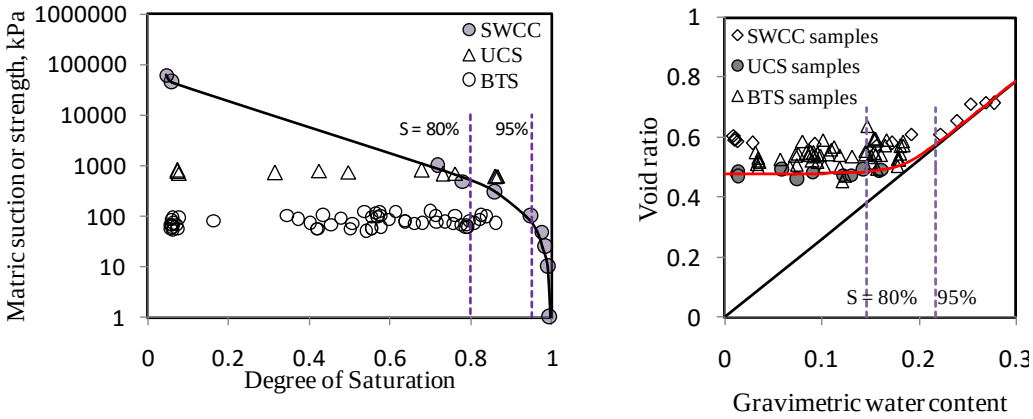

b) Sample set E

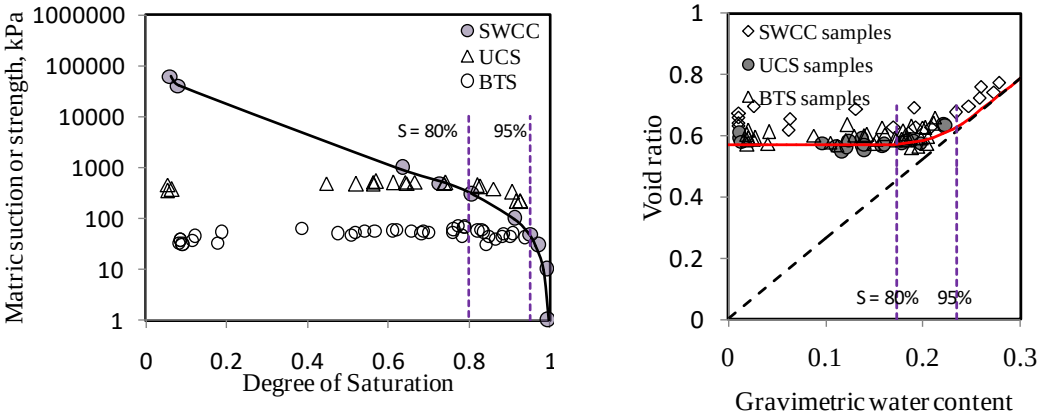

c) Sample set F

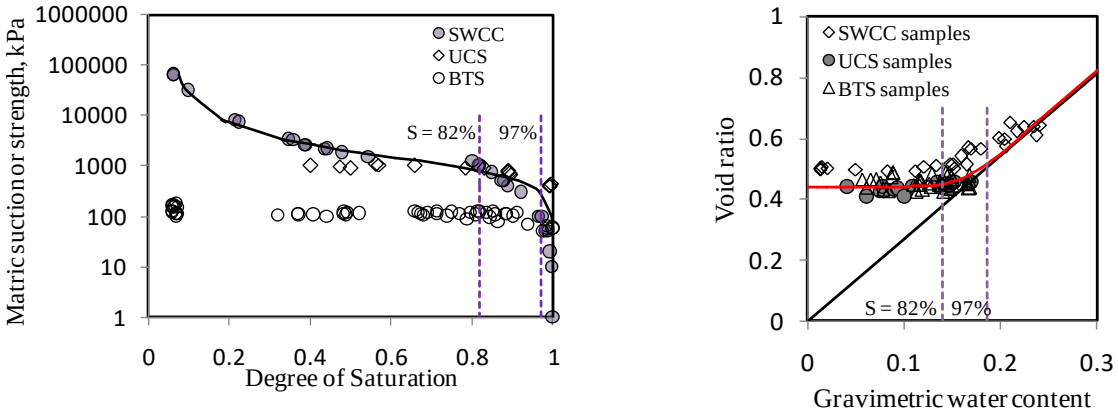

d) Sample G

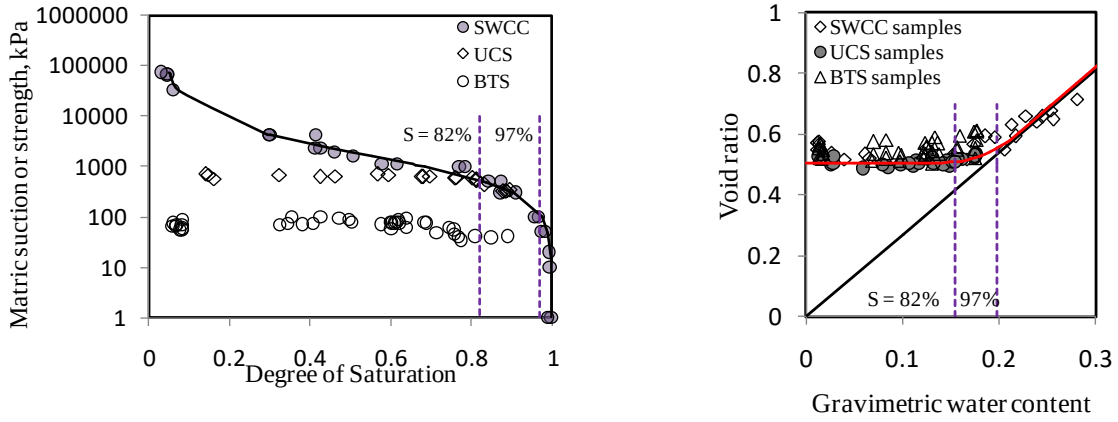

e) Sample H

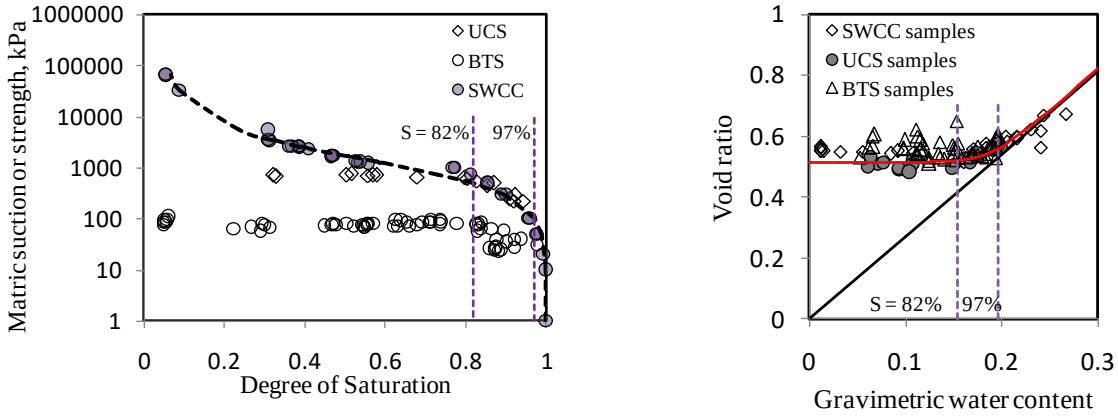

f) Sample I

Appendix D-UC and UU data

Contains Appendices D1-D6 (Referenced to in Chapter 7)

APPENDIX D1- UCS and UU stress-strain plots

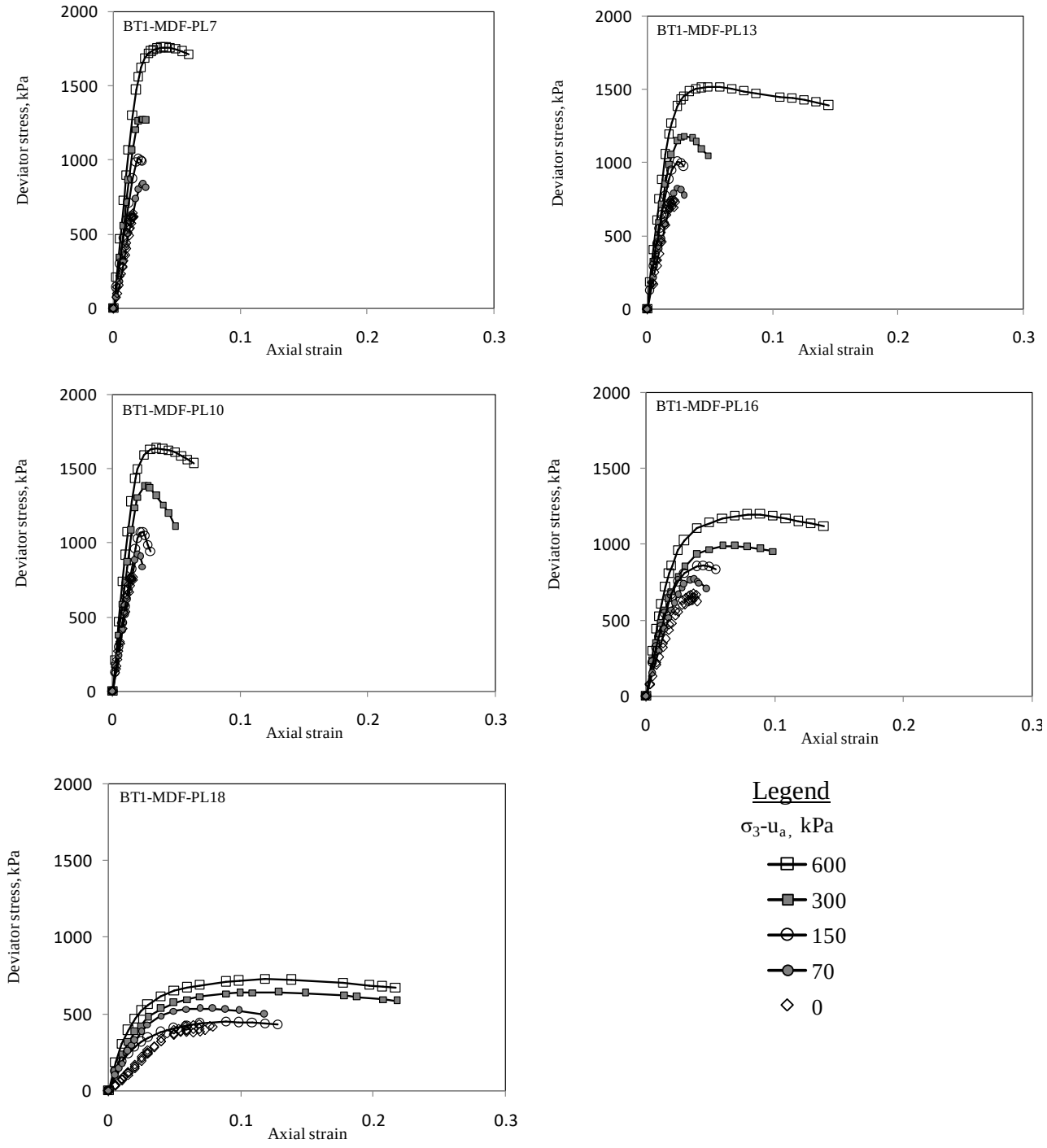

Figure D1-1: UC and UU stress-strain plots for BT1 soil specimens

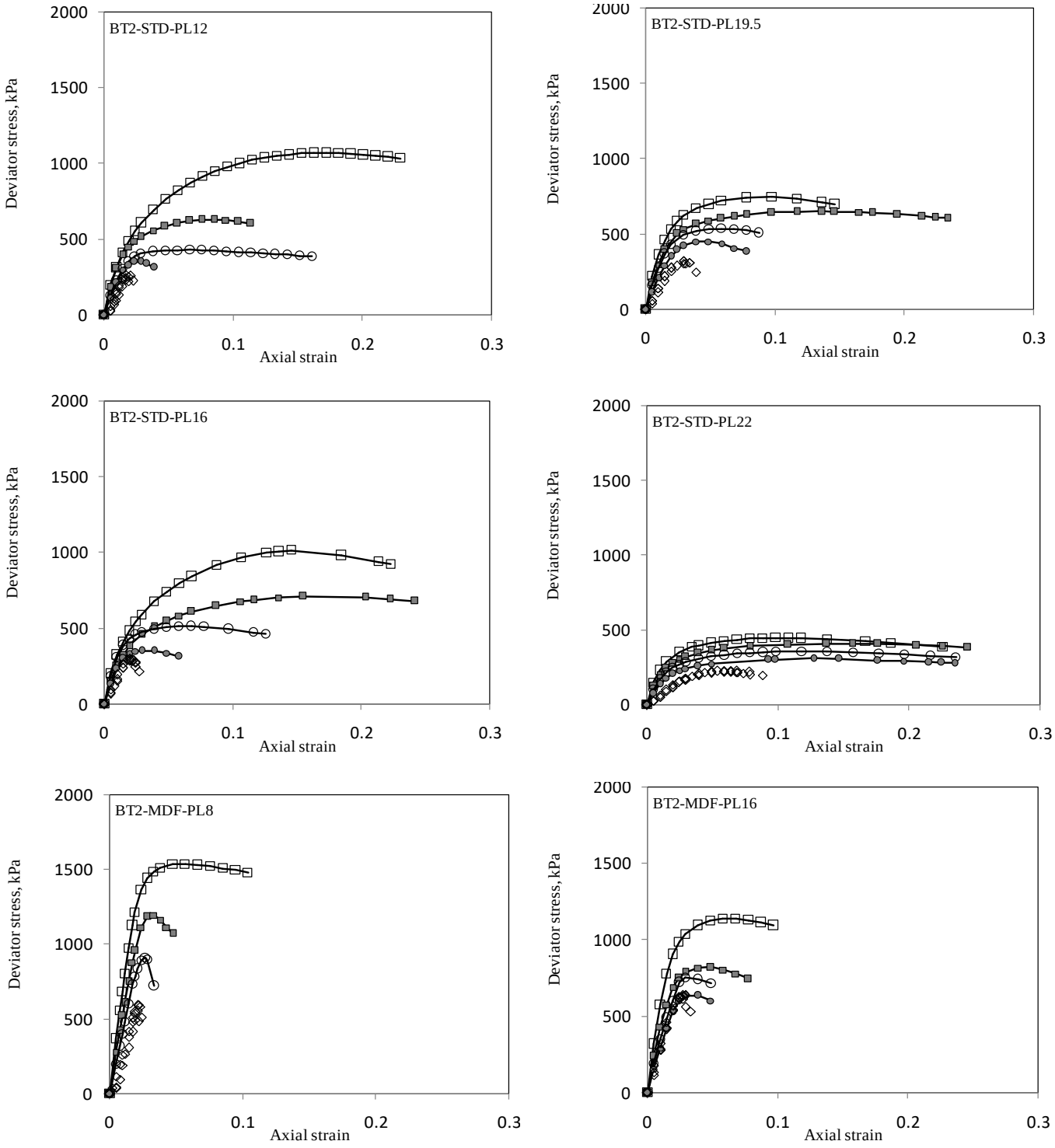

Figure D1-2: UC and UU stress-strain plots for BT2 soil specimens

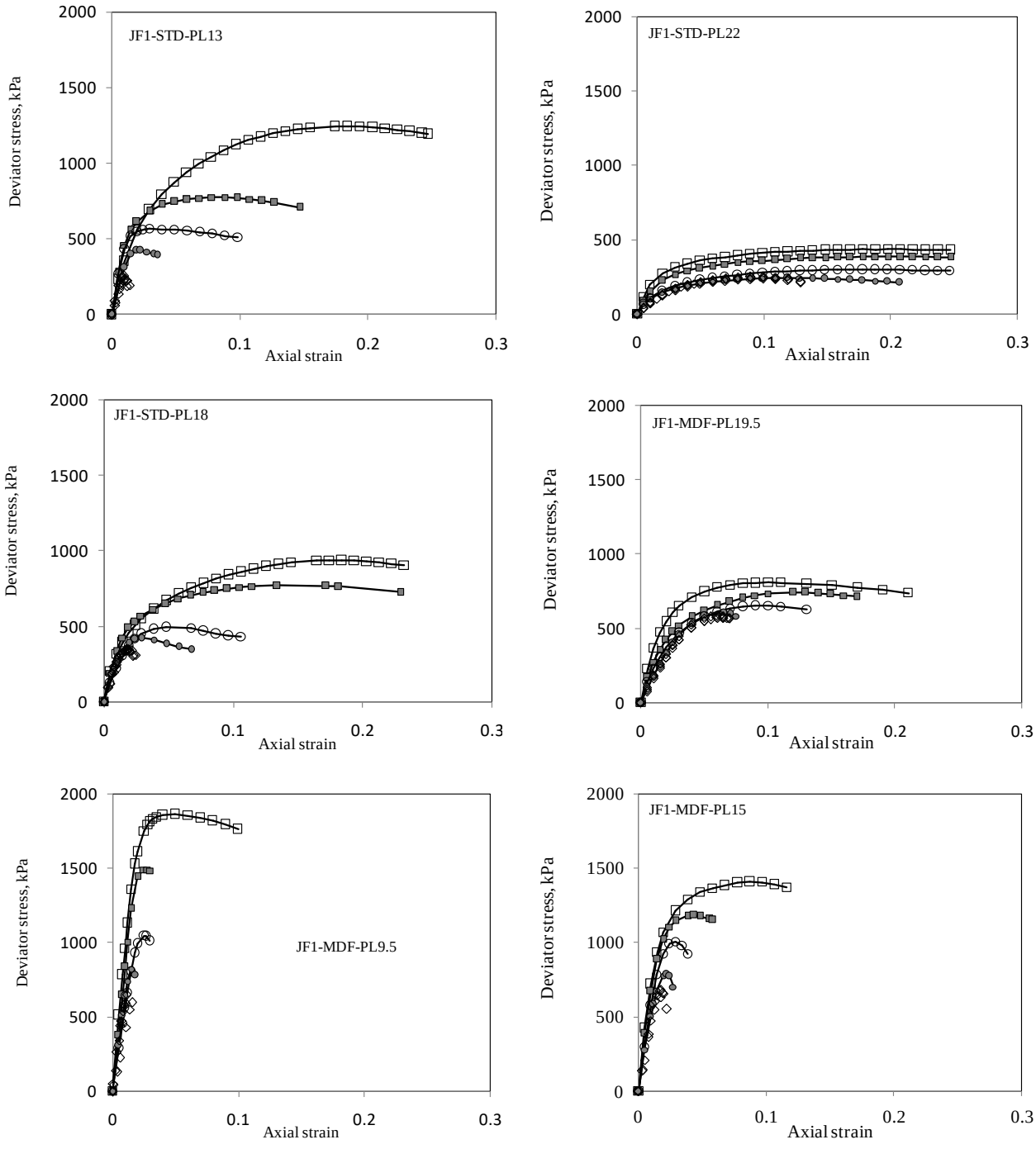

Figure D1-3: UC and UU stress-strain plots for JF1 soil specimens

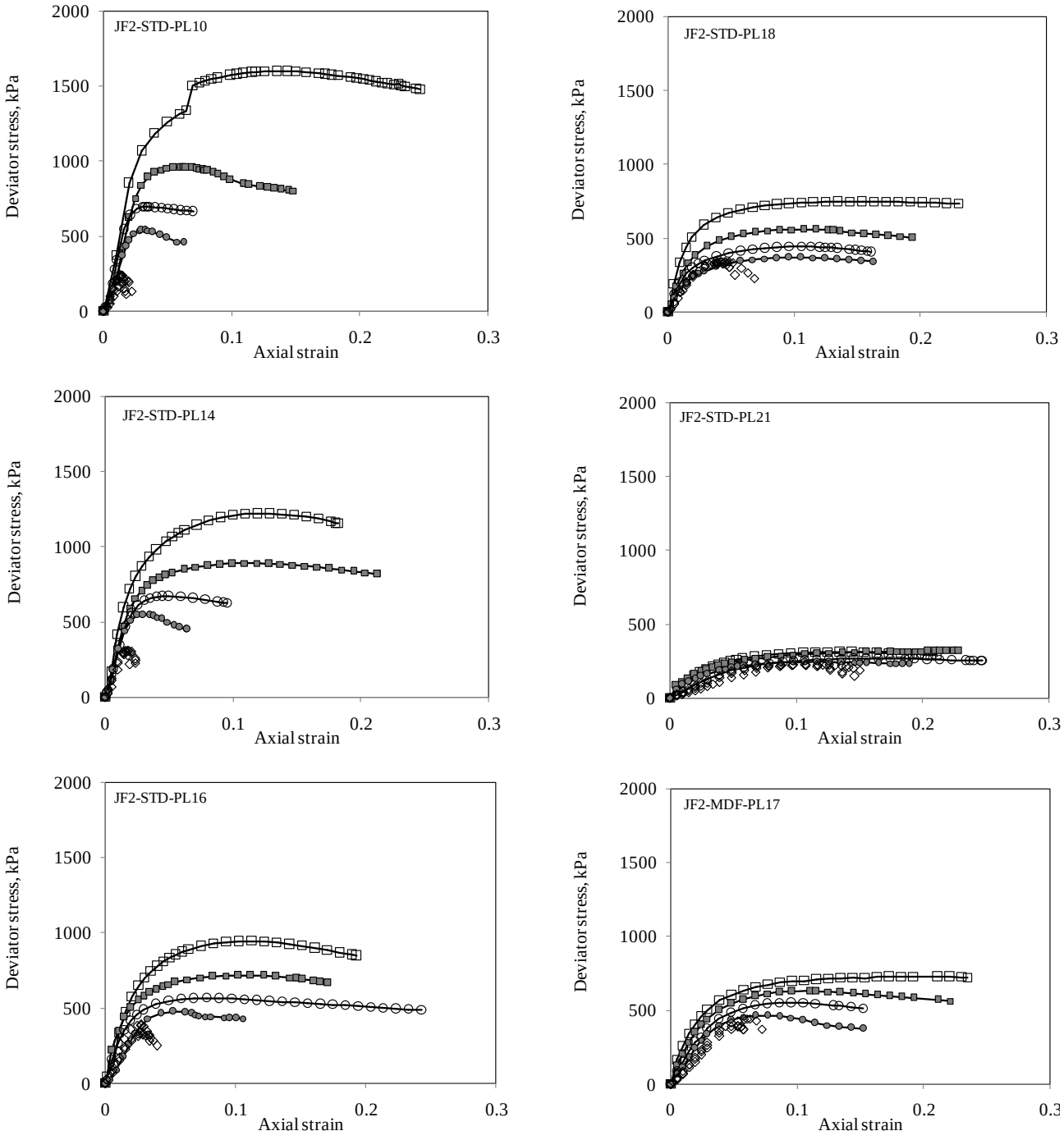

Figure D1-4: UC and UU stress-strain plots for JF2 soil specimens

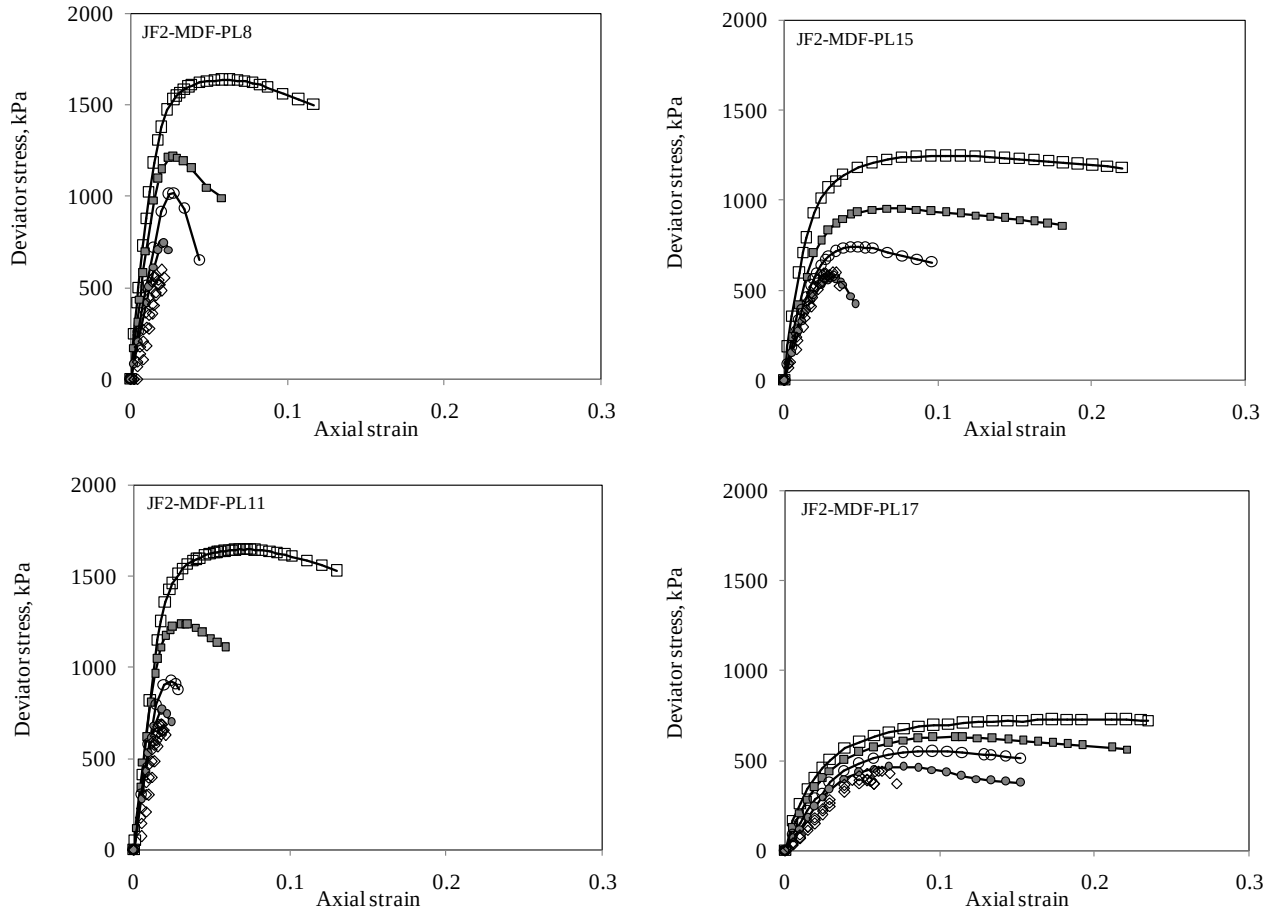

Figure D1-4: UC and UU stress-strain plots for JF2 soil specimens

Appendix D2: Effect of confining pressure on the stress-strain behavior

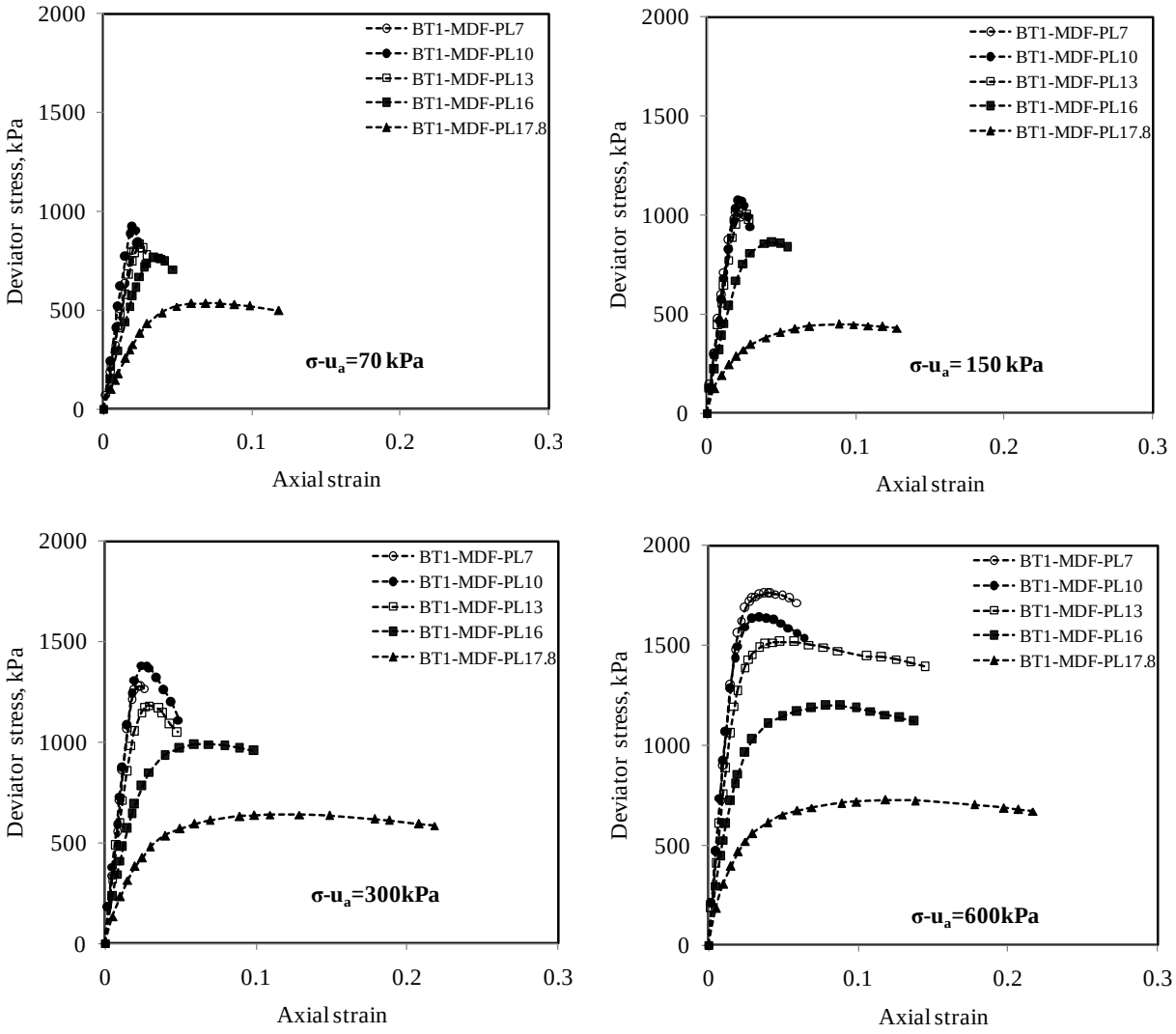

Figure D2-1: Effect of net confining pressure on the stress-strain plots of BT1 soil specimens compacted at modified Proctor

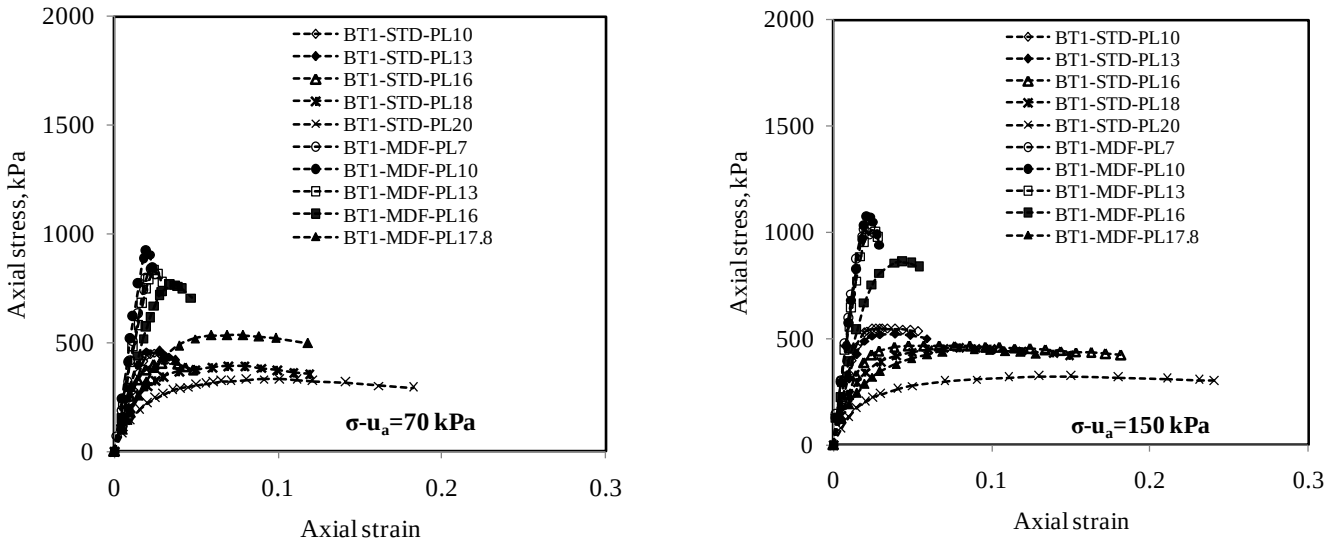

Figure D2-2: Effect of net confining pressure on the stress-strain plots comparing specimens compacted at standard and modified Proctor energy - BT1 soil specimens

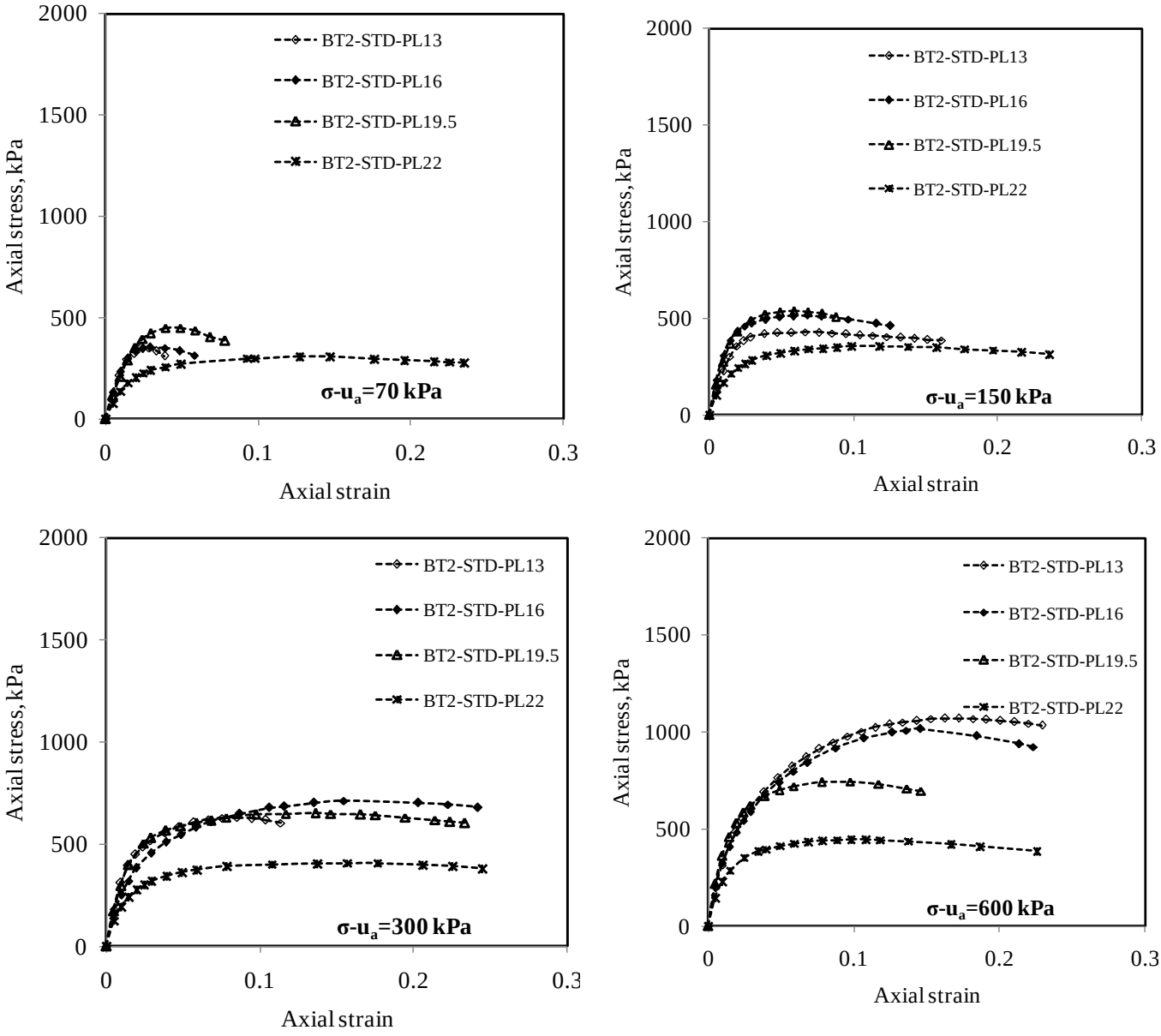

Figure D2-3: Effect of net confining pressure on the stress-strain plots of BT2 soil specimens compacted at standard Proctor

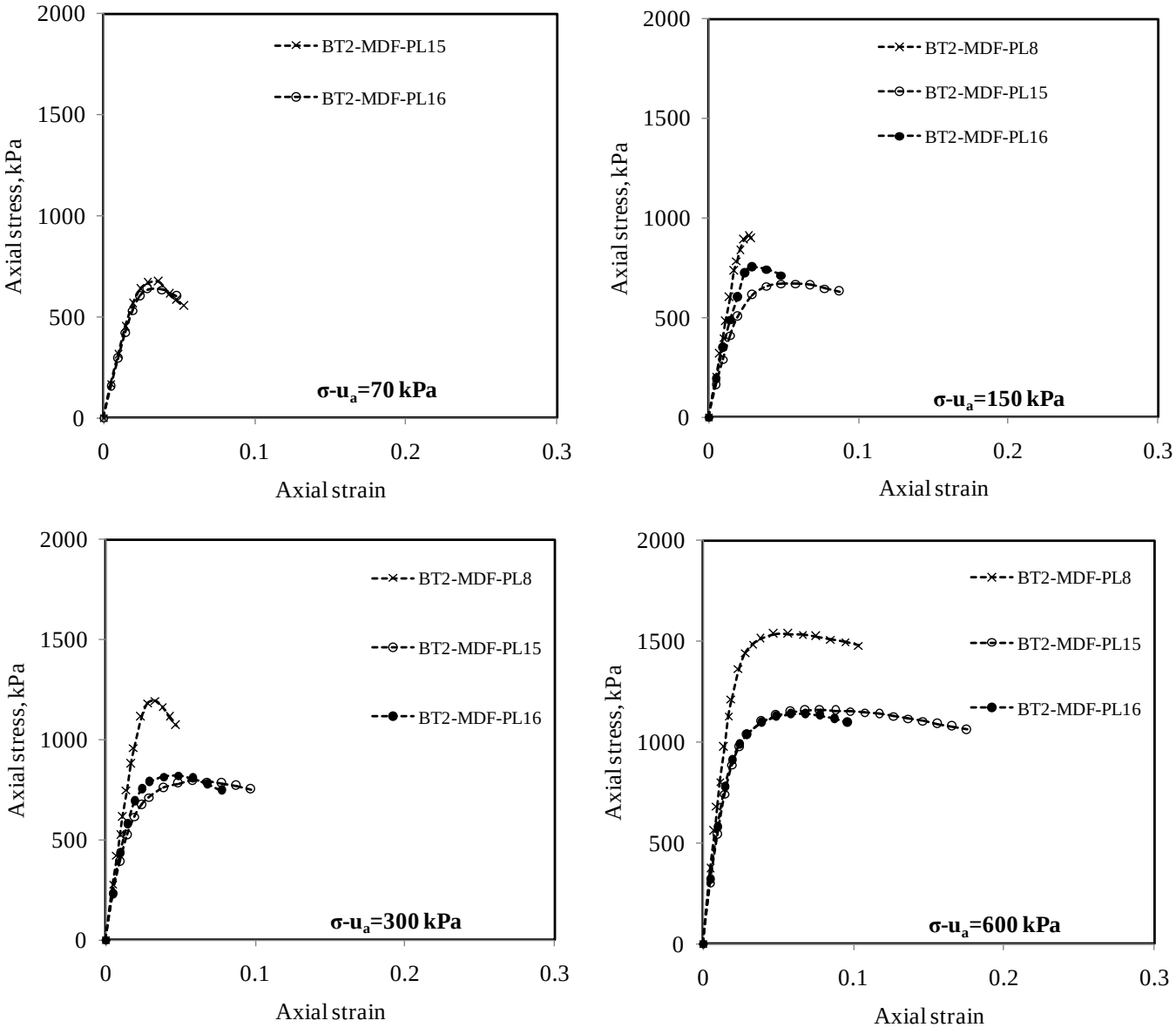

Figure D2-4: Effect of net confining pressure on the stress-strain plots of BT2 soil specimens compacted at modified Proctor

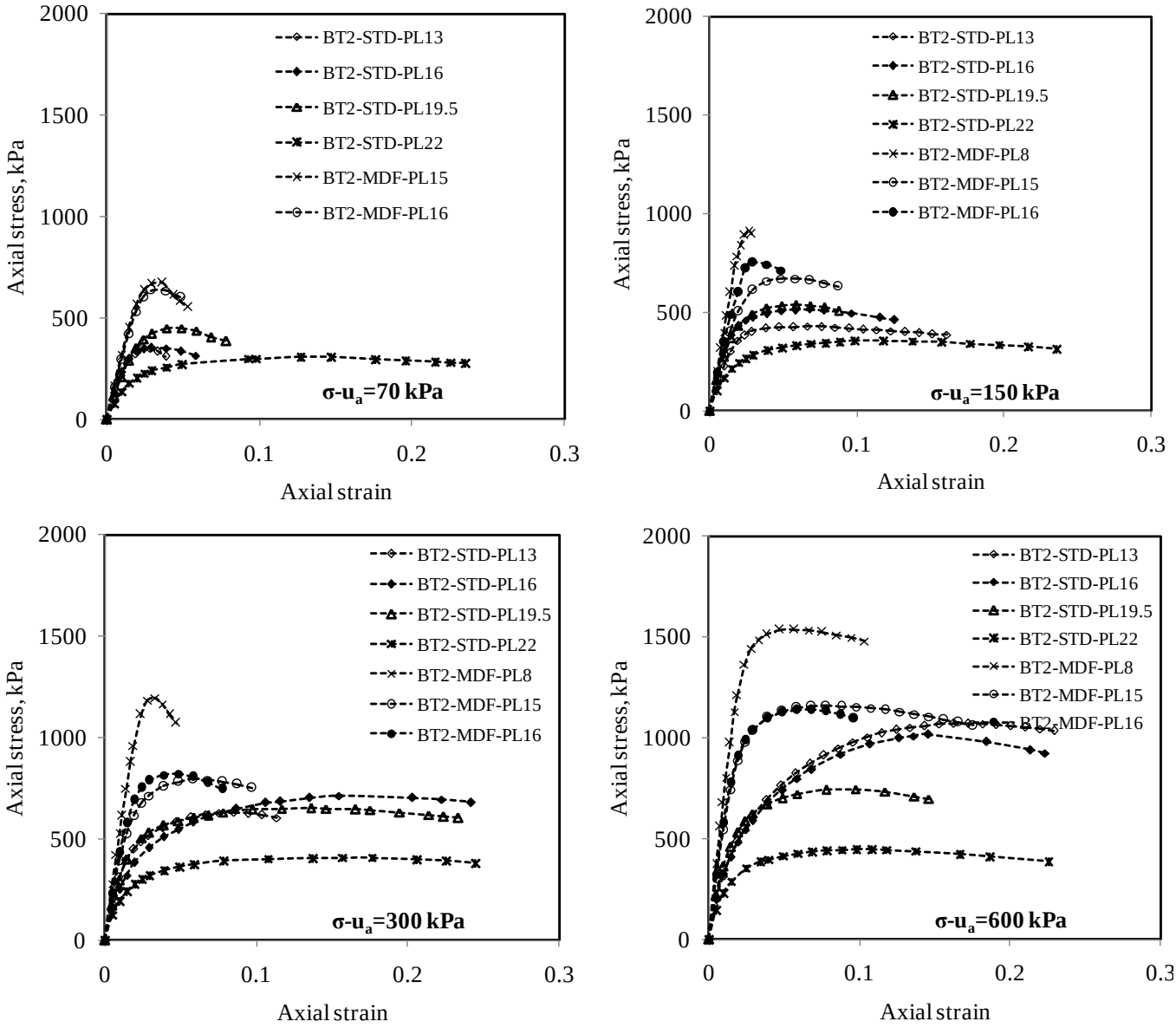

Figure D2-5: Effect of net confining pressure on the stress-strain plots comparing specimens compacted at standard and modified Proctor energy – BT2 soil specimens

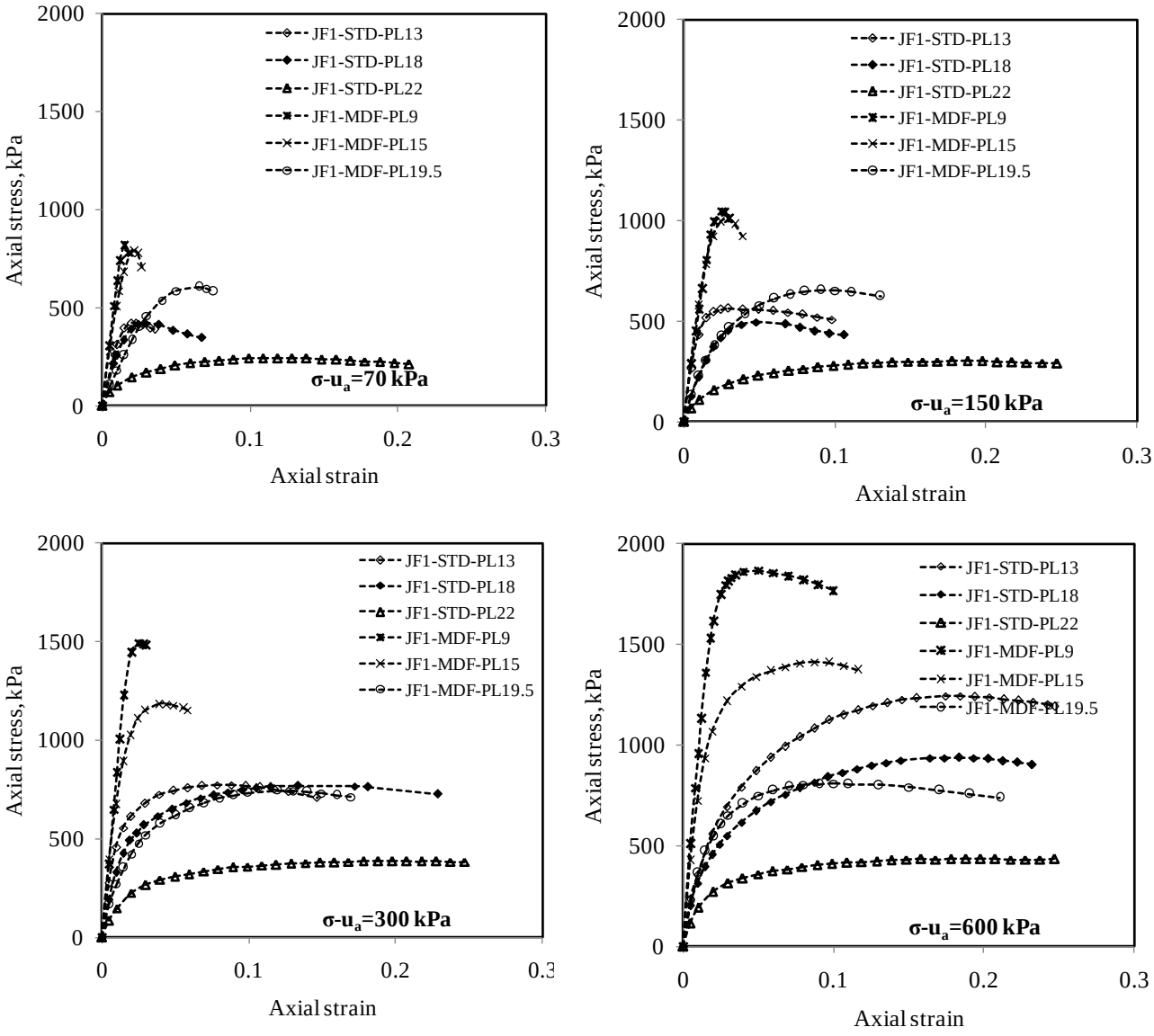

Figure D2-6: Effect of net confining pressure on the stress-strain plots comparing specimens compacted at standard and modified Proctor energy – JF1 soil specimens

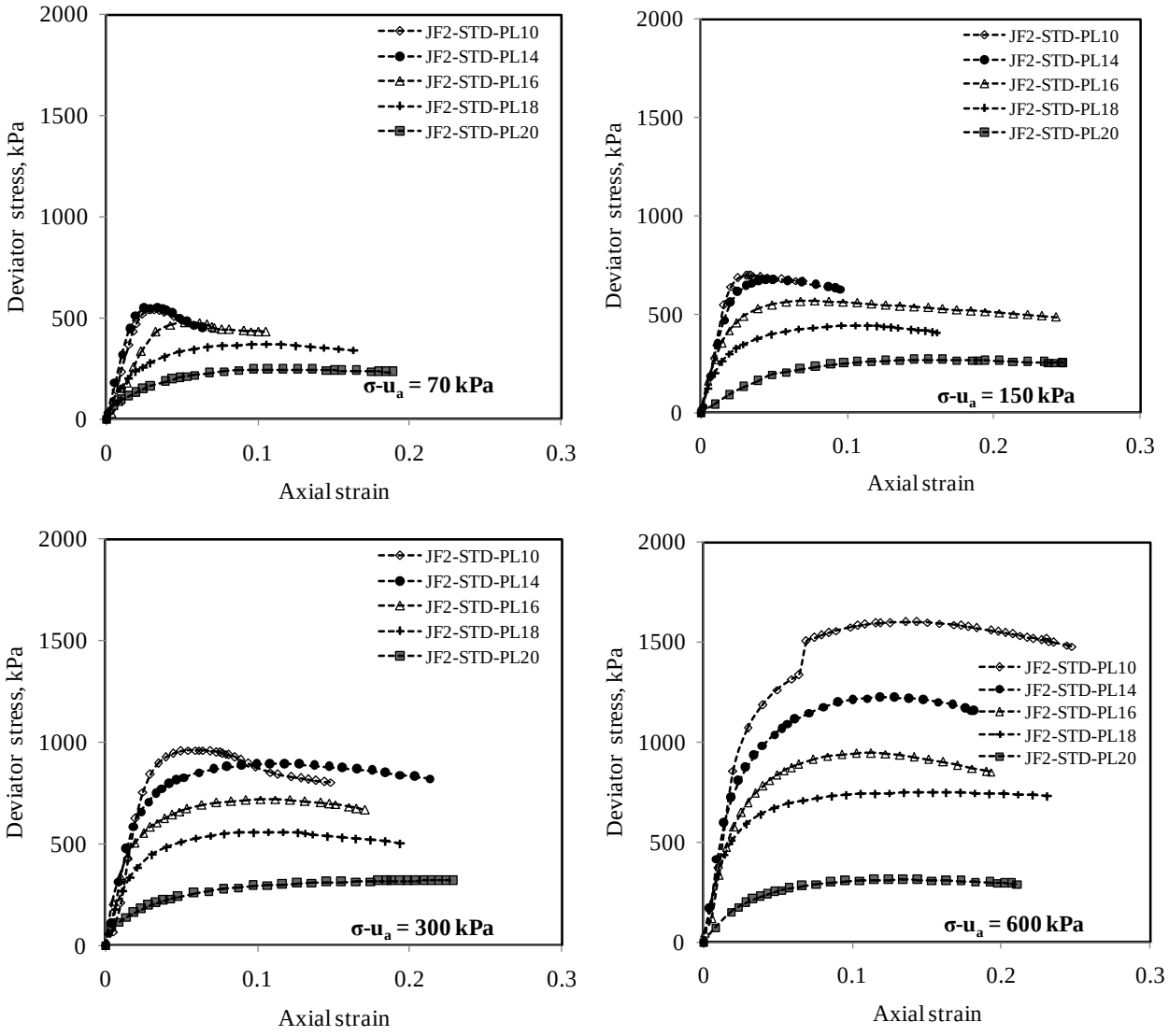

Figure D2-7: Effect of net confining pressure on the stress-strain plots of JF2 soil specimens compacted at standard Proctor

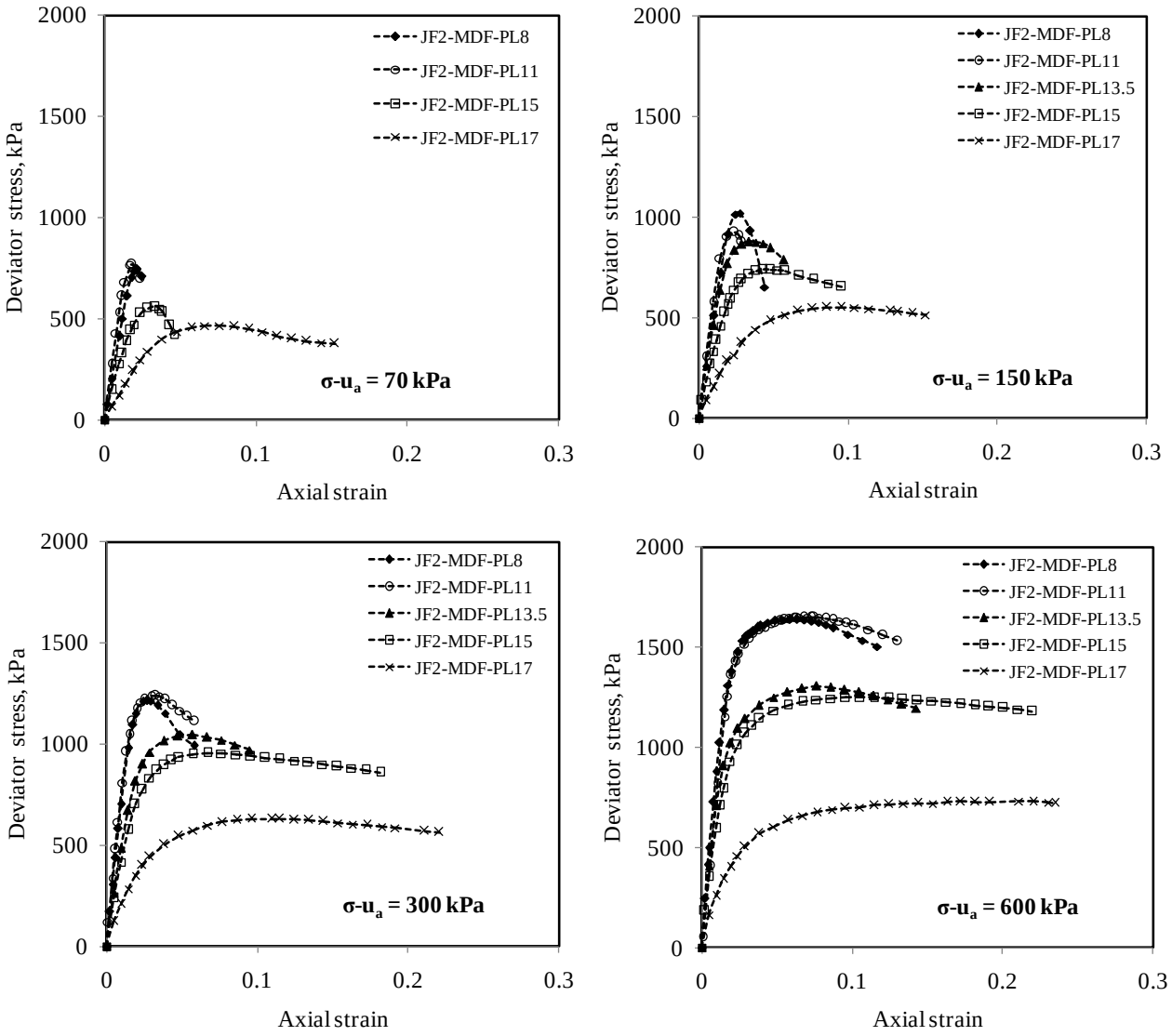

Figure D2-8: Effect of net confining pressure on the stress-strain plots of JF2 soil specimens compacted at modified Proctor

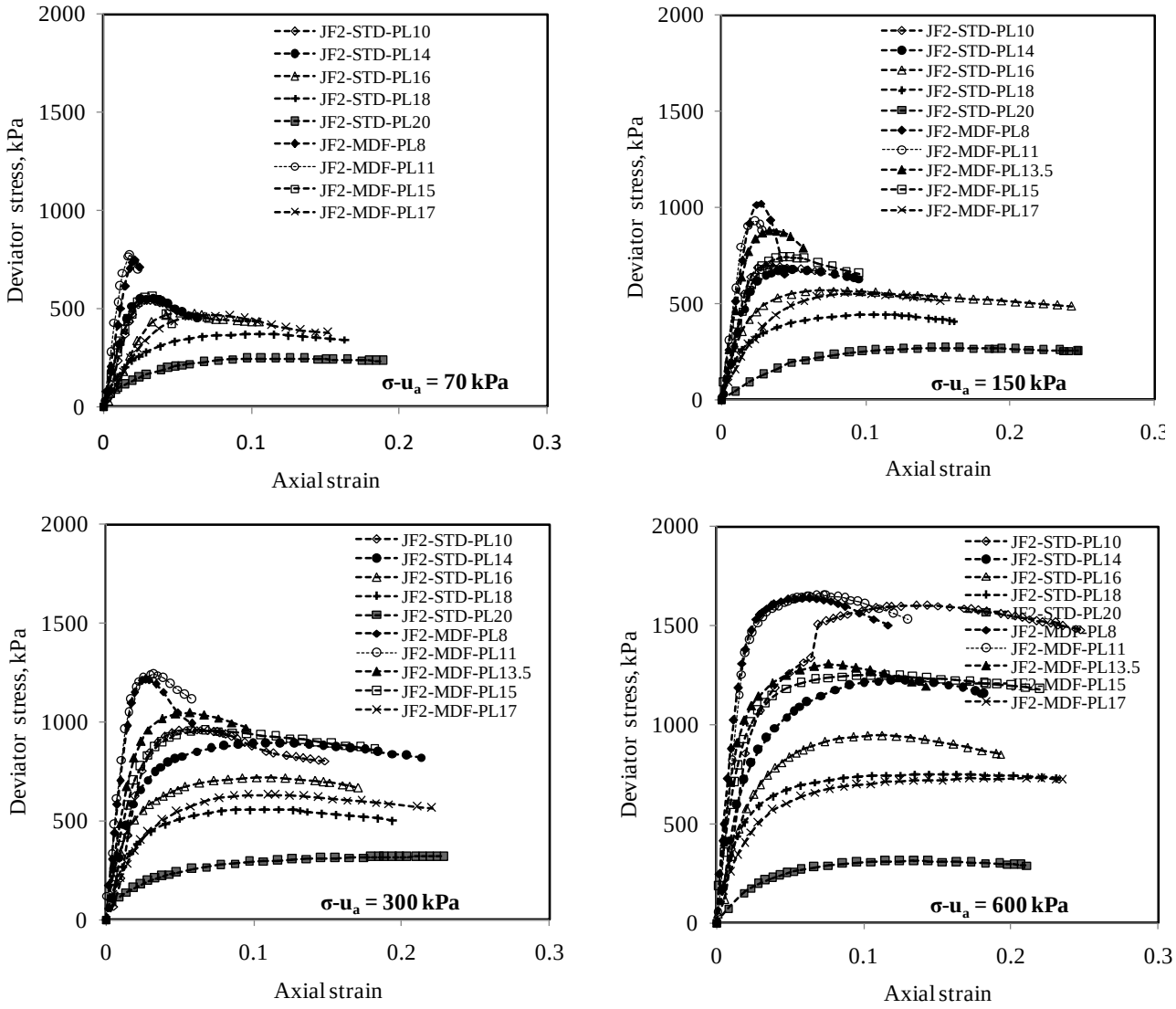

Figure D2-9: Effect of net confining pressure on the stress-strain plots comparing specimens compacted at standard and modified Proctor energy – JF2 soil specimens

Appendix D3- Variation of q_u with net confining pressure, compaction water content and compaction effort

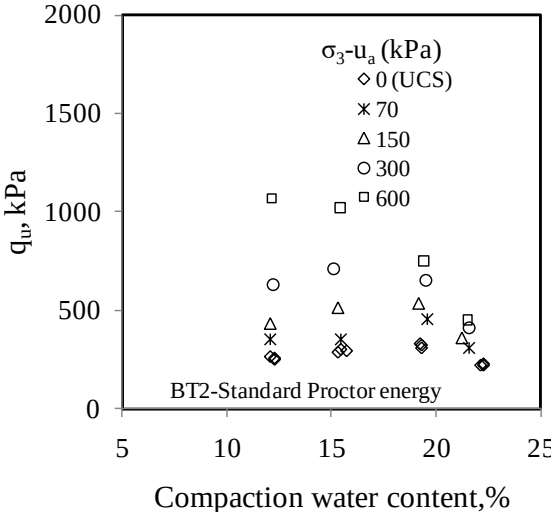

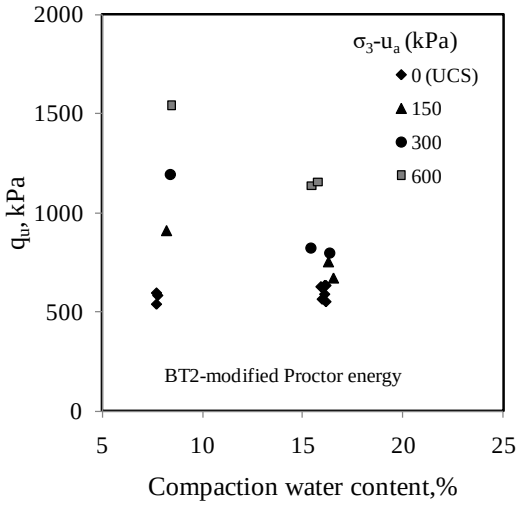

a) BT2 soil

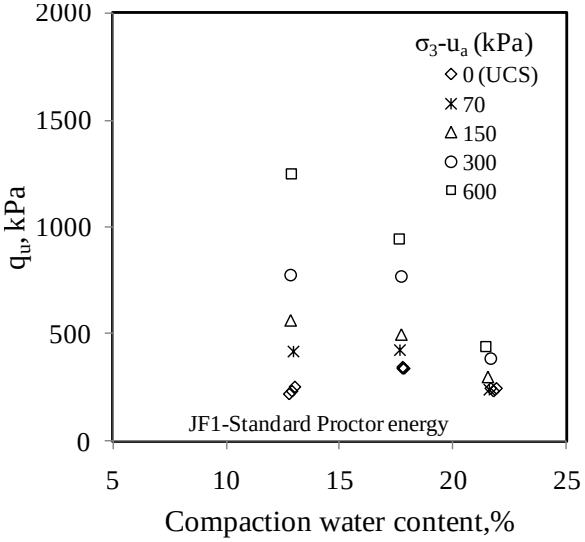

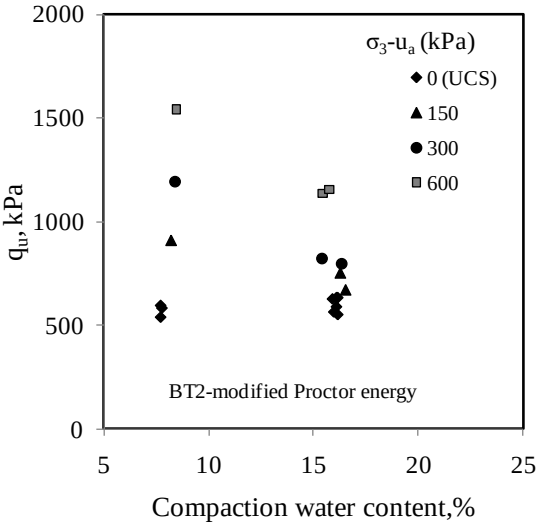

b) JF1 soil

Figure D3-1:Variation of q_u with net confining pressure, compaction water content and compaction effort for BT2 and JF1

Appendix D4- CU Multi-stage test- summary of results

Table D4-1: Saturated shear strength parameters for BT1

Sample id	stage	σ_{3f}, kPa	$(\sigma_1 - \sigma_3)_f$, kPa	u_f, kPa	ε_f, %	φ'°	c', kPa
BT1-STD-PL10	1	320	76.5	283.7	20.0	29.0	3
	2	390	141.8	312.6			
	3	540	400.0	339.4			
BT1-STD-PL13	1	270	78.7	237.2	12.5	30.6	1
	2	340	157.1	255.2			
	3	490	332.5	330.3			
BT1-STD-PL16	1	320	73.0	281.6	19.6	28.0	3
	2	390	143.7	313.5			
	3	540	307.5	371.4			
BT1-STD-PL18	1	370	82.5	327.1	12.0	27.5	4
	2	440	160.3	355.1			
	3	590	312.8	415.6			
BT2-STD-PL20	1	320	99.6	265.4	18.5	27.5	3
	2	390	178.6	291.6			
	3	540	373.7	331.9			
BT2-MDF-PL7	1	420	118.4	374.1	10.2	29.0	7
	2	490	189.4	403.6			
	3	640	354.1	465.3			
BT1-MDF-PL10	1	420	106.2	3770	20.0	27.0	10
	2	490	199.1	402.4			
	3	640	406.3	415.2			
BT1-MDF-PL13	1	370	90.4	325.6	20.0	27.0	14
	2	440	192.3	350.1			
	3	590	429.3	359.5			
BT1-MDF-PL16	1	270	133.0	221.0	18.0	26.0	16
	2	340	225.7	260.0			
	3	490	405.9	260.0			
BT1-MDF-PL18	1	270	174.4	204.0	17.0	27.5	16
	2	340	298.6	226.2			
	3	490	490.6	233.6			

Table D4-2: Saturated shear strength parameters for BT2

Sample id	stage	σ_{3f}, kPa	$(\sigma_1 - \sigma_3)_f$, kPa	u_f, kPa	ε_f, %	φ'°	c', kPa
BT2-STD-PL12	1	320	83.4	281	20	31	1
	2	390	146.4	311.8			
	3	540	340.3	385.5			
BT2-STD-PL16	1	320	92	281.5	20	32	1
	2	390	169.6	312.1			
	3	540	366.4	377.9			
BT2-STD-PL19.5	1	420	134	358.3	20	29.5	3
	2	490	189.1	389.7			
	3	640	415.1	430.5			
BT2-STD-PL22	1	420	125	366	20	32	0
	2	490	204.1	398.3			
	3	640	428.9	448.2			
BT2-MDF-PL8	1	320	218	245.1	12	30	12
	2	390	292	284			
	3	540	499.2	344.2			
BT2-MDF-PL16*	1	420	137	372.7	12	29.5	15
	2	490	240.8	397			
	3	640	496.3	420.5			
BT2-MDF-PL16	1	370	150.5	319.4	21	30	12
	2	440	249	346.9			
	3	590	543	335.9			

*Two samples at nearly same water content, 16% were tested at modified Proctor energy

Table D4-3: Saturated shear strength parameters for JF1

Sample id	stage	σ_{3f}, kPa	$(\sigma_1 - \sigma_3)_f$, kPa	u_f, kPa	ε_f, %	φ'°	c', kPa
JF1-STD-PL13	1	420	98.2	372.6	20	27.5	9
	2	490	166	404.3			
	3	640	333.3	445.6			
JF1-STD-PL18	1	420	78	384	20	26.5	7
	2	490	155	411			
	3	640	338.6	447.1			
JF1-STD-PL22	1	420	116.2	362.2	20	26.5	7
	2	490	192.3	394.1			
	3	640	395.7	449			
JF1-MDF-PL9	1	320	103	268	19	28	15
	2	390	149.3	304.4			
	3	540	416	328			
JF1-MDF-PL15	1	420	97	275	20	25.5	12
	2	490	168.2	404.1			
	3	640	397	398.1			
JF1-MDF-PL19.5	1	420	142.3	367.9	12	28	15
	2	490	234.5	394.4			
	3	640	449.5	414.4			

Table D4-4: Saturated shear strength parameters for JF2

Sample id	stage	σ_{3f}, kPa	$(\sigma_1 - \sigma_3)_f$, kPa	u_f, kPa	ε_f, %	φ'°	c', kPa
JF2-STD-PL10	1	370	96.4	326.2	12.2	31	1
	2	440	134.4	358.7			
	3	590	362.6	419.8			
JF2-STD-PL14	1	170	99.2	116.7	16.1	31	0
	2	240	197.8	144.8			
	3	390	413.3	195.5			
JF2-STD-PL16	1	320	87.6	269.3	16	30	3
	2	390	173.5	348.0			
	3	540	391	348.0			
JF2-STD-PL18	1	220	98.1	178.8	16.1	30	5
	2	290	198.2	204.7			
	3	440	428.2	233.2			
JF2-STD-PL20*	1	310	113	263.3	14.3	24*	10*
	2	390	169.3	295.6			
	3	540	323.1	325.4			
JF2-MDF-PL8	1	420	117.5	372.6	20	29	8
	2	490	207.5	397.5			
	3	640	481	398.7			
JF2-MDF-PL11	1	320	128.5	269.6	14.7	30	8
	2	390	237.3	292.8			
	3	540	509.3	299.5			
JF2-MDF-PL13.5	1	190	123	143.0	14.0	29	12
	2	260	240.4	160.0			
	3	410	463.6	187.6			
JF2-MDF-PL15	1	370	144.4	308.0	12.6	29	10
	2	440	260	337.2			
	3	590	473.3	359.3			
JF2-MDF-PL17	1	370	154	314.1	12.2	30	10
	2	440	240.2	341.7			
	3	590	538	337.8			

*Result is suspect.

Appendix D5- Summary of UCS and UU test data

Table D5-1 Summary of UCS and UU test data –BT1

Sample id	σ_3, kPa	$(\sigma_1-\sigma_3)$, kPa	ε_f, %	w, %	ρ_d (Mg/m^3)	Sample id	σ_3, kPa	$(\sigma_1-\sigma_3)$, kPa	ε_f, %	w, %	ρ_d (Mg/m3)
BT1-STD-PL10	0	225.8	1.1	10	1.65	BT1-MDF-PL7	0	626.4	1.5	6.9	1.80
	70	452.7	2.5	9.9	1.66		70	839.2	2.4	7.1	1.79
	150	548	2.9	9.8	1.64		150	1010.9	2	7.0	1.78
	300	860.2	12.8	9.8	1.64		300	1278	2.4	6.8	1.78
	600	1352	15.8	9.8	1.66		600	1761.6	4	6.8	1.78
BT1-STD-PL13	0	299.4	1.4	12.9	1.66	BT1-MDF-PL10	0	767.1	1.4	9.9	1.83
	70	460.5	2.7	12.8	1.67		70	922.5	2	9.8	1.82
	150	522.6	3.9	12.8	1.67		150	1074.2	2.4	9.7	1.82
	300	782	9.8	12.8	1.67		300	1383	2.5	9.8	1.81
	600	1053	14.6	12.7	1.66		600	1640	3.4	9.8	1.83
BT1-STD-PL16	0	321.6	2.0	15.8	1.67	BT1-MDF-PL13	0	730.2	2	12.8	1.83
	70	407	2.9	15.7	1.68		70	829.6	2.4	12.8	1.84
	150	468	7.6	15.9	1.68		150	1009.7	2.4	12.8	1.84
	300	715.6	14.4	15.8	1.67		300	1182.9	2.9	12.7	1.83
	600	896.7	16.3	15.7	1.68		600	1518.2	4.8	12.8	1.85
BT1-STD-PL18	0	305.2	4.2	18	1.70	BT1-MDF-PL16	0	651	3.7	15.9	1.82
	70	393	7.9	17.8	1.69		70	767.6	3.7	16.0	1.83
	150	459	7.9	17.7	1.70		150	861	4.4	15.8	1.81
	300	514	16.9	17.8	1.71		300	989.5	6.9	15.9	1.82
	600	644	16.9	17.8	1.71		600	1199.3	8.9	15.8	1.82
BT1-STD-PL20	0	218.3	9.0	20.4	1.66	BT1-MDF-PL18	0	404.9	6.5	17.7	1.77
	70	332	9.1	19.7	1.67		70	535.4	6.9	17.8	1.78
	150	322.3	13.0	19.8	1.67		150	448.9	8.9	17.8	1.77
	300	397	15.1	19.8	1.68		300	640.8	12.9	17.7	1.78
	600	419	15.0	19.8	1.67		600	726.6	11.9	17.8	1.78

Table D5-2 Summary of UCS and UU test data –BT2

Sample id	σ_3, kPa	(σ_1-σ_3), kPa	ε_f, %	w, %	ρ_d (Mg/m 3)
BT2-STD-PL12	0	257	2	12.2	1.58
	70	352	2.4	12.1	1.57
	150	430	6.6	12.1	1.58
	300	631	8.5	12.2	1.57
	600	1071	16.2	12.1	1.57
BT2-STD-PL16	0	294	2.1	15.8	1.63
	70	352.1	2.9	15.9	1.62
	150	515	6.8	15.9	1.62
	300	713	15.5	15.7	1.63
	600	1016.4	14.5	15.8	1.62
BT2-STD-PL19.5	0	320	3	19.3	1.68
	70	451	4.9	19.6	1.67
	150	534	5.8	19.5	1.68
	300	651.1	13.6	19.5	1.67
	600	745.2	9.7	19.5	1.67
BT2-STD-PL22	0	222	6.1	22	1.61
	70	310	12.7	21.7	1.61
	150	355	9.8	21.7	1.62
	300	408	17.6	21.7	1.61
	600	447.3	9.8	21.7	1.62
BT2-MDF-PL8	0	571.6	2.1	7.8	1.78
	70	-	-	-	
	150	910.8	2.7	8.2	1.77
	300	1195.6	3.3	8.2	1.78
	600	1537	5.7	8.3	1.77
BT2-MDF-PL16*	0	571	3.5	16.1	1.84
	70	673.8	3.7	16	1.83
	150	671	4.9	16.2	1.83
	300	796	5.8	16.1	1.83
	600	1157.7	7.8	15.8	1.83
BT2-MDF-PL16	0	631.5	2.7	16.1	1.82
	70	635.8	2.9	15.8	1.81
	150	735.5	2.9	16.2	1.82
	300	821.3	4.8	15.8	1.82
	600	1139.4	6.8	15.9	1.82

Table D5-3 Summary of UCS and UU test data –JF1

Sample id	σ_3, kPa	$(\sigma_1-\sigma_3)$, kPa	ε_f, %	w, %	ρ_d (Mg/m3)
JF1-STD-PL13	0	236.3	1.2	12.9	1.61
	70	422	2.3	13.0	1.60
	150	464	2.9	12.8	1.59
	300	773.9	7.8	12.8	1.59
	600	1243.7	17.4	12.9	1.60
JF1-STD-PL18	0	341.4	1.9	17.8	1.64
	70	422.8	2.9	17.7	1.63
	150	496.2	4.8	17.7	1.63
	300	770.3	13.4	17.7	1.63
	600	939.6	18.4	17.7	1.64
JF1-STD-PL22	0	244	9.9	21.8	1.63
	70	243.2	11	21.6	1.63
	150	300.7	17.8	21.5	1.63
	300	386.5	19	21.7	1.63
	600	436.6	19.8	21.5	1.64
JF1-MDF-PL9	0	612.1	1.5	9.1	1.75
	70	822.8	1.5	9.1	1.75
	150	1048	2.5	9.2	1.75
	300	1493.6	2.5	9.1	1.74
	600	1868.1	5	9.2	1.74
JF1-MDF-PL15	0	661.4	1.8	14.5	1.78
	70	788.2	2.22	14.6	1.79
	150	1004.4	2.9	14.6	1.78
	300	1184.3	4.3	14.6	1.80
	600	1412.6	8.7	14.6	1.79
JF1-MDF-PL19.5	0	578.6	6	19.2	1.74
	70	606	6.5	19.1	1.74
	150	654	9	19.1	1.75
	300	744	12	19.1	1.74
	600	808.5	10	19.1	1.74

Table D5-4 Summary of UCS and UU test data –JF2

Sample id	σ_3, kPa	$(\sigma_1-\sigma_3)$, kPa	ε_f, %	w, %	ρ_d (Mg/m^3)	Sample id	σ_3, kPa	$(\sigma_1-\sigma_3)$, kPa	ε_f, %	w, %	ρ_d (Mg/m3)
JF2-STD-PL10	0	225.1	1.4	9.7	1.72	JF2-MDF-PL8	0	560.3	1.8	8.2	1.83
	70	542.4	3.0	10.0	1.71		70	745.9	2.1	8.1	1.84
	150	697.2	3.6	10.1	1.72		150	1019.7	2.7	8.2	1.83
	300	960.3	6.1	9.7	1.72		300	1216.4	2.7	8.2	1.83
	600	1602.4	14.3	9.9	1.72		600	1640.8	5.8	8.2	1.84
JF2-STD-PL14	0	304.3	1.6	14.0	1.73	JF2-MDF-PL11	0	671	1.8	11	1.86
	70	550	2.9	13.7	1.74		70	769	1.8	11	1.85
	150	673	4.9	13.6	1.74		150	927	2.4	11	1.85
	300	892	11.8	13.7	1.73		300	1239	3.3	11	1.85
	600	1224	11.9	13.8	1.74		600	1650	7.3	11	1.86
JF2-STD-PL16	0	347.8	3.1	16.0	1.76	JF2-MDF-PL13.5	0	643.2	2.4	13.5	1.88
	70	476.5	5.2	15.9	1.77		70	-			
	150	567.1	7.8	16.0	1.76		150	880	3.3	13.4	1.87
	300	719.5	11.7	16.2	1.76		300	1046.8	5.7	13.5	1.87
	600	946.5	11.2	16.2	1.76		600	1305.4	7.6	13.3	1.87
JF2-STD-PL18	0	331.3	4.1	17.6	1.75	JF2-MDF-PL15	0	593	3.2	15.1	1.85
	70	370.9	10.5	17.7	1.75		70	561	3.4	15.2	1.84
	150	444	10.6	17.7	1.74		150	741	4.3	15.2	1.84
	300	558.7	11.5	17.7	1.74		300	956.3	6.7	15.3	1.85
	600	748.5	16.4	17.7	1.75		600	1249	11.5	15.3	1.85
JF2-STD-PL20	0	225.7	10.7	19.7	1.71	JF2-MDF-PL17	0	411.5	5.7	16.9	1.80
	70	245.9	11.6	20.0	1.71		70	465.4	7.6	17.0	1.80
	150	268.9	15.5	20.2	1.72		150	552.5	9.5	17.0	1.79
	300	319.4	23.4	20.1	1.72		300	631.5	11.0	17.2	1.80
	600	312.6	15.4	19.9	1.72		600	7302	20.0	17.2	1.78

Appendix D6- UC and UU Mohr circles fitted with tangents inclined at ϕ’

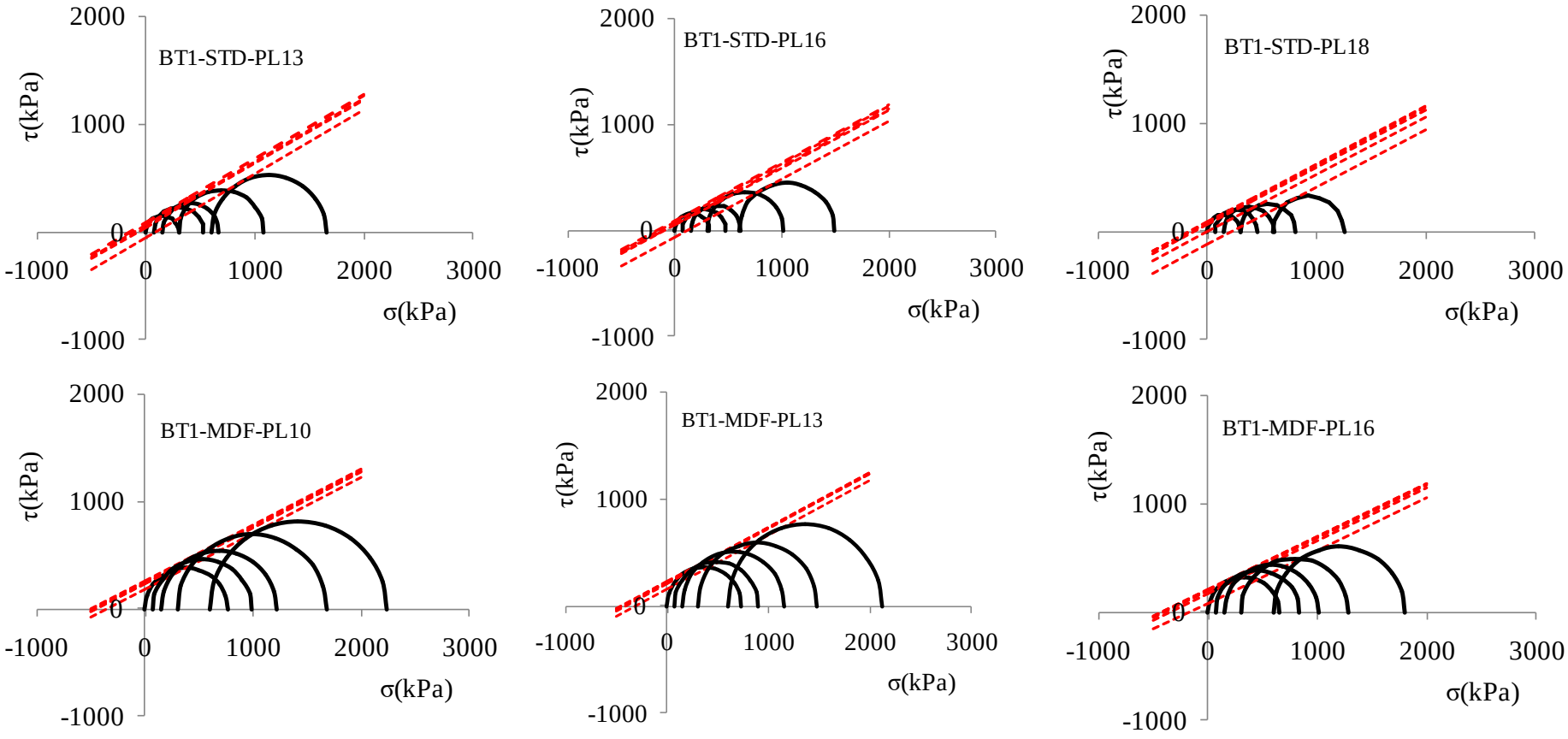

Figure D6-1: UC and UU Mohr circles fitted with tangents inclined at ϕ’- BT1

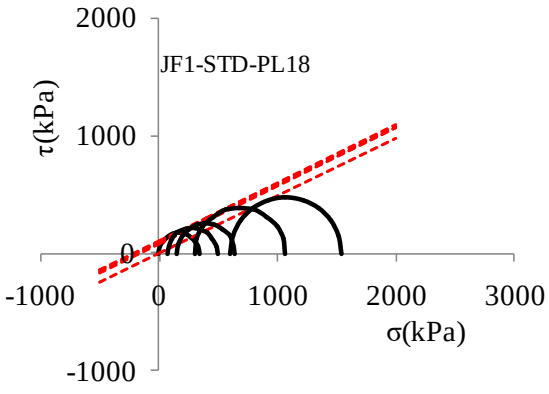
JF1-STD-PL18
τ(kPa)
σ(kPa)
2000
1000
0
-1000
-1000
0
1000
2000
3000

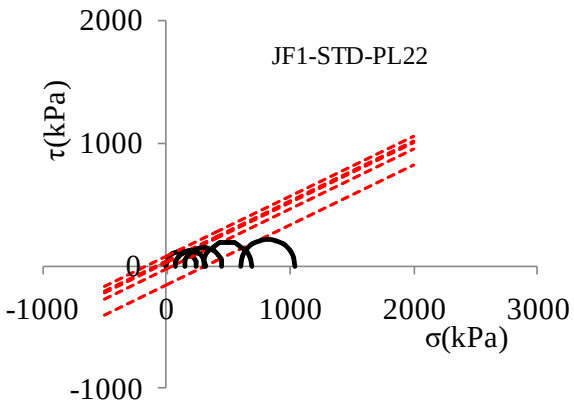
JF1-STD-PL22
τ(kPa)
σ(kPa)
2000
1000
0
-1000
-1000
0
1000
2000
3000

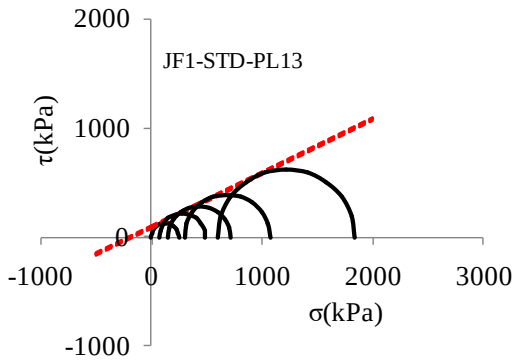
JF1-STD-PL13
τ(kPa)
σ(kPa)
2000
1000
0
-1000
-1000
0
1000
2000
3000

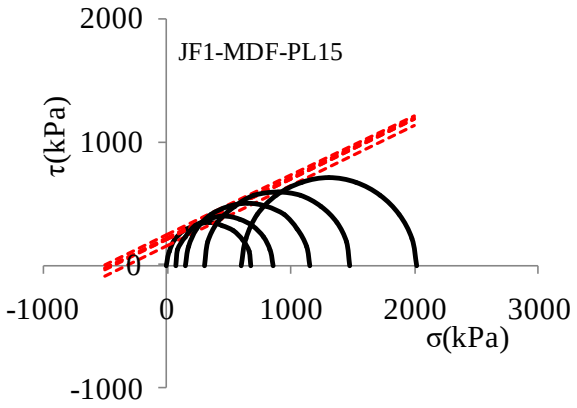
JF1-MDF-PL15
τ(kPa)
σ(kPa)
2000
1000
0
-1000
-1000
0
1000
2000
3000

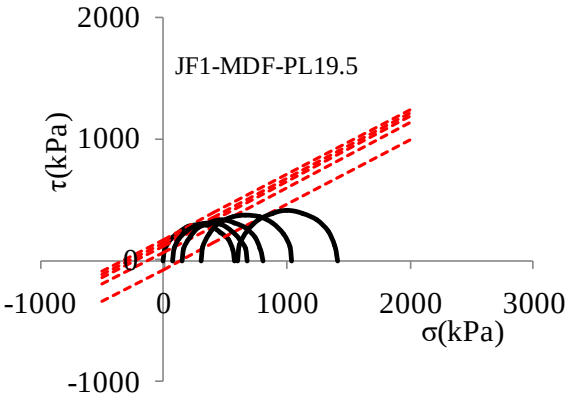
JF1-MDF-PL19.5
τ(kPa)
σ(kPa)
2000
1000
0
-1000
-1000
0
1000
2000
3000

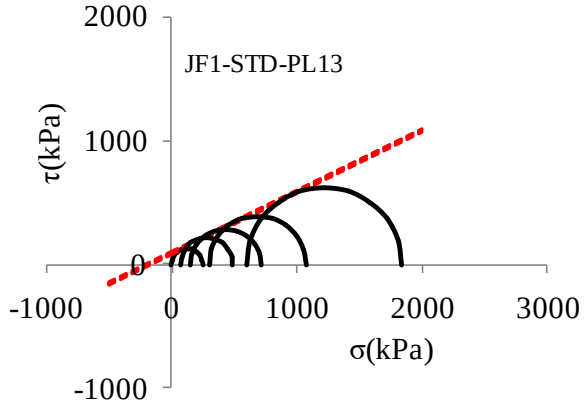
JF1-STD-PL13
τ(kPa)
σ(kPa)
2000
1000
0
-1000
-1000
0
1000
2000
3000

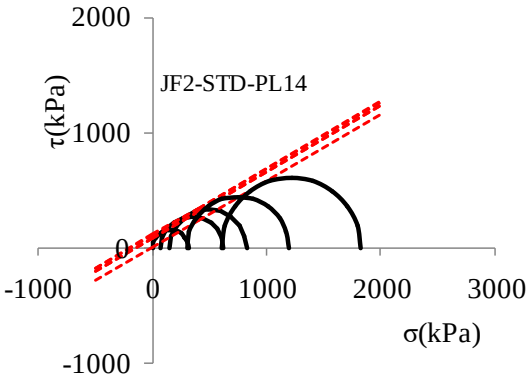
JF2-STD-PL14
τ(kPa)
σ(kPa)
2000
1000
0
-1000
-1000
0
1000
2000
3000

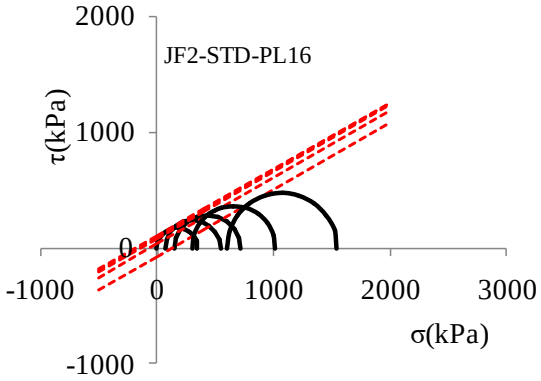
JF2-STD-PL16
τ(kPa)
σ(kPa)
2000
1000
0
-1000
-1000
0
1000
2000
3000

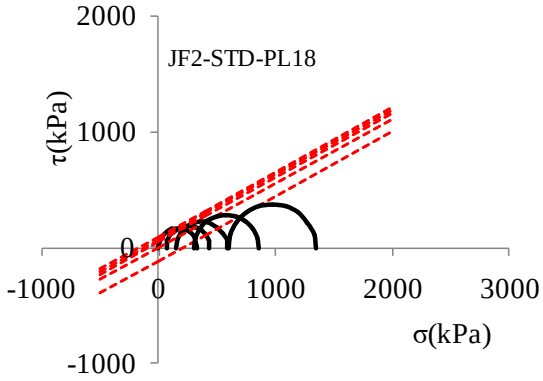
JF2-STD-PL18
τ(kPa)
σ(kPa)
2000
1000
0
-1000
-1000
0
1000
2000
3000

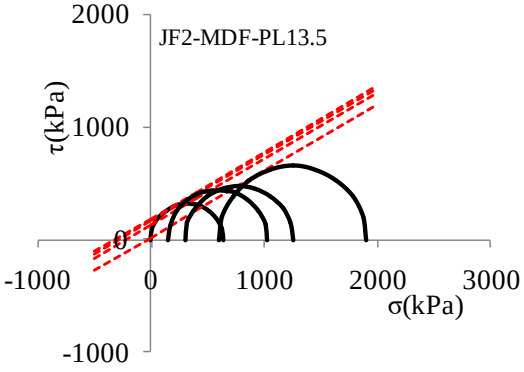
JF2-MDF-PL13.5
τ(kPa)
σ(kPa)
2000
1000
0
-1000
-1000
0
1000
2000
3000

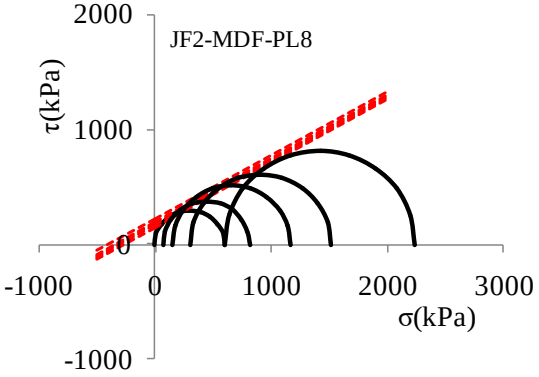
JF2-MDF-PL8
τ(kPa)
σ(kPa)
2000
1000
0
-1000
-1000
0
1000
2000
3000

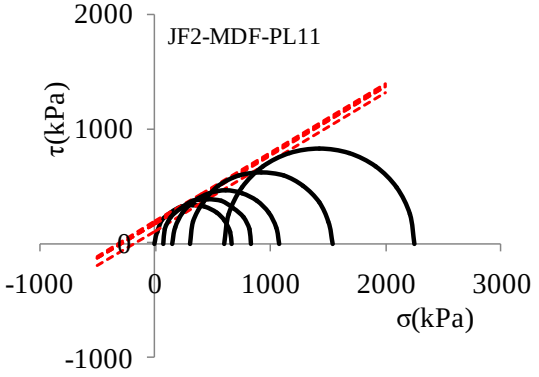
JF2-MDF-PL11
τ(kPa)
σ(kPa)
2000
1000
0
-1000
-1000
0
1000
2000
3000

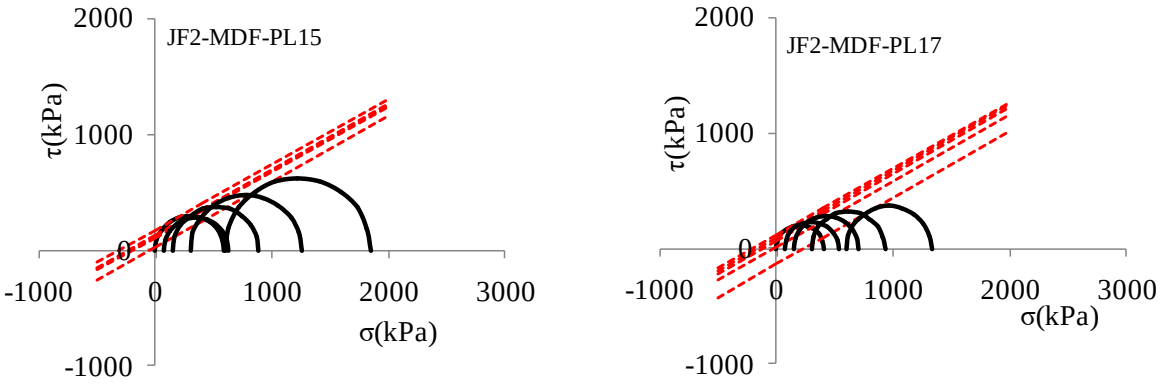

Figure D6-3: UC and UU Mohr circles fitted with tangents inclined at ϕ'- JF2

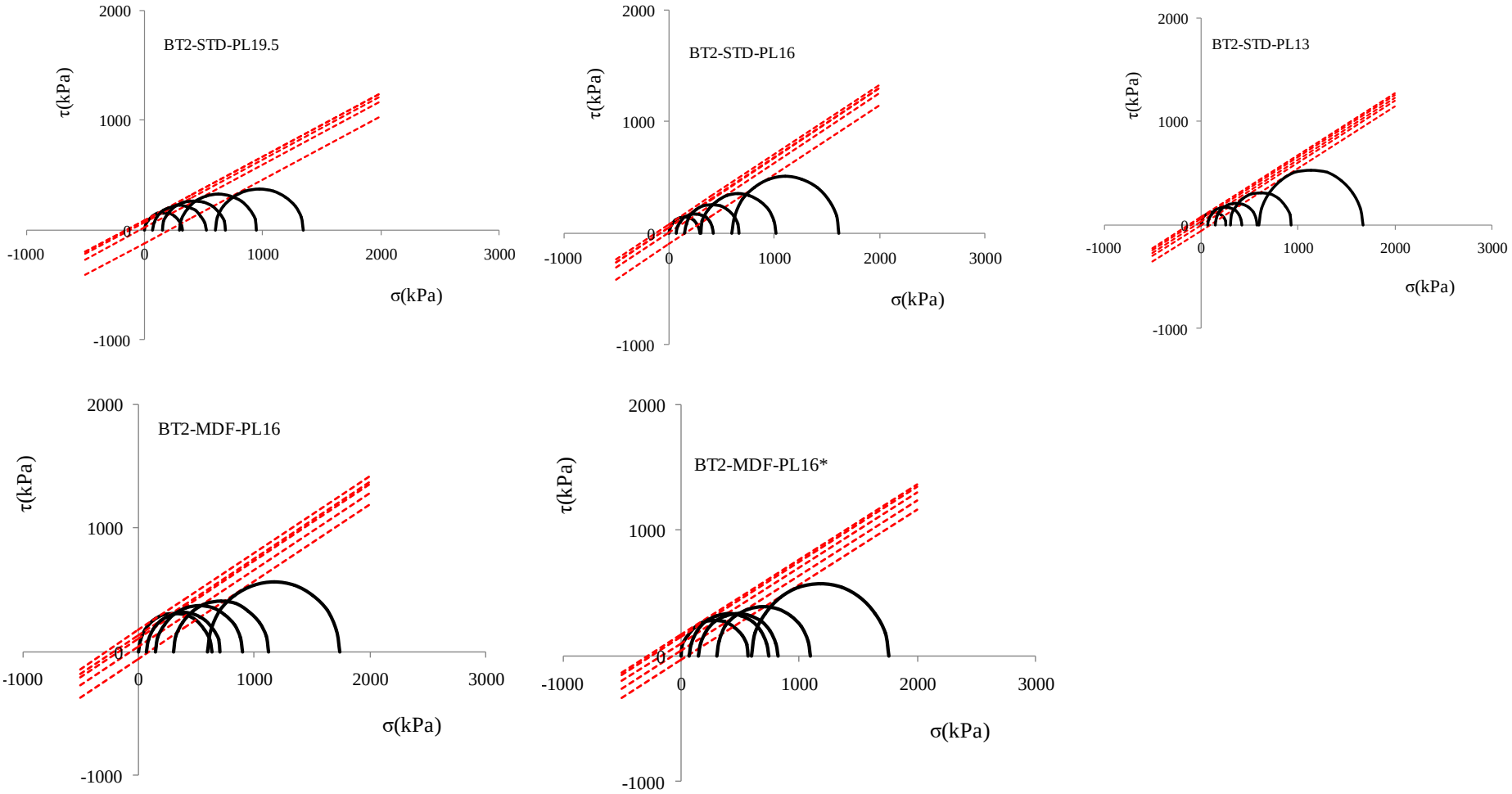

Figure D6-3: UC and UU Mohr circles fitted with tangents inclined at ϕ'- BT2